CARMINE LIMA **Capacity Models for Beam-to-Column Joints in RC Frames Under Seismic Actions**

Dottorato di Ricerca
in Ingegneria delle Strutture e del Recupero Edilizio ed Urbano

Università degli Studi di Salerno
Sede amministrativa

Carmine Lima

CAPACITY MODELS FOR BEAM-TO-COLUMN JOINTS IN RC FRAMES UNDER SEISMIC ACTIONS

IX Ciclo - Nuova Serie (2007- 2010)

DIPARTIMENTO DI INGEGNERIA CIVILE

Dottorato di Ricerca in Ingegneria delle Strutture e del Recupero Edilizio ed Urbano

IX Ciclo N.S. (2007-2010)

CAPACITY MODELS FOR BEAM-TO-COLUMN JOINTS IN RC FRAMES UNDER SEISMIC ACTIONS

Carmine Lima

Il Tutor
Prof. Enzo Martinelli

Il Coordinatore
Prof. Ciro Faella

SUMMARY

Foreword 1

1. Introduction 3
1.1 Beam-to-Column Joints Under Seismic Actions 3
1.2 Basic Concepts on the Mechanical Behaviour of RC Joints 9
1.3 Features of Beam-to-Column Joints 12
1.4 Steel Reinforcement in RC Joints 14

2. Capacity Models for Shear Strength of Joints 17
2.1 Code Formulations 18
2.1.1 ACI-ASCE Committee 352-05 (1985) 18
2.1.2 ACI-ASCE Committee 352–02 (2002) 20
2.1.3 ACI-ASCE Committee 318-05 (2005) 20
2.1.4 AIJ 1990 (1990) 21
2.1.5 AIJ 1999 (1999) 21
2.1.6 NZS 3101 (1995) 22
2.1.7 FEMA 273 (1997) and FEMA 356 (2000) 23
2.1.8 Eurocode 8 (EN 1995-1, 1995) 23
2.1.9 Eurocode 8 (EN 1998-3, 2005) and NTC (2008) 24
2.1.10 NTC (2008) for Existing Joints and OPCM 3431/05 (2005) 25
2.2 Models for both Interior and Exterior Joints 26
2.2.1 The Model by Pantazopoulo & Bonacci (1992) 26
2.2.2 The Model by Paulay & Priestley (1992) 31
2.2.3 The Model by Parker & Bullman (1997) 36
2.2.4 The Model by Hwang & Lee (2002) 39
2.2.5 The Model by Parra-Montesinos & Wight (2002) 44
2.2.6 The Model by Hegger et Al. (2003) 47
2.2.7 The Model by Attaalla (2004) 50
2.2.8 The Model by Kim et Al. (2009) 53
2.3 Specific Models for Interior Joints 55
2.3.1 The Model by Kitayama et Al. (1991) 56
2.3.2 The Model by Hwang & Lee (2000) 56
2.4 Specific Models for Exterior Joints 61
2.4.1 The Model by Zhang & Jirsa (1982) 61
2.4.2 The Model by Sarsam & Phillips (1985) 63
2.4.3 The Model by Ortiz (1993) 64

2.4.4 The Model by Scott et Al. (1994) 67
2.4.5 The Model by Vollum & Newman (1999) 68
2.4.6 The Model by Hwang & Lee (1999) 69
2.4.7 The Model by Bakir & Boduroglu (2002) 74
2.4.8 The Model by Russo & Somma (2006) 75
2.4.9 The Model by Tsonos (2007) 79
2.4.10 The Model by Vollum & Parker (2008) 82
2.5 Remarks 88

3. Parametric Comparison of the Capacity Models 91
3.1 Sensitivity Analysis of the Capacity Models for Exterior Joints 92
3.1.1 Column width b_c 93
3.1.2 Beam width b_b 94
3.1.3 Aspect ratio (h_b / h_c) 95
3.1.4 Horizontal Reinforcement Index 96
3.1.5 Beam Reinforcement Index 98
3.1.6 Column Reinforcement Index 99
3.1.7 Axial Load N_c 100
3.1.8 Concrete Strength f_c 102
3.2 Sensitivity Analysis of the Models for Interior Joints 103
3.2.1 Column width b_c 104
3.2.2 Beam width b_b 105
3.2.3 Aspect ratio (h_b/h_c) 106
3.2.4 Horizontal Reinforcement Index 107
3.2.5 Beam Reinforcement Index 109
3.2.6 Column Reinforcement Index 110
3.2.7 Axial Load N_c 111
3.2.8 Concrete Strength f_c 112

4. The Experimental Database 115
4.1 Exterior Joints 115
4.2 Interior Joints 124
4.3 Evaluation of the Experimental Shear Strength 128
4.4 Parametric Examination of the Databases 130
4.4.1 Exterior Joints 130
4.4.2 Interior Joints 135
4.5 Remarks 140

5. Experimental Assessment of the Capacity Models 143

5.1 Experimental Observation vs. Theoretical Predictions 143
5.1.1 Experimental Assessment of Code Formulations for Exterior Joints 144
5.1.2 Experimental Assessment of Capacity Models for Exterior Joints Available in the Literature 155
5.1.3 Experimental Assessment of Code Formulations for Interior Joints 175
5.1.4 Experimental Assessment of Capacity Models Available in the Literature for Interior Joints 186
5.2 Error and Scatter Measures 197
5.3 Insights about Reliability-related Aspects 210
5.3.1 Overview of Reliability Assessment in Seismic Analysis 210
5.3.2 Correlation Index of Capacity Models for Reliability Analysis 213

6. Recalibration of the Capacity Models 225
6.1 Recalibration of Capacity Models 225
6.1.1 Recalibration of Code Formulations for Exterior Joints 226
6.1.2 Recalibration of Capacity Models Available in the Literature for Exterior Joints 239
6.1.3 Recalibration of Code Formulations for Interior Joints 260
6.1.4 Recalibration of Capacity Models Available in the Literature for Interior Joints 271
6.2 Probabilistic Assessment 281
6.2.1 Exterior Joints 283
6.2.2 Interior Joints 311
6.3 The Proposed Formula for Exterior Joints 330
6.3.1 Assessment of the Proposed Formula 333

7. Monotonic and Cyclic Strength 339
7.1 Specimens Under Cyclic Loads 339
7.2 Low Cycle Fatigue 341
7.3 Fatigue Curves 343
7.3.1 Interior Joints 344
7.3.2 Exterior Joints 348

8. Modelling Joints in Nonlinear Structural Analyses 353
8.1 Overview of Joints Models 353
8.1.1 The Model by Biddha & Ghobarah (1999) 355
8.1.2 The Model by Youssef & Ghobarah (2001) 364

8.1.3 The Model by Pampanin et al. (2003) 372
8.1.4 The Model by Lowes & Altoontash (2003) and Mitra & Lowes (2007) 374
8.1.5 The Model by Trowland (2003) 385
8.1.6 The Model by Shin & LaFave (2004) 386
8.2 Preliminary Simulation of the Cyclic Behaviour of Joints 396
8.2.1 Simulation of the Model by Biddha & Ghobarah (1999) 396
8.2.2 Simulation of Interior Joint 397
8.2.3 Simulation of Exterior Joint 400
8.3 Development and Assessment of a Hysteretic Nonlinear Model for Exterior Joints 403
8.3.1 Joint Strength Model 405
8.3.2 Joint Stiffness Model 406
8.3.3 The Experimental Database 406
8.3.4 Calibration of Model Parameters 411

9. Joint Behaviour in Frame Analyses 419
9.1 Seismic Analysis of Frame Structures 419
9.1.1 Static Nonlinear Analysis 420
9.1.2 Nonlinear Time History Analysis 425
9.1.3 Vulnerability Evaluation 429
9.2 Application 434
9.2.1 The Analysed Structure 435
9.2.2 Static Nonlinear Analysis Results 441
9.2.3 Results of Seismic Assessment 443
9.2.4 Nonlinear Time History Analysis Results 446

10. Conclusions 449
10.1 Assessment of Capacity Models 450
10.2 Assessment of Recalibrated Capacity Models and Proposed Formula 459
10.3 Reliability Analysis 464
10.4 Monotonic and Cyclic Strength 469
10.5 Nonlinear Joints in Seismic Analysis of Frames 470

Appendix A1- Database for Exterior Joints 473

Appendix A2- Database for Interior Joints 509

References 525

List of Figures 539

List of Tables 555

FOREWORD

This thesis reports a detailed study on the behaviour of beam-to-column joints in reinforced concrete (RC) structures. They represent one of the most critical regions in frame structures under seismic actions.

The work is organised in ten chapters. In the first one general aspects about beam-to-column joints in RC structures are presented.

The second chapter collects the code formulations and the capacity models currently available in the scientific literature for evaluating the shear strength of both exterior and interior joints. Some authors have provided models for evaluating the shear capacity of only exterior or interior joints, while other ones have developed formulations for determining the strength of generic joints (both interior and exterior). Furthermore, the difference between theoretical and analytical models is specified by considering if the model has been developed by the authors through equilibrium, compatibility and constitutive laws or through calibration of experimental evidence, respectively. For each model the procedure for evaluating the capacity is explained through some flow-charts.

In the third chapter the models outlined in the previous chapter are analysed through a parametric assessment with the aim of pointing out the sensitivity of the various models to the relevant mechanical parameters.

In chapter 4 a wide experimental database has been collected and a comparison between the experimental evidence. The database is subdivided in interior and exterior subassemblies.

The comparison between the theoretical results collected in the database and the theoretical shear strength is made in chapter 5 for assessing the presented models.

In chapter 6, by considering the experimental results collected in the database, the models have been recalibrated and, by considering the increasing importance of probabilistic analyses in seismic assessment, the relevant coefficients describing the average error and the dispersion of the models have

been evaluated. Furthermore, a new formulation for evaluating the shear strength of exterior joints is proposed.

In the last sections the behaviour of reinforced concrete beam-to-column joints under cyclic loading is analysed and a simple model for dynamic non-linear analyses is proposed. In particular, in chapter 7 the shear strength of joints under cyclic loading is evaluated starting from the monotonic strength evaluated through the mentioned capacity models and considering the number of cycles of load and unload with the low fatigue theory.

In chapter 8 the main models currently available in the scientific literature for simulating the cyclic behaviour of RC joints in frame structures are presented. A model that can be easily used in seismic assessment of RC frames for taking into account the damage of beam-to-column joint is calibrated and assessed.

In chapter 9 further applications are reported about seismic assessment of existing RC structures including joint damage simulated through the model calibrated in chapter 8.

Finally, chapter 10 includes the resume of the main results and the conclusions.

CHAPTER I

1. Introduction

Reinforced concrete (RC) buildings designed during the 1960s and 1970s still widely exist in Italy. Furthermore, they are often strategic structures such as schools or hospitals which are vulnerable to seismic events due to insufficient capacity in terms of either strength or ductility, namely due to widely spaced column ties, and little or no transverse reinforcement within beam-column joint regions.

The studies on seismic vulnerability of structures have been intensified in the last two decades by considering the damage observed after the recent earthquakes of Assisi (1996), Molise (2002) and L'Aquila (2009). The reports of damage observed on existing structures pointed out the key importance of beam-to-column joints on the global performance of RC structures. Several theoretical and analytical formulations have been proposed for evaluating the shear strength of beam-to-column joints. The present thesis deals with the formulations for evaluating the shear strength of exterior and interior connections currently available in both the scientific literature and the main seismic codes.

In this chapter an overview of damage due to seismic events is reported showing the key influence of beam-to-column joints on seismic response of frame structures. Then, the features of RC joints are outlined and a preliminary classification of joints is proposed with reference to the amount of steel reinforcement in the panel zone.

1.1 Beam-to-Column Joints Under Seismic Actions

By observing the damages of the existing RC structures due to the recent seismic events (Bursi et al., 2009; Cimellaro, 2009) the vulnerability is mainly due to shear failure and/or plastic hinges made at the top and the bottom of the

column with consequently soft storey mechanism, bond slip of bars in column and beam and failure of the beam-to-column joints. These mechanisms are generally due to the absence of seismic details in the structural elements; these critical zones develop a brittle failure and accordingly low available ductility.

Fig. 1.1 shows a typical joint failure at the intersection with the column and an example of wrong detail of stirrup with smooth bars.

(a) (b)

Fig. 1.1: Joint failure and wrong detail of stirrup (Bursi et al., 2009).

The worst and unfortunately the most frequent mechanism of collapse is the one due to soft story, as it is the mechanism resulting in the minimum ductility capacity. It generally occurs at the lower floors, especially in the cases of buildings with a colonnade at the first floor.

(a) (b)

(c) (d)

Fig. 1.2: Soft story mechanisms due to the earthquake of L'Aquila (Bursi et al., 2009).

(a) (b) (c)

Fig. 1.3: Joint failures due to the earthquake of L'Aquila (Bursi et al., 2009).

Shear failure in the column is very common in the squat elements located near the windows (Fig. 1.4).

(a) (b)

Fig. 1.4: Shear failure of squat column due to seismic events (Cimellaro, 2009).

The recent seismic codes take into account that under seismic actions excursions in plastic field can be expected in the structures. Therefore, in the design the capacity of the structures of dissipating the energy introduced by the earthquake is considered. This philosophy, called "Capacity Design", distinguishes the various parts of the structure in dissipative and non-dissipative zones. The first ones consist of elements and mechanisms of ductile members, the others account crises characterised by brittle mechanisms. The ductile mechanisms are "controlled by the displacements" (displacement controlled), or they are characterized by high displacement capacity that allows to obtain a non-linear response of the structure. On the contrary, brittle mechanisms are "controlled by the forces" (force controlled); in particular, they occur at a fixed value of force generally in the elastic range.

The corresponding design criterion is called Capacity Design and has two basic rules:

- ductile elements and mechanisms are designed considering the maximum stress that they can receive if earthquake occurs;

- brittle elements and mechanisms are designed considering the maximum stress that the ductile elements and mechanisms are able to transfer when they reach the ultimate conditions (or their plasticity starts).

In RC structures the beams are generally considered the ductile elements as well as the bending failures are accounted as ductile mechanisms. Instead, the shear failures are identified as brittle mechanisms

Beam-to-column joints are characterised by a shear failure so, in frame structures they are considered as brittle elements.

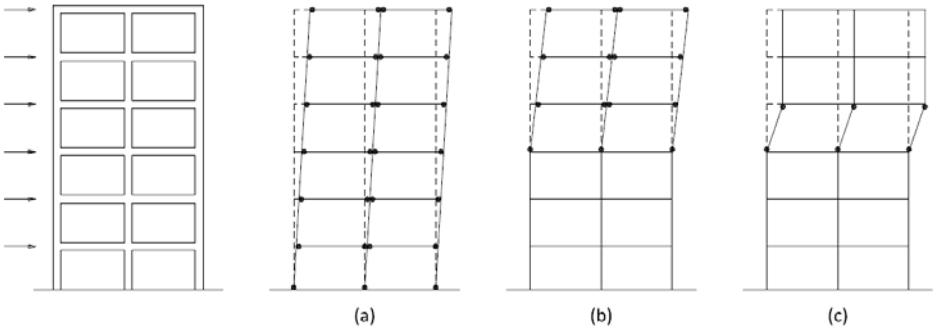

Fig. 1.5: Modes of collapse of RC frame structures.

The result of the Capacity Design approach in RC structures is a system namely with strong column and weak beam. This design approach tends to preserve the integrity of the columns and supports the formation of plastic hinges at the ends of the beams. The type of collapse that occurs is, therefore, global or partial [Fig. 1.5 (a) and (b)] avoiding the most inconvenient local mechanism also called soft story mechanism [Fig. 1.5 (c)].

The advantage of achieving global collapses than local ones is that they allow to dissipate energy greater the one dissipated in the latter type of failure. In global mechanisms there are multiple zones of plasticity that dissipate the energy input due to earthquakes.

The criteria for obtaining a correct behaviour of joints in ductile seismic resistant structures according to the requirements of the Capacity Design can be summarized as follows (Paulay & Priestley, 1992):

- the strength of the joint must not be smaller than the maximum demand corresponding to the development of plastic hinge in the adjacent beams;

- the capacity of the column must not be compromised by a strength reduction of the joint, considered as a part of the column;
- under low seismic actions the response of beam-to-column joints should be elastic;
- the joint deformation should not significantly affect the interstory drift and then the global displacement of the structure;
- the steel reinforcement in the pane zone should not lead complex details.

It has been observed that it is not convenient to solve the problems of strength by increasing the horizontal reinforcement in the joint, because it causes severe construction problems (Kim & LaFave, 2009).

Fig. 1.6 reports an example of two types of joints: one for buildings designed for only vertical loads according old design criteria and the other one detailed according to the recent seismic codes for buildings designed by considering the Capacity Design approach.

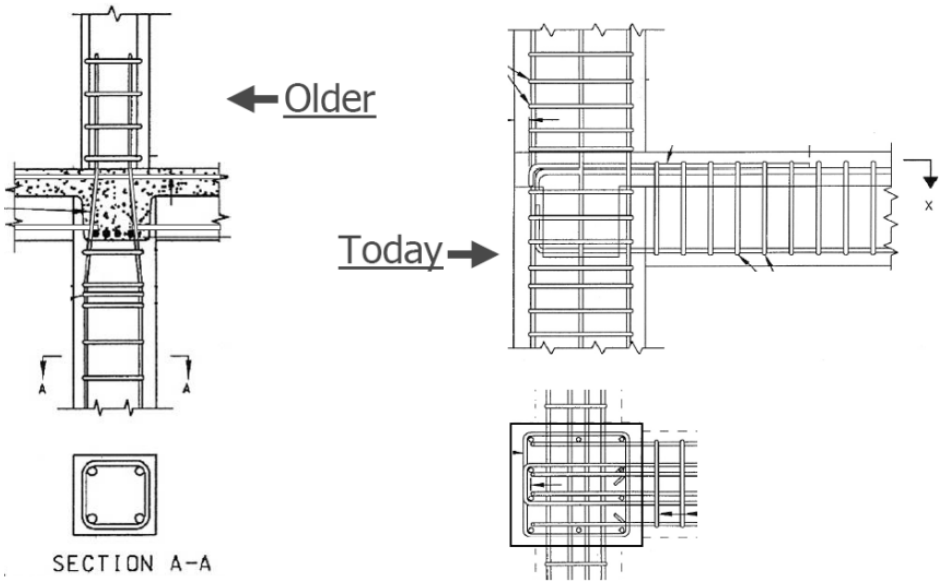

Fig. 1.6: Comparison between old and compliant with recent seismic codes joint details (Deierlein et al., 2006).

Fig. 1.7 shows the details of an exterior and an interior joint designed according to the modern seismic codes accounting the Capacity Design criteria.

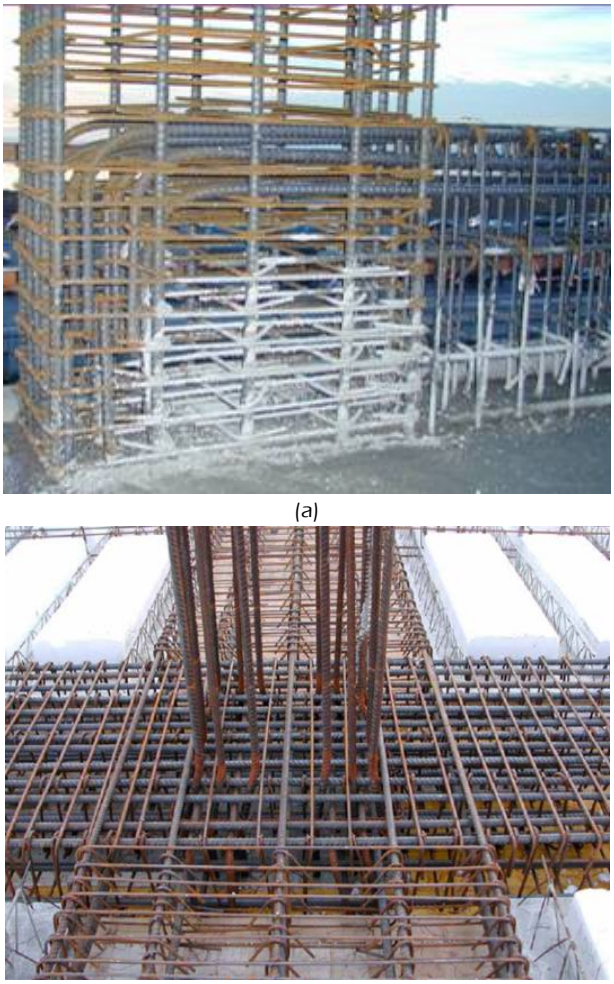

(a)

(b)

Fig. 1.7: Comparison between old and compliant with recent seismic codes joint details (Deierlein et al., 2006).

1.2 Basic Concepts on the Mechanical Behaviour of RC Joints

A significant amount of research on the seismic performance of RC beam-to-column joints has been carried out in the last four decades. The researches available in the scientific literature have emphasized the improvement of the

performance of RC beam-to-column joints through new design concepts and improved details such as hoops in the panel zone and improved anchorage. Several researches have focused on an array of different variables, including the geometry, the transverse reinforcement ratio, the effect of column axial load, etc., which are of interest in the present study.

The joints can be classified according to the geometry in *exterior* and *interior* ones; as shown in Fig. 1.8 in a generic RC structure both interior and exterior joints can be identified.

Various types of exterior beam-to-column connections are shown in Fig. 1.10; some of these ones have in-plane behaviour [Fig. 1.9 (a) and (b)], the other ones develop a three-dimensional response. The type (b) and (e) (Fig. 1.9) are identified as corner joints because they have two sides free. Particular considerations are needed about the so-called knee joints [Fig. 1.9 (a)] outlined as an exterior joint without the top column.

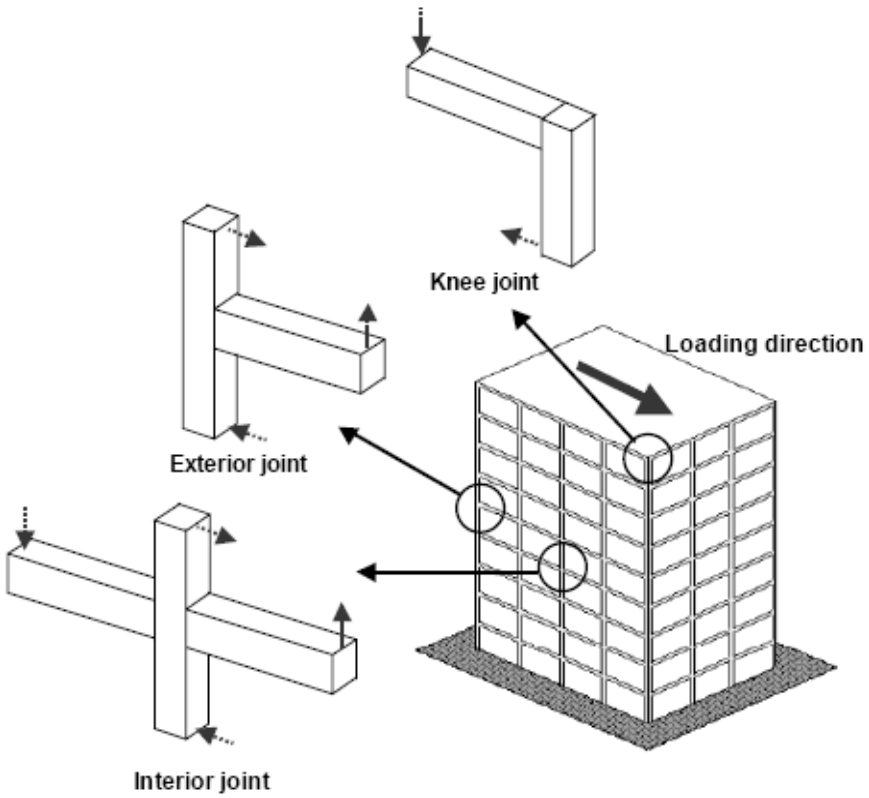

Fig. 1.8: Beam-to-column connections in RC structures (Kim et al., 2009).

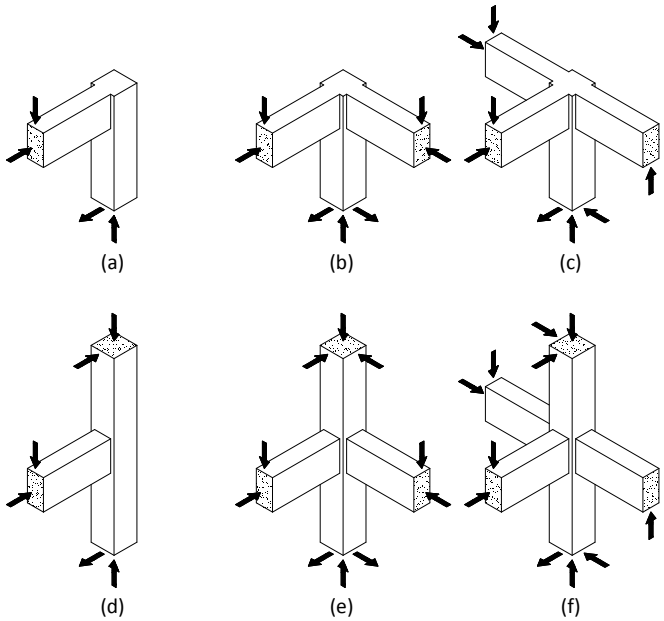

Fig. 1.9: Exterior beam-to-column joints (Paulay & Priestley, 1992).

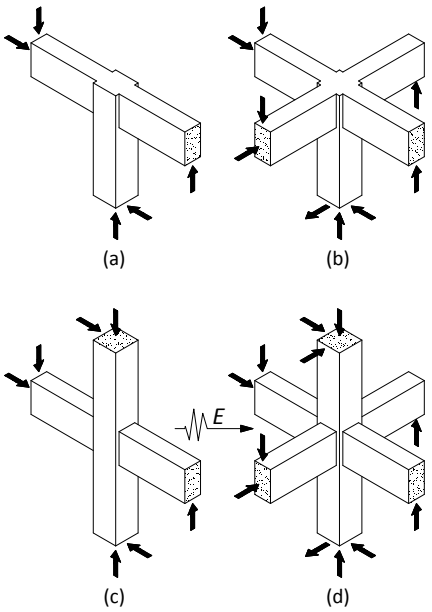

Fig. 1.10: Interior beam-to-column joints (Paulay & Priestley, 1992).

Fig. 1.10 shows the corresponding plane and three-dimensional configurations of interior joints. The represented arrows point out possible forces on the joint subjected to seismic action.

1.3 Features of Beam-to-Column Joints

Plastic hinges can develop under seismic action in beams immediately adjacent to the column faces. In this case large shear forces result on beam-to-column joints leading to possible failure in the joint core due to the breakdown of shear or bond mechanisms or both.

Such a joint is also part of a column (Paulay & Priestley, 1992), the equilibrium problem can be examined as a column component. By considering an interior column extracted by a frame structure at approximately half-story heights (corresponding to the ideal points of contraflexure under seismic load), the actions introduced by symmetrically reinforced beams to the column are shown in Fig. 1.11 being T_b and C_b the horizontal tension and compression forces, respectively and V_b the vertical beam shear forces.

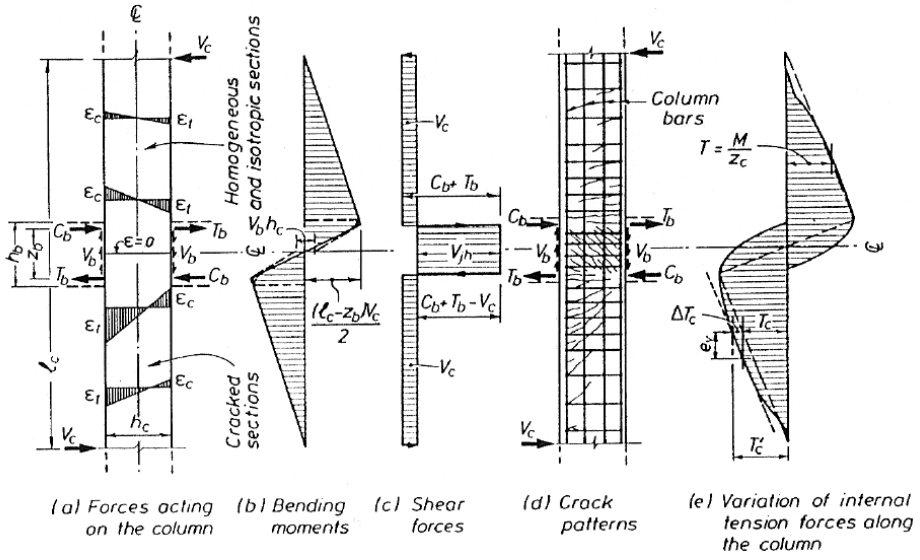

Fig. 1.11: Features of column and joint behaviour (Paulay & Priestley, 1992).

Assuming that $C_b = T_b$ and that beam shear on opposite sides of the joint are equal, equilibrium of the free body shown requires a horizontal column shear force:

$$V_{col} = \frac{2 \cdot T_b \cdot z_b + V_b \cdot h_c}{L_c} \tag{1.1}$$

where the variables are readily identified in Fig. 1.11 and Fig. 1.12.

The horizontal shear force across the joint region is:

$$V_{jh,E} = C_b + T_b - V_{col} \ . \tag{1.2}$$

Similar to the previous equation, the shear force acting an interior joint can be evaluated as follows:

$$V_{jh,E} = T + T' - V_{col} \tag{1.3}$$

in which T and T' are the tensile strength of the top and bottom beam reinforcement, respectively.

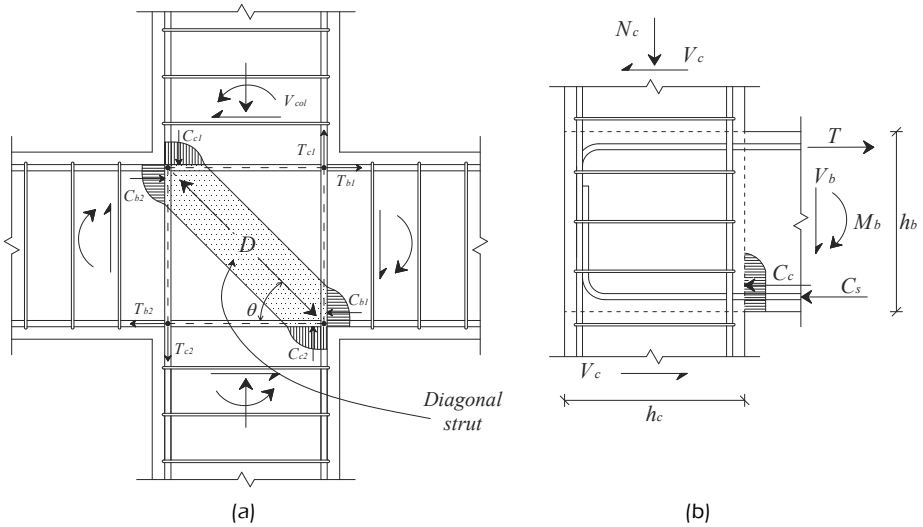

(a) (b)

Fig. 1.12: Equilibrium for interior (a) and exterior (b) joints.

As the quantities of top flexural reinforcement $A_{sb,sup}$ and bottom flexural reinforcement $A_{sb,inf}$ in the beam are known and the tensile steel is assumed to have developed its overstrength $\lambda_0 f_{yb}$, the maximum intensity of the horizontal joint shear force to be used in the design and the assessment is:

$$V_{jh,E} = \left(A_{sb,\sup} + A_{sb,\inf}\right) \cdot \lambda_0 \cdot f_{yb} - V_{col} = \left(1+\beta\right) \cdot A_{sb,\sup} \cdot \lambda_0 \cdot f_{yb} - V_{col} \tag{1.4}$$

where

$$\beta = A_{sb,\inf} \Big/ A_{sb,\sup} \,. \tag{1.5}$$

By considering an exterior joint in which only one beam converges into the column, it is evident that similar to Eqn. (1.3) the horizontal joint shear force is:

$$V_{jh,E} = T - V_{col} \tag{1.6}$$

where only the tension force T of the top beam reinforcement is taken into account.

1.4 Steel Reinforcement in RC Joints

By considering the purpose of this thesis a further classification has been developed taking into account the amount the horizontal reinforcement in the panel zone. The amount of stirrups in the panel zone can be read as a measure of the seismic details of the joint; in particular, the strong reinforced joint can be considered like new joints designed according to the modern capacity design principles, while the unreinforced joints are representative of joints of existing RC structure designed without seismic details.

Thus, the following three classes can be defined on the basis of the amount of transversal reinforcement within the joint panel:

- **Unreinforced** joints;
- **Under-reinforced** joints;
- **EC8-compliant** joints (EN 1998-3, 2005).

The third class collects the joints with an amount of transversal stirrups A_{sjh} complying with the EC8 provisions for RC frames in seismic areas:

$$A_{sjh} \geq A_{sjh,EC8} = \left[\frac{\left(\dfrac{V_{jh,E}}{b_j \cdot h_{jc}} \right)^2}{\left(f_{ctd} + \nu_d \cdot f_{cd}\right)} - f_{ctd} \right] \cdot \frac{b_j \cdot h_{jb}}{f_{yj}} \tag{1.7}$$

The complete definition of the parameters in Eqn. (1.7) is omitted herein for the sake of brevity and can be found in Eurocode 8 (EN 1998-3, 2005).

In particular, the shear stress $V_{jh,E}$ should be evaluated as follows:

$$V_{jh,E} = 1,2 \cdot A_{sb,\sup} \cdot f_{yb} - V_c^{\exp} \tag{1.8}$$

where V_c^{exp} is the shear stress in the top column, which is related to the ultimate load P_u^{exp} also depending on the test layout. All joints whose amount of stirrups A_{sjh} is

$$0 \le A_{sjh} < A_{sjh,EC8} \tag{1.9}$$

are considered as "under-reinforced", while in "unreinforced" ones no stirrups at all are present in the joint panel.

CHAPTER II

2. Capacity Models for Shear Strength of Joints

This chapter is devoted to an overview of the capacity model available in the scientific literature. Those models can be classified using several criteria.

As a first classification the capacity models can be subdivided in three classes based on the layout of the joint they deal with:

- capacity models for generic joint (both interior and exterior);
- capacity models for interior joints;
- capacity models for exterior joints.

As a second classification, the difference between theoretical and analytical model can be proposed by subdividing the capacity models developed by the authors by equilibrium, constitutive laws and compatibility considerations and the capacity models developed by experimental evidence. In this last group two classes can be identified: the models developed regarding only experimental evidence without any theoretical foundation and the analytical models developed by theoretical models opportunely modified by numerical coefficients calibrated on the bases of experimental evidence.

Another classification consists in subdividing the capacity models developed for evaluating shear strength of beam-to-column joints under monotonic loads from the ones useful in evaluating the shear strength under cyclic loading.

An important classification in seismic assessment of existing structures consists in subdividing the model based on the amount of stirrups in the joint; for these purposes three classes have been identified:

- unreinforced joints;
- joints with low horizontal reinforcement (in which the amount of stirrups is lower than the limit proposed by seismic codes), namely under-reinforced;
- joints with normal and high horizontal reinforcement compliant with recent seismic, namely EC8-compliant.

Finally, as a last classification the models developed by the author for design purpose can be divided from the models developed for assessment purpose.

In the following, after a brief treatment of the features of beam-to-column joints, useful for evaluating the shear demand, the recommendations of the main international codes of the last two decades are reported. Finally, a comprehensive collection of capacity models available in the scientific literature are exposed by adopting the first classification of models for generic joint, for only interior joints and for only exterior ones.

2.1 Code Formulations

In the last two decades the importance of beam-to-column joints in RC structures has quickly increased. Many codes have focused their attention on those elements to insure proper structural performance under earthquake shakes that may reasonably be expected to occur and to alert the designer to possible congestion of reinforcement.

The present section deals with the most important code recommendations available worldwide for evaluating the seismic of joints in both new and existing RC structures with the purpose of providing the reader with important tools about design and assessment of beam-to-column RC joints.

2.1.1 ACI-ASCE Committee 352-05 (1985)

The recommendations provided by the *American Concrete Institute* through ACI 352–85 (1985) can be used for evaluating beam-to-column joints size and designing of the longitudinal and transverse reinforcement at the intersection of beams and columns. The code specifically excludes the slab-to-column connections and precast structures in which connections are made near the beam-to-column region. The recommendations take into account two types of joints:

- Type 1 takes into account the joints designed on the basis strength without considering special ductility requirements (i.e. joints in typical frame designed to resist gravity and normal wind loads);
- Type 2 takes into account the joints that connect members which are required to dissipate energy through reversals of deformation into the inelastic range (i.e. joints designed to resist earthquake motions, very high winds, or blast effects).

Considering the joints in type 2 the ACI 352-85 (1985) recommendations are suitable for connections where the beam bars are located inside the column core, in other words the ACI 352-85 (1985) formulation is applicable to the joints Type 2 if the beam width is less or equal to the column width.

The ultimate shear force is evaluated using Eqn. (2.1) in which 0.083 is the conversion factor from psi to MPa, h_c is the thickness of the column in the direction of loading and b_j is the effective width of the joint.

$$\begin{aligned} V_{jh} &= \gamma \cdot \sqrt{f_c} \cdot b_j \cdot h_c \qquad (psi) \\ V_{jh} &= 0.083 \cdot \gamma \cdot \sqrt{f_c} \cdot b_j \cdot h_c \qquad (MPa)\,. \end{aligned} \tag{2.1}$$

The effective width b_j of the joint can be evaluated starting from the equivalent beam width b_b and the column width b_c. When there is only one beam in the direction of load (i.e. exterior joints) the equivalent beam width b_b should be taken equal the width of that beam. If there are two beams in the loading direction (i.e. interior joints) the equivalent base is taken as the average between the widths of those two beams. The effective joint width is evaluated as follows considering that the first case in which b_b is greater than b_c is suitable for only the joints type 1.

$$\begin{aligned} &\text{if } b_b > b_c \text{ then} \qquad b_j = b_c \\ &\text{if } b_b \le b_c \text{ then} \qquad b_j = {(b_b + b_c)}/{2}\,. \end{aligned} \tag{2.2}$$

However, the effective joint width b_j should not be greater than the equivalent beam width b_b plus one half of the column depth h on each side of the beam.

Finally, the constant γ depends on the joint classification and joint type as defined above and is given by Table 2.1.

Table 2.1: Values of γ for beam-to-column joints provided by ACI 352-85. (1985)

JOINT TYPE	JOINT CLASSIFICATION		
	Interior	Exterior	Knee
(1)	24	20	15
(2)	20	15	12

A further limitation is given about the concrete strength; in particular, the ACI 352-85 (1985) formulation is unsuitable in the case of concrete compressive strength lower than 6000 psi (42 MPa) because at that time no research studies were available for connections constructed using high strength concrete.

2.1.2 ACI-ASCE Committee 352–02 (2002)

The ACI 352-02 (2002) (*"Joints and Connections in Monolithic Concrete Structures"*) defines nominal ultimate shear strength for modern RC beam-to-column connections similarly to the ACI 352-85 (1985) mentioned above as follows:

$$V_{jh} = \gamma \cdot \sqrt{f_c} \cdot b_j \cdot h_c \qquad (MPa). \tag{2.3}$$

The shear strength factor is provided in $MPa^{0,5}$ (Table 2.2) depending on the same joint classification and joint type defined by ACI 352-85 (1985).

A different law is provided for evaluating the effective joint width b_j; in particular, the following equation should be used for this purpose:

$$b_j = \min\left(\frac{b_b + b_c}{2}; b_b + \sum\frac{m \cdot h_c}{2}; b_c\right) \tag{2.4}$$

in which b_b and b_c are the beam and column width respectively, h_c is the column thickness and m is the slope to define the effective width of joint transverse to the direction of shear. The value of m should be 0.3 when the eccentricity between the beam centerline and the column centroid exceeds $b_c / 8$ and 0.5 in other cases. Finally, the term $m\, h_c / 2$ should not be taken greater than the extension of the column beyond the edge of the beam.

Table 2.2: Values of γ for beam-to-column joints provided by ACI 352-02 (2002).

JOINT TYPE	JOINT CLASSIFICATION		
	Interior	Exterior	Knee
(1)	1,67	1,25	1,00
(2)	1,25	1,00	0,67

2.1.3 ACI-ASCE Committee 318-05 (2005)

The formulation provided by ACI 318-05 (2005) for evaluating the shear strength of RC beam-to-column joints is the same as the one already adopted in ACI 325-02 (2002). Also the philosophy is the same except for a few points:

ACI 318-05 (2005) does not consider column discontinuity in determining the joint shear strength factor γ: no difference is considered between exterior and knee joints; the effective joint width is evaluated as follows:

$$b_j = \min\left(b_b + h_c ; b_b + 2x\right) \tag{2.5}$$

where x is the smaller of the distance beam face to column face.

2.1.4 AIJ 1990 (1990)

The AIJ 1990 (1990) provides a simple formulation for evaluating the shear strength of interior and exterior joints; in particular the following equation is recommended:

$$V_{jh} = k \cdot f_c \cdot b_j \cdot D_j \qquad (MPa) \tag{2.6}$$

where k is a factor equal to 0.30 for interior joint and 0.18 for exterior ones, f_c is the concrete compression strength in MPa, D_j is the effective column depth defined as the column depth for interior joints and the projected development length of anchored beam bars with 90 degree hooks for exterior and knee connections. The effective joint width b_j is defined as:

$$b_j = b_b + b_{a1} + b_{a2} \tag{2.7}$$

in which b_{a1} and b_{a2} are the smaller of ¼ of column depth h_c and ½ of distance between beam and column face on either side of beam.

2.1.5 AIJ 1999 (1999)

AIJ 1999 (1999) (*"Design guidelines for earthquake resistant reinforced concrete building based on ultimate strength concept and commentary"*) has recommended nominal joint shear strength in the following form:

$$V_{jh} = k \cdot \phi \cdot F_j \cdot b_j \cdot D_j \qquad (MPa). \tag{2.8}$$

In Eqn. (2.8), k is the factor dependent on the shape of in-plane geometry (1.0 for interior joints, 0.7 for exterior and T-shape connections and 0.4 for knee ones), ϕ is the factor for the effects of out-of-plane geometry (1.0 for joints with transverse beams and 0.85 for other cases), F_j is the standard value of the joint shear strength and b_j and D_j are the effective joint width the effective column depth respectively evaluated as recommended by the previous AIJ 1990 (1990).

$$F_j = 0.8 \cdot f_c^{0,7} \tag{2.9}$$

The standard value of the joint shear strength is assumed to be function of the concrete strength by Eqn. (2.9).

2.1.6 NZS 3101 (1995)

The *"Concrete structure standard"* NZS 3101 (1995) has suggested of evaluating the shear strength of joints as follows:

$$V_{jh} = v_{jh} \cdot b_j \cdot h_c \tag{2.10}$$

where v_{jh} is the horizontal joint shear stress, h_c is the column thickness and b_j is the effective joint width.

The joint shear stress v_{jh} is provided by Eqn. (2.11) as a function of the axial load, the horizontal stirrups inside the joint A_{sjh}, the greater area between the top and bottom beam reinforcement passing through the joint A_s^* and the concrete compression strength f_c:

$$v_{jh} = \frac{f_c}{6 \cdot \alpha} \frac{A_{sjh} \cdot f_{yj}}{A_s^* \cdot f_{yb}}. \tag{2.11}$$

The parameter α taking into account the axial load on the column is computed as follows:

$$\begin{aligned} \alpha &= 1.4 - 1.6 \frac{C_j \cdot N_{col}}{f_c \cdot A_c} && \text{(interior joints)}, \\ \alpha &= \beta \left(0.7 - \frac{C_j \cdot N_{col}}{f_c \cdot A_c} \right) && \text{(exterior joints)} \end{aligned} \tag{2.12}$$

in which C_j takes into account the beneficial effects of axial compression load to the 2 direction of the lateral design force (C_j = 1.00 for unidirectional joints and symmetrical two-way frames subjected to axial tension, C_j = 0.50 for symmetrical two-way frames subject to axial compression), β is the area ratio of compression to tension beam reinforcement ($\beta = A_s'/A_s$), N_{col} is the column axial load (takes positive in compression) and A_c is the column cross-sectional area.

$$b_j = \min\left(b_c ; b_b + h_c/2 \right) \tag{2.13}$$

Finally the effective joint width b_j is the smaller of column width b_c and beam width plus ½ of column thickness h_c as shown in Eqn. (2.13).

2.1.7 FEMA 273 (1997) and FEMA 356 (2000)

According the FEMA 273 (1997) the shear strength V_{jh} shall be calculated as follows:

$$V_{jh} = \lambda \cdot \gamma \cdot \sqrt{f_c} \cdot A_g \qquad (psi) \tag{2.14}$$

in which λ = 0.75 for lightweight aggregate concrete and 1.00 for normal weight aggregate concrete, A_g is the effective horizontal joint area and γ is provided by Table 2.3 where the joints are classified in two types considering the volumetric ratio of horizontal confinement reinforcement in the joint.

Table 2.3: Values of γ for beam-to-column joints provided by FEMA 273 (1997).

JOINT TYPE	JOINT CLASSIFICATION				
	Interior with transverse beams	Interior without transverse beams	Exterior with transverse beams	Exterior without transverse beams	Knee
$\gamma < 0.003$	12	10	8	6	4
$\gamma \geq 0.003$	20	15	15	12	8

The cross-sectional area A_g is defined by the product between the column depth h_c in the direction of framing and the effective joint width b_j assumed to be equal the smallest of the column width, the beam width plus the joint depth, and twice the smaller perpendicular distance from the longitudinal axis of the beam to the column side like shown in Eqn. (2.15):

$$b_j = \min\left(b_c \quad ; \quad b_b + h_c \quad ; \quad b_b + 2\left(\frac{b_c - b_b}{2} - e_b \right) \right) \tag{2.15}$$

in which e_b is the eccentricity between the centerline of the beam and the column centroid.

2.1.8 Eurocode 8 (EN 1995-1, 1995)

According the Eurocode 8 (EN 1995-1, 1995) the shear strength of beam-to-column joints should be evaluated as follows:

$$V_{jh} = \gamma \cdot \tau_c \cdot b_j \cdot h_c \tag{2.16}$$

where γ is a coefficient equal to 20 for interior joints and 15 for exterior ones, h_c is the column thickness and τ_c is the concrete tangential strength. The effective joint width b_j depends on the beam and column width thorough the following relationship:

$$\begin{aligned} b_j &= \min\left(b_c\,;\, b_b + h_c/2\right) \qquad \text{for } b_c \geq b_b \\ b_j &= \min\left(b_b\,;\, b_c + h_c/2\right) \qquad \text{for } b_c < b_b\,. \end{aligned} \tag{2.17}$$

Finally, according to the EC8 (EN 1995-1, 1995) recommendations the tangential concrete strength should be evaluated as follows:

$$\tau_c = 0.25 \cdot f_{ct}\,, \tag{2.18}$$

$$f_{ct} = 0.21 \cdot \left(f_c\right)^{2/3}, \tag{2.19}$$

in which f_c is the average concrete compression strength.

2.1.9 Eurocode 8 (EN 1998-3, 2005) and NTC (2008)

The EC8 (EN 1998-3, 2005), following the Italian Code NTC (2008), provides a model suitable for evaluating shear strength of exterior and interior joints accounting for both the diagonal compression and tension of the strut-and-tie mechanism developing inside the joint core.

The diagonal compression induced into the joint by the diagonal strut mechanism shall not exceed the compressive strength of concrete; in particular, the following expression can be adopted to evaluate the shear strength due to the diagonal compression:

$$V_{jhc} = \eta \cdot f_c \cdot \sqrt{1 - \frac{\upsilon_d}{\eta}} \cdot b_j \cdot h_{jc} \tag{2.20}$$

where h_{jc} is the distance between the extreme layers of column reinforcement, b_j is the effective joint width evaluated as shown in Eqn. (2.17) for Eurocode8 (EN 1995-1, 1995), υ_d is the normalized axial force in the column above the joint $\left[\upsilon_d = N_{col}/\left(A_c \cdot f_c\right)\right]$, f_c is the concrete compressive strength in MPa and η is given by Eqn. (2.21) in which the parameter α is 0.60 for interior joints and 0.48 for exterior ones.

$$\eta = \alpha \cdot \left(1 - \frac{f_c}{250}\right). \tag{2.21}$$

The shear strength due to the diagonal tensile stress of concrete may be provided by the following expression:

$$\frac{A_{sjh} \cdot f_{yj}}{b_j \cdot h_{jb}} = \frac{\left(\frac{V_{jhs}}{b_j \cdot h_{jc}}\right)^2}{f_{ct} + \upsilon_d \cdot f_c} - f_{ct} \tag{2.22}$$

in which the symbols not previously mentioned have the following meaning:

- A_{sjh} is the total area of horizontal hoops;
- h_{ib} is the distance between the top and the bottom reinforcement of the beam;
- f_{ct} is the tensile strength of the concrete evaluate according the Eurocode 2 (EN 1992-1, 2004) as follows:

$$f_{ct} = 0.30 \cdot \left(f_c\right)^{2/3} . \tag{2.23}$$

Finally, the shear strength of joint V_{jh} is assumed to be the smallest value between the shear strength provided by the diagonal strut V_{jhc} and the one provided by the diagonal tie V_{jhs}.

2.1.10 NTC (2008) for Existing Joints and OPCM 3431/05 (2005)

The NTC (2008) and the previous OPCM 3431/05 (2005) provide a general rule for evaluating the shear strength of beam-to-column joints part of existing RC structure designed without seismic details. As matter of principle, it should be verified the diagonal stress of the strut-and-tie mechanism.

The tensile stress of the diagonal tie is limited by the following equation:

$$0.30 \cdot \sqrt{f_c} = \left| \frac{N_c}{2 \cdot A_g} - \sqrt{\left(\frac{N_c}{2 \cdot A_g}\right)^2 + \left(\frac{V_{jhs}}{A_g}\right)^2} \right|, \tag{2.24}$$

while the compressive stress of the diagonal strut evaluated by Eqn. (2.25) should not exceed 0.50 f_c.

$$f_c = \frac{N_c}{2 \cdot A_g} + \sqrt{\left(\frac{N_c}{2 \cdot A_g}\right)^2 + \left(\frac{V_{jhc}}{A_g}\right)^2} \quad . \tag{2.25}$$

The joint cross-section A_g is provided by the effective joint width b_j and the distance between extreme layers of column reinforcement h_{jc} according the recommendations reported in section 2.1.9.

2.2 Models for both Interior and Exterior Joints

The scientific literature provide a wide number of models for evaluating shear strength of beam-to-column joints in RC structures demonstrating the importance of those regions in analyses of framed structures.

By classifying the theoretical models according to the classes already introduced in section 2, the present section deals with the general models suitable for both interior and exterior joints.

2.2.1 The Model by Pantazopoulo & Bonacci (1992)

The author (Pantazopoulo & Bonacci, 1992) provided a theoretical model on the basis of the basic mechanisms of joint behaviour. For developing the model the joint is idealized as a three-dimensional solid with dimensions d_w, b and h and lateral forces are considered parallel to one principal direction t (Fig. 2.1).

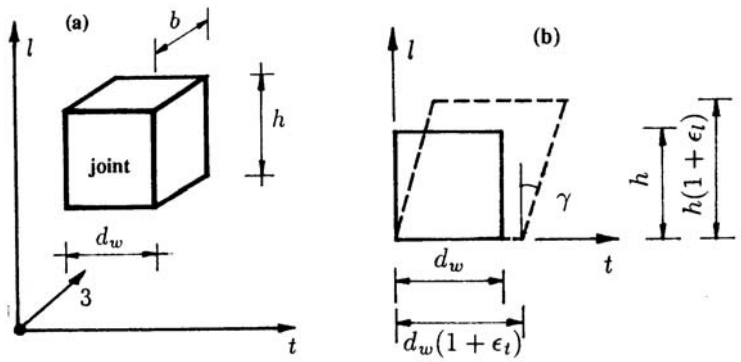

Fig. 2.1: Joint geometry (Pantazopoulo & Bonacci, 1992).

After deformation, the overall geometry of the joint is described by the average angle of shear distortion γ and by the average longitudinal and transverse strains, denoted by ε_t and ε_l, respectively.

$$\varepsilon = \begin{pmatrix} \varepsilon_t & 0{,}5\gamma & 0 \\ 0{,}5\gamma & \varepsilon_l & 0 \\ 0 & 0 & \varepsilon_3 \end{pmatrix}. \tag{2.26}$$

Studying the kinematics of the system some useful relationship between the entries of the average tensor in (*t, l, 3*) system shown in Eqn. (2.26) expressed in various coordinate systems are:

$$\varepsilon_1 + \varepsilon_2 = \varepsilon_l + \varepsilon_t \ , \tag{2.27}$$

$$\gamma = \frac{2\left(\varepsilon_1 - \varepsilon_t\right)}{\tan\alpha} = 2\left(\varepsilon_1 - \varepsilon_l\right)\tan\alpha \ , \tag{2.28}$$

$$\tan^2\alpha = \frac{\varepsilon_1 - \varepsilon_t}{\varepsilon_1 - \varepsilon_l} = \frac{\varepsilon_2 - \varepsilon_l}{\varepsilon_2 - \varepsilon_t} \ , \tag{2.29}$$

where α is the direction of the principal strains in the joint and ε_1 and ε_2 represent the values of principal strains.

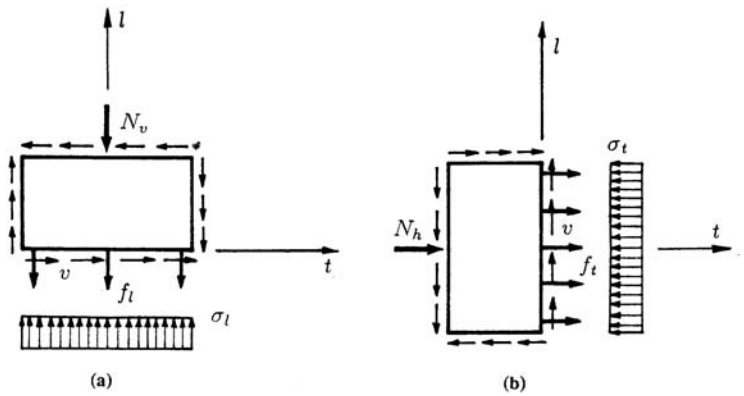

Fig. 2.2: Stress equilibrium: (a) in vertical direction, (b) in horizontal direction (Pantazopoulo & Bonacci, 1992).

The model should also satisfy equilibrium requirements on the joint core as shown in Fig. 2.2 where, for simplicity, the shear stress υ is assumed to be uniform.

The equilibrium of vertical and horizontal forces (Fig. 2.2) provides the following expressions:

$$\sigma_l = -\rho_l \cdot f_l - \frac{N_v}{b \cdot d_c}, \tag{2.30}$$

$$\sigma_t = -\rho_s \cdot f_t^s - \rho_b \cdot f_t^b - \frac{N_h}{b \cdot h}, \tag{2.31}$$

where, referring Eqn.(2.30), f_l is the average stress of the longitudinal reinforcement of the column, ρ_l is the available reinforcement ratio, d_c is the column depth and N_v is the axial load of the column. In Eqn. (2.31) ρ_s and ρ_b represent the area ratios of horizontal stirrups in the joint and the total longitudinal beam reinforcement, respectively, while f_t^s and f_t^b are the average stress of the same components. To simplify the final equation reducing the number of variables, Eqn. (2.31) is simplified as follows:

$$\sigma_t = -\rho_t \cdot f_t - \frac{N_h}{b \cdot h} \tag{2.32}$$

in which $f_t = f_t^s$ and $\rho_t = \rho_s + \beta\ \rho_b$ are assumed. The factor β related the magnitude of stresses in longitudinal beam reinforcement to the average stirrup stresses; in particular, for perfect bond $\beta = 0$ while for negligible bond resistance $\beta = 1$.

Also the average stress tensor of the joint concrete core can be defined:

$$\sigma = \begin{pmatrix} \sigma_t & \nu & 0 \\ \nu & \sigma_l & 0 \\ 0 & 0 & \sigma_3 \end{pmatrix}, \tag{2.33}$$

$$\sigma_1 = 0 \quad \textit{and} \quad \sigma_2 = \sigma_t + \sigma_l \quad (\text{first stress invariant}), \tag{2.34}$$

$$\sigma_1 - \sigma_t = \nu \cdot \tan\theta \qquad \textit{and} \quad \sigma_t = -\nu \cdot \tan\theta, \tag{2.35}$$

$$\sigma_1 - \sigma_l = \frac{\nu}{\tan\theta} \quad \textit{or} \quad \sigma_t = -\frac{\nu}{\tan\theta}, \tag{2.36}$$

where σ_1 and σ_2 are the principal stresses of concrete and θ is the angle of inclination from the t-axis.

Upon substitution of Eqn. (2.35) and (2.36) in Eqn. (2.34), the nonzero principal stress of concrete is expressed in terms of the average shear stress:

$$\sigma_2 = -\nu\left(\tan\theta + \frac{1}{\tan\theta}\right). \tag{2.37}$$

Generally, the directions of principal strains and stresses are unknown; considering the behaviour of hoops before yielding it is reasonable to assume $\alpha = \theta$ (the principal strain directions are also principal stress directions). For this assumption it is possible to evaluate the angle from the entries of the two tensors:

$$\tan^2\theta = \tan^2\alpha = \frac{\varepsilon_2 - \varepsilon_l}{\varepsilon_2 - \varepsilon_t} = \frac{\left(\frac{\sigma_2}{E_c(\varepsilon)} - \frac{f_l}{E_s}\right)}{\left(\frac{\sigma_2}{E_c(\varepsilon)} - \frac{f_t}{E_s}\right)}. \tag{2.38}$$

The previous equation can be rewritten in terms of the average joint shear stress υ obtaining a quadratic polynomial of $\tan\theta$:

$$\left[1 + \frac{1}{n\cdot\rho_t} - \frac{r}{n\cdot\rho_t(n\cdot\rho_t + r)}}{1 + \frac{1}{n\cdot\rho_l}}\right]\tan^4\theta + \left[\frac{e_v/\varepsilon_t}{(1+n\cdot\rho_l)(n\cdot\rho_t + r)}\right]\tan^2\theta - 1 = 0\,, \tag{2.39}$$

where $n = E_s/E_c$ is the ratio of material modules, $r = e_h/\varepsilon_t$ is the strain ratio that reflects the amount of lateral restraint, while the quantities $e_h = N_h/E_c(\varepsilon)hb$ and $e_h = N_h/E_c(\varepsilon)hb$ represent the deformations occurring in the joint under purely axial forces.

From this point, the author, showing experimental evidence, developed two different solutions of the problem considering the behaviour before and after yielding of joint reinforcement. Finally, two different formulations are provided for evaluating the shear strength of beam-to-column joints by considering that the hoop yielding can be followed by (a) yielding of the longitudinal column reinforcement or (b) crushing of concrete in the direction principal compressive stress. For the first case, the stress in the longitudinal steel reaches the yield stress f_y. Thus the shear strength is evaluated as follows:

$$\nu_{n,1} = \sqrt{\left\{\rho_t\cdot f_y + \frac{N_h}{b\cdot h}\right\}\left\{\rho_l\cdot f_y + \frac{N_v}{b\cdot d_b}\right\}}. \tag{2.40}$$

For the second case, failure occurs when the principal compressive stress σ_2 reaches the crushing strength of concrete f_c^{max}. It is assumed that f_c^{max} depends

on the amount of tensile deformation in the perpendicular direction characterized by ε_1.

$$f_c^{max} = \lambda \cdot f_c \,, \tag{2.41}$$

$$\lambda = \frac{K}{0{,}8 - 0{,}34 \, \varepsilon_1 / \varepsilon_0} \,. \tag{2.42}$$

where ε_o is the concrete deformation at yielding, while K is carried out as follows:

$$K = 1 + \rho_s \left| f_y / f_c \right| \,. \tag{2.43}$$

In Eqn. (2.42) and (2.43), f_c and ε_0 carry negative sign for calculations.

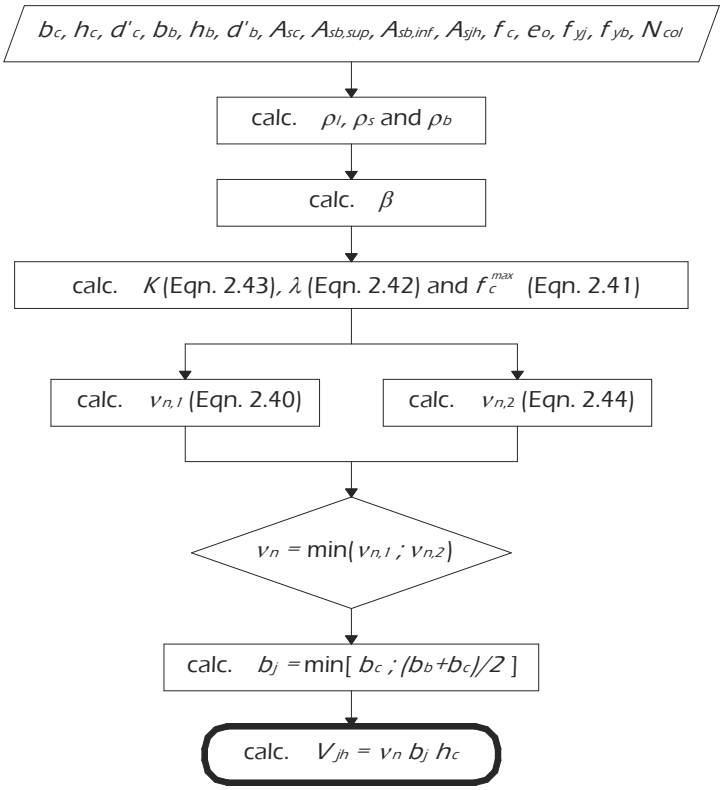

Fig. 2.3: Evaluating the shear strength according to Pantazopoulo & Bonacci (1992)

$$v_{n,2} = \sqrt{\left(\left|f_c^{\max}\right| - \rho_t \cdot f_y - \frac{N_h}{b \cdot h}\right)\left(\rho_t \cdot f_y + \frac{N_h}{b \cdot h}\right)}\,. \tag{2.44}$$

Finally, for the second case in which concrete crushing occurs, the ultimate shear strength is provided by Eqn. (2.44).

For sake of clarity, the flow-chart shown in Fig. 2.3 reports the procedure used for evaluating the shear strength of beam-to-column joints according to the model by Pantazopoulo & Bonacci (1992).

2.2.2 The Model by Paulay & Priestley (1992)

Referring to the book by Paulay & Priestley (1992), the total shear strength of an interior beam-to-column joint can be estimated using the model shown in Fig. 2.4.

The horizontal joint shear strength is evaluated by the superposition of the two mechanisms as follows:

$$V_{jh} = V_{ch} + V_{sh}\,, \tag{2.45}$$

where the subscripts *c* and *s* denoted the contributions of concrete and stirrups, respectively. The two mentioned contributions are in the following determined referring to Fig. 2.5.

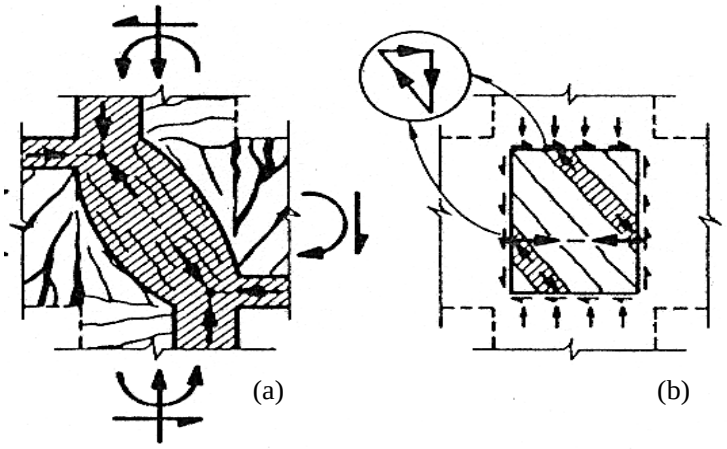

Fig. 2.4: Paulay and Priestley mechanisms of shear transfer at an interior joint: concrete strut (a) and diagonal compression field (b). (Paulay & Priestley, 1992)

The horizontal component of the diagonal compression strut D_c consist of a concrete compression force C_c, a steel force ΔT_c and the shear force from the column V_{col}.

$$V_{ch} = C'_c + \Delta T'_c - V_{col} \ . \tag{2.46}$$

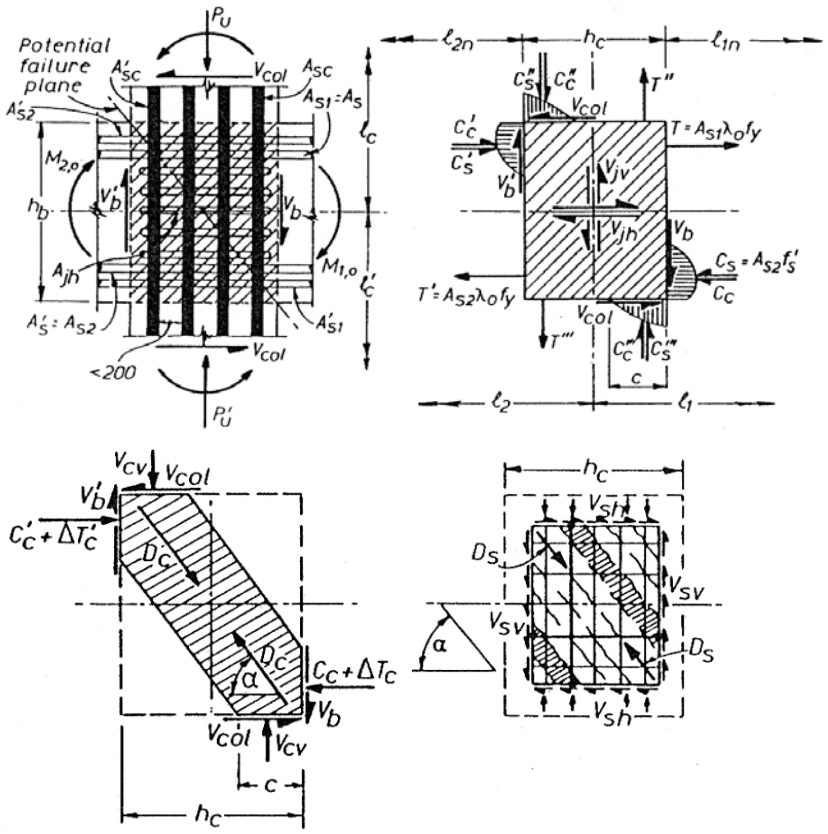

Fig. 2.5: External actions and internal stress resultants at an interior joint (Paulay & Priestley, 1992).

The fraction of the total bond force at the top beam bars $\Delta T'_c$ that can be transmitted to the strut depends to the distributions of bond forces along these bars. The maximum value of the horizontal bond force introduced over the flexural compression zone of the column is approximately 1.25 times the average unit bond force u_o. It may be assumed that the bond force is introduced to the diagonal strut over an effective distance of only $0.8\,c$, where

c is the depth of the flexural compression zone of the elastic column, which can be approximated by:

$$c = \left(0.25 + 0.85 \frac{N_{col}}{f_c \cdot A_g} \right) h_c \ , \tag{2.47}$$

$$\Delta T'_c = (1.25 \cdot u_0)(0.8 \cdot c) = u_0 \cdot c = (C'_s + T) \frac{c}{h_c} \ , \tag{2.48}$$

where A_g is the cross-sectional area of joint individuate by the column thickness and the effective joint width evaluated as the minimum value between the column width and the average of column and beam width $b_j = \min\left[b_c \ ; (b_c + b_b)/2 \right]$.

To evaluate the relative magnitudes of the internal forces C'_s and C'_c, the steel compression force is limited based on yield strength f_{yb}.

$$T = \lambda \cdot f_{yb} \cdot A_{sb} \ , \tag{2.49}$$

$$C'_s = \gamma \cdot f_{yb} \cdot A_{sb} = \frac{\gamma}{\lambda} \cdot T \ , \tag{2.50}$$

$$C'_s + T = \left(1 + \frac{\gamma}{\lambda} \right) T \ . \tag{2.51}$$

By considering the range of values of typical steel overstrength factor $1.2 \le \lambda \le 1.4$ and relative compression reinforcement contents in beam sections $\left[0.5 \le \left(\beta = A_{sb,\inf} / A_{sb,\sup} \right) \le 1.0 \right]$, it is shown that $\gamma / \lambda = 0.55$ can be assumed.

Hence, with this value, from Eqn. (2.48) is found:

$$\Delta T'_c = 1.55 \frac{c}{h_c} T \ , \tag{2.52}$$

while the concrete compression force C'_c is provided by the following equation:

$$C'_c = T' - C'_s = \beta \cdot T - \frac{\gamma}{\lambda} T = (\beta - 0.55) T \ . \tag{2.53}$$

Finally, the contribution of the strut mechanism is obtained as follows:

$$V_{ch} = \left(1.55 \frac{c}{h_c} + \beta - 0.55 \right) T - V_{col} \ . \tag{2.54}$$

The joint shear resistance to be assigned to the truss mechanism V_{sh} can be obtained by difference using Eqn. (2.45); in particular, being the joint strength V_{jh} unknown, the following expression can be used:

$$V_{sh} = \left(1.15 + 1.3\frac{N_{col}}{f_c \cdot A_g}\right) T \,. \tag{2.55}$$

The resistance of the truss mechanism V_{sh} can be used to estimate the minimum stirrups needed in the joint; the corresponding area is evaluated by the following equation:

$$V_{sh} = A_{sjh} \cdot f_{yj} \,. \tag{2.56}$$

In an assessment problem the Eqn. (2.56) is a tool for evaluating the contribution of stirrups to the shear strength of the interior joint; clearly, for the case of unreinforced joint the horizontal shear strength V_{jh} is assumed to be equal to the horizontal contribution of the strut mechanism V_{ch}.

A similar mechanism (Fig. 2.6), is useful for evaluating shear strength of exterior joints.

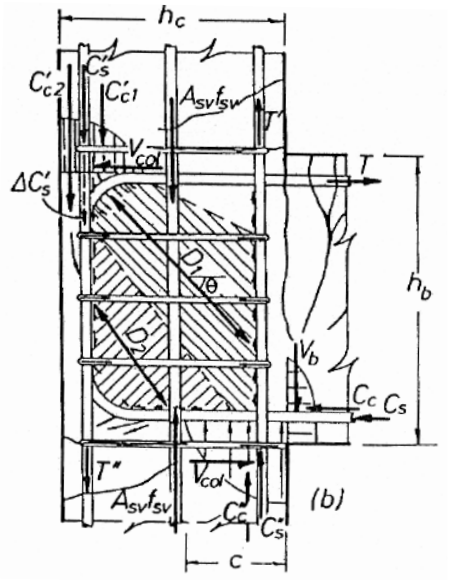

Fig. 2.6: Mechanism for exterior joint (Paulay & Priestley, 1992)

The relationships provided for interior joints can be easily modified for the case of exterior ones as follows:

$$C_s \le A_{sb,\inf} \cdot f_{yb} = \beta \frac{T}{\lambda}, \tag{2.57}$$

$$C_c \ge T - C_s = \left(1 - \frac{\beta}{\lambda}\right) T. \tag{2.58}$$

The assumption of an effective anchorage length of $0.7\ h_c$ for the bottom beam bars; hence the unit bond force is:

$$u_0 = 1.4 \, C_s / h_c, \tag{2.59}$$

while the anchorage force introduced to the diagonal strut is:

$$\Delta T_c = u_0 \cdot c = 1.4 \cdot C_s \cdot \frac{c}{h_c} = \frac{1.4 \cdot c \cdot \beta}{\lambda \cdot h_c} T. \tag{2.60}$$

By assuming that effective bond transfer to the diagonal strut occurs over only 80% of compression zone c of the column, defined by Eqn. (2.47), it is possible to determine the concrete contribution V_{ch} by substituting Eqn. (2.58) and (2.60) in (2.46):

$$V_{ch} = \left(1 - \frac{\beta}{\lambda}\right) T + \frac{1.4 \cdot c \cdot \beta}{\lambda \cdot h_c} T - V_{col}. \tag{2.61}$$

Also for exterior joints the truss force for design of stirrups can be evaluated by difference:

$$V_{sh} = V_{jh} - V_h = \frac{\beta}{\lambda} \left(0.7 - \frac{N_{col}}{f_c \cdot A_g}\right) T = A_{sjh} \cdot f_{yj}. \tag{2.62}$$

Furthermore, for both interior and exterior joints without transverse beams, to avoid brittle diagonal compression failure, it is suggested that the horizontal shear stress should be limited as follows:

$$v_{jh} = \frac{V_{jh,\lim}}{A_g} \le 0.25 \cdot f_c \le 9\ MPa. \tag{2.63}$$

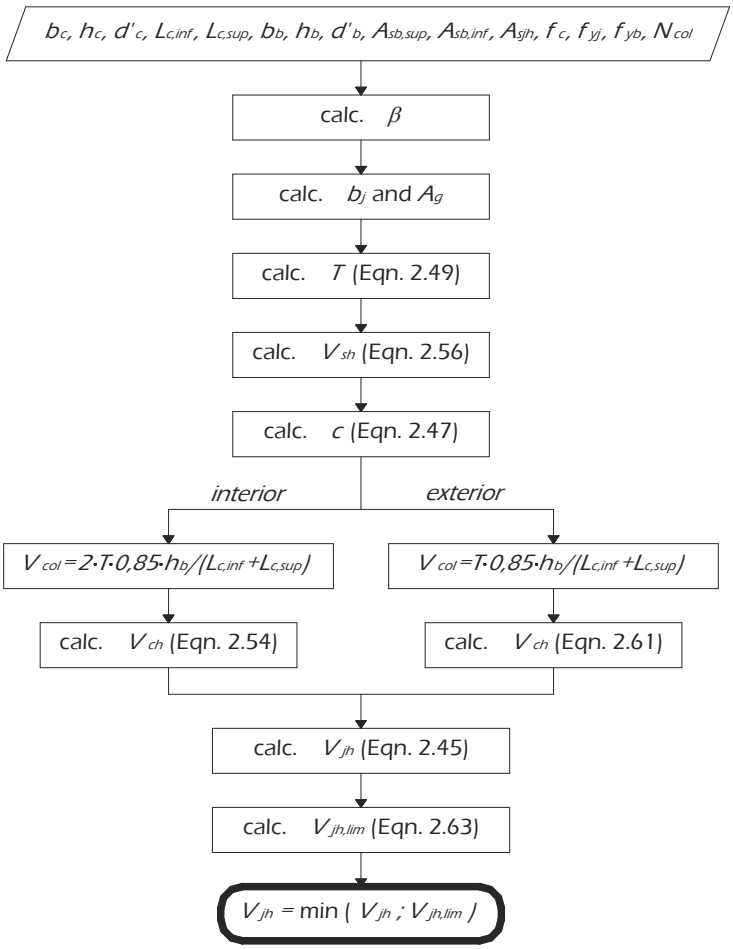

Fig. 2.7: Evaluating the shear strength according to Paulay & Priestley (1992)

Fig. 2.7 reports the flow-chart of the algorithm used for evaluating the shear strength of interior and exterior beam-to-column joint according to Paulay & Priestley (1992).

2.2.3 The Model by Parker & Bullman (1997)

The authors (Parker & Bullman, 1997) developed a model for predicting the shear strength of beam-to-column joints based on one previously developed by them (Parker & Bullman, 1995) to predict the shear strength of RC beams.

The effective shear span a_v of the connection is taken as:

$$a_v = 0.8 \cdot \left(h_b - d'_b\right) - 0.8 \cdot R \,, \tag{2.64}$$

where R is the radius of the centreline of the beam bars which is taken positive if the bars bent down into the joint and negative for bars bent up

$$\chi = \frac{a_v}{h_c - d'_c} \,. \tag{2.65}$$

Evaluating a factor χ by Eqn. (2.65), the critical angle of inclination θ_{crit} of the direct strut is evaluated as follows:

$$for \quad \chi < 0.5 \quad \rightarrow \quad \tan\theta_{crit} = 1 - \chi/2 \,, \tag{2.66}$$

$$for \quad \chi \geq 0.5 \quad \rightarrow \quad \tan\theta_{crit} = \frac{1}{2 \cdot \chi} + \frac{\left(\chi^2 - 0.75\right)}{\left(6 \cdot \chi^3 + 2.5 \cdot \chi\right)} \,. \tag{2.67}$$

A first value V_1 of shear is given below:

$$V_1 = \left(A_{sc} \cdot f_{yc} + N_{col}\right) \cdot \tan\theta_{crit} \,, \tag{2.68}$$

where A_{sc} is the total area of reinforcement in column.

A second value of shear strength is provided by the shear capacity of the concrete strut evaluated as following:

$$V_2 = \alpha \cdot \nu \cdot R_c \cdot b_c \cdot \left(h_c - d'_c\right) \,, \tag{2.69}$$

where:

$$\alpha = \frac{\left(1 - \chi \cdot \tan\theta_{crit}\right)}{\left(\tan\theta_{crit} + \cot\theta_{crit}\right)} \,, \tag{2.70}$$

$$\nu = 0{,}56 - R_c/310 \geq 0.4 \,, \tag{2.71}$$

in which R_c is the concrete compressive cube strength.

If joint stirrups are provided the joint shear strength is assumed to be given by:

$$V_3 = V_2 + A_{sjh} \cdot f_{yj} \cdot \left(\frac{a_v}{s} - 1\right) \,, \tag{2.72}$$

where A_{sjh} is the area of stirrups, f_{yj} is the yield stress and s is the spacing of the stirrups. Finally the shear strength is assumed to be limited by the strength of concrete between the stirrups which is obtained as follows:

$$V_4 = \beta \cdot V_2 \,, \tag{2.73}$$

where:

$$\beta = \frac{\left(d_v - s \cdot \tan\theta_{crit}\right)}{\left(h_c - d'_c - a_v \cdot \tan\theta_{crit}\right)} \geq 1 \,, \tag{2.74}$$

$$d_v = 0.9 \cdot \left(h_c - d'_c\right) . \tag{2.75}$$

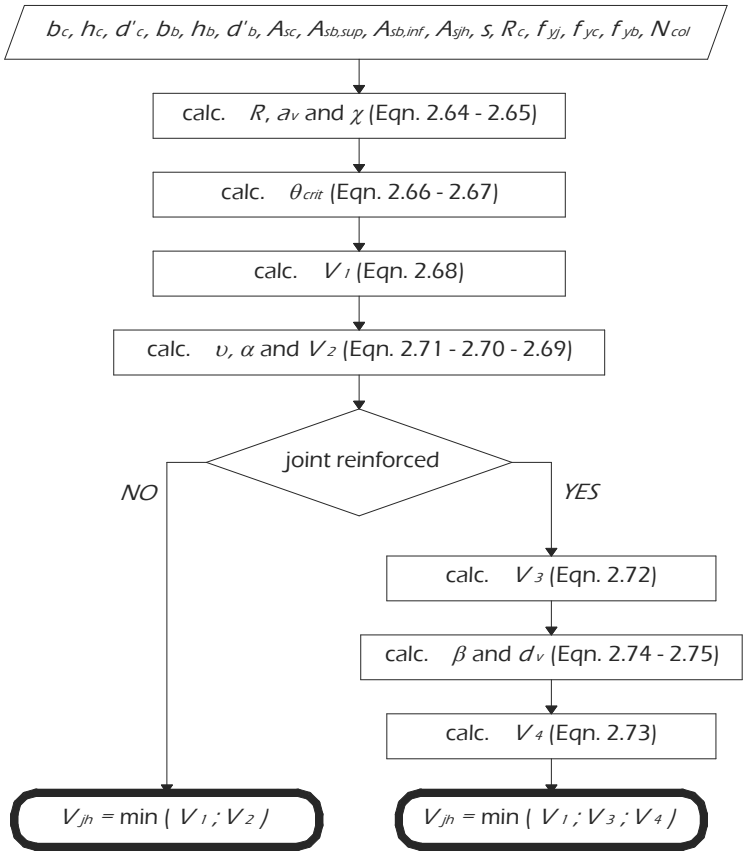

Fig. 2.8: Evaluating the shear strength according to Parker & Bullman (1997).

The flow-chart reported in Fig. 2.8 shows the implemented algorithm for evaluating shear strength according Parker & Bullman (1997).

2.2.4 The Model by Hwang & Lee (2002)

The model (Hwang & Lee, 2002) derives by two previous ones developed by the authors in 1999 (Hwang & Lee, 1999) and 2000 (Hwang & Lee, 2000) for exterior and interior joints, respectively and presented in the special sections of this thesis. In particular this model is a simplification of the two predecessors based on a strut-and-tie model (Fig. 2.9).

The equilibrium of the represented model is provided by the following three equations:

$$V_v = C_d \cdot \sin\theta \,, \tag{2.76}$$

$$V_h = C_d \cdot \cos\theta \,, \tag{2.77}$$

$$\frac{V_v}{V_h} = \frac{l_v}{l_h} = \tan\theta \,, \tag{2.78}$$

where V_v = vertical shear force, V_h = horizontal shear force, C_d = diagonal compression, h = angle of inclination of the diagonal compression with respect to the horizontal h axis and l_h and l_v = internal lever arms of the vertical and horizontal shear couples (Hwang & Lee, 1999 and 2000, respectively).

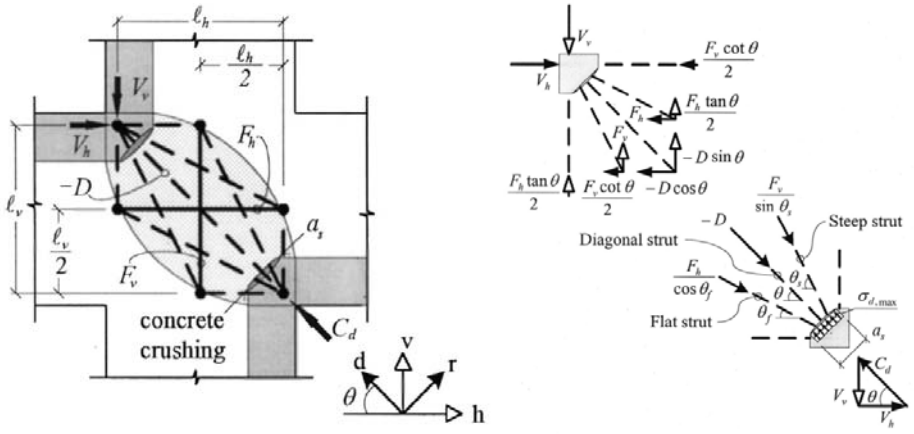

Fig. 2.9: Hwang & Lee's strut-and-tie modelling of interior joint (Hwang & Lee, 2002).

The diagonal compression is provided as follows:

$$C_d = -D + \frac{F_h}{\cos\theta} + \frac{F_v}{\sin\theta}, \tag{2.79}$$

in which D is the compression force in the diagonal strut, and F_h and F_v are the tension forces in the horizontal and vertical ties, respectively.

The authors assumed that the ratios of the diagonal compression C_d assigned among the three mechanisms are defined as:

$$-D : \frac{F_h}{\cos\theta} : \frac{F_v}{\sin\theta} = R_d : R_h : R_v . \tag{2.80}$$

The strut mechanism is statically indeterminate to the second degree; by using two additional equations on the stiffness ratios among the resisting mechanism, the values of R_d, R_h and R_v can be fully defined.

$$\gamma_h = \left(2 \cdot \tan\theta - 1\right) \Big/ 3 \qquad 0 \le \gamma_h \le 1, \tag{2.81}$$

$$\gamma_v = \left(2 \cdot \cot\theta - 1\right) \Big/ 3 \qquad 0 \le \gamma_v \le 1. \tag{2.82}$$

The relative stiffness ratios between the horizontal and diagonal mechanism and the vertical and diagonal one are:

$$R_h : R_d = \gamma_h : \left(1 - \gamma_h\right), \tag{2.83}$$

$$R_v : R_d = \gamma_v : \left(1 - \gamma_v\right), \tag{2.84}$$

$$R_d + R_h + R_v = 1. \tag{2.85}$$

The researched values are obtained as follows by solving Eqn. (2.83), (2.84) and (2.85):

$$R_d = \frac{\left(1-\gamma_h\right)\left(1-\gamma_v\right)}{1 - \gamma_h \cdot \gamma_v}, \tag{2.86}$$

$$R_h = \frac{\gamma_h\left(1-\gamma_v\right)}{1 - \gamma_h \cdot \gamma_v}, \tag{2.87}$$

$$R_v = \frac{\gamma_v\left(1-\gamma_h\right)}{1 - \gamma_h \cdot \gamma_v}. \tag{2.88}$$

In order to check whether the failure stress is reached, the area of the nodal zone which bears the diagonal pressure must be estimated. The effective area of the diagonal strut A_{str} is defined as:

$$A_{str} = a_s \cdot b_j \ , \tag{2.89}$$

$$a_s = \left(0.25 + 0.85 \frac{N_{col}}{f_c \cdot A_c} \right) h_c \ , \tag{2.90}$$

in which b_j is the effective joint width (the authors do not provide a formulation, so it will be assumed $b_j = \min\left[b_c \ ; (b_c + b_b)/2 \right]$), while a_s is the depth of the diagonal strut assumed equal to the depth of the flexural compression zone [Eqn. (2.90)] where A_c is the cross-sectional area of the column.

The maximum compressive stress $\sigma_{d,max}$ of the nodal zone (assumed negative in compression) is evaluated in the following:

$$-\sigma_{d,\max} = \frac{1}{A_{str}} \left[-D + \frac{F_h}{\cos\theta} \left(1 - \frac{\sin^2\theta}{2} \right) + \frac{F_v}{\sin\theta} \left(1 - \frac{\cos^2\theta}{2} \right) \right]. \tag{2.91}$$

The authors considered that the shear failure is also governed by the phenomenon of softening of concrete; for this purpose the following softened law is taken:

$$\sigma_d = -\zeta \cdot f_c \left[2 \left(\frac{-\varepsilon_d}{\zeta \cdot \varepsilon_0} \right) - \left(\frac{-\varepsilon_d}{\zeta \cdot \varepsilon_0} \right)^2 \right] \qquad for \ \frac{-\varepsilon_d}{\zeta \cdot \varepsilon_0} \le 1 , \tag{2.92}$$

$$\zeta = \frac{5.8}{\sqrt{f_c}} \frac{1}{\sqrt{1 + 400 \cdot \varepsilon_r}} \le \frac{0.9}{\sqrt{1 + 400 \cdot \varepsilon_r}} , \tag{2.93}$$

where σ_d is the average principal stress of concrete in the d direction (negative in compression), ζ is the softening coefficient, ε_d and ε_r are the average principal strains in d and r directions respectively and ε_0 is the concrete strain corresponding to the cylinder stress f_c.

If the maximum compressive stress exerting on the nodal zone $-\sigma_{d,max}$ is less than the capacity of the cracked concrete ζf_c, the diagonal compression could be increased. The shear strength of the discontinuity region is obtained when the acting stress $-\sigma_{d,max}$ exceeds the concrete capacity ζf_c.

In order to calculate the value of ζ, the principal tensile strain ε_r should be determined. It is assumed that the two-dimensional membrane elements of the discontinuity regions should satisfy Mohr's circular compatibility:

$$\varepsilon_r + \varepsilon_d = \varepsilon_h + \varepsilon_v \ , \tag{2.94}$$

where ε_h and ε_v are the averaged normal strains in h and v directions, respectively and can be obtained from the forces of the tension ties:

$$\left(F_h = A_{sjh} \cdot E_s \cdot \varepsilon_h\right) \le \left(F_{yh} = A_{sjh} \cdot f_{yj}\right), \tag{2.95}$$

$$\left(F_v = A_{sjv} \cdot E_s \cdot \varepsilon_v\right) \le \left(F_{yv} = A_{sjv} \cdot f_{yj}\right). \tag{2.96}$$

The solution of the above procedure can be obtained through an iterative analysis as done by the two previous models (Hwang & Lee, 1999 0 and 2000 0) or using the simplified procedure listed below.

A factor representing the beneficial effects of the tie force on the shear strength is developed in the following:

$$K = \frac{C_d}{-\sigma_{d,\max} A_{str}} = \frac{-D + \dfrac{F_h}{\cos\theta} + \dfrac{F_v}{\sin\theta}}{-D + \dfrac{F_h}{\cos\theta}\left(1 - \dfrac{\sin^2\theta}{2}\right) + \dfrac{F_v}{\sin\theta}\left(1 - \dfrac{\cos^2\theta}{2}\right)} \ge 1. \tag{2.97}$$

The nominal diagonal compressive strength $C_{d,n}$ is estimated as:

$$C_{d,n} = K \cdot \zeta \cdot f_c \cdot A_{str}\ . \tag{2.98}$$

With the aim of simplifying the problem, some constant values are assumed for ε_d and ε_r; in particular, $\varepsilon_d = -0.001$ and $\varepsilon_r = 0.005$ are considered. As a result the stiffness coefficient is approximated to:

$$\zeta = \frac{3.35}{\sqrt{f_c}} \le 0.52\,. \tag{2.99}$$

The additional contribution of the sufficient horizontal tie for the diagonal compressive strength is provided by the below simplified equation:

$$\overline{K_h} = \frac{1}{1 - 0.2\left(\gamma_h - \gamma_h^2\right)}, \tag{2.100}$$

and consequently, the horizontal tie force is:

$$\overline{F_h} = \gamma_h \cdot \left(\overline{K_h} \cdot \zeta \cdot f_c \cdot A_{str}\right) \cdot \cos\theta\,. \tag{2.101}$$

In the case of under-reinforced joint, the index K_h can be approximated by a linear interpolation using the balanced amount of the horizontal tie force.

$$K_h = 1 + \left(\overline{K_h} - 1\right) \cdot \frac{F_{yh}}{\overline{F_h}} \le \overline{K_h} \,. \tag{2.102}$$

The presence of vertical reinforcement results in steeper sub-struts, so that more concrete is summoned for shear resistance. The set of equations for vertical tie is the same as Eqn. (2.100), (2.101) and (2.102), except that all the subscripts *h* are replaced by *v* and $\cos\theta$ and $\sin\theta$ are interchanged.

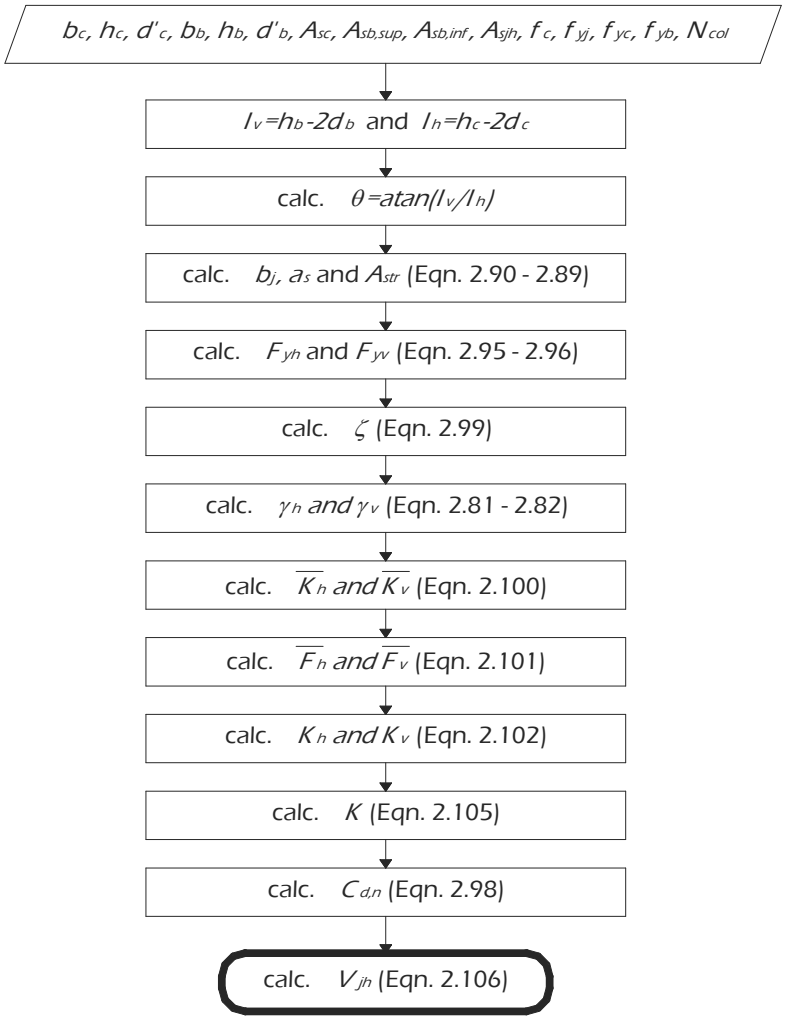

Fig. 2.10: Evaluating the shear strength according to Hwang & Lee (2002).

The maximum beneficial effect of the sufficient tension ties in increasing the shear strength can be calculated by Eqn. (2.97):

$$\overline{K} = \frac{R_d + R_h + R_v}{R_d + R_h\left(1-\frac{\sin^2\theta}{2}\right) + R_v\left(1-\frac{\cos^2\theta}{2}\right)} \geq 1. \tag{2.103}$$

In order to simplify the whole process, it is recommended that the value of $\overline{K}$ be approximated by simple addition as follows:

$$\overline{K} = \overline{K_h} + \overline{K_v} - 1, \tag{2.104}$$

$$K = K_h + K_v - 1. \tag{2.105}$$

Finally, the shear strength of beam-to-column joint is provided by the projection of the diagonal nominal strength $C_{d,n}$:

$$V_{jh} = C_{d,n} \cdot \cos\theta. \tag{2.106}$$

The exposed procedure can be easily understood if shown by the flow-chart reported in Fig. 2.10 that explains the main phases of the evaluation of beam-to-column joint shear strength according to Hwang & Lee (2002).

2.2.5 The Model by Parra-Montesinos & Wight (2002)

The joint model developed by Parra-Montesinos & Wight 0 is based on the state of plane strains in the connection through the development of a ratio between the joint principal strains, which was determined by experimental results.

The state of plane strains in a beam-to-column joint can be defined by the following expressions:

$$\varepsilon_c = \frac{\varepsilon_x + \varepsilon_y}{2} + \frac{\varepsilon_x - \varepsilon_y}{2}\cos(2\theta) + \frac{\gamma}{2}\sin(2\theta), \tag{2.107}$$

$$\varepsilon_t = \frac{\varepsilon_x + \varepsilon_y}{2} + \frac{\varepsilon_x - \varepsilon_y}{2}\cos\left[2(\theta+90°)\right] + \frac{\gamma}{2}\sin\left[2(\theta+90°)\right], \tag{2.108}$$

$$\gamma = \tan(2\theta)\left(\varepsilon_x - \varepsilon_y\right), \tag{2.109}$$

where ε_c and ε_t are the principal compression and tensile strains, respectively, ε_x and ε_y are the horizontal and vertical strains, γ is the joint shear distortion and θ is the principal compression angle.

By assuming that the principal angle θ is known, from Eqn. (2.107) to (2.109) four unknown variables are present, and thus a fourth relationship is required. This has been overcome by defining a factor, k_{tc}, that relates the principal tensile and compression strains as follows:

$$k_{tc} = -\frac{\varepsilon_t}{\varepsilon_c}. \tag{2.110}$$

The k_{tc} factor is affected by the joint type (i.e. interior, exterior, eccentric) and confinement. For modelling purposes a linear relationship between the k_{tc} factor and the joint shear distortion γ is used:

$$k_{tc} = 2 + k_s \cdot \gamma, \tag{2.111}$$

where k_s represents the slope of the k_{tc} vs. γ relationship and is influenced by the amount of joint confinement. The minimum value of $k_{tc} = 2$ for $\gamma = 0$ indicates that a cracked response is assumed for all levels of joint shear distortion.

It is accepted that the shear strength of RC beam-to-column connections is provided by two mechanisms: a strut mechanism activated by direct bearing on the concrete from the adjoining beam and column compression zone and a truss mechanism dependant on the amount of force transferred to the joint by bond between the beam and column bars passing through the joint core.

The angle of inclination of the diagonal compression strut with respect to the beam axis, θ, is assumed to be fixed and can be estimated as follows:

$$\theta = \arctan\frac{h_b - 2\cdot d'_b}{h_c}, \tag{2.112}$$

where h_b and h_c denote the beam and column thickness, respectively, while d'_b is the concrete cover of the beam.

The depth of the concrete strut is assumed to be:

$$d_{strut} = \frac{(h_b - 2\cdot d'_b)h_c}{\sqrt{(h_b - 2\cdot d'_b)^2 + h_c^2}}. \tag{2.113}$$

From this point, the authors provide several parametric analyses for calibrating the factors affecting the strength of the concrete strut and thus the shear strength of the joint.

$$C_d = f_c\left(\varepsilon_c\right)\cdot A_{strut} \tag{2.114}$$

$$V_{jh} = C_d \cdot \cos\theta \tag{2.115}$$

In particular, the k_s and k_{tc} factors and the principal strains ε affect directly the concrete compressive strength. In Eqn. (2.114), A_{strut} is the sectional area of the strut evaluated as follows:

$$A_{strut} = b_j \cdot d_{strut} \ , \tag{2.116}$$

where b_j is evaluated according to ACI 352 recommendation where e_b is the eccentricity between the beam centreline and the column centroid:

$$b_j = \min\left(\frac{b_b + b_c}{2}\,;\, b_b + \frac{h_c}{2}\right) \qquad \text{if } e_b = 0 \ , \tag{2.117}$$

$$b_j \le b_b + \frac{0.3\cdot h_{col}}{2} \qquad \text{if } e_b \neq 0 \ . \tag{2.118}$$

As a result of the parametric study developed, the authors provide the following analytical equation for evaluating the shear strength of exterior and interior beam-to-column joints:

$$V_{jh} = v_{jh} \cdot b_j \cdot h_c \ , \tag{2.119}$$

where v_{jh} is the shear stress capacity estimated as follows:

$$v_{jh} = \alpha_1 \cdot \alpha_2 \cdot f_c \ . \tag{2.120}$$

The parameters α_1 and α_2 take into account the influence of k_s and f_c and can be defined by the following equations:

$$\alpha_1 = 0.34 - 0.00018 \cdot k_s \ , \tag{2.121}$$

$$\alpha_2 = 0.00018 \cdot f_c^2 - 0.03 \cdot f_c + 1.7 \ , \tag{2.122}$$

in which f_c is expressed in MPa.

The k_s factor, for interior joints, is provided by the following equation in terms of eccentricity e_b and column width b_c:

$$k_s = 500 + 2000\frac{e_b}{b_c}, \tag{2.123}$$

while, for exterior joints, a single value of $k_s = 500$ is proposed.

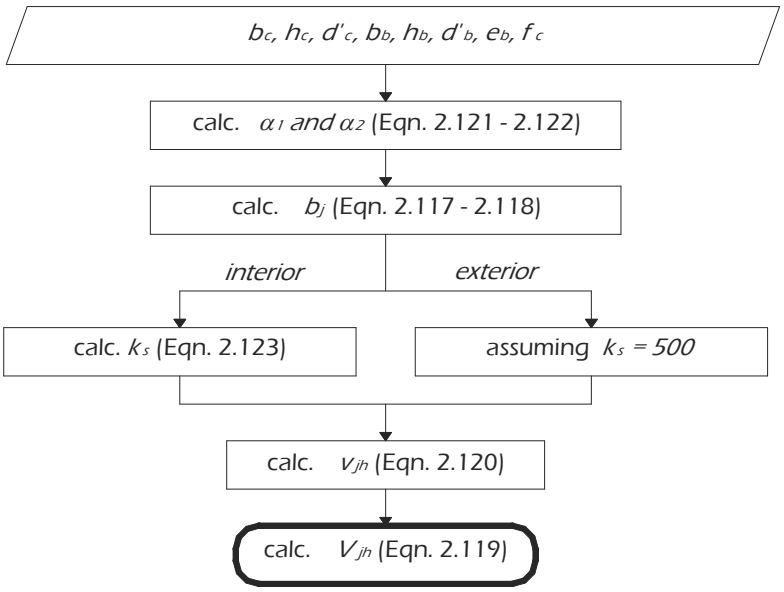

Fig. 2.11: Evaluating shear strength according to Parra-Montesinos & Wight (2002).

Fig. 2.11 shows the flow-chart about the simple exposed procedure

2.2.6 The Model by Hegger et Al. (2003)

Hegger et al. (2003) proposed a model based on various experimental results. As generally suggested the shear force resistance V_{jh} of exterior beam-to-column joint can be attributed to the concrete resistance V_{ch} and the resistance provided by the shear reinforcement V_{sh}:

$$V_{jh} = V_{ch} + V_{sh}. \tag{2.124}$$

The concrete contribution may be expressed in the following form:

$$V_{ch} = \alpha_1 \cdot A \cdot B \cdot C \cdot b_j \cdot h_c, \tag{2.125}$$

where α_1 is an anchorage factor reflecting the efficiency of the anchorage of the beam reinforcement, A is a factor taking into account the joint slenderness, B takes into account the column reinforcement ratio ρ_{col}, C is a function of the concrete compressive strength and b_j is evaluated according ACI 352–02 (2002) through Eqn. (2.4). The shear resistance of the stirrups inside the joint V_{sh} can be expressed as:

$$V_{sh} = \alpha_2 \cdot A_{sjh} \cdot f_{yj} \ , \tag{2.126}$$

in which α_2 is the efficiency factor for the shear reinforcement and A_{sjh} is the area of shear reinforcement within the joint.

For evaluating the factors α_1 and α_2 affecting the two contributions to the shear strength, an iterative regression analysis was performed by the authors (Hegger et al., 2003).

The effect of the beam reinforcement anchorage on the shear resistance of exterior beam-to-column connections is taken into account by assigning $\alpha_1 = 0.85$ or $\alpha_1 = 0.95$ for the case of 180 degree bend bars and 90-degree bend, respectively. Furthermore, from experimental tests it was observed that the shear resistance decreases with increasing joint slenderness, so, through a regression analysis the following expression was provided for A:

$$A = 1.2 - 0.3\frac{h_b}{h_c} . \tag{2.127}$$

It was registered that the anchorage efficiency inside the joint, the stiffness and the height of the compression zone of the column increased by increasing the longitudinal column reinforcement ratio ρ_{col}; the following equation is suggested for the factor B:

$$B = 1.0 - \frac{\rho_{col} - 0.5}{7.5} . \tag{2.128}$$

The concrete strength factor C is assumed to be provided by the following equation:

$$C = 2 \cdot \left(f_c\right)^{1/3} \tag{2.129}$$

with $20 \le f_c \le 100\ MPa$.

The shear reinforcement efficiency factor α_2 was evaluated using the short beam analogy; the author suggested different values for α_2 for different detailing as shown in Table 2.4.

Table 2.4: Shear reinforcement coefficient factor α_2.

Anchorage type	Hairpins	Closed stirrups
90-degree bend or headed bars	0.7	0.6
180-degree bend bars	0.6	0.5

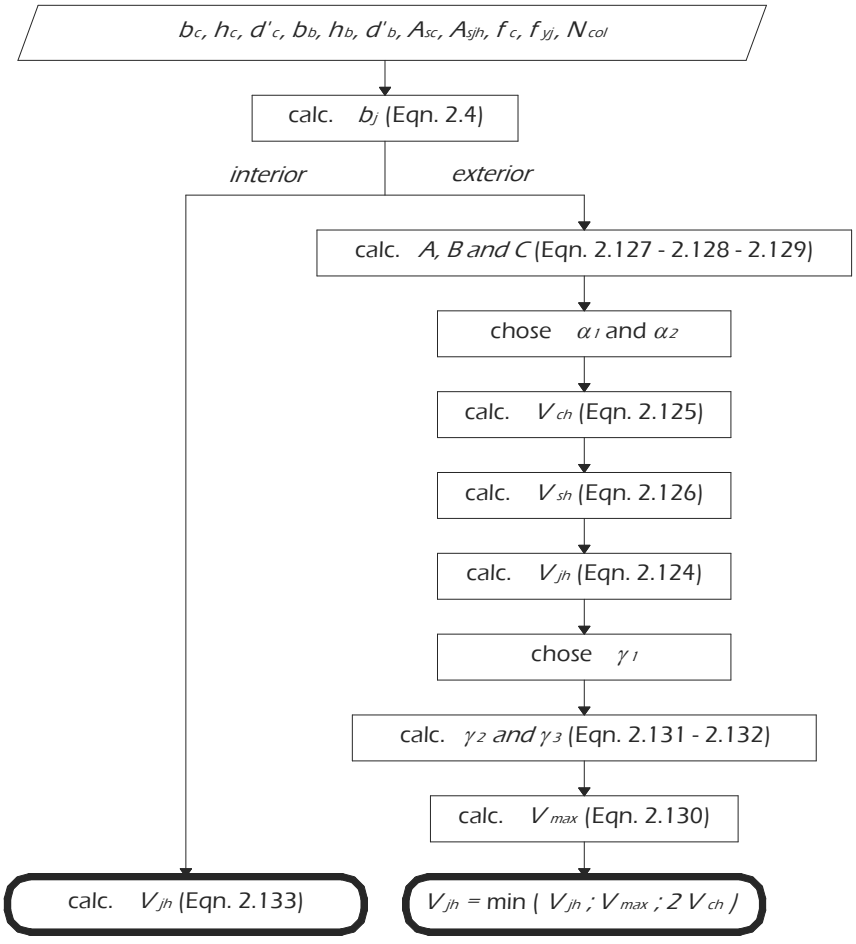

Fig. 2.12: Evaluating shear strength according to Hegger et al. (2003).

An upper limit of the shear force V_{max} was provided according to experimental results:

$$V_{\max} = \gamma_1 \cdot \gamma_2 \cdot \gamma_3 \cdot 0.25 \cdot f_c \cdot b_j \cdot h_c \le 2 \cdot V_{ch} \,, \tag{2.130}$$

where γ_1, γ_2 and γ_3 are coefficients to account for the anchorage efficiency of the beam reinforcement, the column normal force and the joint slenderness of the connection, respectively. Hegger et. al. (2003) suggested a value of 1.0 for γ_1 for bend bars and 1.2 for headed ones, while the following two equations were proposed for the other two coefficients:

$$\gamma_2 = 1.5 - 1.2\frac{\sigma_{col}}{f_c} \le 1.0 \,, \tag{2.131}$$

$$\gamma_3 = 1.9 - 0.6\frac{h_b}{h_c} \le 1.0 \,, \tag{2.132}$$

in which σ_{col} is the column normal stress $\sigma_{col} = N_{col} / A_c$.

The following simple equation has been proposed for interior joints:

$$V_{jh} = 0.25 \cdot f_c \cdot b_j \cdot h_c \,. \tag{2.133}$$

The procedure used in this thesis for evaluating the shear strength of beam-to-column joints according to the model by Hegger et al. (2003) is shown in Fig. 2.12.

2.2.7 The Model by Attaalla (2004)

The model by Attalla (2004) is a modification of a previous one developed by the same author in 1997 (Attaalla, 2004) that required an iterative procedure not easily implementable for assessment and design use.

The shear strength of joint is assumed to be function of the average principal compressive stress in the joint concrete f_{c2} evaluated as recommended by Zhang & Hsu (1998):

$$f_{2c} = \zeta \cdot f_c \left[2\left(\frac{\varepsilon_2}{\zeta \cdot \varepsilon_0}\right) - \left(\frac{\varepsilon_2}{\zeta \cdot \varepsilon_0}\right)^2 \right] \qquad for \ \frac{\varepsilon_2}{\zeta \cdot \varepsilon_0} \le 1 \,, \tag{2.134}$$

$$f_{2c} = \zeta \cdot f_c \left[1 - \left(\frac{\frac{\varepsilon_2}{\zeta \cdot \varepsilon_0} - 1}{\frac{2}{\zeta} - 1} \right)^2 \right] \qquad for \ \frac{\varepsilon_2}{\zeta \cdot \varepsilon_0} > 1, \tag{2.135}$$

where the softening coefficient ζ is

$$\zeta = \frac{5.8}{\sqrt{f_c}} \frac{1}{\sqrt{1+400\varepsilon_1}} \le \frac{0.9}{\sqrt{1+400\varepsilon_1}} \tag{2.136}$$

and f_{c2} can reach a maximum value of:

$$f_c^{\max} = \frac{0.9 \cdot f_c}{\sqrt{1+400\varepsilon_1}} \le f_c \ , \tag{2.137}$$

in which ε_1 and ε_2 are the average principal compressive and tensile strains, respectively.

As a simplified tool for evaluating the nominal shear stress of joints, Attalla proposed the following equation:

$$v_{jj} = \pm 0.45 \cdot \zeta \cdot f_c \left[\frac{\sqrt{\left(\rho_t \cdot f_{yt} - N_b / b_b h_b\right)\left(\rho_t \cdot f_{yt} - N_c / b_c h_c\right)}}{\rho_t \cdot f_{yt} + \rho_l \cdot f_{yl} - \left(N_b / b_b h_b + N_c / b_c h_c\right)} \right] \tag{2.138}$$

where ρ_t and ρ_l are the joint reinforcement ratio in transverse and longitudinal direction with their corresponding yield stresses f_{yt} and f_{yl}, respectively, while N_b and N_{col} are the axial forces in beam and column assumed positive in tension.

The main simplification consists in considering the softening coefficient provided by the following expression neglecting the dependence by ε_1:

$$\zeta = 0.40 \left[1 + \left(\frac{110 - f_c}{69} \right)^3 \right] \le 1 \qquad \left[f_c \ in \ MPa \right]. \tag{2.139}$$

Furthermore, the contribution of the transverse reinforcement is due to both the reinforcement ratio of joint tie ρ_{jh} and the reinforcement ratio of beam flexural bars passing through the joint (top and bottom) in the investigate direction ρ_b:

$$\rho_t \cdot f_{yt} = \rho_{jh} \cdot f_{yj} + \frac{1}{3} \rho_b \cdot f_{yb} \ . \tag{2.140}$$

Considering the yield strength identical for all column bars, the longitudinal reinforcement ratio in the joint can be calculated as follows:

$$\rho_l = \rho_{jv} + \frac{1}{3}\rho_c \ , \tag{2.141}$$

in which ρ_{jv} is the reinforcement ratio of intermediate column bars and ρ_c is the reinforcement ratio of column bars at the two faces of the joint.

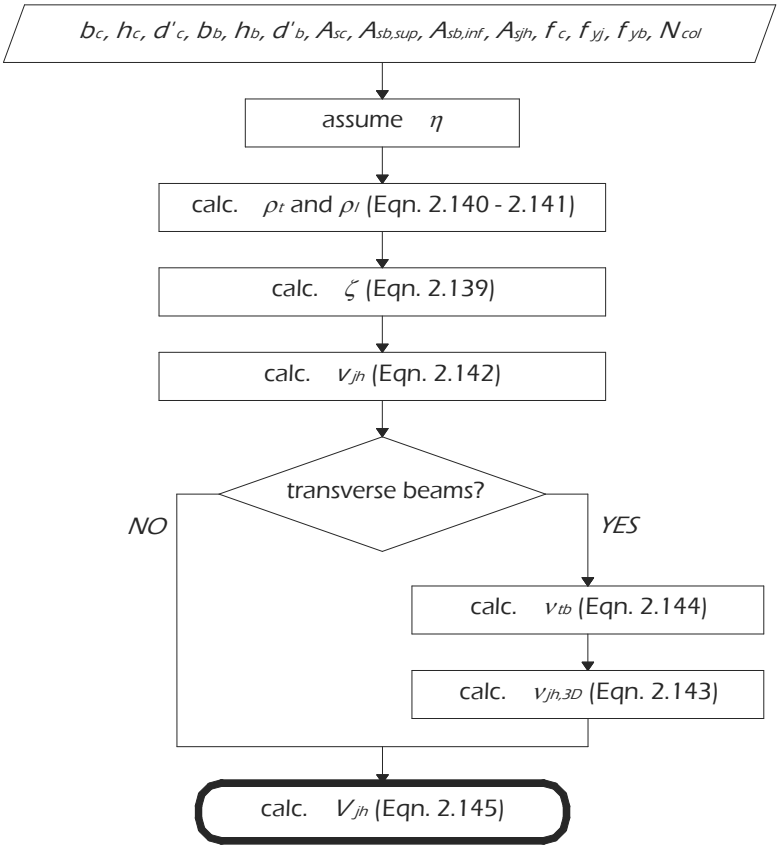

Fig. 2.13: Evaluating shear strength according Attaalla (2004).

With the aim of accounting the different behaviour between interior and exterior joints, a coefficient of geometry η, equal to 1.00 and 0.79 for interior and exterior joint respectively, was introduced in Eqn. (2.138) providing:

$$v_{ij} = \pm 0.45 \cdot \eta \cdot \zeta \cdot f_c \left[\frac{\sqrt{\left(\rho_t \cdot f_{yt} - N_b / b_b h_b\right)\left(\rho_t \cdot f_{yt} - N_c / b_c h_c\right)}}{\rho_t \cdot f_{yt} + \rho_l \cdot f_{yl} - \left(N_b / b_b h_b + N_c / b_c h_c\right)} \right]. \qquad (2.142)$$

Finally, for taking into account the effects of confinement provided by transverse beam in three-dimensional elements, if there are transverse beams the shear stress of the joint is evaluated as follows:

$$v_{ij,3D} = v_{jh} + v_{tb} \qquad (2.143)$$

where the contribution of transverse beams v_{tb} is obtained through Eqn. (2.144) in which b_{bt} and h_{bt} are the width and the thickness of the transverse beam respectively:

$$v_{tb} = \frac{0{,}29 \cdot \sqrt{f_c} \cdot b_{tb} \cdot h_{tb}}{b_c \cdot h_c}. \qquad (2.144)$$

Starting from the shear stress evaluated by Eqn. (2.142) in plane problems or Eqn. (2.144) in three dimensions, the shear strength of beam-to-column joints is derived by the following product:

$$V_{jh} = v_{jh} \cdot b_c \cdot h_c. \qquad (2.145)$$

The flow-chart in Fig. 2.13 shows the procedure adopted for evaluating the shear strength of beam-to-column connections according to the exposed model.

2.2.8 The Model by Kim et Al. (2009)

The authors in 2007 (Kim et al., 2007) developed a model based on the results of a wide experimental database (Kim & LaFave, 2007) including only reinforced joints; after having observed that the model was not suitable for evaluating shear strength of unreinforced beam-to-column joint collecting in a database wider than the first one (Kim & LaFave, 2009), Kim et al. (2009) modified the model by limiting a parameter obtaining the model suitable for interior and exterior joints reinforced or not (Kim et al., 2009).

As a result of the probabilistic method used by the authors, the shear strength can be evaluated as follows:

$$v_{jh} = \alpha_t \cdot \beta_t \cdot \eta_t \cdot \lambda_t \cdot \left(JI\right)^{0.15} \left(BI\right)^{0.30} \left(f_c\right)^{0.75} \qquad [MPa] \qquad (2.146)$$

in which α_t is a parameter for describing in-plane geometry: 1.0 for interior joints, 0.7 for exterior connections and 0.4 for knee ones; β_t is a parameter describing out-of-plane geometry: 1.0 for joints without or with one transverse beam and 1.18 for connections with two opposite transverse beams; λ_t is equal to 1.31 for setting the overall average of the ratios of Eqn. (2.146) as 1.0 and η_t is a parameter that accounts for the beam eccentricity e_b evaluate in the following:

$$\eta_t = \left(1 - \frac{e_b}{b_c}\right)^{0.67} . \tag{2.147}$$

The parameter *BI* is defined beam reinforcement index and is provided by the following equation:

$$BI = \frac{\rho_b \cdot f_{yb}}{f_c} , \tag{2.148}$$

while *JI* is the joint transverse reinforcement index:

$$JI = \frac{\rho_j \cdot f_{yj}}{f_c} \geq 0.0139 \tag{2.149}$$

where the limitation above to 0.0139 was introduced by the author in 2009 as difference from the model previously developed in 2007 for taking into account the shear strength of joints without transverse reinforcement.

In particular, the beam reinforcement ratio ρ_b and the volumetric joint transverse reinforcement ratio are evaluated as follows:

$$\rho_b = \frac{A_{sb,\sup} + A_{sb,\inf}}{b_b \cdot h_b} , \tag{2.150}$$

$$\rho_j = \frac{A_{sjh} \cdot h_c}{h_c \cdot b_c \cdot \left(h_b - 2 \cdot d'_b\right)} . \tag{2.151}$$

Finally, the shear strength of the joint is:

$$V_{jh} = v_{jh} \cdot b_j \cdot h_c \tag{2.152}$$

where the effective joint width is provided by the minimum value between the column width and $\left(b_b + b_c\right)/2$.

The flow-chart resuming the procedure is shown in Fig. 2.14.

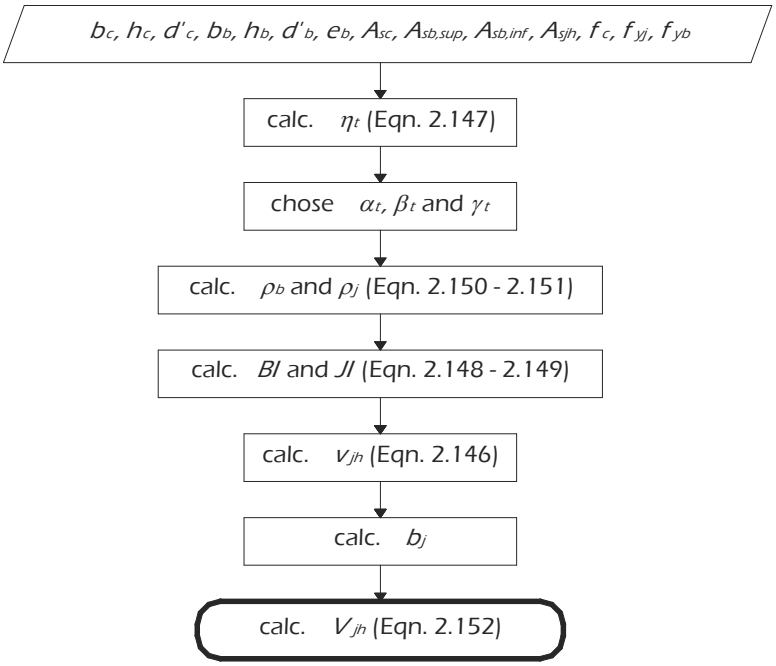

Fig. 2.14: Evaluating shear strength according to Kim et al. (2009).

2.3 Specific Models for Interior Joints

Having in the past individuate the most critical aspects in exterior beam-to-column joints, the interior ones have been little studied obtaining the relationship for those elements as an extrapolation from the models developed for exterior connections. As a result, plenty of models valid for interior joints are also strong for exterior ones and have been reported in the previous section.

In this section two models suitable for only interior joints are presented; in particular, the model by Kitayama et al. (1991) and the model by Hwang & Lee (2002) are proposed. The first one is a simple model and the authors did not provide any dual model for exterior joints, while the second model is exactly the dual of another one suitable for exterior joints only by the same author in 1999 and reported in section 2.4.6.

2.3.1 The Model by Kitayama et Al. (1991)

The authors (Kitayama et al., 1991) provided an analytical model for interior joints based on two sets of experimental subassemblages.

The following equation should be used for evaluating the nominal shear stress of interior joint in plane configuration (without transverse beams) or with transverse beams in which less than two-thirds of each joint face is covered by framing beams:

$$v_{jh} = 0.25 \cdot f_c \,. \tag{2.153}$$

Therefore, the nominal shear strength v_{jh} of a joint may be enhanced up to 1.3 times if beams into four vertical faces of the joint and if at last two-thirds of each joint face is covered by framing beams; in particular the previous equation can be modified as follows:

$$v_{jh} = 0.33 \cdot f_c \,. \tag{2.154}$$

Finally, the shear strength can be evaluated as follows:

$$V_{jh} = v_{jh} \cdot b_j \cdot h_c \tag{2.155}$$

where the joint core width b_j is chosen as the minimum between the column width and the average between this last and the beam width.

2.3.2 The Model by Hwang & Lee (2000)

The present model proposed by the authors in 2000 (Hwang & Lee, 2000), suitable for only exterior joints, was the first version of the model by Hwang & Lee (2002) previously described in section 2.2.4. The proposed softened strut-and-tie model has been already discussed with their simplifications developed in 2002 (Hwang & Lee, 2002). In this section the model is briefly recalled without the simplification tools according to the original one (Hwang & Lee, 2000).

The angle of inclination of the compression strut is:

$$\theta = \arctan\left(\frac{h_b - 2 \cdot d_b}{h_c - 2 \cdot d_c}\right), \tag{2.156}$$

and the affective area is evaluated by Eqn. (2.89) and (2.90). Considering the horizontal mechanism, it is composed of horizontal tie and flat struts; the joint hoops within the centre half of the core are considered fully effective when computing the cross area of the horizontal tie, and that the other joint core hoops are included at a rate of 50% (Fig. 2.15).

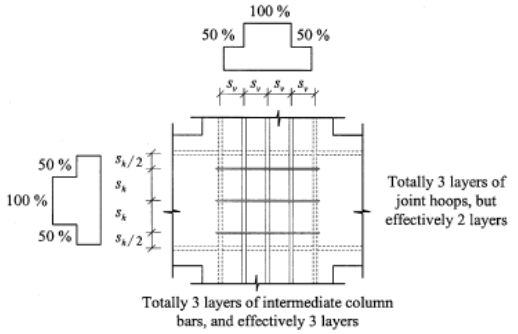

(a)

– For the joint hoops :

Total layers	1	2	3	4	5	6	7	8
Effective layers	1	2	2	3	4	5	5	6

– For the intermediate column bars :

Total layers	1	2	3	4	5	6	7	8
Effective layers	1	2	3	3	4	5	6	6

(b)

Fig. 2.15: Determination of areas of horizontal and vertical ties.

The horizontal shear to be resisted by the strut-and-tie model is found as:

$$V_{jh} = -D \cdot \cos\theta + F_h + F_v \cdot \cot\theta \,. \tag{2.157}$$

The statically indeterminate tie-force F_h in the reduced mechanism is assumed to be:

$$F_h = \gamma_h \cdot V_{jh} \,, \tag{2.158}$$

$$\gamma_h = \frac{2 \cdot \tan\theta - 1}{3} \qquad for \quad 0 \le \gamma_h \le 1 \,, \tag{2.159}$$

while the fraction of the vertical shear assigned to the vertical tie is:

$$F_v = \gamma_v \cdot V_{jv} \,, \tag{2.160}$$

$$\gamma_v = \frac{2 \cdot \cot\theta - 1}{3} \qquad for \quad 0 \le \gamma_v \le 1 \,. \tag{2.161}$$

It is assumed that the ratios of the horizontal shear V_{jh} are assigned among the three mechanisms as follows:

$$-D\cos\theta : F_h : F_v \cot\theta = R_d : R_h : R_v \tag{2.162}$$

where R_d, R_h and R_v are the ratios of the joint shears resisted by the diagonal, horizontal and vertical mechanisms, respectively, and are defined by Eqn. (2.86), (2.87) and (2.88). By a substitution in Eqn. (2.162) it can be obtained:

$$D = \frac{-1}{\cos\theta} \cdot \frac{R_d}{\left(R_d + R_h + R_v\right)} V_{jh} \,, \tag{2.163}$$

$$F_h = \frac{R_h}{\left(R_d + R_h + R_v\right)} V_{jh} \,, \tag{2.164}$$

$$F_v = \frac{1}{\cot\theta} \cdot \frac{R_d}{\left(R_d + R_h + R_v\right)} V_{jh} \,. \tag{2.165}$$

The maximum compressive stress $\sigma_{d,max}$ acting on the nodal zone is assumed to govern the failure. With some algebraic efforts, the value of $\sigma_{d,max}$ is given by:

$$\sigma_{d,\max} = \frac{1}{A_{str}} \left(D - \frac{\cos\left(\theta - \tan^{-1}\left(\frac{h_b - 2\cdot d'_b}{2(h_c - 2\cdot d'_c)}\right)\right)}{\cos\left(\tan^{-1}\left(\frac{h_b - 2\cdot d'_b}{2(h_c - 2\cdot d'_c)}\right)\right)} F_h - \frac{\cos\left(\tan^{-1}\left(\frac{2(h_b - 2\cdot d'_b)}{h_c - 2\cdot d'_c}\right) - \theta\right)}{\sin\left(\tan^{-1}\left(\frac{2(h_b - 2\cdot d'_b)}{h_c - 2\cdot d'_c}\right)\right)} F_v \right). \tag{2.166}$$

Considering the constitutive laws of concrete by Zhang & Hsu (1998), the ascending branch of the softened stress-strain curve of the cracked concrete is governed by Eqn. (2.92) and (2.93) where the cylinder strain corresponding to the cylinder strength f_c that can be defined approximately as:

$$\varepsilon_0 = 0{,}002 + 0{,}001\left(\frac{f_c - 20}{80}\right) \qquad \textit{for } 20 \le f_c \le 100 \textit{ MPa} \,. \tag{2.167}$$

The shear strength of the joint is assumed to be reached whenever the compressive stress and strain of the concrete diagonal strut arrive at the following situations:

$$\sigma_d = -\zeta \cdot f_c \,, \tag{2.168}$$

$$\varepsilon_d = -\zeta \cdot \varepsilon_0 \,. \tag{2.169}$$

If the stress-strain relationships of bare mild steel for the joint hoops and the intermediate column bars are assumed to be elastic-perfectly-plastic, then

$$f_s = E_s \cdot \varepsilon_s \qquad \textit{for} \quad \varepsilon_s < \varepsilon_y \,, \tag{2.170}$$

$$f_s = f_y \qquad \textit{for} \quad \varepsilon_s \ge \varepsilon_y \,. \tag{2.171}$$

The stress f_s becomes f_h or f_v, ε_s becomes ε_h or ε_v and f_y becomes f_{yh} or f_{yv} when applied to joint hoop reinforcement or intermediate column bars, respectively.

The relationship between forces and strains of the tension ties can be constructed by Eqn. (2.95) and (2.96).

Furthermore the Mohr's circle compatibility [Eqn. (2.94)] should be satisfied.

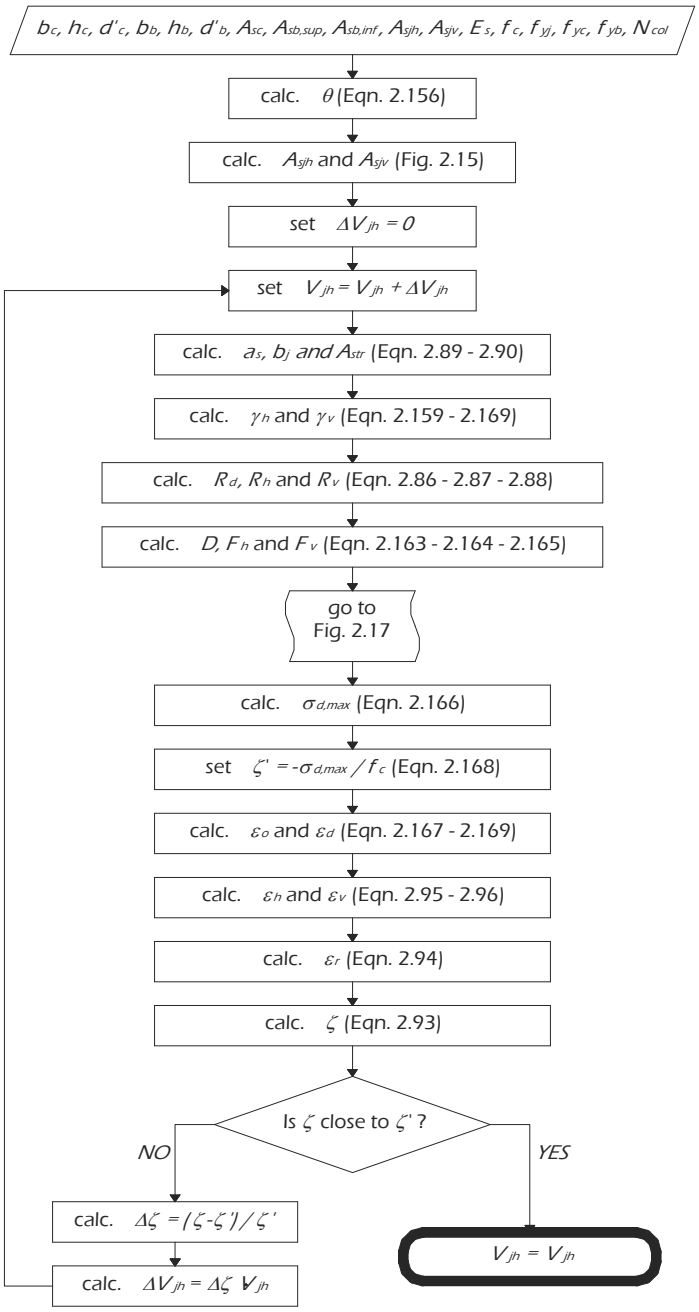

Fig. 2.16: Evaluating shear strength according to Hwang & Lee (2000).

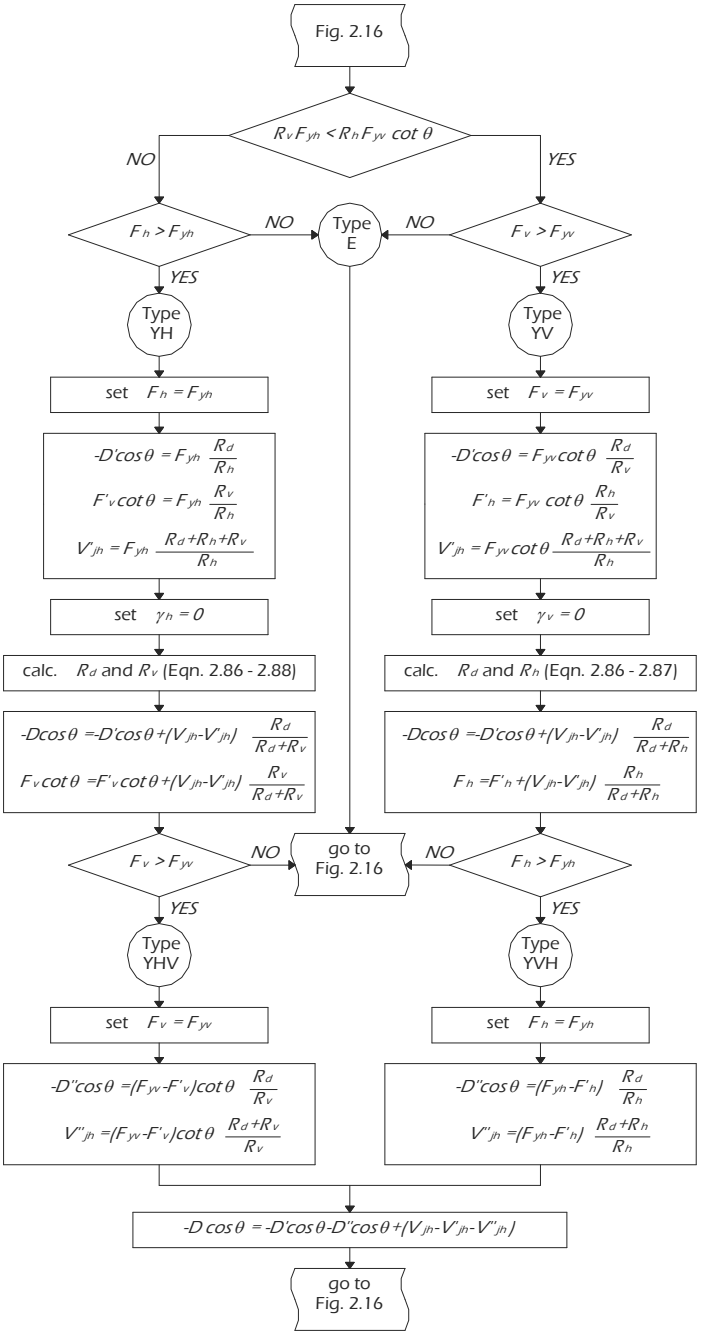

Fig. 2.17: Algorithm for post-yielding cases according to Hwang & Lee (2000).

The proposed procedure is iterative; the author proposed 0 a solution procedure categorized into five types of analyses (Type E, YH, YV, YHV and YVH) for varied yielding conditions of the ties. The set of solution procedures is reproduced in the flow-charts in Fig. 2.16 and Fig. 2.17. The case of Type E means that the concrete strut reaches its strength while the horizontal and vertical ties are in the elastic range. Type YH deals with the case that the yielding of horizontal ties occurs before the reaching of the concrete strength, whereas the vertical ties are still elastic; Type YV treats the dual case of vertical ties yielded and horizontal ones elastic. The scope of Type YHV includes the case where the yielding of the horizontal tie occurs first then the vertical tie yields, and finally the concrete strut arrives at its capacity while the dual case of Type YVH is in reverse.

2.4 Specific Models for Exterior Joints

The scientific literature provides several models for evaluating the shear strength of exterior beam-to-column joints as those elements have been identified as critical zone already in '80. After a detailed research, in the following, only the models for which the original paper is available and the procedure is clearly identified are reported.

2.4.1 The Model by Zhang & Jirsa (1982)

Zhang and Jirsa (1982) developed an approach to determine the shear strength and behaviour of beam-column joints under monotonic and cyclic loading from a large number of published test data. The joint shear strength is governed by the failure of a single diagonal strut affected by: the concrete strength, the hinge mechanism, the column axial load, the transverse reinforcement ratio, the joint aspect ratio and the existence of lateral beams.

The joint shear strength, depending on forming plastic hinges due to beam reinforcement yielding in the beams adjacent to the joint, is evaluated as follows:

$$V_{jh} = K \cdot \zeta \cdot \gamma \cdot f_c \cdot b_c \cdot \sqrt{a_c^2 + a_b^2} \cos\theta \quad \text{for joints without beam hinge,} \qquad (2.172)$$

$$V_{jh} = K \cdot \zeta \cdot \gamma \cdot f_c \cdot b_c \cdot a_c \cdot \cos\theta \quad \text{for joints with beam hinge,} \qquad (2.173)$$

where K represents the effect of concrete strength [Eqn. (2.174)], ζ represents the effect of the volumetric transverse reinforcement ratio ρ_j [Eqn. (2.175)] and γ

represents the effects of the lateral beams [Eqn. (2.176)] in which W_L is the width of the lateral beam.

$$K = 1{,}2 - 0{,}1 \cdot f_c \qquad [ksi], \tag{2.174}$$

$$\zeta = 0{,}95 + 4{,}5 \cdot \rho_j \le 1{,}20 \qquad with\ 0{,}01 \le \rho_j \le 0{,}06, \tag{2.175}$$

$$\gamma = 0{,}85 + 0{,}30 \frac{W_L}{h_c} \qquad with\ 0{,}5 \le \frac{W_L}{h_c} \le 1{,}0. \tag{2.176}$$

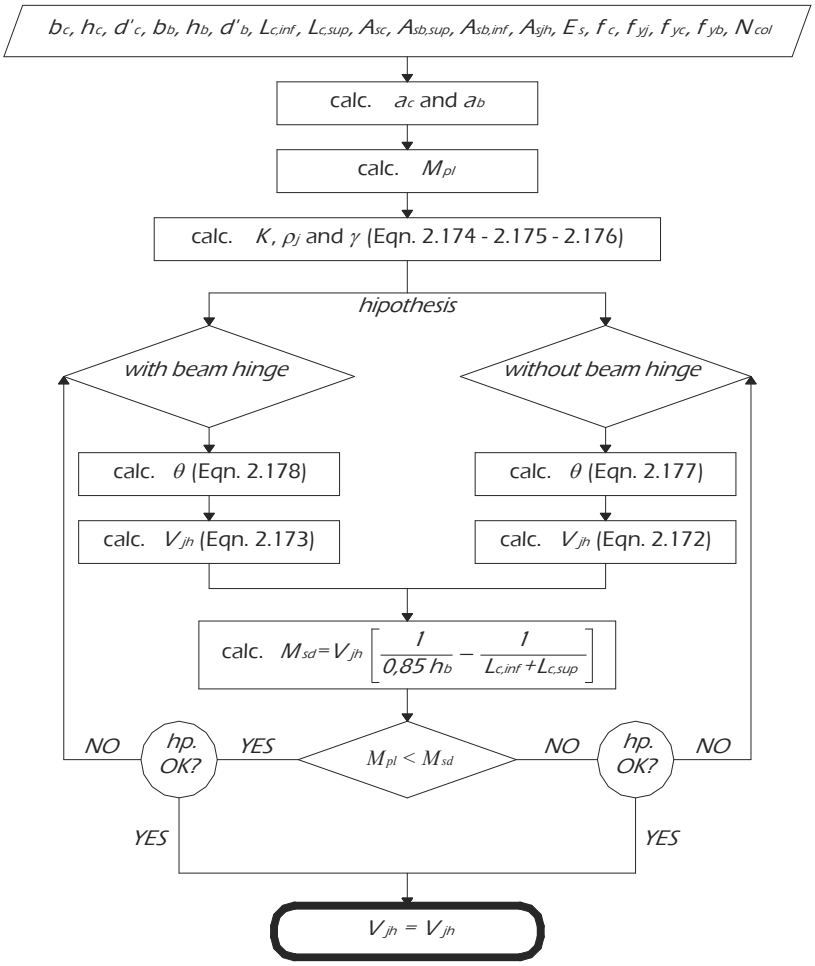

Fig. 2.18: Evaluating shear strength according to Zhang & Jirsa (1982).

The depth of the compression zone in column a_c and beam a_b should be determined considering the effect of column and beam axial load, respectively.

The angle of inclination of the strut is:

$$\theta = \tan^{-1}\left(\frac{h_b - \frac{2}{3}a_b}{h_c - \frac{2}{3}a_c}\right) \quad \text{for joints without beam hinge ,} \tag{2.177}$$

$$\theta = \tan^{-1}\left(\frac{h_b}{h_c - \frac{2}{3}a_c}\right) \quad \text{for joints with beam hinge .} \tag{2.178}$$

The algorithm implemented for solving the equations developed by Zhang & Jirsa (1982) is shown in Fig. 2.18.

2.4.2 The Model by Sarsam & Phillips (1985)

According to the proposed model (Sarsam & Phillips, 1985) the following equations for the design of exterior beam-column joints under monotonic loading can be used:

$$V_{ch} = 5.08\left(R_c \cdot \rho_c\right)^{0.33}\left(\frac{d_c}{d_b}\right)^{1.33} b_c \cdot d_c \cdot \sqrt{1 + 0.29\frac{N_c}{A_c}}\,, \tag{2.179}$$

$$V_{sh} = 0.87 \cdot A_{sjh} \cdot f_{yj}\,, \tag{2.180}$$

$$V_{jh} = V_{ch} + V_{sh}\,. \tag{2.181}$$

where R_c is the concrete cube strength in MPa, ρ_c is the column longitudinal reinforcement ratio $\left[\rho_c = \frac{A_{sc,0}}{b_c \cdot d_c}\right]$, d_c and d_b are the column and beam depth, respectively, $A_{sc,0}$ is the area of the layer of steel farthest from the maximum compression face in a column and A_{sjh} is the total area of the transverse reinforcement into the joint.

The following upper limits were proposed:

$$\rho_c \le 0.02\,, \tag{2.182}$$

$$N_{col}/A_c \le R_c/3\,, \tag{2.183}$$

$$V_{jh} \le 2.4\left(R_c\right)^{0.33} b_c \cdot d_c \qquad with \quad R_c \le 70 MPa\,. \tag{2.184}$$

2.4.3 The Model by Ortiz (1993)

Ortiz (1993) developed a simple strut and tie model for the design of exterior beam-to-column joints both with and without stirrups (Fig. 2.19).

The horizontal joint shear force can be evaluated as follows:

$$V_{jh} = T_b - V_{col} \tag{2.185}$$

where T_b is the tensile force in the beam reinforcement at the inner face of the column and R_t is the shear force in the upper column which, without axial force in the beam, is function of the moment M_j of the beam load about the centre line of the column by:

$$V_{col} = \frac{M_j}{\left(L_{c,\inf} + L_{c,\sup}\right)}\,. \tag{2.186}$$

The resultants of the vertical forces F_v that act on the internal and external faces of the column are defined in the following:

$$F_{ve} = N_c + T_{si} + T_{se}\,, \tag{2.187}$$

$$F_{vi} = N_c + N_b + T_{si} + T_{se}\,, \tag{2.188}$$

where the tensile force in the column bars have been defined as T_s indicating with the subscripts e and i the external and internal faces of the column.

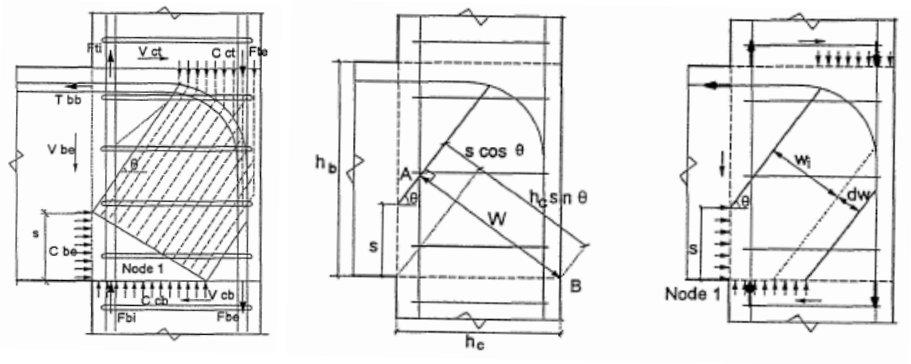

(a) (b) (c)

Fig. 2.19: Definition of the Ortiz (1993) strut-and-tie model.

The joint shear force is assumed to be transferred across the joint by an inclined strut; in particular, the following equations can be written:

$$D \cdot \sin\theta = F_{ve} \,, \tag{2.189}$$

$$D \cdot \cos\theta = V_{ch} \,, \tag{2.190}$$

in which D is the force in the inclined strut and θ is the angle that the strut makes to the horizontal.

$$\theta = \arctan\frac{F_{ve}}{V_{ch}} \,. \tag{2.191}$$

The strength of the inclined strut should be established adopting a semi-rational approach whereby the concrete strength is taken as σ_d (CEB Model Code, 1990) and the width of the inclined strut is chosen to give a good fit to the experimental results for specimens without joint stirrups developed by Ortiz.

$$\sigma_d = 0.6 \cdot f_c \left(1 - \frac{f_c}{250}\right) \tag{2.192}$$

On this basis Ortiz adopted a strut width of:

$$w_i = 0.45 \cdot W \tag{2.193}$$

where

$$W = h_c \cdot \sin\theta + a_b \cdot \cos\theta \,, \tag{2.194}$$

and a_b is the depth to the neutral axis of the beam from the extreme compression fibre at the intersection with the column, evaluated assuming plane sections.

Finally the shear strength of exterior beam-to-column unreinforced concrete joints is given by:

$$D = \sigma_d \cdot b_c \cdot w_i \,, \tag{2.195}$$

$$V_{jh} = V_{ch} = \sigma_d \cdot b_c \cdot w_i \cdot \cos\theta \,. \tag{2.196}$$

It is important to note that W depends on both a_b and θ which are related to the applied loads; this indicates that an iterative solution procedure is required to calculate the joint shear strength (Fig. 2.20).

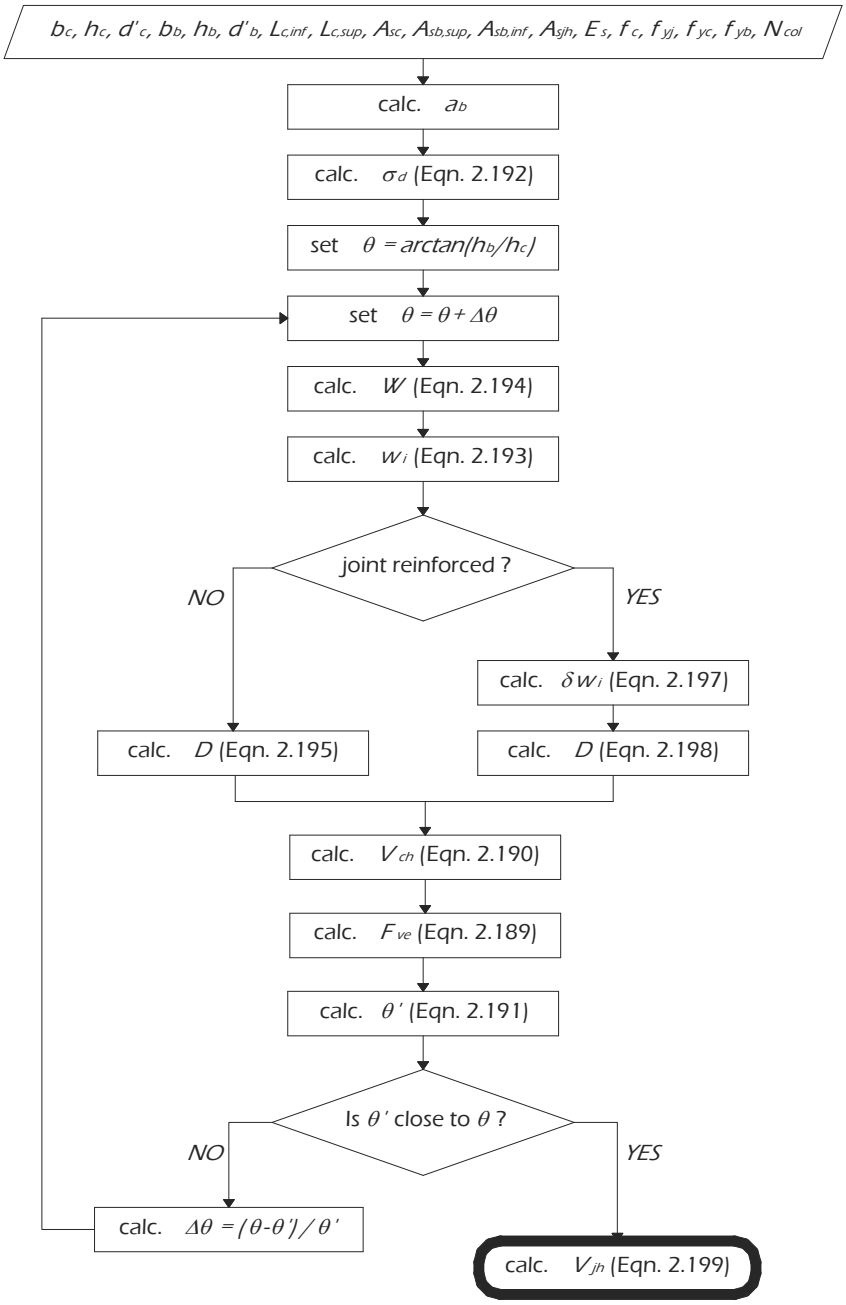

Fig. 2.20: Evaluating shear strength according to Ortiz (1993).

When stirrups are provided, the strut width is assumed to increase by an amount δw_i that corresponds to the shear force resisted by the stirrups; the stirrups are assumed to yield at failure:

$$\delta w_i = \frac{\delta D}{f_c \cdot b_c} = \frac{A_{sjh} \cdot f_{yj}}{\cos\theta} \frac{1}{f_c \cdot b_c}. \tag{2.197}$$

The total strut width $w_i + \delta w_i$ must not exceed W:

$$D = \sigma_d \cdot b_c \cdot (w_i + \delta w_i). \tag{2.198}$$

Then joint failure load is then given by:

$$V_{jh} = V_{ch} + A_{sjh} \cdot f_{yj}. \tag{2.199}$$

The flow-chart reporting the iterative solution procedure used for evaluating the shear strength of reinforced concrete beam-to-column joints according to Ortiz, is shown in Fig. 2.20.

2.4.4 The Model by Scott et Al. (1994)

The authors 0(Scott et al., 1994) proposed a simple model to predict the shear strength of exterior beam-to-column joints based on a single diagonal strut neglecting both the vertical and horizontal contributions of stirrups:

$$v_{jh} = \frac{2 \cdot \sqrt{f_c}}{\left(z_c / z_b + z_b / z_c \right)}. \tag{2.200}$$

The ultimate joint shear stress v_{jh} is function of the concrete strength f_c and geometric characteristics of the column and the beam; in particular in Eqn. (2.200) z_c is the distances between the centres of two outer bars in the column and z_b is the distance between the bars in tension and the resultant of the compression stresses in the sectional analysis of the beam.

Finally, the shear strength of exterior joints is evaluated as follows:

$$V_{jh} = v_{jh} \cdot b_c \cdot d_c \tag{2.201}$$

in which b_c and d_c are the column width and depth.

2.4.5 The Model by Vollum & Newman (1999)

Vollum & Newman (1999) analysed several specimens available in the scientific literature tested under monotonically loads determining the influences on joint shear strength of concrete strength, column load, joint aspect ratio, reinforcement detailing and stirrups.

After a parametric study a simple design equation was proposed:

$$V_{jh} = V_{ch} + \left(A_{sjh} \cdot f_{yj} - \alpha \cdot b_j \cdot h_c \cdot \sqrt{f_c} \right) \tag{2.202}$$

in which A_{sjh} is the cross-sectional area of the joint stirrups within the top five-eighths of the beam depth, α is a coefficient including the effects of the column axial load, the concrete strength, the stirrup index and the joint aspect ratio (conservatively the authors suggest α = 0.2 [MPa$^{0.5}$]), V_c is the joint shear strength without stirrups (2.204) and b_j is the effective joint width evaluated as follows:

$$\begin{aligned} b_j &= \min\left(\frac{b_c + b_b}{2} ; b_b + \frac{h_c}{2} \right) && \text{if } b_b \le b_c \text{ ,} \\ b_j &= \min\left(b_b ; b_c + \frac{h_c}{2} \right) && \text{if } b_b > b_c \text{ .} \end{aligned} \tag{2.203}$$

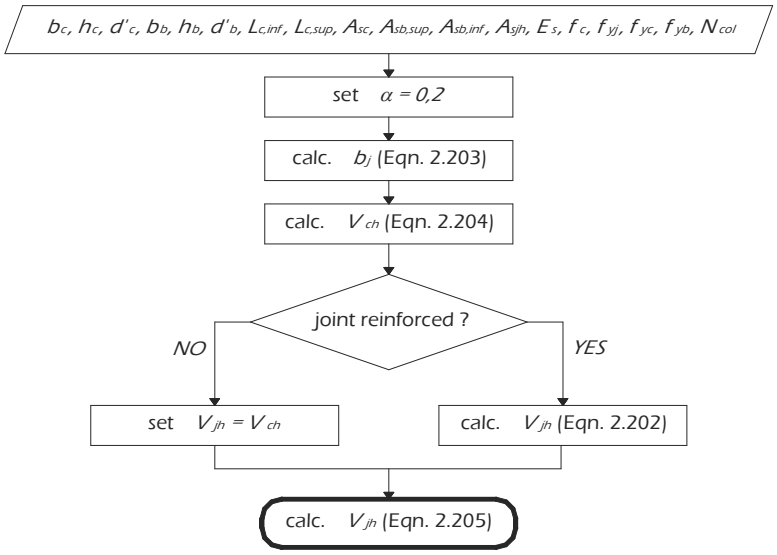

Fig. 2.21: Evaluating shear strength according to Vollum & Newman (1999).

The joint shear strength without stirrups can be estimated by:

$$V_{ch} = 0.642 \cdot \beta \cdot \left[1 + 0.555 \cdot \left(2 - {h_b}/{h_c}\right)\right] \cdot b_j \cdot h_c \cdot \sqrt{f_c} \qquad (2.204)$$

where β is 1.00 for connection with L bars and 0.90 for connections with U bars.

The maximum joint shear strength should be limited to:

$$V_{jh} \le 0.97 \cdot b_j \cdot h_c \cdot \sqrt{f_c} \cdot \left[1 + 0.555 \cdot \left(2 - {h_b}/{h_c}\right)\right] \le 1.33 \cdot b_j \cdot h_c \cdot \sqrt{f_c} \ , \qquad (2.205)$$

based on the assumption that the joint shear strength reduces linearly as the joint aspect ratio is increased. The flow-chart describing the Vollum and Newman model (1999) is shown in Fig. 2.21.

2.4.6 The Model by Hwang & Lee (1999)

The present model proposed by Hwang & Lee (1999) represents the first model developed by the authors about the joint shear strength. This model, suitable for only exterior joints, was the starting point of the model proposed in 2000 (Hwang & Lee, 2000) for suitable for only interior joints and the final simplified model developed in 2002 (Hwang & Lee, 2002) and exposed in section 2.2.4 used for evaluating the shear strength of both interior and exterior joints.

The proposed model is based on a strut-and-tie mechanism satisfying equilibrium, compatibility and constitutive laws of materials at the ultimate load stage. The model is composed of the diagonal, horizontal and vertical mechanisms as shown in Fig. 2.22.

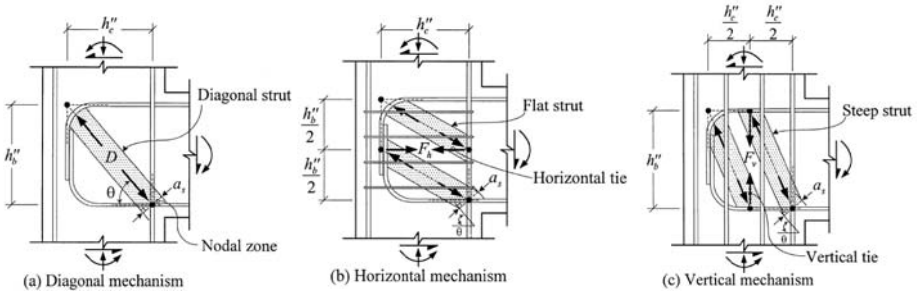

Fig. 2.22: Joint shear resisting mechanisms: (a) diagonal mechanism, (b) horizontal mechanism and (c) vertical mechanism (Hwang & Lee, 1999).

The effective area of the diagonal strut A_{str} is defined as a function of the strut depth a_s and the effective width of the joint according Eqn. (2.89) and (2.90).

Since the forces meeting at a node must be in equilibrium, the horizontal joint shear to be resisted by the strut-and-tie model is found from:

$$V_{jh} = D \cdot \cos\theta + F_h + F_v \cdot \cot\theta \,, \tag{2.206}$$

having denoted with θ the angle of inclination of the single diagonal strut [Fig. 2.22 (a)] evaluated using Eqn. (2.156).

As suggested for the model for interior joint discussed in section 2.3.2 the tie horizontal force F_h and the tie vertical force F_v can be evaluated by Eqn. (2.158), (2.159), (2.160) and (2.161).

The ratio of the horizontal shear V_{jh} assigned among three mechanisms is defined as:

$$D \cdot \cos\theta : F_h : F_v \cdot \cot\theta = R_d : R_h : R_v \,, \tag{2.207}$$

and Eqn. (2.206) can be restated as:

$$D = \frac{1}{\cos\theta} \cdot \frac{R_d}{R_d + R_h + R_v} \cdot V_{jh} \,, \tag{2.208}$$

$$F_h = \frac{R_h}{R_d + R_h + R_v} \cdot V_{jh} \,, \tag{2.209}$$

$$F_v = \frac{1}{\cot\theta} \cdot \frac{R_v}{R_d + R_h + R_v} \cdot V_{jh} \,, \tag{2.210}$$

in which the values of the ratios of the joint shears resisted by the diagonal R_d, horizontal R_h and vertical R_v mechanisms are provided by Eqn. (2.86), (2.87) and (2.88). If the vertical tie is absent or yielding, by assigning $\gamma_v = 0$, the value R_h converts to γ_h for the reduced mechanisms; the same situation occurs between R_v and γ_v.

For evaluating if the ultimate strength is reached, the compressive forces of the diagonal strut should be checked by assuming the maximum compressive stress $\sigma_{d,max}$ given by:

$$\sigma_{d,\max} = \frac{1}{A_{str}} \left\{ D + \frac{\cos\left(\theta - \tan^{-1}\left(\frac{h_b - 2d'_b}{2(h_c - 2d'_c)}\right)\right)}{\cos\left(\tan^{-1}\left(\frac{h_b - 2d'_b}{2(h_c - 2d'_c)}\right)\right)} F_h + \frac{\cos\left(\tan^{-1}\left(\frac{2(h_b - 2d'_b)}{h_c - 2d'_c}\right) - \theta\right)}{\sin\left(\tan^{-1}\left(\frac{2(h_b - 2d'_b)}{h_c - 2d'_c}\right)\right)} F_v \right\}. \tag{2.211}$$

The so-called compression softening phenomenon can be taken into account using Eqn. (2.212) and (2.213) for the ranging of interest from 20 to 100 MPa.

$$\sigma_d = \zeta \cdot f_c \left[2\left(\frac{\varepsilon_d}{\zeta \cdot \varepsilon_0} \right) - \left(\frac{\varepsilon_d}{\zeta \cdot \varepsilon_0} \right)^2 \right] \qquad for \ \frac{\varepsilon_d}{\zeta \cdot \varepsilon_0} \le 1, \tag{2.212}$$

$$\zeta = \frac{5.8}{\sqrt{f_c}} \cdot \frac{1}{\sqrt{1+400\varepsilon_r}} \le \frac{0.9}{\sqrt{1+400\varepsilon_r}}, \tag{2.213}$$

in which the concrete cylinder strains ε_0 corresponding to the cylinder strength f_c can be defined approximately as:

$$\varepsilon_0 = -0.002 - 0.001\left(\frac{f_c - 20}{80} \right) \qquad for \ 20 \le f_c \le 100 \ MPa. \tag{2.214}$$

The shear strength of the joint is reached whenever the compressive stress and strain of concrete diagonal strut conform to the following formulations:

$$\sigma_d = \zeta \cdot f_c, \tag{2.215}$$

$$\varepsilon_d = \zeta \cdot \varepsilon_0. \tag{2.216}$$

Finally, the behaviour of the steel bars is assumed to be elastic-perfectly-plastic [Eqn. (2.95) and Eqn. (2.96)] as done for the models developed by the same author (Hwang & Lee, 2000 and 2002) and exposed in section 2.2.4 and section 2.3.2.

Accepting the predetermined direction of the principal compressive stress θ, the principal tensile strain ε_r can be related to the horizontal strain ε_h, the vertical strain ε_v and the magnitude of the principal compressive strain ε_d as follows:

$$\varepsilon_r = \varepsilon_h + (\varepsilon_h - \varepsilon_d)\cot^2\theta, \tag{2.217}$$

$$\varepsilon_r = \varepsilon_v + (\varepsilon_v - \varepsilon_d)\tan^2\theta. \tag{2.218}$$

The authors proposed an iterative procedure for the solution (Hwang & Lee, 1999) reported in the following flow-charts starting from a hypothetic small value of V_{jh}.

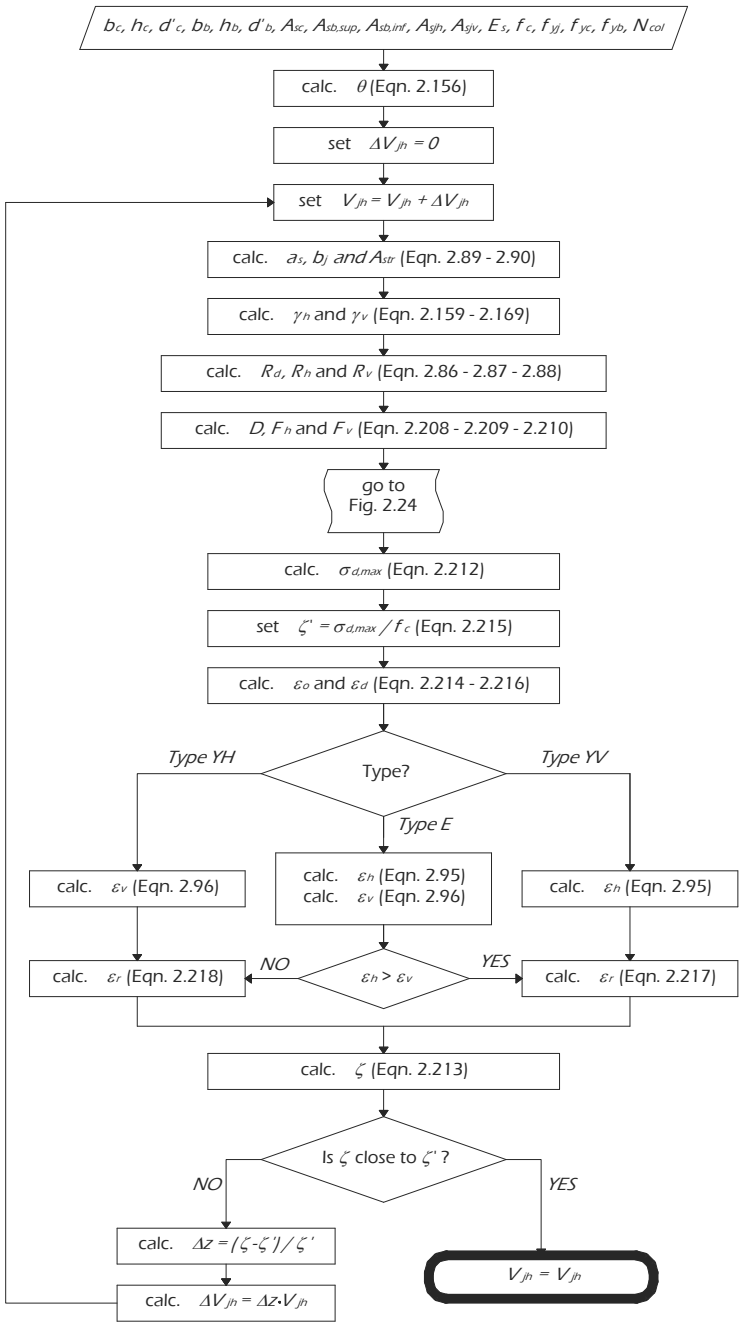

Fig. 2.23: Evaluating shear strength according to Hwang & Lee (1999).

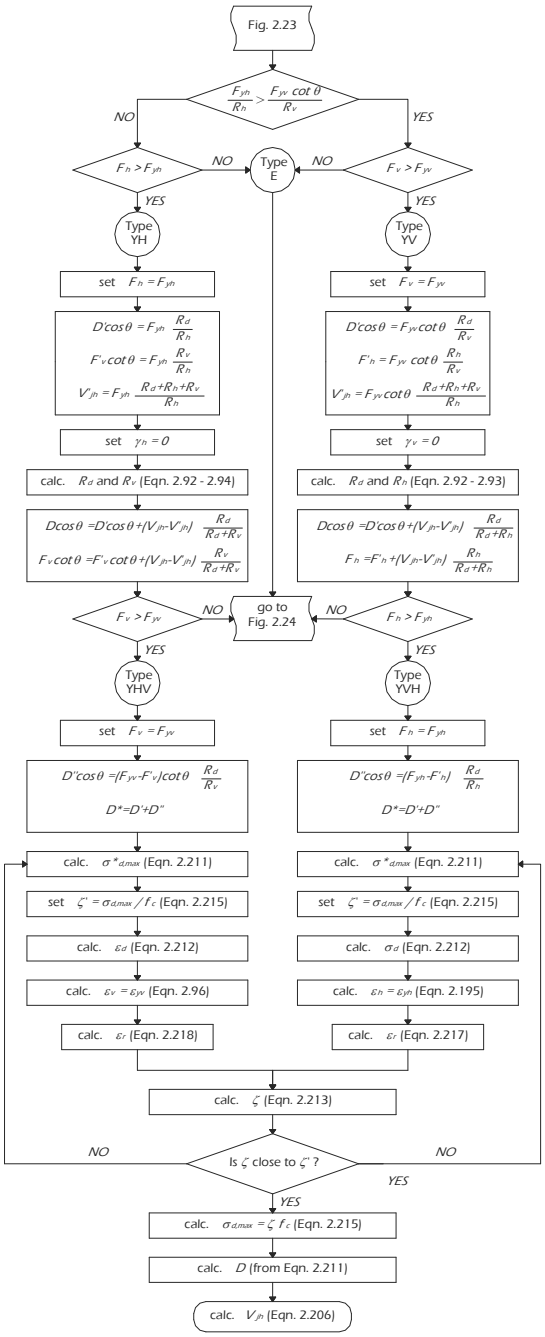

Fig. 2.24: *Algorithm of Hwang & Lee (1999) for post yielding cases.*

The procedure reported in Fig. 2.23 and Fig. 2.24 is categorized into five types:

- *Type E* : $F_h < F_{yh}$ *and* $F_v < F_{yv}$, (2.219)
- *Type YH* : $F_h = F_{yh}$ *and* $F_v < F_{yv}$, (2.220)
- *Type YV* : $F_h < F_{yh}$ *and* $F_v = F_{yv}$, (2.221)
- *Type YHV* : $F_h = F_{yh}$ *and then* $F_v = F_{yv}$, (2.222)
- *Type YVH* : $F_v = F_{yv}$ *and then* $F_h = F_{yh}$. (2.223)

Type E means that the concrete reaches its strength while the horizontal and vertical ties are elastic yet. Type YH and Type YV basically follow Type E including the yielding of horizontal and vertical ties, respectively, without yielding of the ties in the perpendicular direction. Finally Type YHV and Type YVH respectively describe the cases in which the yielding of vertical or horizontal ties follows the inelastic excursion of the perpendicular ones.

2.4.7 The Model by Bakir & Boduroglu (2002)

Through a parametric study on joint shear strength based on 58 tests carried out in Europe, the authors (Bakir & Boduroglu, 2002) proposed a new design equation for exterior joints.

According to the experimental results, the shear strength of exterior beam-to-column joints depends on the concrete cylinder strength, the column and beam reinforcement ratios, the beam reinforcement detailing (U or L bars anchored into the connection), the aspect ratio and the stirrups of joints.

It is assumed that the shear strength is given by the addition of concrete resistance to shear V_{ch} and stirrup yield capacity V_{sh}:

$$V_{jh} = V_{ch} + V_{sh} \ . \tag{2.224}$$

The contribution of joint stirrups is made as follows:

$$V_{sh} = \alpha \cdot A_{sjh} \cdot f_{yj} \tag{2.225}$$

in which α depends from the amount of stirrups and in particular $\alpha = 0.664$ for joint with low amount of stirrups, $\alpha = 0.600$ for joints with medium amount of stirrups and $\alpha = 0.370$ for joint with high amount of stirrups. Indeed, the amount of stirrups is measured by the stirrup ratio ρ_{jh}:

$$\rho_{jh} = \frac{A_{sjh}}{b_j \cdot h_c} \tag{2.226}$$

where b_j is taken as the minimum between the column width and the average of the column and the beam width.

The low, medium and high amount of stirrups is defined as follows:

$$\begin{aligned} &\textit{if} \quad \rho_{jh} < 0.0030 \quad \rightarrow \quad \textit{low amount of stirrups}, \\ &\textit{if} \quad 0.0030 \le \rho_{jh} \le 0.0055 \quad \rightarrow \quad \textit{medium amount of stirrups}, \\ &\textit{if} \quad 0.0055 \le \rho_{jh} \quad \rightarrow \quad \textit{high amount of stirrups}. \end{aligned} \tag{2.227}$$

The contribution provided by the concrete strut V_{ch} is evaluated through the following equation in which $\beta = 0.85$ for joints detailed by U bars and $\beta = 1.00$ for joints detailed by L bars, $\gamma = 1.37$ for inclined bars into the joint and $\gamma = 1.00$ for others:

$$V_{ch} = \frac{0.71 \cdot \beta \cdot \gamma \cdot \left(100 \frac{A_{sb,\sup}}{b_b \cdot d_b}\right)^{0.4289}}{\left(h_b / h_c\right)^{0.61}} b_j \cdot h_c \cdot \sqrt{f_c}\ . \tag{2.228}$$

The authors applied their equation on the experimental database of 58 joints determining that the average $V_{jh} \,/\, V_{jh}^{exp}$ value is 0.88 and the standard deviation is 0.10 demonstrating extremely good results.

2.4.8 The Model by Russo & Somma (2006)

The expression proposed by the authors (Russo & Somma, 2006) takes into account the three following contributions to joint shear strength: the vertical stresses transmitted by the column to the concrete v_{ch}, the longitudinal beam reinforcement v_l and the passive confinement due to the stirrups into the joint v_{sh} (if present).

$$v_{jh} = v_{ch} + v_l + v_{sh}\ . \tag{2.229}$$

The concrete contribution to the shear strength v_{ch} depends on the concrete compressive strength f_c and on the two vertical stresses σ_a and σ_v respectively due to the axial load and vertical reinforcement.

By considering a horizontal plane between the upper and lower beam longitudinal reinforcements and the Mohr's circle, the principal tensile and

compressive stresses, ρ_t and ρ_c, are expressed in function of a mean shear stress $\tau_{h,c}$, a mean axial compressive stress σ_a and a mean vertical stress σ_v.

$$\rho_t = \frac{-\sigma_a + \sigma_v}{2} + \sqrt{\left(\frac{\sigma_a + \sigma_v}{2}\right)^2 + {\tau_{h,c}}^2}\,, \tag{2.230}$$

$$\rho_c = \frac{-\sigma_a + \sigma_v}{2} - \sqrt{\left(\frac{\sigma_a + \sigma_v}{2}\right)^2 + {\tau_{h,c}}^2}\,, \tag{2.231}$$

$$\tau_{h,c} = \rho_t \sqrt{1 + \frac{|\sigma_a + \sigma_v|}{\rho_t}}\,. \tag{2.232}$$

In the joint panel there is a biaxial state of tension-compression in two orthogonal directions as shown in Fig. 2.25.

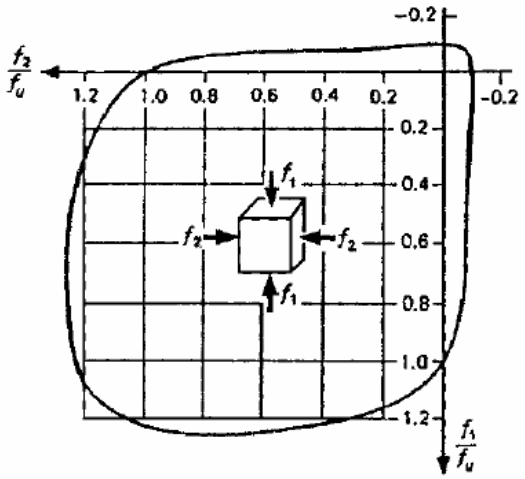

Fig. 2.25: Biaxial strength of concrete (Russo & Somma, 2006).

The portion of the diagram in Fig. 2.25 in the first quadrant (pure tension) can be approximated by the following expression:

$$\rho_t = 0.1 \cdot f_c \left[1 - \left(\frac{\rho_c}{f_c}\right)^2\right] \tag{2.233}$$

where, by adding Eqn. (2.230) and Eqn. (2.231) it is obtained:

$$p_t = f_c \cdot \sqrt{26 + 10\frac{\sigma_a - \sigma_v}{f_c}} - 5 \cdot f_c - \sigma_a + \sigma_v \ . \tag{2.234}$$

To obtain the concrete shear strength contribution v_{ch} the vertical stress σ_v is taken as the maximum vertical action f_v obtained when the longitudinal bars in the column $A_{s,col}$ are yielded:

$$f_v = k_v \frac{A_{s,col} \cdot f_{yc}}{A_g} \tag{2.235}$$

in which k_v = 0.29 is a coefficient calibrated by the authors through the analysis of 89 exterior reinforced concrete joints tested by various authors (Russo & Somma, 2006) and A_g is the area of the joint transverse section provided by the column thickness h_c and the effective joint width b_j. Russo and Somma (2006) did not provide a formulation for evaluating b_j; for this purpose in the present study it is assumed as the minimum value between the column width b_c and the average of the column b_c and the beam width b_b.

Therefore, the shear strength contribution provided by the concrete is:

$$v_{ch} = \overline{p}_t \sqrt{1 + \frac{|\sigma_a - f_v|}{\overline{p}_t}} \tag{2.236}$$

where $\overline{p}_t$ is obtained from Eqn. (2.234) by putting $\sigma_v = f_v$ and σ_a depends on the column axial load:

$$\sigma_a = \frac{N_{col}}{A_g} \ . \tag{2.237}$$

The contribution of the beam longitudinal reinforcement v_l is assumed to be proportional to the steel yielding strength f_{yb} and the area of the beam bottom longitudinal reinforcement $A_{sb,inf}$; consequently the shear strength due to beam reinforcement is:

$$v_l = k_l \cdot \frac{f_{yb} \cdot A_{sb,\inf}}{A_g} \tag{2.238}$$

where the numerical coefficient k_l was determined by experimental data as the coefficient k_v mentioned above.

Finally, the contribution of horizontal stirrups is expressed as:

$$v_{sh} = k_h \cdot \frac{f_{yj} \cdot A_{sjh}}{A_g} \tag{2.239}$$

where k_h is a third numerical coefficient calibrated by the authors through experimental results.

On the basis of Eqn. (2.229) the shear stress of an exterior beam-to-column joint is provided by the following equation:

$$v_{jh} = k_0 \left[\overline{\rho}_t \sqrt{1 + \frac{|\sigma_a - f_v|}{\overline{\rho}_t}} + c_l \frac{f_{yb} \cdot A_{sb,\inf}}{A_g} + c_h \frac{f_{yj} \cdot A_{sjh}}{A_g} \right] \tag{2.240}$$

in which $c_l = k_l / k_0$ and $c_h = k_h / k_0$.

From experimental results, the author found $k_0 = 0.3$, $c_l = 1.97$ and $c_h = 2.88$, which provided the exact mean equality between experimental and computed shear strength, i.e. $AVG = 1$, and a minimum coefficient of variation $COV = 0.31$.

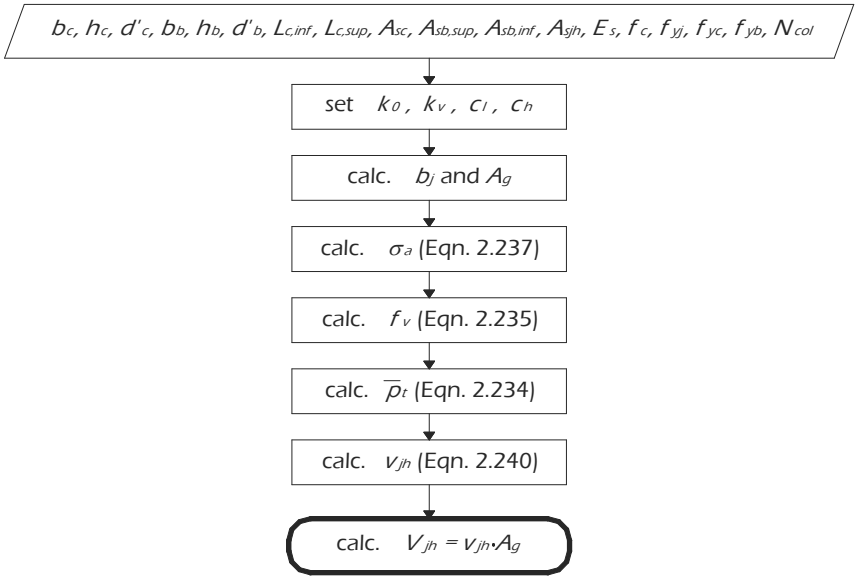

Fig. 2.26: Evaluating shear strength according to Russo & Somma (2006).

The algorithm for evaluating shear strength of exterior joint according Russo & Somma (2006) is shown in Fig. 2.26.

2.4.9 The Model by Tsonos (2007)

In the proposed model (Tsonos, 2007) the shear force acting in the joint core is resisted partly by a diagonal compression strut that acts between diagonally opposite corners of the joint core and partly by a truss mechanism formed by horizontal and vertical reinforcement (Fig. 2.27).

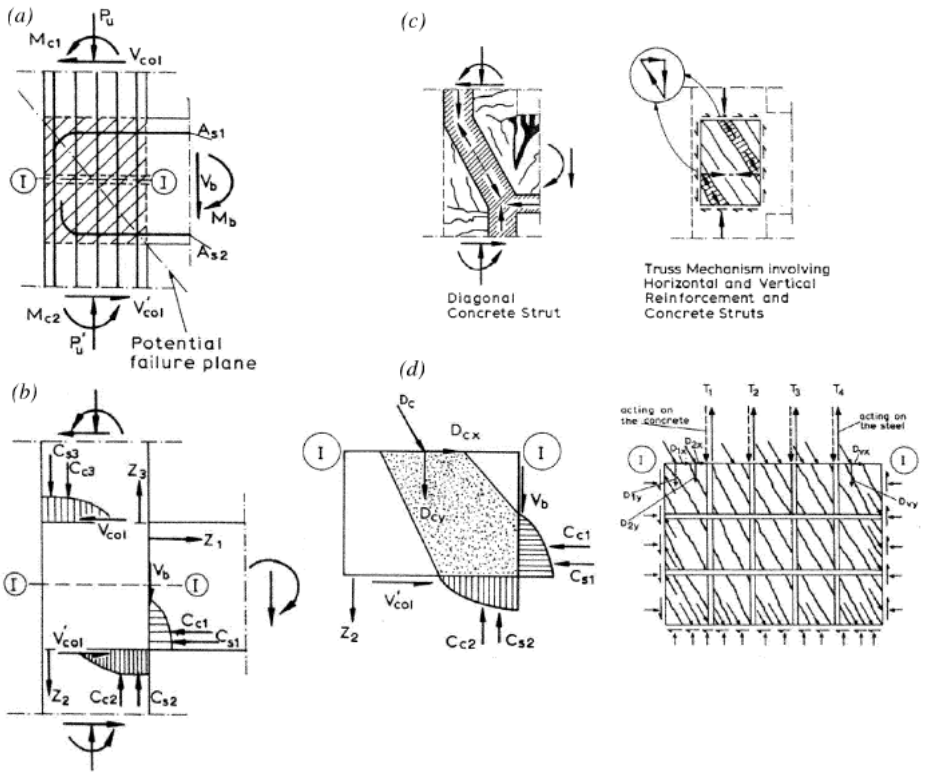

Fig. 2.27: Exterior beam-to-column joint: (a) resultant of seismic action; (b) internal forces; (c) two mechanisms of shear transfer; (d) forces acting in joint core through section I-I (Tsonos, 2007)

The summation of horizontal forces of concrete strut D_{ch} and of reinforcement D_{sh} equals the horizontal joint shear force V_{jh}:

$$V_{jh} = D_{ch} + D_{sh} \,. \tag{2.241}$$

About vertical direction an analogous equation can be written between the vertical forces and the vertical joint shear V_{jv}:

$$V_{jv} = D_{cv} + D_{sv} \tag{2.242}$$

where D_{cv} and D_{sv} are the vertical components of the forces in the concrete strut and reinforcements, respectively.

The vertical compressive stress v_{jv} and the shear stress v_{jh} uniformly distributed over section I-I (Fig. 2.27) are given in the following:

$$v_{jv} = \frac{V_{jv}}{h_c \cdot b_j}, \tag{2.243}$$

$$v_{jh} = \frac{V_{jh}}{h_c \cdot b_j}, \tag{2.244}$$

in which the effective joint width b_j is evaluated as the average between the column and the beam width. The relationship between the normal and shear stresses is:

$$v_{jv} = \frac{V_{jv}}{V_{jh}} \cdot v_{jh} \ . \tag{2.245}$$

The joint aspect ratio α can be evaluated as follows:

$$\alpha = \frac{V_{jv}}{V_{jh}} = \frac{h_b}{h_c} \ . \tag{2.246}$$

The principle stresses σ_I and σ_{II} are calculated by analysing the Mohr's circle:

$$\sigma_{I,II} = \frac{v_{jv}}{2} \pm \frac{v_{jv}}{2} \sqrt{1 + \frac{4 \cdot v_{jh}^{\ 2}}{v_{jv}^{\ 2}}}, \tag{2.247}$$

and the following equation the authors adopted for the representation of the concrete biaxial strength curve:

$$-10 \frac{\sigma_I}{K \cdot f_c} + \left(\frac{\sigma_{II}}{K \cdot f_c} \right)^5 = 1 \tag{2.248}$$

where K is a parameter that increases the joint concrete compressive strength due to the confinement by joint hope reinforcement evaluated as follows:

$$K = 1 + \frac{\rho_{jh} \cdot f_{yj}}{f_c} \tag{2.249}$$

with

$$\rho_{yj} = \frac{A_{sjh} \cdot h_c}{b_c \cdot h_c \cdot \left(h_b - 2 \cdot d_b^{'}\right)} \tag{2.250}$$

in which ρ_{yj} is the volume ratio of transverse reinforcement.

The author (Tsonos, 2007) considers:

$$v_{jh} = \gamma \cdot \sqrt{K \cdot f_c} \ . \tag{2.251}$$

By substituting Eqn. (2.243) through Eqn. (2.245) into Eqn. (2.248) it is obtained:

$$\left[\frac{\alpha \cdot \gamma}{2 \cdot \sqrt{f_c}} \left(1 + \sqrt{1 + \frac{4}{\alpha^2}}\right)\right]^5 + \frac{5 \cdot \alpha \cdot \gamma}{\sqrt{f_c}} \left(\sqrt{1 + \frac{4}{\alpha^2}} - 1\right) = 1. \tag{2.252}$$

By considering:

$$x = \frac{\alpha \cdot \gamma}{2 \cdot \sqrt{f_c}} , \tag{2.253}$$

and

$$\psi = \frac{\alpha \cdot \gamma}{2 \cdot \sqrt{f_c}} \sqrt{1 + \frac{4}{\alpha^2}} , \tag{2.254}$$

the Eqn. (2.252) becomes:

$$\left(x + \psi\right)^5 + 10 \cdot \psi - 10 \cdot x = 1. \tag{2.255}$$

The solution of the system of three equations [Eqn. (2.253), (2.254) and (2.255)] provides the parameter γ and through Eqn. (2.251) the shear stress of the joint can be evaluated.

Finally, the shear strength of exterior beam-to-column joint is derived:

$$V_{jh} = v_{jh} \cdot h_c \cdot b_j \ . \tag{2.256}$$

The proposed model has been solved using the iterative algorithm shown in the flow-chart in Fig. 2.28.

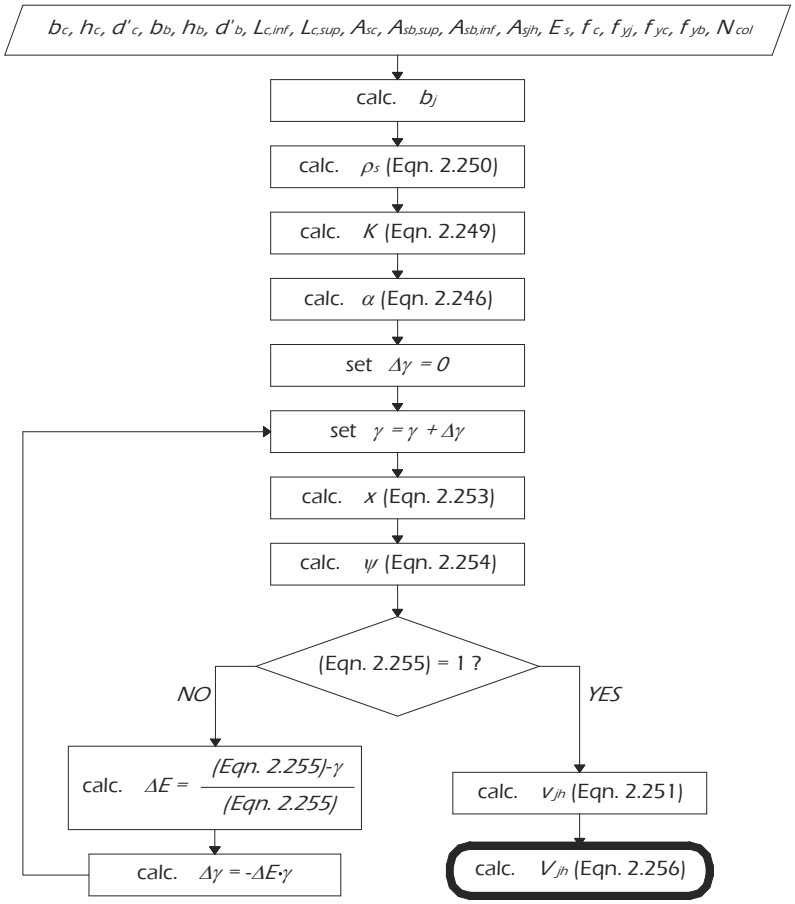

Fig. 2.28: Evaluating shear strength according to Tsonos (2007).

2.4.10 The Model by Vollum & Parker (2008)

The authors (Vollum & Parker, 2008) proposed a rational strut and tie model for the design of external beam-to-column joints which is consistent with the recommendations of EC2 (EN 1992-1, 2004).

The joint shear strength can be expressed in terms of the node dimensions as follows:

$$V_{jh} = b_j \cdot k \cdot \nu' \cdot f_c \cdot (x - y) \tag{2.257}$$

where

$$k \cdot \nu' \cdot f_c = k \cdot \left(1 - \frac{f_c}{250}\right) \cdot f_c \,. \tag{2.258}$$

The coefficient k is taken equal to 0.6 for concrete struts in cracked compression zones, 0.85 for compression-tension nodes with anchored ties in one direction and 0.75 for compression-tension nodes with anchored ties in more than one direction.

By assuming $k = 0.6$ a coefficient ν can be introduced:

$$\nu = k \cdot \nu' = 0.6 \cdot \left(1 - \frac{f_c}{250}\right). \tag{2.259}$$

The effective joint width b_j is assumed to equal the average width of the beam and column as commonly assumed, but an upper limit is introduced to limit the compressive stresses in the beam to $0.85 \cdot (1 - f_c/250) \cdot f_c$:

$$b_j = \frac{b_c + b_b}{2} \le \frac{0.85}{0.6 \cdot b_b} \,. \tag{2.260}$$

The joint shear strength is related to the maximum moment that can be developed in the beam at the face of the column, which is defined in terms of the maximum moment which can be transferred through the joint into the upper and lower columns. The width of the node x_c (Fig. 2.29.a) is taken as half the column width to maximise the moment transferred into the columns through the concrete at the joint boundaries. It follows that in the absence of joint shear reinforcement, the maximum moment that can be transferred through the joint into the columns above and below the beam is given by:

$$M_{col} = 0.125 \cdot b_j \cdot h_c^2 \cdot \nu \cdot f_c \,. \tag{2.261}$$

The strut-and-tie model is modified by the presence of joint shear reinforcement as shown in Fig. 2.29.b. Therefore, joint stirrups are considered to be effective in increasing joint shear strength if placed within the top $5/8^{ths}$ of the beam depth below the tensile beam reinforcement as previously recommended by Vollum & Newman (1999).

Joint stirrups increase joint shear capacity by increasing the maximum moment that can be transferred into the column through the mobilisation of the column bars.

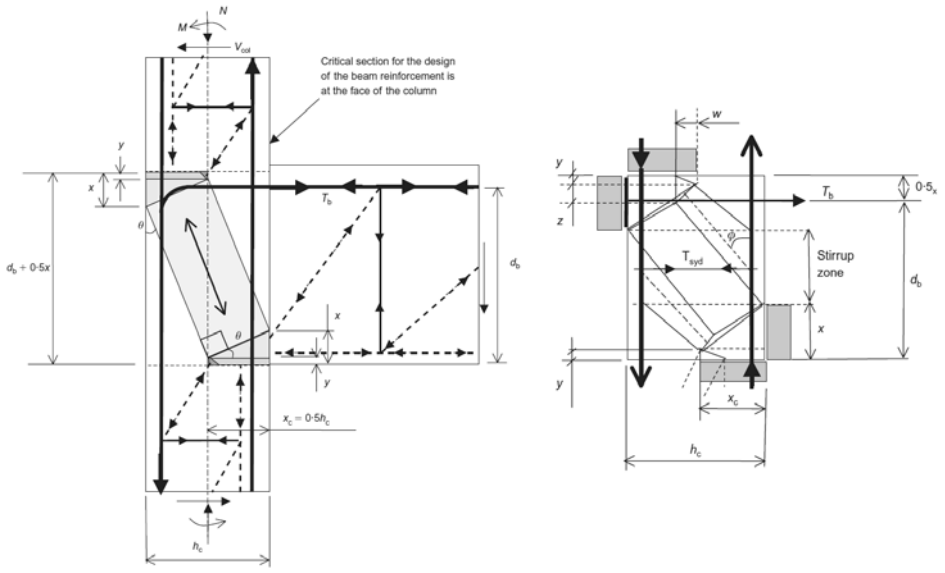

(a) (b)

Fig. 2.29: Strut and tie model for external beam-to-column joint without stirrups (a) and with stirrups (b) (Vollum & Parker, 2008).

The depth of the stress block in the beam is assumed to be proportional increasing to maintain the hydrostatic state of stress in the nodes. Therefore, it is assumed that the centroid of the joint stirrups is at the mid-height of the beam.

Joint stirrups increase the moment capacity of the column at the top and bottom of the beam by:

$$\Delta M = \left(2 \cdot d_c - h_c\right) \Delta T \tag{2.262}$$

where ΔT is half the vertical force transferred from the inclined strut into the internal and external column bars. The force ΔT is given by:

$$\Delta T = 0.5 \cdot T_{sy} \cdot \cot \phi \tag{2.263}$$

where

$$T_{sy} = A_{sjh} \cdot f_{yj} \tag{2.264}$$

in which A_{sjh} is the area of joint shear reinforcement within the top 5/8^{ths} of the beam depth below the tensile beam reinforcement and

$$\cot\phi = \frac{\left(d_b + 0.5\cdot x - 2y - z\right)}{\left(2d_c - h_c + w\right)} \tag{2.265}$$

where

$$x = d_b\left(1 - \sqrt{\left(1 - 2\frac{M_b}{b_j \cdot d_b^2 \cdot v \cdot f_c}\right)}\right) \le 0.5\cdot h_b\ , \tag{2.266}$$

$$y = M_b \frac{\left(1 + 0.5\cdot {h_c}/{L_b}\right)}{\left(L_c \cdot b_j \cdot v \cdot f_c\right)}, \tag{2.267}$$

$$w = \frac{2\cdot\Delta T}{b_j \cdot v \cdot f_c} \le 0.5\cdot h_c\ , \tag{2.268}$$

$$z = \frac{T_{sy}}{b_j \cdot v \cdot f_c}, \tag{2.269}$$

in which L_c is the distance between the points of contraflexure in the upper and lower columns, L_b is the distance to the point of contraflexure in the beam from the column face and M_b is the moment in the beam at the column face.

In accordance with the EC2, the maximum permissible joint shear force is limited to:

$$V_{jh,\max} \le 0.45\cdot v \cdot f_c \cdot b_c \cdot d_c\ . \tag{2.270}$$

The authors (Vollum & Parker, 2008) explained the algorithm to determine joint moment capacity of existing exterior joints. If the stirrups force T_{sy} is known, Eqn. (2.263) can be expressed in the form:

$$\Delta T = 0.5\cdot\left(-b + \sqrt{\left(b^2 - 4c\right)}\right) \tag{2.271}$$

where

$$b = 0.5\cdot\left(2d_c - h_c\right)\cdot v \cdot f_c \cdot b_j\ , \tag{2.272}$$

$$c = -0.25\cdot T_{sy}\cdot\left(h^* - z\right)\cdot v \cdot f_c \cdot b_j\ , \tag{2.273}$$

in which

$$h^* = d_b + 0.5\cdot x - 2y\ . \tag{2.274}$$

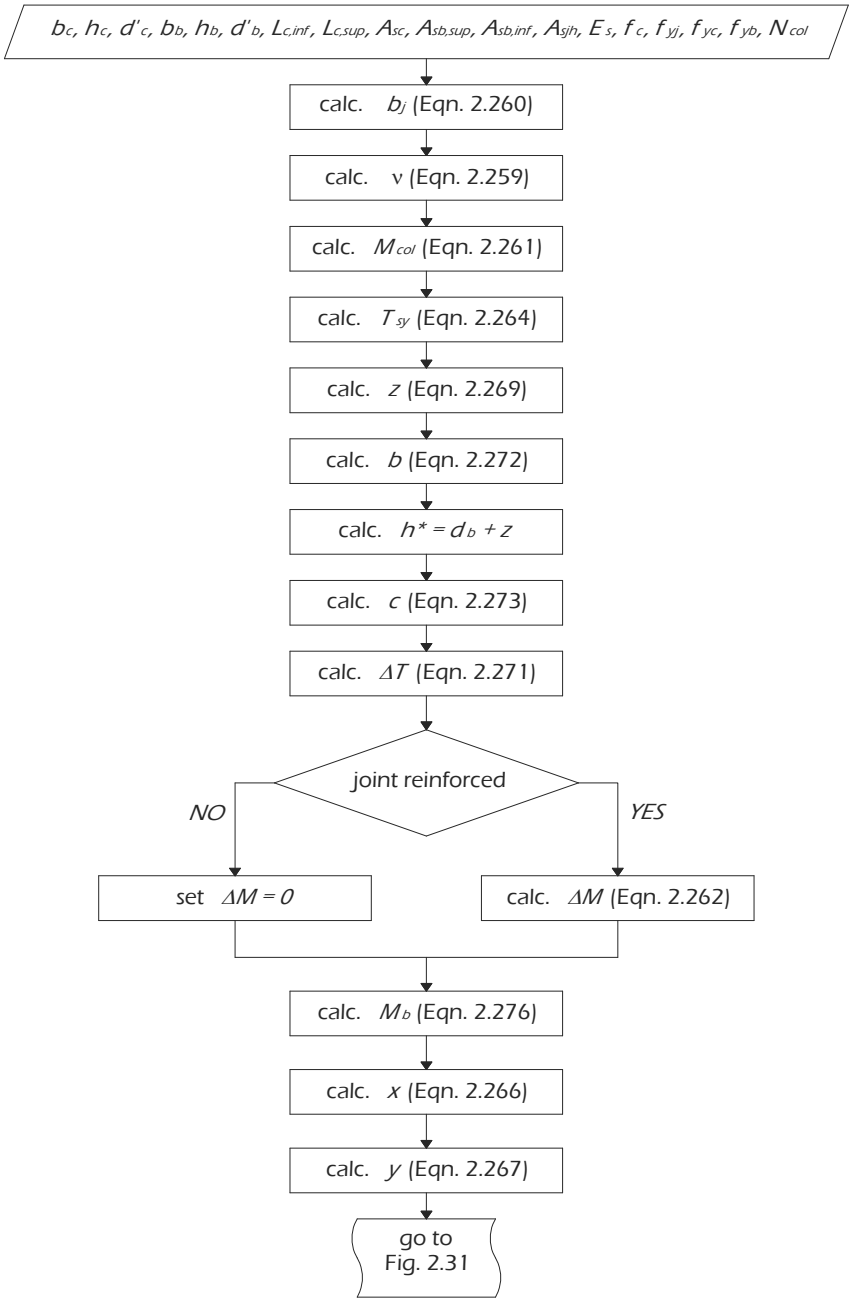

Fig. 2.30: Evaluating shear strength according to Vollum & Parker (2008) – part.1.

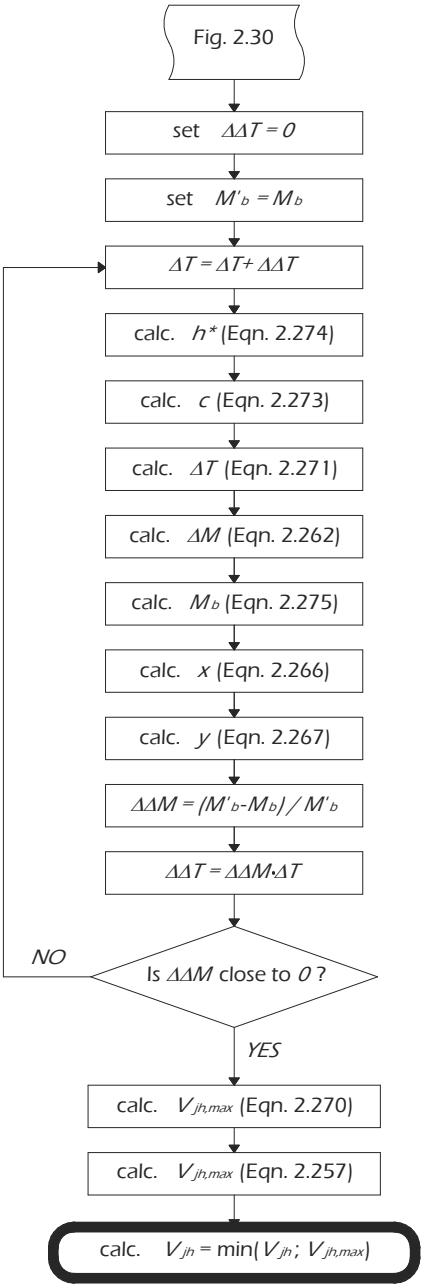

Fig. 2.31: Evaluating shear strength according to Vollum & Parker (2008) – part.2.

The maximum moment which can be transferred into the joint at the beam face M_b is given by:

$$M_b = 2\frac{M_{col} + \Delta M}{1 - \frac{\left(1 + 0.5 \cdot h_c / L_b\right) \cdot \left(d_b + 0.5 \cdot x - y\right)}{L_c}}, \tag{2.275}$$

$$M_b \approx 2\frac{M_{col} + \Delta M}{1 - \frac{\left(1 + 0.5 \cdot h_c / L_b\right) \cdot d_b}{L_c}}, \tag{2.276}$$

where M_b is given by Eqn. (2.261), ΔM by Eqn. (2.262) and M_b can be evaluated through the following iterative procedure:

- calculate ΔT with Eqn. (2.271) assuming $h^* - z = d_b$ in Eqn. (2.273);
- calculate $M_{col} + \Delta M$ with Eqn. (2.261) and (2.262), respectively;
- calculate M_b with Eqn. (2.276) in the first iteration and with Eqn. (2.275) subsequently;
- calculate the node dimensions x and y with Eqn. (2.266) and (2.267) respectively in terms of M_b from step 3;
- recalculate ΔT with Eqn. (2.271) and the current value of h^*;
- repeat steps 2 to 5 until values of M_b from successive iterations converge.

The iterative strategy adopted in this thesis for evaluating the shear strength of exterior beam-to-column joints according to the Vollum & Parker model (2008) is shown in Fig. 2.30 and Fig. 2.31.

2.5 Remarks

The capacity models reported above take into account a wide set of parameters. In all models available in both the scientific literature and the code formulations, the shear strength V_{jh} is supposed to be directly depending on the geometric dimensions of the joint such as the column b_c and the beam b_b width. Other properties, such as the amount of reinforcement in the beam and/or column are generally taken into account by only some models, while are not considered in other ones.

The code formulations generally depends on the column b_c and beam b_b widths, the column depth h_c and the concrete strength f_c (i.e. ACI 352-02, 2002, FEMA 273, 1997 and AIJ 1999). Only recent European and Italian codes [EN

1998, 2005 and NTC (2008)] account the amount of stirrups into the panel zone and the axial load N_c at the bottom of the top column as key parameters for evaluating the shear strength of beam-to-column joints.

Capacity models available in the scientific literature generally depend on a set of parameter wider than the one take into account by the code formulations. However, in adjoin to the parameters taken into account by the code formulation, such as b_c, b_b, h_c, f_c and A_{sjh}, the following geometric and mechanical quantities are of concern in the models outlined in the previous sections:

- the joint aspect ratio h_b / h_c;
- the amount of longitudinal reinforcement in beam $A_{sb,sup}$ and $A_{sb,inf}$;
- the amount of longitudinal reinforcement in column A_{sc};

Almost the analysed models take into account the parameters listed above as dimensional quantities, while some of them [i.e. the models by Pantazopoulo & Bonacci (1992) and by Kim et al. (2009)] consider no-dimensional quantities for accounting the key parameters.

CHAPTER III

3. Parametric Comparison of the Capacity Models

The capacity models reported in section 2 take into account a wide set of parameters. In all models available in both the scientific literature and the code formulations, the shear strength V_{jh} is supposed to be directly depending on the geometric dimensions of the joint such as the column b_c and the beam b_b width. Other properties, such as the amount of reinforcement in the beam and/or column are generally taken in account by only some models, while are not considered in other ones.

In this section a comprehensive study of those capacity models about the geometric and mechanical parameters influencing the prediction of shear strength in both exterior and interior joints is presented. In particular, two experimental subassemblies (one for exterior joints and another one for interior) have been considered as a reference and the following parameters will be examined:

- column and beam widths, b_c and b_b respectively;
- joint aspect ratio h_b / h_c;
- amount of joint stirrups A_{sjh};
- amount of longitudinal reinforcement in beam $A_{sb,sup} + A_{sb,inf}$;
- amount of longitudinal reinforcement in column A_{sc};
- axial load N_c at the bottom of the top column;
- concrete strength f_c.

In particular, the influence of the amount of stirrups into the panel zone A_{sjh} is investigated through the Horizontal Reinforcement Index HRI defined as follows:

$$HRI = \frac{A_{sjh} \cdot f_{yj}}{b_c \cdot (h_b - 2 \cdot d') \cdot f_c}, \tag{3.1}$$

being d' the thickness of the cover concrete.

The relationship between the theoretical shear strength evaluated through the capacity models mentioned in the previous section and the amount of longitudinal reinforcement in beam $A_{sb,sup} + A_{sb,inf}$ is studied by defining the no-dimensional Beam Reinforcement Index BRI evaluated as follows:

$$BRI = \frac{\left(A_{sb,\sup} + A_{sb,\inf}\right) \cdot f_{yb}}{b_c \cdot \left(h_b - 2 \cdot d'\right) \cdot f_c}. \tag{3.2}$$

The Column Reinforcement Index CRI defined as the mechanical ratio between the total longitudinal reinforcement in the column A_{sc} and the cross section of the column is used for accounting the influence of the amount of column reinforcement on the various capacity models:

$$CRI = \frac{A_{sc} \cdot f_{yc}}{b_c \cdot h_c \cdot f_c}. \tag{3.3}$$

Finally, the dependence of the shear strength of exterior beam-to-column joints from the column axial load N_c through the no-dimensional axial load ν evaluated in the following:

$$\nu = \frac{N_c}{b_c \cdot h_c \cdot f_c}. \tag{3.4}$$

The following sections investigate the influence of the above parameters on the prediction of shear strength through the models outlined in section 2.

3.1 Sensitivity Analysis of the Capacity Models for Exterior Joints

The specimen tested by Ehsani et al. (1987) has been considered as starting point for providing the sensitivity analysis on the models for exterior beam-to-column reinforced concrete joints.

Table 3.1: Original specimen provided by Ehsani et al. (1987).

Specimen	L_c	L_b	$b_c = h_c$	d_{1c}	d_{2c}	A_{s1c}	A_{s2c}	N_{col}
	mm	mm	mm	mm	mm	mm^2	mm^2	kN
	1727	1725	300	249	150	1400	774	325
4	h_b	b_b	d_{1b}	d_{2b}	A_{s1b}	A_{s2b}	f_c	f_y
	mm	mm	mm	mm	mm^2	mm^2	MPa	MPa
	439	259	391	340	1161	397	67.2	428

Table 3.1 reports the relevant geometric and mechanical properties of the original specimen, while Fig. 3.1 shows the original sketch taken from the original work by Ehsani et al. (1987).

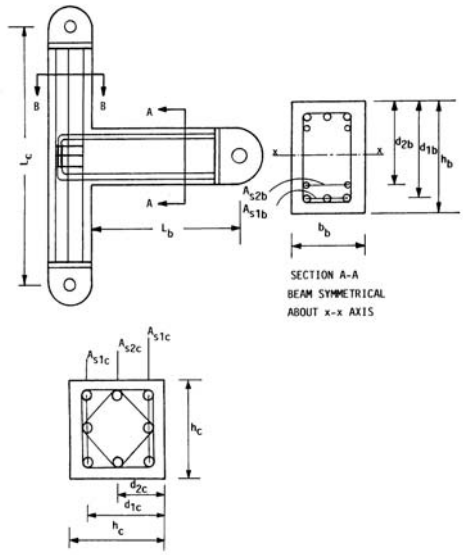

Designation	Specimen number				
	1	2	3	4	5
L_c, in.	136.0	136.0	136.0	136.0	84.0
L_b, in.	62.0	62.0	62.0	62.0	60.0
h_c, in.	13.4	13.4	11.8	11.8	11.8
d_{1c}, in.	11.4	11.4	9.8	9.8	9.6
d_{2c}, in.	6.7	6.7	5.9	5.9	5.9
A_{s1c}	2 No. 7 + 1 No. 6	2 No. 7 + 1 No. 6	2 No. 7 + 1 No. 6	2 No. 8 + 1 No. 7	4 No. 6
A_{s2c}	2 No. 6	2 No. 6	2 No. 6	2 No. 7	2 No. 6
h_b, in.	18.9	18.9	17.3	17.3	17.3
b_b, in.	11.8	11.8	10.2	10.2	10.2
d_{1b}, in.	16.9	16.9	15.4	15.4	15.4
d_{2b}, in.	15.0	15.0	13.4	13.4	13.4
A_{s1b}	2 No. 6 + 1 No. 5	3 No. 6	3 No. 6	3 No. 7	3 No. 7
A_{s2b}	2 No. 5	2 No. 6	2 No. 5	2 No. 5	3 No. 6

Note: 1 in. = 25.4 mm.

Fig. 3.1: Sketch of the original specimen provided by Ehsani et al. (1987).

3.1.1 Column width b_c

Values of the column width b_c ranging from 100 mm to 1000 mm have been considered for assessing the sensitivity of the analysed capacity models.

In Fig. 3.2 the sensitivity of the capacity models about the column width is analysed by reporting on the x-axis the column width b_c and on the y-axis the shear strength V_{jh} evaluated through the various capacity models. Both the code provisions and the models available in the scientific literature are rather sensitive to the column width b_c . In particular, a high sensitivity about the column width b_c is shown for the ACI 352-85 (1985) formulation and for the models by Ortiz (1993), Pantazopoulo & Bonacci (1992), Zhang & Jirsa (1982), and Tsonos (2007). The models by Ortiz (1993), Scott et al. (1994), Tsonos (2007) and Russo & Somma (2006) provide a linear increasing relationship between the column width b_c and the shear strength V_{jh}, while other models, such as the one by Zhang & Jirsa (1982) and by Vollum & Parker (2008), develop a non-linear relationship or a bilinear one in which after a first linear

increasing branch the prediction keeps constant. Particular cases are the ones of the FEMA 273 (1997) and the Italian NTC (2008) for existing joints and OPCM 3431/05 (2005) formulations; in the first model the law relating the shear strength V_{jh} to the column beam b_c is increasing in the first branch, constant in the second one and has a sharp jump corresponding to $b_c = 800\ mm$ and then remains constant. Instead, the model provided by the Italian NTC (2008) for existing joints and OPCM 3431/05 (2005) shows a nearly constant relationship between the geometric dimension of the column b_c and the joint shear strength V_{jh}.

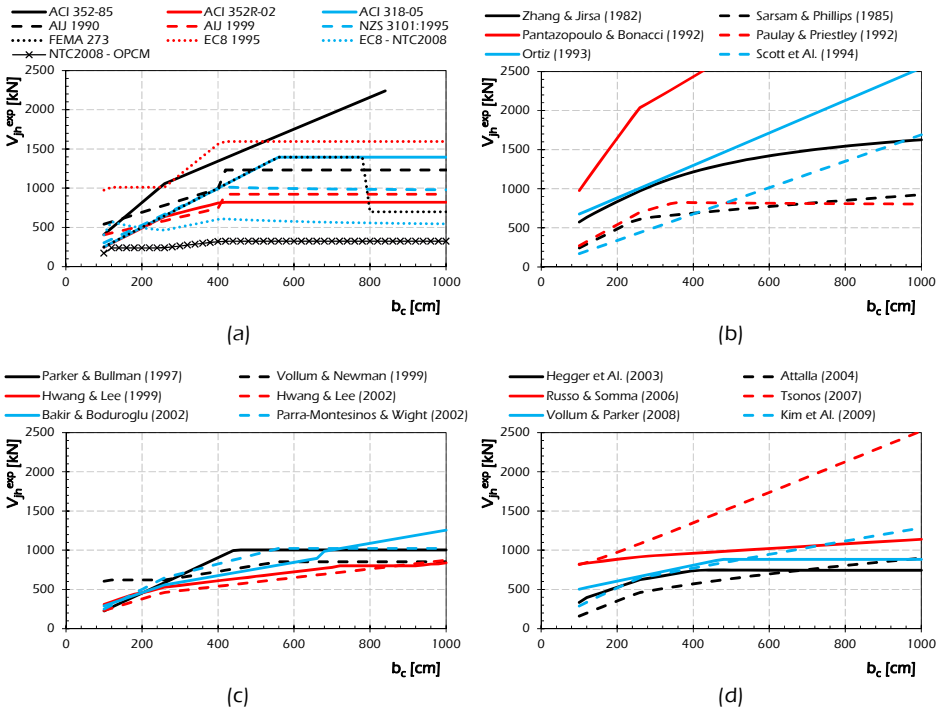

Fig. 3.2: Models for exterior joints: sensitivity to the column width b_c.

3.1.2 Beam width b_b

Fig. 3.3 shows the influence of values of the beam width b_b ranging from the value of 99 mm to the one of 999 mm (around the original value of 259 mm).

The two models by Tsonos (2007) and by Vollum & Parker (2008) and the Japanese code formulations (AIJ 1990 and AIJ 1999) result a linear increasing

relationship between the beam width b_b and the shear strength V_{jh} . on the contrary the shear strength provided by the model by Pantazopoulo & Bonacci (1992) results in a decreasing law with the beam width; in particular this model develops high value of shear strength V_{jh} associated to small values of the beam width b_b decreasing when the analysed geometric dimension increases.

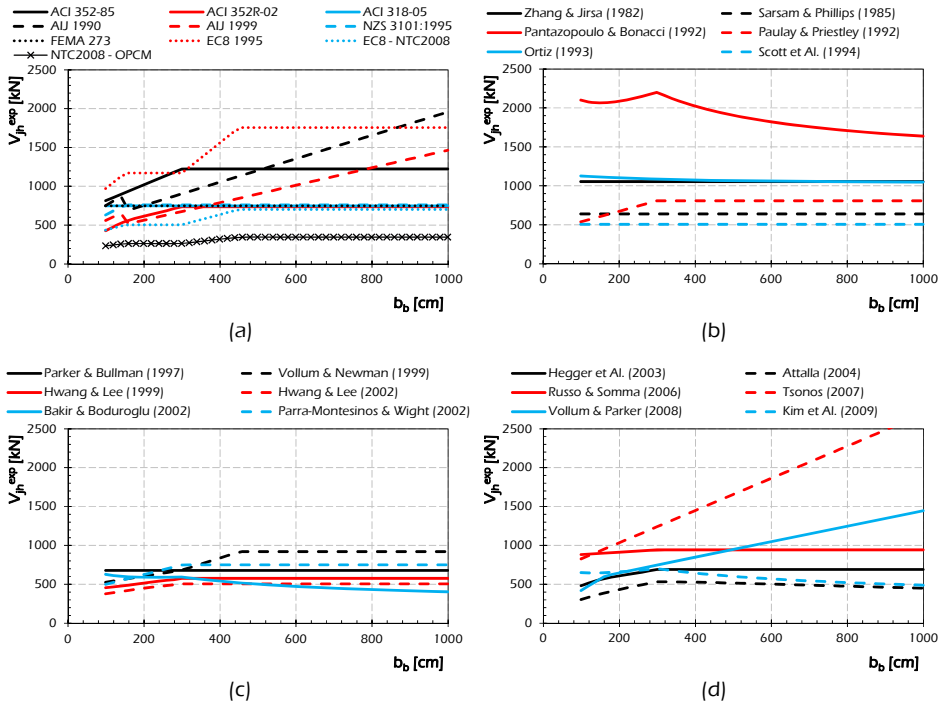

Fig. 3.3: Models for exterior joints: sensitivity to the beam width b_b .

Other models result in constant or bilinear, yet low sensitive, relationship with respect to the beam width b_b.

3.1.3 Aspect ratio (h_b/h_c)

A very important parameter influencing the prediction of the shear strength V_{jh} is the joint aspect-ratio h_b/h_c. With the aim of investigating how the various models depend on this parameter, the beam depth h_b of the original specimen has been varied while the column depth h_c has been considered fixed. Thus, a range from 0.5 to 3.0 has been considered for the aspect ratio (Fig. 3.4).

Generally, the code formulations are not influenced by the joint aspect ratio h_b/h_c as the joint shear strength V_{jh} in constant law with the analysed parameter [Fig. 3.4(a)]. The same trend is observed for the models by Paulay & Priestley (1992), by Parker & Bullman (1997), Parra-Montesinos & Wight (2002) and Russo & Somma (2006) which provide a horizontal line in the chart in Fig. 3.4 (b), (c) and (d).

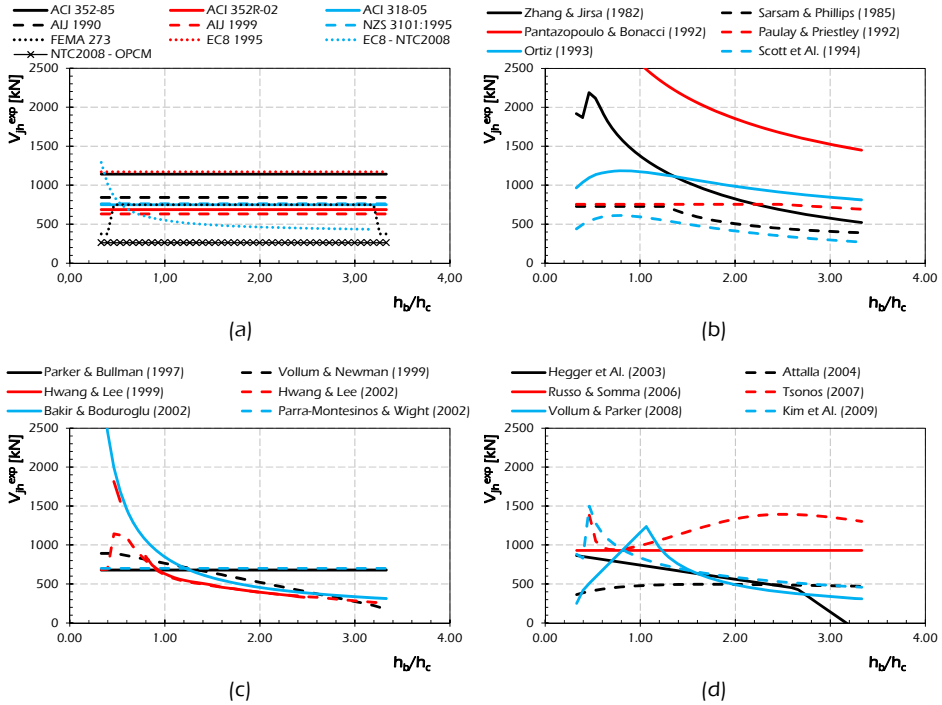

Fig. 3.4: Models for exterior joints: sensitivity to the joint aspect ratio h_b / h_c.

Other models develop a non-linear relationship between the evaluated shear strength V_{jh} and the joint aspect ratio h_b / h_c generally resulting in decreasing laws.

3.1.4 Horizontal Reinforcement Index

The influence of the amount of stirrups A_{sjh} in the panel zone of exterior beam-to-column joints is analysed through a parametric study of the shear strength V_{jh} provided by the capacity models outlined in section 2. The amount

of horizontal reinforcement has been taken in account by using the Horizontal Reinforcement Index *HRI* as defined in Eq. (3.1).

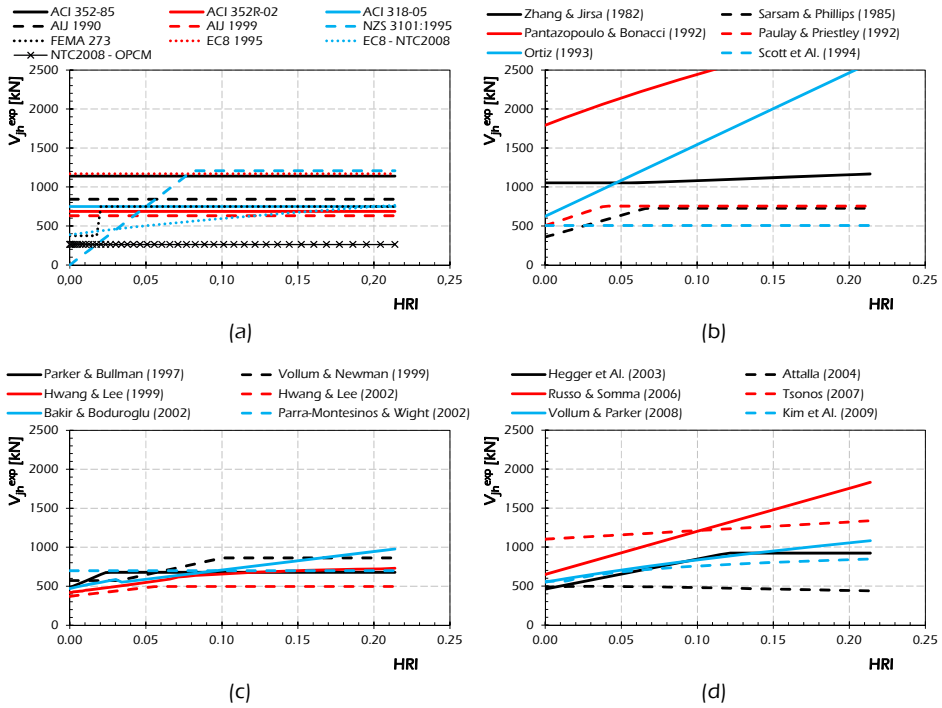

Fig. 3.5: Models for exterior joints: sensitivity to the Horizontal Reinforcement Index *HRI*.

Fig. 3.5 shows the relationship between the shear strength V_{jh} (on the y-axis) and the *HRI* (on the x-axis) for the various capacity models.

As far as the code formulations, a generally constant trend of the shear strength V_{jh} in respect of the amount of stirrups A_{sjh} is observed demonstrating that the code formulations do not take in account the amount of stirrups providing the shear strength in function of the failure of the concrete strut. Predictions based on the provisions of NZS 3101 (1995) and Eurocode 8 (EN 1998-3, 2005) – NTC (2008) present an exception to that general rule. The first model develops a linear increasing relationship between the shear strength V_{jh} and the *HRI* for small values of the horizontal reinforcement and then a constant plateau is achieved, while the second ones [Eurocode 8 (EN 1998-3, 2005) and NTC (2008)] provide an increasing (less than linear) law of the strength in respect of the amount of stirrups.

The capacity models available in the scientific literature, generally, account for the influence of the amount of horizontal reinforcement on the shear strength V_{jh} of exterior beam-to-column reinforced concrete joints, which result in growing relationship between the shear strength V_{jh} and the Horizontal Reinforcement Index *HRI* (Fig. 3.5). The models by Pantazopoulo & Bonacci (1992), Ortiz (1993), Zhang & Jirsa (1982), Bakir & Boduroglu (2002), Russo & Somma (2006) and Vollum & Parker (2008) show an increasing law of the shear strength V_{jh} with the increasing of the *HRI*, while the models by Paulay & Priestley (1992), Sarsam & Phillips (1985), Parker & Bullman (1997), Vollum & Newman (1999), Hwang & Lee (1999 and 2002), Hegger et al. (2003) and Kim et al. (2009) result influenced by the *HRI* for law amount of horizontal stirrups, while are not sensitive to the amount of stirrups A_{sjh} in the panel zone for high values of *HRI*.

Other models (i.e. the one by Scott et al., 1994) are not influenced by the amount of stirrups resulting in constant relationship between V_{jh} and *HRI* (Fig. 3.5) because in their formulation the amount of reinforcement into the panel zone is not taken into account.

3.1.5 Beam Reinforcement Index

Fig. 3.6 shows the relationship between the shear strength V_{jh}, evaluated through the capacity models under consideration, and the amount of longitudinal reinforcement $A_{sb,inf} + A_{sb,sup}$, in the beam taken in account through the Beam Reinforcement Index *BRI* [Eq. (3.2)].

Generally, both code formulations and capacity models available in the scientific literature are not sensitive to the variation of the amount of longitudinal reinforcement in the beam.

Exceptions are represented by the models by Pantazopoulo & Bonacci (1992), Paulay & Priestley (1992), Bakir & Boduroglu (2002), Russo & Somma (2006) and Kim et al. (2009) which result in higher values of shear strength for higher BRI values.

A different behaviour is shown by the model taken in account by the NZS 3101 (1995) in which the shear strength V_{jh} is not influenced by small values of the Beam Reinforcement Index *BRI*, while it decreases by increasing the amount of longitudinal reinforcement in beam when the value of $BRI = 0.12$ is overlapped.

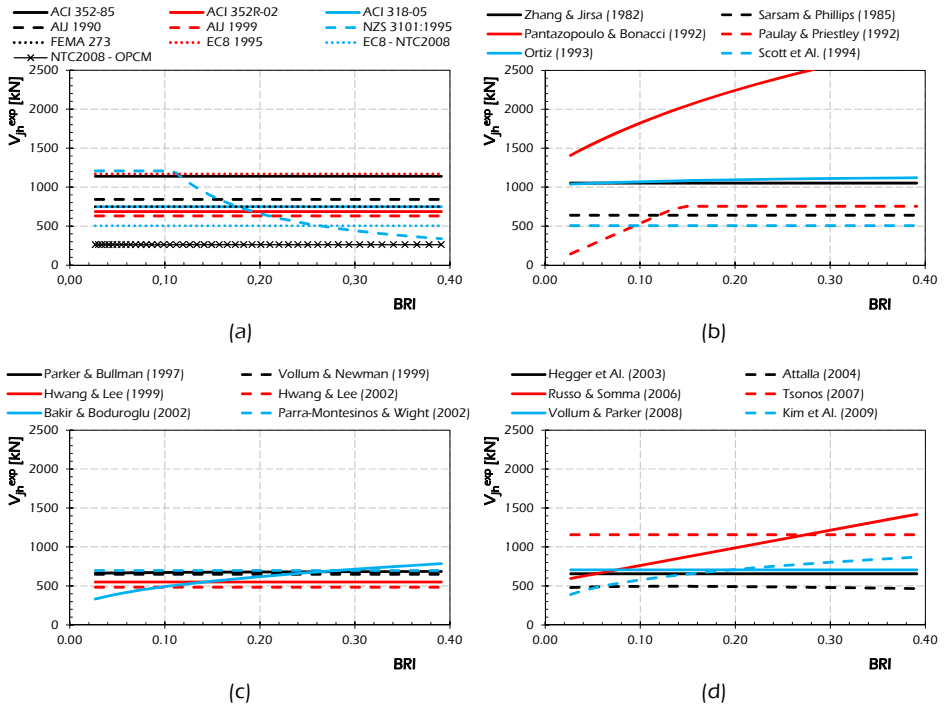

Fig. 3.6: Models for exterior joints: sensitivity to the Beam Reinforcement Index *BRI*.

3.1.6 Column Reinforcement Index

Fig. 3.7 deals with the sensitivity of the capacity models for the amount of longitudinal reinforcement in the column A_{sc}. In particular, the amount of reinforcement in the column has been taken into account by the Column Reinforcement Index *CRI* as defined by Eq. (3.3).

Fig. 3.7 (a) shows that the code formulations do not take in account the amount of longitudinal reinforcement in the column for evaluating the shear strength V_{jh} of exterior beam-to-column reinforced concrete joints resulting in constant law in respect to the variation of the *CRI*.

About the capacity models available in the scientific literature, only five models are influenced by the amount of reinforcement in column. They are the ones by Zhang & Jirsa (1982), Sarsam & Phillips (1985), Parker & Bullman (1997), Russo & Somma (2006) and Attaalla (2004). In particular, the first three models are sensitive to low amount of reinforcement in column resulting in increasing law, while they provide small variations of shear strength V_{jh} for high values of

CRI. The model by Russo & Somma (2006), instead, results in constant values of V_{jh} for values of *CRI* smaller than 0.15 and an increasing relationship between V_{jh} and *CRI* for high values.

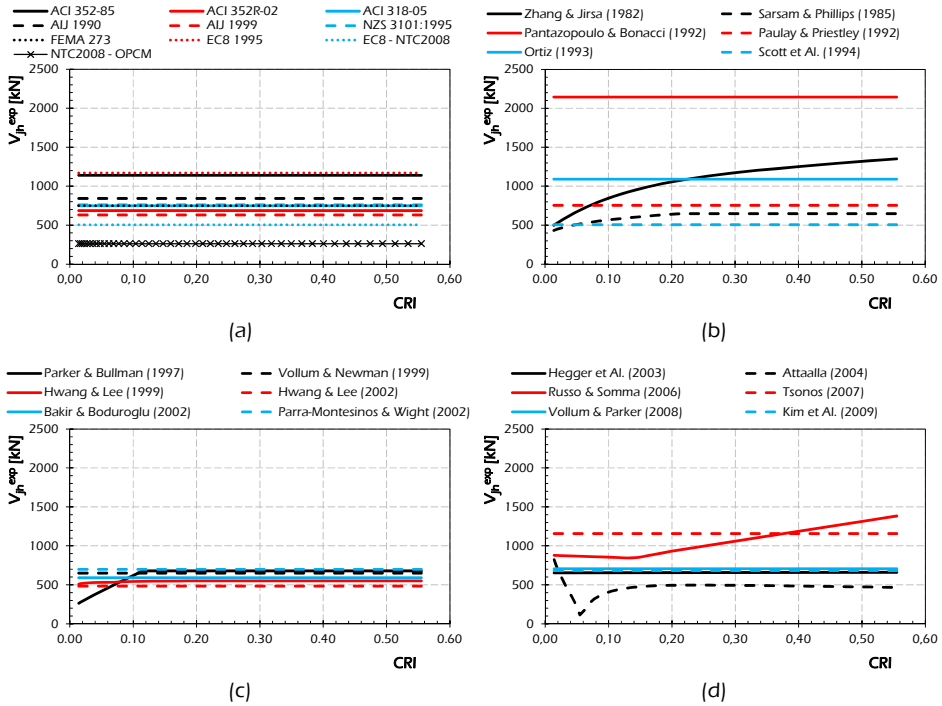

Fig. 3.7: Models for exterior joints: sensitivity to the Column Reinforcement Index *CRI*.

Finally, the model by Attaalla (2004) develops a particular relationship between the shear strength V_{jh} and the Column Reinforcement Index *CRI* for low amount of reinforcement and then becomes constant [Fig. 3.7 (d)].

3.1.7 Axial Load N_c

Fig. 3.8 shows the parametric analysis of the capacity models for evaluating the shear strength V_{jh} of exterior beam-to-column joints about the axial load N_c at the bottom of the top column of the joint. In particular, the study of the shear strength V_{jh} in respect of the variation of the axial load N_c at the bottom of the top column is provided by taking into account the non-dimensional axial stress ν defined in Eq. (3.4).

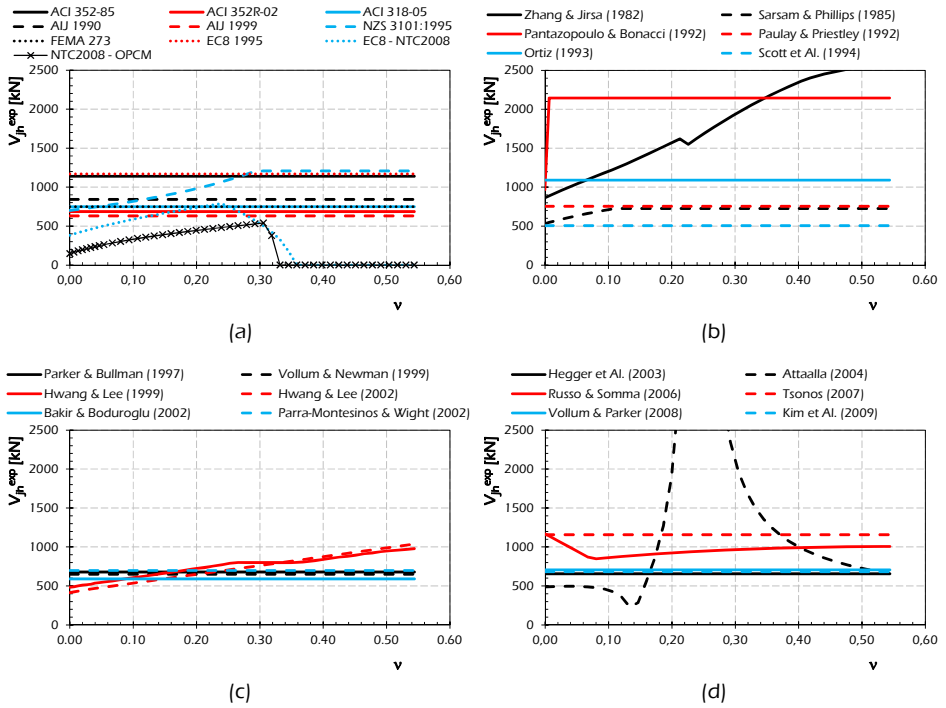

Fig. 3.8: Models for exterior joints: sensitivity to the non-dimensional axial stress ν in the top column.

The influence of the axial load N_c in the top column is taken into account in three code formulations and six theoretical models, while the other analysed models are insensitive to non-dimensional axial stress ν. In particular, the models proposed in the NZS 3101 (1995), the Eurocode 8 (EN 1998-3, 2005) and the NTC (2008), and the OPCM 3431/05 (2005) for existing structures develop an increasing relationship between V_{jh} and ν for small value of the axial stress. After a certain value of ν the shear strength V_{jh} evaluated by the European (EN 1998-3, 2005) and Italian (NTC, 2008 and OPCM 3431/05, 2005) codes decreases rapidly and becomes equal to zero, while the value V_{jh} becomes constant if evaluated by the NZS 3101 (1995) formulation.

The other analysed capacity models are generally slightly affected by the variation of the axial stress in the top column as the shear strength V_{jh} in constant or low sensitive law with the non-dimensional axial stress ν. Two exceptions are represented by the models by Zhang & Jirsa (1982) and by Attaalla (2004). The former develops an increasing relationship between the shear strength V_{jh} and the non-dimensional axial stress ν in the top column,

while the latter provides a complex relationship characterized by a high maximum value.

3.1.8 Concrete Strength f_c

Fig. 3.9 shows the sensitivity of the capacity models outlined in section 2 in respect of the concrete strength f_c.

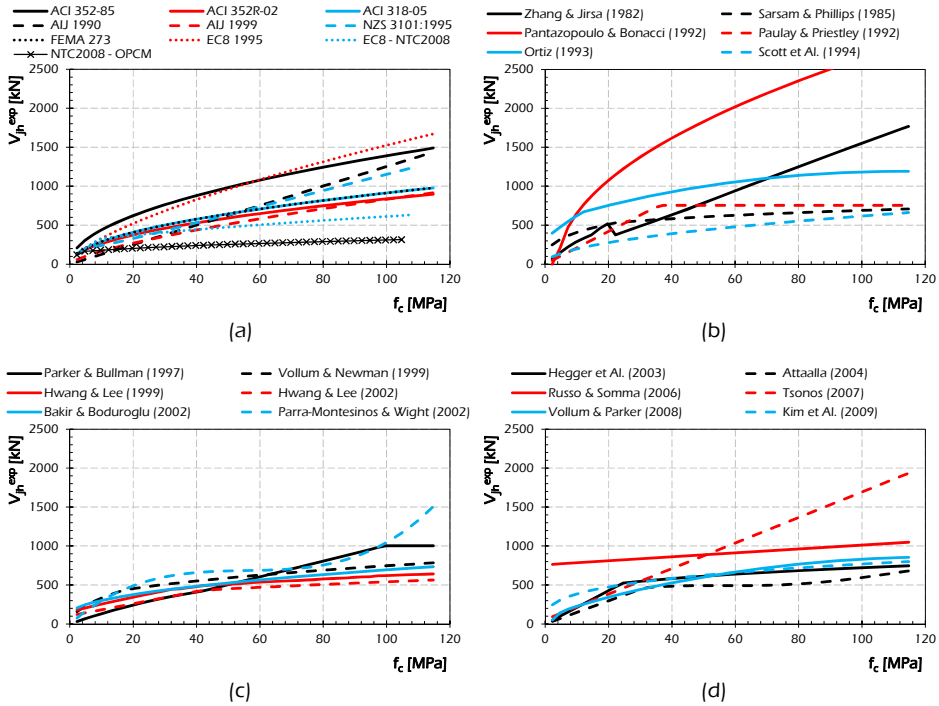

Fig. 3.9: Models for exterior joints: sensitivity to the concrete strength f_c.

The considered models are rather sensitive to the variation of concrete strength resulting in increasing relationship between V_{jh} and f_c. The most sensitive models are the ones by Pantazopoulo & Bonacci (1992), by Zhang & Jirsa (1982) and by Tsonos (2007).

3.2 Sensitivity Analysis of the Models for Interior Joints

The specimen provided by Kitayama et al. (1991) has been taken into account for developing the parametric study of the capacity models outlined in section 2 about interior beam-to-column reinforced concrete joints. In particular, the specimen denoted by the Authors as B1 has been considered.

Table 3.2: Original specimen provided by Kitayama et al. (1991).

Specimen	L_c	L_b	b_c	h_c	d'_c	A_{s1c}	A_{s2c}	N_{col}
	mm	mm	mm	mm	mm	mm^2	mm^2	kN
	1470	1350	300	300	30	664	664	180
B2	h_b	b_b	d'_b	A_{sjh}	$A_{sb,sup}$	$A_{sb,inf}$	f_c	f_y
	mm	mm	mm	mm^2	mm^2	mm^2	MPa	MPa
	300	200	30	226	1061	1061	25	498

Table 3.2 reports the geometric and mechanical properties of the original specimen taken in account, while Fig. 3.10 shows the original sketch taken from the original work of Kitayama et al. (1991).

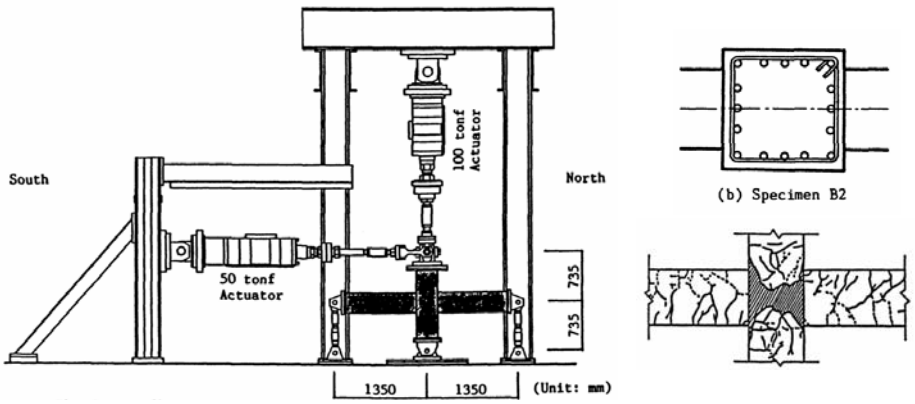

Fig. 3.10: Sketch of the original specimen provided by Kitayama et al. (1991).

Some of the sensitivity analysis of interior joints is provided in the following subsections by varying the geometric and mechanical properties around the values of the original specimen outlined above.

3.2.1 Column width b_c

The column width b_c of the interior beam-to-column subassemblies tested by Kitayama et al. (1991) has been ranged between 100 mm and 1000 mm with the aim of investigating the sensitivity of the analysed capacity models.

The graphs shown in Fig. 3.11 outline the results of this parametric analysis by reporting the shear strength V_{jh} evaluated by the capacity models on the y-axis and the column width b_c on the x-axis.

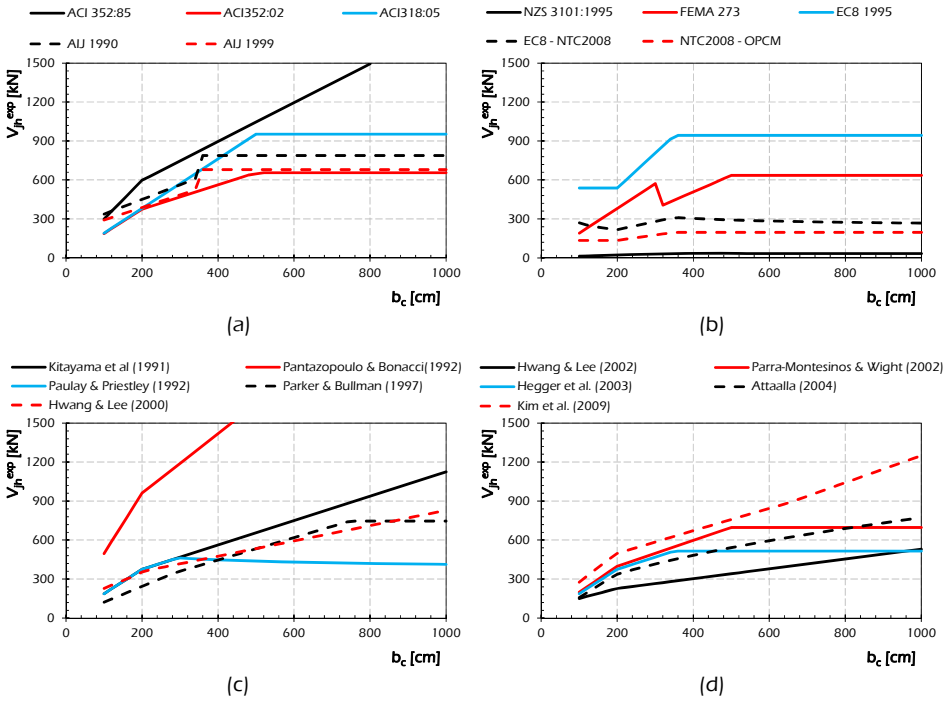

Fig. 3.11: Models for interior joints: sensitivity to the column width b_c.

The evidence shown a generalised increasing relationship between the shear strength V_{jh} and the column width b_c. Only three code formulations are low sensitive to the variation of the column width b_c: the NZS 3101 (1995), the Eurocode 8 (EN 1998-3, 2005) and NTC (2008), and the Italian codes (NTC, 2008 and OPCM 3431/05, 2005) for existing structures. The models by AIJ 1990 (1990) and AIJ 1999 (1999) have the same trend resulting the last one in conservative law. The same consideration can be made for the models adopted by NTC (2008) for new and existing structures, respectively.

Finally, some models (i.e. Parra-Montesinos & Wight, 2002 and Paulay & Priestley, 1992) develop an increasing relationship between the shear strength V_{jh} and the column width b_c for small values of the width of the column, while the law becomes constant for high values of b_c.

3.2.2 Beam width b_b

The parametric analysis of the models in respect of the beam width b_b is shown in Fig. 3.12. by ranging the beam width b_b from the value of 100 mm to the one of 1000 mm around the original value of 300 mm.

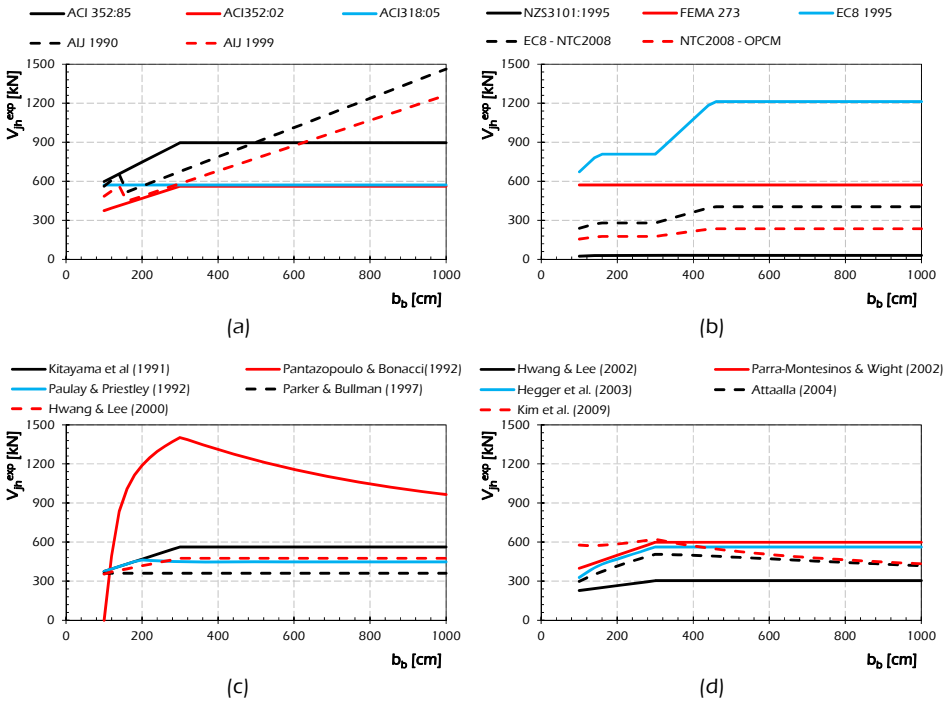

Fig. 3.12: Models for interior joints: sensitivity to the beam width b_b.

The models by the Japanese (AIJ 1990 and AIJ 1999), European (EN 1995-1, 1995, EN 1998-3, 2005) and Italian (NTC, 2008 and OPCM 3431/05, 2005) code formulations provide an increasing relationship between the beam width b_b and the shear strength V_{jh} of exterior joints. The prediction of the model by Pantazopoulo & Bonacci (1992) is not monotone with respect to b_b . In particular, this model develops increasing value of shear strength V_{jh} for small

values of the beam width b_b (smaller than 1.5 times the column width b_c) while turns to a decreasing trend as the width increases beyond that value.

Other models result in constant or in bilinear, yet low sensitive, relationships with the beam width b_b.

3.2.3 Aspect ratio (h_b/h_c)

The joint aspect ratio h_b / h_c has been considered by the models available in the scientific literature as a relevant parameter affecting the shear strength of both exterior and interior joints.

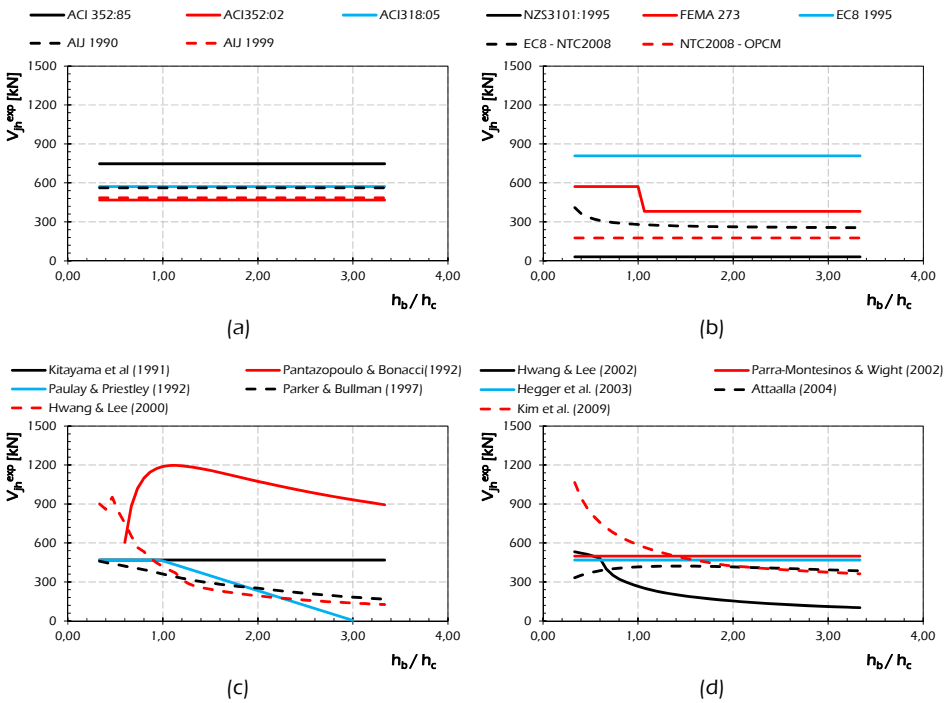

Fig. 3.13: Models for interior joints: sensitivity to the joint aspect ratio h_b / h_c.

In the following, the influence of the joint aspect ratio h_b / h_c on the shear strength V_{jh} evaluated through the analysed capacity models for interior joints is investigated. The study has been made by fixing the column depth h_c and ranging the beam depth between 100 mm and 1000 mm around the original value of the specimen provided by Kitayama et al. (1991) equal to 300 mm.

The predictions of shear strength based on the code formulations are not sensitive to the variation of the joint aspect ratio h_b / h_c. Only the formulations suggest by the FEMA 273 (1997), FEMA 356 (2000) and by the Eurocode 8 (EN 1998-3, 2005) – NTC (2008) are influenced by values of the joint aspect ratio. In particular, the first model (FEMA 273, 1997 and FEMA 356, 2000) develops for small values of h_b / h_c a value of V_{jh} greater than the one provided for high values of the aspect ratio resulting in a sharp gap around the value $h_b / h_c = 1$ corresponding to the beam depth h_b equal to the column depth h_c (Fig. 3.13).

The capacity models available in the scientific literature are generally more sensitive to the joint aspect ratio h_b / h_c than the ones accounted for the codes under consideration. The relationship shown in Fig. 3.13 outlines a decreasing rule of the prediction of shear strength V_{jh} corresponding to the increasing of the joint aspect ratio (i.e. the models by Hwang & Lee, 2000 and 2002, by Kim et al., 2009, by Parker & Bullman, 1997 and by Paulay & Priestley, 1992). On the contrary, the models by Kitayama et al. (1991), by Parra-Montesinos & Wight (2002), by Hegger et al. (2003) and by Attaalla (2004) are not sensitive to the variation of the joint aspect ratio h_b / h_c.

Finally, as already observed about the sensitivity in respect of the beam width b_b, the model by Pantazopoulo & Bonacci (1992) provides an initial increasing relationship between V_{jh} and h_b / h_c and then a decreasing law starting from the point corresponding to the beam depth h_b equal to the column one h_c.

3.2.4 Horizontal Reinforcement Index

The influence of the amount of stirrups A_{sjh} in the panel zone of interior beam-to-column joints is analysed through a parametric study of the shear strength V_{jh} provided by the capacity models outlined in section 2. The amount of horizontal reinforcement has been taken in account by using the Horizontal Reinforcement Index *HRI* as defined in Eq. (3.1).

Fig. 3.14 shows the relationship between the shear strength V_{jh} (on the y-axis) and the *HRI* (on the x-axis) for the various capacity models.

About the code formulations, a generally constant trend of the shear strength V_{jh} in respect of the amount of stirrups A_{sjh} is observed demonstrating that the code formulations do not take into account the amount of stirrups providing the shear strength in function of the failure of the concrete strut. As already observed in the case of exterior joints, the exceptions are represented by the formulations provided by NZS 3101 (1995) and Eurocode 8 (EN 1998-3, 2005) – NTC (2008). The first model develops a linear increasing relationship

between the shear strength V_{jh} and the *HRI* for small value of the horizontal reinforcement and then a constant relationship for high value, while the second one [Eurocode 8 (EN 1995-3, 2005) and NTC (2008)] provide an increasing law less than linear of the strength in respect of the amount of stirrups.

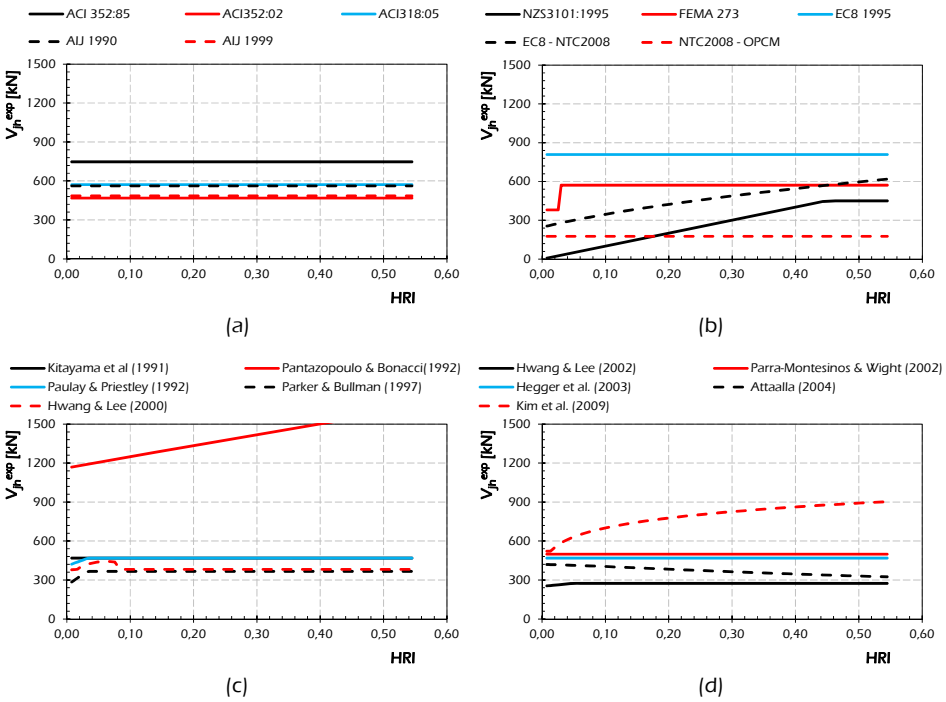

Fig. 3.14: Models for interior joints: sensitivity to the Horizontal Reinforcement Index *HRI*.

Regarding interior joints (Fig. 3.14), the models available in the scientific literature result less sensitive than the models for exterior joints (Fig. 3.5) with respect to the amount of horizontal stirrups in the panel zone. The models by Pantazopoulo & Bonacci (1992) and Kim et al. (2009) lead to higher prediction corresponding to higher values of the *HRI*, while the models by Paulay & Priestley (1992), Parker & Bullman (1997), and Hwang & Lee (2000 and 2002), result influenced by the *HRI* for law amount of horizontal stirrups, while are not sensitive to the amount of stirrups A_{sjh} in the panel zone for high values of *HRI*.

Other models (i.e. the one by Hegger et al., 2003) provide values of the shear strength substantially insensitive to the amount of stirrups resulting in constant relationships between V_{jh} and *HRI* (Fig. 3.14).

3.2.5 Beam Reinforcement Index

The relationship between the shear strength V_{jh}, evaluated through the analysed capacity models, and the amount of longitudinal reinforcement in the beam $A_{sb,inf} + A_{sb,sup}$, taken in account through the Beam Reinforcement Index *BRI* [Eq. (3.2)], is shown in the following.

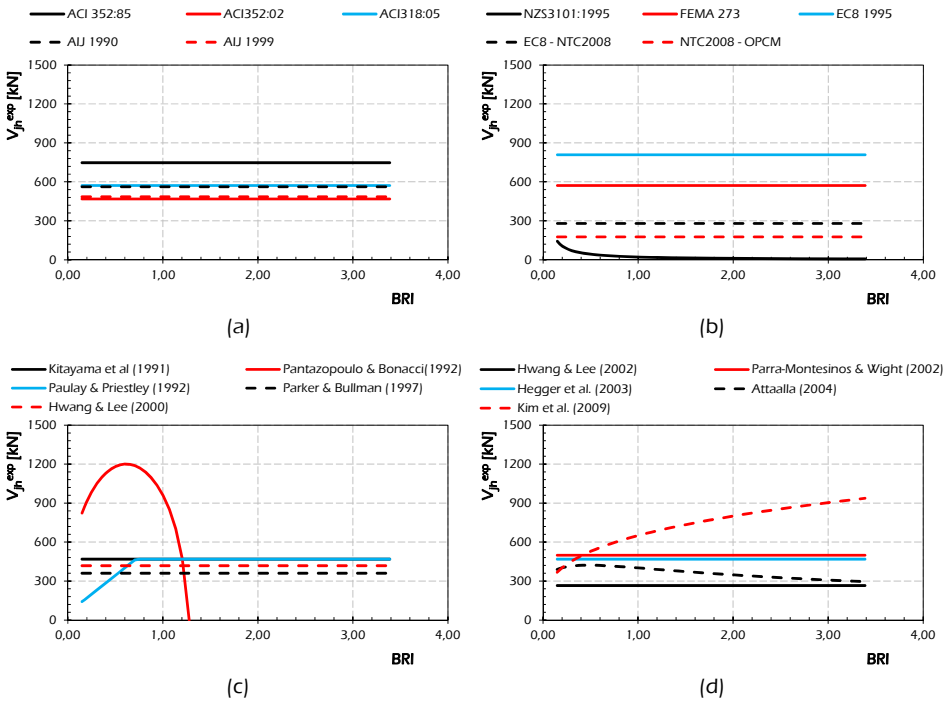

Fig. 3.15: Models for interior joints: sensitivity to the Beam Reinforcement Index *BRI*.

Generally, both the code formulations and the capacity models collected from the scientific literature are not sensitive to the variation of the amount of longitudinal reinforcement in the beam. Exceptions are represented by the models by Pantazopoulo & Bonacci (1992), Paulay & Priestley (1992), and Kim et al. (2009) that account the increment of the shear strength V_{jh} related to the increasing of amount of reinforcement in beam *BRI*.

A different behaviour is shown by the model taken into account by the NZS 3101 (1995) and the model by Attaalla (2004) in which the shear strength V_{jh} decreases by increasing the amount of longitudinal reinforcement in beam.

3.2.6 Column Reinforcement Index

Fig. 3.16 shows the sensitivity to the amount of longitudinal reinforcement in the column A_{sc} of the capacity models. In particular, the amount of reinforcement in the column has been taken into account by the Column Reinforcement Index *CRI* as defined by Eq. (3.3).

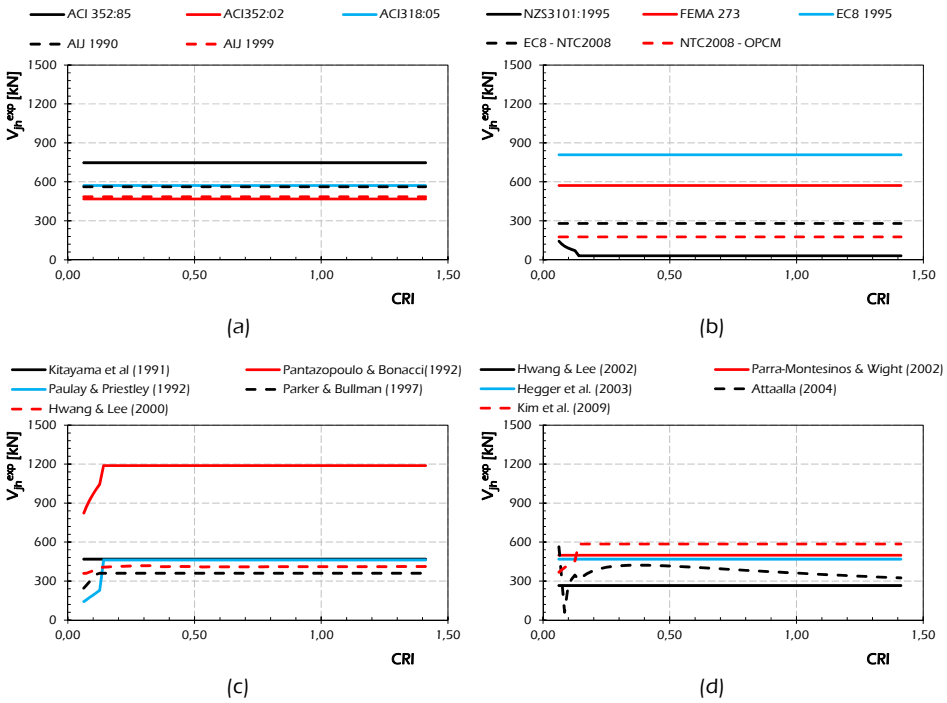

Fig. 3.16: Models for interior joints: sensitivity to the Column Reinforcement Index *CRI*.

Fig. 3.16 shows that the code formulations do not take into account the amount of longitudinal reinforcement in the column for evaluating the shear strength V_{jh} of interior beam-to-column reinforced concrete joints resulting in constant law in respect to the variation of the *CRI*.

The models of the scientific literature are influenced by the amount of reinforcement in column. In particular, for low amount of longitudinal reinforcement the prediction of the shear strength results increasing, while the models do not provide variations of shear strength V_{jh} for high values of *CRI*. Finally, the model by Attaalla (2004) develops a particular relationship between the shear strength V_{jh} and the Column Reinforcement Index *CRI* for low amount of reinforcement and then becomes constant (Fig. 3.16).

3.2.7 Axial Load N_c

Fig. 3.17 shows the parametric analysis of the capacity models for evaluating the shear strength V_{jh} of interior beam-to-column joints about the axial load N_c at the bottom of the top column of the joint.

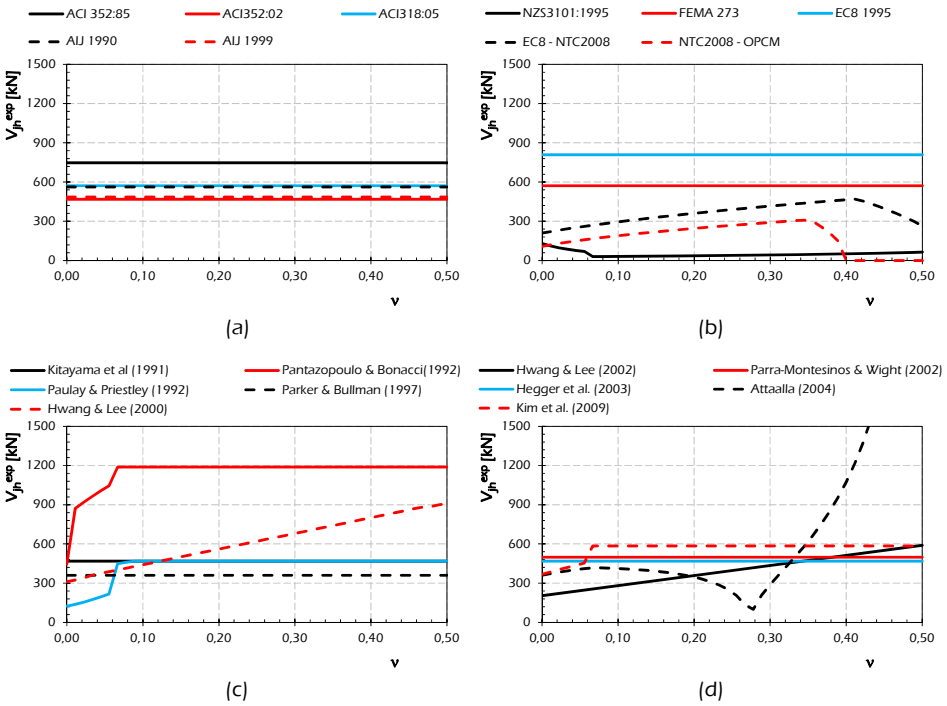

Fig. 3.17: Models for interior joints: sensitivity to the non-dimensional axial stress in the top column ν.

In particular, the study of the shear strength V_{jh} in respect of the variation of the axial load N_c at the bottom of the top column is provided taking into account the no dimensional axial stress ν defined in Eq. (3.4).

The influence of the axial load N_c in the top column is taken into account from three code formulations and six theoretical models available in the scientific literature, while the other analysed models provide a constant value of the shear strength V_{jh} in respect of the variation of the no dimensional axial stress ν. In particular the models taken into account by the Eurocode 8 (EN 1998-3, 2005) and the NTC (2008), and this last one and the OPCM 3431/05 (2005) for existing structures develop an increasing relationship between V_{jh}

and ν for small value of the axial stress. After a determinate value of ν the shear strength V_{jh} evaluated by the European (EN 1998-3, 2005) and Italian [NTC (2008) and OPCM 3431/05 (2005)] codes decreases rapidly and becomes equal to zero, while the value V_{jh} decreasing for small value of ν if evaluated by the NZS 3101 (1995) formulation and then becomes constant.

The other analysed capacity models affected by the variation of the axial stress in the top column develop increasing relationship between V_{jh} and ν. The model by Attaalla (2004) represents an exception because it provide a complex relationship characterized by a small minimum value.

3.2.8 Concrete Strength f_c

Fig. 3.18 shows the sensitivity of the capacity models outlined in section 2 in respect of the concrete strength f_c considered ranging between 2.5 MPa and 115 MPa.

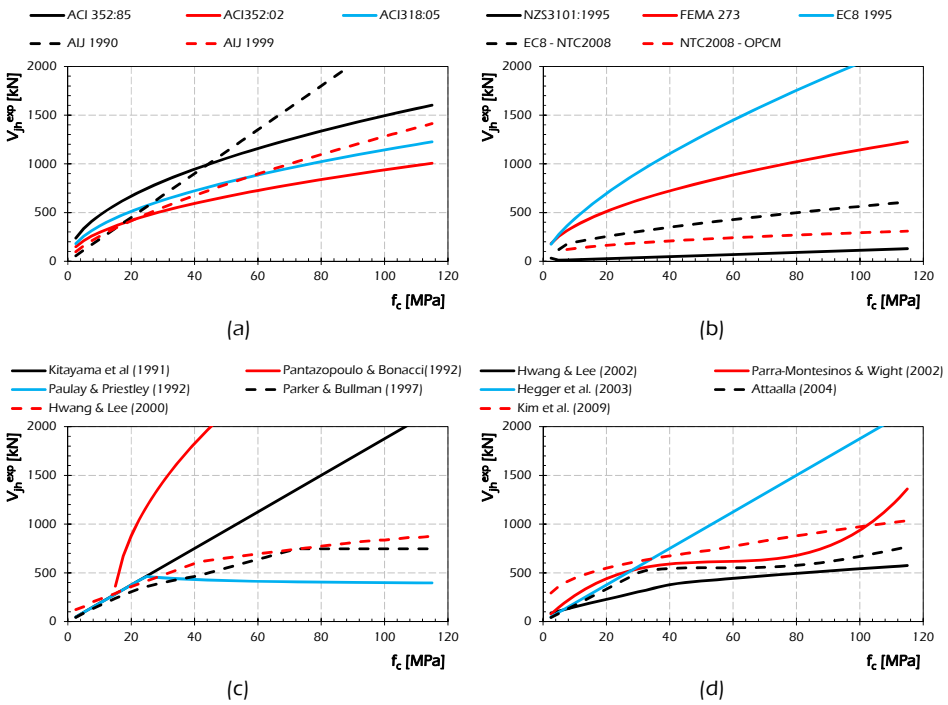

Fig. 3.18: Models for interior joints: sensitivity to the concrete strength f_c.

The considered models are sensitive to the variation of concrete strength resulting in increasing relationship between V_{jh} and f_c. The models by AIJ 1990 (1990), Kitayama et al. (1991) and Hegger et al. (2003) provide the shear strength V_{jh} in linear law with the concrete strength f_c.

CHAPTER IV

4. The Experimental Database

A wide experimental database about interior and exterior beam-to-column joints has been assembled with the aim of studying the behaviour of these structural components and assessing the accuracy of the capacity models presented in the previous sections.

The database collects results of experimental tests performed on interior and exterior subassemblages and available in the scientific literature. The specimens have been carried out in different years and countries. Thus ensures the heterogeneity of the results that makes it possible to take into account all the parameters affecting the shear strength of exterior beam-to-column joints.

The following two subsections describe the collection of data regarding exterior and interior joints, respectively.

4.1 Exterior Joints

The database collecting the specimens on exterior beam-to-column connections is composed of 224 joints. In Table 4.1 the subassemblies are listed reporting the reference, the name of the specimen, the type of loading *(monotonic M or cyclic C)*, the main notes and the type of failure.

Table 4.1: Experimental database collecting exterior beam-to-column joints.

Author	Specimen	Load Type	Notes	Failure Type
Alva, 2004	LVP1	C	-	J
Alva et al., 2007	LVP2	C	-	J
	LVP3	C	-	J
	LVP4	C	-	J
	LVP5	C	-	J

Table 4.1: Experimental database collecting exterior beam-to-column joints.

Author	Specimen	Load Type	Notes	Failure Type
Binbhu & Jaya, 2008	A1	C	one-third scaled	BJ
	A2	C	one-third scaled	B
	B1	C	one-third scaled - X-bars	B
	B2	C	one-third scaled - X-bars	B
Calvi et al., 2001	T1	C	2/3 scaled-50's & 70's	BJ
Chalioris et al., 2008	JA-0	C	-	J
	JA-s5	C	-	BJ
	JA-X12	C	X-bars	BJ
	JA-X14	C	X-bars	BJ
	JB-0	C	-	J
	JB-s1	C	-	J
	JB-X10	C	X-bars	BJ
	JB-X12	C	X-bars	BJ
	JCa-0	C	-	J
	JCa-X10	C	X-bars	BJ
	JCa-s1	C	-	BJ
	JCa-s1-X10	C	X-bars	BJ
	JCa-s2	C	-	BJ
	JCa-s2-X10	C	X-bars	BJ
	JCb-0	C	-	J
	JCb-X10	C	X-bars	BJ
	JCb-s1	C	-	J
	JCb-s1-X10	C	X-bars	BJ
	JCb-s2	C	-	J
	JCb-s2-X10	C	X-bars	BJ
Chun & Kim, 2004	JC-1	C	-	B
	JM-1	C	headed bars	B
	JC-2	C	-	J
	JM-2	C	headed bars	J
Chun et al., 2007	JC-1	C	-	B
	JM-1	C	headed bars	B
	JC-2	C	-	J
	JM-2	C	headed bars	J
	JC-No. 11-1	C	-	J
	JM-No. 11-1a	C	headed bars	BJ
	JM-No. 11-1b	C	headed bars	BJ
Chutarat & Aboutaha, 2003	A -Group 2	C	-	B
	B - Group 2	C	headed bars	B
	I -Group 1	C	-	J
	II - Group 1	C	headed bars	J
Clyde et al., 2000	#2	C	0,5 scaled, bad anchorage of longitudinal beam bars in the connection	J
	#4	C	-	J

Table 4.1: Experimental database collecting exterior beam-to-column joints.

Author	Specimen	Load Type	Notes	Failure Type
	#5	C	-	J
	#6	C	-	J
Durrani & Zerbe, 1987	J1	C	-	BJ
	J2	C	transv. beams of 1778mm tot. length	BJ
	J5	C	transv. beams+slab of 1168,4mm width	BJ
	J7	C	transv. beams+slab of 1778mm width	BJ
Ehsani & Alameddine, 1991	LL8	C	CLS high str.	-
	LH8	C	CLS high str.	-
	HL8	C	CLS high str.	-
	HH8	C	CLS high str.	-
	LL11	C	CLS high str.	BJ
	LH11	C	CLS high str.	BJ
	HL11	C	CLS high str.	BJ
	HH14	C	CLS high str.	BJ
	LL14	C	CLS high str.	BJ
	LH14	C	CLS high str.	BJ
	HH11	C	CLS high str.	-
Ehsani et al., 1987	1	C	CLS high str.	BJ
	2	C	CLS high str.	BJ
	3	C	CLS high str.	BJ
	4	C	CLS high str.	J
	5	C	-	BJ
Ehsani & Wight, 1985 (a)	1S	C	transverse beams and slab	BJ
	2S	C	transverse beams and slab	BJ
	3S	C	transverse beams and slab	BJ
	6S	C	transverse beams and slab	BJ
Ehsani & Wight, 1985 (b)	1B	C	specimens designed in the fall of 1978	BJ
	2B	C	specimens designed in the fall of 1979	BJ
	3B	C	specimens designed in the fall of 1980	BJ
	4B	C	specimens designed in the fall of 1981	BJ
	5B	C	specimens designed in the fall of 1982	BJ
	6B	C	specimens designed in the fall of 1983	BJ
Genesan et al., 2007	HPr	C	high performance concrete	B
Gencoglu & Eren,	#1	C	-	B

Table 4.1: Experimental database collecting exterior beam-to-column joints.

Author	Specimen	Load Type	Notes	Failure Type
2002	#2	C	-	J
Hamil, 2000	C6LN0	C	U-bars for the main beam steel	J
	C6LN1	C	U-bars for the main beam steel	J
	C6LN3	C	U-bars for the main beam steel	J
	C6LN5	C	U-bars for the main beam steel	J
	C6LH0	C	U-bars for the main beam steel	J
	C6LH1	C	U-bars for the main beam steel	J
	C6LH3	C	U-bars for the main beam steel	J
	C6LH5	C	U-bars for the main beam steel	B
	C4ALN0	C	the main beam steel bent down into the column (D)	J
	C4ALN1	C	the main beam steel bent down into the column (D)	J
	C4ALN3	C	the main beam steel bent down into the column (D)	J
	C4ALN5	C	the main beam steel bent down into the column (D)	J
	C4ALH0	C	the main beam steel bent down into the column (D)	J
	C4ALH1	C	the main beam steel bent down into the column (D)	B
	C4ALH3	C	the main beam steel bent down into the column (D)	B
	C4ALH5	C	the main beam steel bent down into the column (D)	B
Hakuto et al., 2000	O6	C	-	BJ
	O7	C	-	BJ
Hegger et al., 2003	RK1	M	-	B
	RK2	M	U bar column+ diagonal bar beam	B
	RK3	M	-	B
	RK4	M	-	J
	RK5	M	-	J
	RK6	M	-	J
	RK7	M	-	J
	RK8	M	-	J
Hwang et al., 2004	70-3T44	C	-	B

Table 4.1: Experimental database collecting exterior beam-to-column joints.

Author	Specimen	Load Type	Notes	Failure Type
	70-3T4	C	-	B
	70-2T5	C	-	BJ
	70-1T55	C	-	BJ
	28-3T4	C	-	BJ
	28 - 0T0	C	-	J
Hwang et al., 2005	0T0	C	-	BJ
	3T44	C	-	B
	1B8	C	-	BJ
	3T3	C	-	BJ
	2T4	C	-	BJ
	1T44	C	-	BJ
	3T4	C	-	B
	2T5	C	-	B
	1T55	C	-	B
Idayani, 2007	S1	M	-	J
	S2	M	-	J
	S3	M	-	J
Karayannis et al., 2008	A0	C	-	J
	A1	C	-	BJ
	A2	C	-	BJ
	A3	C	-	BJ
	B0	C	-	J
	B1	C	-	J
	C0	C	-	J
	C2	C	-	BJ
	C3	C	-	BJ
	C5	C	-	BJ
Karayannis & Sirkelis, 2005	AJ1sp	C	rectangular spiral shear reinforcement	B
	AJ1s	C	-	J
Karayannis & Sirkelis, 2008	A1	C	-	J
	A2	C	-	J
	B1	C	-	BJ
	B2	C	-	BJ
Kuang & Wong, 2006	BS-OL	C	Beam bars bent away from joint	J
	BS-LL	C	beam bars bent into joint	J
	BS-U	C	U-anchorage	J
	BS-L-LS	C	Beam bars bent into joint; Laps in column bars at end zone of upper column	J
Kusuhara & Shiohara, 2008	E1	C	-	J
	E2	C	-	J
	B2	C	-	J

Table 4.1: Experimental database collecting exterior beam-to-column joints.

Author	Specimen	Load Type	Notes	Failure Type
Lee & Ko, 2007	S0	C	e_b=0mm	B
	S50	C	e_b=50mm	B
	W0	C	e_b=0mm	BJ
	W75	C	e_b=75mm	BJ
	W150	C	e_b=150mm	BJ
Liu, 2006	RC - 1	C	-	J
	RC - 6	C	-	B
	NZ - 7	C	was designed by New Zealand concrete design code NZS3101:1995	B
Masi et al., 2009	T1	C	ERD: NE; Type beam: RB	B
	T2	C	ERD: Z2; Type beam: RB	B
	T3	C	ERD: Z2; Type beam: FB	B
	T4	C	ERD: Z4; Type beam: FB	B
	T5	C	ERD: Z2; Type beam: RB	BJ
	T6	C	ERD: NE; Type beam: RB	B
	T7	C	ERD: NE; Type beam: FB	B
	T8	C	ERD: Z4; Type beam: FB	B
	T9	C	ERD: Z2; Type beam: RB	BJ
	T10	C	ERD: Z2; Type beam: RB	BJ
Pampanin et al., 2002	T2	C	2/3 scaled-50's & 70's	J
Pantelides et al., 2002	1	C	$l_{anch.}$ bottom beam bar=152,4mm; upper beam bar U-bent type	J
	2	C	-	J
	3	C	$l_{anch.}$ bottom beam bar=355,6mm; upper beam bar U-bent type	J
	4	C	-	CJ
	5	C	bottom beam bar and upper beam bar U-bent type	BJ
	6	C	-	CJ
Parker & Bullman, 1997	4a	M	-	J
	4b	M	-	J
	4c	M	-	J
	4d	M	-	J
	4e	M	-	J
	4f	M	-	J
	5a	M	-	J
	5b	M	-	J
	5c	M	-	J
	5d	M	-	J

Table 4.1: Experimental database collecting exterior beam-to-column joints.

Author	Specimen	Load Type	Notes	Failure Type
	5e	M	-	J
	5f	M	-	J
Scott, 1996	C1	M	beam reinf. bent down into column	B
	C1A	M	beam reinf. bent down into column	B
	C1AL	M	beam reinf. bent down into column	J
	C2	M	beam reinf. bent up into column	J
	C3	M	beam reinf. Bent into U-bar	B
	C3L	M	beam reinf. Bent into U-bar	J
	C4	M	beam reinf. bent down into column	J
	C4A	M	beam reinf. bent down into column	J
	C4AL	M	beam reinf. bent down into column	J
	C5	M	beam reinf. bent up into column	J
	C6	M	beam reinf. Bent into U-bar	J
	C6L	M	beam reinf. Bent into U-bar	J
	C7	M	beam reinf. bent down into column	J
	C8	M	beam reinf. bent up into column	J
	C9	M	beam reinf. Bent into U-bar	J
Tsonos, 1999	M1	C	-	CJ
	M2	C	-	CJ
Tsonos, 2007	A1	C	-	BJ
	E2	C	-	BJ
	E1	C	-	J
	G1	C	-	J
Tsonos et al., 1992	S1	C	-	BJ
	X1	C	INCL. BARS	B
	S2	C	-	J
	X2	C	INCL. BARS	B
	S6	C	-	J
	X6	C	INCL. BARS	J
	S'6	C	-	J
	F2	C	-	J
Wong and Kuang, 2008	BS-L-300	C	-	J
	BS-L-450	C	-	J
	BS-L-600	C	-	J

Table 4.1: Experimental database collecting exterior beam-to-column joints.

Author	Specimen	Load Type	Notes	Failure Type
	BS-L-V2	C	-	J
	BS-L-V4	C	-	J
	BS-L-H1	C	-	J
	BS-L-H2	C	-	J
Wallace et al., 1998	BCEJ1	C	stub beam + headed bars	B
	BCEJ2	C	stub beam + headed bars	-

Further details about the experimental tests can be found in both the Appendix A1 and the original works of the authors mentioned in the table above. The specimens are tested under monotonic and cyclic loading. Fig. 4.2(a) shows the composition of the database accounting for the type of loading for exterior beam-to-column joints.

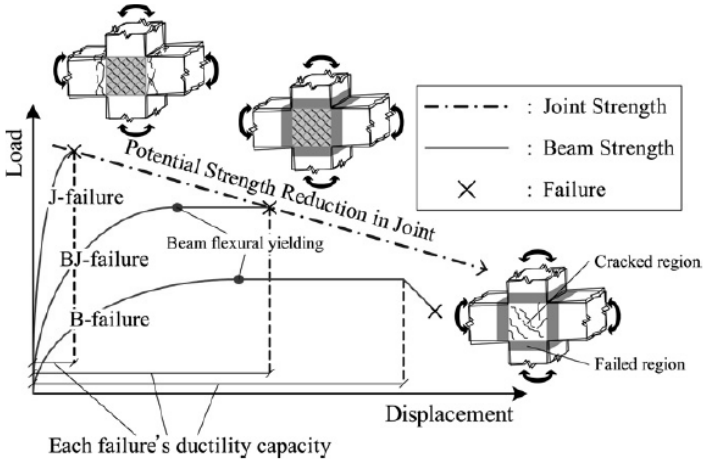

Fig. 4.1: Ductility capacity function of type of failure (Lee et al., 2009)

Another important variable in Table 4.1 is the type of failure observed from the experimental evidence [Fig. 4.1 (Lee et al., 2009)]. In fact, by analysing the original papers of the authors, the following type of failure have been observed:

- **Joint failure (J)**, in which the joint failure occurs before plastic hinges develop at the ends of adjacent beams;
- **Beam failure (B)** where the beam failure is achieved while the joint remains elastic;

- **Beam-Joint failure (BJ)**, in which the joint failure occurs after plastic hinges develop at both ends of adjacent beams;
- **Column-Joint failure (CJ)**, in which the joint failure occurs after plastic hinges develop in columns;
- **Unknown failure (U)**, as the authors do not provide any information about the type of failure observed in testing phase.

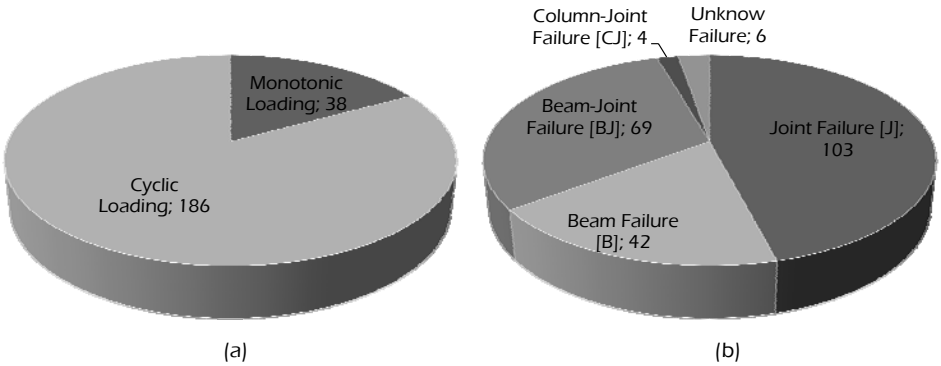

Fig. 4.2: Type of loading and failure for the database of exterior joints

Fig. 4.2(b) shows the composition of the database in respect of the type of failure resulting by the experimental evidence. It is noted that the greater number of specimens failed with plastic hinges developing at end of adjacent beam. The beam failure (B) is achieved for 42 specimens while the failure type is unknown (U) for 6 experimental tests.

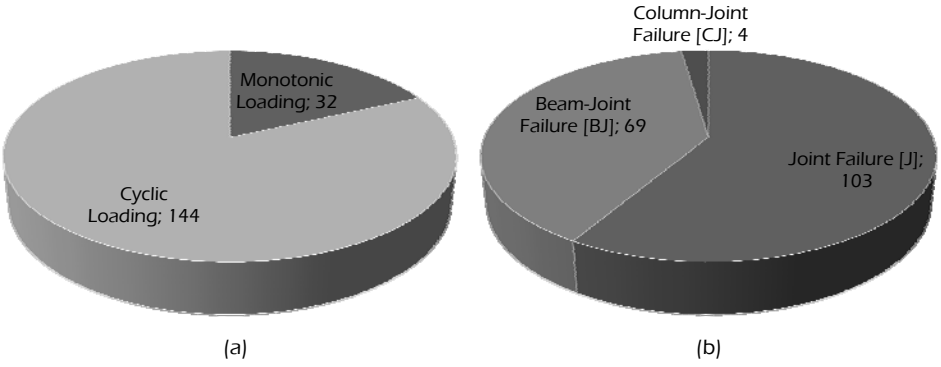

Fig. 4.3: Type of loading and failure for the reduced database of exterior joints

A reduction of the database can be made by considering the several specimens collected. In particular, the specimens characterized by a beam failure (B) and the ones where the failure mode is unknown (U) have been neglected. Indeed, the considered specimens are 176 in which:

- 69 tests attain Beam-Joint failure (BJ);
- 103 tests attain Joint Failure (J);
- 4 tests attain Column-Joint failure (CJ).

In Fig. 4.3 the composition of the database for exterior joints is shown in respect of the type of loading [Fig. 4.3(a)] and the type of failure [Fig. 4.3(b)].

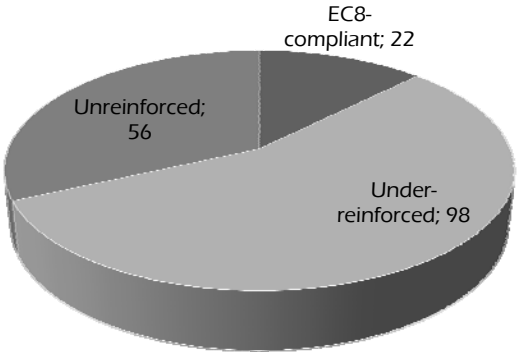

Fig. 4.4: Amount of stirrups in respect of Eurocode 8 requirements.

By considering the classification reported in section 1.4 about the amount of stirrups the collected database is composed as shown in Fig. 4.4.

4.2 Interior Joints

A database collecting the specimens on 85 interior beam-to-column connections has been collected. Table 4.2 lists the considered specimens reporting the reference, the name, the type of loading *(monotonic M or cyclic C)*, the main notes and the type of failure.

Table 4.2: Experimental database collecting interior beam-to-column joints.

Author	Specimen	Load Type	Notes	Failure Type
Benevant et al., 2008	IL	C	3/5 scaled wide beam	J
	IU	C	3/5 scaled wide beam	J
Durrani & Wight,	X1	C	-	J

Table 4.2: Experimental database collecting interior beam-to-column joints.

Author	Specimen	Load Type	Notes	Failure Type
1982	X2	C	-	J
	X3	C	-	J
	S1	C	with slab and transverse beam	J
	S2	C	with slab and transverse beam	BJ
	S3	C	with slab and transverse beam	J
Hakuto et al., 2000	O1	C	-	J
	O2	C	-	J
	O3	C	-	CJ
Hegger et al., 2003	RA1	M	-	J
	RA2	M	-	J
	RA3	M	-	J
	RA4	M	-	J
	RA5	M	-	J
	RA6	M	-	J
	RA7	M	-	J
Kitayama et al., 1991	J1	C	-	J
	C1	C	-	BJ
	B1/B2	C	only legged ties	BJ
	B3	C	only legged ties	BJ
Kusuhara et al., 2004	JE-0	C	-	J
	JE-55	C	eccentric beams	J
	JE-558	C	eccentric beams – additional reinforcement	J
Kusuhara & Shiohara, 2008	A1	C	-	BJ
	A2	C	-	BJ
	A3	C	-	J
	C1	C	transverse beam	J
	D1	C	-	J
	D2	C	anchor plates in joint	J
	B1	C	-	BJ
Lee et al., 2009	J1	C	-	J
	BJ1	C	-	BJ
	BJ2	C	-	BJ
	BJ3	C	-	BJ
	B1	C	-	BJ
Leon, 1990	BCJ2	C	-	J
	BCJ3	C	-	J
	BCJ4	C	-	BJ
Li et al., 2002	A1	C	beam bottom bar lap spliced within joint	J

Table 4.2: Experimental database collecting interior beam-to-column joints.

Author	Specimen	Load Type	Notes	Failure Type
	M1	C	-	J
	A2	C	beam bottom bar lap spliced within joint	BJ
	M2	C	-	BJ
Pampanin et al., 2002	C2	C	2/3 scaled-50's & 70's - continuous	CJ
Pampanin et al., 2007	C4	C	2/3 scaled-50's & 70's - end hocked bars	CJ
Shannag & Alhassan, 2005	S1	C	-	CJ
	S2	C	discontinuous beam bottom steel	J
	S5	C	discontinuous beam bottom steel	J
	S8	C	discontinuous beam bottom steel	J
Shin & LaFave, 2004	1	C	eccentric beams with slab	J
	2	C	eccentric beams with slab	J
Shiohara et al., 2000	S3	C	-	J
Soleimani et al., 1979	BC2	C	-	BJ
	BC3	C	-	BJ
Takaine et al., 2008	JH1	C	-	BJ
Teng & Zhou, 2003	S1 (serie 1)	C	-	J
	S2 (serie 1)	C	eccentric beams	J
	S3 (serie 1)	C	eccentric beams	J
	S5 (serie 2)	C	eccentric beams	J
	S6 (serie 2)	C	eccentric beams	J
Wang & Hsu, 2009	KO-JI1	C	-	CJ
	HO-JI1	C	-	J
Supuviriyakit & Pimanmas, 2007	Control	C	-	J
	Debond	C	-	BJ
Shiohara & Kusuhara, 2008	B01	C	-	J
	B02	C	-	J
	B03	C	-	J
	B04	C	-	J
	B05	C	-	J
	B06	C	-	J
	B07	C	-	J
	B08	C	-	J
	B09	C	-	J
	B10	C	-	J
	C01	C	-	J
	C03	C	-	J
	D01	C	-	J

Table 4.2: Experimental database collecting interior beam-to-column joints.

Author	Specimen	Load Type	Notes	Failure Type
	D02	C	-	J
	D03	C	-	J
	D04	C	-	J
	D05	C	-	J
	D06	C	-	J
	D07	C	-	J
	D08	C	-	J

In Fig. 4.5. the composition of the database for interior joints is shown in respect to the type of loading [Fig. 4.5(a)] and the type of failure [Fig. 4.5(b)].

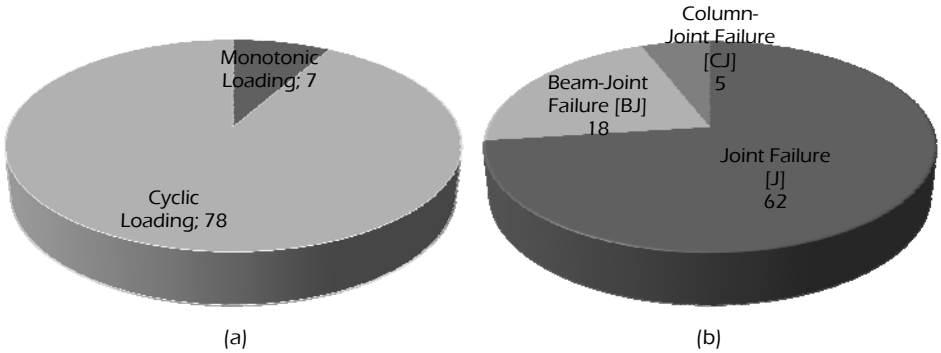

Fig. 4.5: Type of loading and failure for the database of interior joints

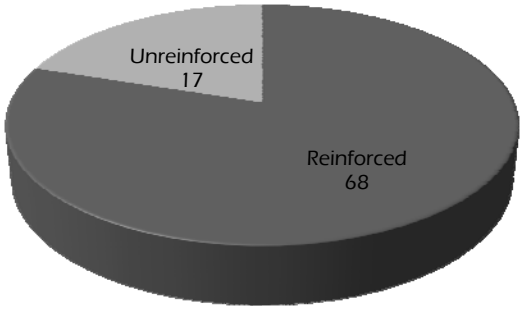

Fig. 4.6: Amount of horizontal stirrups into the panel zone

The database for interior joints has not been reduced because there are no specimens characterised by either beam (B) or unknown (U) failure, while the classification adopted about the amount of stirrups is simplified by considering joints without stirrups into the panel zone (**Unreinforced**) and with horizontal stirrups (**Reinforced**); for details see Fig. 4.6. Further details about the tests on interior joints collected in the database are reported in Appendix A2.

4.3 Evaluation of the Experimental Shear Strength

The reports available in the scientific literature about beam-to-column joints do not provide the exact value of the experimental shear strength; indeed, generally, the authors are interested in the load force or to the deformation measurement. In this thesis the shear strength is evaluated by the load known in the specimens through the actuator.

The possible test configurations for exterior joints are two:

- the configuration in which the load is applied to the end of the beam (Fig. 4.7);
- the one in which the load is applied to the end of the column and the end of the beam can develop horizontal displacement (Fig. 4.8).

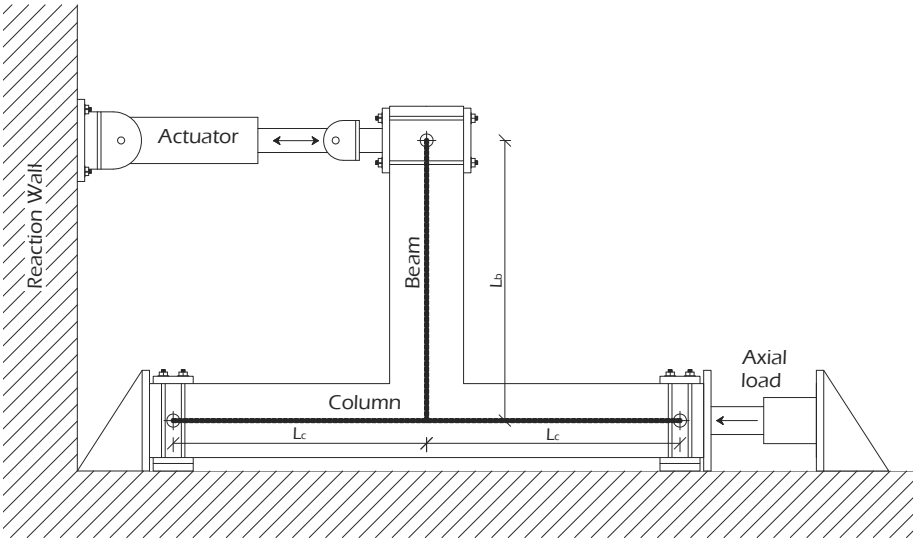

Fig. 4.7: Horizontal test configuration for exterior joints

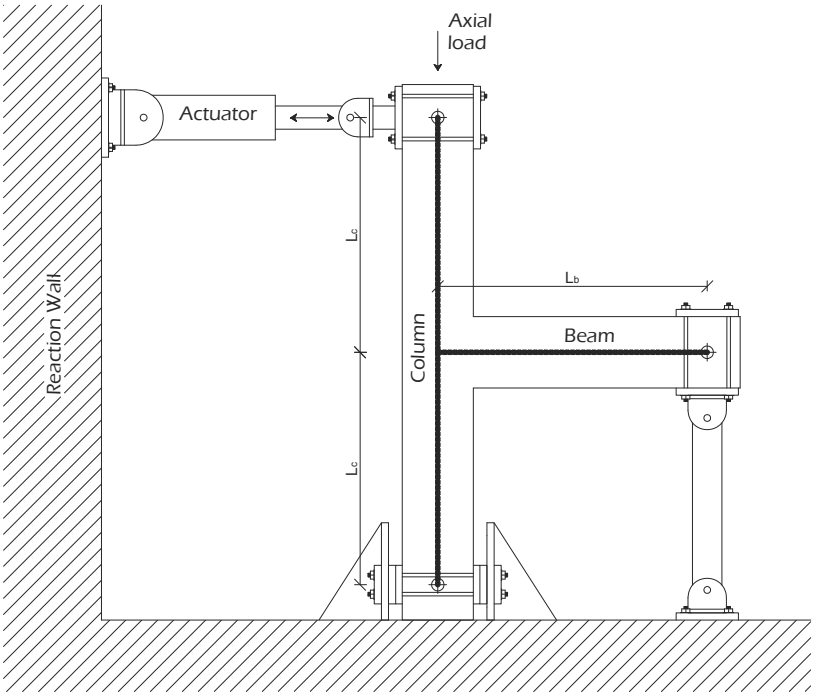

Fig. 4.8: Vertical test configuration for exterior joints

The experimental value of shear strength V_{jh}^{exp} is evaluated as follows:

$$V_{jh}^{\exp} = T^{\exp} - V_c^{\exp} \tag{4.1}$$

in which V_c^{exp} is the ultimate load applied at the top of the column and T^{exp} is the force of the top bars in beam. If joint failure occurs before the yielding in beam ($M^{exp} < M_y$), the force T^{exp} is simply evaluated as follows:

$$T^{\exp} = \frac{M^{\exp}}{M_y} \cdot A_{sb,\sup} \cdot f_{yb} \ . \tag{4.2}$$

If the beam reinforcement is yielded but the ultimate flexural strength M_u is not achieved ($M_y \le M^{exp} < M_u$), the tensile force T^{exp} in the top bars is evaluated through a linear interpolation between M_y and M_u:

$$T^{exp} = A_{sb,\sup} \cdot f_{yb} + \frac{M^{\exp} - M_y}{M_u - M_y} \cdot \left(A_{sb,\sup} \cdot f_{yb} \cdot \lambda - A_{sb,\sup} \cdot f_{yb} \right). \tag{4.3}$$

Finally, if the beam fails before the joint failure ($M^{exp} = M_u$) the top reinforcement attains the maximum tension:

$$T^{\exp} = A_{sb,\sup} \cdot f_{yb} \cdot \lambda \,. \tag{4.4}$$

The moment acting on the joint M^{exp} can be evaluated by equilibrium from the force P^{exp} at the end of the beam; the force P^{exp} in the case of horizontal test configuration (Fig. 4.7) is directly known by the test report, while by analysing the cases tested by using the vertical configuration (Fig. 4.8) the P^{exp} force at the end of beam can be obtained by equilibrium [Eqn. (4.6)] starting from the shear force at the bottom of the top column V_c^{exp}. The bending moment M^{exp} acting on the joint is:

$$P^{\exp} = \frac{V_c^{exp} \cdot 2L_c}{L_b} \,. \tag{4.5}$$

$$M^{exp} = P^{\exp} \cdot L_b \tag{4.6}$$

in which the breadth of the panel zone ($h_c / 2$) has been neglected, by taking in account the translation of the bending action due to the cracking effects (EN 1992-1, 2005).

The yielding M_y and ultimate M_u moments have been evaluated by assuming a bilinear elastic-plastic behaviour with ultimate strain ε_{us} equal to 0.075 for steel and the parabola-rectangle constitutive law for concrete considering the value of 0.0035 for the ultimate strain ε_{cu}.

4.4 Parametric Examination of the Databases

The database collecting the specimens on exterior and interior joints are assessed in respect of the geometrical and mechanical characteristics. The results are useful to quantifying the sensitivity of the behaviour of beam-to-column joints to the various parameters.

4.4.1 Exterior Joints

The database collecting the specimens on exterior beam-to-column joints is assessed in the following by reporting the experimental shear strength V_{jh}^{exp} in function of the various considered parameters.

Fig. 4.9 and Fig. 4.10 show the distribution of the experimental joint shear strength V_{jh}^{exp} (on the y-axis) in respect to the column b_c and beam b_b width (on the x-axis), respectively. By analysing the two mentioned figures it is easily to see that the shear strength increases by increasing the geometrical dimensions of both column and beam.

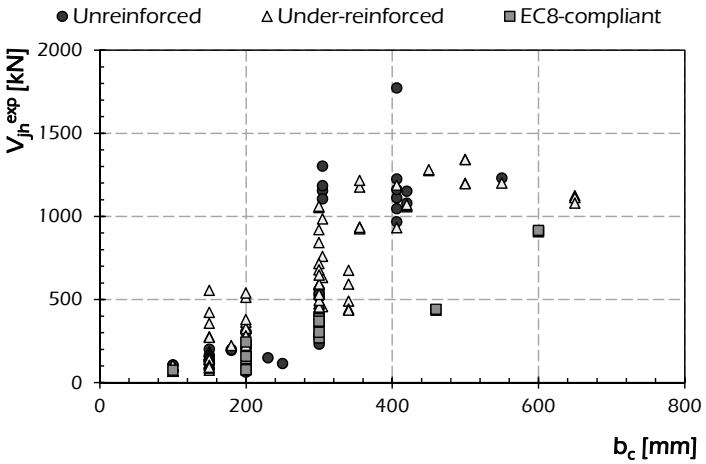

Fig. 4.9: Distribution of the experimental shear strength about the column base for exterior joints.

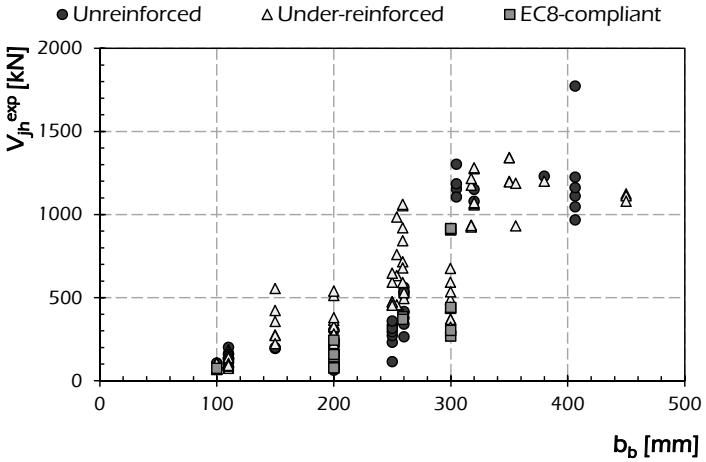

Fig. 4.10: Distribution of the experimental shear strength about the beam base for exterior joints.

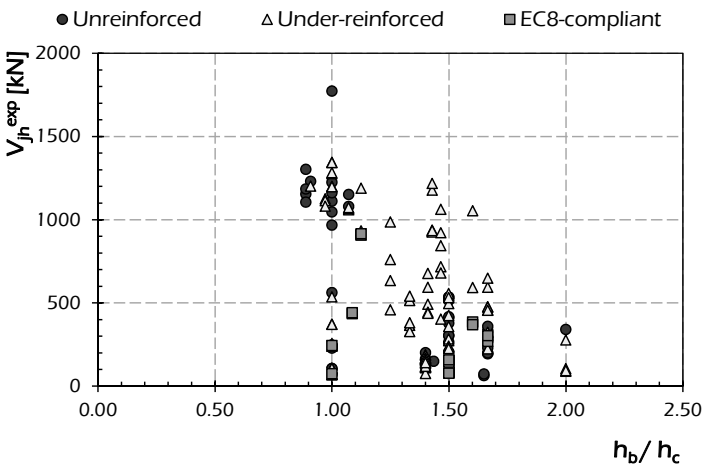

Fig. 4.11: Distribution of the experimental shear strength about the joint aspect ratio for exterior joints.

Fig. 4.11 reports an important correlation between the experimental shear strength V_{jh}^{exp} and the joint aspect ratio h_b / h_c defined as the ratio between the beam h_b and the column h_c depth. The graph shows a reduction of the shear strength by increasing the joint aspect ratio. In all the analysed specimens the value of the joint aspect ratio is smaller than 2 according to consideration that the elements characterised by a value of h_b / h_c greater than 2 are considered squat elements and then can be analysed through different theories. Finally, different consideration should be provided for elements characterized by a value of the joint aspect ratio h_b / h_c smaller than 0.5 that are considered similar to beam element.

Fig. 4.12 shows the distribution of the experimental shear strength V_{jh}^{exp} function of the Horizontal Reinforcement Index defined in Eqn. (3.1).

The trend observed is not well defined, so it may be deduced that the shear strength of exterior beam-to-column joints is not conditioned by the amount of horizontal stirrups in the panel zone. However, looking at the size of the joints it can observed that the reinforced specimens are generally smaller than the reinforced subassemblies. The shear strength V_{jh}^{exp} increases with the size b_c and b_b of column and beam, respectively (Fig. 4.9 and Fig. 4.10), while the graph in Fig. 4.12 returns a trend of V_{jh}^{exp} constant with the parameter HRI. From the above considerations it can be deduced that the shear strength V_{jh}^{exp} resulting from tests performed on exterior beam-to-column joints and collected in the database tends to increase with increasing the amount of the horizontal stirrups into the joint.

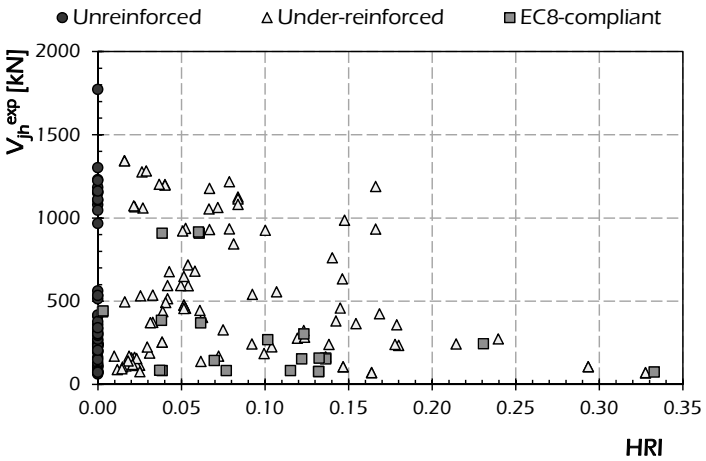

Fig. 4.12: Distribution of the experimental shear strength about the horizontal reinforcement index for exterior joints.

Fig. 4.13 and Fig. 4.14 show the relationship between the experimental shear strength and the Beam Reinforcement Index (BRI) and the Column Reinforcement Index (CRI) respectively. In particular, the BRI is a measure of the amount of longitudinal reinforcement in the beam and is evaluated by Eqn. (3.2) as the mechanical ratio between the sum of the top $A_{sb,sup}$ and bottom $A_{sb,inf}$ layer of the longitudinal reinforcement in the beam and the cross section.

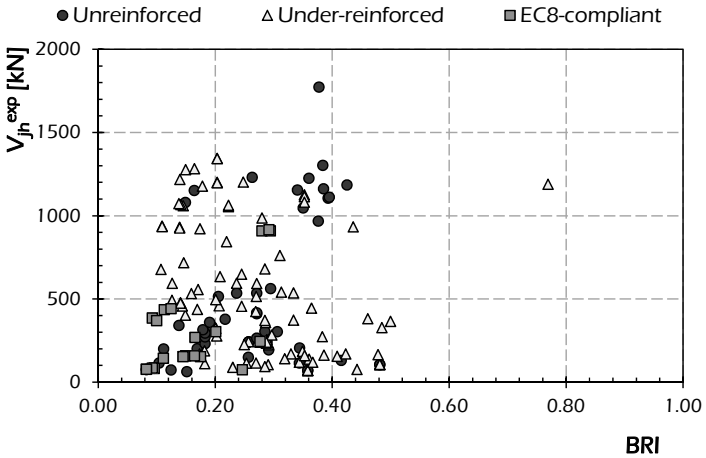

Fig. 4.13: Distribution of the experimental shear strength about the Beam Reinforcement Index for exterior joints.

The Column Reinforcement Index (CRI) is defined by the mechanical ratio between the total longitudinal reinforcement in column and the column cross section. [Eqn. (3.3)].

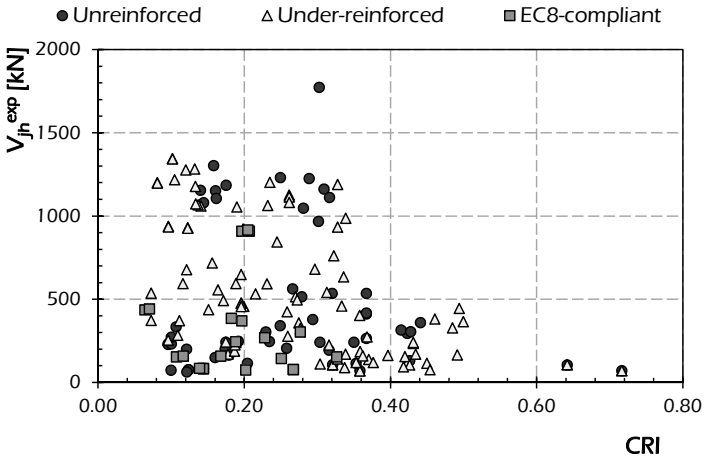

Fig. 4.14: Distribution of the experimental shear strength about the Column Reinforcement Index for exterior joints.

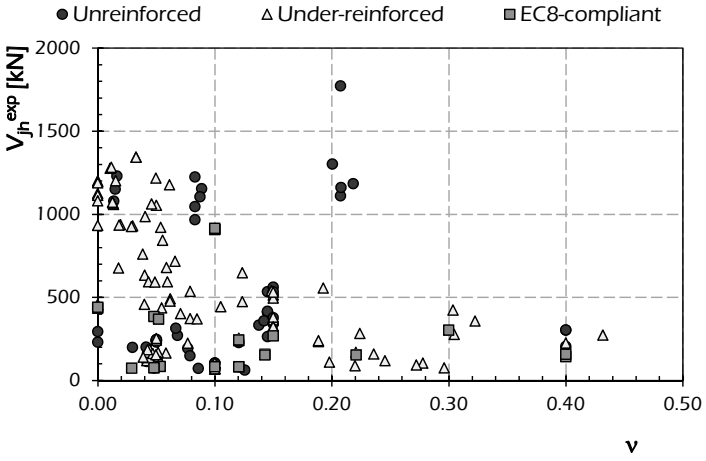

Fig. 4.15: Distribution of the experimental shear strength about the axial load for exterior joints.

The graphs reported in Fig. 4.13 and Fig. 4.14 show that there is not a direct dependence between the joint shear strength V_{jh}^{exp} and the amount of reinforcement in beam and column; maybe, this result is affected by the influence of the geometrical dimension of the considered specimens. A better understanding of the correlation between strength and reinforcement could result by analysing specimens with the same characteristics except for the amount of stirrups.

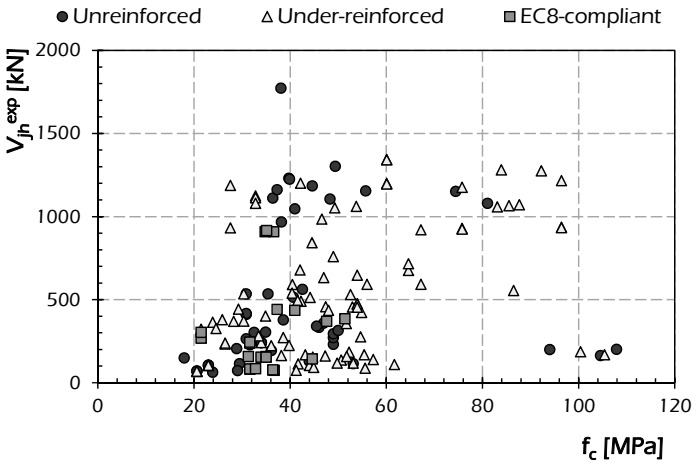

Fig. 4.16: Distribution of the experimental shear strength about the concrete strength for exterior joints.

Fig. 4.15 and Fig. 4.16 show the dependence of the shear strength of exterior beam-to-column joints from the column axial load N_{col} through the no dimensional axial load ν [evaluated by Eqn. (3.4)] and the concrete strength f_c.

In particular, it shows that the database collecting exterior beam-to-column joints is composed of subassemblages tested under different loads applied to the column that ranges between 0 and 0.40 in terms of no dimensional load ν. About the concrete strength f_c a variable value between 20 MPa (ordinary concrete) and 110 MPa (high strength concrete) can be observed.

4.4.2 Interior Joints

In the following, the studies on the experimental shear strength V_{jh}^{exp} of the interior joints which make up the database is reported as done with the exterior ones. The study is produced by subdividing the database in only two main

groups: reinforced joints and unreinforced ones. This subdivision in reinforced and unreinforced type, less accurate than the one operated in the case of exterior joints, is the result of the limited number of tests on both reinforced and EC8-compliant specimens available in the scientific literature.

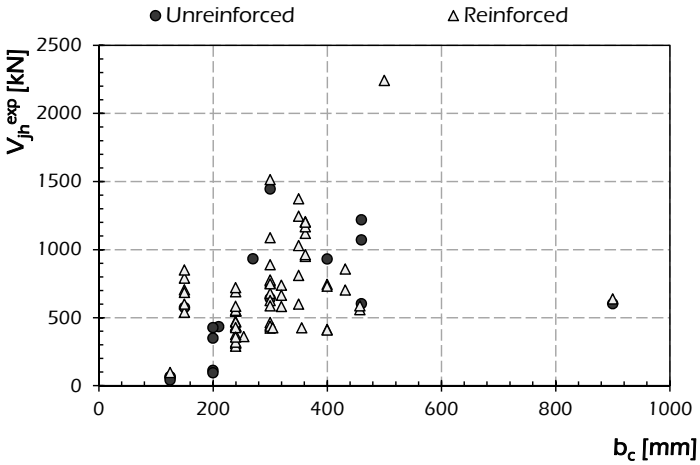

Fig. 4.17: Distribution of the experimental shear strength about the column base for interior joints.

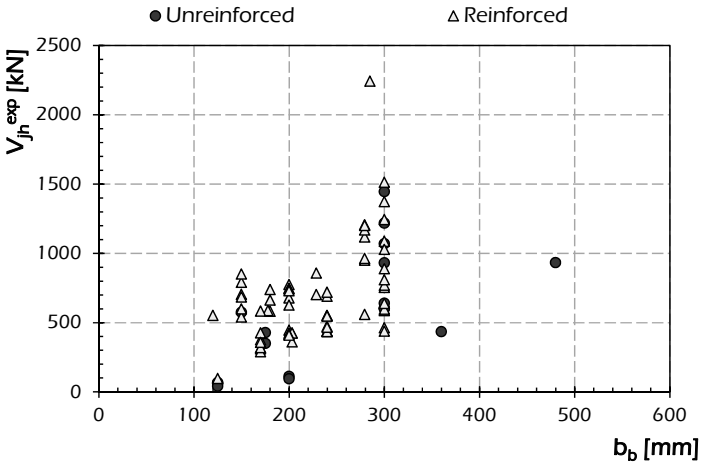

Fig. 4.18: Distribution of the experimental shear strength about the beam base for interior joints.

Fig. 4.17 and Fig. 4.18 show the distribution of the experimental shear strength V_{jh}^{exp} of interior joints in function of the column b_c and beam b_b width. As already observed for the exterior beam-to-column connections, the strength depends on the geometrical dimensions of the beam and of the column resulting in high value when the width increases.

Fig. 4.19 shows the experimental shear strength in function of a variation of the joint aspect ratio h_b / h_c by considering both unreinforced and reinforced interior beam-to-column joints. The trend observed for exterior joints is respected by interior ones resulting in lower shear strength the higher is the joint aspect ratio.

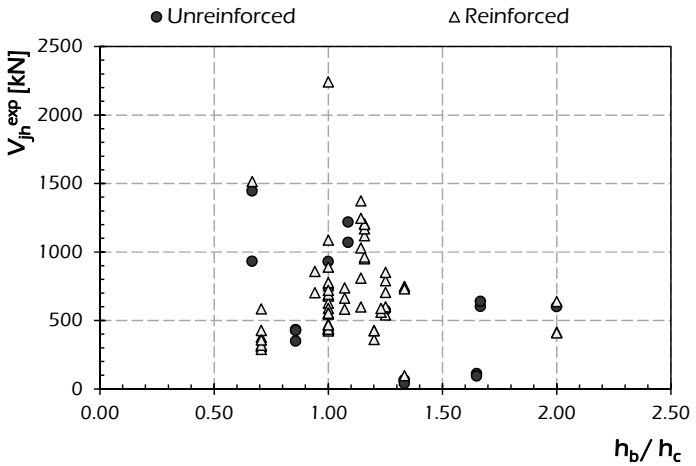

Fig. 4.19: Distribution of the experimental shear strength about the joint aspect ratio for interior joints.

In the following, Fig. 4.20, Fig. 4.21 and Fig. 4.22 report the behaviour of the interior beam-to-column joints analysed considering the variation of the Horizontal Reinforcement Index (HRI), Beam Reinforcement Index (BRI) and Column Reinforcement Index (CRI) [Eqns. (3.1), (3.2) and (3.3), respectively]. As already observed for the case of exterior connections (section 4.4.1), in a preliminary analysis it might seem that the shear strength V_{jh}^{exp}, resulting from experimental tests, does not depend on the amount of the reinforcement of the panel zone and of the connected element. Also in this case, instead, the correlation should be studied by considering the joint characterized by the same geometrical dimensions and in particular the same column and beam width. By considering this particularity, it has been observed that the small specimens achieving small values of the shear strength (see Fig. 4.17 and Fig.

4.18) are characterised by high amount of reinforcement both in the panel zone and in the connected beam and column.

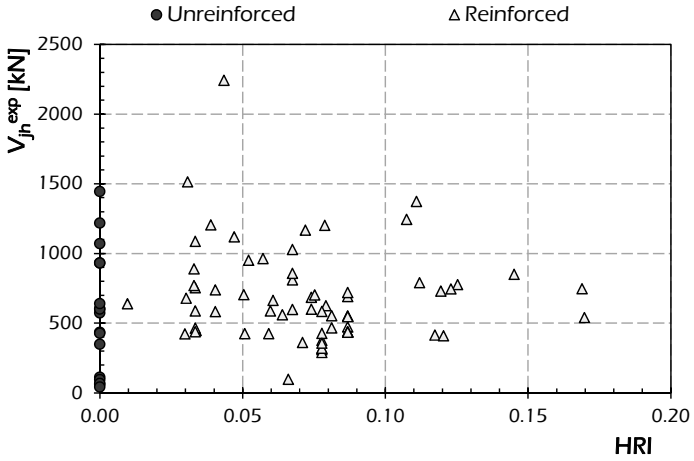

Fig. 4.20: Distribution of the experimental shear strength about the Horizontal Reinforcement Index (HRI) for interior joints.

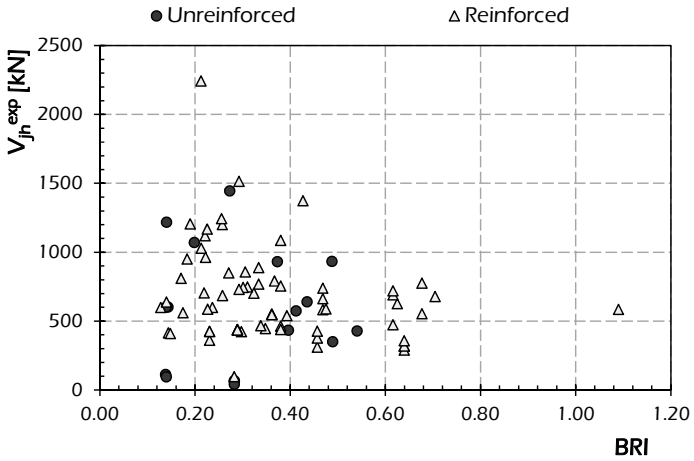

Fig. 4.21: Distribution of the experimental shear strength about the Beam Reinforcement Index (BRI) for interior joints.

Through the consideration listed above, and taking into account that Fig. 4.20, Fig. 4.21 and Fig. 4.22 show an invariable strength of the interior joints

about the steel reinforcement, it can be considered that the shear strength increases the greater is the horizontal steel reinforcement in the panel zone (HRI) and the longitudinal reinforcement in beam and column (BRI and CRI, respectively).

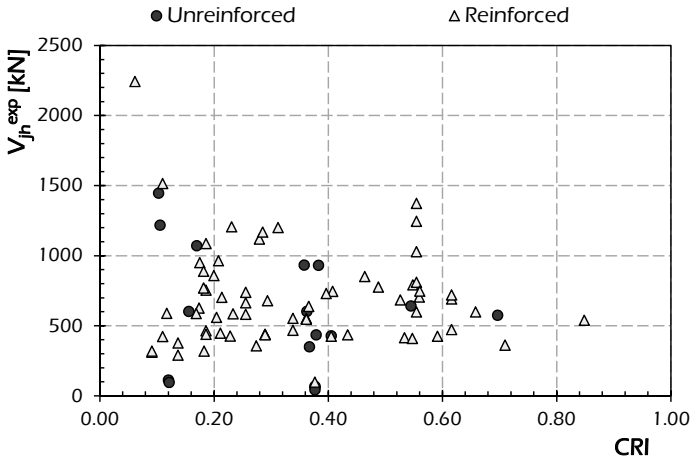

Fig. 4.22: Distribution of the experimental shear strength about the Column Reinforcement Index (CRI) for interior joints.

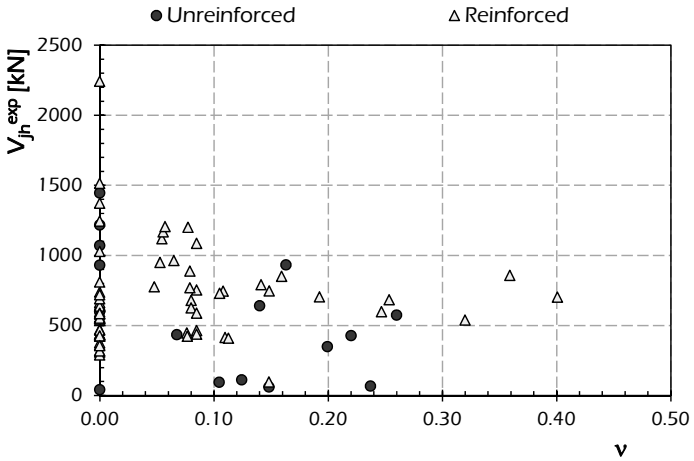

Fig. 4.23: Distribution of the experimental shear strength about the axial load for interior joints.

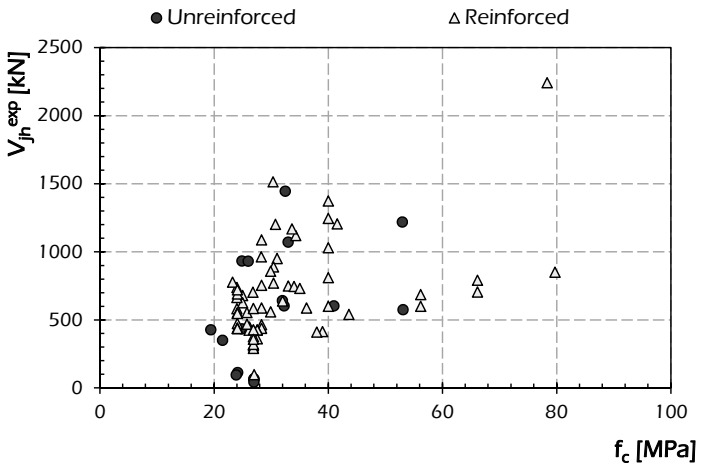

Fig. 4.24: Distribution of the experimental shear strength about the concrete strength for interior joints.

Finally, the trends of the experimental shear strength with the variation of the axial load applied to the top column and the variation of the concrete cylinder strength are reported in Fig. 4.23 and Fig. 4.24, respectively.

The non-dimensional axial load ν (eqn. 2.11) is variable between 0 (specimens in which axial load has not been applied to the top column) and 0.40 (Fig. 4.23), while, by analysing Fig. 4.24, a concrete cylinder strength ranger between 20 MPa and 80 MPa is shown.

4.5 Remarks

The database collecting the specimens on exterior and interior joints have been examined in respect of the geometrical and mechanical characteristics affecting the capacity models for evaluating the shear strength of those structural elements. The results are useful to quantifying the sensitivity of the behaviour of beam-to-column joints to the various parameters.

The capacity of beam-to-column joints is strongly influenced by the size of the specimens. In particular, the shear strength results in directly proportional relationships with the column and beam widths, while a strength reduction is achieved by increasing the joint aspect ratio.

The comparison between the shear strength and the amount of horizontal steel reinforcement in the panel zone provides increasing values of the capacity

by increasing the Horizontal Reinforcement Index, but the points representing the comparison are characterized by high dispersion. However, the amounts of longitudinal reinforcement in beam and column analysed through the BRI and CRI, as well as the axial load N_c, do not influence the shear strength of both exterior and interior joints.

Finally, a clear increasing relationship is achieved between V_{jh}^{exp} and the concrete strength f_c.

CHAPTER V

5. Experimental Assessment of the Capacity Models

The accuracy of the models recalled in section 2 is assessed in the present section by comparing the experimental values of shear strength V_{jh}^{exp} with the corresponding theoretical predictions V_{jh}.

The assessment of the various models can be first of all carried out in a qualitative way by analysing the equivalence charts between the experimental values V_{jh}^{exp} and the corresponding theoretical ones V_{jh}. Then, further quantitative parameters are introduced for assessing the capacity models.

All the analyses and validations presented in following are reported for both exterior and interior joints by specialising the results about the amount of reinforcement in the panel zone in unreinforced, under-reinforced and EC8-compliant exterior joints and unreinforced and reinforced interior joints, respectively, according to the classification made in section 1.4.

5.1 Experimental Observation vs. Theoretical Predictions

In this section the assessment of the code formulations and the capacity models available in the scientific literature is carried out in a qualitative way.

The results are provided through the so-called equivalence charts in which, for each specimen, the experimental shear strength V_{jh}^{exp} is reported on the x-axis while the corresponding theoretical strength V_{jh} evaluated through the analysed capacity model is reported on the y-axis.

The equivalence between the experimental evidence and the calculated strength results from the bisector segment reported in every figure as reference. The model can be deemed as accurate as the bunch of points is close to that segment, being either conservative or non-conservative as the points tend to be mainly below or above the same segment, respectively.

Section 5.1.1 to 5.1.4 report the equivalence charts for exterior and interior joints and the comments are listed in simple points.

For every capacity model for exterior beam-to-column joints four equivalence charts are represented: the first one deals with the results of the database as a whole while the other three ones refer to unreinforced, under-reinforced and EC8-compliant joints.

About interior joints, three equivalence charts are represented for every capacity model: the first one includes all the specimens on interior beam-to-column subassemblies and the other two ones are specialised for unreinforced and reinforced joints.

5.1.1 Experimental Assessment of Code Formulations for Exterior Joints

Fig. 5.1 shows the equivalence charts plotted for the ACI 352-85 (1985) formulation for exterior joints.

The model by ACI 352-85 (1985) results (Fig. 5.1) in non-conservative law for all the analysed joints providing for unreinforced, under-reinforced and EC8-compliant joints the branch of points above the bisector segment.

Fig. 5.2 shows the assessment provided for the model proposed by the ACI 352-02 (2002) demonstrating that the last version of the ACI 352 developed in 2002 provides results more accurate than the ones provided by the old code version (ACI 352-85, 1985) shown in Fig. 5.1.

The formulation adopted by the ACI 352-02 (2002) (Fig. 5.2):

- provides non-conservative results for both unreinforced and EC8-compliant low strength joints,
- in respect of the under-reinforced joints and for both unreinforced and EC8-compliant joints with high strength the model meanly results equivalent.
- high dispersion around the bisector equivalence can be observed in Fig. 5.2.

Fig. 5.3 shows the equivalence charts for the ACI 318-05 (2005) formulation for exterior joints.

The behaviour of the ACI 318-05 (2005) results substantially equal to the one shown for the ACI 352-02 (2002). Indeed, about the code formulation analysed in Fig. 5.3:

- non-conservative results are achieved for both unreinforced and EC8-compliant low strength joints;

- a better correlation between experimental V_{jh}^{exp} and theoretical V_{jh} values is shown for under-reinforced and unreinforced high strength joints.
- high dispersion of the values around the bisector segment results demonstrating the low accuracy of the code formulation.

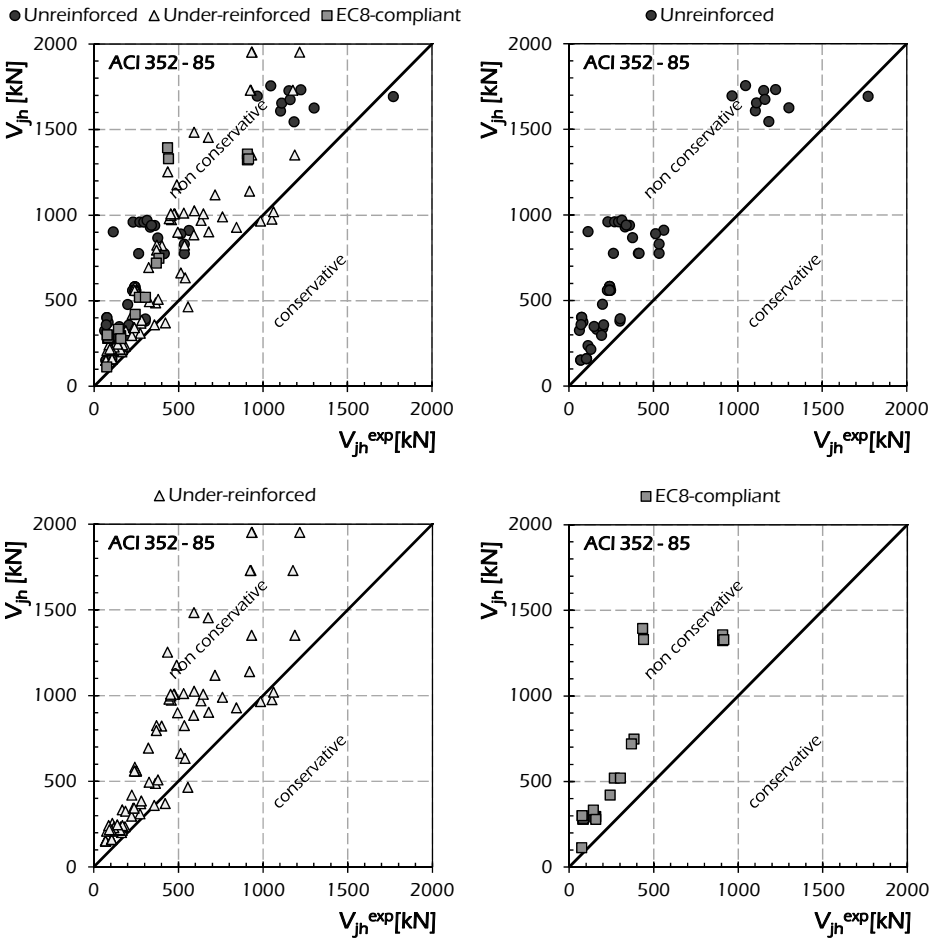

Fig. 5.1: Assessment of the ACI 352-85 (1985) for exterior joints.

The Japanese codes AIJ 1990 (1990) and AIJ 1999 (1999) are qualitatively analysed in Fig. 5.4 and Fig. 5.5, respectively.

About the first one (AIJ 1990):

- it results in good correlation with the experimental evidence for unreinforced joints and non-compliant low strength joints;
- non-conservative trend is shown in Fig. 5.4 for reinforced and EC8-compliant exterior joints.

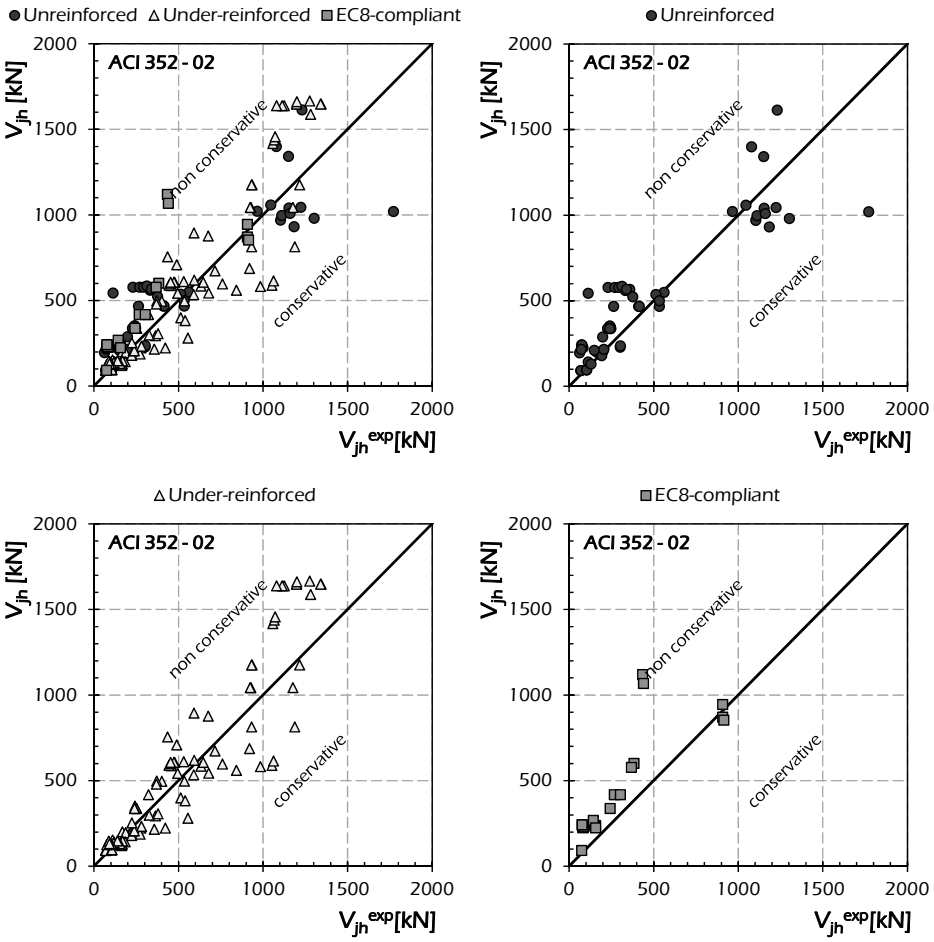

Fig. 5.2: Assessment of the ACI 352-02 (2002) for exterior joints.

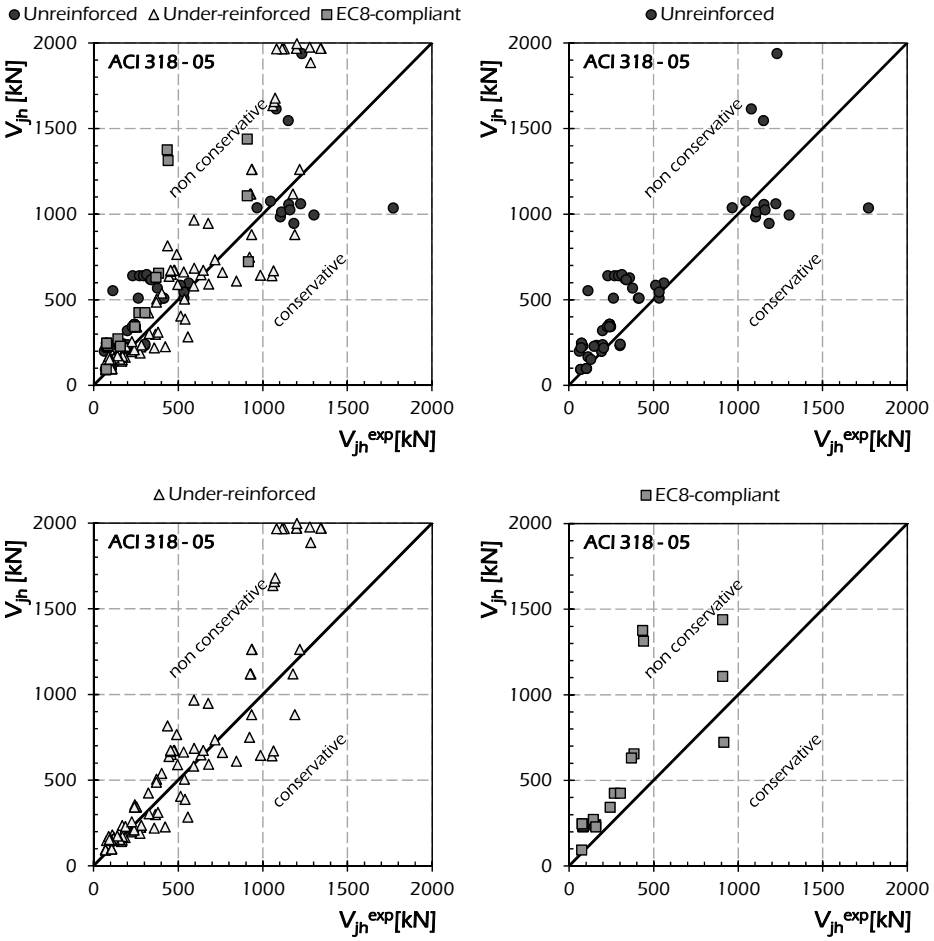

Fig. 5.3: Assessment of the ACI 318-05 0 for exterior joints.

The assessment of the last version of the Japanese code (AIJ 1999) is reported in Fig. 5.5. The trend is the same as that already observed for the old version (AIJ 1990):

- it results in equivalent law with the experimental evidence for unreinforced and non-compliant joints;
- slightly non-conservative trend results for EC8-compliant joints.

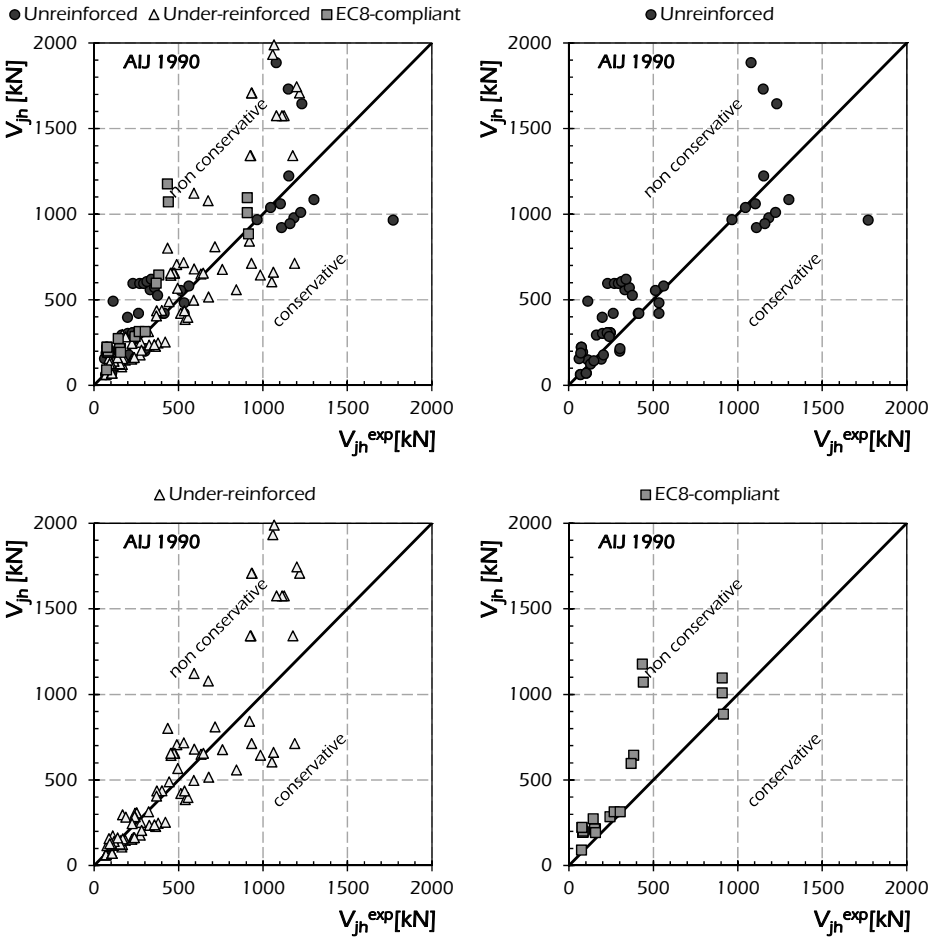

Fig. 5.4: Assessment of the AIJ 1990 (1990) for exterior joints.

As already observed in the case of the American codes (ACI 352-85, 1985 and ACI 352-02, 2002), the latest Japanese code leads to predictions more accurate than the ones provided by the old one.

In particular, the results provided by the AIJ 1999 are closer to the bisector segment than the ones obtained by applying the AIJ 1990 formulation (Fig. 5.5).

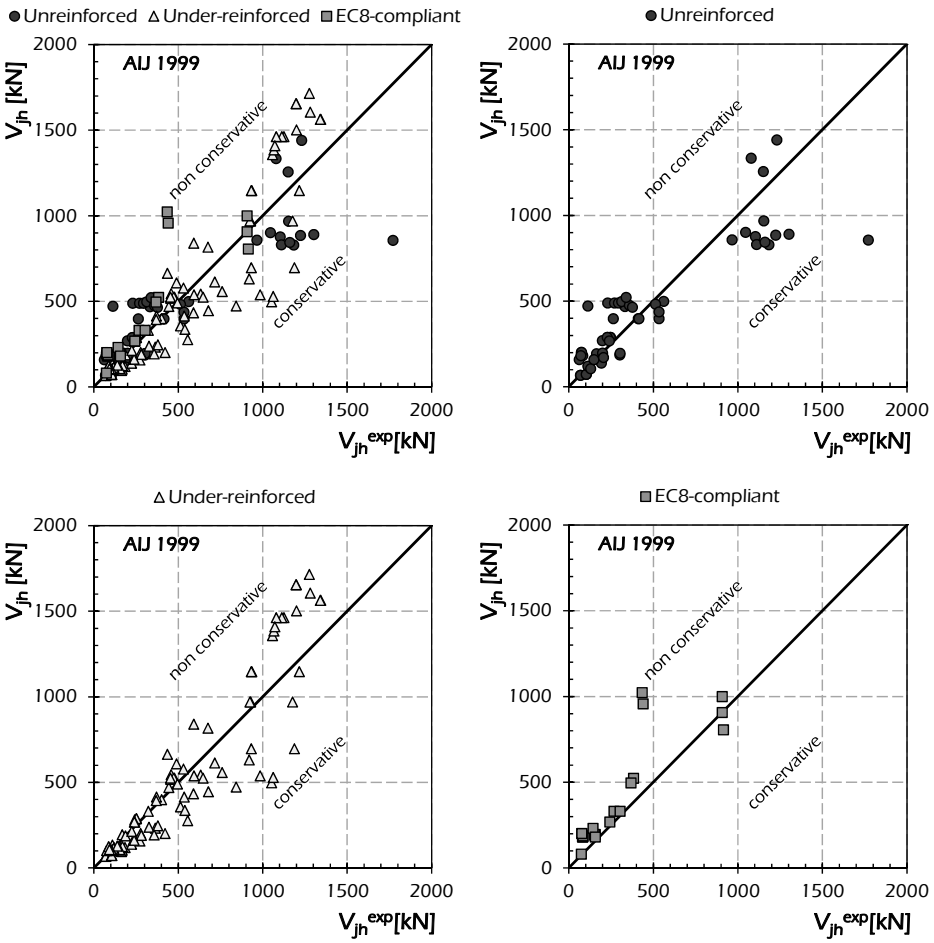

Fig. 5.5: Assessment of the AIJ 1999 (1999) for exterior joints.

Fig. 5.6 shows the qualitative assessment of the NZS 3101 (1995) formulation. The following comments can be listed about the New Zealand code:

- the unreinforced beam-to-column joints are not taken into account providing a shear strength $V_{jh} = 0$ when there are not horizontal stirrups in the panel zone;
- the models results meanly in equivalence law with the experimental results;
- high dispersion around the 45° equivalence line is shown in Fig. 5.6.

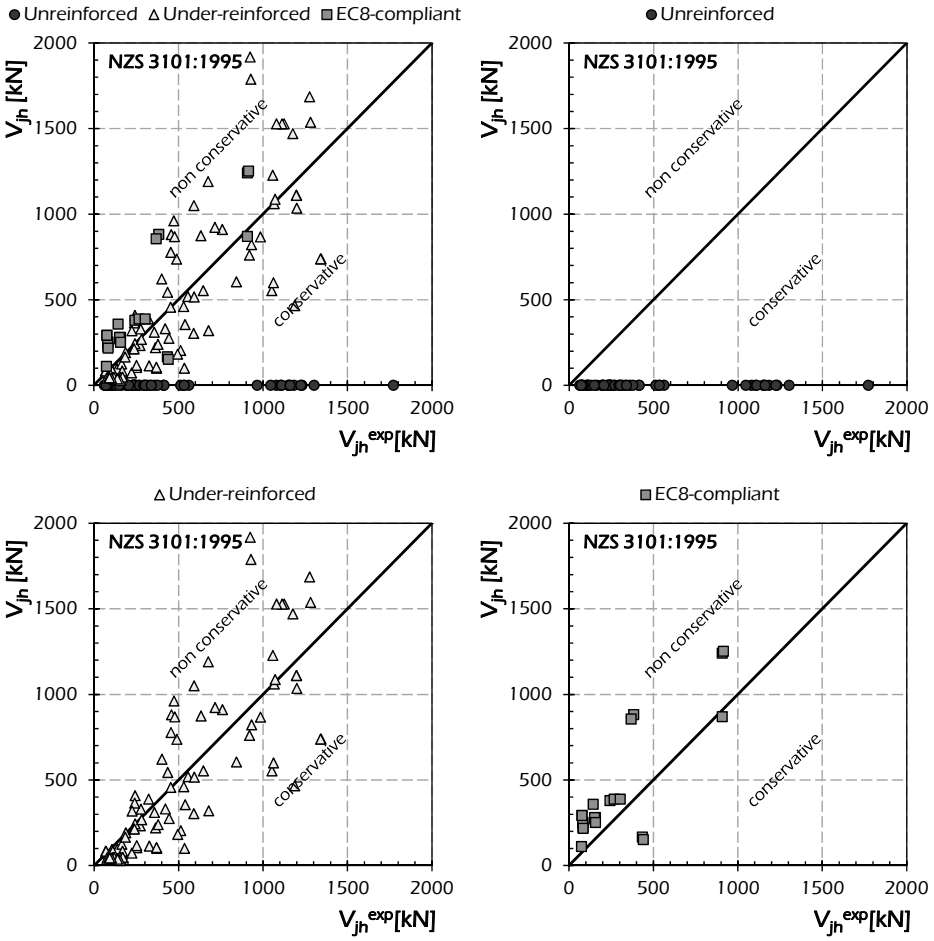

Fig. 5.6: *Assessment of the NZS 3101 (1995) for exterior joints.*

The equivalence charts for unreinforced, under-reinforced and EC8-compliant exterior beam-to-column joints about the model recommended by the FEMA 273 (1997) and FEMA 356 (2000) are shown in Fig. 5.7. The analysed predictions:

- result conservative in evaluating the shear strength V_{jh} of unreinforced joints;
- provide non-conservative results for compliant joints.

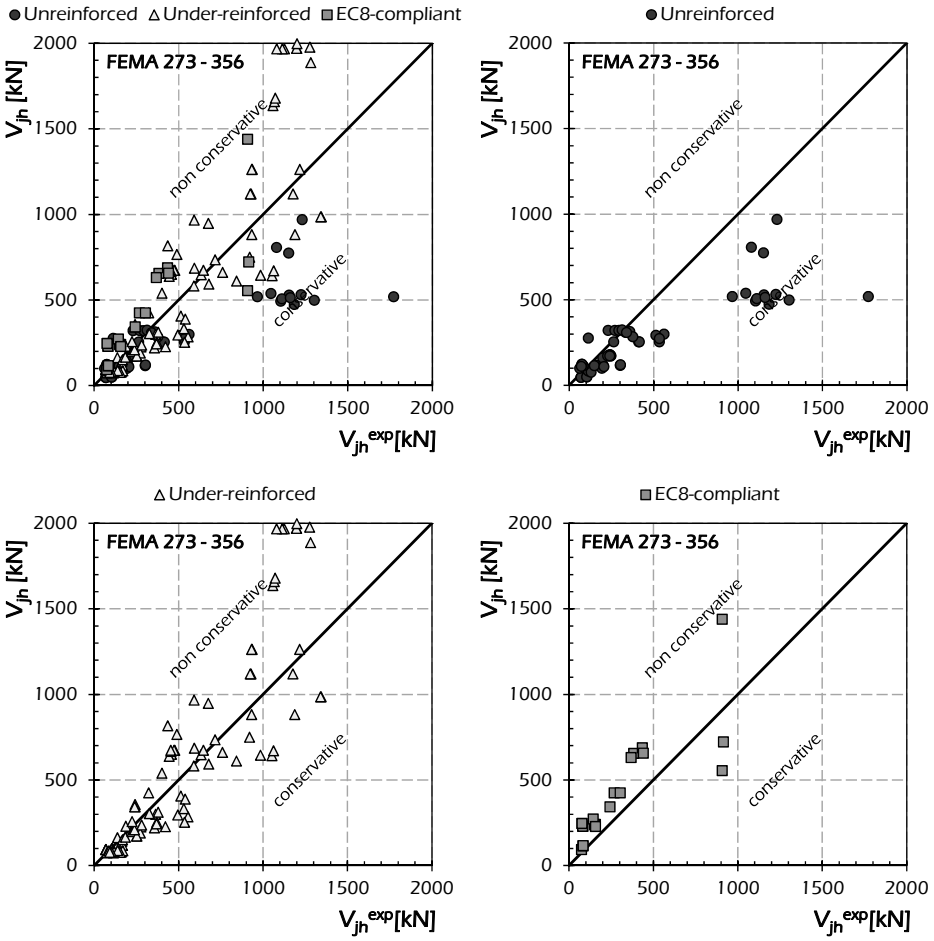

Fig. 5.7: Assessment of the FEMA 273 (1997) - 356 (2000) for exterior joints.

The assessment of the formulation provided by Eurocode 8 (EN 1995-1, 1995) is shown in Fig. 5.8. The model results in non-conservative law for all the specimens taken into account.

In fact, the bunch of points representing the comparison between experimental shear strength V_{jh}^{exp} and the theoretical one V_{jh} is distributed above the bisector segment.

Finally, high dispersion of the results provided by the Eurocode 8 (EN 1995-1, 1995) is shown in Fig. 5.8 especially in the case of unreinforced and under-

reinforced joints, while by analysing the equivalence chart about EC8-compliant joints the theoretical shear strength V_{jh} compared with the experimental evidence V_{jh} results in linear relationship. In this last case the exception is represented by two experimental tests providing a shear strength V_{jh}^{exp} equal to around 500 kN, while by applying the code formulation 0 a shear strength four time greater (around 2000 kN) than the first one is found.

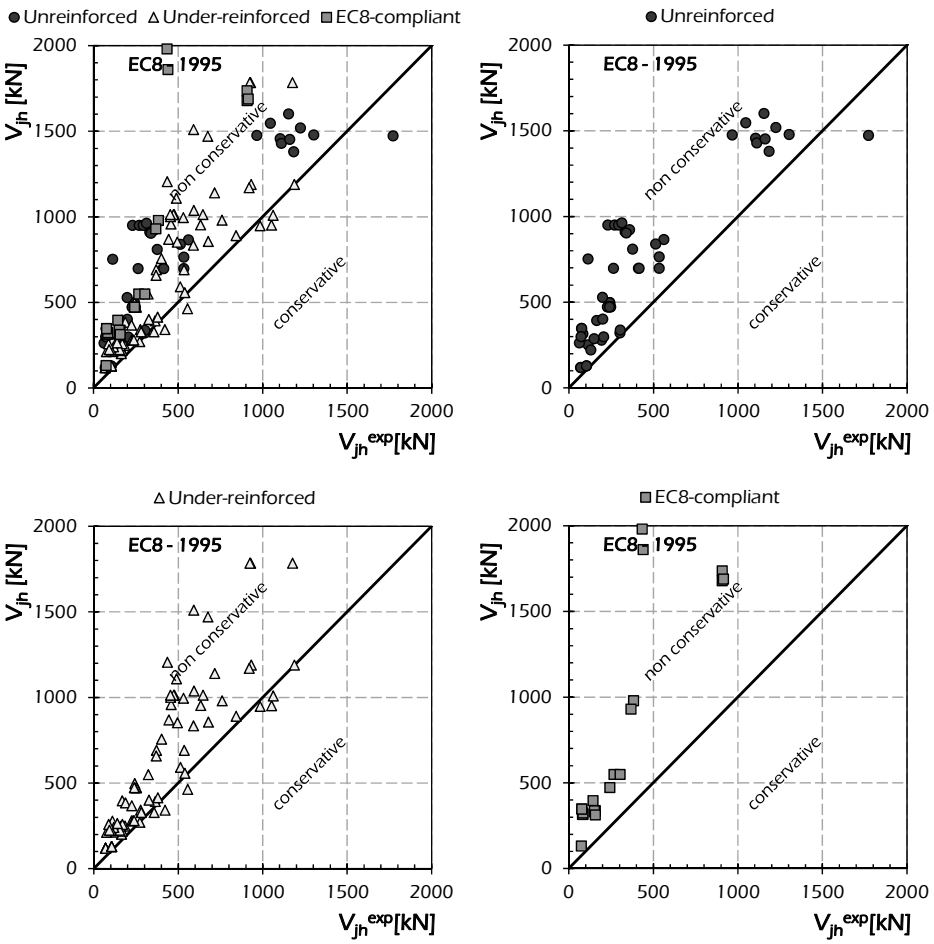

Fig. 5.8: Assessment of the Eurocode 8 (EN 1995-1, 1995) for exterior joints.

Fig. 5.9 reports the equivalence charts comparing the experimental shear strength V_{jh}^{exp} and the one V_{jh} evaluated by applying the Eurocode 8 (EN 1998-3, 2005) and NTC (2008) recommendations.

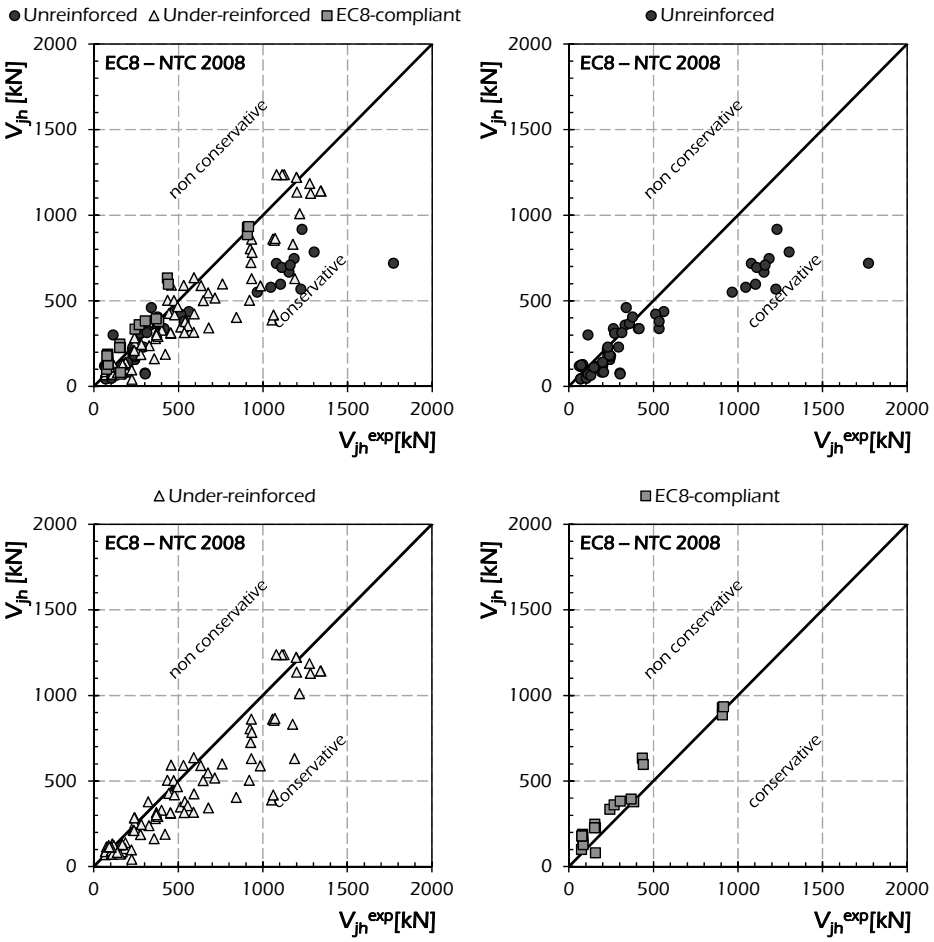

Fig. 5.9: Assessment of the Eurocode 8 (EN 1998-3, 2005) and NTC (2008) for exterior joints.

Regarding the shear strength V_{jh} predicted by applying the Eurocode 8 (EN 1998-3, 2005) and NTC (2008) formulation:

- it results in meanly equivalent law with the experimental evidence providing a huge number of points near the 45° segment;
- a conservative relationship is shown for unreinforced joints with high strength;
- results more accurate than the ones observed for the old version of the Eurocode 8 (EN 1995-1, 1995) are shown.

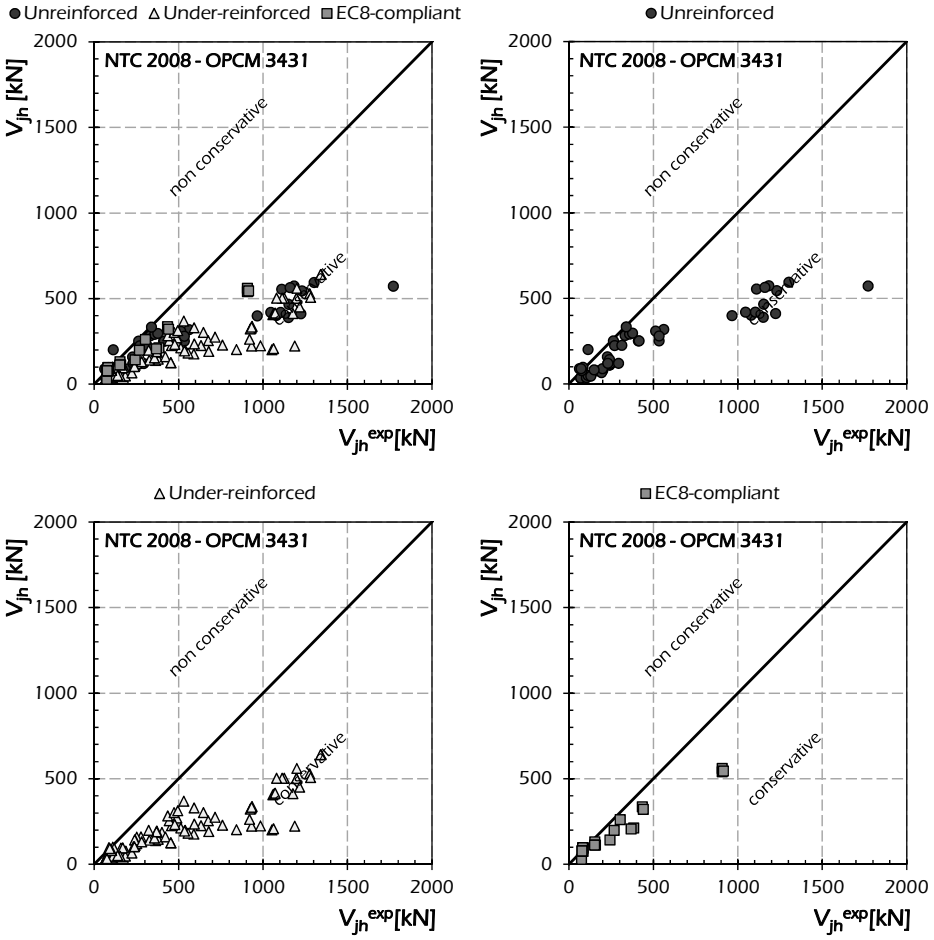

Fig. 5.10: Assessment of the NTC (2008) and OPCM 3431/05 (2005) for exterior joints.

The predictions resulting by the NTC (2008) and OPCM 3431/05 (2005) taking into account the behaviour of beam-to-column joints of existing structure designed with substandard seismic details is assessed in Fig. 5.10.

The following considerations are made:

- the model results over-conservative in evaluating the shear strength V_{jh} of unreinforced and under-reinforced joints;
- the relationship between the experimental shear strength V_{jh}^{exp} and the theoretical one is characterised by low dispersion.

5.1.2 Experimental Assessment of Capacity Models for Exterior Joints Available in the Literature

The capacity models available in the scientific literature for evaluating the shear strength V_{jh} of exterior beam-to-column reinforced concrete joints and outlined in section 2.2 and 2.4 are assessed in this section.

Fig. 5.11 shows the equivalence charts comparing the shear strength V_{jh} predicted through the model by Pantazopoulo & Bonacci (1992) and the experimental evidence V_{jh} for unreinforced, under-reinforced and EC8-compliant exterior joints. The model (Pantazopoulo & Bonacci, 1992) results in non-conservative law with respect to the value V_{jh} of the considered database providing all the comparison points above the bisector segment reported in each graphs as a reference.

Although there is no difference between unreinforced, under-reinforced and EC8-compliant joints in the results obtained by applying the model by Pantazopoulo & Bonacci (1992) (Fig. 5.11).

The comparison between the shear strength V_{jh} evaluated through the model by Paulay & Priestley (1992) and the experimental shear strength V_{jh}^{exp} is shown in Fig. 5.12. The analysed model provides results which are in good correlation with the experimental evidence; in fact:

- the points representing unreinforced joints are gathered around the bisector segment with a little trend toward conservative values;
- the points representing under-reinforced specimens are located around the bisector segment providing a meanly equivalent law;
- the points representing EC8-compliant joints are gathered near the 45° equivalence segment resulting above this one and so in little unconservative law.

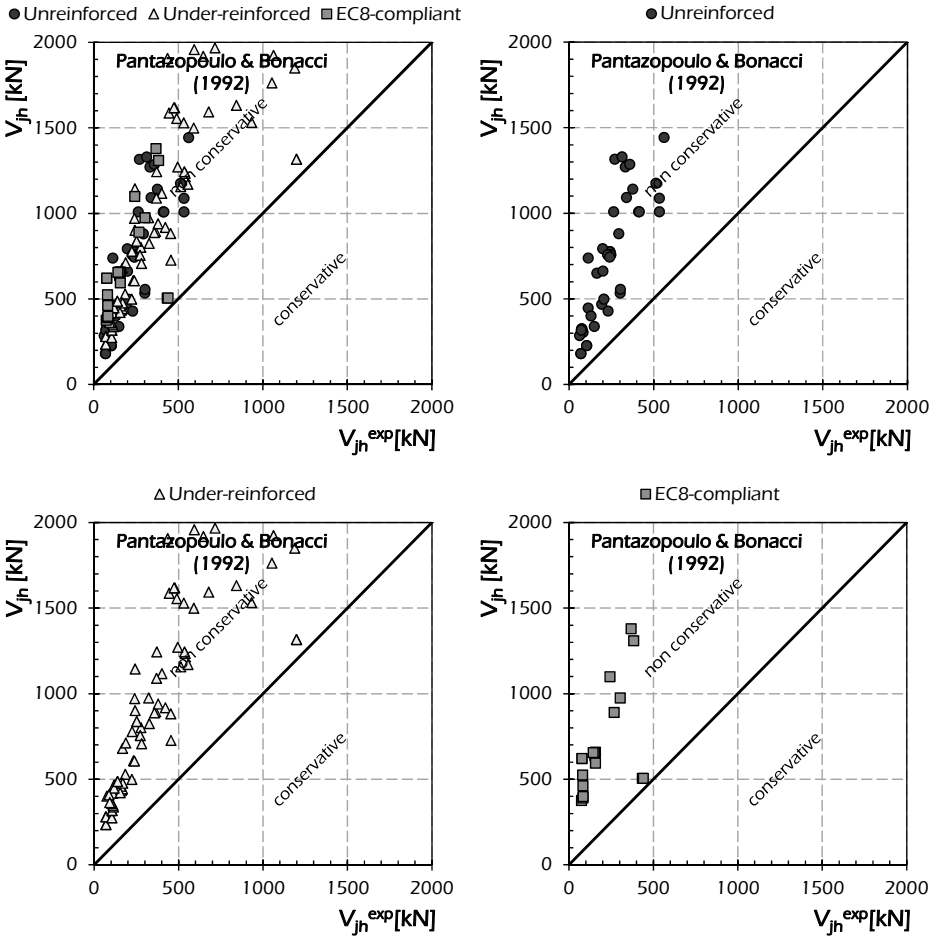

Fig. 5.11: Assessment of the model by Pantazopoulo & Bonacci (1992) for exterior joints.

In Fig. 5.13 the equivalence charts about the model by Parker & Bullman (1997) are shown. The following considerations about comparison between experimental evidence V_{jh}^{exp} and theoretical shear strength V_{jh} evaluated through the analysed model can be made:

- the results about unreinforced joints are characterised by high dispersion around the 45° equivalence segment resulting meanly conservative;
- high dispersion of the results is also observed in the case of under-reinforced joints;

- a good relationship between V_{jh} and V_{jh}^{exp} results in the case of EC8-compliant exterior beam-to column joints; in particular the majority of points lie close to the bisector segment, except for the EC8-compliant joints with high values of the shear strength which results in non-conservative law.

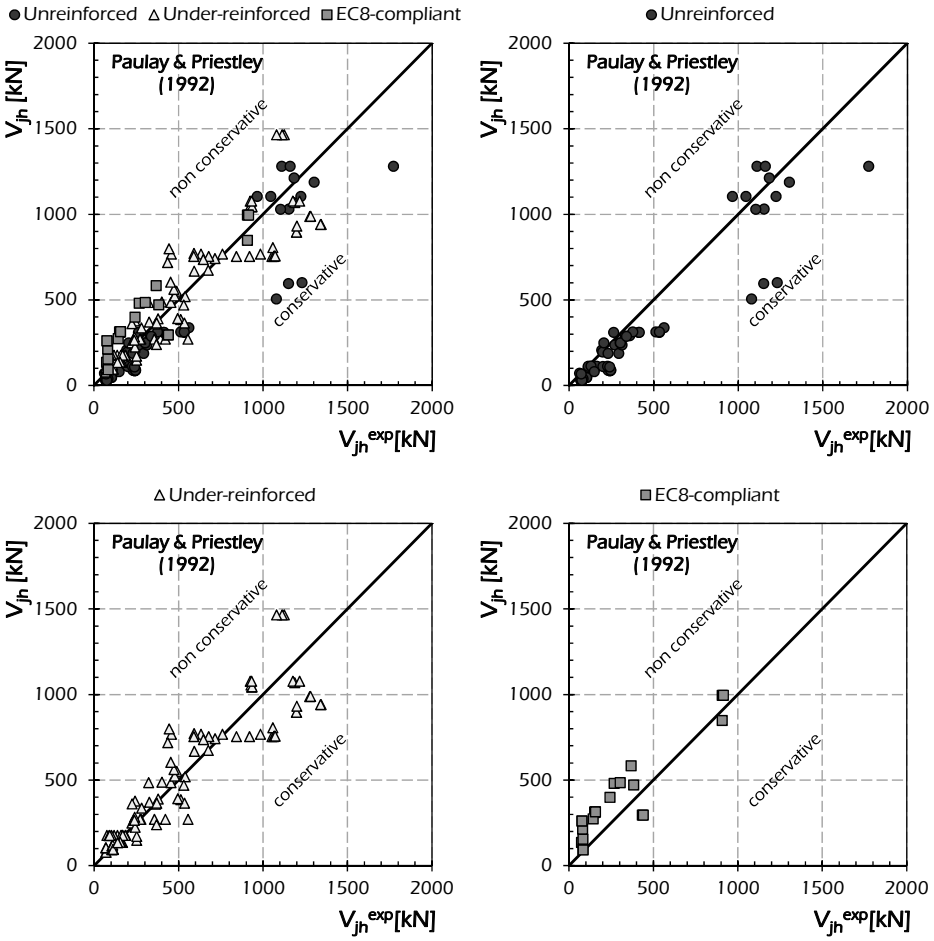

Fig. 5.12: Assessment of the model by Paulay & Priestley (1992) for exterior joints.

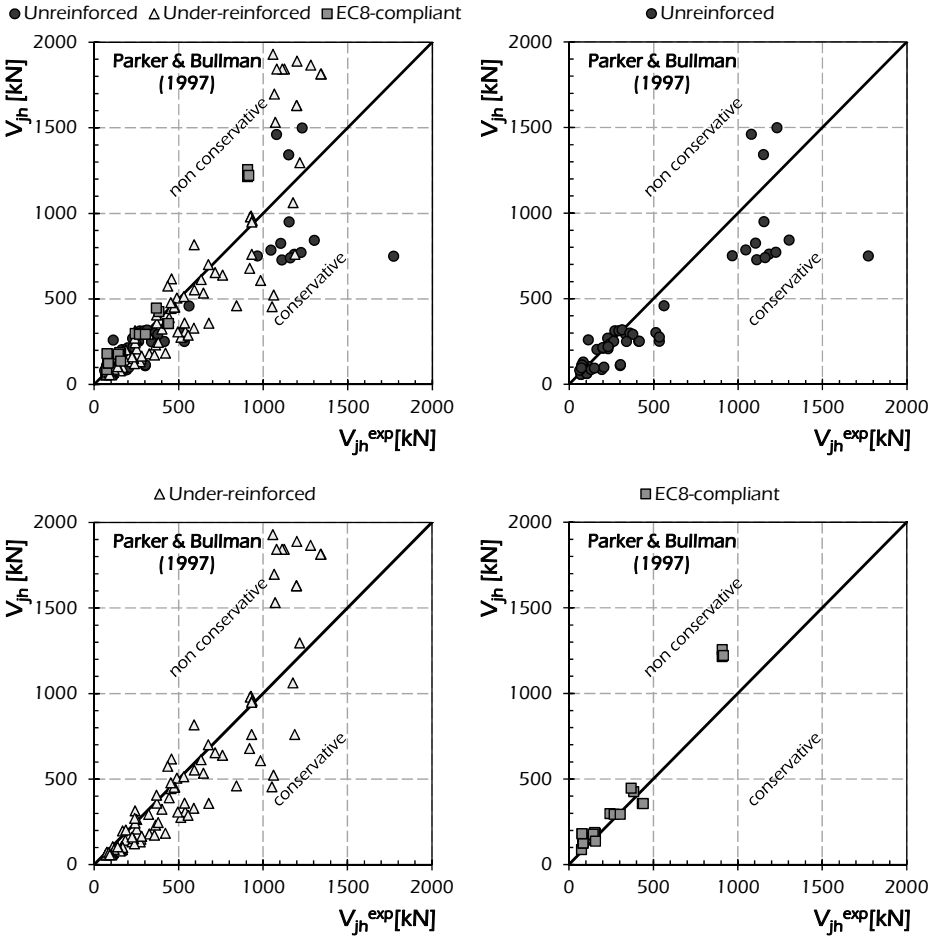

Fig. 5.13: Assessment of the model by Parker & Bullman (1997) for exterior joints.

Fig. 5.14 shows the equivalence charts for the model by Hwang & Lee (2002). The model results meanly conservative where applied on the database as a whole, providing a huge number of points below the bisector segment. In particular:

- the model by Hwang & Lee (2002) provides conservative results for unreinforced and under-reinforced exterior joints;
- a substantial equivalence between the prediction V_{jh} and the experimental evidence V_{jh}^{exp} is found about EC8-compliant joints;
- the dispersion around the 45° equivalence segment is rather low.

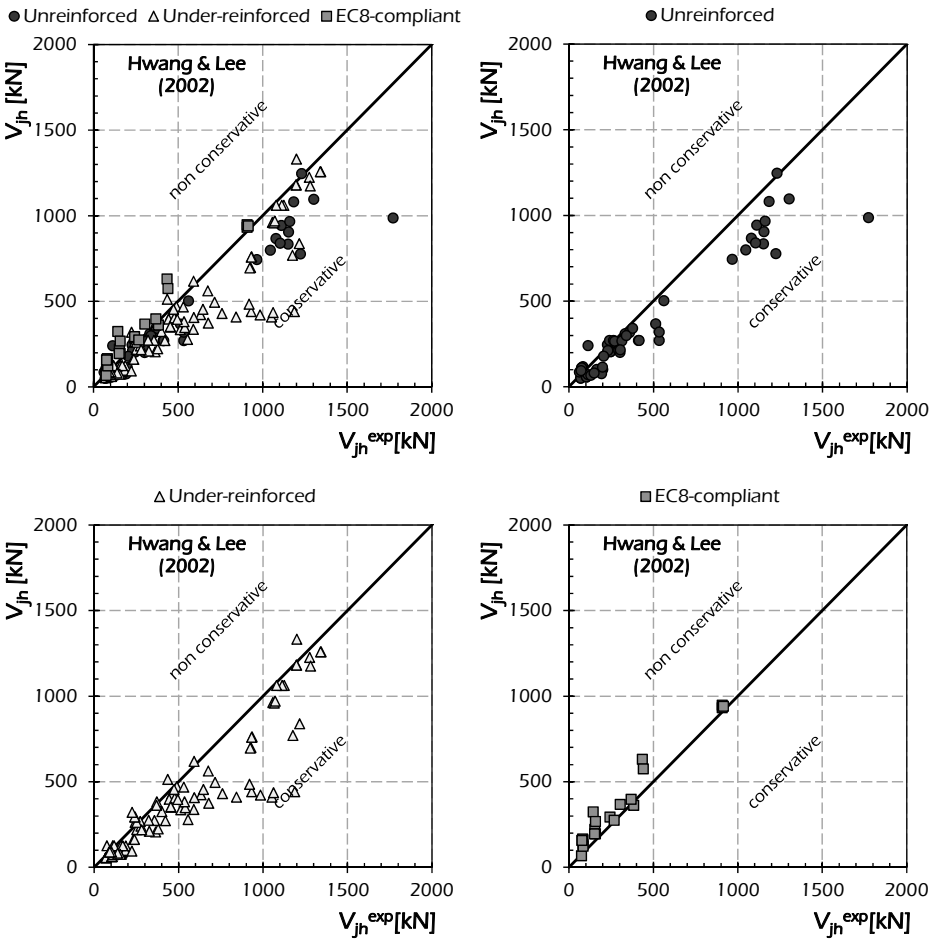

Fig. 5.14: Assessment of the model by Hwang & Lee (2002) for exterior joints.

The model developed by Parra-Montesinos & Wight (2002) is assessed in Fig. 5.15. It results generally non-conservative, as the bunch of points lies above the bisector segment. In particular:

- the theoretical shear strength V_{jh} is greater than the experimental one V_{jh}^{exp} in the case of unreinforced, under-reinforced and EC8-compliant joints;
- the dispersion of the points is very high because the model in some cases provide values of the shear strength V_{jh} equal to the experimental

one V_{jh}^{exp}, while theoretical values five times greater than the experimental shear strength V_{jh}^{exp} results in other case (Fig. 5.15).

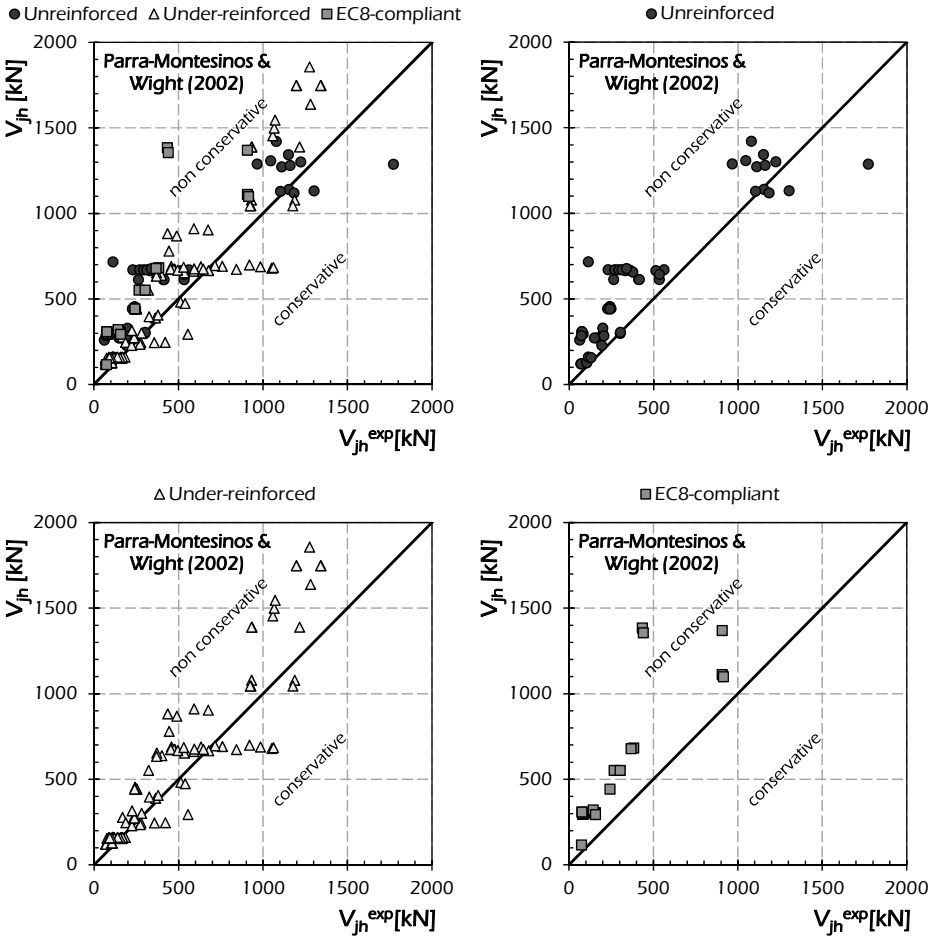

Fig. 5.15: Assessment of the model by Parra-Montesinos & Wight (2002) for exterior joints.

Fig. 5.16 reports the equivalence charts comparing the experimental shear strength V_{jh}^{exp} and the theoretical one V_{jh} evaluated by applying the model by Hegger et al. (2003). The results obtained through the analysed model are different by considering unreinforced or reinforced joints. In particular:

- a conservative trend of the model by Hegger et al. (2003) is shown for unreinforced joints characterised by high values of strength;
- a meanly equivalent relationship exists between the theoretical shear strength V_{jh} and the experimental evidence V_{jh}^{exp};
- the model is non-conservative for EC8-compliant joints.

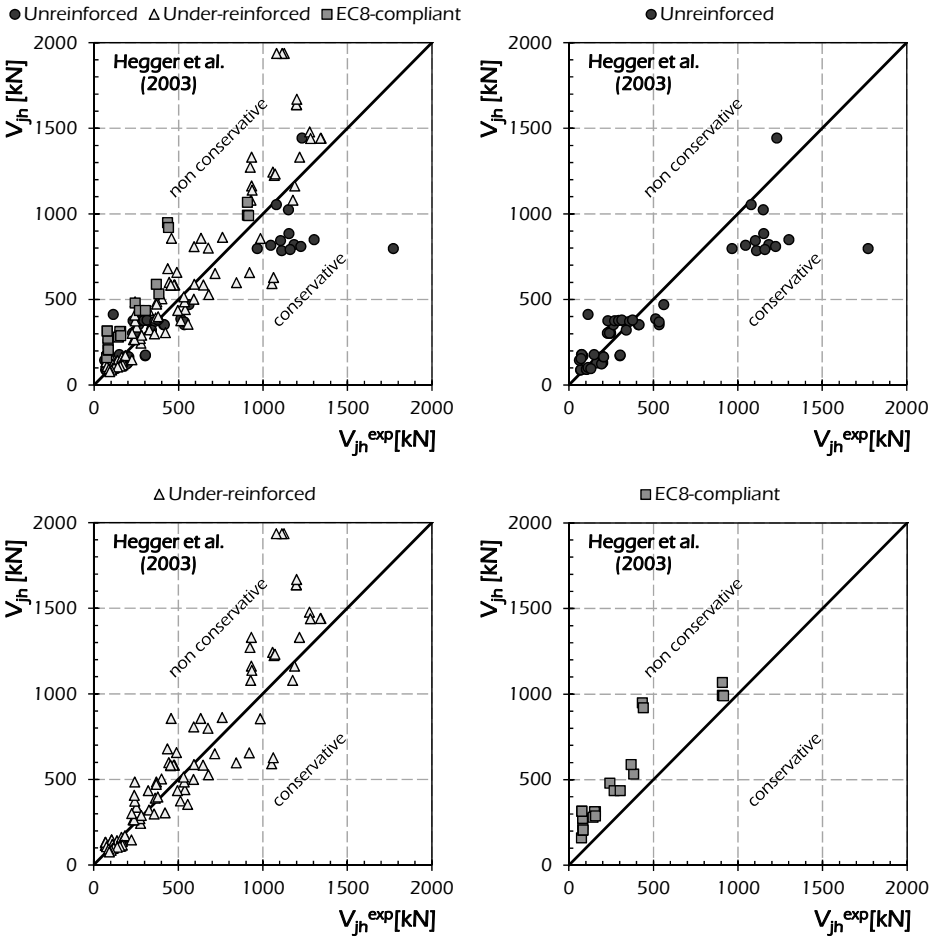

Fig. 5.16: Assessment of the model by Hegger et al. (2003) for exterior joints.

Fig. 5.17 deals with the model by Attaalla (2004). It shows general inaccuracy of this model resulting a high dispersion of the points representing

the comparison between the theoretical V_{jh} and the experimental V_{jh}^{exp} strength.

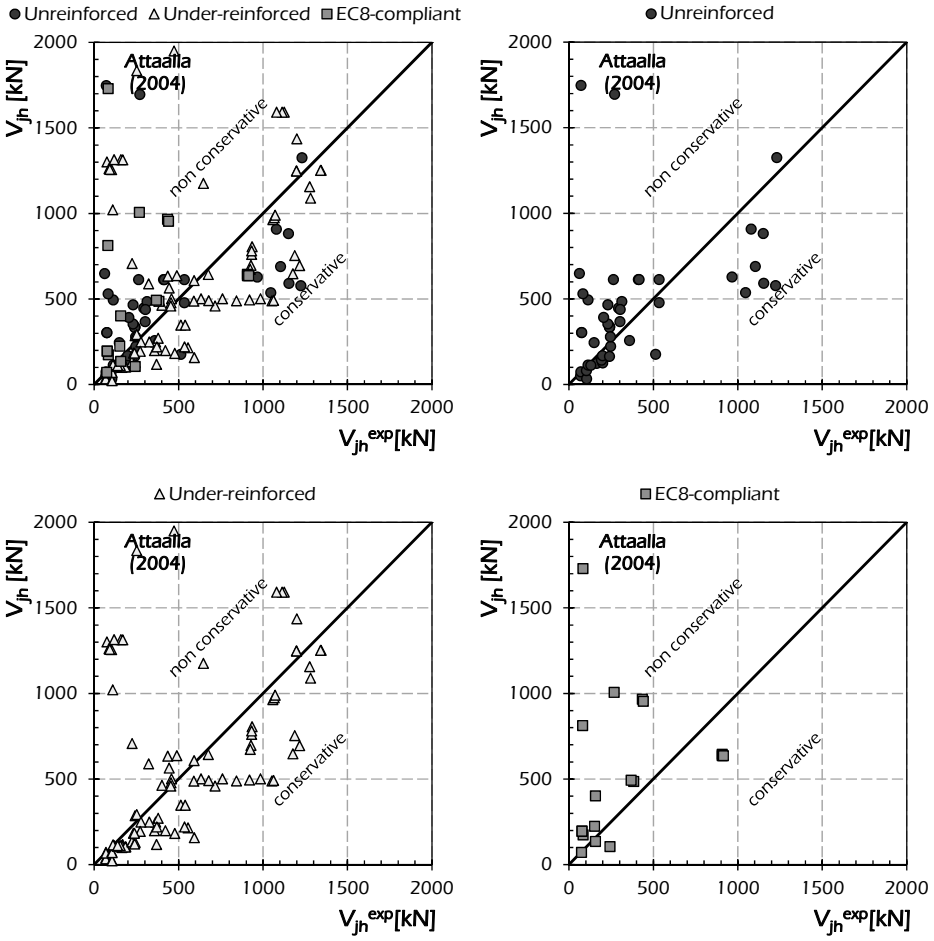

Fig. 5.17: Assessment of the model by Attaalla (2004) for exterior joints.

Fig. 5.17 shows that the model by Attaalla (2004):

- provides results not correlated with the experimental evidence;
- is characterized by high dispersion especially for low strength joint (from Fig. 5.17 can be observed great values of the theoretical shear

strength V_{jh} when the experimental shear strength V_{jh}^{exp} is less than 500 kN).

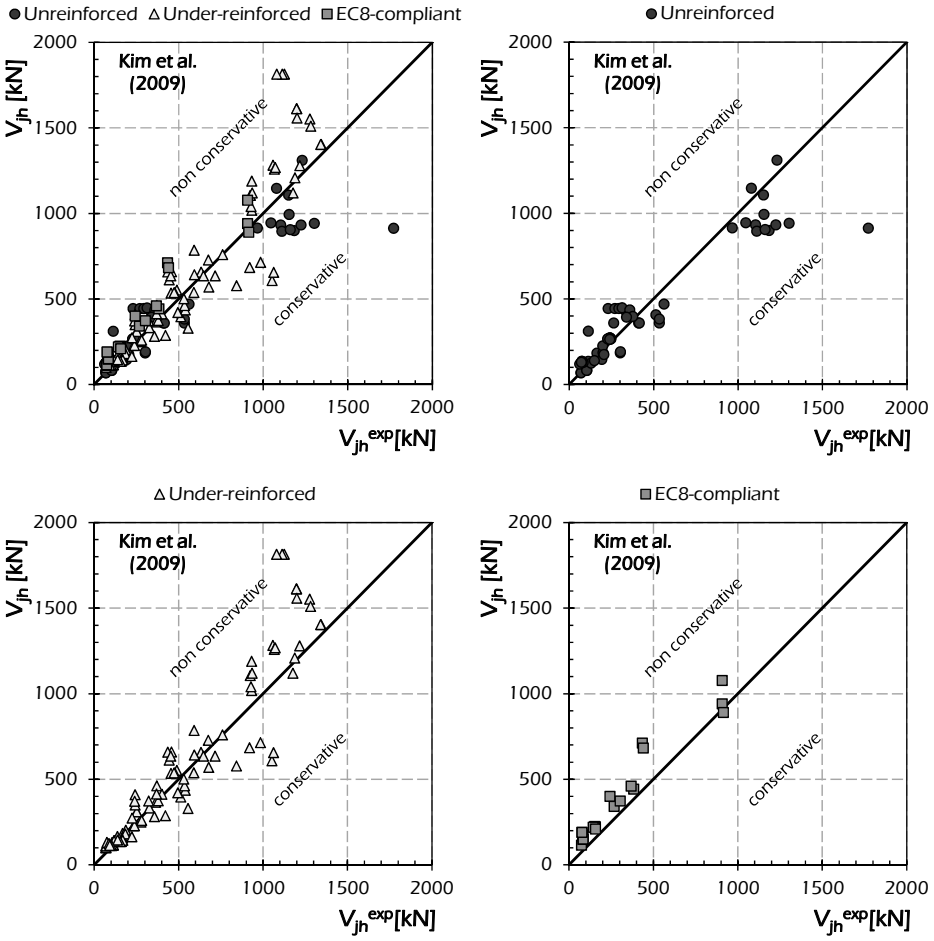

Fig. 5.18: Assessment of the model by Kim et al. (2009) for exterior joints.

Fig. 5.18 shows the comparison between the shear strength V_{jh} evaluated through the model by Kim et al. (2009) and the experimental evidence V_{jh}^{exp}. The equivalence charts reported in Fig. 5.18 show a good correlation between theoretical and experimental shear strength for unreinforced, under-reinforced and EC8-compliant joints. In particular:

- the theoretical shear strength V_{jh} is meanly equal to the experimental one V_{jh}^{exp} in the case of unreinforced low strength and under-reinforced joints;
- the model by Kim et al. (2009) results conservative by analysing the unreinforced joints characterised by high experimental shear strength V_{jh}^{exp};
- a slightly unconservative trend is achieved for EC8-compliant joints being the points located above the bisector segment.

Fig. 5.19 shows the assessing of the model by Zhang & Jirsa (1982) by reporting the equivalence chart for all the analysed specimens and the three charts take into account separately unreinforced, under-reinforced and EC8-compliant joints.

The model (Zhang & Jirsa, 1982) results non-conservative providing a huge number of comparison points above the equivalence segment. In particular:

- non-conservative relationships are observed for all the unreinforced and EC8-compliant joints;
- the theoretical shear strength V_{jh} evaluated for some under-reinforced joints is smaller than the corresponding experimental value V_{jh}^{exp}, so the model (Zhang & Jirsa, 1982) returns results around the bisector segment in the case of under-reinforced joints;
- the dispersion of the points is rather significant.

Fig. 5.20 shows the comparison between the experimental shear strength V_{jh}^{exp} and the theoretical value V_{jh} evaluated through the model by Sarsam & Phillips (1985). From the analysis of Fig. 5.20, the following considerations can be made for the model by Sarsam & Phillips (1985):

- the model results in conservative predictions for unreinforced joints, as a huge number of points lie below the bisector segment representing the equivalence between the theoretical values and the experimental evidence;
- the relationship between V_{jh}^{exp} and V_{jh} is meanly in equivalent law by considering under-reinforced joints;
- a slightly non-conservative behaviour is shown by analysing EC8-compliant exterior joints (Fig. 5.20).

The assessment of the model by Ortiz (1993) is shown in Fig. 5.21. Different results can be observed about unreinforced, under-reinforced and EC8-compliant joints:

- about exterior unreinforced joints the theoretical shear strength V_{jh} evaluated through the model by Ortiz (1993) is meanly equal to the experimental evidence;

- the model result non-conservative by considering reinforced joints providing a bunch of points above the equivalence segment.

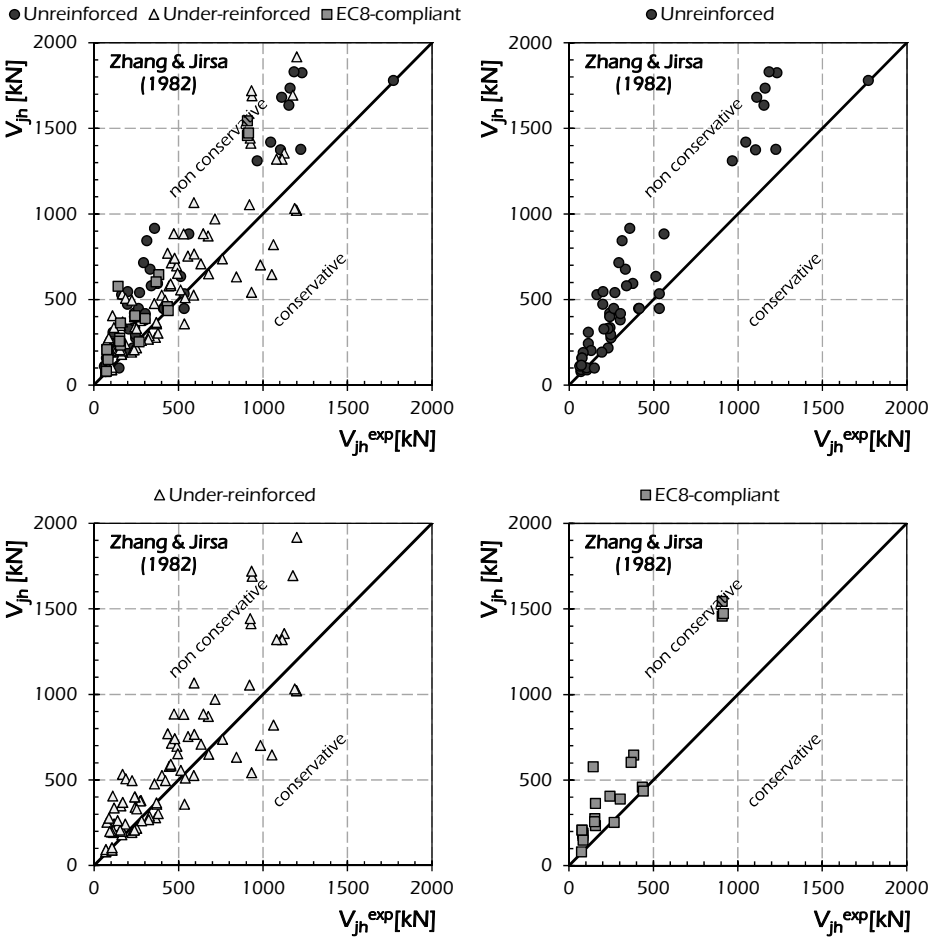

Fig. 5.19: Assessment of the model by Zhang & Jirsa (1982) for exterior joints.

In summary, the model by Ortiz (1993) provides good results for unreinforced joints (Fig. 5.21).

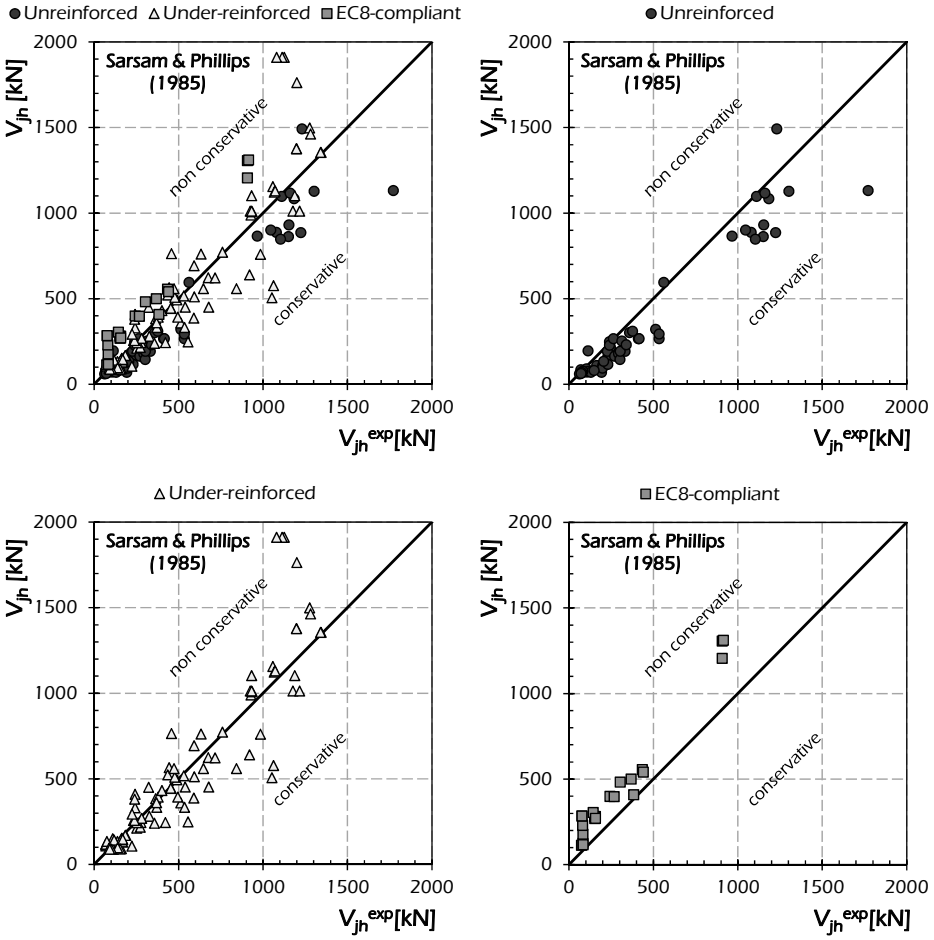

Fig. 5.20: Assessment of the model by Sarsam & Phillips (1985) for exterior joints.

Fig. 5.22 shows the comparison between the experimental shear strength V_{jh} and the theoretical one evaluated by applying the model by Scott et al. (1994). The relationship shown in Fig. 5.22 outlines good results of the analysed models; in particular:

- theoretical results close on average to the experimental ones are provided in the case of unreinforced, under-reinforced and EC8-compliant exterior joints characterised by low values of strength;
- non-conservative predictions are observed for under-reinforced and EC8-compliant joints with high strength;

- high dispersion is observed for the model by Scott et al. (1994).

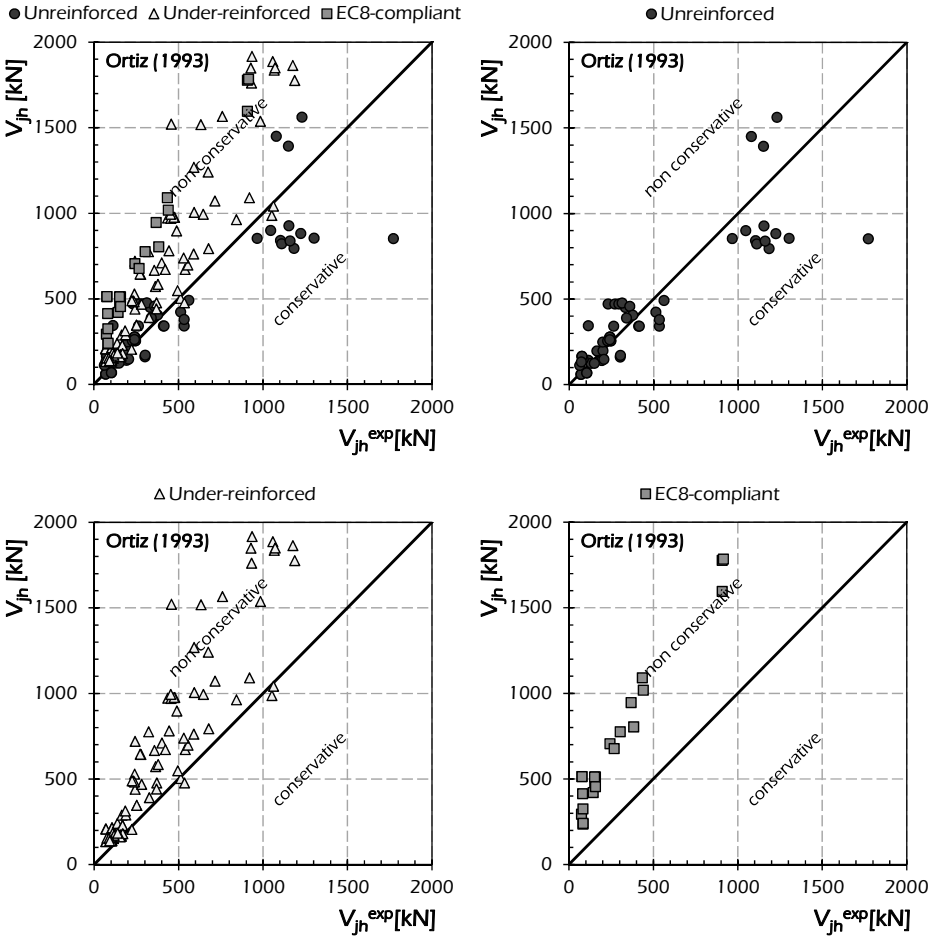

Fig. 5.21: Assessment of the model by Ortiz (1993) for exterior joints.

The equivalence charts for the model by Vollum & Newman (1999) are shown in Fig. 5.23. This model (Vollum & Newman, 1999) provides the following results:

- good correlation is shown in Fig. 5.23 between experimental and theoretical values in the cases of unreinforced and under-reinforced exterior joints;

- non-conservative predictions are obtained for EC8-compliant joints being the bunch of points located above the bisector segment.

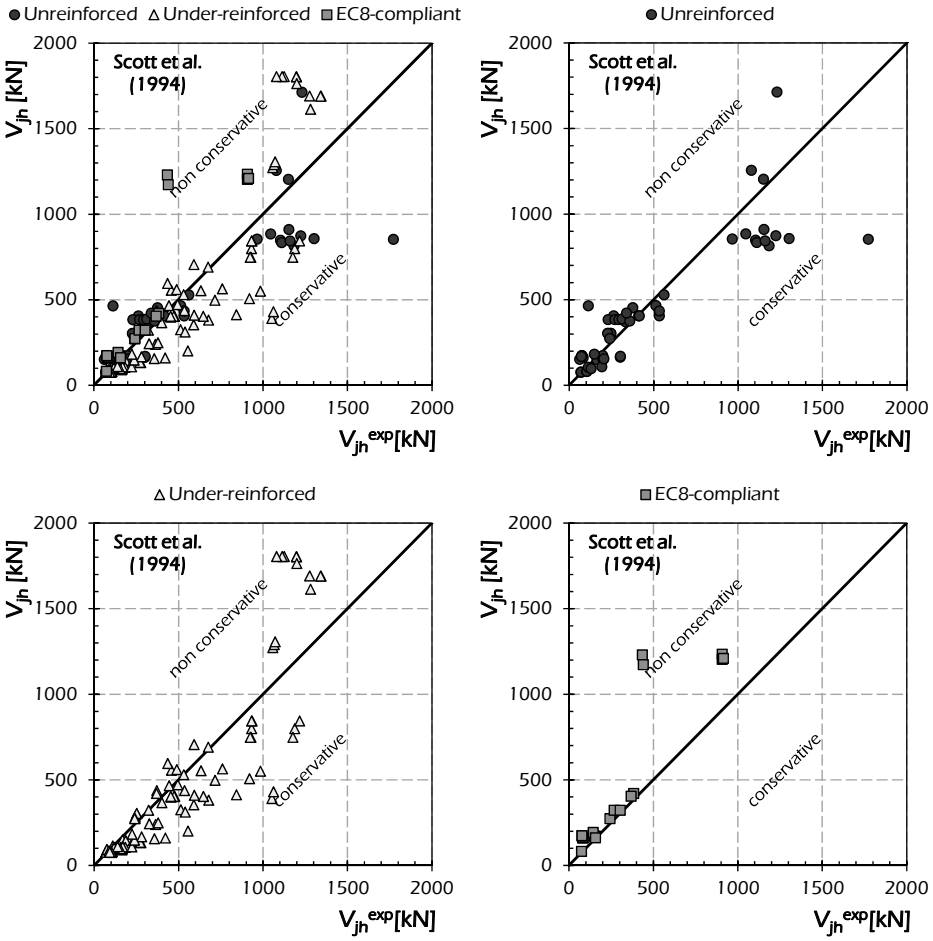

Fig. 5.22: Assessment of the model by Scott et al. (1994) for exterior joints.

Fig. 5.24 shows the equivalence charts reporting the comparison between experimental shear strengths V_{jh}^{exp} and the corresponding theoretical values V_{jh} evaluated through the model by Hwang & Lee (1999). The following considerations can be made:

- very accurate results are obtained for all the considered joints resulting the points well distributed around the equivalence segment;
- conservative predictions are achieved for unreinforced and under-reinforced joints;
- non-conservative trend results by evaluating the shear strength V_{jh} of complain joints through the model by Hwang & Lee (1999) being the bunch of points located above the 45° segment;
- low dispersion of the points around the bisector segment is observed.

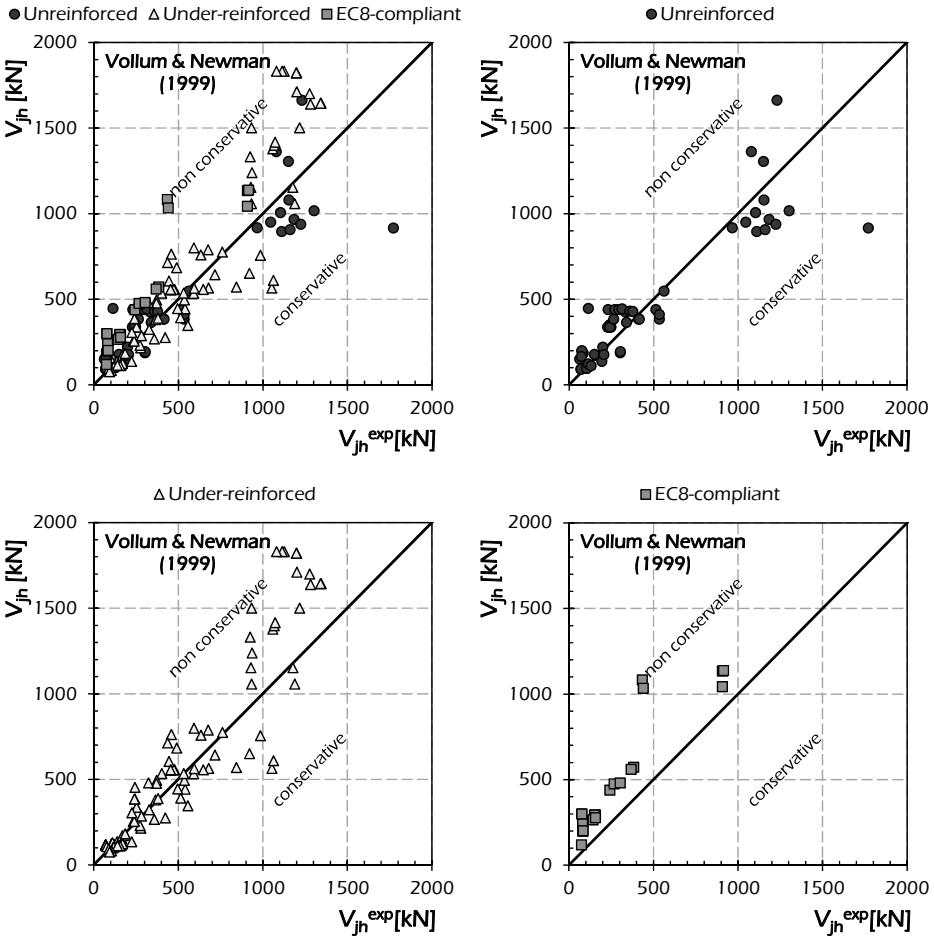

Fig. 5.23: Assessment of the model by Vollum & Newman (1999) for exterior joints.

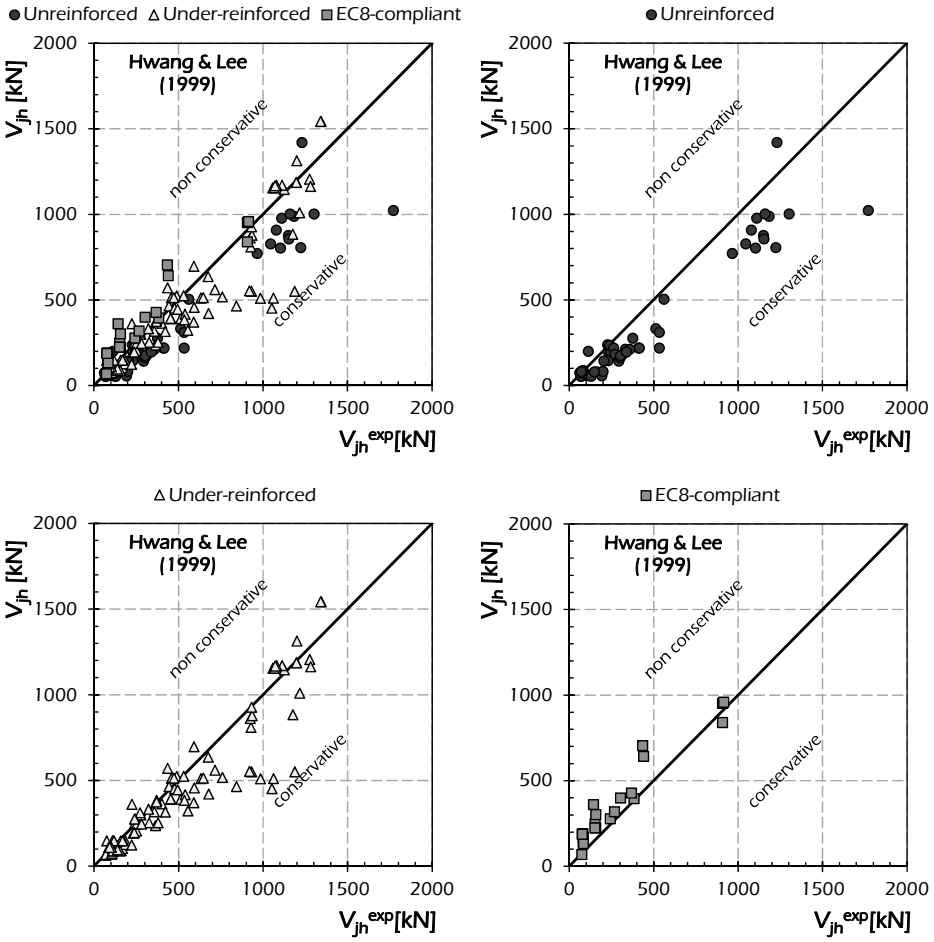

Fig. 5.24: *Assessment of the model by Hwang & Lee (1999) for exterior joints.*

The model by Bakir & Boduroglu (2002) is assessed in the equivalence charts shown in Fig. 5.25. The shear strength V_{jh} evaluated through the mentioned capacity model results in good correlation with the experimental evidence:

- a slightly conservative trend is obtained about unreinforced exterior joints;
- very good results with low dispersion of the points are shown about under-reinforced and EC8-compliant joints.

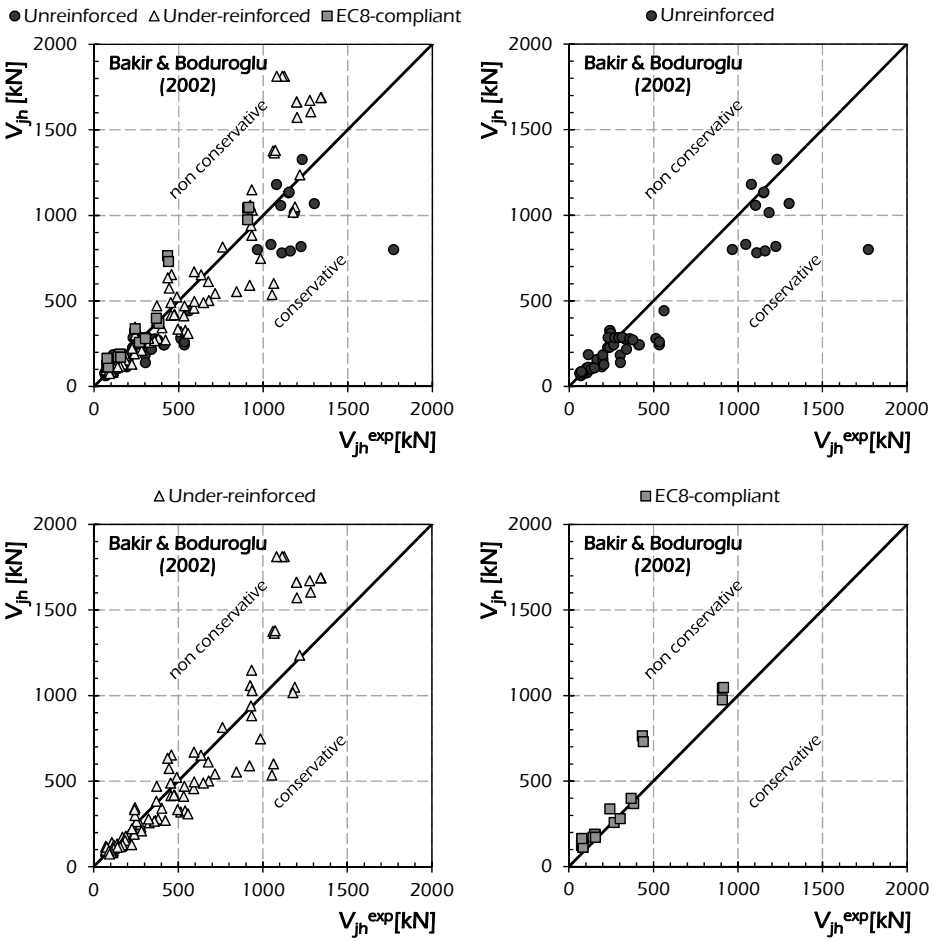

Fig. 5.25: Assessment of the model by Bakir & Boduroglu (2002) for exterior joints.

Fig. 5.26 deals with the model by Russo & Somma (2006). This model (Russo & Somma, 2006) results mainly non-conservative and characterised by high dispersion. The main following considerations are made by analysing separately unreinforced, under-reinforced and EC8-complain joints:

- the predictions resulting by the model by Russo & Somma (2006) for unreinforced joints are rather close to the experimental evidence, as a similar number of points lie above and below the bisector segment;
- the model is non-conservative for reinforced joints both EC8-compliant and under-reinforced;

- the prediction is affected by a significant scatter.

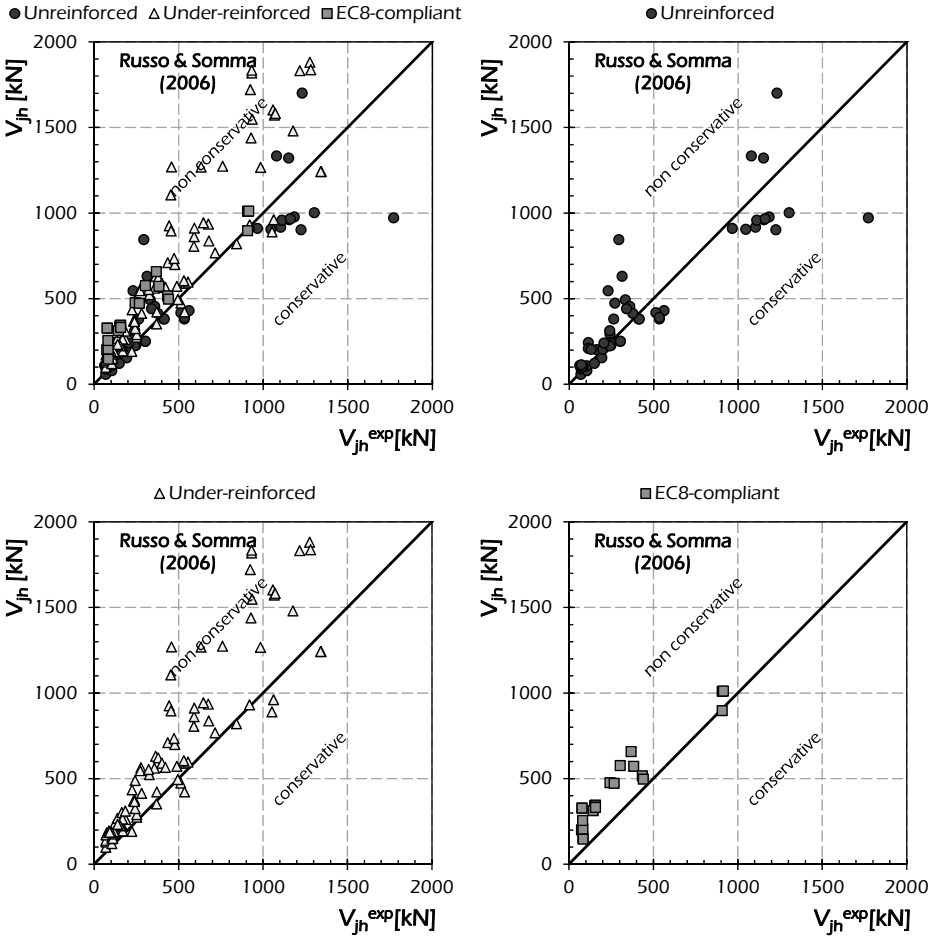

Fig. 5.26: Assessment of the model by Russo & Somma (2006) for exterior joints.

The model by Tsonos (2007) is assessed in the equivalence charts shown in Fig. 5.27. The model does not result in accurate prediction as the points are highly dispersed around the 45° equivalent segment. In particular:

- non-conservative results are made for unreinforced exterior joints characterised by low values of the experimental shear strength;

- good results are shown for under-reinforced joints characterised by low shear strength, while non-conservative results are observed in Fig. 5.27 for under-reinforced joints with high values of experimental strength;
- non-conservative results are provided by the model by Tsonos (2007) for all the considered EC8-compliant specimens.

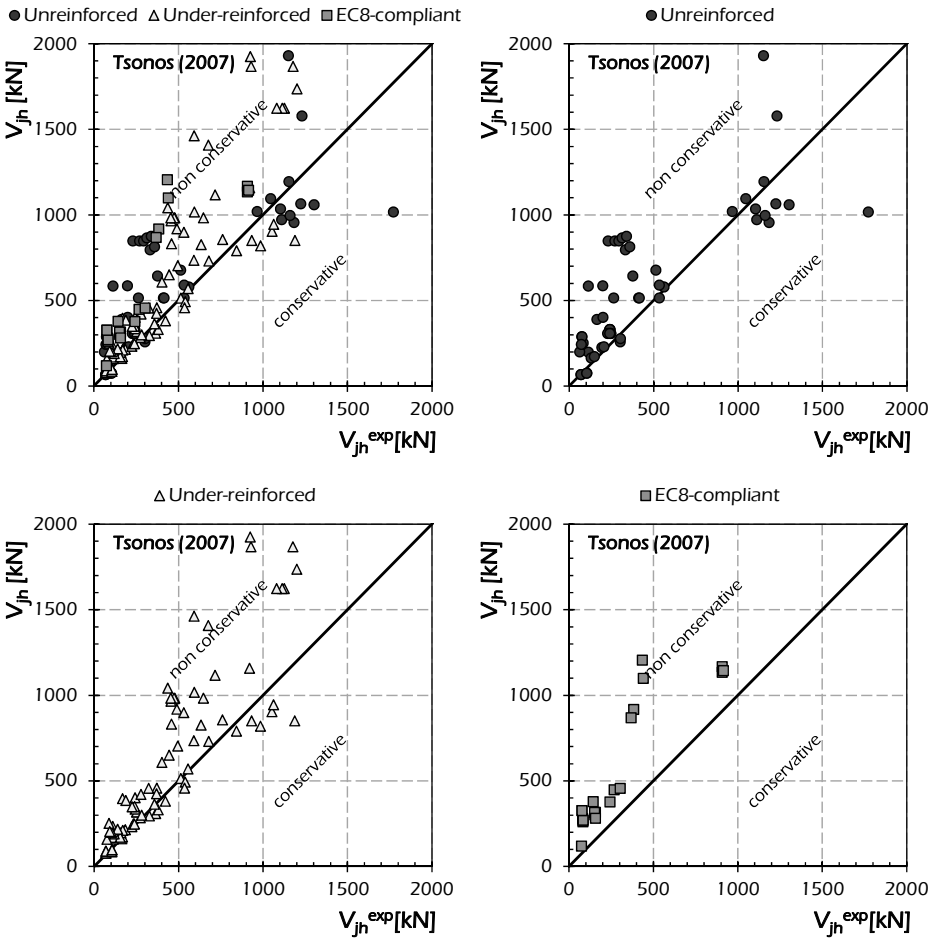

Fig. 5.27: Assessment of the model by Tsonos (2007) for exterior joints.

The last analysed model about exterior beam-to-column joints is the one by Vollum & Parker (2008). The comparison between the experimental shear

strength V_{jh}^{exp} and the theoretical values V_{jh} provided by the model by Vollum & Parker (2008) is shown in Fig. 5.28. The following behaviour is observed:

- good prediction for unreinforced and under-reinforced joints are achieved, as a huge number of points is close the bisector segment especially for joints characterised by low strength;
- non-conservative results are provided for EC8-compliant joints resulting the comparison points located above the 45° equivalence line.

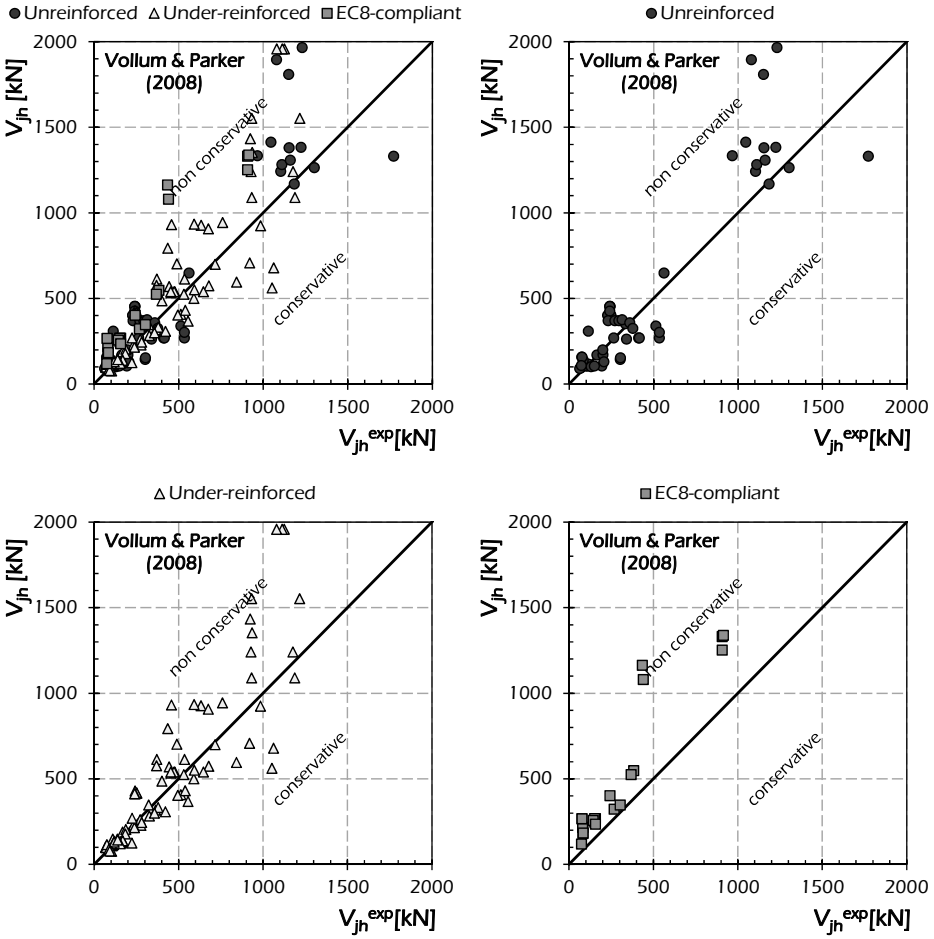

Fig. 5.28: Assessment of the model by Vollum & Parker (2008) for exterior joints.

5.1.3 Experimental Assessment of Code Formulations for Interior Joints

In the following, the shear strength V_{jh} of interior beam-to-column joints evaluated through the code formulation outlined in section 2 is compared with the corresponding experimental V_{jh}^{exp}.

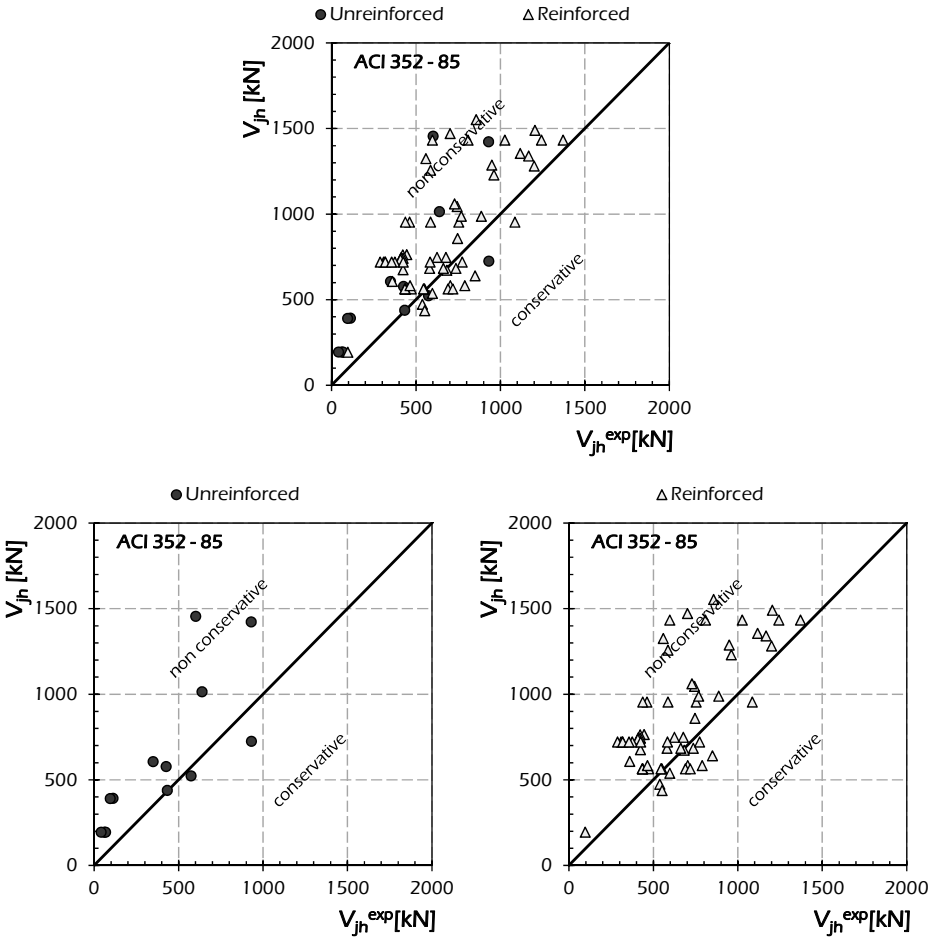

Fig. 5.29: Assessment of the ACI 352–85 (1985) for interior joints.

The comparison is made by the equivalence charts reporting, for each model, the experimental values V_{jh}^{exp} on the x-axis and the theoretical one V_{jh}

on the y-axis. Three equivalence charts are provided: the first chart includes all the collected specimens on interior joints, while the other ones deal with the results about unreinforced and reinforced interior joints, respectively. Although, the bisector segment is reported for representing the equivalence between the experimental evidence and the theoretical value, leading non-conservative or conservative relationships if the bunch of points is located above or below the equivalence 45° segment, respectively.

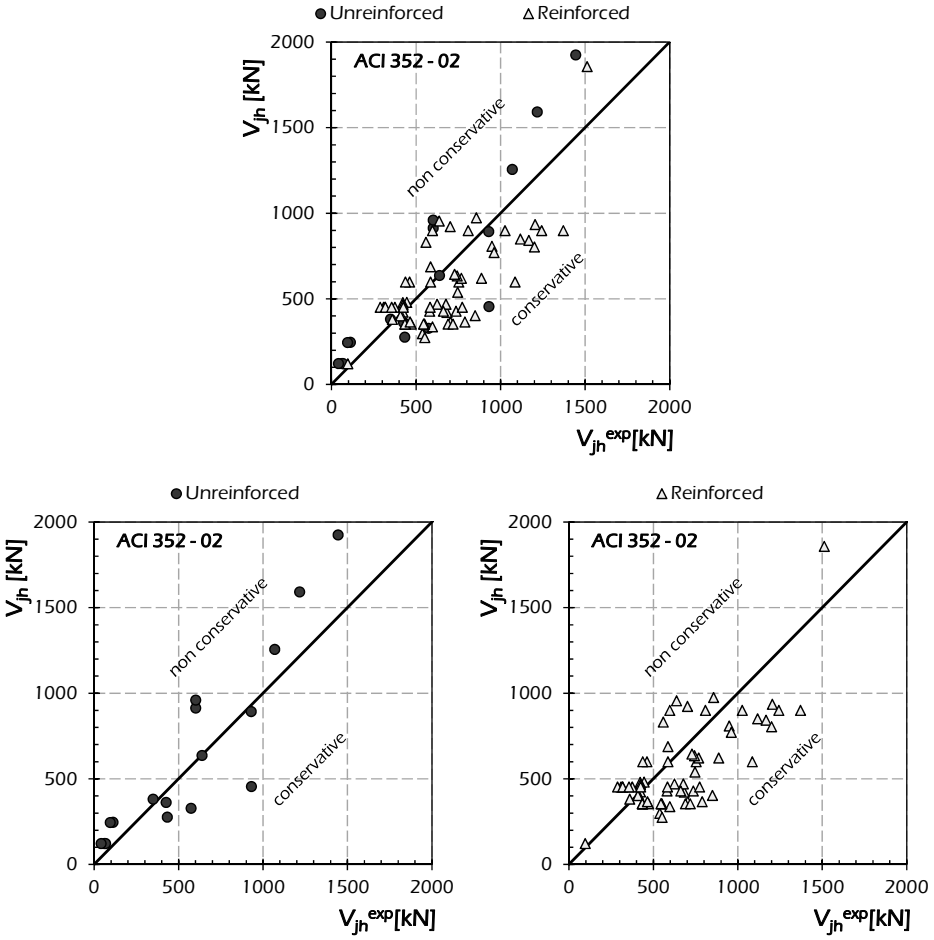

Fig. 5.30: Assessment of the ACI 352–02 (2002) for interior joints.

Fig. 5.29 shows the equivalence charts obtained by applying the formulation provided by the ACI 352 – 85 (1985). The results are mainly in non-conservative prediction, as the bunch of points is mainly located above the bisector segment. In particular:

- no differences are observed on the predictions for both unreinforced and reinforced interior joints, resulting in an often non-conservative relationship between experimental and theoretical strength;
- the predictions are generally affected by high dispersion.

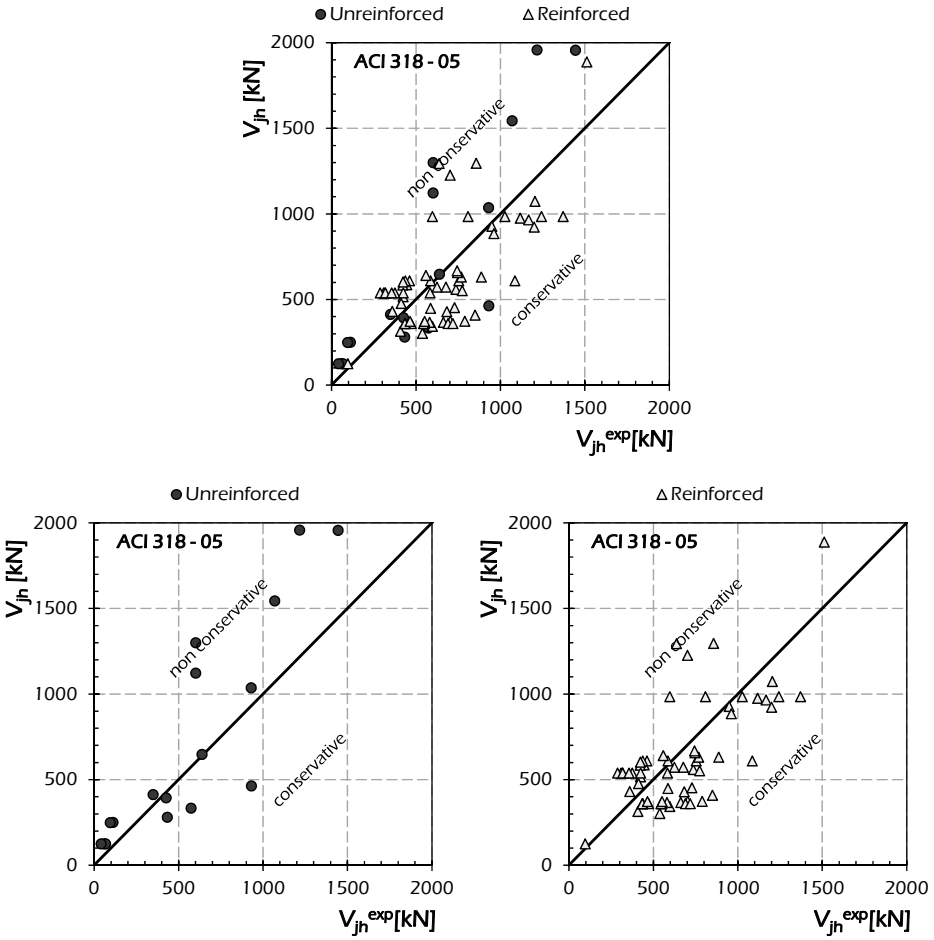

Fig. 5.31: Assessment of the ACI 318–05 (2005) for interior joints.

The last version of ACI 352 (ACI 352-02, 2002) generally leads to non-accurate results than the old version (ACI 352–85, 1985). The following considerations can be made by analysing Fig. 5.30:

- on average, the ACI 352–02 (2002) provides accurate results for unreinforced interior joints;
- the relationship between experimental evidence V_{jh}^{exp} and evaluated strength V_{jh} is meanly conservative for reinforced joints;
- a dispersion of the points lower than the one observed for the old version of the code (ACI 352–85, 1985) is shown.

The results provided by the ACI 318–05 (2005) are compared with the experimental evidence in the equivalence charts reported in Fig. 5.31.

Similar observations can be drawn out from Fig. 5.30 and Fig. 5.29. However:

- on average, the relationship between code results and experimental evidence for unreinforced interior joints is equivalent by specialising a non-conservative law for high strength unreinforced connections;
- a slightly conservative trend can be observed for reinforced interior beam-to-column joints.

The formulations provided by the Japanese codes, AIJ 1990 (1990) and AIJ 1999 (1999), for interior joints are analysed in Fig. 5.32 and Fig. 5.33, respectively.

The AIJ 1990 (1990) provides:

- non-conservative results for unreinforced interior joints;
- shear strength values generally equivalent to the experimental evidence in the case of reinforced joints;
- the prediction is generally affected by low dispersion of the comparison points around the bisector segment.

Fig. 5.33 shows the results of the assessment of the AIJ 1999 (1999) formulation. The accuracy of the last Japanese code with respect to the older one (AIJ 1990) is shown by resulting:

- a generally equivalent relationship between the experimental shear strength V_{jh}^{exp} and the theoretical value V_{jh} evaluated through the AIJ 1999 (1999) for unreinforced interior joints;
- a concentration of the bunch of points representing the comparison around the bisector segment for reinforced joints;
- low dispersion for both unreinforced and reinforced joints.

However, the results provided by the AIJ 1999 (1999) are more accurate than the ones obtained by applying the AIJ 1990 (1990).

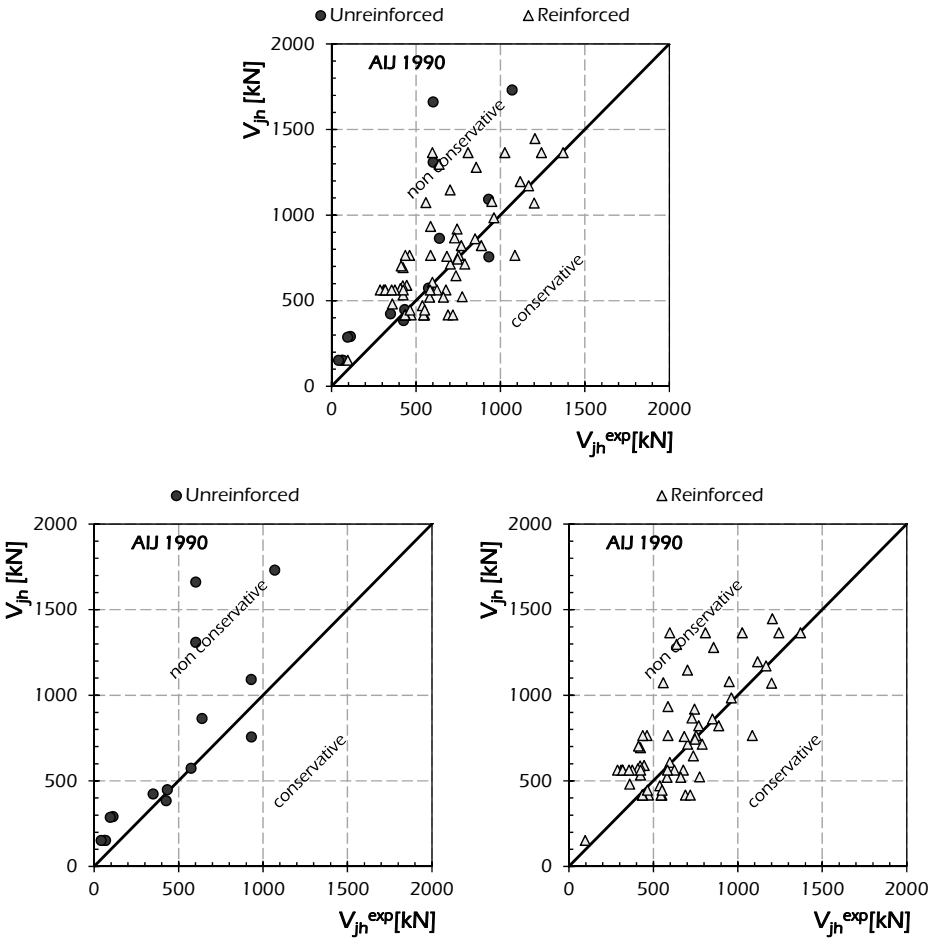

Fig. 5.32: *Assessment of the AIJ 1990 (1990) for interior joints.*

Fig. 5.34 reports the equivalence charts obtained for the NZS 3101 (1995). The comparison shows the very conservative results provided by the code formulation with respect to the shear strength of exterior beam-to-column joints. In particular:

- the applied model does not take into account unreinforced joints providing a shear strength V_{jh} equal to zero if there are not stirrups into the panel zone;
- the values of theoretical predictions V_{jh} are often smaller than the corresponding experimental ones.

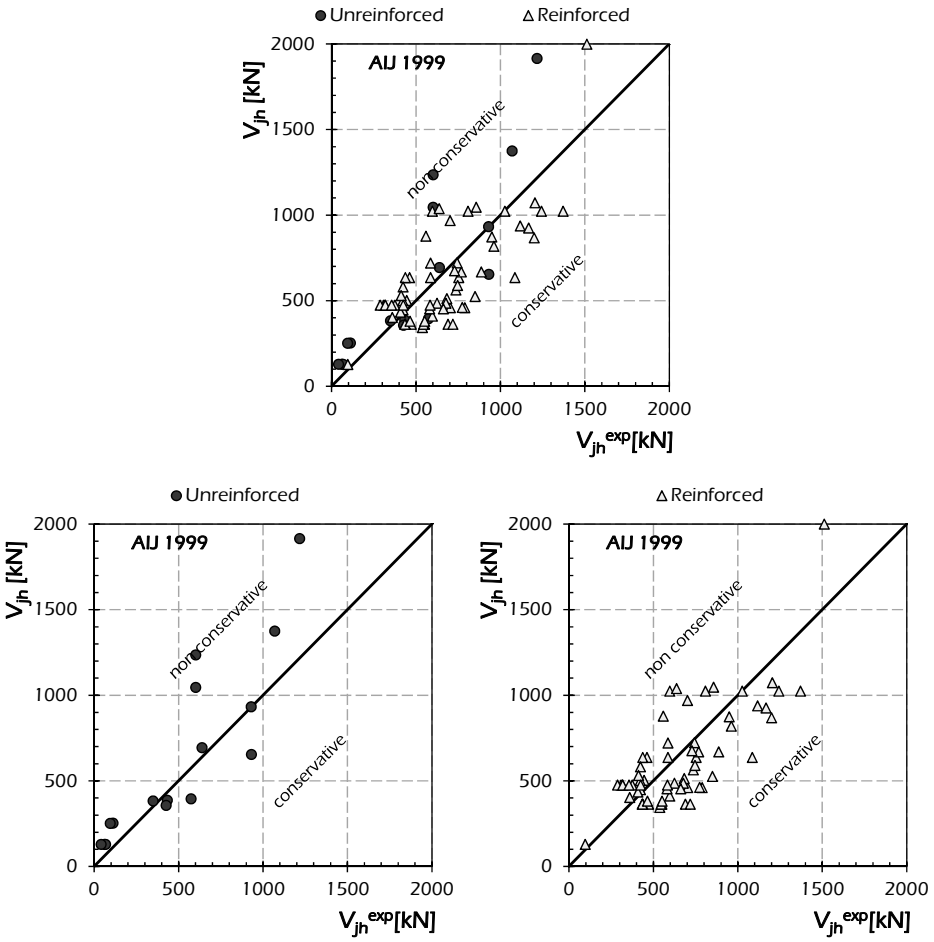

Fig. 5.33: *Assessment of the AIJ 1999 (1999) for interior joints.*

The formulation provided by both the FEMA 273 (1997) and FEMA 356 (2000) is assessed in Fig. 5.35 for interior reinforced concrete beam-to-column joints.

For each specimen, the comparison between the experimental evidence V_{jh}^{exp} and the shear strength V_{jh} evaluated according to the code formulation (FEMA 273, 1997 and FEMA 356, 2000) is carried out through the equivalence charts. The accuracy of the code in evaluating the shear strength of interior column is shown resulting in the bunch of points close to the bisector segment reported on each graph as reference of the equivalence law. The following

evidence is observed by specialising the considerations for unreinforced and reinforced joints:

- generally good results are provided by the FEMA 273 (1997) and FEMA 356 (2000) for unreinforced joints;
- a slightly conservative trend emerges from Fig. 5.35, as a lot of points lie below the equivalence segment;
- almost equal dispersion is observed for both unreinforced and reinforced interior joints.

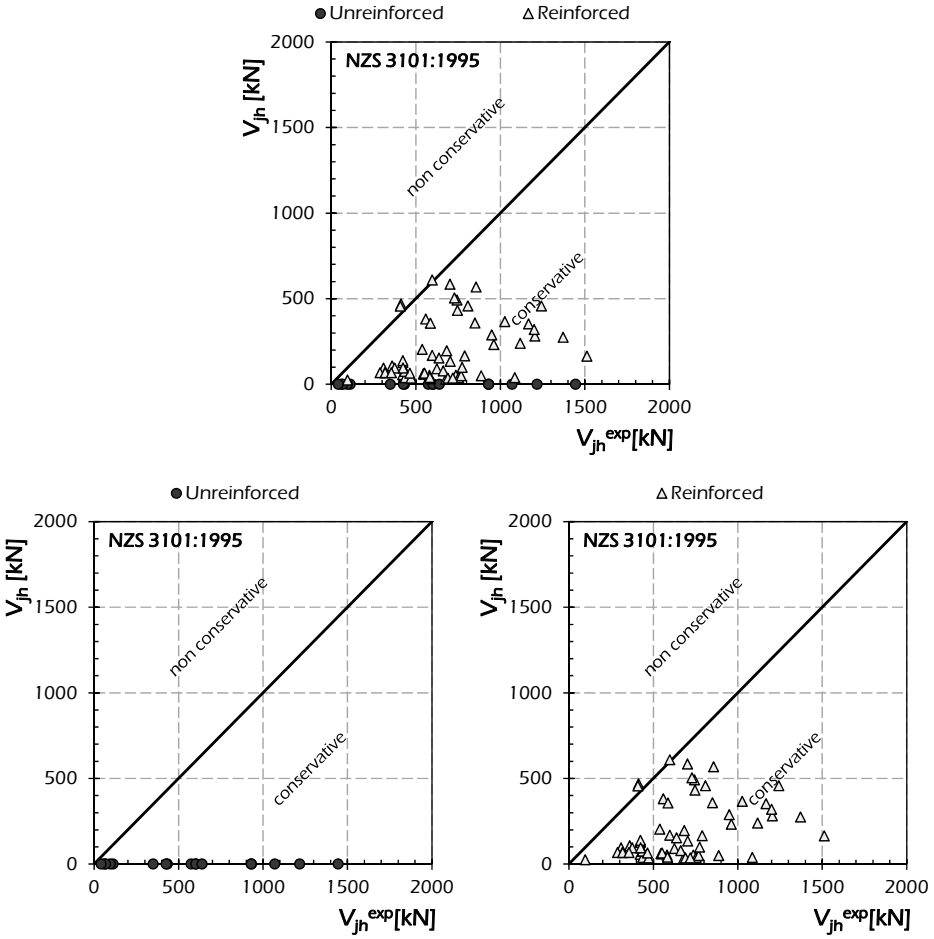

Fig. 5.34: Assessment of the NZS 3101 (1995) for interior joints.

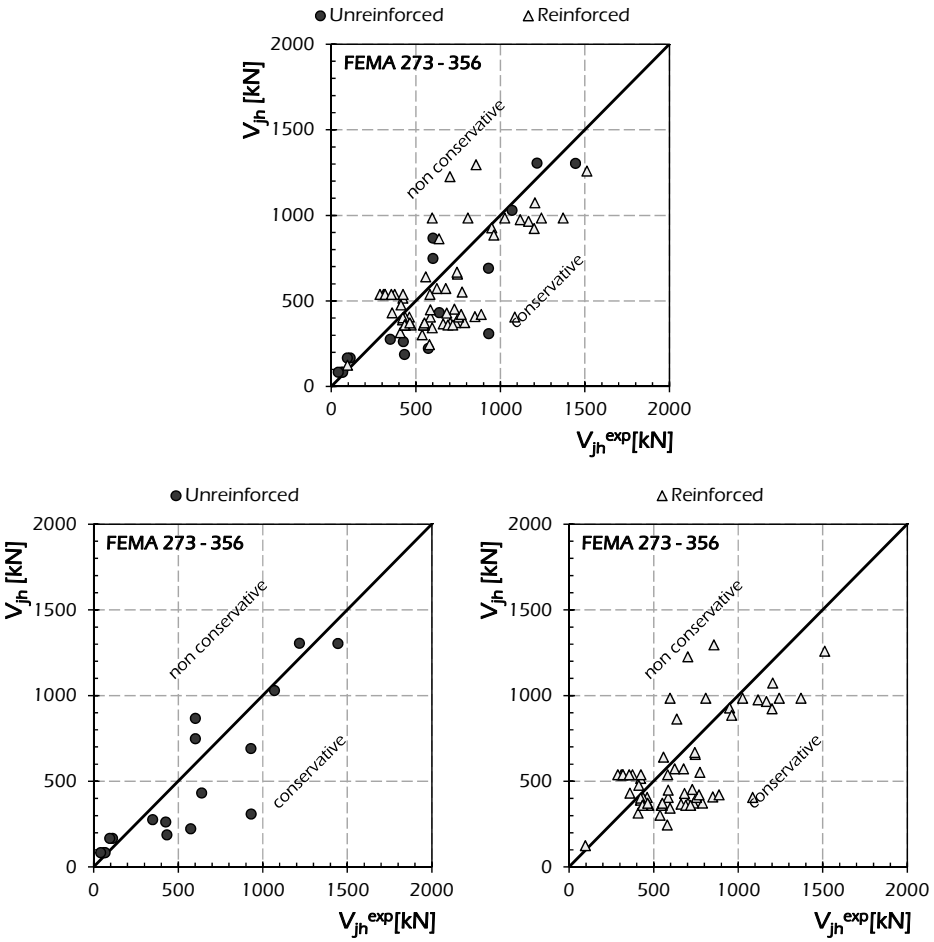

Fig. 5.35: Assessment of the FEMA 273 (1997) – FEMA 356 (2000) for interior joints.

Fig. 5.36 shows the comparison between the experimental shear strength V_{jh}^{exp} of interior joints and the theoretical capacity V_{jh} evaluated by applying the formulation suggested in Eurocode 8 (EN 1995-1, 1995). The equivalence charts reporting the bunch of comparison points and the bisector segment as a reference show the generally non-conservative trend of the Eurocode 8 (EN 1995-1, 1995) formulation. In particular:

- non-conservative results are provided for all the unreinforced interior joints, resulting the bunch of points above the equivalence 45° segment;

- often non-conservative relationship between experimental V_{jh}^{exp} and theoretical V_{jh} values are shown in Fig. 5.36 for interior reinforced joints, as a lot of comparison points lie above the bisector segment and a few ones above.

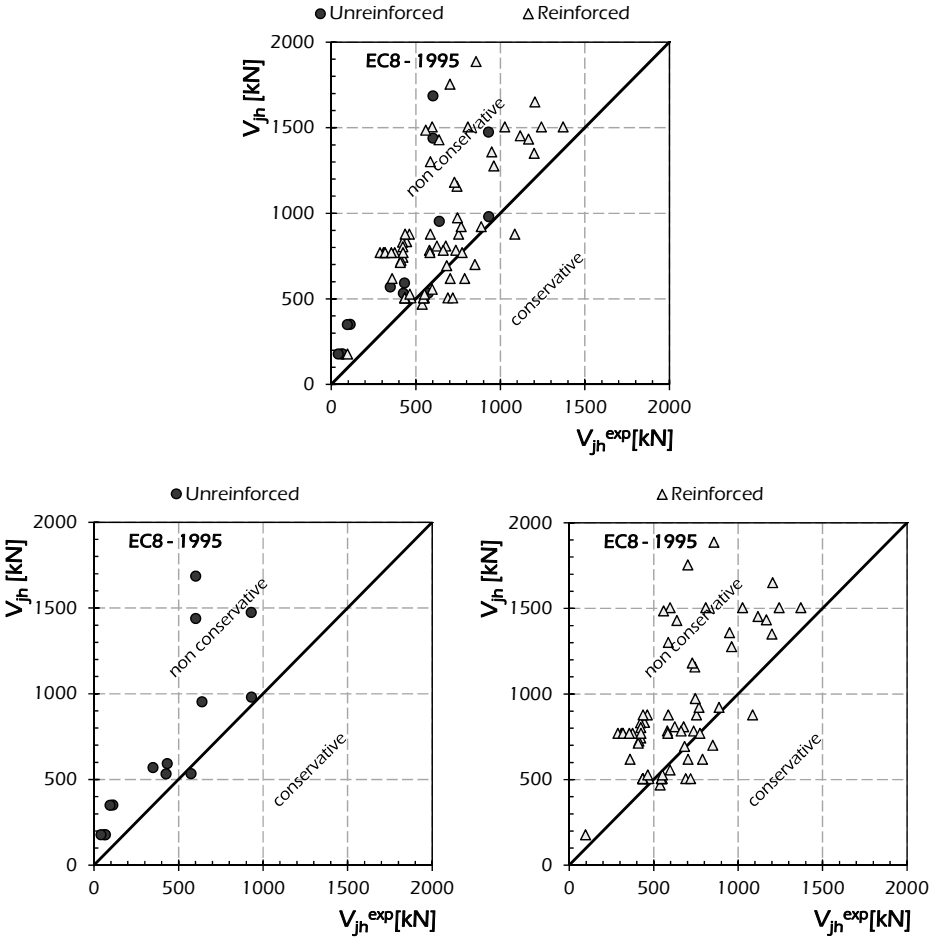

Fig. 5.36: Assessment of the Eurocode 8 (EN 1995-1, 1995) for interior joints.

The Eurocode 8 (EN 1998-3, 2005) providing the same formulation recommended by the NTC (2008) for joints of new RC structures is assessed in Fig. 5.37.

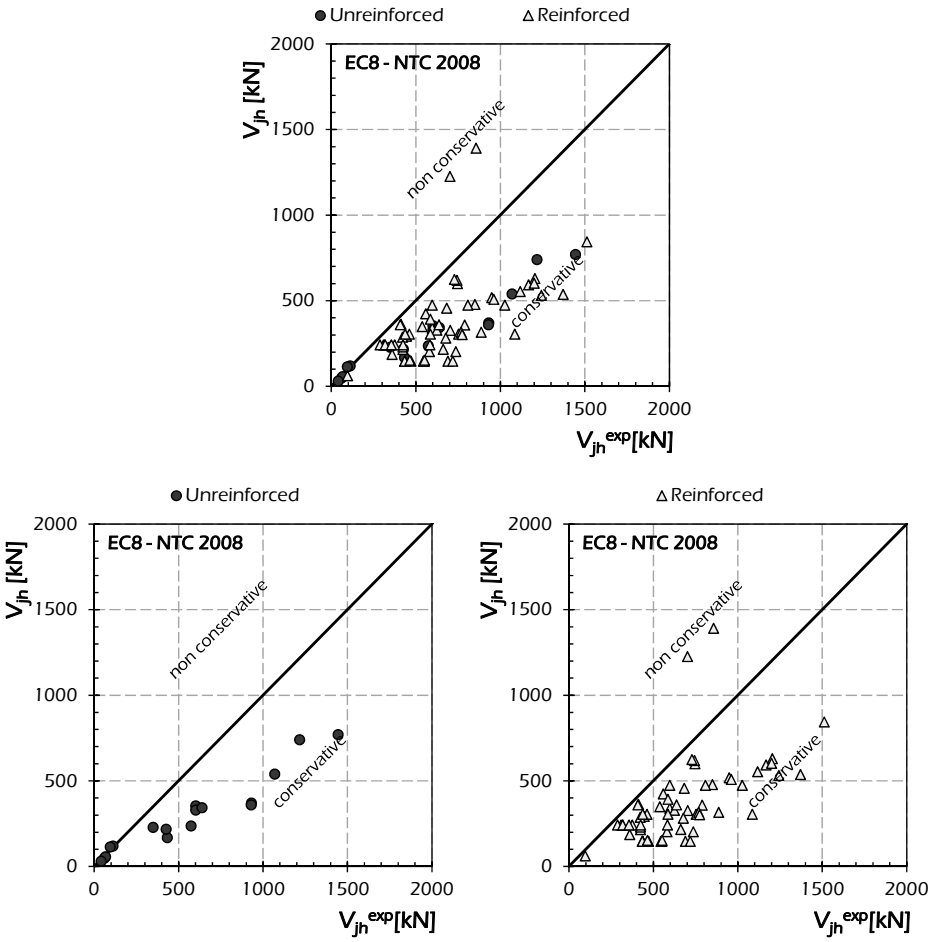

Fig. 5.37: *Assessment of the Eurocode 8 (EN 1998-3, 2005) and NTC (2008) for interior joints.*

The analysed formulation (Fig. 5.37) provides very conservative results for both unreinforced and reinforced interior joints:

- the results provided by Eurocode 8 (EN 1998-3, 2005) and NTC (2008) for unreinforced interior joints lie below the bisector segment;
- the comparison points for reinforced joints lie in the conservative region of the chart, except for two specimens whose prediction is higher than the corresponding experimental observation. In particular, those specimens are characterised by high axial load in the top column.

Substantially, the latest version of Eurocode 8 (EN 1998-3, 2005) is more accurate than the older one (EN 1995-1, 1995) resulting conservative for both unreinforced and reinforced interior joints.

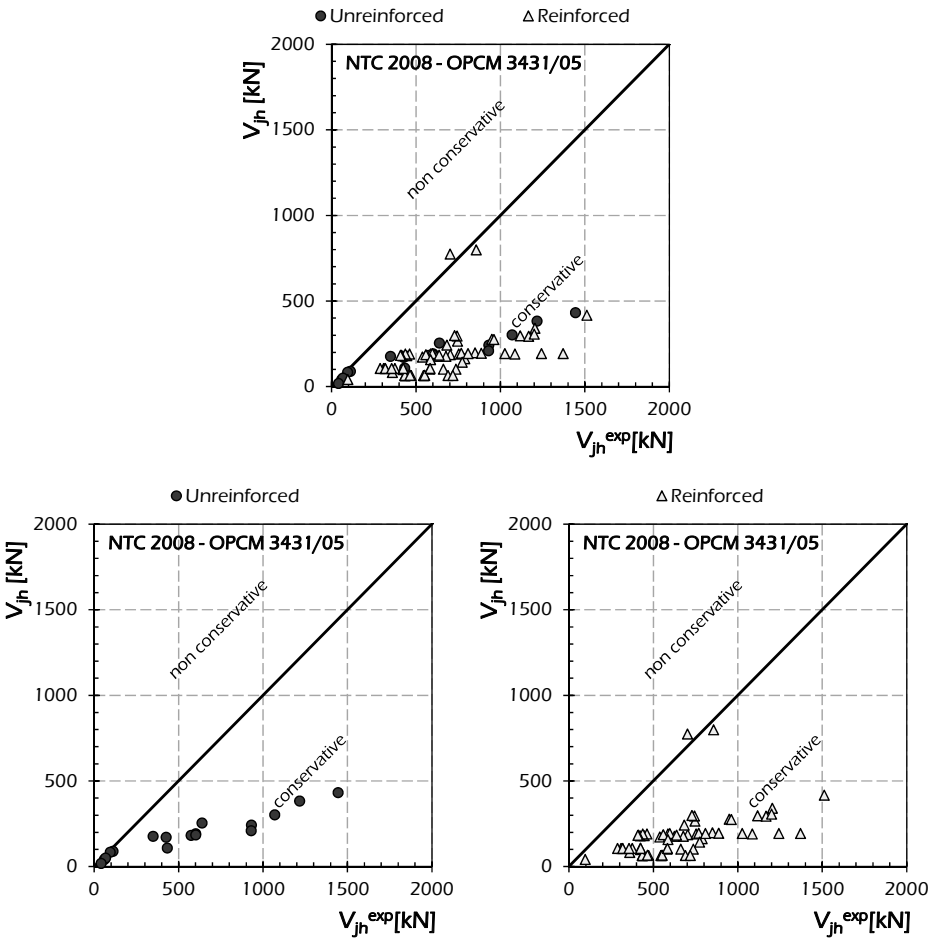

Fig. 5.38: Assessment of the NTC (2008) and OPCM 3431/05 (2005) for interior joints.

Finally, the comparison between experimental evidence V_{jh}^{exp} and theoretical shear strength V_{jh} evaluated through the NTC (2008) and the OPCM 3431/05 (2005) is shown in Fig. 5.38. The equivalence charts show:

- very conservative results for both unreinforced and reinforced interior joints;
- good predictive capacity only for the same two specimens characterised by high axial load in the top column.

However, by comparing Fig. 5.37 reporting the assessment of NTC (2008) formulation and Fig. 5.38 showing the equivalence charts for the formulation provided by NTC (2008) and OPCM 3431/05 (2005) for joints in existing structures, a more conservative trend is shown for the last one.

5.1.4 Experimental Assessment of Capacity Models Available in the Literature for Interior Joints

The comparison between the experimental shear strength V_{jh}^{exp} and the corresponding theoretical prediction V_{jh} evaluated through the capacity models available in the scientific literature and outlined in section 2 are reported in the following.

Fig. 5.39 shows the equivalence charts comparing the theoretical shear strength V_{jh} evaluated by applying the model by Pantazopoulo & Bonacci (1992) and the experimental evidence V_{jh} for both unreinforced and reinforced interior joints. The model (Pantazopoulo & Bonacci, 1992) results in non-conservative predictions as almost all points lie above the equivalent segment. The two equivalence charts dealing with the two cases of unreinforced and reinforced joints confirm that this trend characterises both kinds of joints (Fig. 5.39).

Fig. 5.40 shows the comparison between the prediction V_{jh} based on the model by Paulay & Priestley (1992) and the experimental shear strength V_{jh}^{exp}. The model leads to conservative predictions and:

- the points representing unreinforced joints are gathered below the bisector segment;
- the points representing reinforced specimens lie also below the bisector segment, but a less conservative trend can be observed.

Fig. 5.41 shows the equivalence charts representing the performance of the model by Parker & Bullman (1997). The following considerations can be drawn out:

- the prediction for unreinforced joints are characterised by high dispersion around the 45° equivalence segment resulting generally conservative;
- the prediction for reinforced joints is affected by high dispersion;

- the relationship between V_{jh} and V_{jh}^{exp} for reinforced interior beam-to-column joints results less conservative than the one observed for unreinforced connections. In particular, the majority of points are located below the bisector segment except for some reinforced joints which result in non-conservative law.

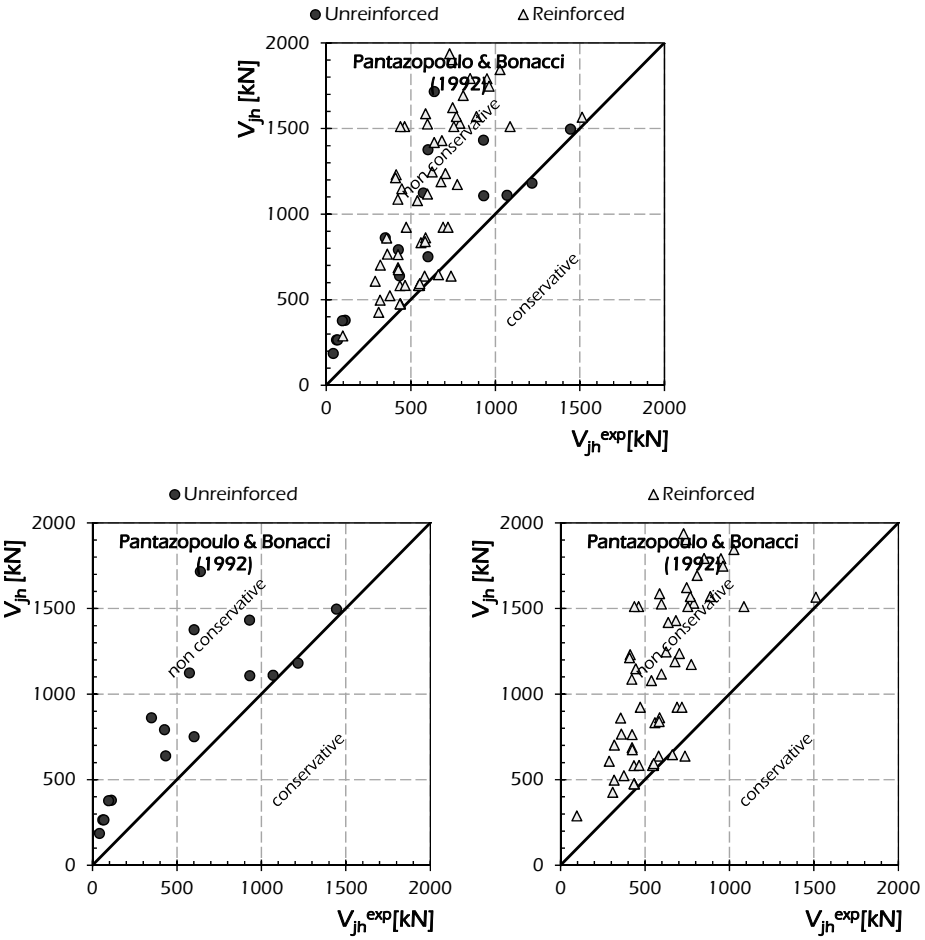

Fig. 5.39: Assessment of the model by Pantazopoulo & Bonacci (1992) for interior joints.

Fig. 5.42 shows the equivalence charts provided for the model by Hwang & Lee (2002):

- the model leads to conservative results for unreinforced joints;
- a substantially conservative trend is found for reinforced joints;
- the dispersion is rather limited.

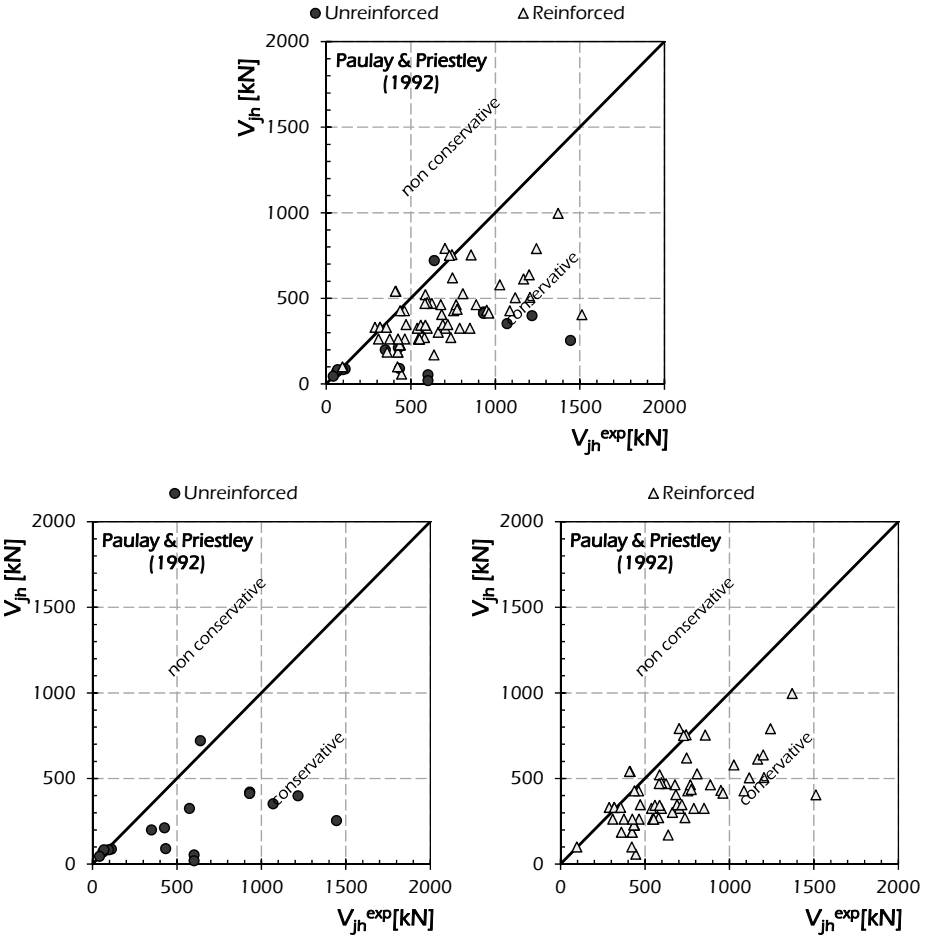

Fig. 5.40: Assessment of the model by Paulay & Priestley (1992) for interior joints.

The model developed by Parra-Montesinos & Wight (2002) is assessed in Fig. 5.43. The model results generally in accurate predictions, as the bunch of points is close to the bisector segment. In particular:

- the theoretical shear strength V_{jh} is generally equal to the experimental one V_{jh}^{exp} in the case of unreinforced joints;
- a slightly conservative relationship between V_{jh}^{exp} and V_{jh} is achieved for reinforced interior beam-to-column joints;
- the dispersion affecting the theoretical prediction is rather high.

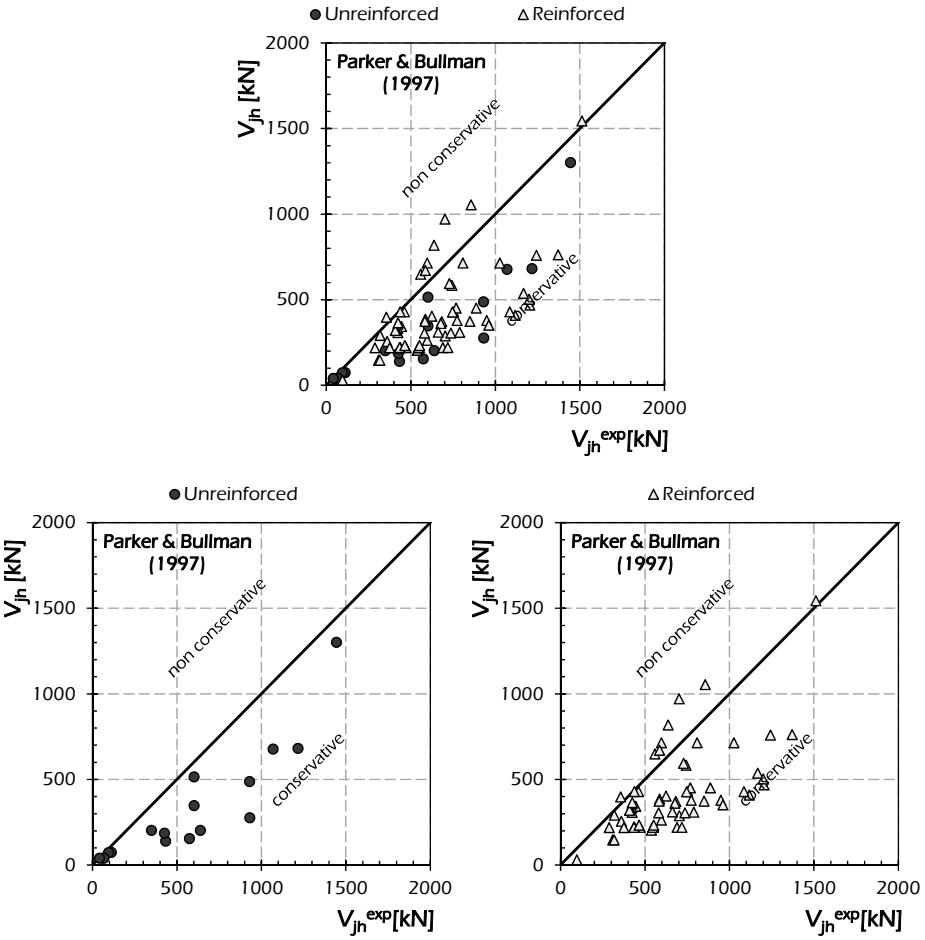

Fig. 5.41: Assessment of the model by Parker & Bullman (1997) for interior joints.

Fig. 5.44 reports the equivalence charts for the model by Hegger et al. (2003). On average the results obtained through the analysed model are in

good correlation with the experimental evidence by considering unreinforced or reinforced joints. In particular:

- a generally equivalent trend of the model by Hegger et al. (2003) is shown for unreinforced joints;
- the dispersion is limited as the bunch of points is located close to the equivalence 45° segment.

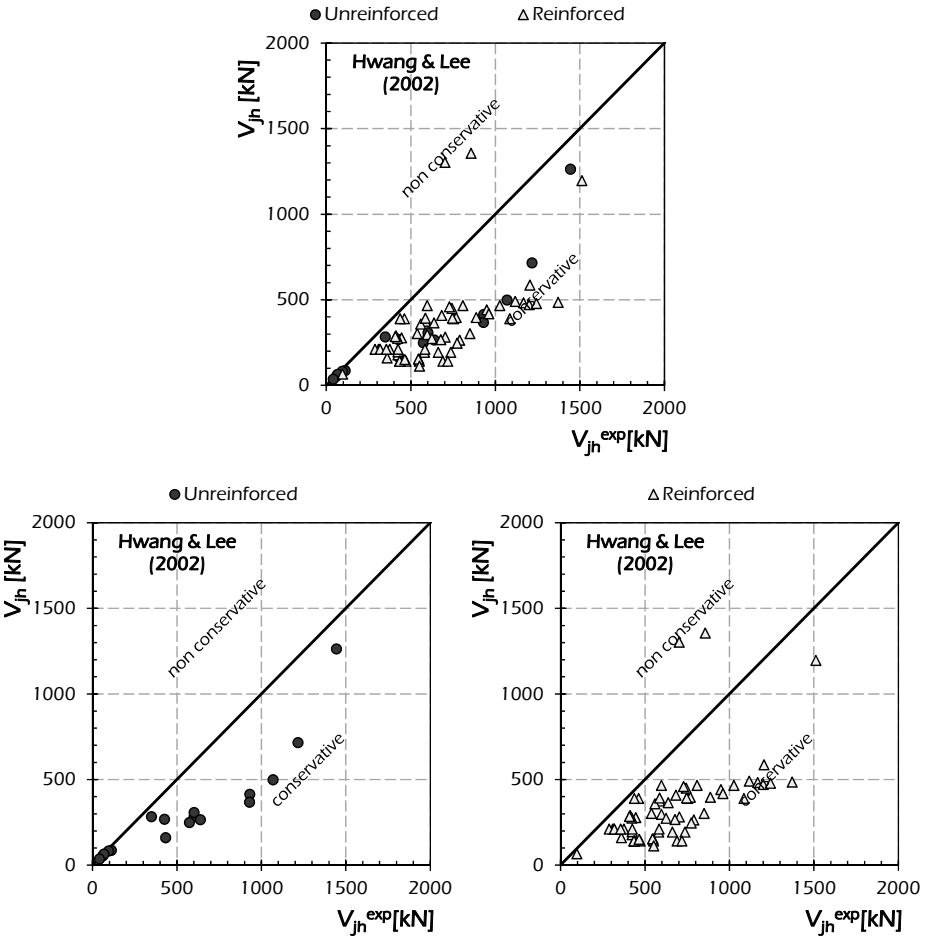

Fig. 5.42: Assessment of the model by Hwang & Lee (2002) for interior joints.

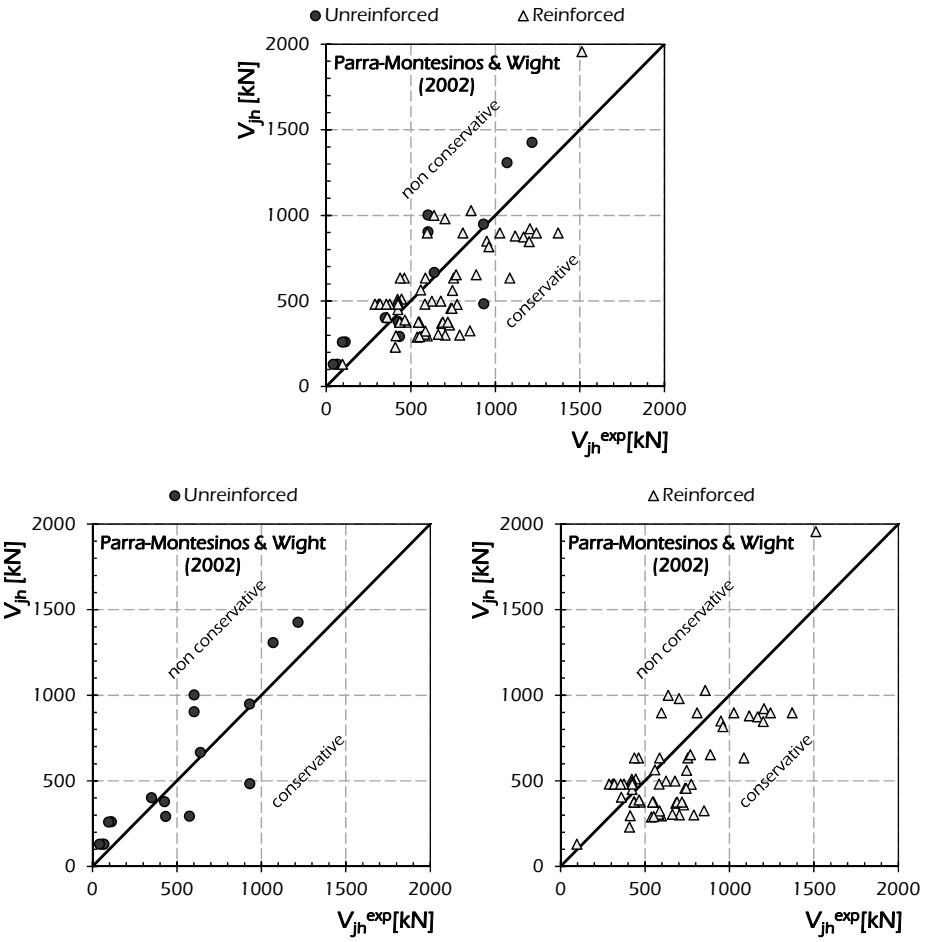

Fig. 5.43: *Assessment of the model by Parra-Montesinos & Wight (2002) for interior joints.*

Fig. 5.45 shows the assessment of model by Attaalla (2004) by reporting the equivalence charts for both unreinforced and reinforced interior joints.

The charts shown in Fig. 5.45 outline a general not accuracy of the model by Attaalla (2004) resulting a high dispersion of the points representing the comparison between the theoretical V_{jh} and the experimental V_{jh}^{exp} strength. Fig. 5.45 shows that the model by Attaalla (2004):

- provides non-accurate predictions;

- is affected by high dispersion especially for low strength joints (from Fig. 5.45 can be observed great values of the theoretical shear strength V_{jh} when the experimental shear strength V_{jh}^{exp} is less than 500 kN).

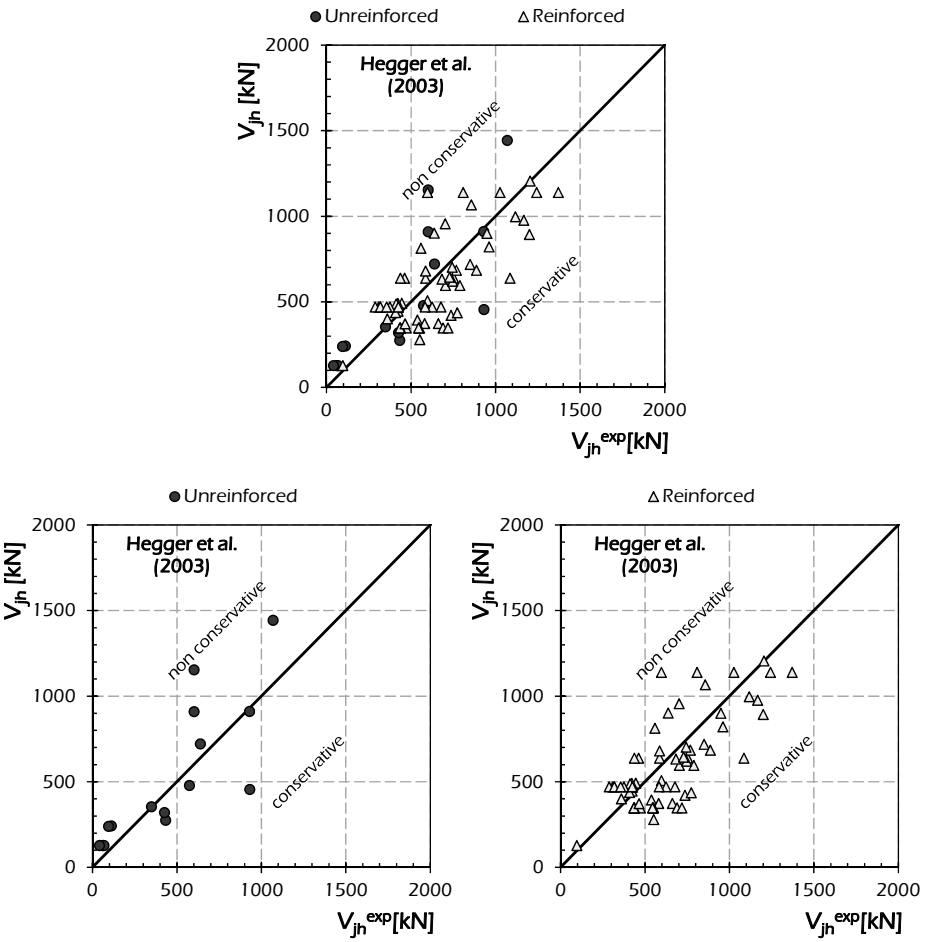

Fig. 5.44: Assessment of the model by Hegger et al. (2003) for interior joints.

Fig. 5.46 shows the comparison between the shear strength V_{jh} evaluated through the model by Kim et al. (2009) and the experimental evidence V_{jh}^{exp}. The equivalence charts show a good correlation between theoretical and

experimental shear strength for both unreinforced and reinforced joints. In particular:

- on average the prediction V_{jh} is equal to the experimental shear strength V_{jh}^{exp} for both unreinforced and reinforced joints, as a huge number of points lie around the bisector segment;
- the dispersion of the comparison points is rather low.

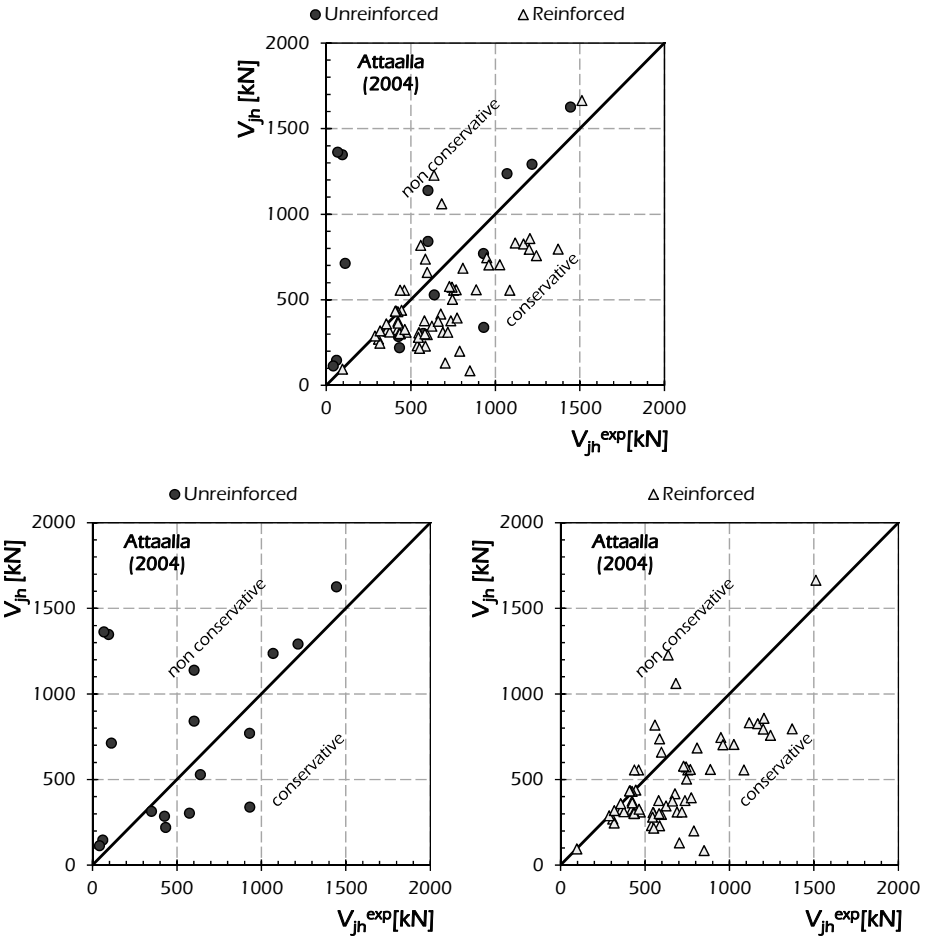

Fig. 5.45: Assessment of the model by Attaalla (2004) for interior joints.

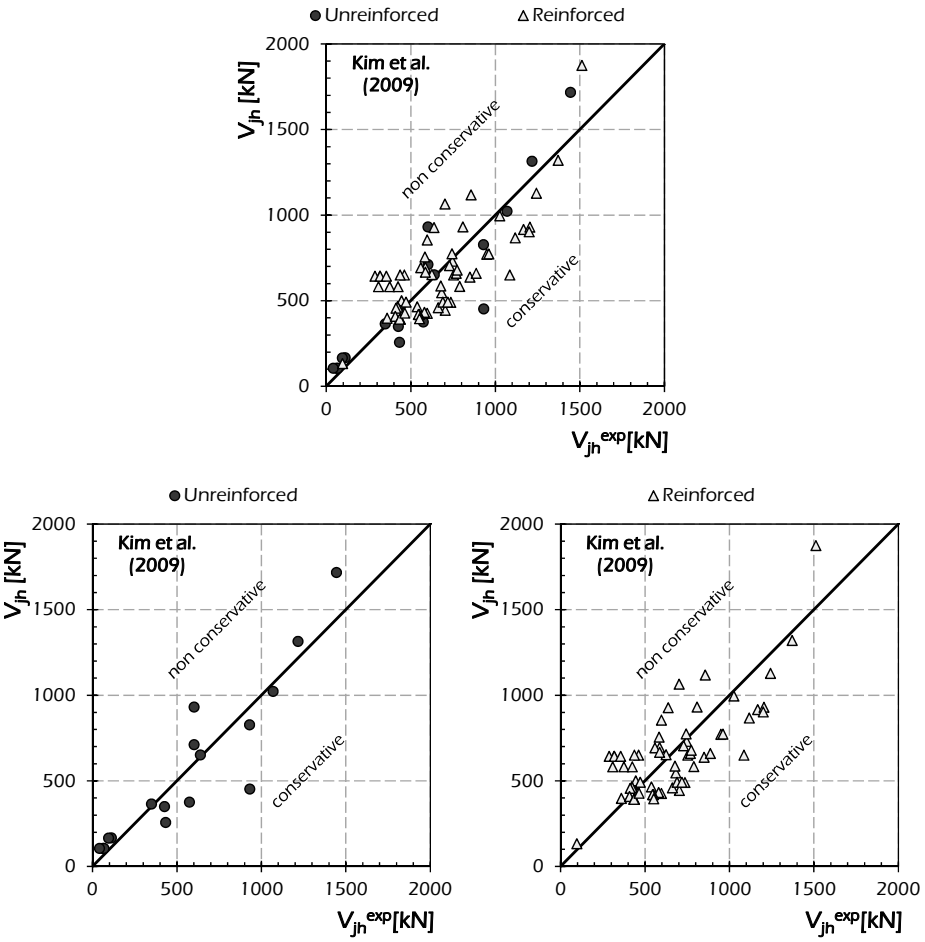

Fig. 5.46: Assessment of the model by Kim et al. (2009) for interior joints.

Fig. 5.47 shows the equivalence charts reporting the comparison between experimental shear strengths V_{jh}^{exp} and the corresponding theoretical values V_{jh} evaluated through the model by Kitayama et al. (1991). The following considerations can be drawn out:

- accurate results are obtained for all the considered joints, as the points lie around the equivalence segment;
- non-conservative predictions are achieved for unreinforced beam-to-column joints;

- generally equivalent trend results by evaluating the shear strength V_{jh} of reinforced joints through the model by Kitayama et al. (1991), as the bunch of points lies above the 45° equivalent segment;
- the model is affected by high dispersion of the points around the bisector segment.

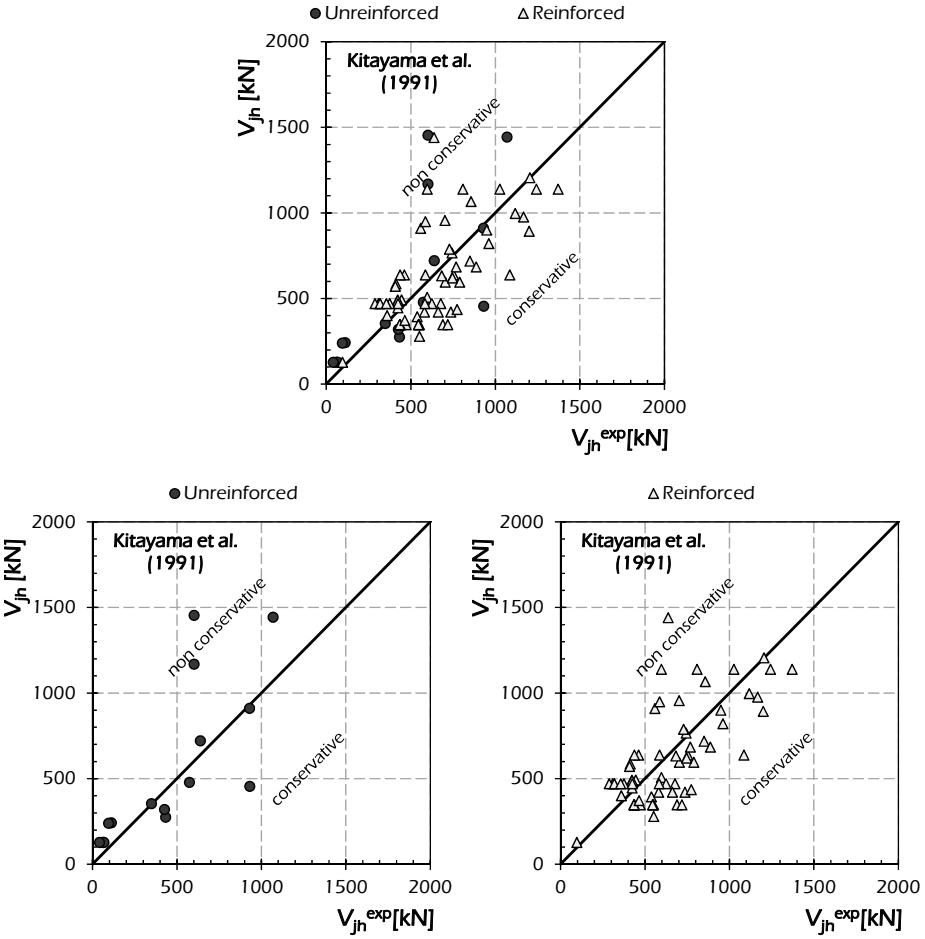

Fig. 5.47: Assessment of the model by Kitayama et al. (1991) for interior joints.

Fig. 5.48 shows the equivalence charts for the model by Hwang & Lee (2000). The following considerations can be drawn out:

- accurate predictions are obtained for all the considered joints, as the points are well lied around the equivalence segment;
- conservative results are provided for both unreinforced and reinforced joints;
- low dispersion of the points around the bisector segment is observed.

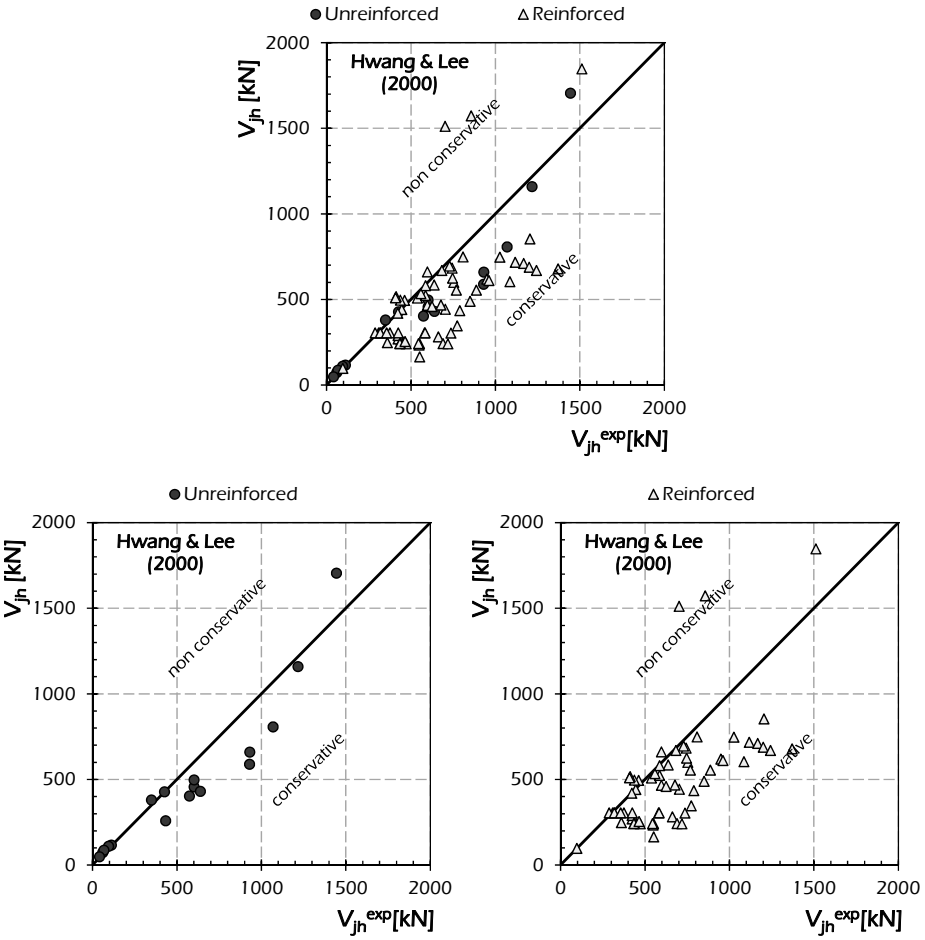

Fig. 5.48: Assessment of the model by Hwang & Lee (2000) for interior joints.

5.2 Error and Scatter Measures

After the qualitative observation reported in section 5.1 for describing the predictive capacity of the theoretical models for shear strength of RC joint, quantitative parameters describing the error and the dispersion will be defined for each model in the following pages.

The first simple parameter is the so-called *Average Quadratic Error* Δ defined as follows (Everitt, 2002):

$$\Delta = \sqrt{\frac{1}{n}\sum_{i=1}^{n}\left(V_{jh,i}^{\exp} - V_{jh,i}\right)^2}\ , \tag{5.1}$$

being n the total number of specimens considered in this study. This parameter denotes the mean difference between the experimental V_{jh}^{exp} and theoretical V_{jh} values of shear strength. As a matter of principle, the lower Δ, the more accurate is the model. However, its value depends on the units adopted for shear strength, as it is expressed in the same units of the shear strength.

A non-dimensional index representing the scatter between the experimental evidence and the theoretical result is the *Relative Average Quadratic Error* δ evaluated as follows (Everitt, 2002):

$$\delta = \sqrt{\frac{1}{n}\sum_{i=1}^{n}\left(\frac{V_{jh,i}^{\exp} - V_{jh}}{V_{jh,i}^{\exp}}\right)^2} \tag{5.2}$$

The Relative Average Quadratic Error δ is a measure of the accuracy of the model resulting equal to 0 if the model provides theoretical values equal to the experimental evidence; the lower the δ, the more accurate is the model.

Over the average quadratic error, the *correlation index of Pearson* that returns a measure of the linear correlation characterising the experimental results is also included (Everitt, 2002):

$$r = \frac{\sum_{i=1}^{n}\left(V_{jh,i}^{\exp} - \bar{V}_{jh}^{\exp}\right)\left(V_{jh,i} - \bar{V}_{jh}\right)}{\sqrt{\sum_{i=1}^{n}\left(V_{jh,i}^{\exp} - \bar{V}_{jh}^{\exp}\right)^2 \cdot \sum_{i=1}^{n}\left(V_{jh,i} - \bar{V}_{jh}\right)^2}}\ , \tag{5.3}$$

having denoted with $\overline{V_{jh}^{\exp}}$ and $\overline{V_{jh}}$ the average values of the experimental and theoretical shear strength, respectively. The square value of the correlation index of Pearson, namely *Coefficient of Determination* R^2, is defined in the following (Everitt, 2002):

$$R^2 = r^2 = \frac{\left[\sum_{i=1}^{n}\left(V_{jh,i}^{\exp} - \overline{V_{jh}^{\exp}}\right)\cdot\left(V_{jh,i} - \overline{V_{jh}}\right)\right]^2}{\sum_{i=1}^{n}\left(V_{jh,i}^{\exp} - \overline{V_{jh}^{\exp}}\right)^2 \cdot \sum_{i=1}^{n}\left(V_{jh,i} - \overline{V_{jh}}\right)^2}. \tag{5.4}$$

The coefficient of determination R^2 is a measure of the correlation between the experimental shear strength V_{jh}^{exp} and the theoretical one V_{jh}; in particular it assumes values ranging between 0 and 1. Values of R^2 equal to 1 denote the perfect alignment of the comparison point on a line. Indeed, if R^2 is close to 1, the model can be corrected by a linear recalibration providing an exact correspondence between V_{jh}^{exp} and V_{jh} for all the analysed specimens.

In the following the numerical results of error and dispersion measures are reported for each model either considering the experimental database as a whole or focusing on its subsections.

Table 5.1: Error and scatter measures for Code Formulation for exterior joints.

Model	Total			Unreinforced			Under-reinforced			EC8-compliant		
	Δ [kN]	δ	R^2	Δ [kN]	δ	R^2	Δ [kN]	δ	R^2	Δ [kN]	δ	R^2
ACI 352-85 (1985)	566.27	1.408	0.815	495.38	1.917	0.813	636.32	0.934	0.847	370.11	1.620	0.809
ACI 352-02 (2002)	205.17	0.685	0.799	194.46	0.900	0.813	204.87	0.298	0.847	231.38	1.135	0.689
ACI 318-05 (2005)	283.53	0.759	0.755	233.50	0.961	0.754	298.18	0.393	0.826	329.04	1.253	0.645
AIJ 1990 (1990)	309.11	0.657	0.750	232.54	0.817	0.744	357.85	0.415	0.811	237.37	0.991	0.734

Table 5.1: Error and scatter measures for Code Formulation for exterior joints.

Model	Total			Unreinforced			Under-reinforced			EC8-compliant		
	Δ [kN]	δ	R^2	Δ [kN]	δ	R^2	Δ [kN]	δ	R^2	Δ [kN]	δ	R^2
AIJ 1999 (1999)	195.30	0.529	0.785	199.32	0.693	0.795	195.17	0.274	0.838	185.26	0.824	0.759
NZS 3101 (1995)	377.76	0.746	0.364	-	-	-	357.13	0.534	0.632	232.66	1.331	0.700
FEMA 273 (1997) - 356 (2000)	294.21	0.512	0.611	328.02	0.457	0.754	291.36	0.373	0.783	201.07	0.971	0.699
EC8 (1995)	630.91	1.368	0.756	476.60	1.627	0.733	711.73	0.926	0.827	591.35	2.102	0.747
EC8 (2005) NTC (2008)	205.85	0.413	0.799	270.06	0.462	0.862	179.61	0.302	0.852	87.03	0.649	0.939
NTC (2008) OPCM (2005)	376.99	0.531	0.795	373.31	0.496	0.860	409.95	0.584	0.809	157.91	0.309	0.944

Table 5.1 reports the error and dispersion measures related to the code predictions for exterior beam-to-column joints.

By considering all the analysed specimens on exterior subassemblies:

- the lower Average Quadratic Error Δ is achieved for the AIJ 1999 (1999) that provides also the lower Relative Quadratic Error δ;
- predictions based on ACI 352–85 (1985) result in the higher R^2;

- the models that provides the lower Coefficient of Determination R^2 and the higher Average Error Δ with respect to the total number of exterior specimens taken into account are the NZS 3101 (1995) and the Eurocode 8 (EN1995, 1995), respectively.

By considering only unreinforced exterior joints:

- the best fitting model are the ACI 352-02 (2002) providing the lower Average Quadratic Error Δ and the Eurocode 8 (EN 1998, 2005) and NTC (2008) which develop the lower Relative Quadratic Error δ and the higher Coefficient of Determination R^2;
- the formulation provided by the NZS 3101 (1995), does not take into account unreinforced joints;
- about under-reinforced exterior joints, Table 5.1 shows that the formulation providing the lower error index and the higher correlation is the one recommended by the Eurocode 8 (EN 1998, 2005) and NTC (2008);
- the ACI 352-02 (2002) provides the lower Relative Average Error δ for under-reinforced exterior joins.

The results reported in Table 5.1 for EC8-compliant exterior joints show that:

- the Eurocode 8 (EN 1998, 2005) and NTC (2008) formulation provides the lower Average Quadratic Error Δ;
- the lower Relative Average Quadratic Error δ and the higher Coefficient of Determination R^2 are developed for the NTC (2008) and OPCM 3431/05 (2005).

Table 5.2 reports the error and dispersion measures evaluated for the capacity models available in the scientific literature and outlined in section 2 with reference to exterior beam-to-column joints.

Table 5.2: Error and dispersion measures for the Capacity Models available in literature for exterior joints.

Model	Total			Unreinforced			Under-reinforced			EC8-compliant		
	Δ [kN]	δ	R^2	Δ [kN]	δ	R^2	Δ [kN]	δ	R^2	Δ [kN]	δ	R^2
Pantazopoulo & Bonacci (1992)	1263.23	2.461	0.796	1066.71	2.248	0.895	1426.17	2.234	0.759	899.58	3.656	0.864

Table 5.2: Error and dispersion measures for the Capacity Models available in literature for exterior joints.

Model	Total			Unreinforced			Under-reinforced			EC8-compliant		
	Δ [kN]	δ	R^2	Δ [kN]	δ	R^2	Δ [kN]	δ	R^2	Δ [kN]	δ	R^2
Paulay & Priestley (1992)	165.72	0.481	0.829	182.11	0.381	0.871	161.48	0.327	0.829	138.36	1.001	0.860
Parker & Bullman (1997)	247.64	0.384	0.749	226.57	0.363	0.767	277.54	0.358	0.805	129.72	0.524	0.953
Hwang & Lee (2002)	177.13	0.362	0.857	170.11	0.330	0.929	195.69	0.313	0.837	82.23	0.577	0.961
Parra-Montesinos & Wight (2002)	288.76	1.012	0.781	251.09	1.313	0.824	291.88	0.467	0.819	356.47	1.685	0.727
Hegger et al. (2003)	212.76	0.643	0.766	205.02	0.572	0.829	216.57	0.349	0.847	214.99	1.389	0.861

Table 5.2: Error and dispersion measures for the Capacity Models available in literature for exterior joints.

Model	Total			Unreinforced			Under-reinforced			EC8-compliant		
	Δ [kN]	δ	R^2	Δ [kN]	δ	R^2	Δ [kN]	δ	R^2	Δ [kN]	δ	R^2
Attalla (2004)	Very high	Very high	Very low	Very high	Very high	Very low	Very high	Very high	Very low	Very high	Very high	Very low
Kim et al. (2009)	172.25	0.393	0.837	166.13	0.412	0.882	186.04	0.274	0.871	113.66	0.685	0.946
Zhang & Jirsa (1982)	395.36	0.829	0.783	373.40	0.822	0.862	430.92	0.766	0.726	261.52	1.079	0.920
Sarsam & Phillips (1985)	183.80	0.475	0.820	152.81	0.308	0.924	199.93	0.312	0.824	181.05	1.063	0.966
Ortiz (1993)	470.45	1.153	0.688	206.04	0.498	0.774	567.45	0.879	0.861	477.66	2.561	0.965

Table 5.2: Error and dispersion measures for the Capacity Models available in literature for exterior joints.

Model	Total			Unreinforced			Under-reinforced			EC8-compliant		
	Δ [kN]	δ	R^2	Δ [kN]	δ	R^2	Δ [kN]	δ	R^2	Δ [kN]	δ	R^2
Scott et al. (1994)	236.30	0.505	0.724	201.28	0.615	0.789	248.64	0.326	0.768	261.13	0.779	0.808
Vollum & Newman (1999)	222.23	0.651	0.797	181.40	0.652	0.822	236.99	0.341	0.856	247.25	1.338	0.842
Hwang & Lee (1999)	163.25	0.388	0.856	181.29	0.359	0.918	162.16	0.266	0.855	111.35	0.748	0.926
Bakir & Boduroglu (2002)	191.76	0.317	0.815	186.77	0.275	0.857	208.12	0.284	0.852	111.55	0.504	0.934
Russo & Somma (2006)	339.49	0.754	0.735	192.82	0.472	0.796	422.93	0.683	0.822	175.00	1.378	0.921

Table 5.2: Error and dispersion measures for the Capacity Models available in literature for exterior joints.

Model	Total			Unreinforced			Under-reinforced			EC8-compliant		
	Δ [kN]	δ	R^2	Δ [kN]	δ	R^2	Δ [kN]	δ	R^2	Δ [kN]	δ	R^2
Tsonos (2007)	422.75	1.031	0.713	311.64	1.221	0.636	492.84	0.683	0.812	317.12	1.624	0.782
Vollum & Parker (2008)	369.05	0.613	0.792	227.59	0.525	0.845	444.87	0.473	0.811	275.95	1.143	0.876

The model by Attaalla (2004) is not accurate in predicting the shear strength of exterior joints; it provides very high values of Δ and δ for both unreinforced and reinforced joints, while very low values of the Coefficient of Determination R^2 are evaluated (Table 5.2)

About the complete database collecting specimens on exterior joints:

- the models providing the lower Average Quadratic Error Δ are the ones by Hwang & Lee (1999), Paulay & Priestley (1992) and Kim et al. (2009);
- the lower Relative Average Quadratic Error δ is provided by the models by Hwang & Lee (1999 and 2002), Parker & Bullman (1997) and Bakir & Boduroglu (2002);
- the models by Hwang & Lee (1999 and 2002) provide the higher Coefficient of Determination R^2.

The evaluation of the error index made taking into account only the unreinforced joints shows:

- the lower Average Quadratic Error Δ for the model by Sarsam & Phillips (1985);
- the lower Relative Average Error δ is achieved for the model by Bakir & Boduroglu (2002);
- the higher Coefficient of Determination R^2 for unreinforced exterior joints is provided by the model by Hwang & Lee (1999).

By analysing exterior under-reinforced joints:

- the model by Paulay & Priestley (1992) and by Hwang & Lee (1999) result the more accurate developing the lower Δ and the lower δ, respectively;
- the higher Coefficient of Determination R^2 is provided by the model by Kim et al. (2009).

For EC8-compliant joints:

- the models Hwang & Lee (1999), Bakir & Boduroglu (2002) and Kim et al. (2009) provide the lower Average Quadratic Error Δ;
- the lower Relative Average Quadratic Error δ is observed for the models by Parker & Bullman (1997) and Bakir & Boduroglu (2002);
- the higher Coefficient of Determination R^2 is provided by the models by Sarsam & Phillips (1985) and Ortiz (1993).

Table 5.3: Error and dispersion measures for Code Formulation for interior joints.

Model	Total			Unreinforced			Reinforced		
	Δ [kN]	δ	R^2	Δ [kN]	δ	R^2	Δ [kN]	δ	R^2
ACI 352-85 (1985)	496.97	0.988	0.625	717.76	1.719	0.772	424.18	0.695	0.625
ACI 352-02 (2002)	227.71	0.456	0.668	242.74	0.799	0.816	223.79	0.316	0.666
ACI 318-05 (2005)	272.27	0.523	0.630	356.85	0.885	0.769	246.63	0.382	0.631
AIJ 1990 (1990)	437.90	0.678	0.685	599.91	1.214	0.786	386.94	0.454	0.700

Table 5.3: Error and dispersion measures for Code Formulation for interior joints.

Model	Total			Unreinforced			Reinforced		
	Δ [kN]	δ	R^2	Δ [kN]	δ	R^2	Δ [kN]	δ	R^2
AIJ 1999 (1999)	242.46	0.486	0.689	324.21	0.884	0.824	217.27	0.316	0.699
NZS 3101 (1995)	554.85	0.760	0.361	-	-	-	554.85	0.760	0.361
FEMA 273 (1997) - 356 (2000)	247.18	0.396	0.651	222.23	0.470	0.769	253.03	0.375	0.622
EC8 (1995)	570.90	0.949	0.671	757.56	1.535	0.830	513.75	0.733	0.656
EC8 (2005) NTC (2008)	383.70	0.501	0.547	349.57	0.435	0.926	391.77	0.516	0.491
NTC (2008) OPCM (2005)	556.96	0.714	0.401	495.21	0.602	0.921	571.35	0.740	0.331

The error and dispersion measures evaluated for the analysed code formulations for interior joints are reported in Table 5.3.

The code formulations for interior joints generally provide results less accurate than the ones obtained by them for exterior connections, resulting higher values of Average Quadric Errors and lower Coefficient of Determination (Table 5.1 vs. Table 5.3).

For all the considered interior joints:

- the most accurate models are the ones recommended by ACI 352-02 (2002) and FEMA 273 (1997) – 356 (2000) providing the lower Δ and the lower δ (Table 5.3), respectively;
- the model by AIJ 1999 (1999) makes the higher Coefficient of Determination R^2.

For unreinforced joints:

- the formulation provided by FEMA 273 (1997) – 356 (2000) provides the lower Average Quadratic Error Δ
- the Italian and European Codes (EN 1998, 2005, NTC, 2008 and OPCM3431/05, 2005), instead, develop the lower Relative Average Error δ and the higher Coefficient of Determination R^2 by considering interior unreinforced joints.

About reinforced joints:

- the most accurate model is the one suggested by AIJ 1999 (1999) providing the lower Average Quadratic Errors Δ and δ with the higher Coefficient of Determination R^2.

Table 5.4 reports the quantitative measures of error and dispersion evaluated by analysing the capacity models available in the scientific literature for interior beam-to-column joints.

The model by Attaalla (2004) does not provide accurate results for both unreinforced and reinforced interior joints, in particular very high Average Quadratic Error Δ and Relative Average Quadratic Error δ values are obtained for reinforced joints.

Table 5.4: Error and dispersion measures for the Capacity Models available in literature for interior joints.

Model	Total			Unreinforced			Reinforced		
	Δ [kN]	δ	R^2	Δ [kN]	δ	R^2	Δ [kN]	δ	R^2
Pantazopoulo & Bonacci (1992)	639.27	1.249	0.523	424.03	1.803	0.656	682.55	1.067	0.514

Table 5.4: Error and dispersion measures for the Capacity Models available in literature for interior joints.

Model	Total			Unreinforced			Reinforced		
	Δ [kN]	δ	R^2	Δ [kN]	δ	R^2	Δ [kN]	δ	R^2
Paulay & Priestley (1992)	394.72	0.470	0.444	487.21	0.563	0.333	367.98	0.444	0.499
Parker & Bullman (1997)	352.89	0.453	0.545	316.66	0.467	0.791	361.38	0.450	0.460
Hwang & Lee (2002)	400.92	0.527	0.522	320.12	0.422	0.811	418.68	0.550	0.448
Parra-Montesinos & Wight (2002)	247.97	0.503	0.611	247.21	0.874	0.814	248.16	0.354	0.595
Hegger et al. (2003)	305.25	0.482	0.696	394.03	0.864	0.779	278.68	0.322	0.710

Table 5.4: Error and dispersion measures for the Capacity Models available in literature for interior joints.

Model	Total			Unreinforced			Reinforced		
	Δ [kN]	δ	R^2	Δ [kN]	δ	R^2	Δ [kN]	δ	R^2
Attalla (2004)	Very high	Very high	Very low	517.81	5.841	0.188	Very high	Very high	Very low
Kim et al. (2009)	190.82	0.403	0.745	178.27	0.541	0.846	193.84	0.361	0.715
Kitayama et al. (1991)	331.30	0.528	0.656	439.81	0.923	0.739	298.06	0.368	0.671
Hwang & Lee (2000)	287.07	0.366	0.576	166.60	0.233	0.885	309.96	0.392	0.485

By considering all the analysed interior joints:

- the model by Kim et al. (1999) provides the lower Δ and the higher Coefficient of Determination R^2, while the lower Relative Average Quadratic Error δ is obtained through the model by Hwang & Lee (2000).

Accounting unreinforced interior joints (Table 5.4):

- the model by Hwang & Lee (2000) provides the lower average errors (both Δ and δ) and the higher R^2.

For reinforced joints:

- the model by Kim et al. (1999) provides the lower Average Quadratic Error Δ and the higher Coefficient of Determination R^2;
- the lower Relative Average Quadratic Error δ is obtained by the model by Hegger et al. (2003).

5.3 Insights about Reliability-related Aspects

In seismic engineering there is a clear trend of the new generation of design codes to set the objectives of the design in terms of the fulfilment of a number of performance levels, whose measure of achievement is quantified by a probability. A sound basis on the theory of probability, on that of stochastic processes and random vibrations, and on the methods that allow probabilities of exceedance of specified levels of response to be evaluated, is becoming a requirement for a correct use of the codes.

The aim of this section is to provide the fundamental parameters accounting for the uncertainty of the capacity needed in the available methods for the probabilistic evaluation of seismic performance (Pinto et al., 2004).

5.3.1 Overview of Reliability Assessment in Seismic Analysis

Various alternative formulations of the reliability problem have been given in the scientific literature (Pinto et al., 2004). They rest on two assumptions, both referring to the time dimensions of the problem: the temporal sequence of the seismic event and the dynamic response of the structure during an event. The first one consists in choosing an appropriate interval of time, normally one year, and considering that if failure is to occur within any such interval, it will do so under the seismic event of larger intensity.

The second assumption of the practical methods is that in a structure subjected to ground acceleration, failure occurs when the response attains its maximum. If more refined versions the dependence of the capacity of some of the failure modes on the demand is accounted for, so that the failure event is defined as:

$$C\left[t, D(t)\right] - D(t) \leq 0 \quad , \tag{5.5}$$

and it may occur when:

$$D(t) = D_{\max} \quad , \tag{5.6}$$

in which C denotes the capacity of the structure and D indicates the seismic demand.

This assumption is quite consequential, since it allows the collection, through a number of dynamic analyses, of the statistics of the maximum responses (demand) so as to obtain a vector of correlated random variables, to be subsequently compared with the corresponding random capacities, as for the case of a time-invariant problem.

The combination of the first and the second assumptions is often referred to the Time-Integrate Approach, due to the fact that time does not appear explicitly in the calculations, the in-time variation of the quantities involved having been absorbed in their extreme values.

In simplified reliability method (i.e. "2000 SAC/FEMA" method, Cornell et al., 2002), the safety factors are considered affecting separately demand and capacity. These factors, however, originate from a full probabilistic treatment of the design/assessment problem, whereby the annual probability of exceeding specified levels of response is computed. The response of the structure of the structure, given the input, is deterministic and the uncertainty on the mechanical parameters which might affect the response is disregarded. Failure occurs when the maximum demand D over the duration of the seismic excitation exceeds the corresponding capacity C. In essence, the method provides a closed form for the risk (annual probability of exceedance) written according to the classical reliability formulation as:

$$P_f = \int_0^{\infty} \left[1 - F_D(\alpha)\right] f_C(\alpha) d\alpha \tag{5.7}$$

in which $F_D(.)$ is the CDF (cumulative distribution function) of the annual maxima demand and $f_C(.)$ is the PDF (probability density function) of the capacity (see Pinto et al., 2004 for further details). The hazard in the site can be expressed in the form:

$$H(S_a) = \Pr(S_a \geq s_a, 1\ year) = k_0 s_a^{-k} \tag{5.8}$$

as the direct result of the hazard analysis.

The second step of the procedure is the passage from the annual probability of S_a to the probability of the response, or demand, D. To make this passage it is assumed that the median value $\overline{D}$ of D can be approximately expressed as a function of S_a as:

$$\overline{D} = a \cdot s_a^b \ . \tag{5.9}$$

The two constant a and b are to be determined by means of a number of non-linear dynamic analyses using recorded accelerograms. The same non-linear analyses provide an estimate of the dispersion of D about its median value. Further, the demand D is assumed to be log-normally distributed about the median, with standard deviation of the natural logarithm (dispersion) equal to β_D. Hence the random variable D can be expressed as:

$$D = \left(a \cdot s_a^b\right)\varepsilon \tag{5.10}$$

where ε is a log-normal random variable with unit median, and dispersion equal to β_D. Eqn. (5.10) can be inverted to give:

$$s_a = \left(\frac{D}{a \cdot \varepsilon}\right)^{\frac{1}{b}} . \tag{5.11}$$

Using this expression and Eqn. (5.9), the annual probability $Pr[D>d]=1-F_D(d)$ is obtained by first conditioning it to random variable ε as follows:

$$\begin{aligned} \Pr(D > d) &= \int_0^\infty \Pr(D > d \mid \varepsilon) f_\varepsilon(\varepsilon) d\varepsilon = \int_0^\infty \Pr\left[S_a > \left(\frac{d}{a \cdot \varepsilon}\right)^{\frac{1}{b}}\right] f_\varepsilon(\varepsilon) d\varepsilon = \\ &= k_0 \left(\frac{d}{a}\right)^{-\frac{k}{b}} \int_0^\infty \left(\frac{1}{\varepsilon}\right)^{-\frac{k}{b}} f_\varepsilon(\varepsilon) d\varepsilon = k_0 \left(\frac{d}{a}\right)^{-\frac{k}{b}} e^{\frac{1}{2}\frac{k^2}{b^2}\beta_D^2} \ . \end{aligned} \tag{5.12}$$

Eqn. (5.12) can be read as saying that the probability of D exceeding any given value d is given by the product of the probability that the hazard exceeds the value necessary to produce $D = d$ assuming the $S_a - d$ relationship as deterministic, times the factor $e^{\frac{1}{2}\frac{k^2}{b^2}\beta_D^2}$. In this latter, three parameters appear with the same weight: the slope k of the hazard curve (for S_a values having a probability of exceedance roughly equal to P_f), the exponent b of the demand as a function of S_a, and the dispersion β_D of the input-output relationship.

The third and final step consists in the probabilistic definition of the random variable expressing the capacity C, and then in carrying out the integration of Eqn. (5.5) analytically. The assumptions on the capacity are two: C is independent from D, and is log-normally distributed:

$$C = \ln\left(\overline{C}, \sigma_{\log C} = \beta_C\right). \tag{5.13}$$

The integral in Eqn. (5.5), taking into account Eqn. (5.12) becomes:

$$P_f = \int_0^{\infty} \left[k_0 \left(\frac{\alpha}{a} \right)^{-\frac{k}{b}} e^{\frac{1}{2}\frac{k^2}{b^2}\beta_D^2} \right] f_C(\alpha) d\alpha \tag{5.14}$$

where $f_C(.)$ is the log-normal PDF (probability density function) of C. Integration of the previous expression gives:

$$\begin{aligned} P_f &= k_0 \left(\frac{1}{a} \right)^{-\frac{k}{b}} e^{\frac{1}{2}\frac{k^2}{b^2}\beta_D^2} \int_0^{\infty} \alpha^{-\frac{k}{b}} f_C(\alpha) d\alpha = k_0 \left(\frac{1}{a} \right)^{-\frac{k}{b}} e^{\frac{1}{2}\frac{k^2}{b^2}\beta_D^2} \overline{C}^{-\frac{k}{b}} e^{\frac{1}{2}\frac{k^2}{b^2}\beta_C^2} = \\ &= H\left[S_a\left(\overline{C}\right) \right] e^{\frac{1}{2}\frac{k^2}{b^2}\left(\beta_D^2 + \beta_C^2\right)} . \end{aligned} \tag{5.15}$$

Similarly to Eqn. (5.12), this last expression can be read as saying that the unconditional probability of failure, or total risk, is given by the product of the probability that the spectral acceleration exceeds the value necessary to produce a demand D equal to the median capacity $\overline{C}$, as if the $S_a - d$ relationship were deterministic, times a factor which now contains in addition the dispersion β_C of the capacity.

5.3.2 Correlation Index of Capacity Models for Reliability Analysis

The reliability capacity factor β_C (Pinto et al., 2004) can be evaluated as the standard deviation of the natural logarithm of the ratios x_i calculated through Eqn. (5.17):

$$\beta_C = \sigma\left[\ln\left(x_i \right) \right], \tag{5.16}$$

$$x_i = \frac{V_{jh,i}^{\exp}}{V_{jh,i}} . \tag{5.17}$$

However, it is noted that the dispersion factor β_C applied to the mean value $\overline{C}$ can be employed for defining the probability levels of 16% and 84% according the following relations:

$$C^{16\%} = \overline{C} \cdot e^{-\beta_c} , \tag{5.18}$$

$$C^{84\%} = \overline{C} \cdot e^{\beta_c} . \tag{5.19}$$

Table 5.5 to Table 5.8 report the Average Quadratic Error Δ, and the Coefficient of Determination R^2 evaluated in section 5.2 as a reference and the

dispersion of the capacity β_C for all the considered specimens and for the classes of joints individuate with reference to the amount of stirrups.

Table 5.5: Measures of error and factor of dispersion of the capacity for code formulations for exterior joints.

Model	Total			Unreinforced			Under-reinforced			EC8-compliant		
	Δ [kN]	R^2	β_C	Δ [kN]	R^2	β_C	Δ [kN]	R^2	β_C	Δ [kN]	R^2	β_C
ACI 352-85 (1985)	566.27	0.815	**0.364**	495.38	0.813	**0.433**	636.32	0.847	**0.285**	370.11	0.809	**0.348**
ACI 352-02 (2002)	205.17	0.799	**0.392**	194.46	0.813	**0.433**	204.87	0.847	**0.285**	231.38	0.689	**0.385**
ACI 318-05 (2005)	283.53	0.755	**0.396**	233.50	0.754	**0.436**	298.18	0.826	**0.307**	329.04	0.645	**0.389**
AIJ 1990 (1990)	309.11	0.750	**0.412**	232.54	0.744	**0.448**	357.85	0.811	**0.355**	237.37	0.734	**0.367**
AIJ 1999 (1999)	195.30	0.785	**0.393**	199.32	0.795	**0.433**	195.17	0.838	**0.302**	185.26	0.759	**0.353**
NZS 3101 (1995)	377.76	0.364	**0.686**	-	-	**-**	357.13	0.632	**0.618**	232.66	0.700	**0.618**

Table 5.5: Measures of error and factor of dispersion of the capacity for code formulations for exterior joints.

Model	Total			Unreinforced			Under-reinforced			EC8-compliant		
	Δ [kN]	R^2	β_C	Δ [kN]	R^2	β_C	Δ [kN]	R^2	β_C	Δ [kN]	R^2	β_C
FEMA 273 (1997) – 356 (2000)	294.21	0.611	**0.466**	328.02	0.754	**0.436**	291.36	0.783	**0.367**	201.07	0.699	**0.389**
EC8 (1995)	630.91	0.756	**0.396**	476.60	0.733	**0.438**	711.73	0.827	**0.323**	591.35	0.747	**0.355**
EC8 (2005) NTC (2008)	205.85	0.799	**0.422**	270.06	0.862	**0.454**	179.61	0.852	**0.333**	87.03	0.939	**0.356**
NTC (2008) OPCM (2005)	376.99	0.795	**0.408**	373.31	0.860	**0.406**	409.95	0.809	**0.334**	157.91	0.944	**0.294**

Table 5.5 reports the factor of dispersion of the capacity of the code formulations about exterior beam-to-column joints.

The formulation recommended by ACI 352 - 85 (1985) results in the lower factor of dispersion β_C by considering all the specimens on exterior joints. The lower β_C about unreinforced and EC8-compliant exterior joints is obtained by applying the NTC (2008) and OPCM 3431/05 (2005) formulation, while the lower dispersion for under-reinforced exterior joints is provided by the ACI 352 – 85 (1985) and ACI 352 – 02 (2002) formulae.

The factor of dispersion β_C of the capacity evaluated for the capacity models for exterior joints are reported in Table 5.6. The lower β_C for the specimens is provided by the model by Kim et al. (2009) which provide the lower factor of dispersion also for both non-compliant and compliant joints.

The lower dispersion about exterior unreinforced joint is obtained through the model by Sarsam & Phillips (1985).

Table 5.6: Measures of error and factor of dispersion of the capacity for the capacity models for exterior joints.

Model	Total			Unreinforced			Under-reinforced			EC8-compliant		
	Δ [kN]	R^2	β_c	Δ [kN]	R^2	β_c	Δ [kN]	R^2	β_c	Δ [kN]	R^2	β_c
Pantazopoulo & Bonacci (1992)	1263.23	0.796	**0.331**	1066.71	0.895	**0.283**	1426.17	0.759	**0.298**	899.58	0.864	**0.477**
Paulay & Priestley (1992)	165.72	0.829	**0.433**	182.11	0.871	**0.386**	161.48	0.829	**0.286**	138.36	0.860	**0.439**
Parker & Bullman (1997)	247.64	0.749	**0.389**	226.57	0.767	**0.382**	277.54	0.805	**0.368**	129.72	0.953	**0.288**
Hwang & Lee (2002)	177.13	0.857	**0.352**	170.11	0.929	**0.315**	195.69	0.837	**0.291**	82.23	0.961	**0.281**
Parra-Montesinos & Wight (2002)	288.76	0.781	**0.413**	251.09	0.824	**0.441**	291.88	0.819	**0.299**	356.47	0.727	**0.382**

Table 5.6: Measures of error and factor of dispersion of the capacity for the capacity models for exterior joints.

Model	Total			Unreinforced			Under-reinforced			EC8-compliant		
	Δ [kN]	R^2	β_c	Δ [kN]	R^2	β_c	Δ [kN]	R^2	β_c	Δ [kN]	R^2	β_c
Hegger et al. (2003)	212.76	0.766	**0.401**	205.02	0.829	**0.416**	216.57	0.847	**0.286**	214.99	0.861	**0.370**
Attalla (2004)	Very high	Very low	**1.265**	Very high	Very low	**1.046**	Very high	Very low	**1.123**	Very high	Very low	**1.861**
Kim et al. (2009)	172.25	0.837	**0.293**	166.13	0.882	**0.327**	186.04	0.871	**0.235**	113.66	0.946	**0.253**
Zhang & Jirsa (1982)	395.36	0.783	**0.383**	373.40	0.862	**0.340**	430.92	0.726	**0.396**	261.52	0.920	**0.356**
Sarsam & Phillips (1985)	183.80	0.820	**0.385**	152.81	0.924	**0.278**	199.93	0.824	**0.306**	181.05	0.966	**0.326**

Table 5.6: Measures of error and factor of dispersion of the capacity for the capacity models for exterior joints.

Model	Total			Unreinforced			Under-reinforced			EC8-compliant		
	Δ [kN]	R^2	β_C	Δ [kN]	R^2	β_C	Δ [kN]	R^2	β_C	Δ [kN]	R^2	β_C
Ortiz (1993)	470.45	0.688	**0.469**	206.04	0.774	**0.392**	567.45	0.861	**0.287**	477.66	0.965	**0.357**
Scott et al. (1994)	236.30	0.724	**0.417**	201.28	0.789	**0.414**	248.64	0.768	**0.354**	261.13	0.808	**0.336**
Vollum & Newman (1999)	222.23	0.797	**0.385**	181.40	0.822	**0.400**	236.99	0.856	**0.290**	247.25	0.842	**0.344**
Hwang & Lee (1999)	163.25	0.856	**0.371**	181.29	0.918	**0.331**	162.16	0.855	**0.270**	111.35	0.926	**0.324**
Bakir & Boduroglu (2002)	191.76	0.815	**0.310**	186.77	0.857	**0.297**	208.12	0.852	**0.281**	111.55	0.934	**0.249**

Table 5.6: Measures of error and factor of dispersion of the capacity for the capacity models for exterior joints.

Model	Total			Unreinforced			Under-reinforced			EC8-compliant		
	Δ [kN]	R^2	β_C	Δ [kN]	R^2	β_C	Δ [kN]	R^2	β_C	Δ [kN]	R^2	β_C
Russo & Somma (2006)	339.49	0.735	**0.361**	192.82	0.796	**0.337**	422.93	0.822	**0.269**	175.00	0.921	**0.402**
Tsonos (2007)	422.75	0.713	**0.430**	311.64	0.636	**0.522**	492.84	0.812	**0.332**	317.12	0.782	**0.379**
Vollum & Parker (2008)	369.05	0.792	**0.393**	227.59	0.845	**0.415**	444.87	0.811	**0.339**	275.95	0.876	**0.319**

The model by AIJ 1999 (1999) provides the lower dispersion for all the analysed interior specimens and for reinforced interior joints (Table 5.7), while the lower β_C about unreinforced interior joints is obtained by applying the Eurocode 8 (EN 1998, 2005) and NTC (2008) formulation.

Table 5.7: Measures of error and factor of dispersion of the capacity for code formulations for interior joints.

Model	Total			Unreinforced			Reinforced		
	Δ [kN]	R^2	β_C	Δ [kN]	R^2	β_C	Δ [kN]	R^2	β_C
ACI 352-85 (1985)	496.97	0.625	**0.417**	717.76	0.772	**0.531**	424.18	0.625	**0.347**

Table 5.7: Measures of error and factor of dispersion of the capacity for code formulations for interior joints.

Model	Total			Unreinforced			Reinforced		
	Δ [kN]	R^2	β_C	Δ [kN]	R^2	β_C	Δ [kN]	R^2	β_C
ACI 352-02 (2002)	227.71	0.668	**0.404**	242.74	0.816	**0.518**	223.79	0.666	**0.333**
ACI 318-05 (2005)	272.27	0.630	**0.437**	356.85	0.769	**0.530**	246.63	0.631	**0.376**
AIJ 1990 (1990)	437.90	0.685	**0.388**	599.91	0.786	**0.469**	386.94	0.700	**0.324**
AIJ 1999 (1999)	242.46	0.689	**0.385**	324.21	0.824	**0.464**	217.27	0.699	**0.317**
NZS 3101 (1995)	554.85	0.361	**0.854**	-	-	**-**	554.85	0.361	**0.854**
FEMA 273 (1997) – 356 (2000)	247.18	0.651	**0.417**	222.23	0.769	**0.530**	253.03	0.622	**0.387**
EC8 (1995)	570.90	0.671	**0.403**	757.56	0.830	**0.443**	513.75	0.656	**0.359**

Table 5.7: Measures of error and factor of dispersion of the capacity for code formulations for interior joints.

Model	Total			Unreinforced			Reinforced		
	Δ [kN]	R^2	β_C	Δ [kN]	R^2	β_C	Δ [kN]	R^2	β_C
EC8 (2005) NTC (2008)	383.70	0.547	**0.412**	349.57	0.926	**0.337**	391.77	0.491	**0.425**
NTC (2008) OPCM (2005)	556.96	0.401	**0.505**	495.21	0.921	**0.430**	571.35	0.331	**0.481**

By analysing the capacity models available in the scientific literature for interior joints (Table 5.8) the model by Kim et al. (2009) provides the lower dispersion factor β_C for the total set of specimens on interior joints and for reinforced joints, while the model by Hwang & Lee (2000) results the one with the lower dispersion.

Table 5.8: Measures of error and factor of dispersion of the capacity for the capacity models about interior joints.

Model	Total			Unreinforced			Reinforced		
	Δ [kN]	R^2	β_C	Δ [kN]	R^2	β_C	Δ [kN]	R^2	β_C
Pantazopoulo & Bonacci (1992)	639.27	0.523	**0.393**	424.03	0.656	**0.539**	682.55	0.514	**0.345**
Paulay & Priestley (1992)	394.72	0.444	**0.587**	487.21	0.333	**0.995**	367.98	0.499	**0.417**

Table 5.8: Measures of error and factor of dispersion of the capacity for the capacity models about interior joints.

Model	Total			Unreinforced			Reinforced		
	Δ [kN]	R^2	β_C	Δ [kN]	R^2	β_C	Δ [kN]	R^2	β_C
Parker & Bullman (1997)	352.89	0.545	**0.387**	316.66	0.791	**0.394**	361.38	0.460	**0.386**
Hwang & Lee (2002)	400.92	0.522	**0.418**	320.12	0.811	**0.338**	418.68	0.448	**0.425**
Parra-Montesinos & Wight (2002)	247.97	0.611	**0.450**	247.21	0.814	**0.535**	248.16	0.595	**0.381**
Hegger et al. (2003)	305.25	0.696	**0.396**	394.03	0.779	**0.516**	278.68	0.710	**0.327**
Attaalla (2004)	Very high	Very low	**1.063**	517.81	0.188	**1.138**	Very high	Very low	**1.010**

Table 5.8: Measures of error and factor of dispersion of the capacity for the capacity models about interior joints.

Model	Total			Unreinforced			Reinforced		
	Δ [kN]	R^2	β_C	Δ [kN]	R^2	β_C	Δ [kN]	R^2	β_C
Kim et al. (2009)	190.82	0.745	**0.334**	178.27	0.846	**0.429**	193.84	0.715	**0.306**
Kitayama et al. (1991)	331.30	0.656	**0.416**	439.81	0.739	**0.536**	298.06	0.671	**0.349**
Hwang & Lee (2000)	287.07	0.576	**0.369**	166.60	0.885	**0.253**	309.96	0.485	**0.381**

CHAPTER VI

6. Recalibration of the Capacity Models

In this section the capacity models outlined in section 2 have been recalibrated by using a database wider than the one generally employed by the authors for calibrating and assessing the same model. The accuracy of the recalibration depends on the average error Δ and the coefficient of determination R^2 defined in the previous section. In fact, to high values of the R^2 and low values of Δ corresponds a recalibration that provides more accurate results.

Further analyses about the capacity models are carried out for the probabilistic parameters in terms of mean μ and standard deviation σ of both original and recalibrated models.

Finally, a formulation for evaluating the shear strength of exterior beam-to-column joints is proposed as a development of a previous model. The comparison between the experimental results V_{jh}^{exp} and the corresponding values evaluated through the proposed formula shows the accuracy of the developed tool in evaluating the capacity of exterior joints providing low dispersion.

6.1 Recalibration of Capacity Models

The proposed recalibration is based on a linear scaling of the shear strength V_{jh} provided by each model (EN 1990, 2006 - Monti et al., 2009) through a factor α selected with the aim of minimizing the average error:

$$V_{jh,rec} = \alpha \cdot V_{jh} \ . \tag{6.1}$$

The factor α has been obtained by performing a least square regression on the available experimental data:

$$\alpha = \arg\min_{\alpha}\left[\sqrt{\frac{\sum_{i=1}^{n}\left(\alpha \cdot V_{jh} - V_{jh}^{\exp}\right)^2}{n}}\right] = \arg\min_{\alpha}\left[\Delta(\alpha)\right]. \qquad (6.2)$$

As a matter of principle, a value of the factor α smaller than 1.00 denotes that the original model is meanly unconservative, while a value greater than one is representative of conservative results provided by the original model.

Finally, it is noted that the recalibration made through the factor α does not provide any variation of the Coefficient of Determination R^2 and of the dispersion parameter β_C, whose values are reported in section 5.3.2.

6.1.1 Recalibration of Code Formulations for Exterior Joints

Table 6.1 reports the recalibration factor α obtained by performing the least square procedure [Eqn. (6.2)]. In particular, the least-square procedure described in Eqn. (6.2) is carried out by considering both the database as a whole and the three subsections collecting EC8-compliant, under-reinforced or reinforced joints. For each group is also reported the Average Quadratic Error Δ evaluated for the recalibrated model through Eqn. (5.1).

Table 6.1: Recalibration factors and Average Quadratic Error of the recalibrated Code Formulation for exterior joints.

Model	Total		Unreinforced		Under-reinforced		EC8-compliant	
	α	Δ [kN]	α	Δ [kN]	α	Δ [kN]	α	Δ [kN]
ACI 352-85 (1985)	0.524	172.34	0.568	190.98	0.506	165.84	0.522	120.33
ACI 352-02 (2002)	0.855	178.92	0.942	190.98	0.839	165.84	0.680	152.13

Table 6.1: Recalibration factors and Average Quadratic Error of the recalibrated Code Formulation for exterior joints.

Model	Total		Unreinforced		Under-reinforced		EC8-compliant	
	α	Δ [kN]	α	Δ [kN]	α	Δ [kN]	α	Δ [kN]
ACI 318-05 (2005)	0.745	201.55	0.862	213.46	0.726	183.85	0.562	162.48
AIJ 1990 (1990)	0.721	212.23	0.873	216.02	0.678	204.83	0.662	139.85
AIJ 1999 (1999)	0.924	189.21	1.067	195.73	0.892	180.04	0.746	133.30
NZS 3101 (1995)	0.726	266.52	-	-	0.732	286.05	0.675	148.55
FEMA 273 (1997) – 356 (2000)	0.837	273.81	1.725	213.46	0.756	213.17	0.734	149.01
EC8 (1995)	0.494	203.93	0.583	220.99	0.475	188.22	0.396	136.39

Table 6.1: Recalibration factors and Average Quadratic Error of the recalibrated Code Formulation for exterior joints.

Model	Total		Unreinforced		Under-reinforced		EC8-compliant	
	α	Δ [kN]	α	Δ [kN]	α	Δ [kN]	α	Δ [kN]
EC8 (2005) NTC (2008)	1.210	178.03	1.547	163.24	1.157	157.67	0.890	71.47
NTC (2008) OPCM (2005)	2.237	180.70	2.164	177.12	2.436	171.06	1.555	73.14

The code formulations recalibrated by using the factor α outlined above have been assessed by comparing the experimental shear strength V_{jh}^{exp} with the recalibrated theoretical one αV_{jh}. The results are shown in the following figures in which the comparison is reported through the equivalence charts already used for assessing the original models (section 5.1). Four equivalence charts are reported for each model; in particular the charts reporting the comparison for all the analysed exterior joints, for unreinforced, under-reinforced and EC8-compliant joints are outlined.

In the equivalence charts the bisector segment is reported as reference of the equivalent rule between the experimental evidence and the theoretical value of the recalibrated model. Moreover, the segments representing the fractile of 84% and 16% evaluated through Eqns. (5.18) and (5.19) are also represented

Finally, the values of the factor α, the Average Quadratic Error Δ and the factor of dispersion β_C are listed in every chart.

Fig. 6.1 shows the equivalence charts plotted for the recalibrated ACI 352-85 (1985) formulation for exterior joints. The values of the factor α evaluated for all the specimens, unreinforced, under-reinforced and EC8-compliant joints are smaller than 1.000 as the original model results non-conservative. The recalibrated model by ACI 352-85 (1985) predicts accurate results for under-reinforced and EC8-compliant joints, while the results for unreinforced joints are rather dispersed.

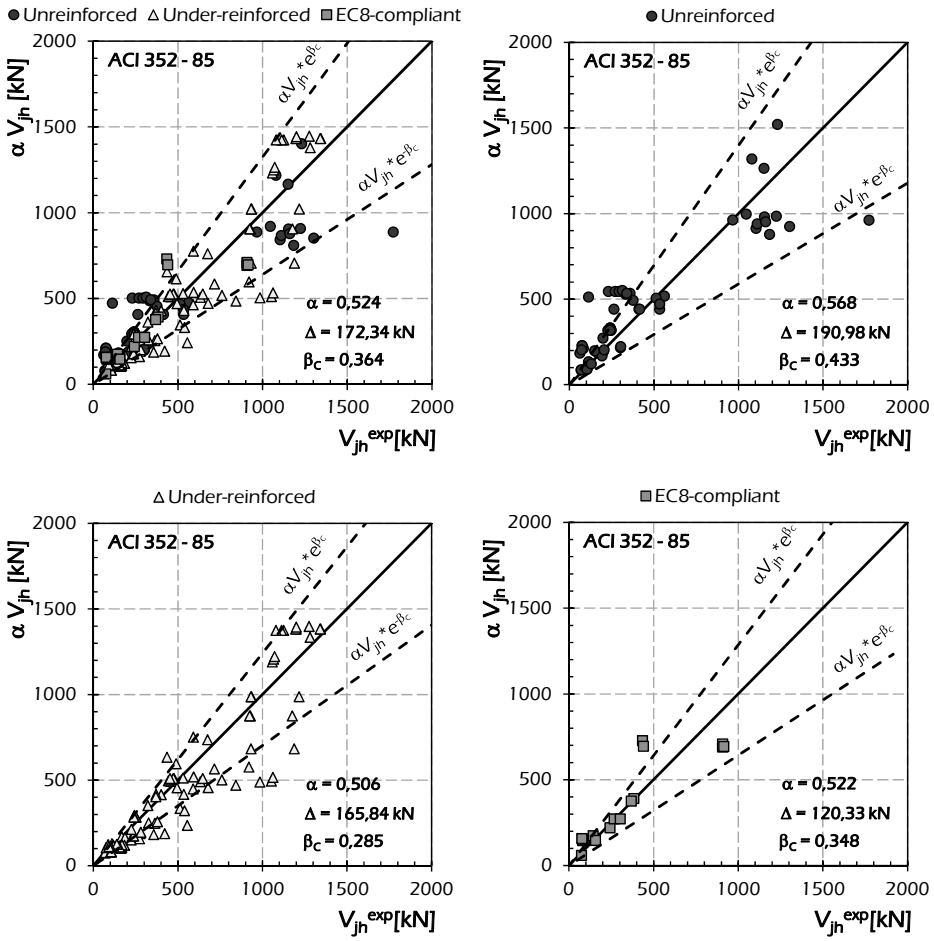

Fig. 6.1: *Assessment of the recalibrated ACI 352-85 (1985) formulation for exterior joints.*

Fig. 6.2 shows the equivalence charts plotted for the recalibrated ACI 352-02 (2002) formulation for exterior joints. The values of the factor α evaluated for all the specimens, unreinforced, under-reinforced and EC8-compliant joints are smaller than 1.000 as the original model results non-conservative. The recalibrated model by ACI 352-02 (2002) predicts accurate results for under-reinforced joints, while the results for unreinforced and for EC8-compliant joints are non-accurate resulting slightly conservative.

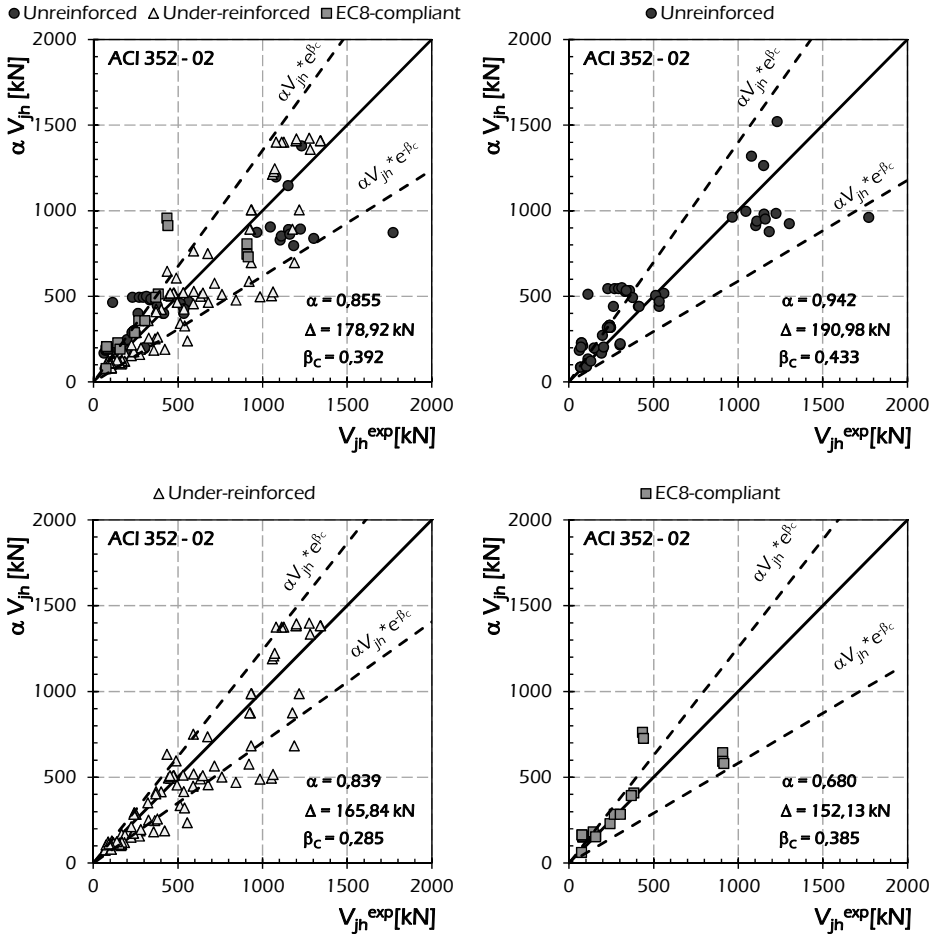

Fig. 6.2: Assessment of the recalibrated ACI 352-02 (2002) formulation for exterior joints.

Fig. 6.3 shows the equivalence charts plotted for the recalibrated ACI 318-05 (2005) formulation for exterior joints. The values of the factor α evaluated for all the specimens, unreinforced, under-reinforced and EC8-compliant joints smaller than 1.000 denote a non-conservative trend of the prediction of the original models for all the analysed classes of joints. The recalibrated model by ACI 318-05 (2005) predicts accurate results for under-reinforced joints. Furthermore, a slightly conservative trend of the strength predicted by using this recalibrated model is shown.

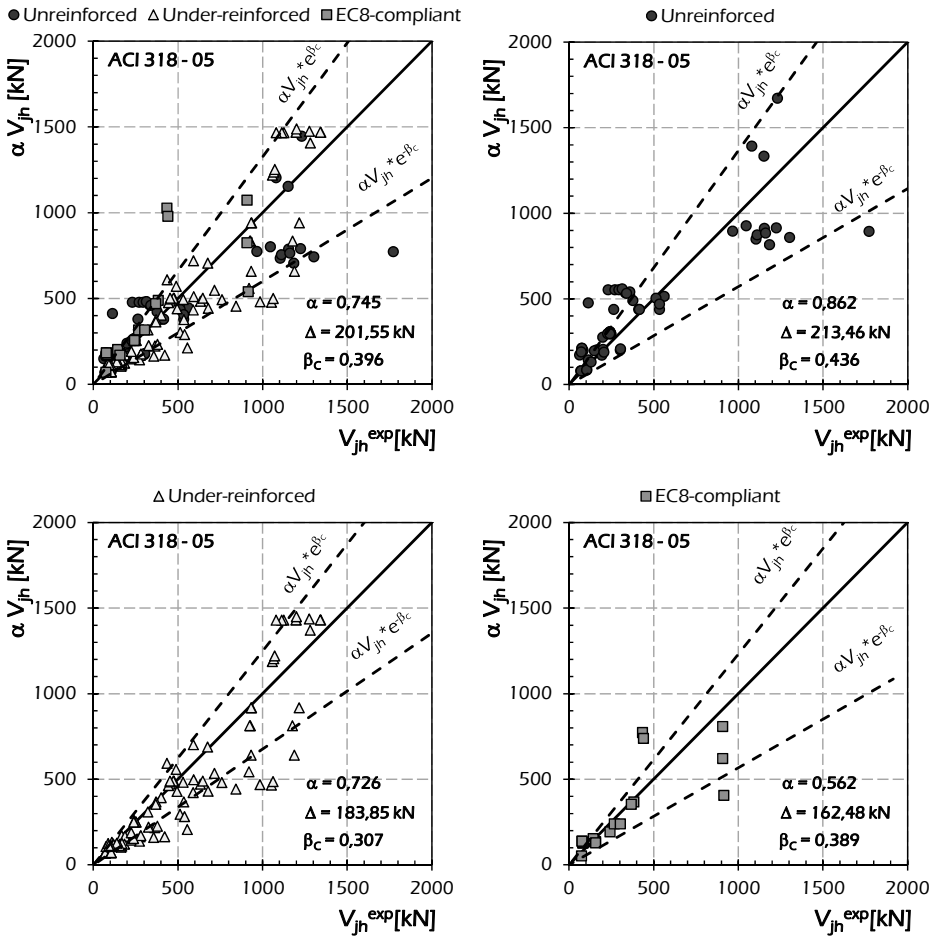

Fig. 6.3: *Assessment of the recalibrated ACI 318-05 (2005) formulation for exterior joints.*

Fig. 6.4 shows the equivalence charts plotted for the AIJ 1990 (1990) formulation for exterior joints recalibrated by using the factor α reported in Table 6.1. The values of the factor α evaluated for all the classes of joints are smaller than 1.000 as the original model results non-conservative. The recalibrated model by AIJ 1990 (1990) predicts slightly conservative results for unreinforced, under-reinforced and EC8-compliant joints, but results are rather dispersed.

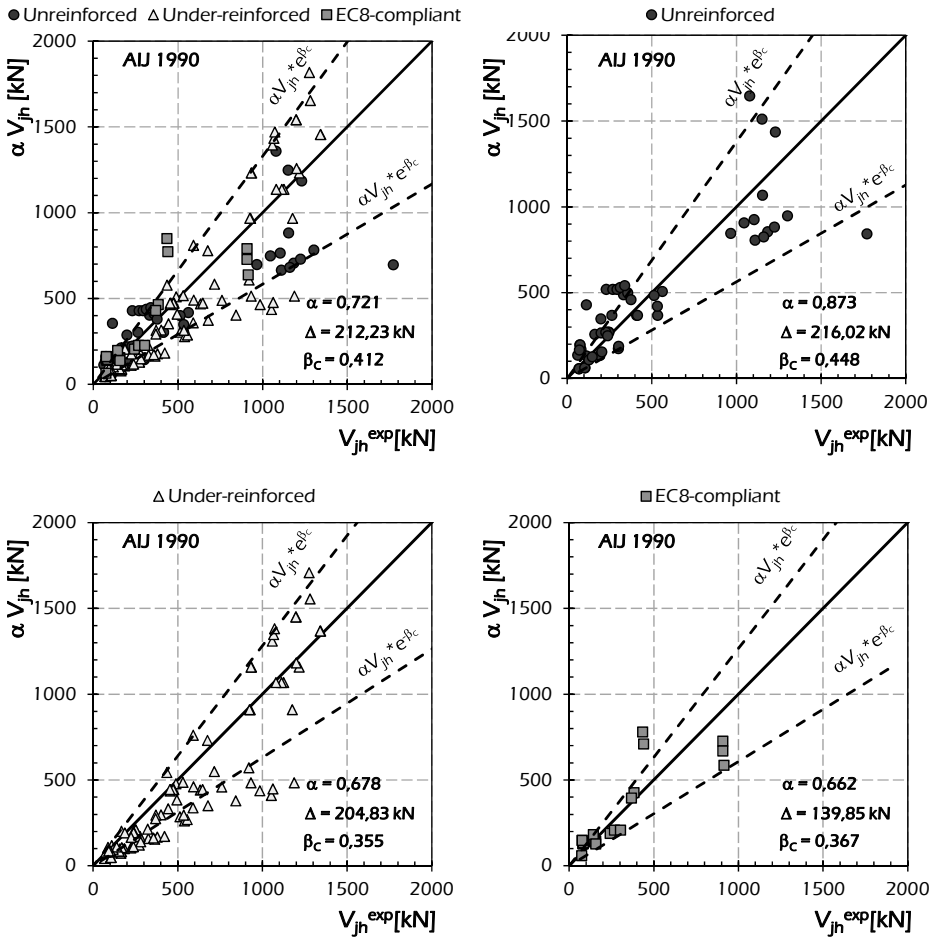

Fig. 6.4: Assessment of the recalibrated AIJ 1990 (1990) formulation for exterior joints.

Fig. 6.5 shows the equivalence charts plotted for the recalibrated AIJ 1999 (1999) formulation for exterior joints. The values of the factor α evaluated for all the specimens, under-reinforced and EC8-compliant joints are smaller than 1.000 as the original model results non-conservative, while α is equal to 1.067 for unreinforced exterior joints as the original model denotes a slightly conservative trend for this kind of joints. The recalibrated model by AIJ 1999

(1999) predicts accurate results for under-reinforced joints, while the results for unreinforced joints are rather dispersed.

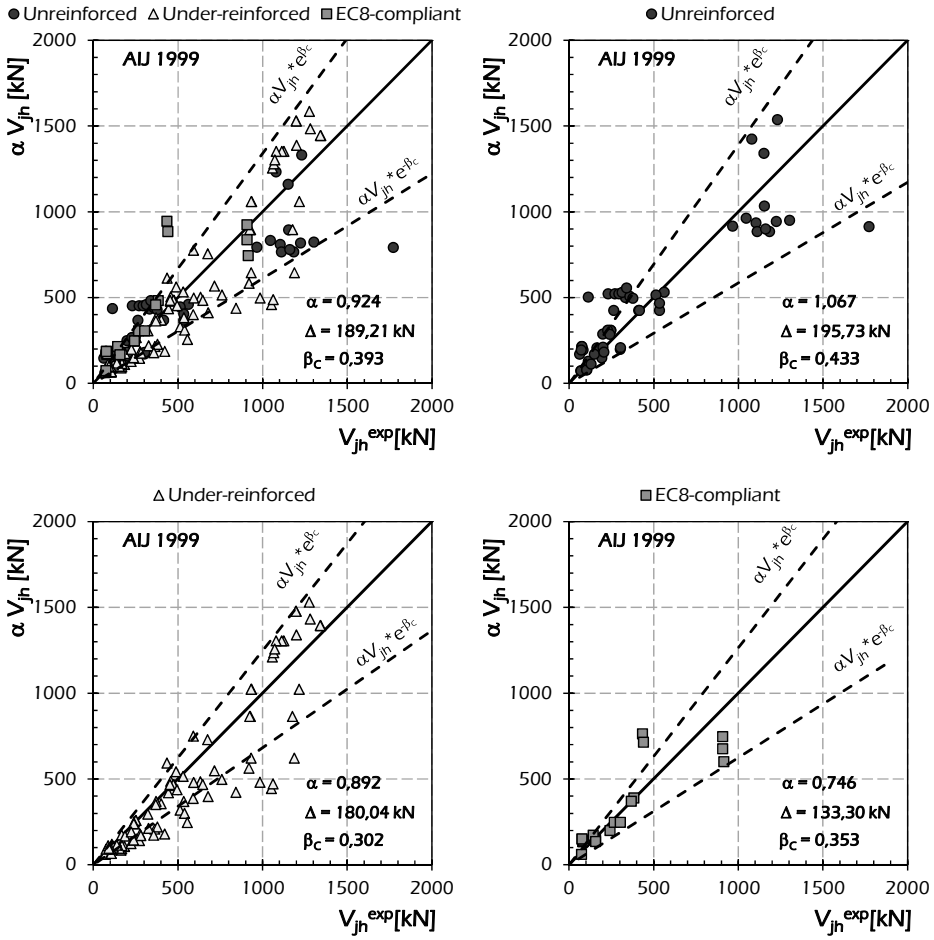

Fig. 6.5: Assessment of the recalibrated AIJ 1999 (1999) formulation for exterior joints.

Fig. 6.6 shows the equivalence charts plotted for the recalibrated NZS 3101 (1995) formulation for exterior joints. The model does not take into account unreinforced joints, as it predicts a shear strength equal to 0 for this kind of joints. The values of the factor α evaluated for all the specimens, under-reinforced and EC8-compliant joints are smaller than 1.000 as the original

model results non-conservative. The prediction of the model by NZS 3101 (1995) is highly dispersed for both under-reinforced and EC8-compliant joints.

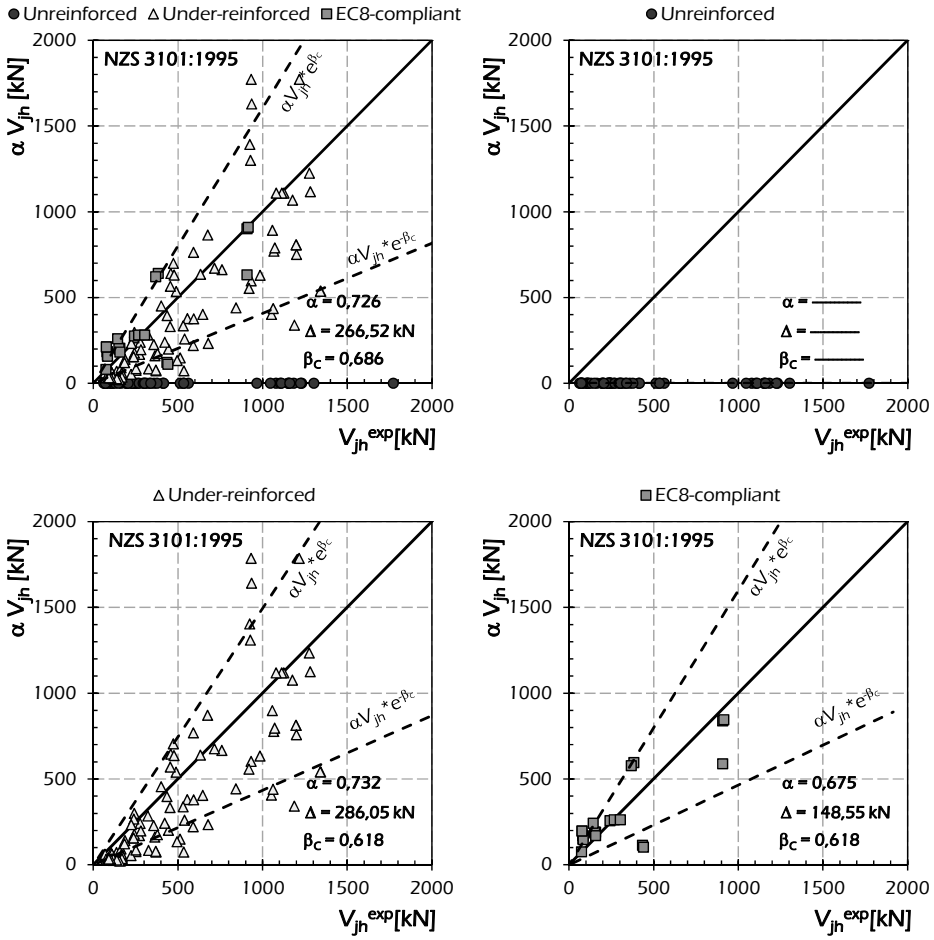

Fig. 6.6: Assessment of the recalibrated NZS 3101 (1995) formulation for exterior joints.

Fig. 6.7 shows the equivalence charts plotted for the recalibrated model by FEMA 273 (1997) - 356 (2000). The values of the factor α evaluated for all the specimens as a whole, under-reinforced and EC8-compliant joints smaller than 1.000 denote a non-conservative trend of the prediction of the original model,

while for unreinforced joints α is equal to 1.725, as the original model is conservative. The recalibrated model by FEMA 273 (1997) and FEMA 356 (2000) predicts slightly conservative results.

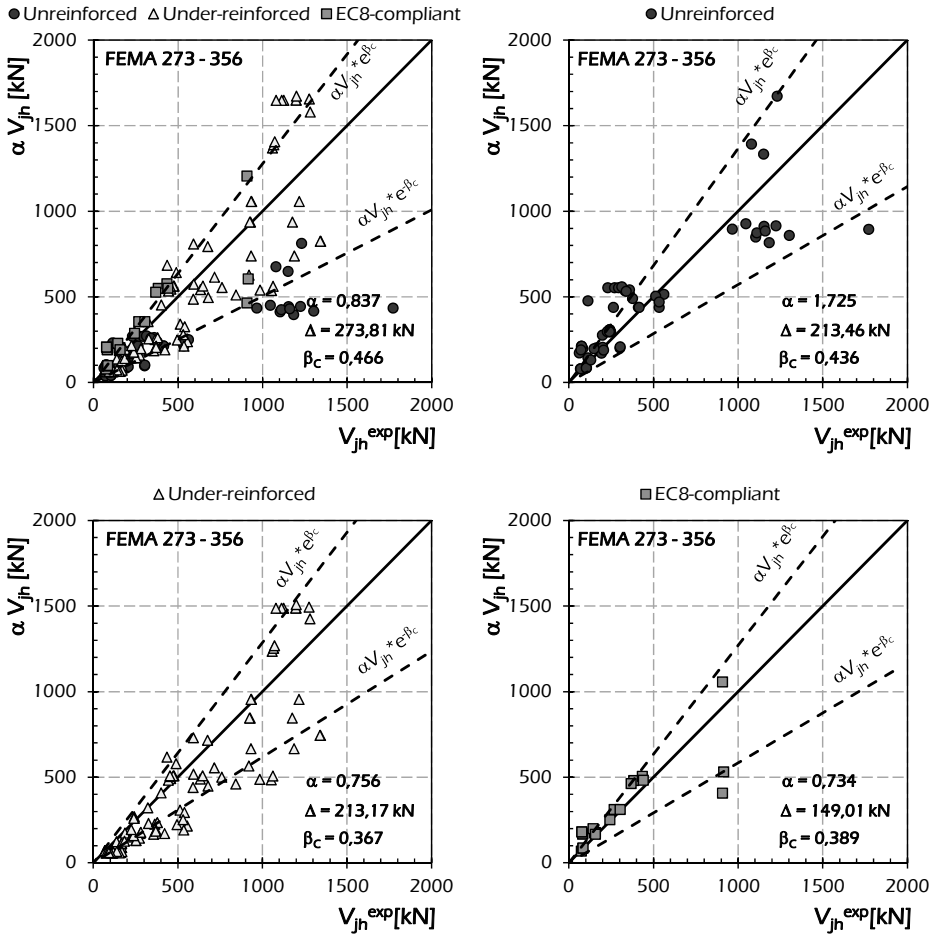

Fig. 6.7: Assessment of the recalibrated FEMA 273 (1997) and 356 (2000) formulation for exterior joints.

Fig. 6.8 shows the equivalence charts plotted for the EC8 (EN 1995, 1995) formulation for exterior joints recalibrated by using the factor α reported in Table 6.1. The values of the factor α evaluated for all the classes of joints are

smaller than 1.000 as the original model results non-conservative. The recalibrated model by EC8 (EN 1995, 1995) predicts slightly conservative results for unreinforced, under-reinforced and EC8-compliant joints. Highly dispersion affects the results for unreinforced joints.

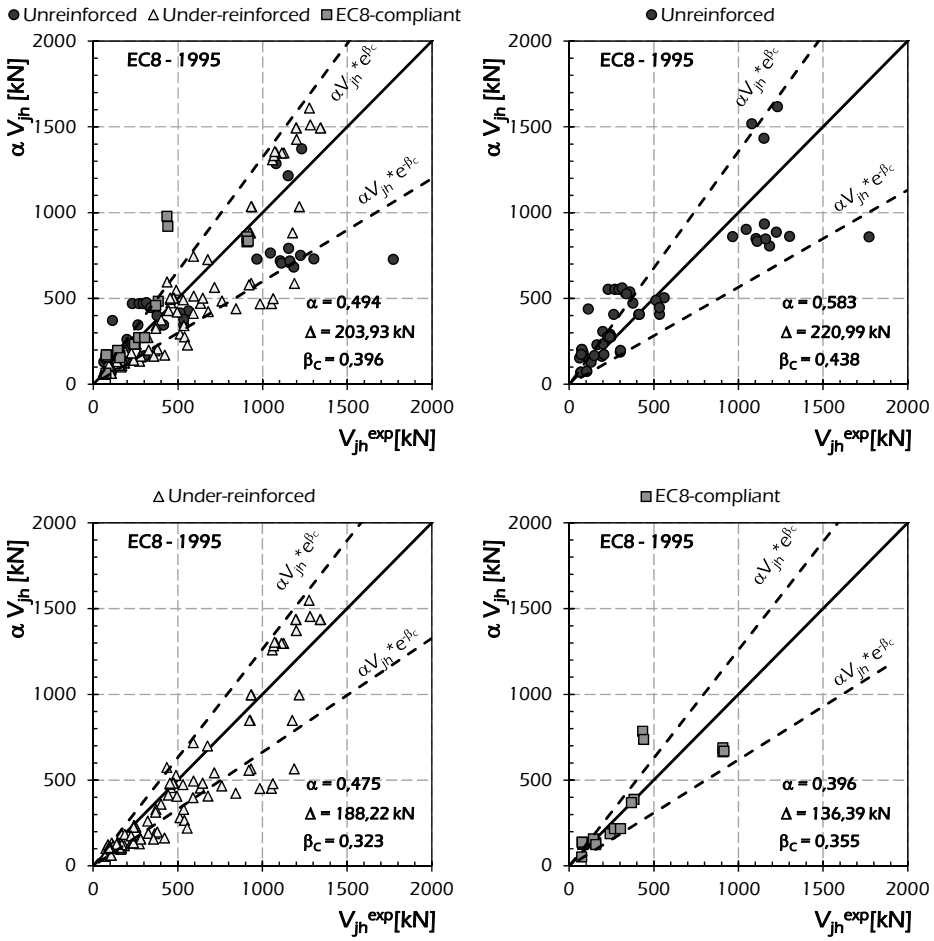

Fig. 6.8: Assessment of the recalibrated Eurocode 8 (EN 1995, 1995) formulation for exterior joints.

Fig. 6.9 shows the equivalence charts plotted for the recalibrated EC8 (EN 1998, 2005) and NTC (2008) formulation for exterior joints. The values of the

factor α evaluated for all the specimens, unreinforced and under-reinforced joints are greater than 1.000 as the original model results conservative, while α is smaller than unit for EC8-compliant exterior joints as the original model denotes a slightly non-conservative trend for this kind of joints. The recalibrated model (EN 1998, 2005 and NTC, 2008) predicts accurate results for under-reinforced and EC8-compliant joints, while the results for unreinforced joints are rather dispersed.

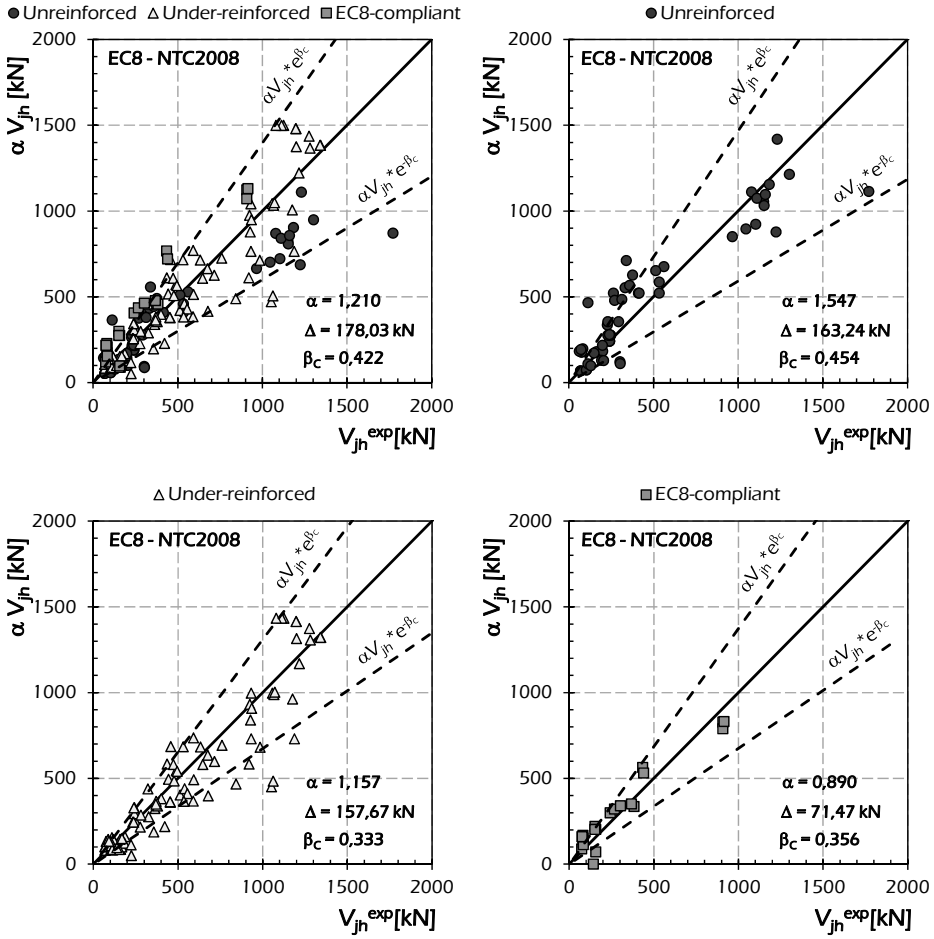

Fig. 6.9: Assessment of the recalibrated Eurocode 8 (EN 1998, 2005) and NTC (2008) formulation for exterior joints.

Fig. 6.10 shows the equivalence charts plotted for the recalibrated model by NTC (2008) and OPCM 3431/05 (2005) for evaluating the shear strength of joints in existing structures. The values of the factor α evaluated for all the specimens as a whole, unreinforced, under-reinforced and EC8-compliant joints greater than 1.000 denote a conservative trend of the prediction of the original model. The recalibrated model (NTC, 2008 and OPCM 3431/05, 2005) predicts accurate results.

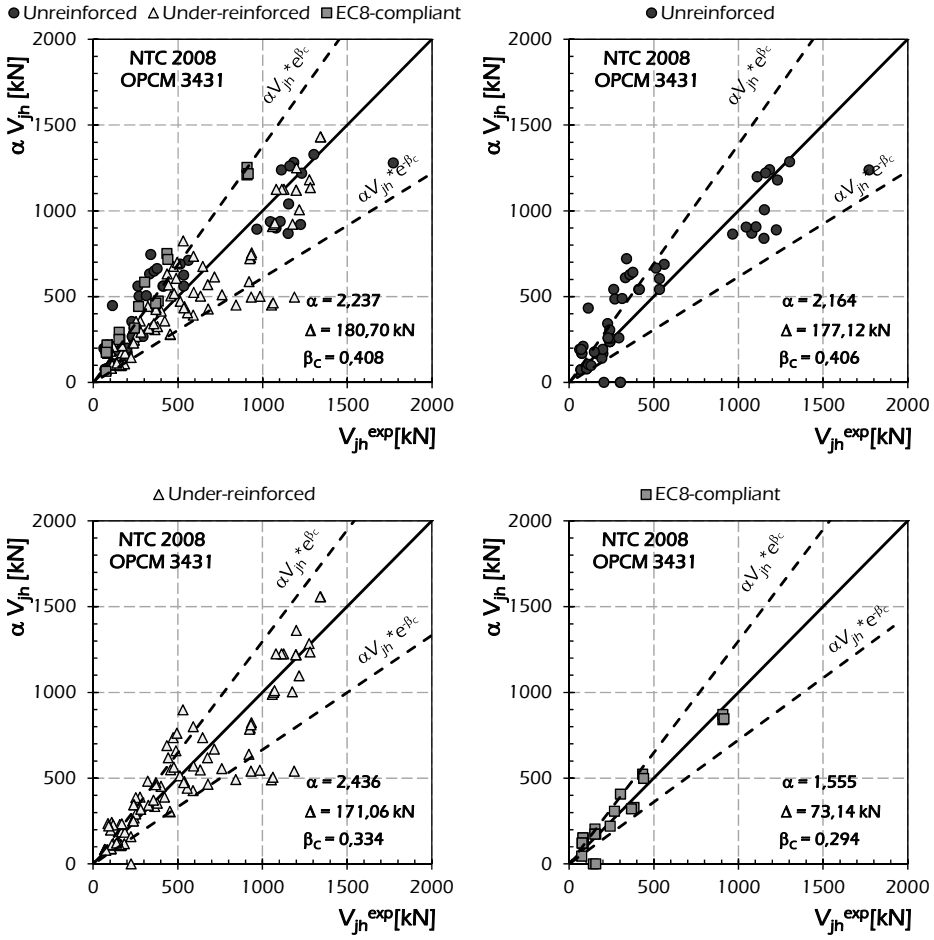

Fig. 6.10: Assessment of the recalibrated NTC (2008) and OPCM 3431/05 (2005) formulation for exterior joints.

6.1.2 Recalibration of Capacity Models Available in the Literature for Exterior Joints

The factors α obtained by performing the least square procedure [Eqn. (6.2)] for the capacity models available in the scientific literature are reported in Table 6.2.

The analysis is provided by considering the total set of exterior specimens, the unreinforced joints and the reinforced ones subdivided in under-reinforced and EC8-compliant. For each group is also reported the Average Quadratic Error Δ evaluated for the recalibrated model through Eqn. (5.1).

Table 6.2: Recalibration factors and Average Quadratic Error of the recalibrated Capacity Models for exterior joints.

Model	Total		Unreinforced		Under-reinforced		EC8-compliant	
	α	Δ [kN]	α	Δ [kN]	α	Δ [kN]	α	Δ [kN]
Pantazopoulo & Bonacci (1992)	0.321	184.05	0.368	138.84	0.304	206.82	0.303	100.42
Paulay & Priestley (1992)	1.027	164.97	1.130	168.23	1.009	161.39	0.827	112.73
Parker & Bullman (1997)	0.854	227.18	1.163	210.65	0.785	221.30	0.776	61.59
Hwang & Lee (2002)	1.178	152.17	1.257	113.69	1.187	168.96	0.885	64.24

Table 6.2: Recalibration factors and Average Quadratic Error of the recalibrated Capacity Models for exterior joints.

Model	Total		Unreinforced		Under-reinforced		EC8-compliant	
	α	Δ [kN]	α	Δ [kN]	α	Δ [kN]	α	Δ [kN]
Parra-Montesinos & Wight (2002)	0.727	185.73	0.787	191.08	0.729	176.63	0.534	143.25
Hegger et al. (2003)	0.872	194.64	1.193	180.26	0.816	163.68	0.681	118.27
Kim et al. (2009)	0.910	161.79	1.129	150.71	0.851	149.76	0.822	74.93
Zhang & Jirsa (1982)	0.630	194.87	0.643	159.22	0.625	228.54	0.612	76.87
Sarsam & Phillips (1985)	0.924	177.28	1.168	124.40	0.880	180.74	0.698	56.73

Table 6.2: Recalibration factors and Average Quadratic Error of the recalibrated Capacity Models for exterior joints.

Model	Total		Unreinforced		Under-reinforced		EC8-compliant	
	α	Δ [kN]	α	Δ [kN]	α	Δ [kN]	α	Δ [kN]
Ortiz (1993)	0.583	231.64	1.066	202.73	0.536	154.02	0.455	85.62
Scott et al. (1994)	0.887	224.74	1.081	196.21	0.864	229.42	0.623	122.25
Vollum & Newman (1999)	0.822	182.09	1.013	181.23	0.786	163.60	0.637	115.22
Hwang & Lee (1999)	1.097	154.48	1.260	128.94	1.066	157.34	0.850	87.27
Bakir & Boduroglu (2002)	0.912	183.17	1.177	162.75	0.847	174.68	0.820	70.18

Table 6.2: Recalibration factors and Average Quadratic Error of the recalibrated Capacity Models for exterior joints.

Model	Total		Unreinforced		Under-reinforced		EC8-compliant	
	α	Δ [kN]	α	Δ [kN]	α	Δ [kN]	α	Δ [kN]
Russo & Somma (2006)	0.686	210.52	1.003	192.81	0.619	173.10	0.744	115.06
Tsonos (2007)	0.615	219.94	0.766	257.49	0.577	189.38	0.568	131.97
Vollum & Parker (2008)	0.654	202.14	0.805	173.92	0.611	210.98	0.601	95.85

The capacity models recalibrated by using the factor α outlined above have been assessed by comparing the experimental shear strength V_{jh}^{exp} with the recalibrated theoretical one αV_{jh}. The results are shown in the following figures in which the comparison is reported in terms of equivalence charts.

Four equivalence charts are reported for each model reporting the comparison for all the analysed exterior joints, for unreinforced, under-reinforced and EC8-compliant joints.

In the equivalence charts, in which the bisector segment is reported as a reference, the segments representing the fractile of 84% and 16% evaluated through Eqns. (5.18) and (5.19) are also shown.

Finally, the values of the factor α used for recalibrating the models, the Average Quadratic Error Δ and the factor of dispersion β_C are listed in every chart.

Fig. 6.11 shows the equivalence charts plotted for the recalibrated model by Pantazopoulo & Bonacci (1992) for exterior joints. The values of the factor α evaluated for all the specimens, unreinforced, under-reinforced and EC8-

compliant joints are smaller than 1.000 as the original model results non-conservative. The recalibrated model by Pantazopoulo & Bonacci (1992) predicts accurate results for unreinforced joints, while the results for EC8-compliant joints are rather dispersed.

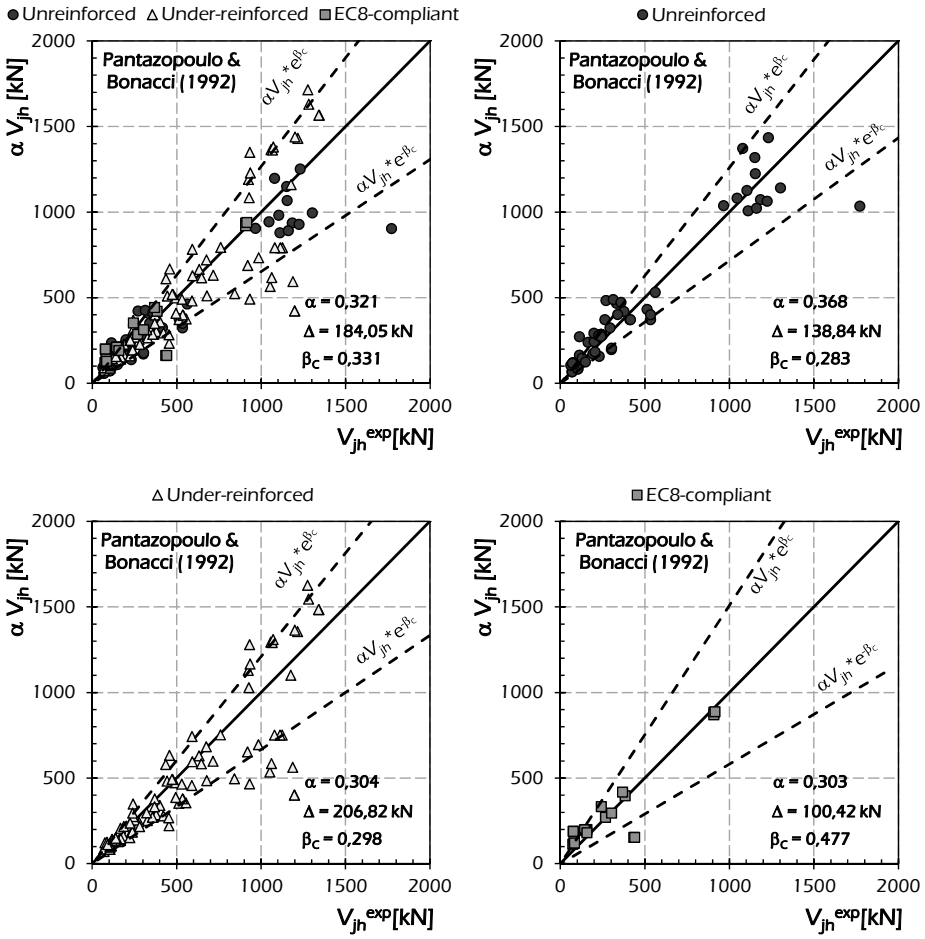

Fig. 6.11: Assessment of the recalibrated model by Pantazopoulo & Bonacci (1992) for exterior joints.

Fig. 6.12 shows the equivalence charts plotted for the recalibrated model by Paulay & Priestley (1992). The values of the factor α evaluated for all the

specimens, unreinforced and under-reinforced joints are greater than 1.000 as the original model results slightly conservative for this kind of joints, while the value α equal to 0.827 for EC8-compliant joint denotes a non-conservative trend of the original model. The recalibrated model by Paulay & Priestley (1992) predicts accurate results for under-reinforced joints, while the results for unreinforced and for EC8-compliant joints are rather dispersed.

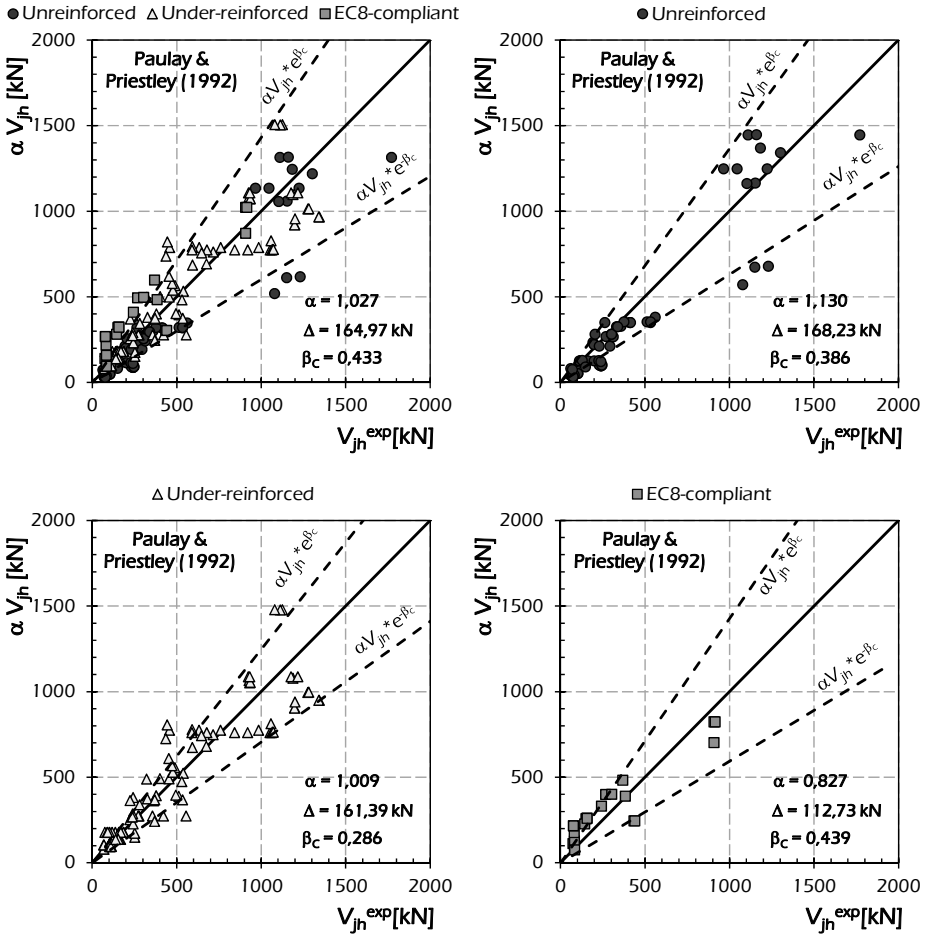

Fig. 6.12: Assessment of the recalibrated model by Paulay & Priestley (1992) for exterior joints.

Fig. 6.13 shows the equivalence charts plotted for the recalibrated model by Parker & Bullman (1997) for exterior joints. The values of the factor α evaluated for all the specimens as a whole, under-reinforced and EC8-compliant smaller than 1.000 denote a non-conservative trend of the prediction of the original model. The recalibrated model by Parker & Bullman (1997) predicts accurate results for EC8-compliant joints. Furthermore, a slightly conservative trend of the strength predicted by using this recalibrated model is shown for unreinforced and under-reinforced joints.

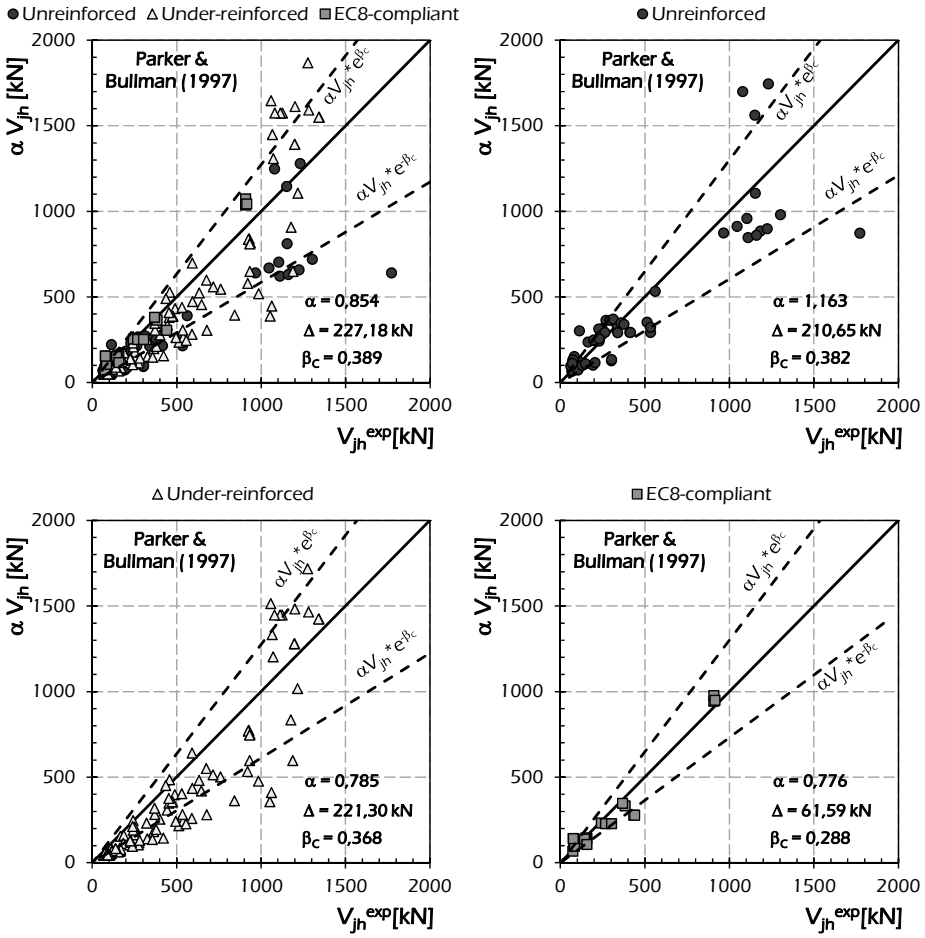

Fig. 6.13: Assessment of the recalibrated model by Parker & Bullman (1997) for exterior joints.

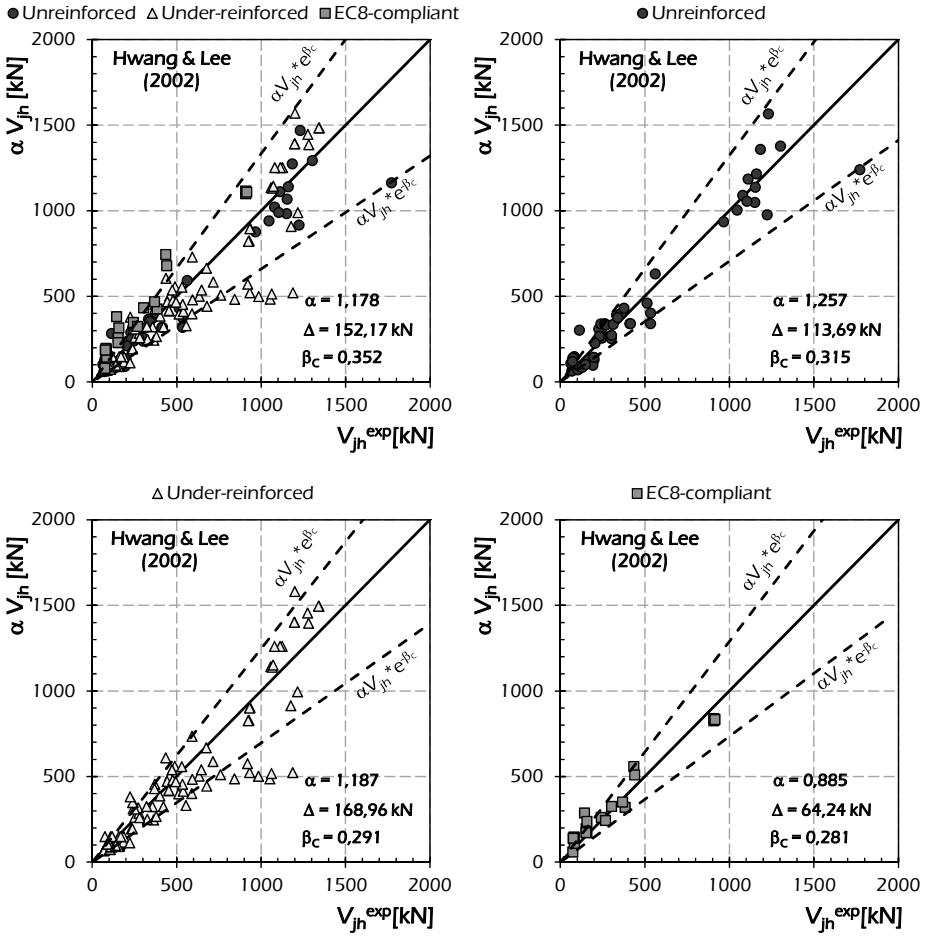

Fig. 6.14: *Assessment of the recalibrated model by Hwang & Lee (2002) for exterior joints.*

Fig. 6.14 shows the equivalence charts plotted for the model by Hwang & Lee (2002) for exterior joints recalibrated by using the factor α reported in Table 6.2. The values of the factor α evaluated for all the specimens as a whole, unreinforced and under-reinforced joints are greater than 1.000 as the original model results conservative. The recalibrated model by Hwang & Lee (2002) predicts accurate results for unreinforced, under-reinforced and EC8-compliant joints.

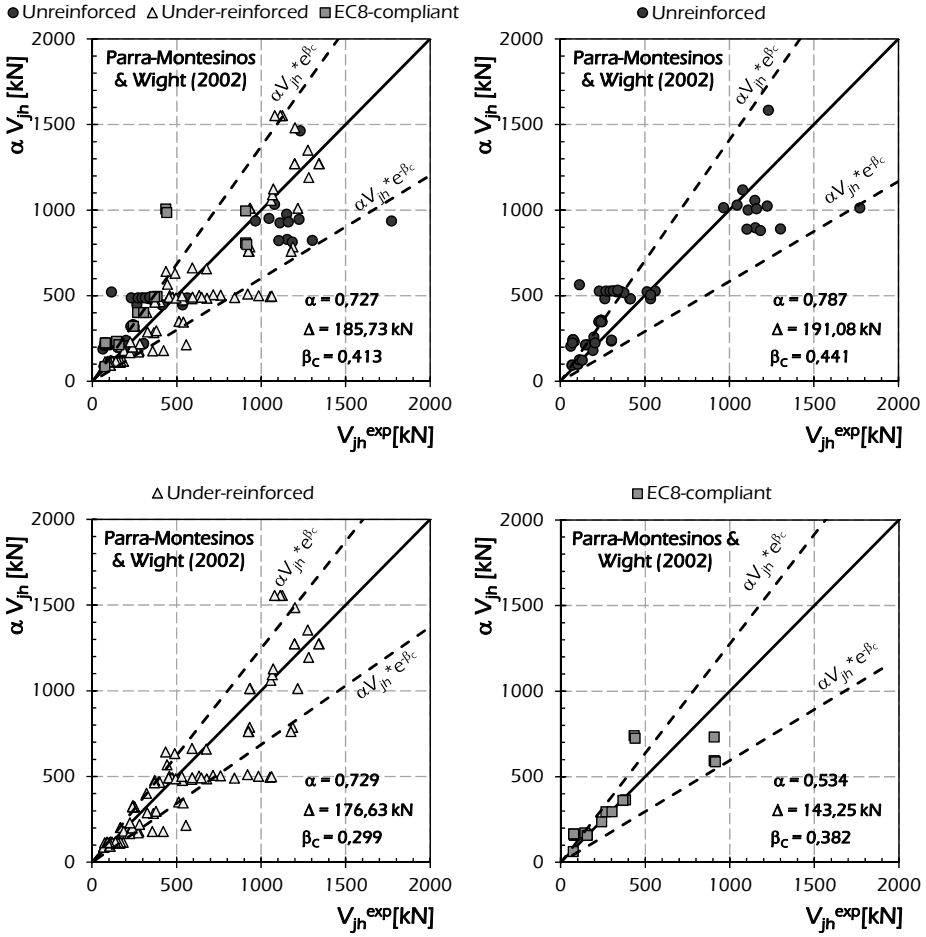

Fig. 6.15: *Assessment of the recalibrated model by Parra-Montesinos & Wight (2002) for exterior joints.*

Fig. 6.15 shows the equivalence charts plotted for the recalibrated model by Parra-Montesinos & Wight (2002) for exterior joints. The values of the factor α evaluated for all the specimens, unreinforced, under-reinforced and EC8-compliant joints are smaller than 1.000 as the original model results non-conservative. The recalibrated model by Parra-Montesinos & Wight (2002) predicts accurate results for under-reinforced joints, while the results for unreinforced and EC8-compliant joints are rather dispersed with a slightly conservative trend.

Fig. 6.16 shows the equivalence charts plotted for the recalibrated model by Hegger et al. (2003) for exterior joints. The values of the factor α evaluated for all the specimens, under-reinforced and EC8-compliant joints are smaller than 1.000 as the original model results non-conservative, while the value of α greater than unit for unreinforced joints denotes a generally conservative trend of the original model by Hegger et al. (2003). The prediction of the recalibrated model is accurate for under-reinforced joints, while results highly dispersed for both unreinforced and EC8-compliant joints.

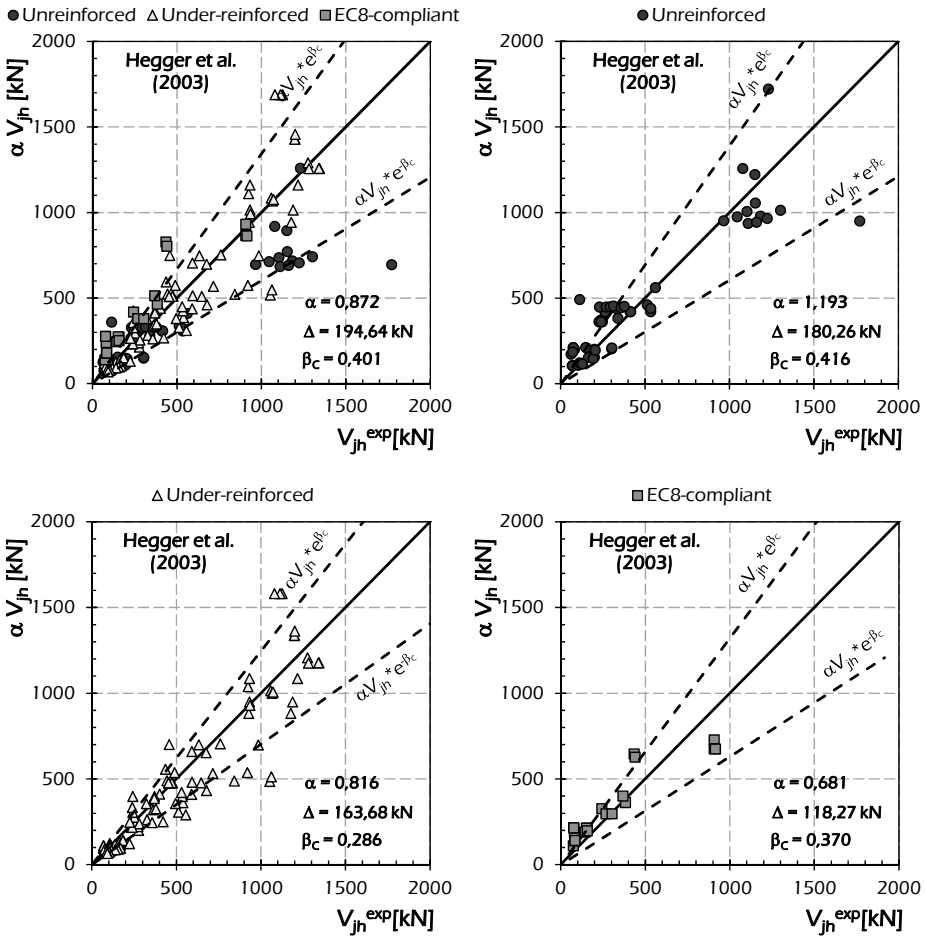

Fig. 6.16: Assessment of the recalibrated model by Hegger et al. (2003) for exterior joints.

Fig. 6.17 shows the equivalence charts plotted for the recalibrated model by Kim et al. (2009). The values of the factor α evaluated for all the specimens as a whole, under-reinforced and EC8-compliant smaller than 1.000 denote a slightly non-conservative trend of the prediction of the original model, while for unreinforced joints α is equal to 1.129, as the original model is conservative. The recalibrated model by Kim et al. (2009) predicts very accurate results for all the classes of joints.

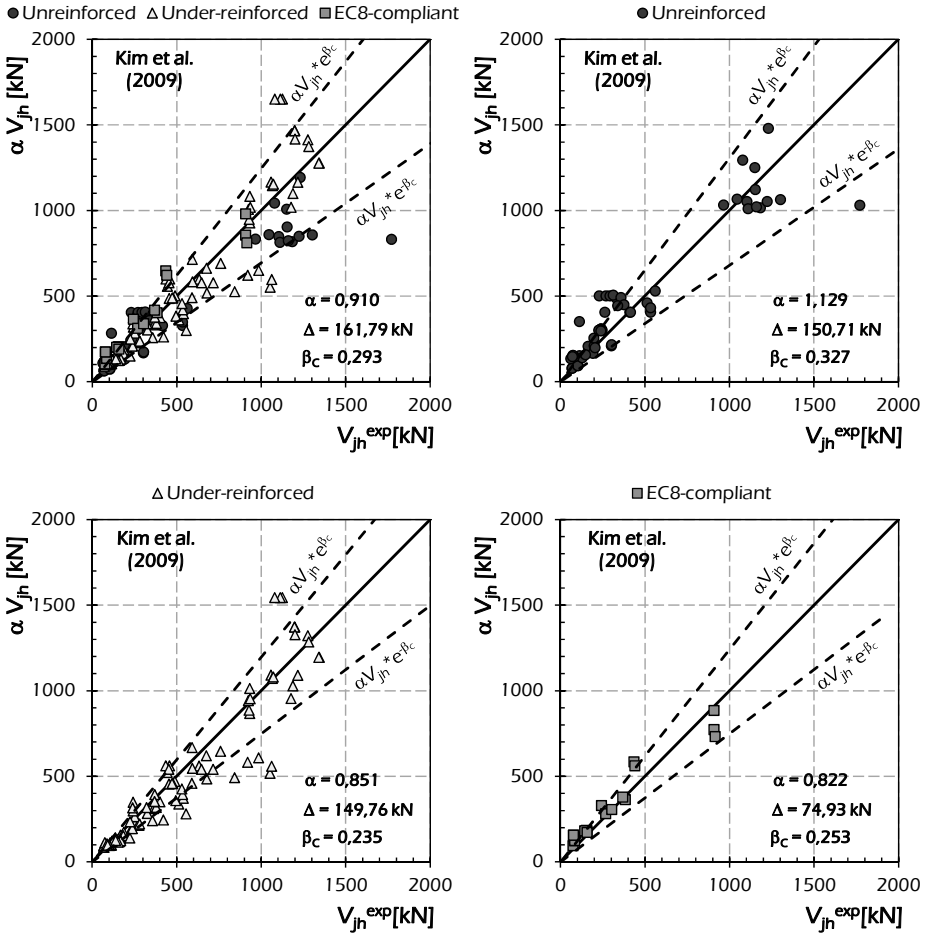

Fig. 6.17: Assessment of the recalibrated model by Kim et al. (2009) for exterior joints.

Fig. 6.18 shows the equivalence charts plotted for the model by Zhang & Jirsa (1982) for exterior joints recalibrated by using the factor α reported in Table 6.2. The values of the factor α evaluated for all the classes of joints are smaller than 1.000 as the original model results non-conservative. The recalibrated model by Zhang & Jirsa (1982) predicts slightly conservative results for under-reinforced joints, but highly dispersion affects the results for this class. On average, accurate predictions are obtained for unreinforced and EC8-compliant joints.

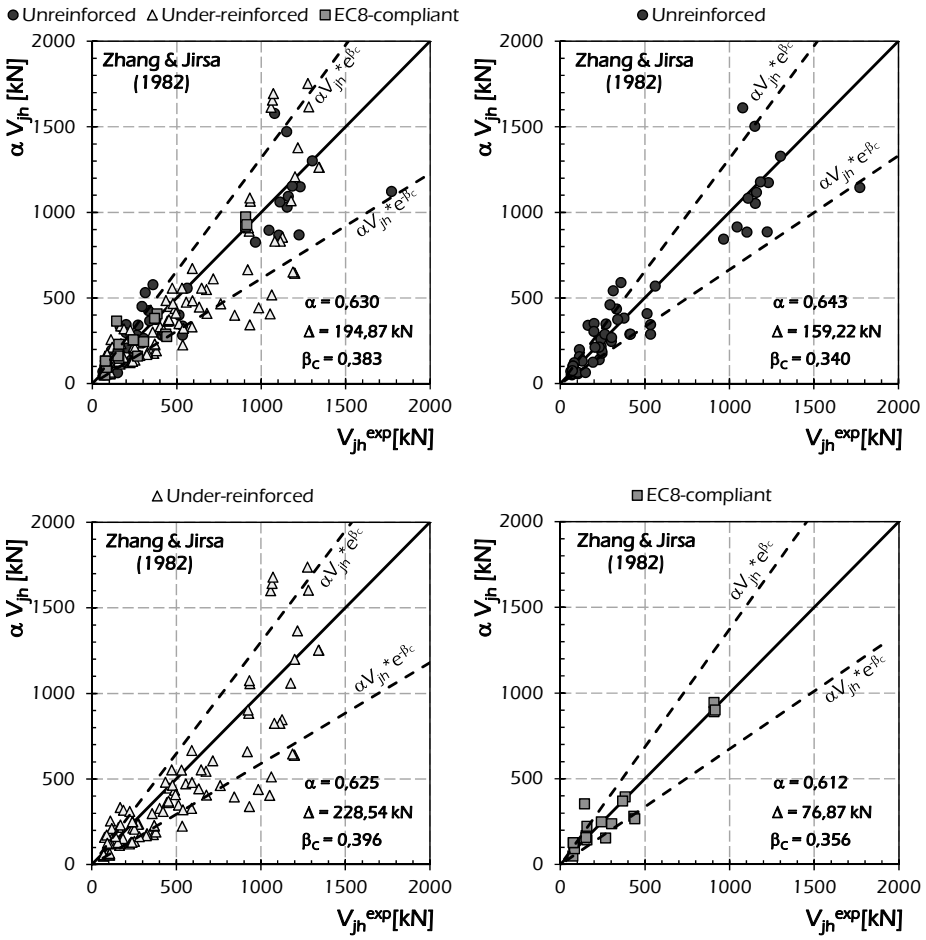

Fig. 6.18: *Assessment of the recalibrated model by Zhang & Jirsa (1982) for exterior joints.*

Fig. 6.19 shows the equivalence charts plotted for the recalibrated model by Sarsam & Phillips (1985) for exterior joints. The values of the factor α evaluated for all the specimens, under-reinforced and EC8-compliant joints are smaller than 1.000 as the original model results non-conservative, while α is greater than unit for unreinforced exterior joints as the original model denotes a slightly conservative trend for this kind of joints. The recalibrated model (Sarsam & Phillips, 1985) predicts accurate results for all the classes of joints. Finally, the results for under-reinforced joints are often slightly conservative.

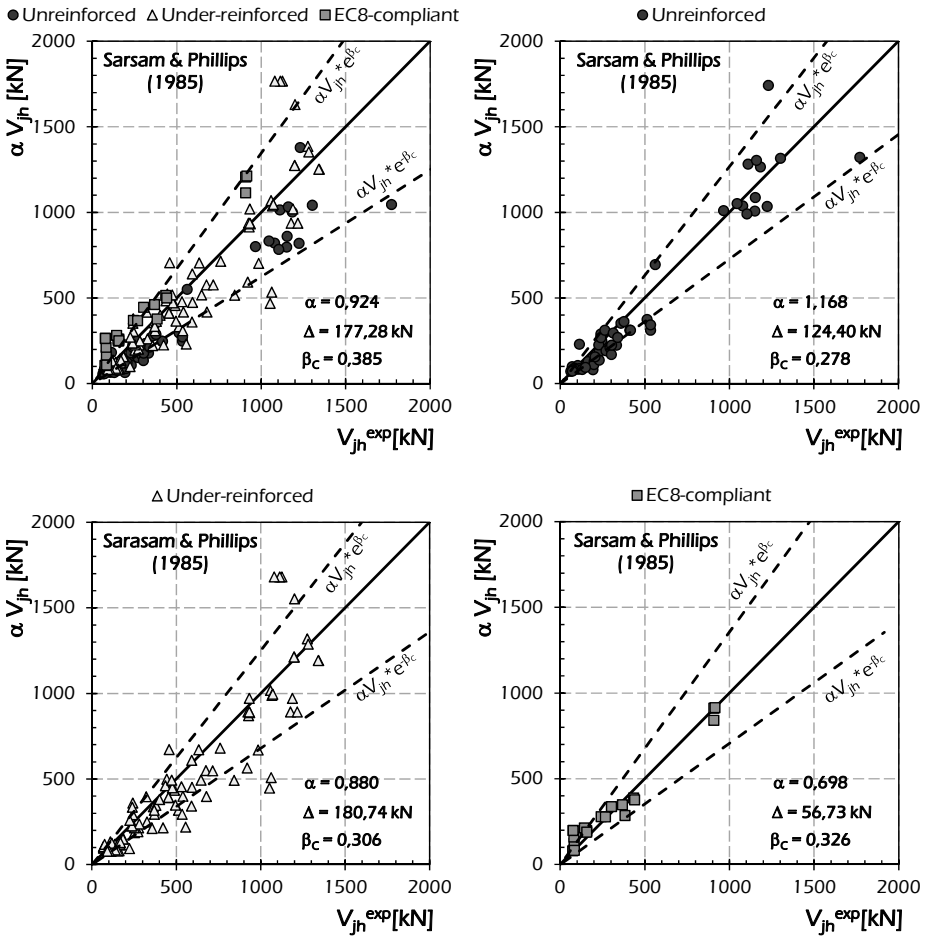

Fig. 6.19: Assessment of the recalibrated model by Sarsam & Phillips (1985) for exterior joints.

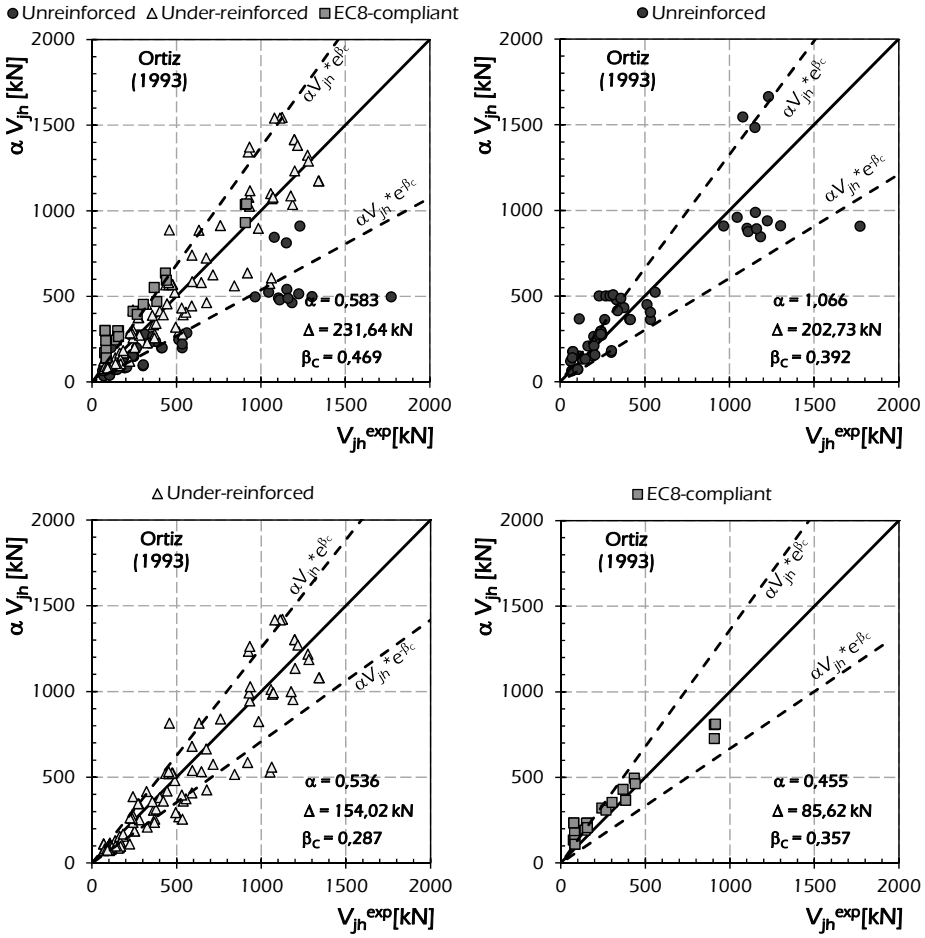

Fig. 6.20: *Assessment of the recalibrated model by Ortiz (1993) for exterior joints.*

Fig. 6.20 shows the equivalence charts plotted for the recalibrated model by Ortiz (1993) for evaluating the shear strength of exterior joints. The values of the factor α evaluated for all the specimens as a whole, under-reinforced and EC8-compliant joints smaller than 1.000 denote a highly conservative trend of the prediction of the original model, while α is equal 1.066 for unreinforced joints, as the original model by Ortiz (1993) predicts accurate results for this kind of joints. The recalibrated model (Ortiz, 1993) predicts accurate results for

under-reinforced joints, while the prediction for unreinforced and EC8-compliant joints is rather dispersed.

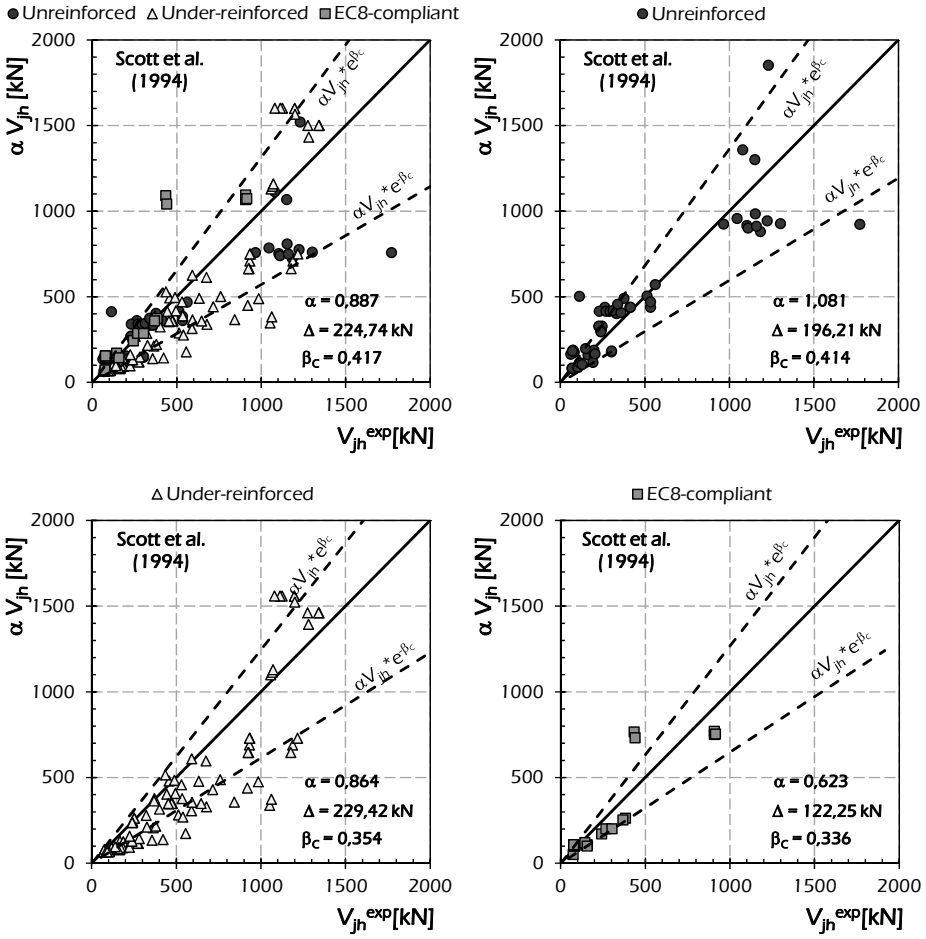

Fig. 6.21: Assessment of the recalibrated model by Scott et al. (1994) for exterior joints.

Fig. 6.21 shows the equivalence charts plotted for the recalibrated model by Scott et al. (1994) for exterior joints. The values of the factor α evaluated for all the specimens, under-reinforced and EC8-compliant joints are smaller than 1.000 as the original model results non-conservative, while α = 1.081 denotes good accordance between the prediction and the experimental evidence. The

recalibrated model by Scott et al. (1994) predicts accurate results for EC8-compliant joints, while the predictions for unreinforced and under-reinforced joint are rather dispersed resulting slightly conservative.

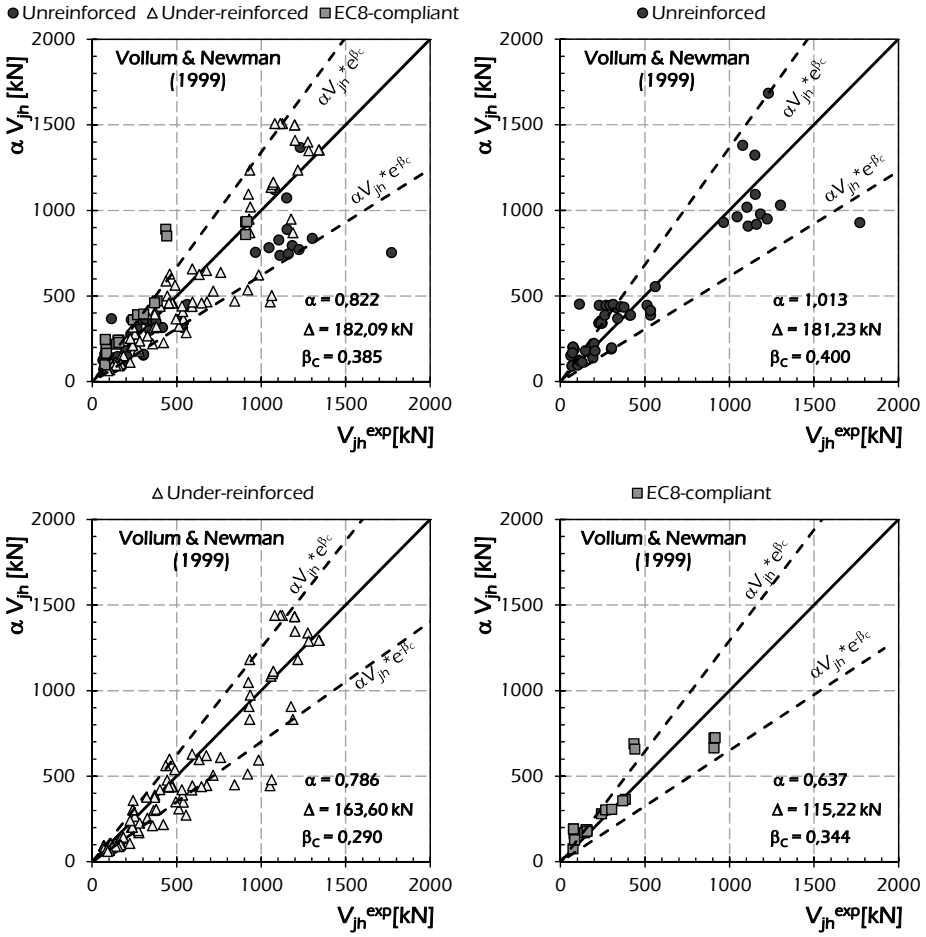

Fig. 6.22: Assessment of the recalibrated model by Vollum & Newman (1999) for exterior joints.

Fig. 6.22 shows the equivalence charts plotted for the recalibrated model by Vollum & Newman (1999). The value of the factor α evaluated for unreinforced joints is greater than 1.000 as the original model results slightly conservative for

this kind of joints, while the values of α smaller than unit for under-reinforced and EC8-compliant joint denotes a non-conservative trend of the original model. The recalibrated model (Vollum & Newman, 1999) predicts accurate results for under-reinforced joints, while the results for unreinforced and for EC8-compliant joints are rather dispersed.

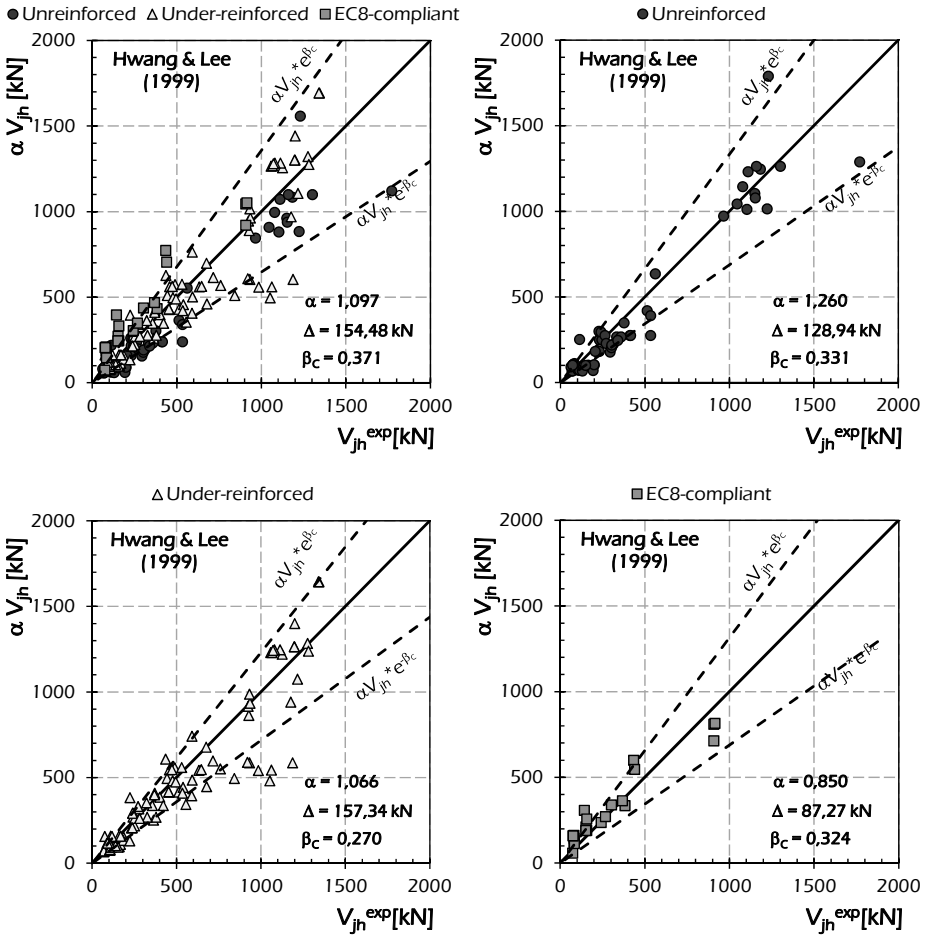

Fig. 6.23: Assessment of the recalibrated model by Hwang & Lee (1999) for exterior joints.

Fig. 6.23 shows the equivalence charts plotted for the recalibrated model by Hwang & Lee (1999) for exterior joints. The values of the factor α evaluated for all the specimens as a whole, unreinforced and under-reinforced greater than 1.000 denote a conservative trend of the prediction of the original model. The recalibrated model by Hwang & Lee (1999) predicts accurate results for all the kinds of joints analysed.

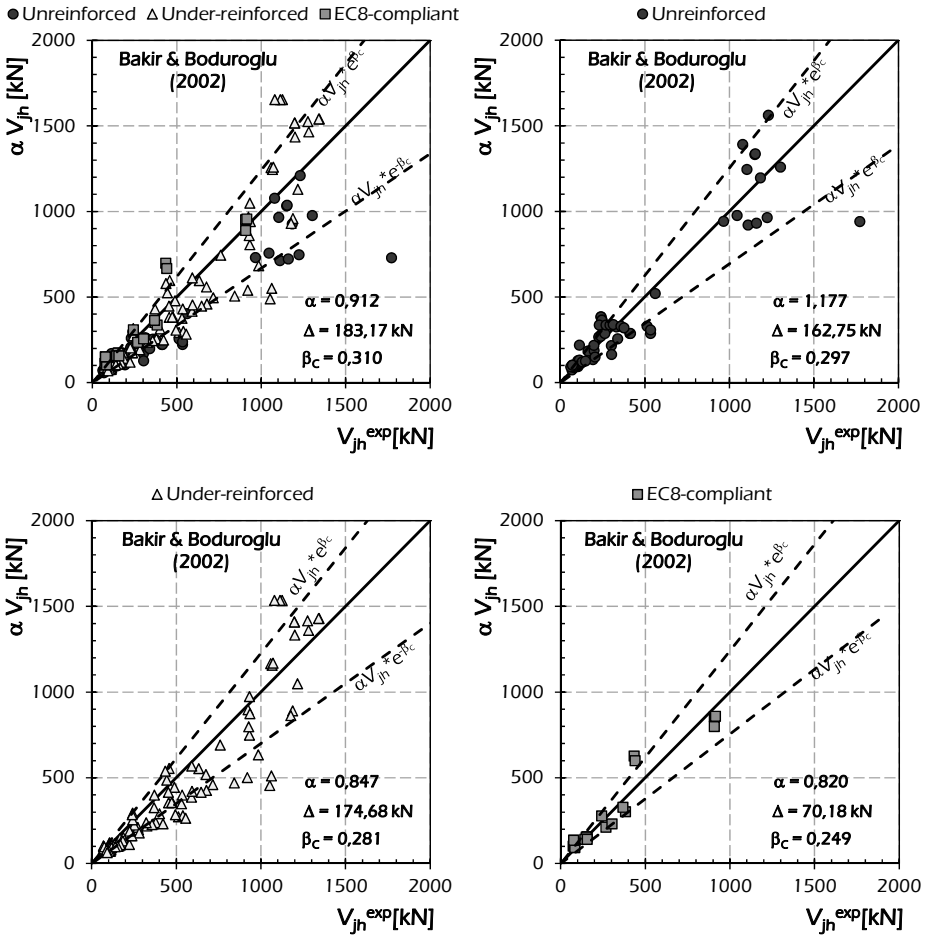

Fig. 6.24: Assessment of the recalibrated model by Bakir & Boduroglu (2002) for exterior joints.

Fig. 6.24 shows the equivalence charts plotted for the model by Bakir & Boduroglu (2002) for exterior joints recalibrated by using the factor α reported in Table 6.2. The values of the factor α evaluated for all the specimens as a whole, under-reinforced and EC8-compliant joints are smaller than 1.000 as the original model results non-conservative. The recalibrated model by Bakir & Boduroglu (2002) predicts accurate results for unreinforced, under-reinforced and EC8-compliant joints as low dispersion affects the prediction.

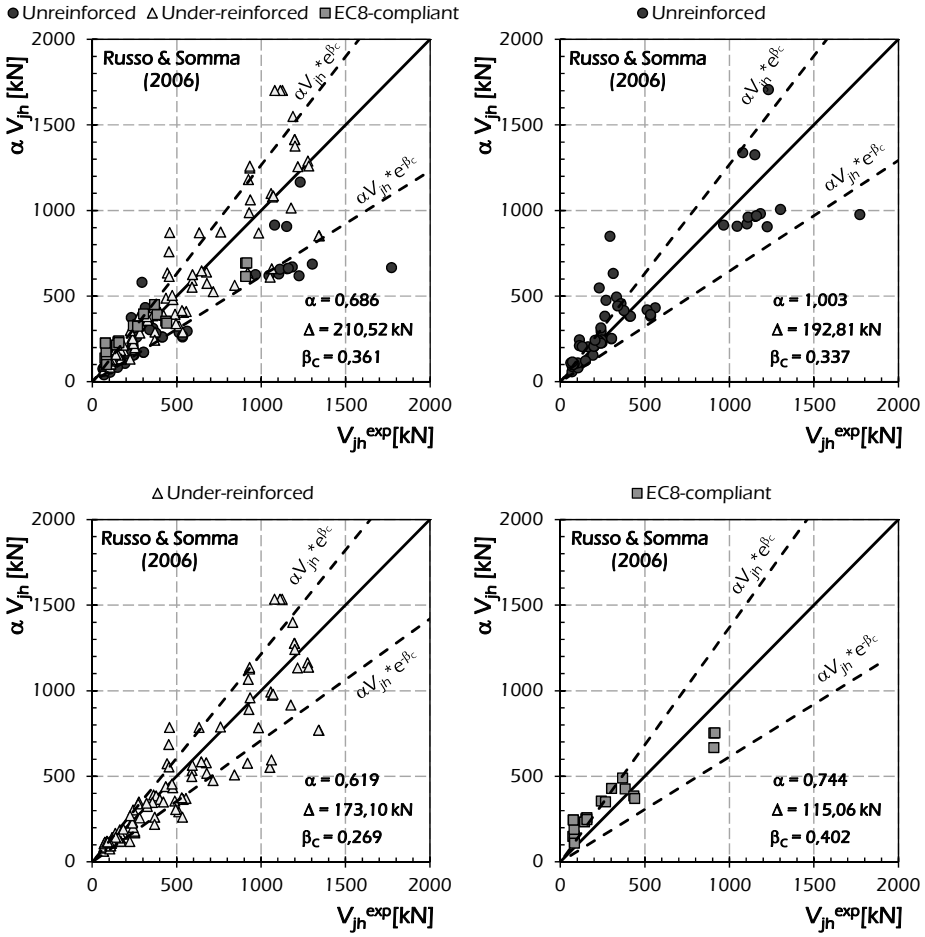

Fig. 6.25: Assessment of the recalibrated model by Russo & Somma (2006) for exterior joints.

Fig. 6.25 shows the equivalence charts plotted for the recalibrated model by Russo & Somma (2006) for exterior joints. The values of the factor α evaluated for unreinforced joints equal to 1.003 denotes the accuracy of the original model for this kind of joints. The recalibrated model by Russo & Somma (2006) predicts accurate results for under-reinforced joints, while the predictions for unreinforced and EC8-compliant joints are rather dispersed with a slightly conservative trend.

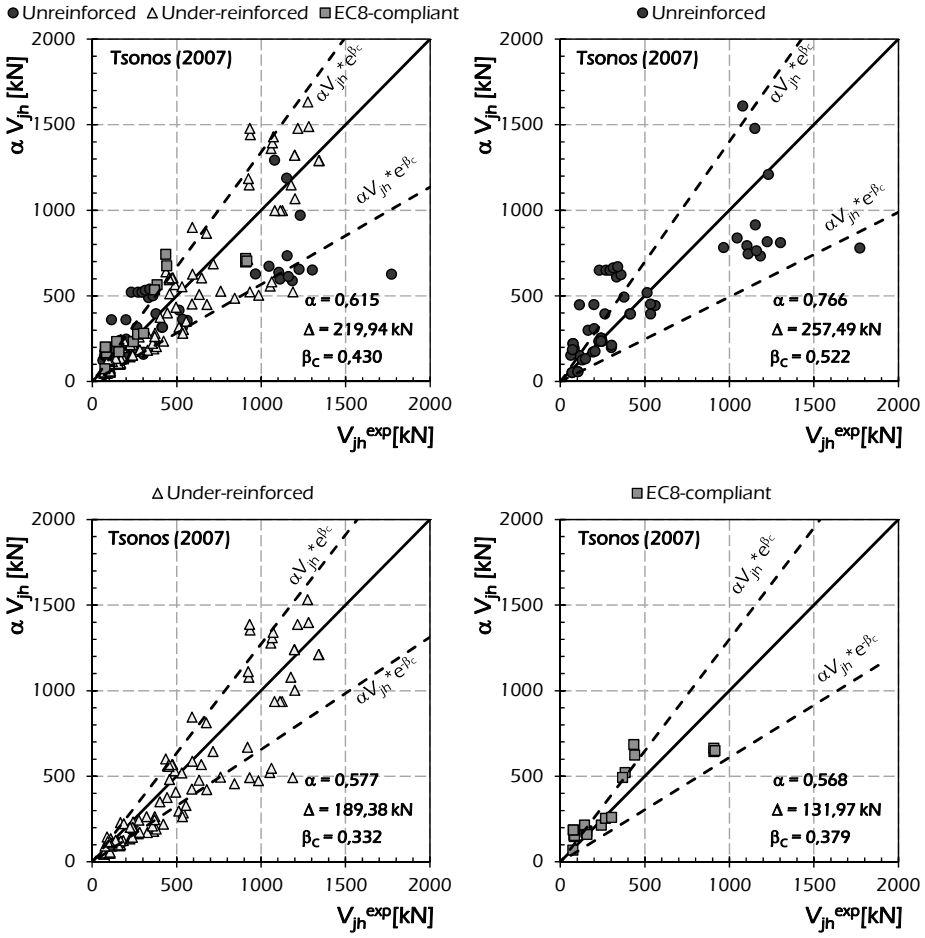

Fig. 6.26: Assessment of the recalibrated model by Tsonos (2007) for exterior joints.

Fig. 6.26 shows the equivalence charts plotted for the recalibrated model by Tsonos. (2007) for exterior joints. The values of the factor α evaluated for all the subclasses of joints are smaller than 1.000 as the original model results non-conservative. The prediction of the recalibrated model is highly dispersed especially for unreinforced joints.

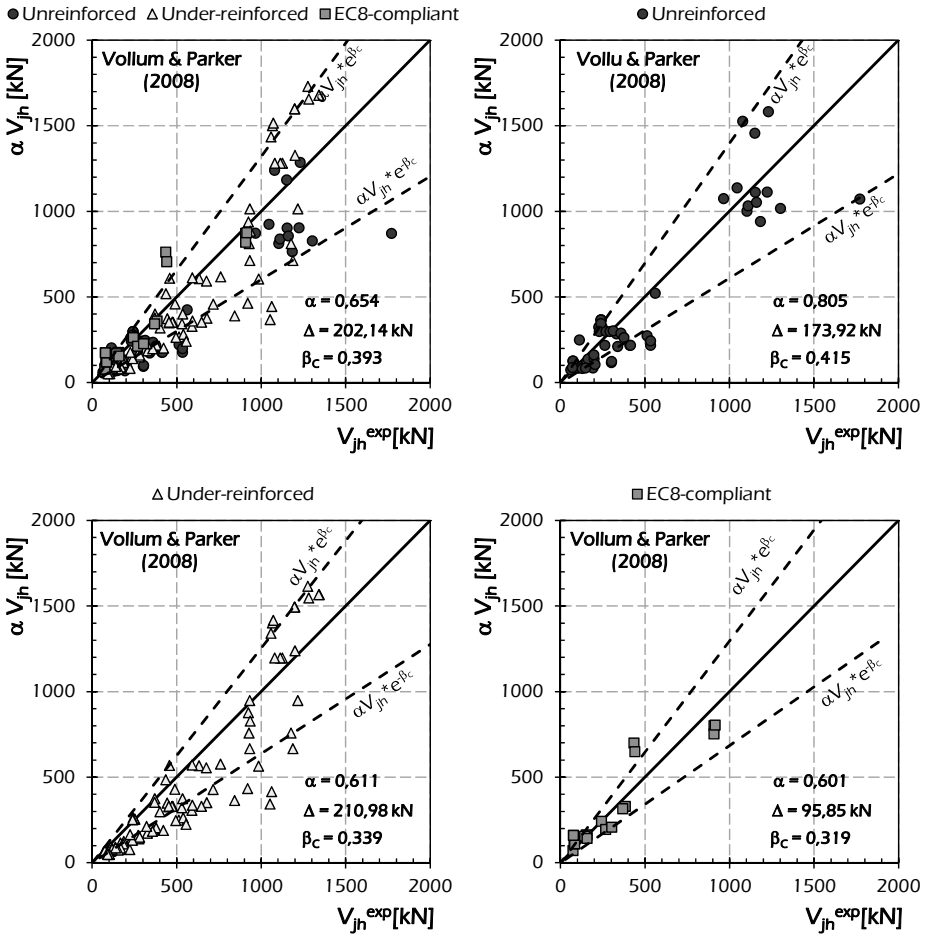

Fig. 6.27: Assessment of the recalibrated model by Vollum & Parker (2008) for exterior joints.

Fig. 6.27 shows the equivalence charts plotted for the recalibrated model by Vollum & Parker (2008). The values of the factor α smaller than 1.000 denote a non-conservative trend of the prediction of the original model

6.1.3 Recalibration of Code Formulations for Interior Joints

Table 6.3 reports the recalibration factor α obtained by performing the minimum square procedure [Eqn. (6.2)] for the analysed code formulations for evaluating the shear strength of interior joints. In particular, the analysis is provided by considering the total set of interior specimens, the unreinforced joints and the reinforced ones. For each group is also reported the Average Quadratic Error Δ evaluated for the recalibrated model through Eqn. (5.1).

Table 6.3: Recalibration factors and Average Quadratic Error of the recalibrated Code Formulation for interior joints.

Model	Total		Unreinforced		Reinforced	
	α	Δ [kN]	α	Δ [kN]	α	Δ [kN]
ACI 352-85 (1985)	0.621	244.12	0.495	214.52	0.671	229.72
ACI 352-02 (2002)	1.018	227.35	0.821	192.32	1.093	214.89
ACI 318-05 (2005)	0.882	255.36	0.704	219.38	0.952	243.93
AIJ 1990 (1990)	0.665	256.89	0.545	216.22	0.710	251.60
AIJ 1999 (1999)	0.899	228.73	0.720	188.24	0.969	215.99
NZS 3101 (1995)	2.065	457.30	-	-	2.065	457.30
FEMA 273 (1997) – 356 (2000)	1.025	246.59	1.056	219.38	1.018	252.70
EC8 (1995)	0.579	244.30	0.481	188.48	0.615	243.16
EC8 (2005) NTC (2008)	1.554	294.38	1.905	114.82	1.499	316.67
NTC (2008) OPCM (2005)	2.909	344.31	3.232	128.16	2.841	377.66

In the following the code formulations recalibrated by using the factor α outlined above have been assessed by comparing the experimental shear strength V_{jh}^{exp} with the recalibrated theoretical one $\alpha\ V_{jh}$.

Three equivalence charts are reported for each model; in particular the charts reporting the comparison for all the analysed interior joints, for unreinforced and reinforced joints are outlined.

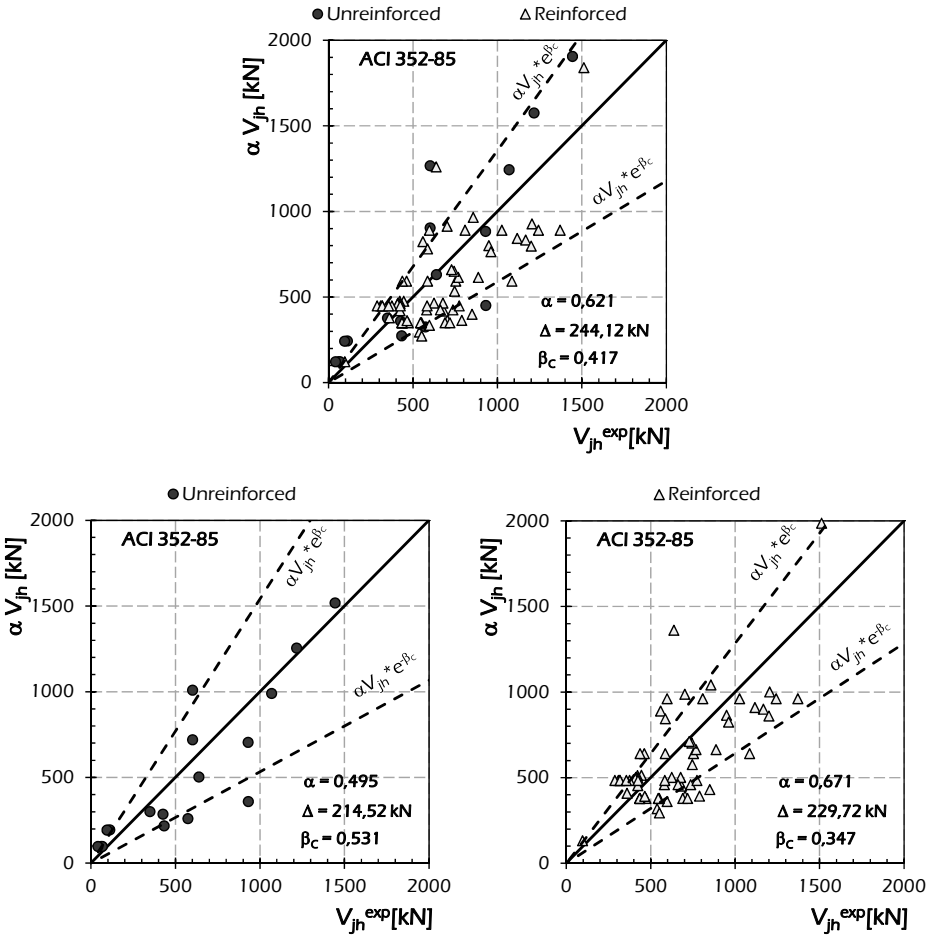

Fig. 6.28: *Assessment of the recalibrated ACI 352-85 (1985) formulation for interior joints.*

Fig. 6.28 shows the equivalence charts plotted for the recalibrated ACI 352-85 (1985) formulation for interior joints. The values of the factor α evaluated for all the specimens, unreinforced and reinforced joints are smaller than 1.000 as the original model results non-conservative. The recalibrated model by ACI 352-85 (1985) predicts accurate results for reinforced interior joints, while the results for unreinforced ones are rather dispersed.

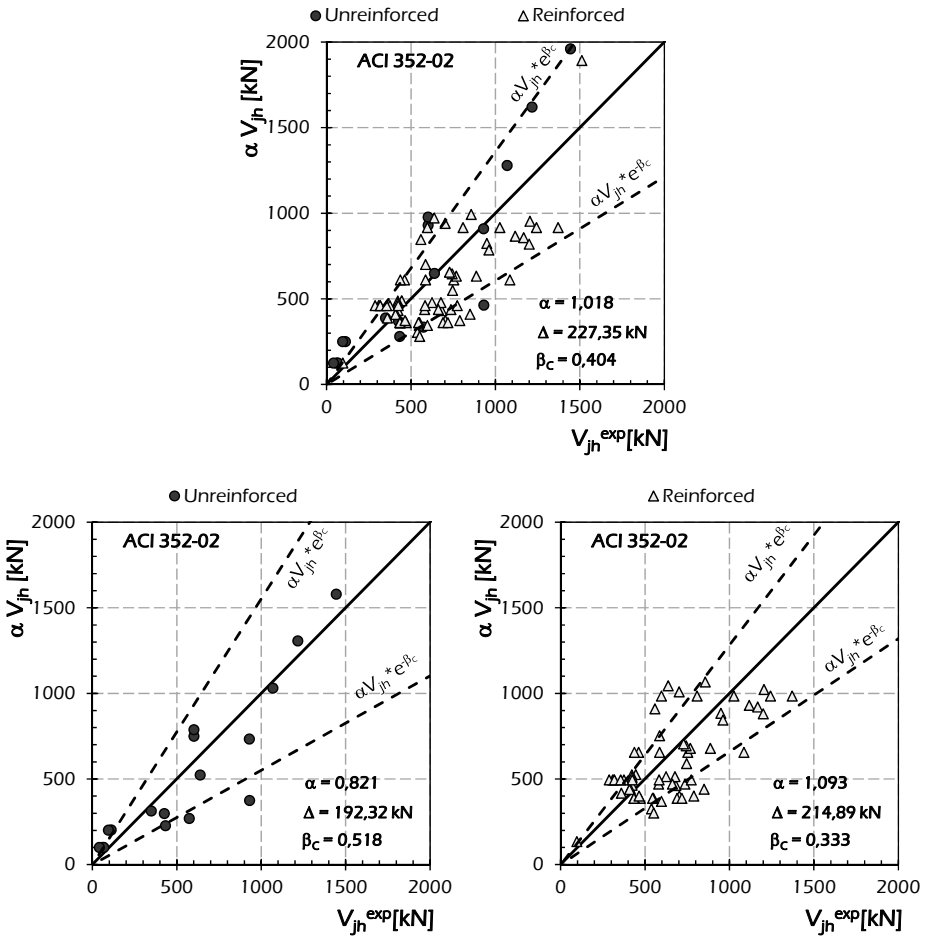

Fig. 6.29: Assessment of the recalibrated ACI 352-02 (2002) formulation for interior joints.

Fig. 6.29 shows the equivalence charts plotted for the recalibrated ACI 352-02 (2002) formulation for interior joints. The values of the factor α evaluated for all the specimens and reinforced joints are greater than 1.000 as the original model results slightly conservative. The recalibrated model by ACI 352-02 (2002) predicts accurate results for reinforced joints, while the results for unreinforced are non-accurate resulting highly dispersed.

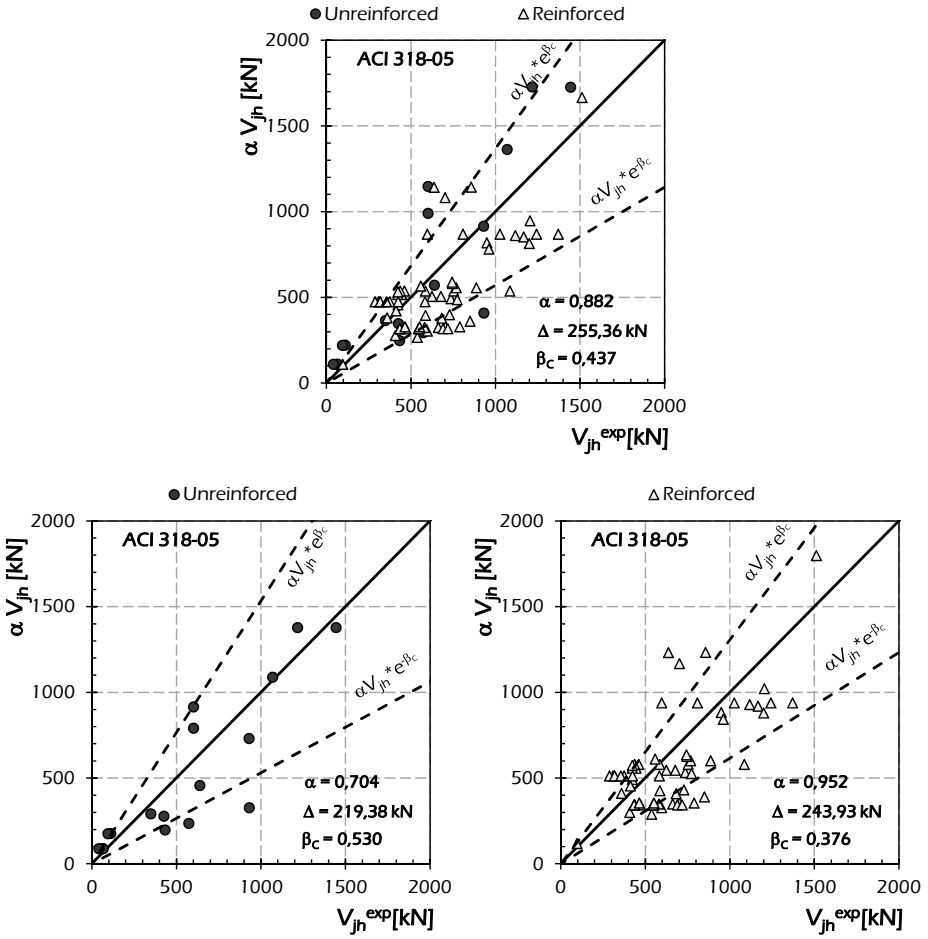

Fig. 6.30: Assessment of the recalibrated ACI 318-05 (2005) formulation for interior joints.

Fig. 6.30 shows the equivalence charts plotted for the recalibrated ACI 318-05 (2005) formulation for interior joints. The values of the factor α smaller than 1.000 denote a non-conservative trend of the prediction of the original model for all the analysed classes of joints. The recalibrated model by ACI 318-05 (2005) predicts accurate results for reinforced joints. Furthermore, a slightly conservative trend of the strength predicted by using this recalibrated model is shown.

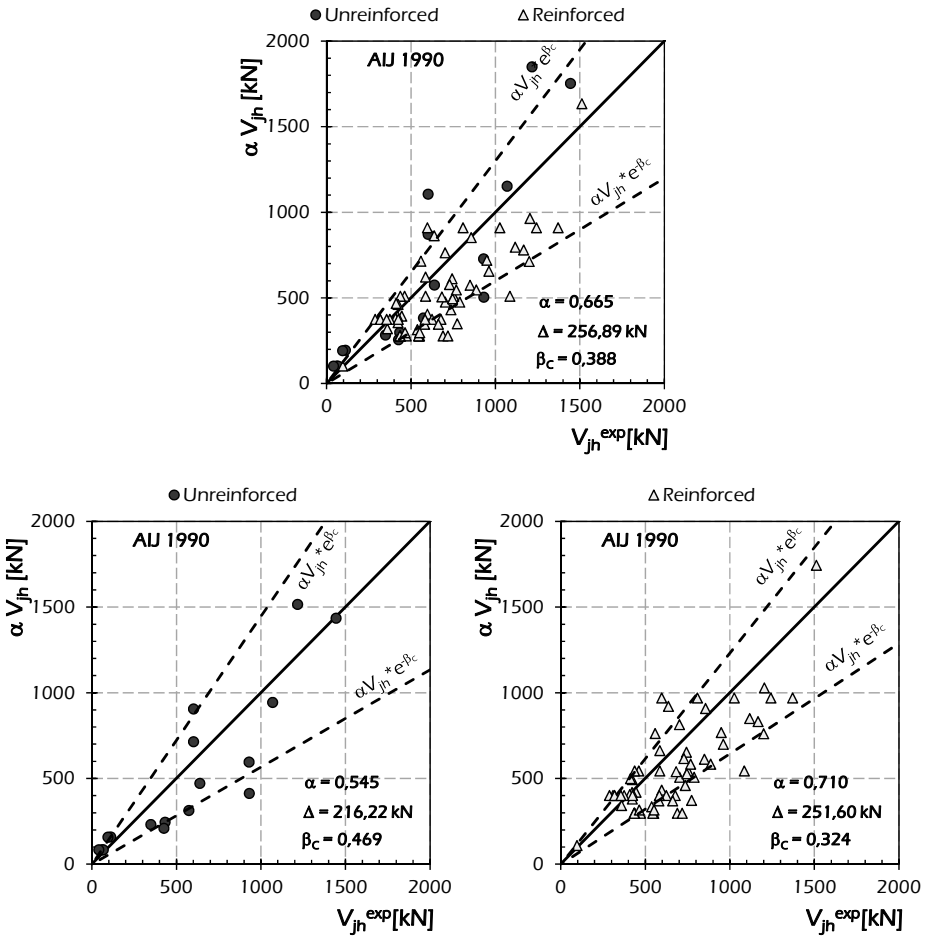

Fig. 6.31: Assessment of the recalibrated AIJ 1990 (1990) formulation for interior joints.

Fig. 6.31 shows the equivalence charts plotted for the AIJ 1990 (1990) formulation for interior joints recalibrated by using the factor α reported in Table 6.3. The values of the factor α evaluated for all the classes of joints are smaller than 1.000 as the original model results non-conservative. The recalibrated model by AIJ 1990 (1990) predicts slightly conservative results for both unreinforced and reinforced joints, but results for the former are rather dispersed.

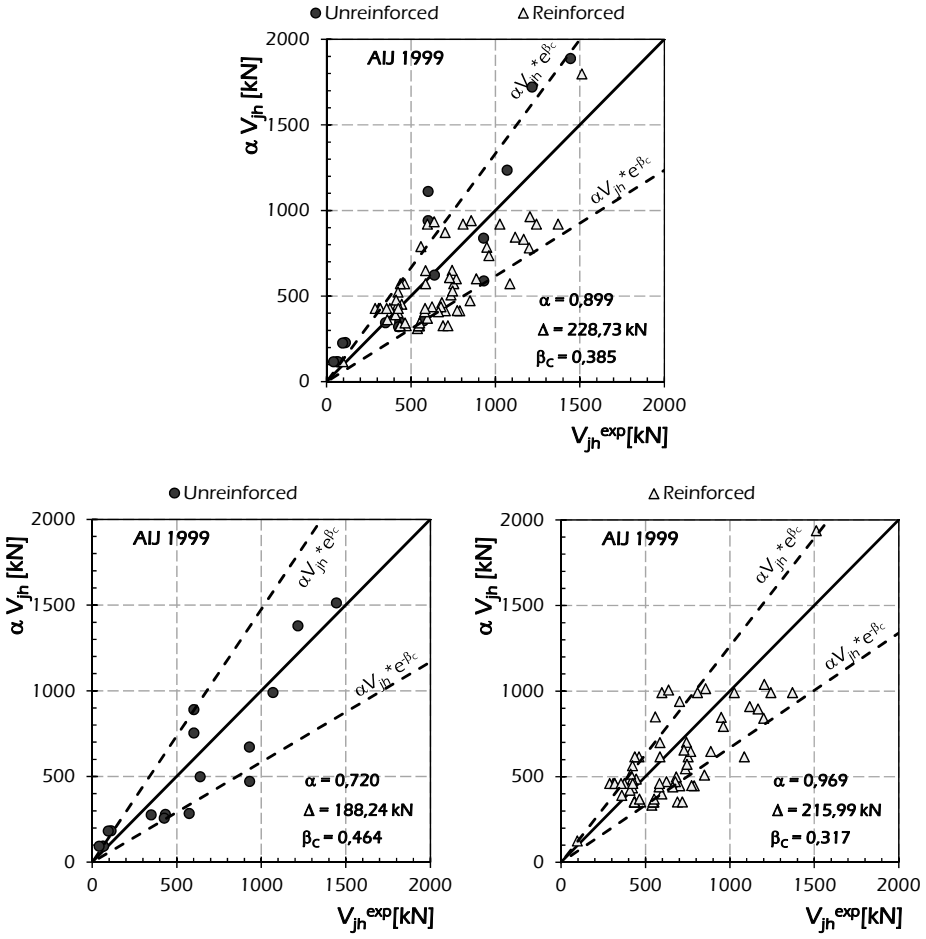

Fig. 6.32: Assessment of the recalibrated AIJ 1999 (1999) formulation for interior joints.

Fig. 6.32 shows the equivalence charts plotted for the recalibrated AIJ 1999 (1999) formulation for interior joints. The values of the factor α evaluated for all the specimens, unreinforced and reinforced joints are smaller than 1.000 as the original model results non-conservative. The recalibrated model by AIJ 1999 (1999) predicts accurate results for reinforced joints, while the results for unreinforced joints are rather dispersed.

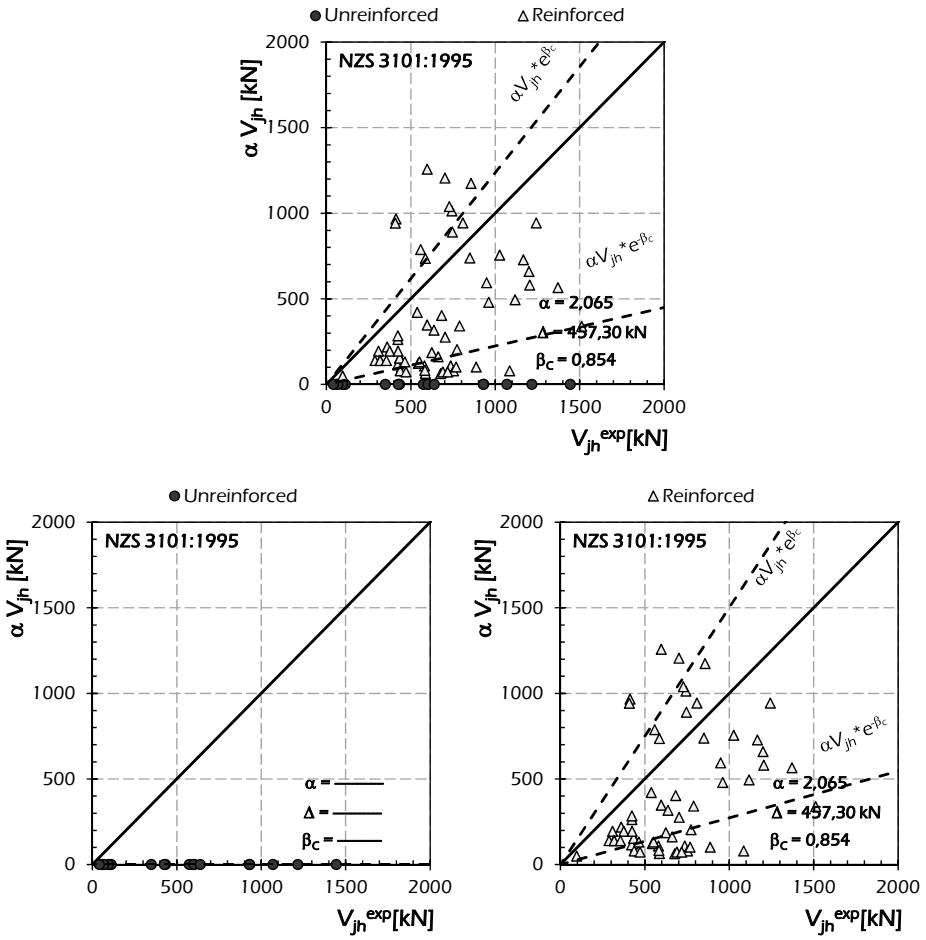

Fig. 6.33: Assessment of the recalibrated NZS 3101 (1995) formulation for interior joints.

Fig. 6.33 shows the equivalence charts plotted for the recalibrated NZS 3101 (1995) formulation for interior joints. The model does not take into account unreinforced joints, as it predicts a shear strength equal to 0 for this kind of joints. The values of the factor α evaluated for reinforced joints are greater than 1.000 as the original model results highly conservative. The prediction of the model by NZS 3101 (1995) is highly dispersed.

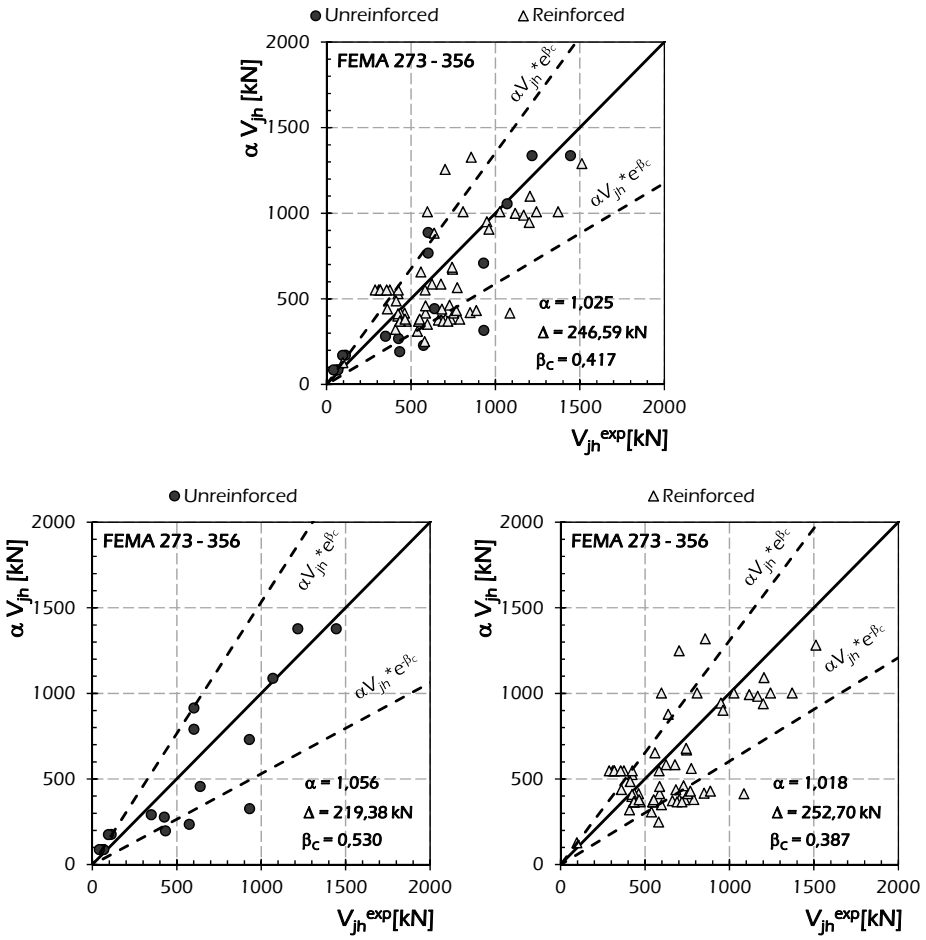

Fig. 6.34: Assessment of the recalibrated FEMA 273 (1997) – 356 (2000) formulation for interior joints.

Fig. 6.34 shows the equivalence charts plotted for the recalibrated model by FEMA 273 (1997) - 356 (2000). The values of the factor α evaluated for all the specimens as a whole, unreinforced and reinforced joints close to 1.000 denote an accurate prediction of the original model. The recalibrated model by FEMA 273 (1997) and FEMA 356 (2000) predicts slightly conservative results.

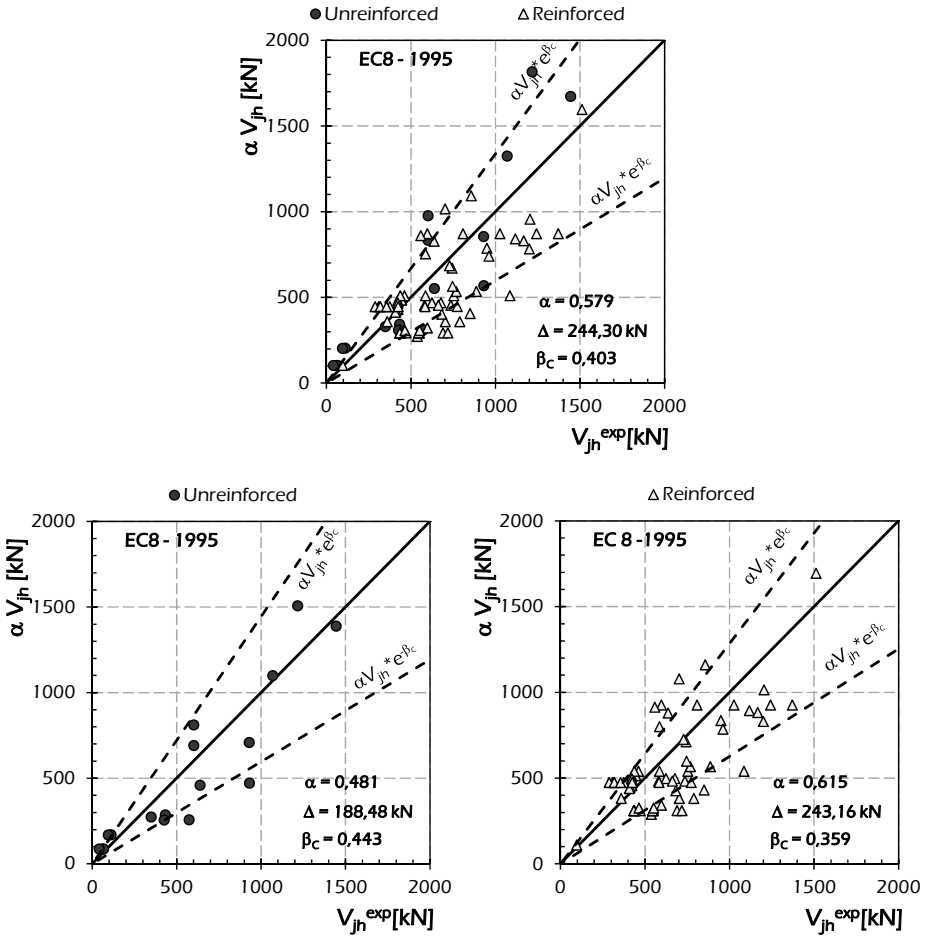

Fig. 6.35: Assessment of the recalibrated Eurocode 8 (EN 1995, 1995) formulation for interior joints.

Fig. 6.35 shows the equivalence charts plotted for the EC8 (EN 1995, 1995) formulation for interior joints recalibrated by using the factor α reported in Table 6.3. The values of the factor α evaluated for all the classes of joints are smaller than 1.000 as the original model results non-conservative. The recalibrated model by EC8 (EN 1995, 1995) predicts slightly conservative results for both unreinforced and reinforced. Highly dispersion affects the results for unreinforced joints.

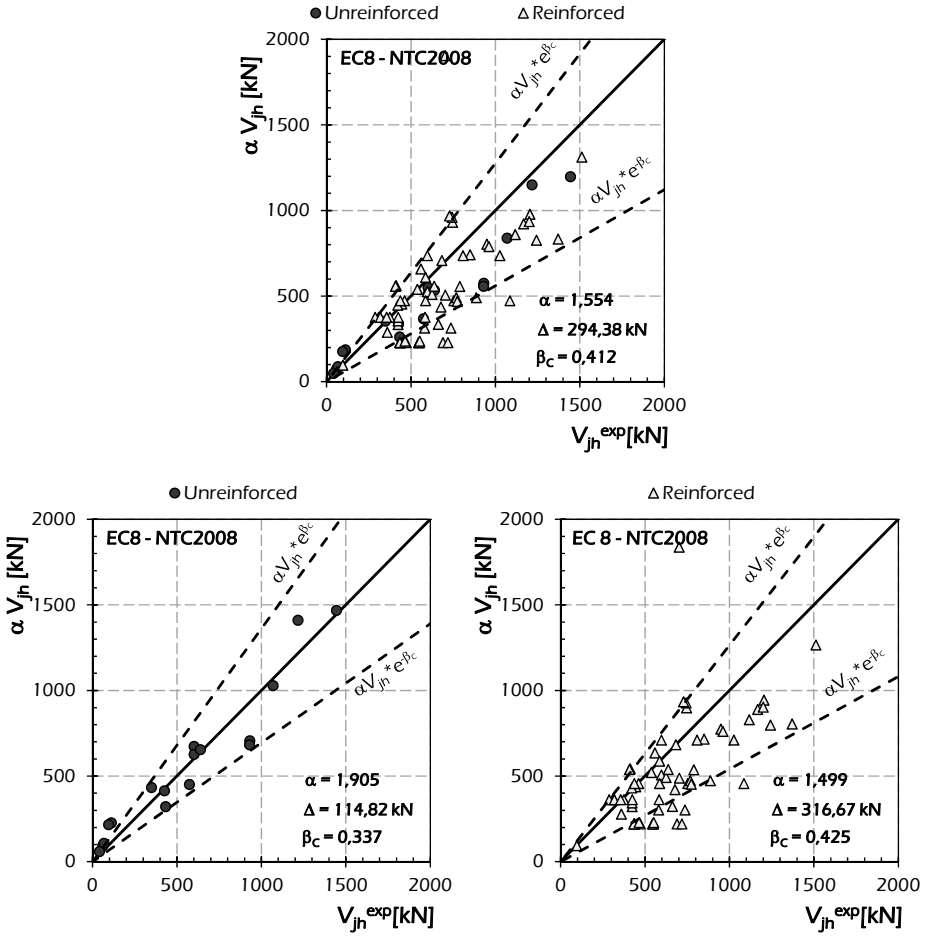

Fig. 6.36: Assessment of the recalibrated Eurocode 8 (EN 1998, 2005) and NTC (2008) formulation for interior joints.

Fig. 6.36 shows the equivalence charts plotted for the recalibrated EC8 (EN 1998, 2005) and NTC (2008) formulation for interior joints. The values of the factor α evaluated for all the specimens, unreinforced and reinforced joints are greater than 1.000 as the original model results conservative. The results predicted by using the recalibrated model (EN 1998, 2005 and NTC, 2008) rather dispersed.

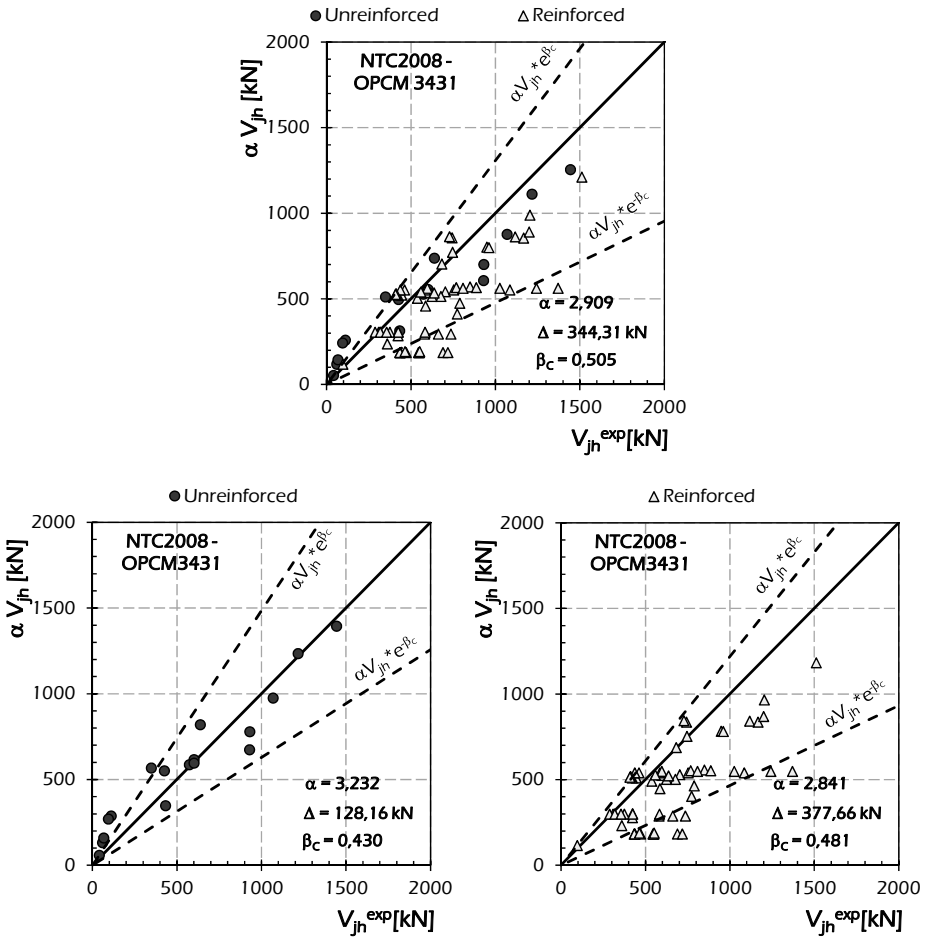

Fig. 6.37: Assessment of the recalibrated NTC (2008) and OPCM 3431/05 (2005) formulation for interior joints.

Fig. 6.37 shows the equivalence charts plotted for the recalibrated model by NTC (2008) and OPCM 3431/05 (2005) for evaluating the shear strength of joints in existing structures. The values of the factor α evaluated for all the specimens as a whole, unreinforced and reinforced joints greater than 1.000 denote a conservative trend of the prediction of the original models. The recalibrated model (NTC, 2008 and OPCM 3431/05, 2005) predicts accurate results.

6.1.4 Recalibration of Capacity Models Available in the Literature for Interior Joints

Table 6.4 reports the factor α obtained by performing the least-square procedure [Eqn. (6.2)] on the analysed capacity models for evaluating shear strength of interior joints.

Table 6.4: Recalibration factors and Average Quadratic Error of the recalibrated Capacity Models for interior joints.

Model	Total		Unreinforced		Reinforced	
	α	Δ [kN]	α	Δ [kN]	α	Δ [kN]
Pantazopoulo & Bonacci (1992)	0.546	253.76	0.658	250.09	0.531	247.61
Paulay & Priestley (1992)	1.630	290.13	2.028	384.51	1.589	254.08
Parker & Bullman (1997)	1.435	283.13	1.467	235.95	1.428	293.64
Hwang & Lee (2002)	1.557	318.75	1.558	210.93	1.557	340.40
Parra-Montesinos & Wight (2002)	1.025	247.35	0.813	191.63	1.113	237.08
Hegger et al. (2003)	0.814	259.04	0.674	226.07	0.863	254.25

Table 6.4: Recalibration factors and Average Quadratic Error of the recalibrated Capacity Models for interior joints.

Model	Total		Unreinforced		Reinforced	
	α	Δ [kN]	α	Δ [kN]	α	Δ [kN]
Kim et al. (2009)	0.960	259.04	0.941	173.03	0.964	188.34
Kitayama et al. (1991)	0.785	270.43	0.643	242.34	0.837	263.52
Hwang & Lee (2000)	1.141	273.84	1.076	159.36	1.158	294.70

The analysis is carried out by considering the total set of interior specimens, the unreinforced joints and the reinforced ones. For each group is also reported the Average Quadratic Error Δ evaluated for the recalibrated model through Eqn. (5.1).

The capacity models recalibrated using the factor α outlined above have been assessed by comparing the experimental shear strength V_{jh}^{exp} with the recalibrated theoretical one αV_{jh}. The results are shown in the following figures in which the comparison is reported in terms of equivalence charts.

Three equivalence charts are reported for each model reporting the comparison for all the analysed interior joints and for both unreinforced and reinforced ones.

In the equivalence charts the bisector segment is reported as a reference of the equivalent rule between experimental evidence and theoretical value of the recalibrated model. Furthermore, the segments representing the fractile of 84% and 16% evaluated through Eqns. (5.18) and (5.19) are also shown. Finally, the values of the factor α, the Average Quadratic Error Δ and the factor of dispersion β_C are listed in every chart.

Fig. 6.38 shows the equivalence charts plotted for the recalibrated model by Pantazopoulo & Bonacci (1992) for interior joints. The values of the factor α evaluated for all the specimens, unreinforced and reinforced joints are smaller than 1.000 as the original model results non-conservative. The recalibrated model by Pantazopoulo & Bonacci (1992) predicts accurate results for reinforced interior joints, while the results for unreinforced joints are rather dispersed.

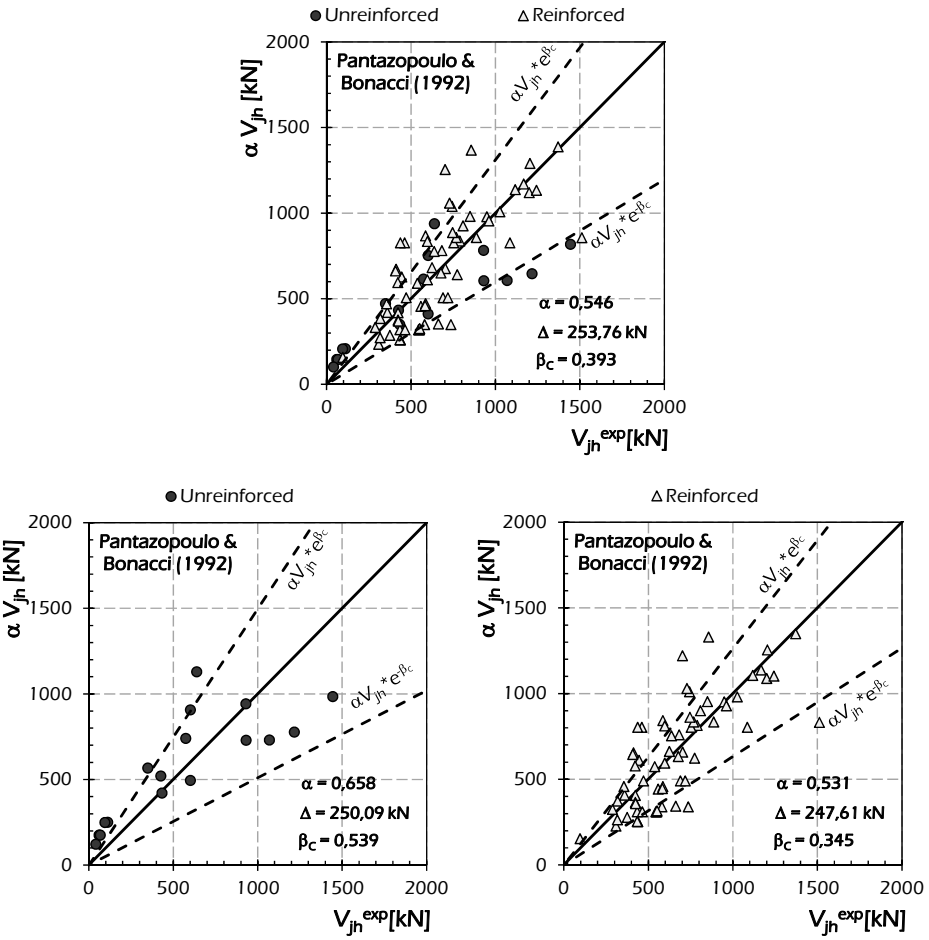

Fig. 6.38: *Assessment of the recalibrated model by Pantazopoulo & Bonacci (1992) for interior joints.*

Fig. 6.39 shows the equivalence charts plotted for the recalibrated model by Paulay & Priestley (1992). The values of the factor α evaluated for all the specimens, unreinforced and reinforced joints are greater than 1.000 as the original model results slightly conservative. The recalibrated model by Paulay & Priestley (1992) predicts accurate results for reinforced joints, while the results for unreinforced interior joints are rather dispersed.

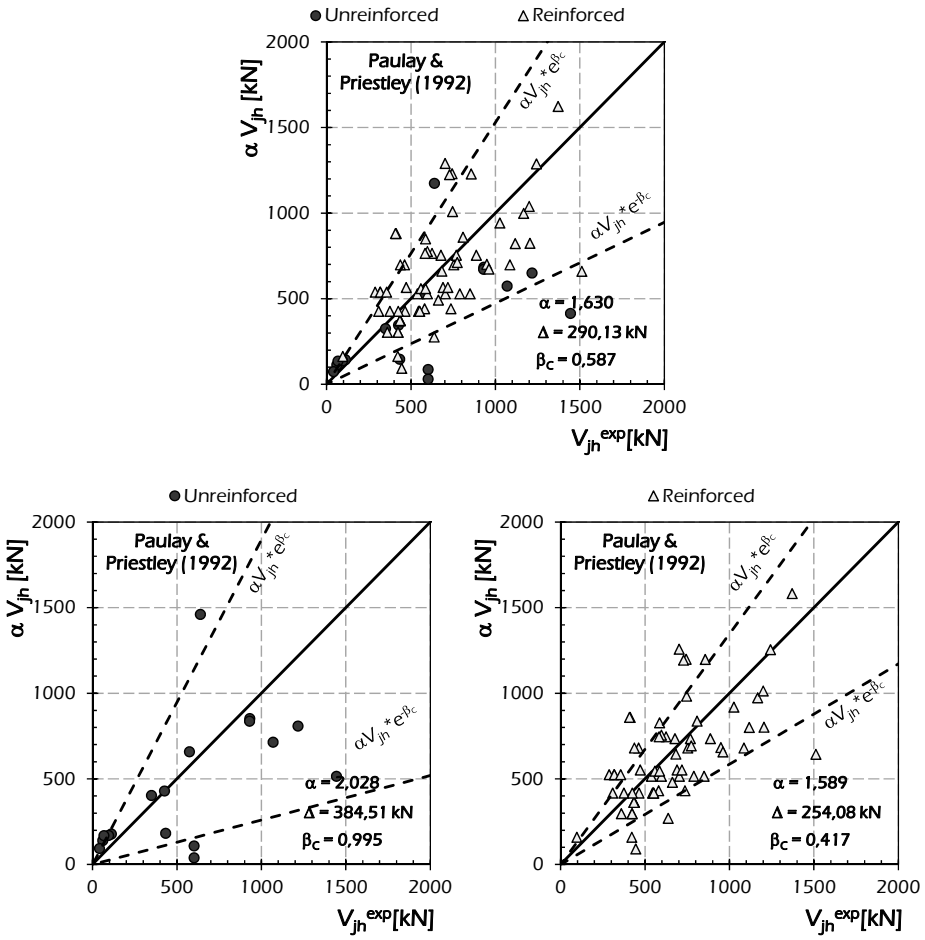

Fig. 6.39: Assessment of the recalibrated model by Paulay & Priestley (1992) for interior joints.

Fig. 6.40 shows the equivalence charts plotted for the recalibrated model by Parker & Bullman (1997) for interior joints. The values of the factor α evaluated for all the specimens as a whole, unreinforced and reinforced joints smaller than 1.000 denote a non-conservative trend of the prediction of the original model. The recalibrated model by Parker & Bullman (1997) predicts accurate results for both unreinforced and reinforced interior joints. Furthermore, a slightly conservative trend of the strength predicted by using this recalibrated model is shown for reinforced joints.

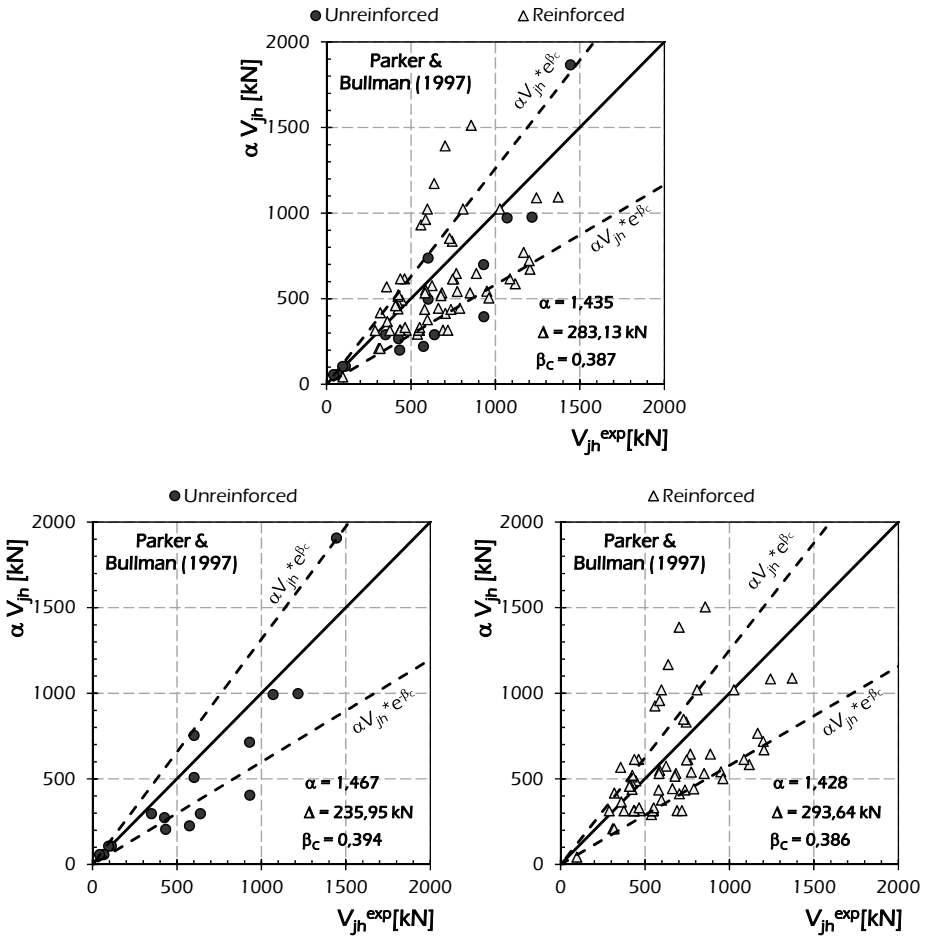

Fig. 6.40: Assessment of the recalibrated model by Parker & Bullman (1997) for interior joints.

Fig. 6.41 shows the equivalence charts plotted for the model by Hwang & Lee (2002) for interior joints recalibrated by using the factor α reported in Table 6.4. The values of the factor α evaluated for all the specimens as a whole, unreinforced and reinforced joints are greater than 1.000 as the original model results conservative. The recalibrated model by Hwang & Lee (2002) predicts accurate results for both unreinforced and reinforced joints. The predictions for unreinforced joints are affected by a dispersion smaller than the one observed for reinforced specimens.

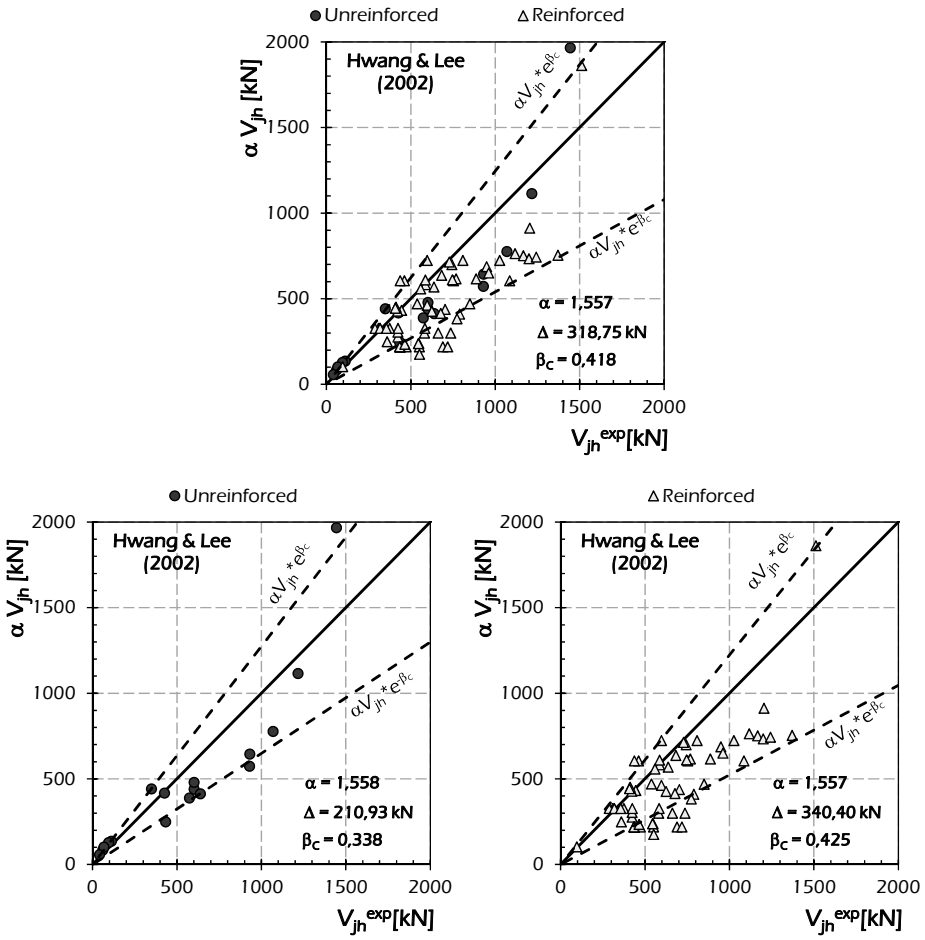

Fig. 6.41: Assessment of the recalibrated model by Hwang & Lee (2002) for interior joints.

Fig. 6.42 shows the equivalence charts plotted for the recalibrated model by Parra-Montesinos & Wight (2002) for interior joints. The values of the factor α evaluated for all the specimens and reinforced joints are greater than 1.000 as the original model results non-conservative., while for unreinforced joints the least-square procedure provides a value of α smaller than 1.000. The recalibrated model by Parra-Montesinos & Wight (2002) predicts accurate results for reinforced joints, while the results for unreinforced connections are rather dispersed with a slightly conservative trend.

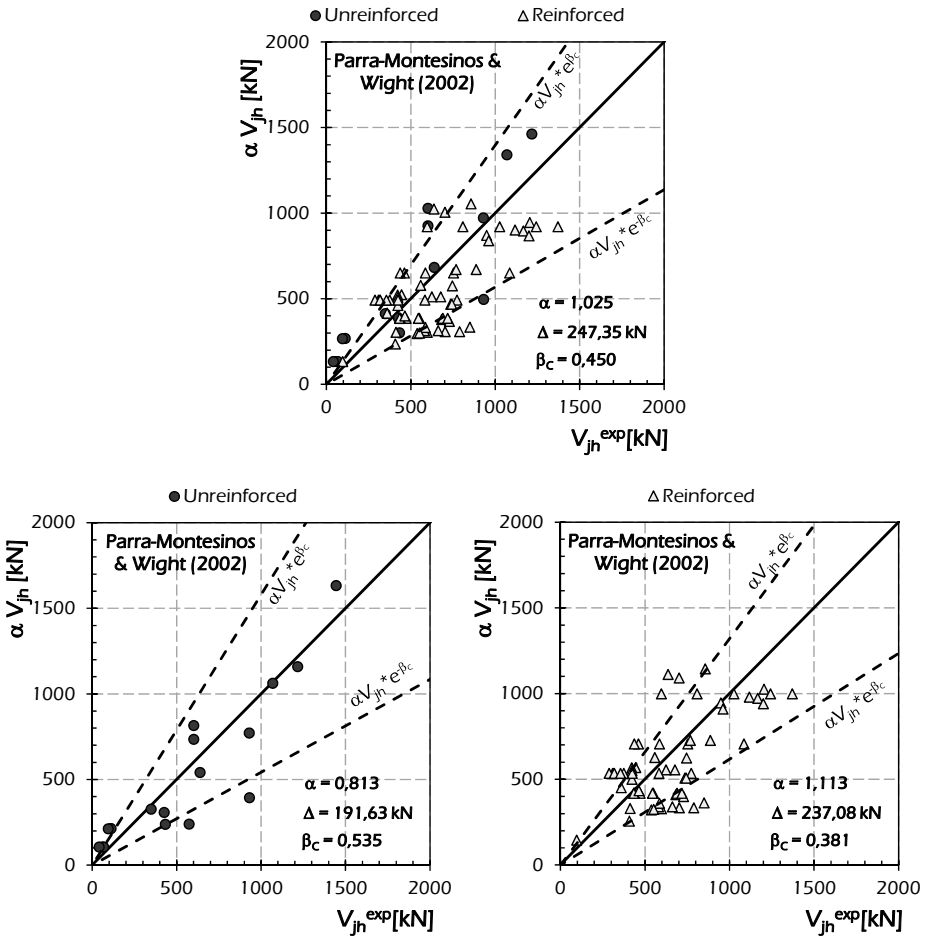

Fig. 6.42: *Assessment of the recalibrated model by Parra-Montesinos & Wight (2002) for interior joints.*

Fig. 6.43 shows the equivalence charts plotted for the recalibrated model by Hegger et al. (2003) for interior joints. The values of the factor α evaluated for all the specimens, unreinforced and reinforced joints are smaller than 1.000 as the original model results non-conservative. The prediction of the recalibrated model is accurate for reinforced joints, while results highly dispersed for unreinforced joints.

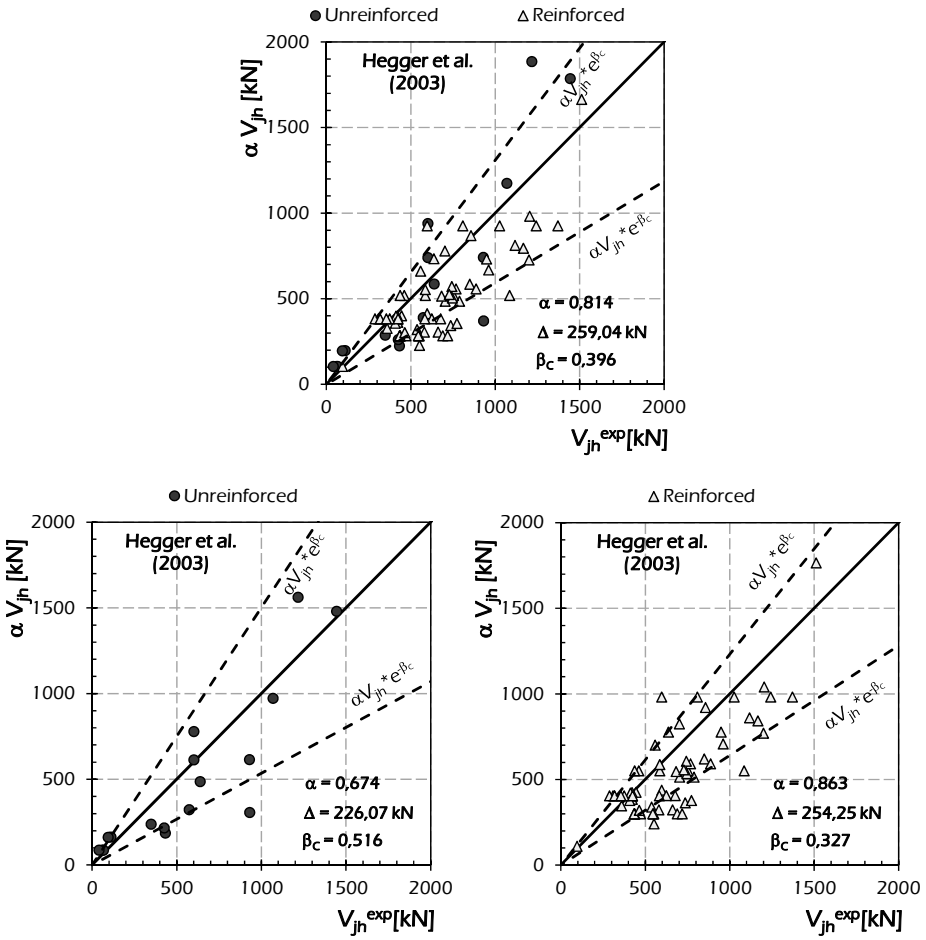

Fig. 6.43: *Assessment of the recalibrated model by Hegger et al. (2003) for interior joints.*

Fig. 6.44 shows the equivalence charts plotted for the recalibrated model by Kim et al. (2009). The values of the factor α evaluated for all the specimens as a whole, unreinforced and reinforced joints close to 1.000 denote a general accuracy of the prediction of the original model. The recalibrated model by Kim et al. (2009) predicts very accurate results for all the classes of joints. In particular, the lower dispersion affects the results for reinforced joints and a slightly conservative trend results for unreinforced joints.

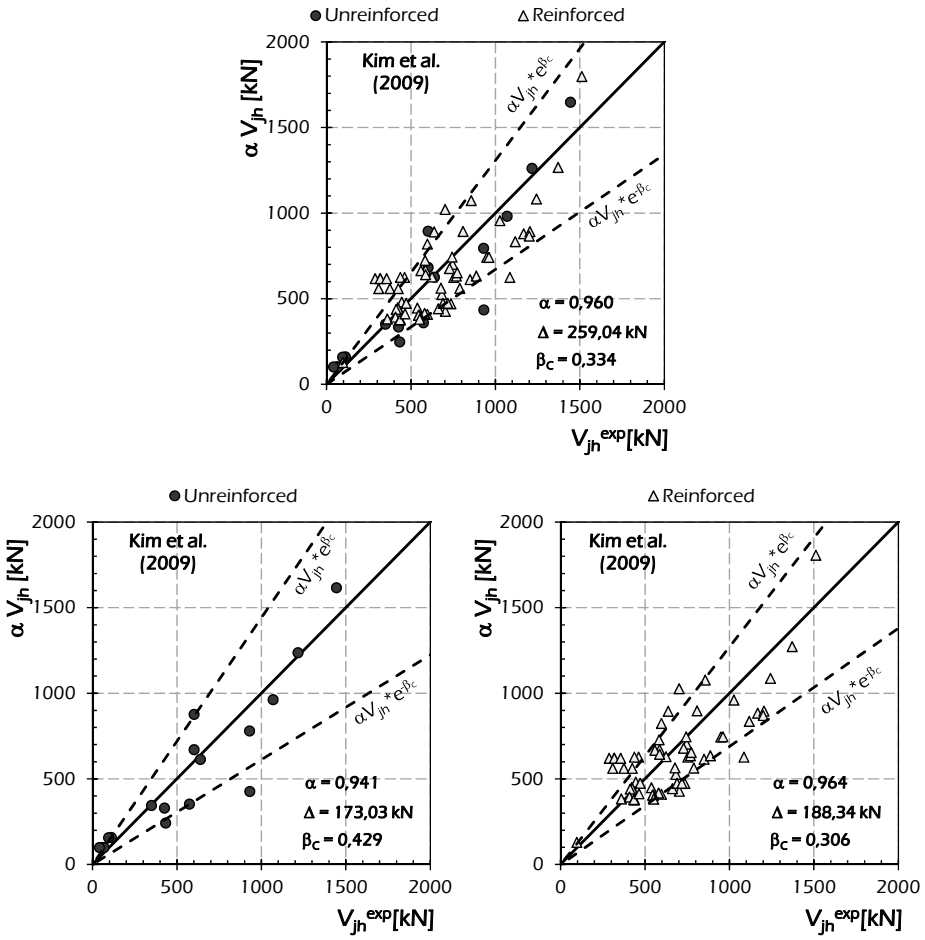

Fig. 6.44: Assessment of the recalibrated model by Kim et al. (2009) for interior joints.

Fig. 6.45 shows the equivalence charts plotted for the model by Kitayama et al. (1991) for interior joints recalibrated by using the factor α reported in Table 6.4. The values of the factor α evaluated for all the specimens as a whole, unreinforced and reinforced joints are smaller than 1.000 as the original model results non-conservative. The recalibrated model by Kitayama et al. (1991) predicts accurate results for reinforced as low dispersion affects the prediction, while predictions for unreinforced joints are characterised by high dispersion.

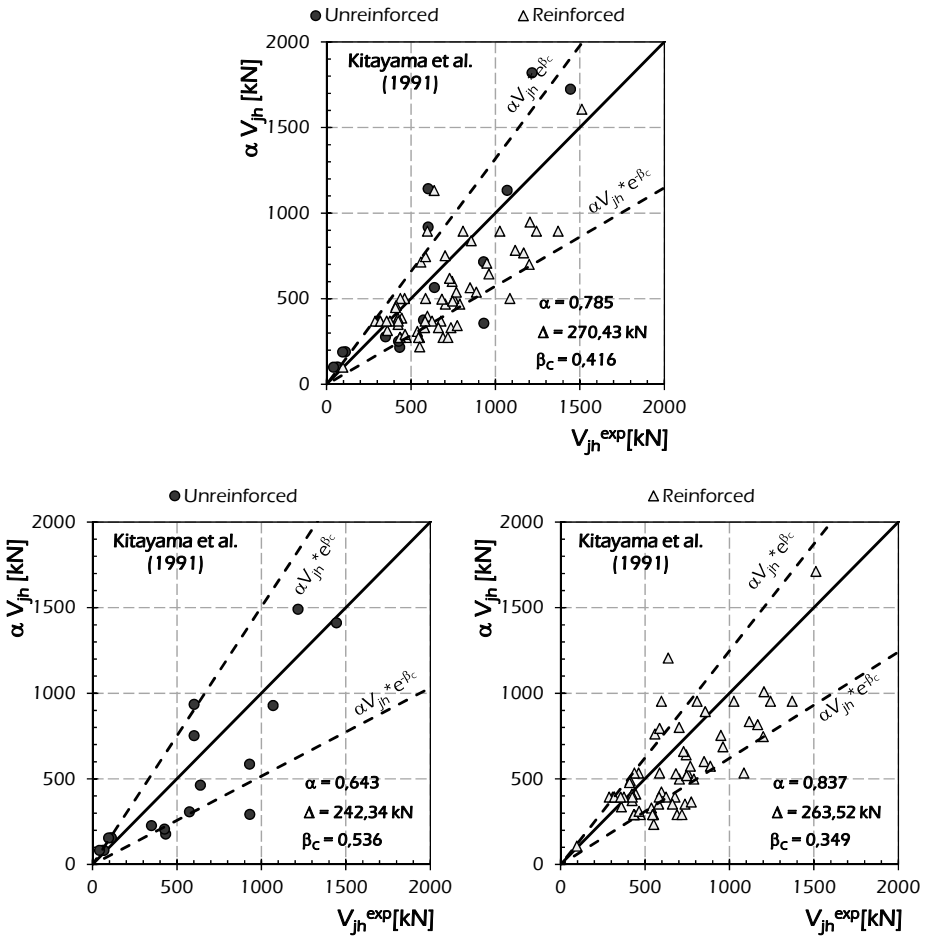

Fig. 6.45: Assessment of the recalibrated model by Kitayama et al. (1991) for interior joints.

Fig. 6.46 shows the equivalence charts plotted for the recalibrated model by Hwang & Lee (2000) for interior joints. The values of the factor α evaluated for all the specimens as a whole, unreinforced and reinforced joints greater than 1.000 denote a conservative trend of the prediction of the original model. The recalibrated model by Hwang & Lee (2000) predicts accurate results for all the kinds of joints analysed. In particular, the recalibrated model provides very accurate predictions for unreinforced interior joints.

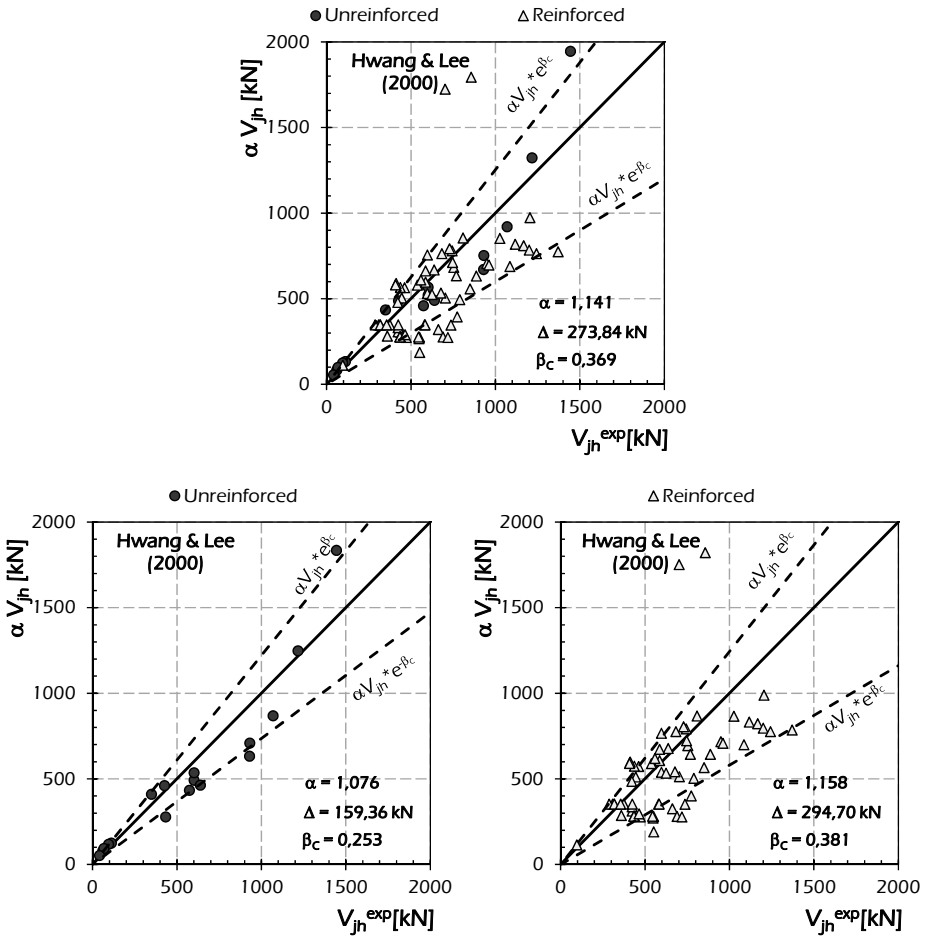

Fig. 6.46: Assessment of the recalibrated model by Hwang & Lee (2000) for interior joints.

6.2 Probabilistic Assessment

Further representations about probabilistic assessment can be made. A simple one is the cumulative probability $P_r(x_i)$ of the experimental-to-theoretical ratio V_{jh}^{exp}/V_{jh}^{th}.

The cumulated distribution of probability density is defined as follows:

$$P_r(x_i) = \sum_{m=1}^{i} f_m(x_m). \tag{6.3}$$

For evaluating the mean μ and the standard deviation σ of the analysed models, the normal distribution of probability, the so called Gauss distribution, is needed:

$$f(x) = \frac{1}{\sigma\sqrt{2\pi}} e^{-\frac{1}{2}\left(\frac{x-\mu}{\sigma}\right)^2} \tag{6.4}$$

in which:

$$\mu = \int_{-\infty}^{\infty} x \cdot f(x), \tag{6.5}$$

$$\sigma^2 = \int_{-\infty}^{\infty} (x-\mu) \cdot f(x). \tag{6.6}$$

The function of the normal cumulated probability density is derived by Eqn. (6.4) as follows:

$$P_{r,c}(x) = \int_{-\infty}^{x} f(y). \tag{6.7}$$

The mean μ and the standard deviation σ of the model will be the values corresponding to the normal distribution that better approximate the distribution of the model. For this purpose, the error ε between the normal distribution and the distribution of probability of the analysed model is evaluated as follows:

$$\varepsilon(\mu,\sigma) = \sum_{i=1}^{n_k} \left[P_r(x_i) - P_{r,c}(x_i,\mu,\sigma)\right]^2 \tag{6.8}$$

where $P_r(x_i)$ is the distribution of probability of the analysed model, while $P_{r,c}(x_i)$ is the normal distribution of cumulated probability with mean μ and standard deviation σ.

Finally, the values of mean μ and standard deviation σ of the model are the ones that minimizing the error ε validating the following condition:

$$\Delta\left(\overline{\mu},\overline{\sigma}\right) = \arg\min \varepsilon(\mu,\sigma). \tag{6.9}$$

In the following the cumulative probabilities for the original models and the recalibrated ones are provided; in particular, the probabilistic assessment is provided for the total specimens, unreinforced and reinforced joints by

developing four subsection reporting code formulations for exterior joints, capacity models available in the scientific literature for exterior joints, code formulations for interior joints and capacity models for interior joints, respectively.

6.2.1 Exterior Joints

The probabilistic assessment of code formulations and capacity models for exterior joints is provided in the following by accounting all the analysed specimens, unreinforced, under-reinforced and EC8-compliant joints.

6.2.1.1 Code Formulations

In the following figures both original code formulations and recalibrated ones are assessed by reporting on each chart the values of mean μ and standard deviation σ.

The predictions are non-conservative if the mean μ (corresponding to the cumulative probability equal to 0.50 on the y-axis) is smaller than 1.000 (on the x-axis). The finding means that there is a probability greater than the 50% that the evaluated theoretical value V_{jh} could be greater than V_{jh}^{exp}. Instead, if the average value is greater than 1.00 the probability of having V_{jh} greater than V_{jh}^{exp} is smaller than the 50% resulting in meanly conservative law.

For example, Fig. 6.47 provides the probabilistic assessment of the original and recalibrated ACI 352-85 (1985) formulation for exterior joints. In every chart are reported the distribution of probability of the model and the normal distribution of cumulated probability (dashed line). As the experimental database is considered as a whole, a non-conservative trend is observed being the mean μ (corresponding to the cumulative probability equal to 0.50 on the y-axis) equal to 0.551 (on the x-axis). Basically, there is a probability of about 95% that the evaluated theoretical value V_{jh} could be greater than V_{jh}^{exp}. The average value becomes 1.052 and the probability of having V_{jh} greater than V_{jh}^{exp} is equal to about 50% by recalibrating the model in respect to the total exterior dataset resulting in meanly equivalent laws. On the contrary, for the entire set of specimens on exterior joints a standard deviation σ greater than the one obtained by the original model is observed by recalibrating the model.

The same considerations provided for the entire set of specimens can be made by considering the analyses separated for unreinforced, under-reinforced and EC8-compliant joints. In fact, the original model by ACI 352-85 (1985) provides very conservative values, while the mean μ results closer to 1.000 by recalibrating the model. About the standard deviation σ, as already observed for

the total specimens, the recalibration provides values higher than the ones obtained with the original model.

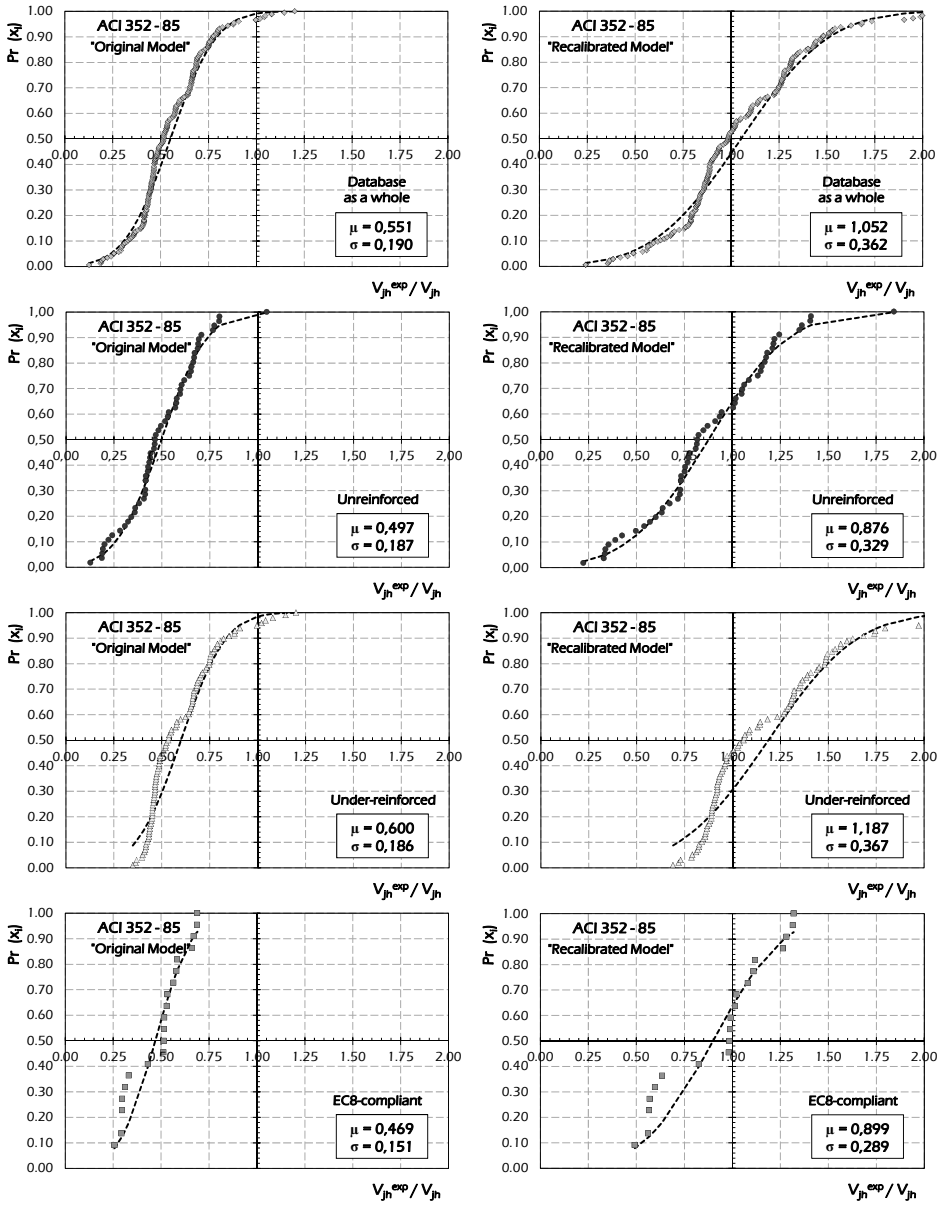

Fig. 6.47: Probabilistic Assessment of the original and recalibrated ACI 352-85 (1985) formulation for exterior joints.

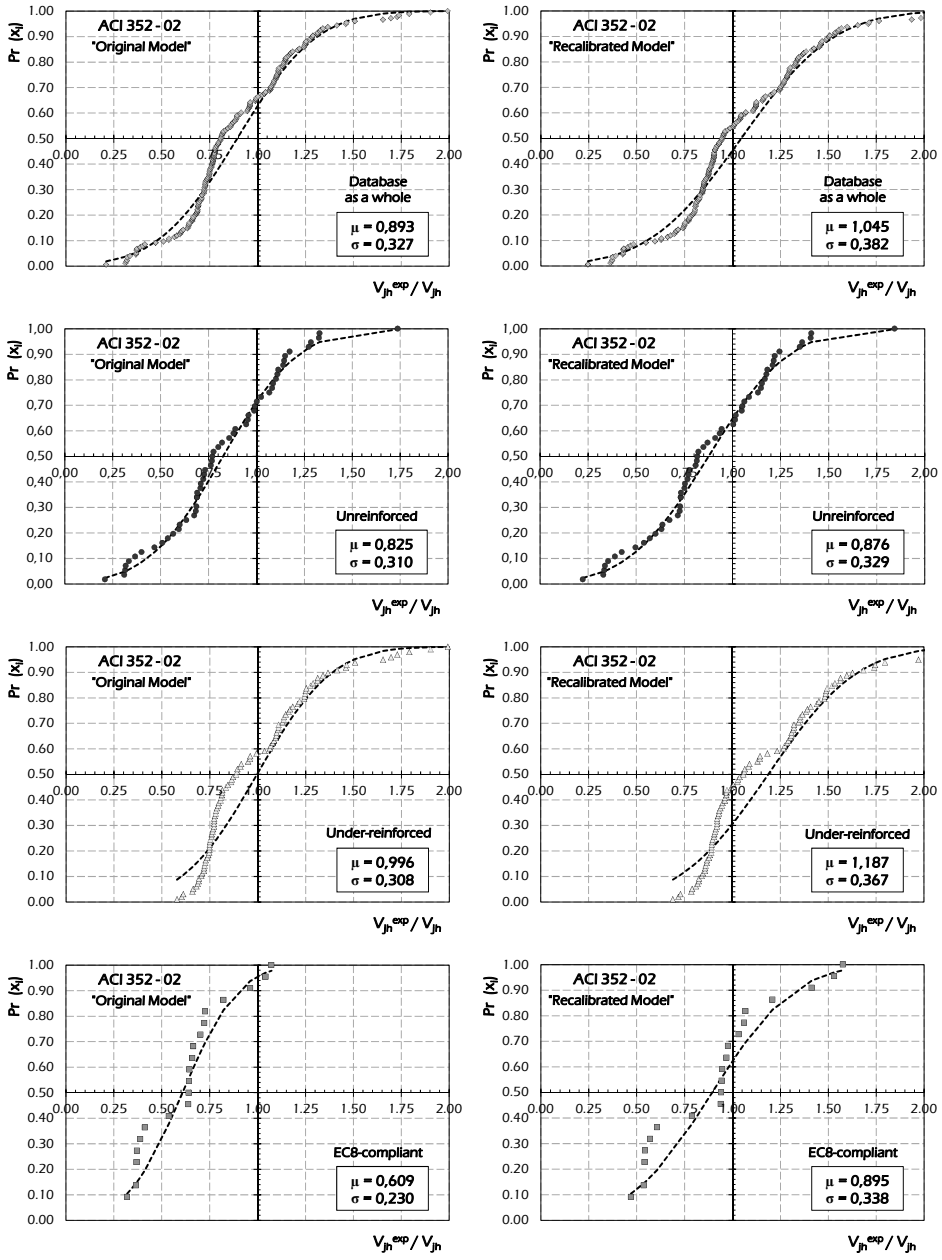

Fig. 6.48: Probabilistic Assessment of the original and recalibrated ACI 352-02 (2002) formulation for exterior joints.

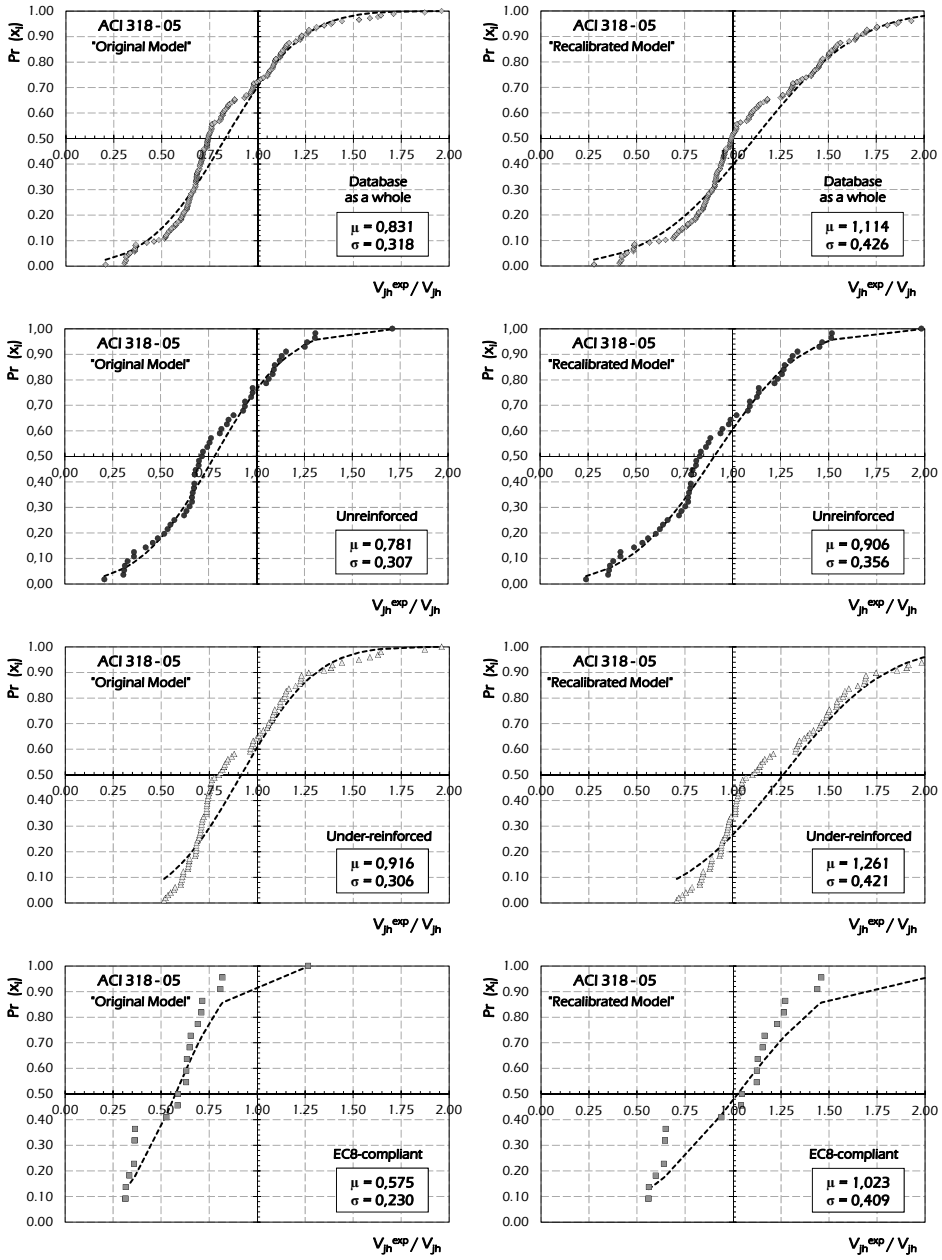

Fig. 6.49: Probabilistic Assessment of the original and recalibrated ACI 318-05 (2005) formulation for exterior joints.

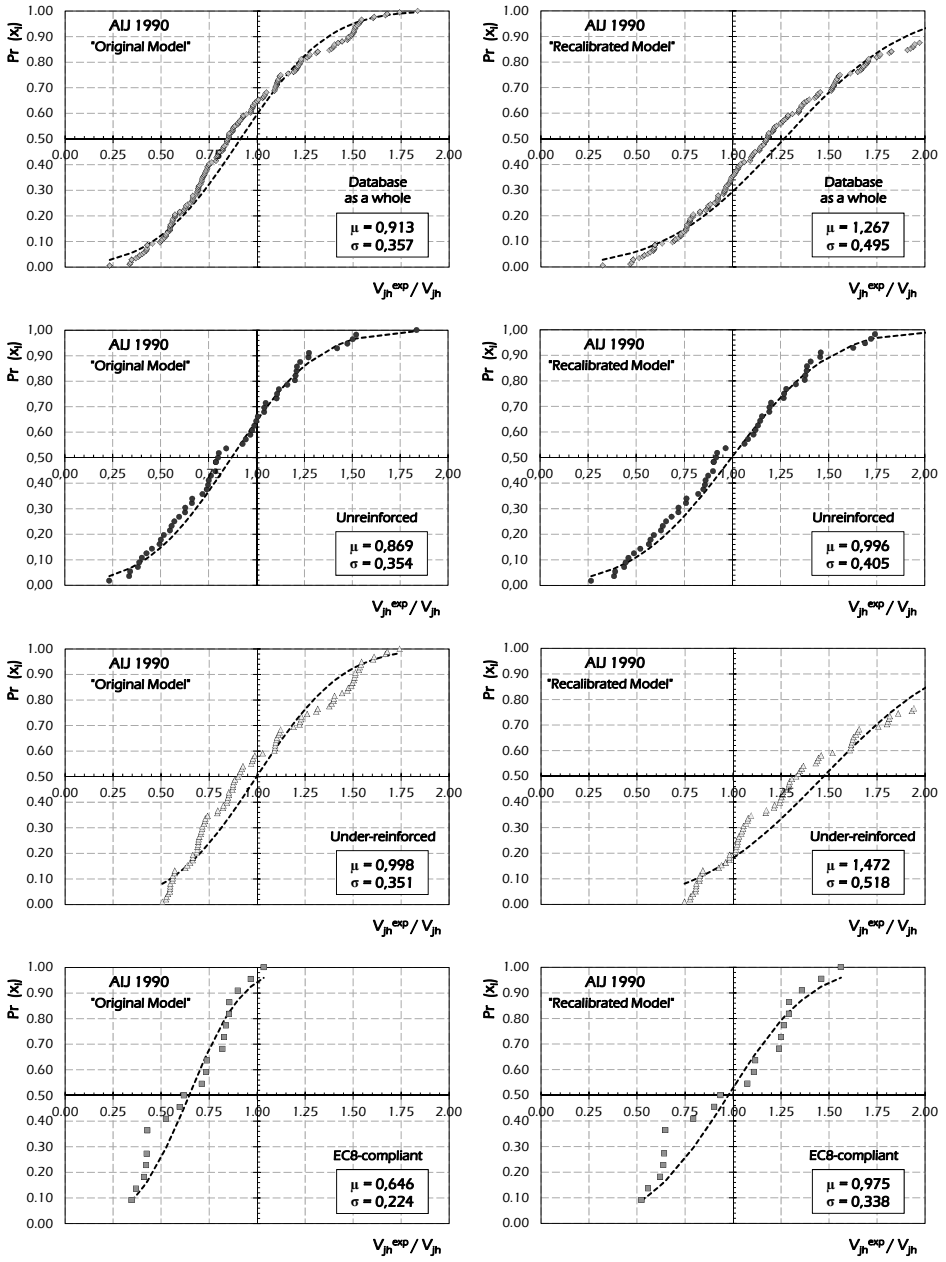

Fig. 6.50: Probabilistic Assessment of the original and recalibrated AIJ 1990 (1990) formulation for exterior joints.

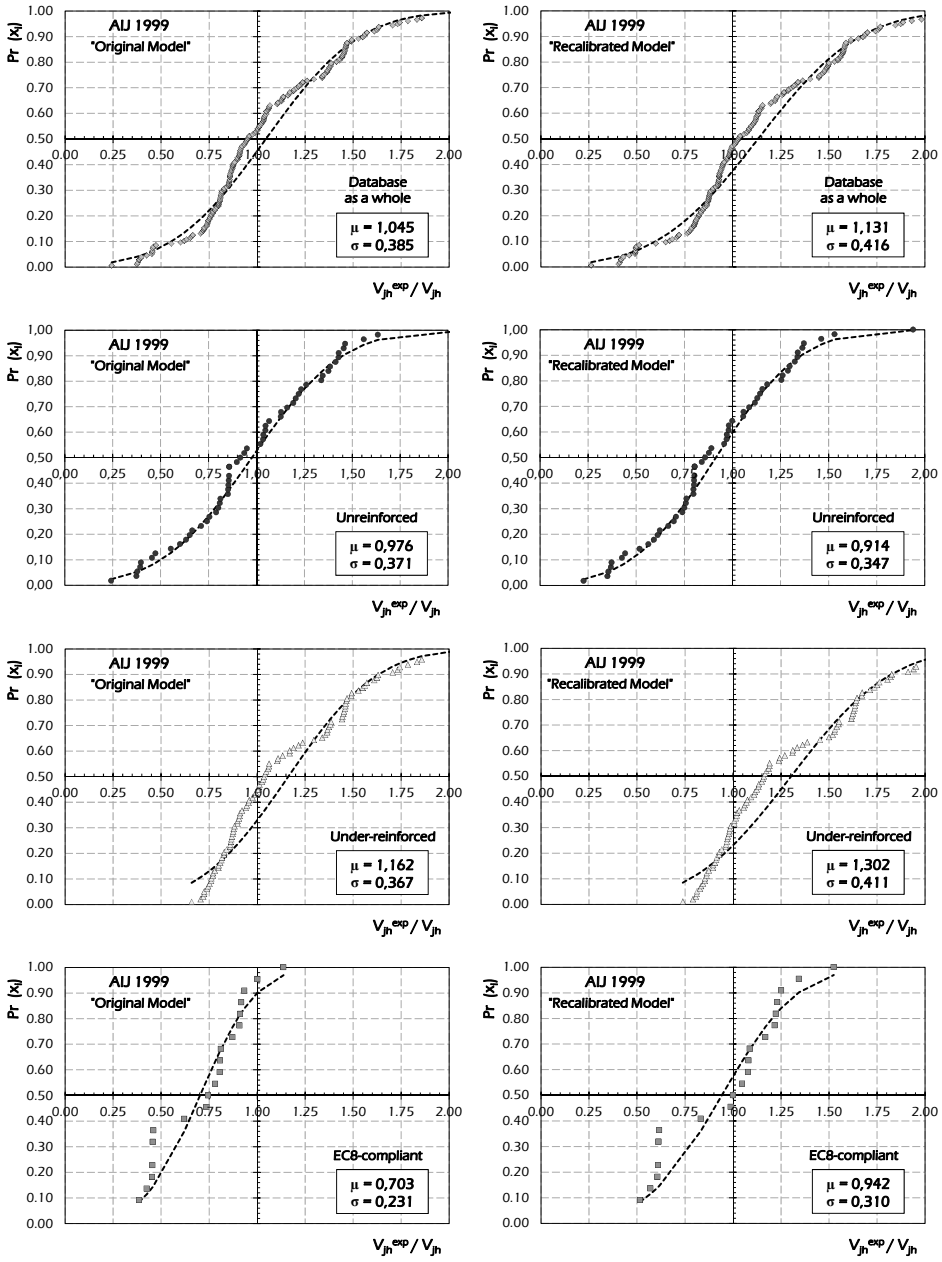

Fig. 6.51: Probabilistic Assessment of the original and recalibrated AIJ 1999 (1999) formulation for exterior joints.

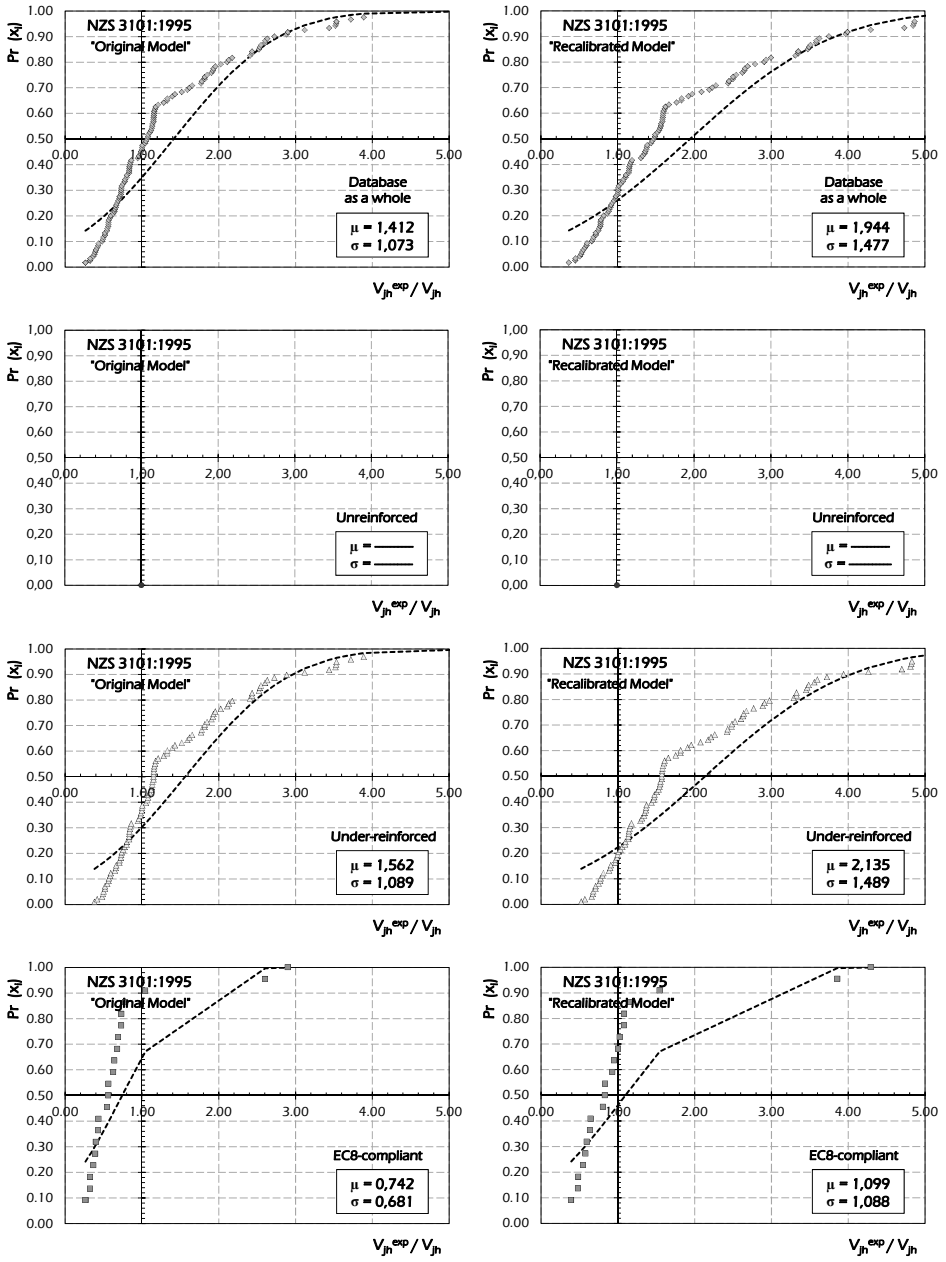

Fig. 6.52: Probabilistic Assessment of the original and recalibrated NZS 3101 (1995) formulation for exterior joints.

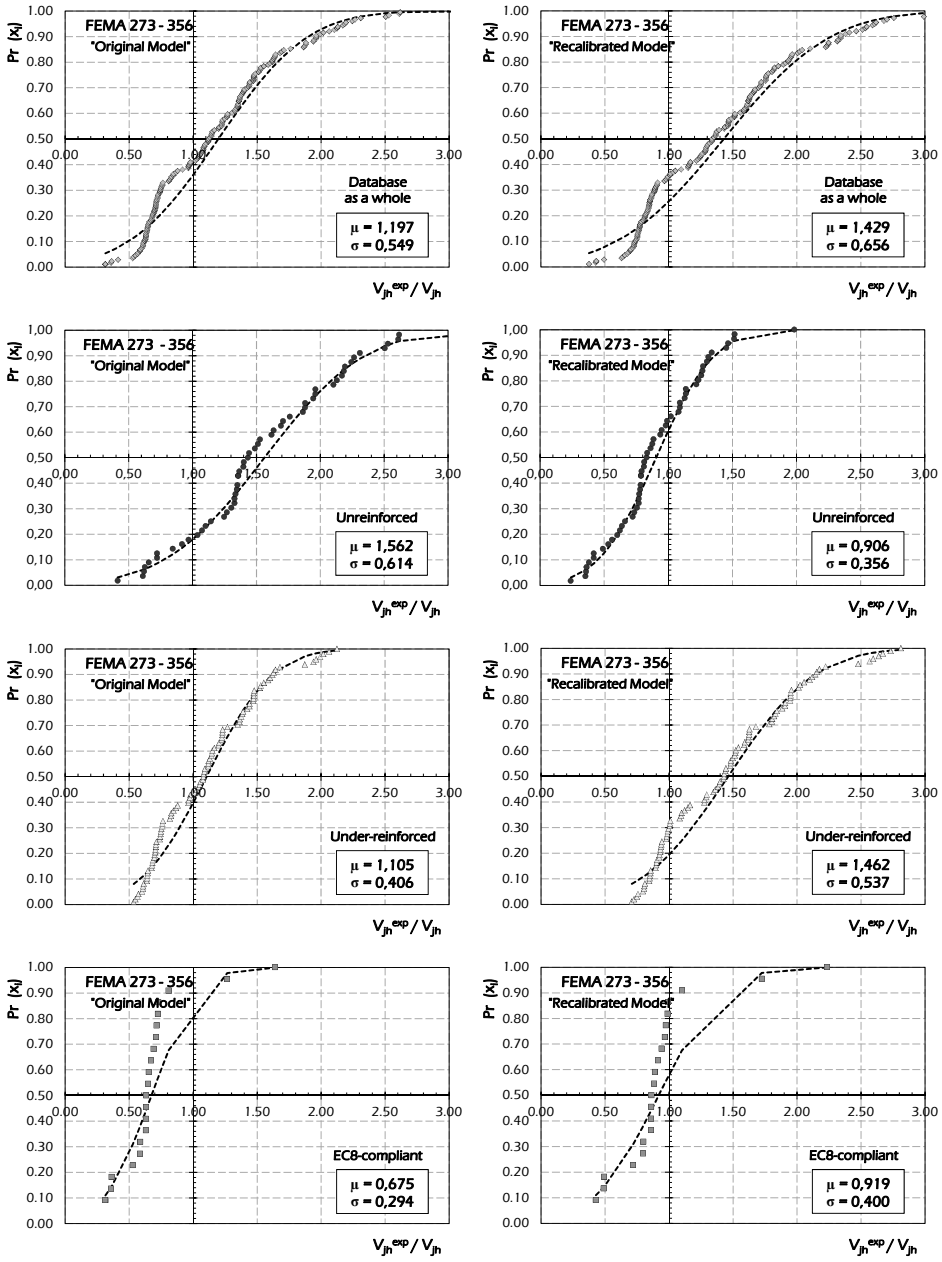

Fig. 6.53: Probabilistic Assessment of the original and recalibrated FEMA 273 (1997) – 356 (2000) formulation for exterior joints.

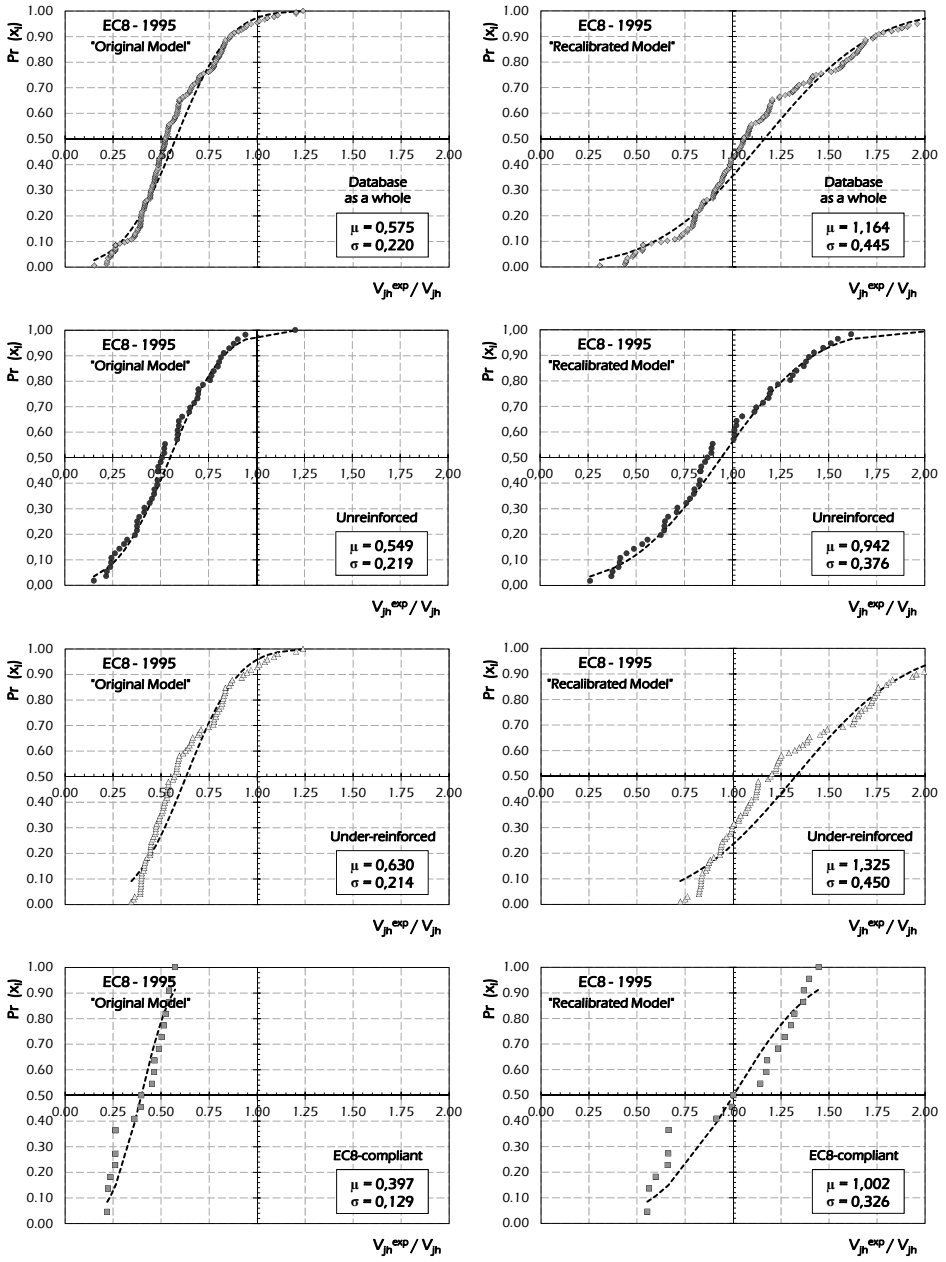

Fig. 6.54: Probabilistic Assessment of the original and recalibrated Eurocode 8 (EN 1995, 1995) formulation for exterior joints.

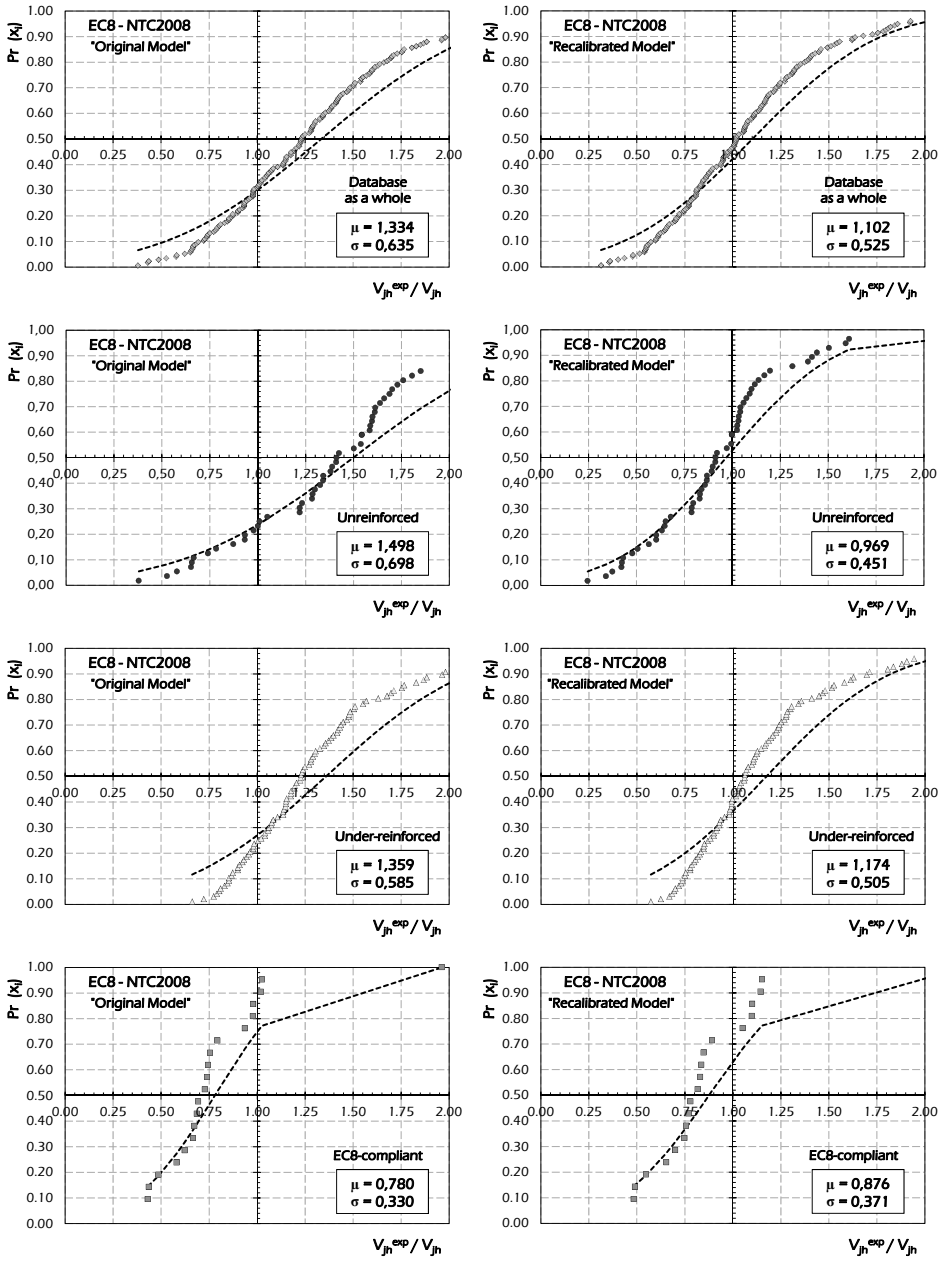

Fig. 6.55: Probabilistic Assessment of the original and recalibrated Eurocode 8 (EN 1998, 2005) and NTC (2008) formulation for exterior joints.

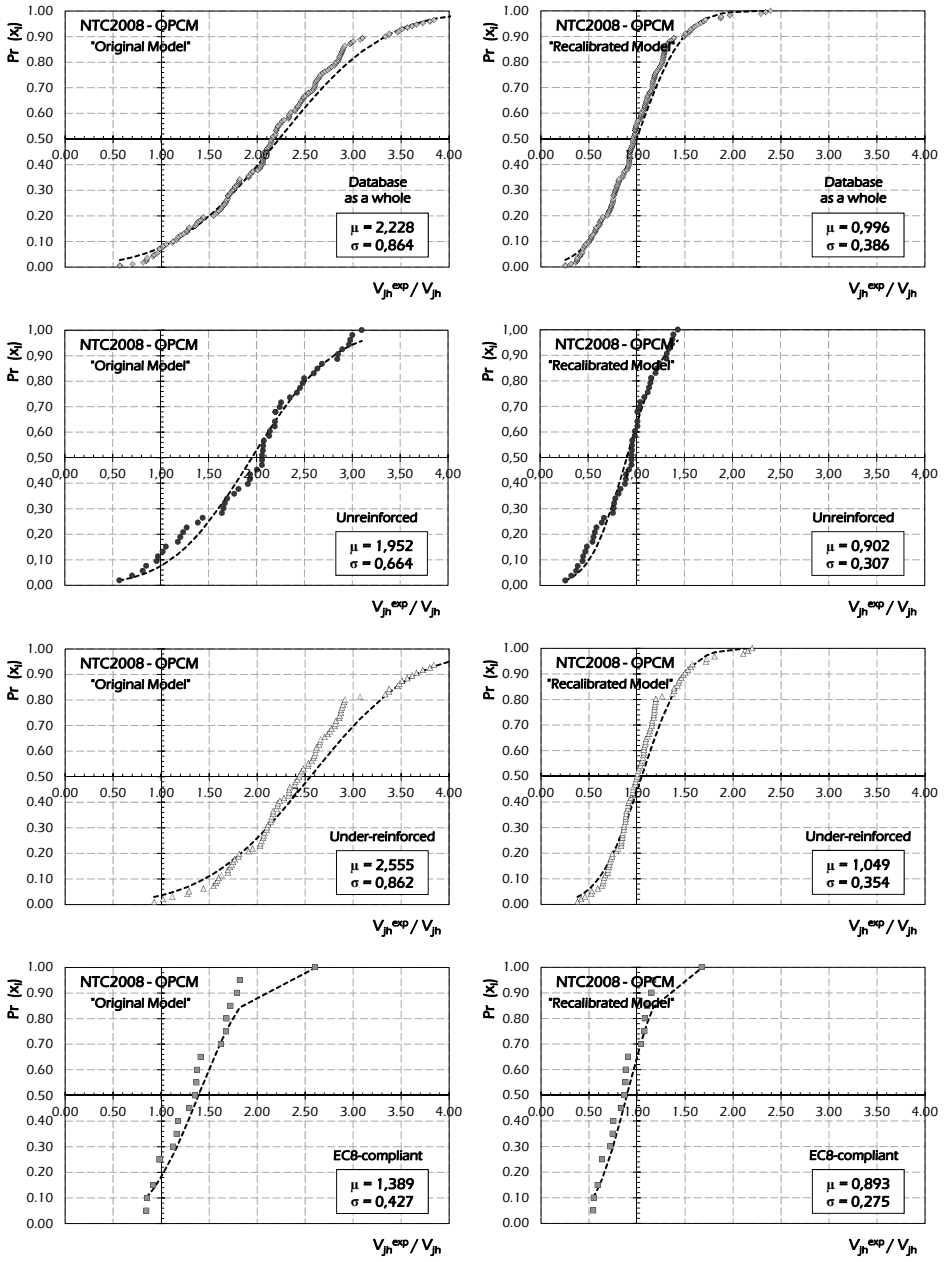

Fig. 6.56: Probabilistic Assessment of the original and recalibrated NTC (2008) and OPCM 3431 (2005) formulation for exterior joints.

6.2.1.2 Scientific Literature

In this section, the probabilistic assessment of the capacity models available in the scientific literature for evaluating the shear strength of exterior joints is carried out.

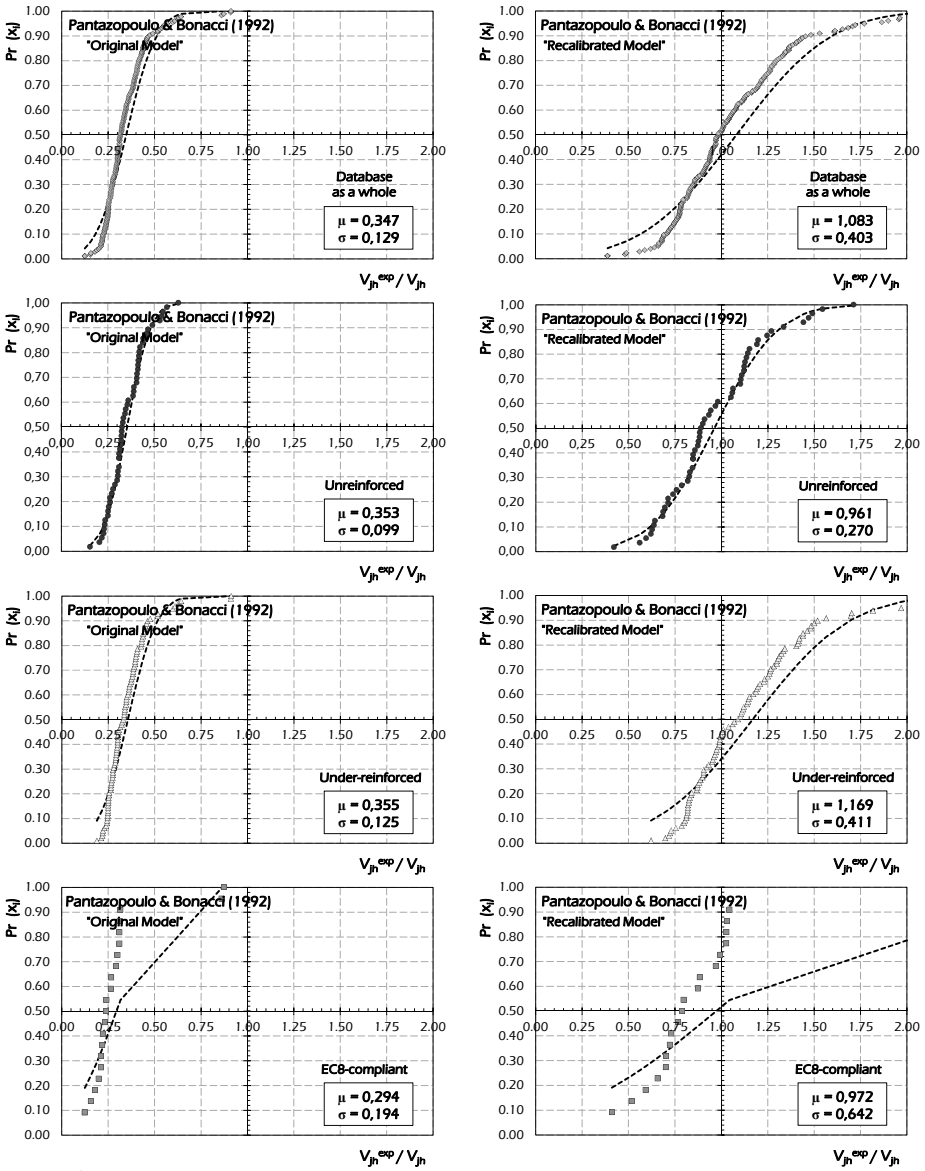

Fig. 6.57: Probabilistic Assessment of the original and recalibrated model by Pantazopoulo & Bonacci (1992) for exterior joints.

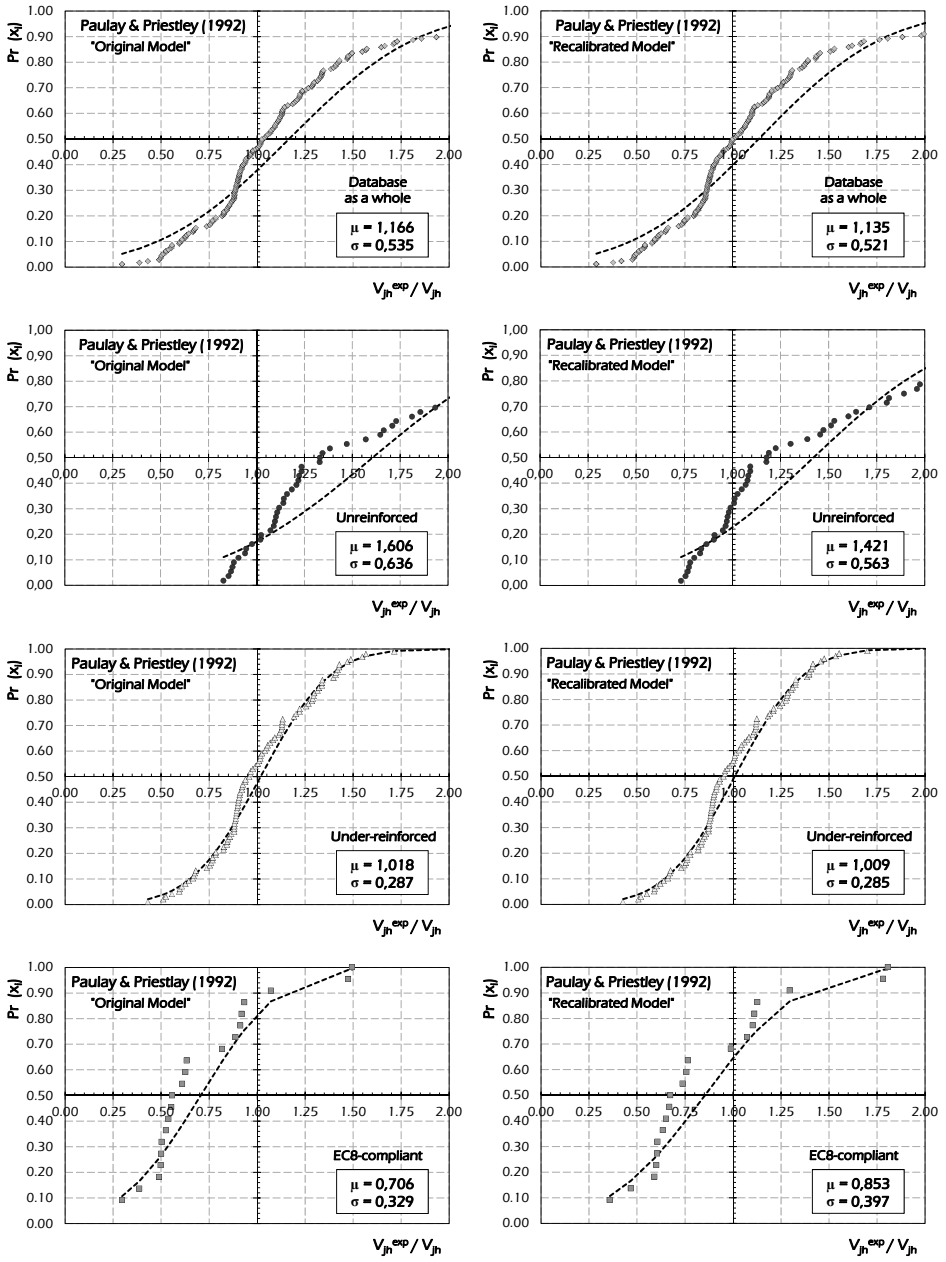

Fig. 6.58: Probabilistic Assessment of the original and recalibrated model by Paulay & Priestley (1992) for exterior joints.

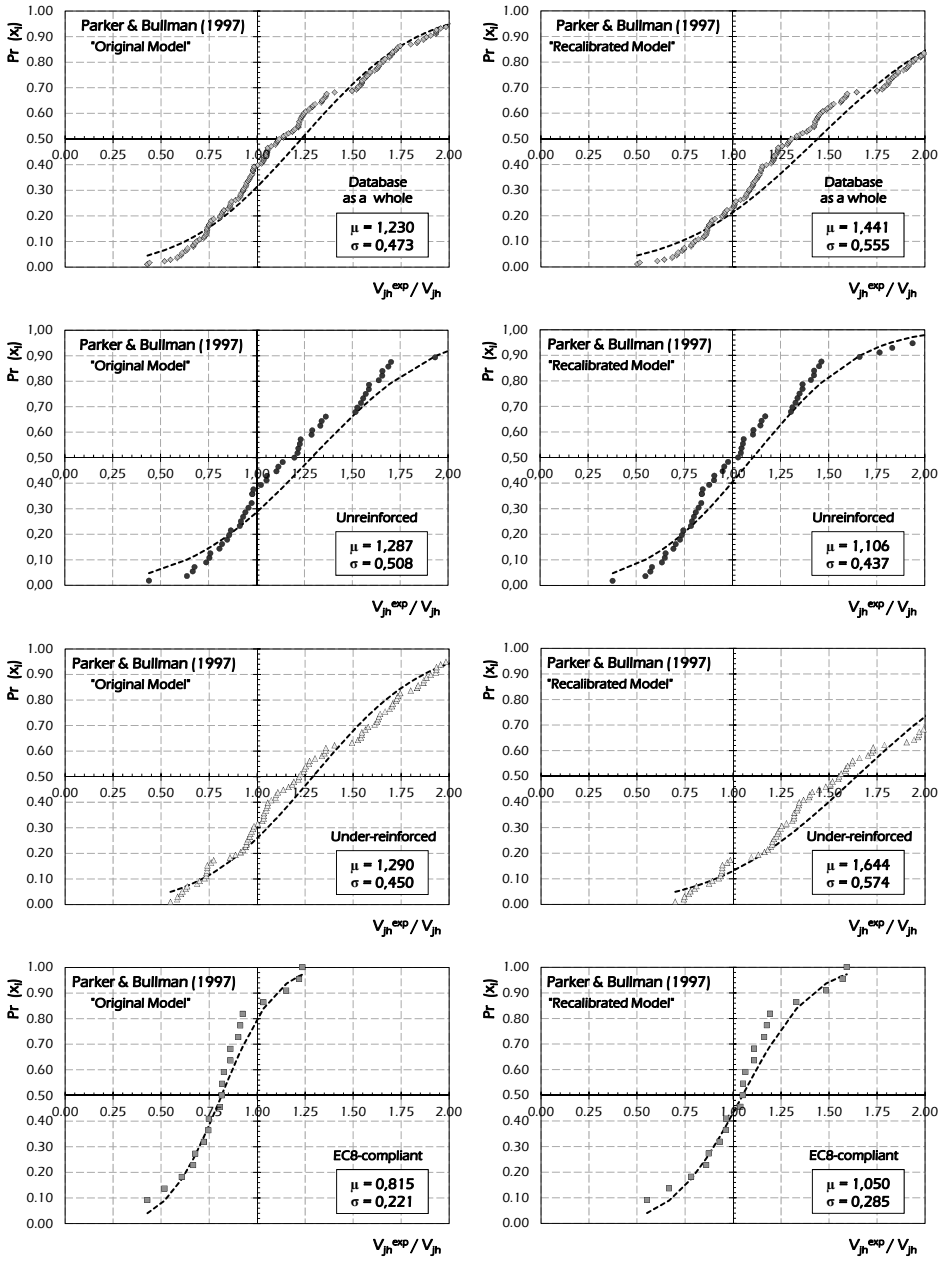

Fig. 6.59: Probabilistic Assessment of the original and recalibrated model by Parker & Bullman (1997) for exterior joints.

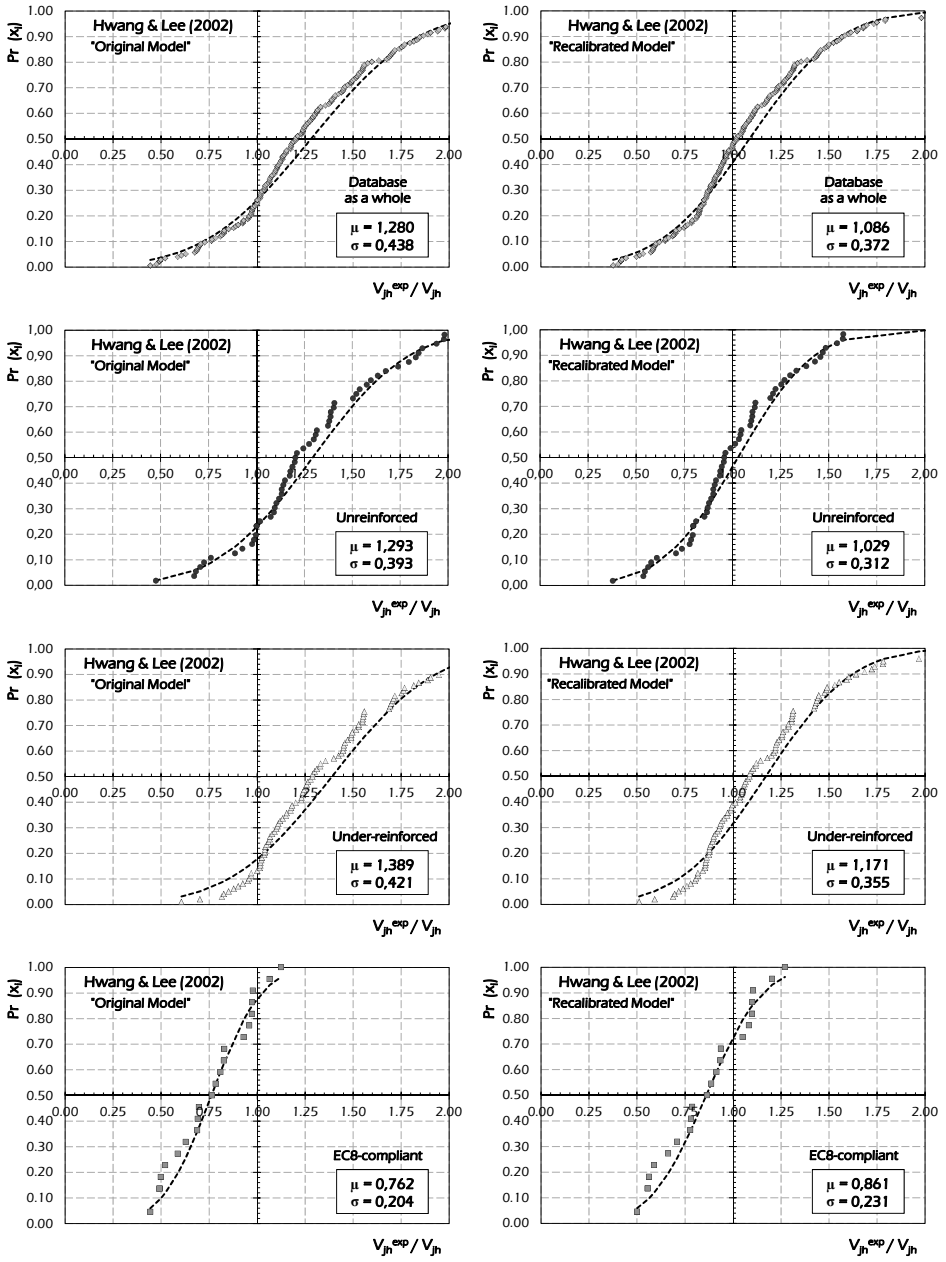

Fig. 6.60: Probabilistic Assessment of the original and recalibrated model by Hwang & Lee (2002) for exterior joints.

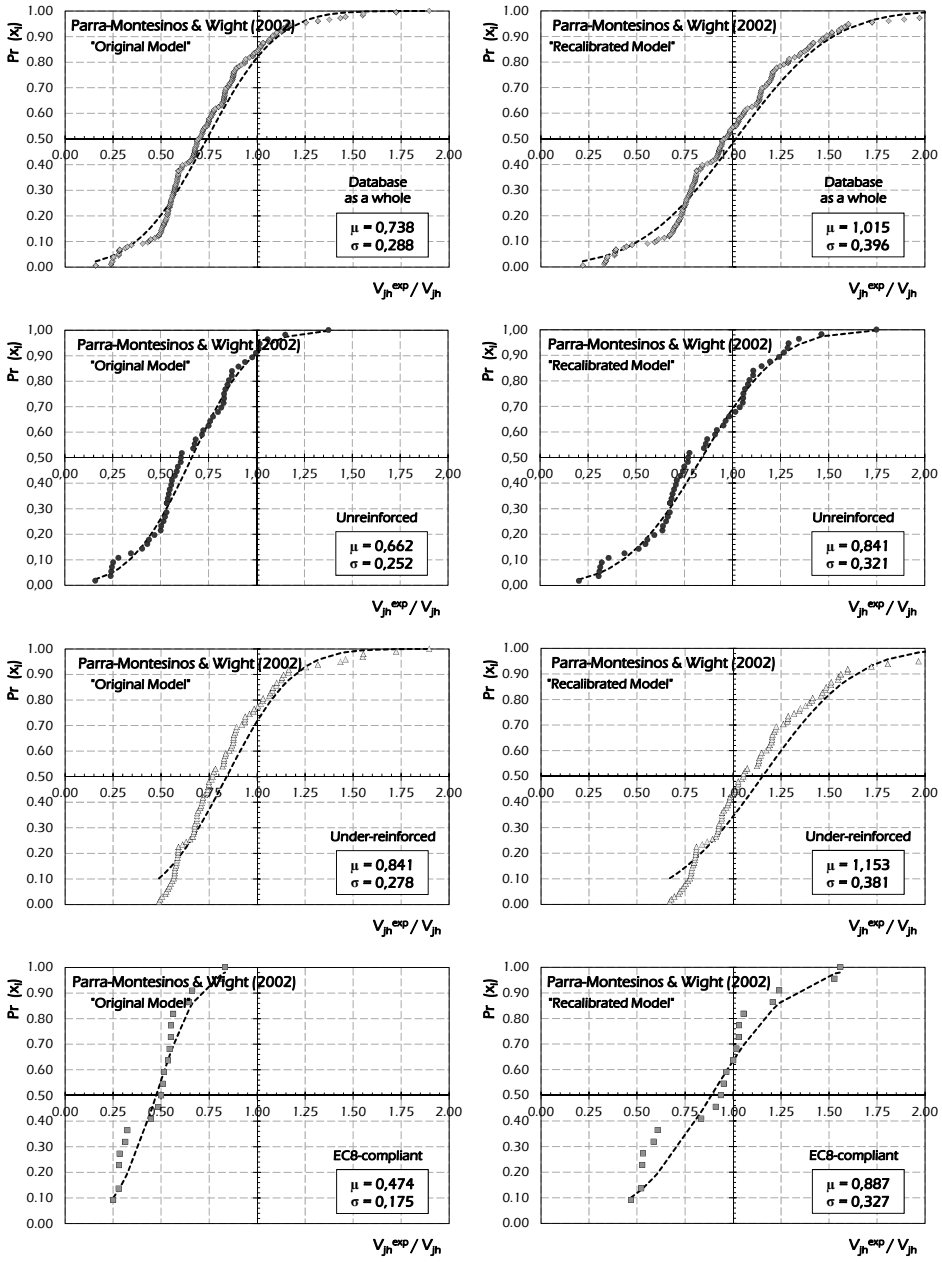

Fig. 6.61: Probabilistic Assessment of the original and recalibrated model by Parra-Montesinos & Wight (2002) for exterior joints.

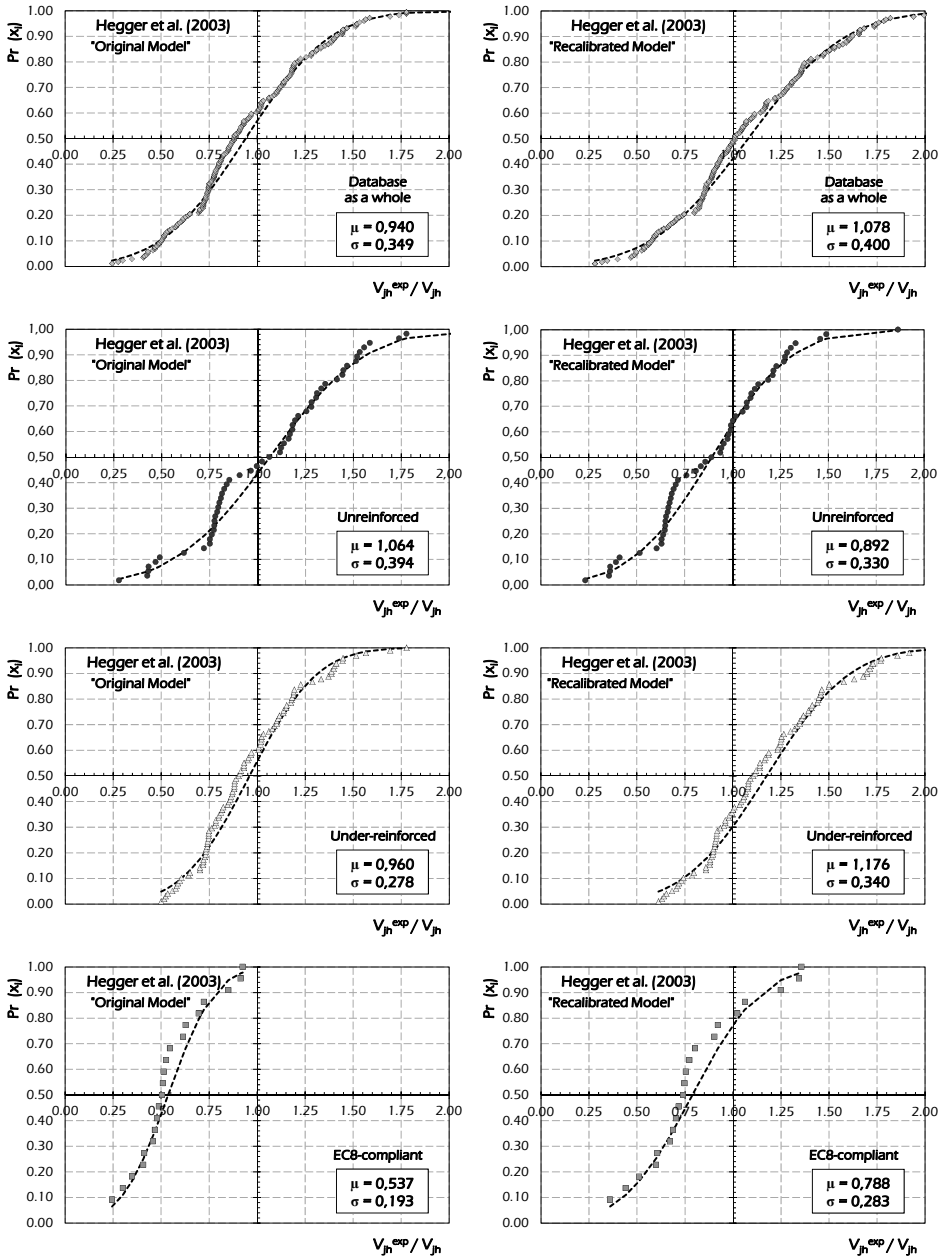

Fig. 6.62: Probabilistic Assessment of the original and recalibrated model by Hegger et al. (2003) for exterior joints.

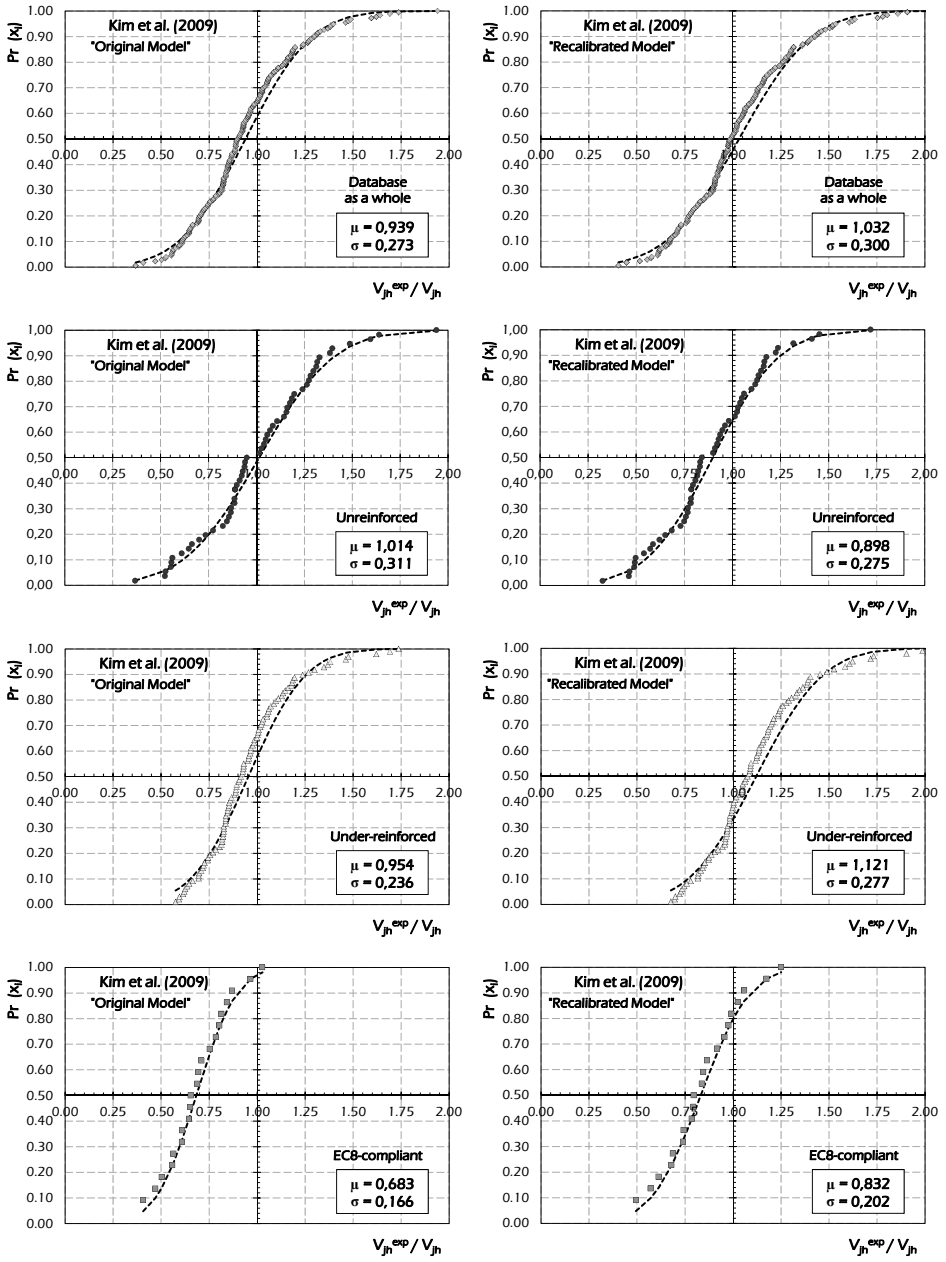

Fig. 6.63: Probabilistic Assessment of the original and recalibrated model by Kim et al. (2009) for exterior joints.

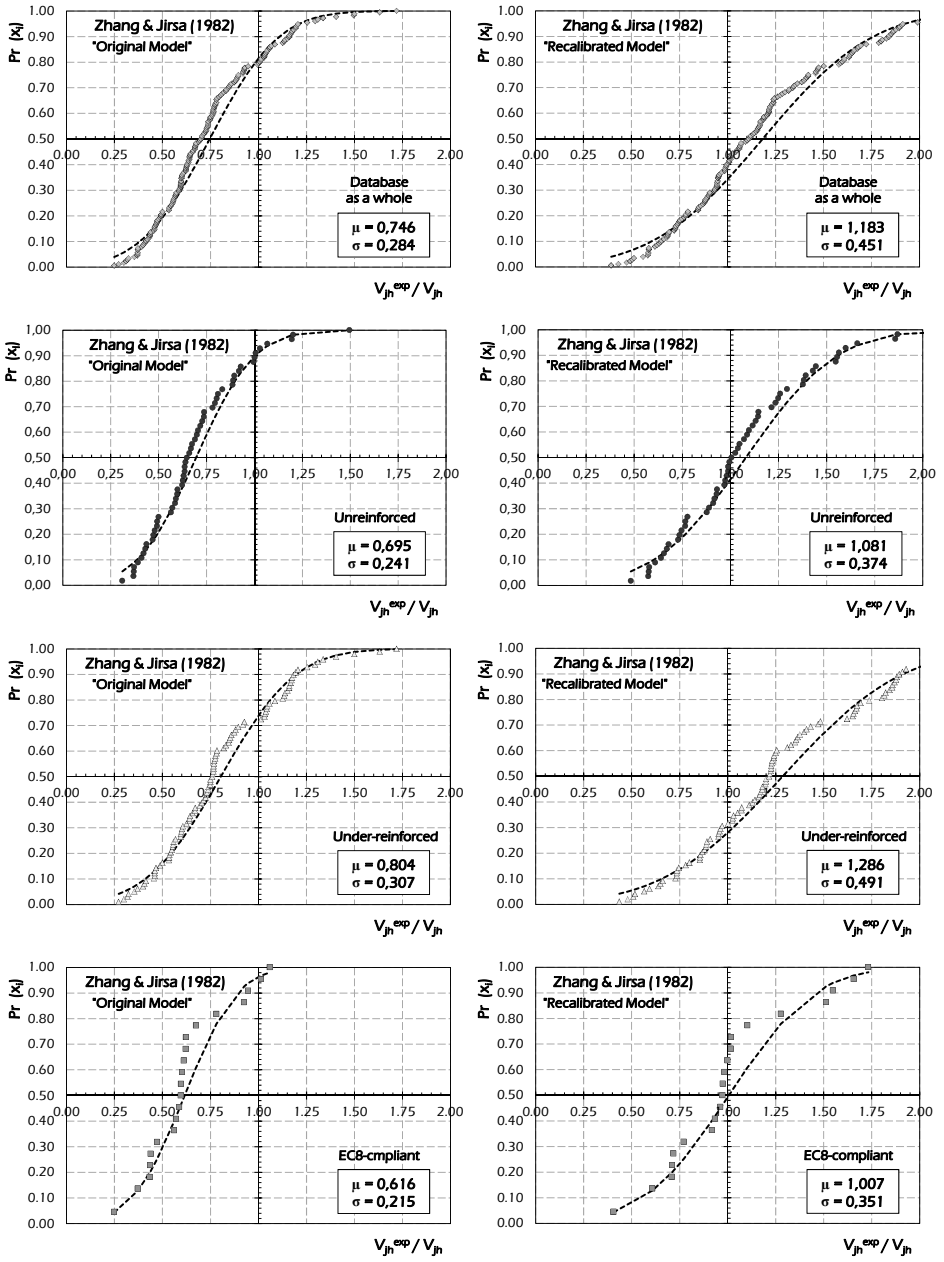

Fig. 6.64: Probabilistic Assessment of the original and recalibrated model by Zhang & Jirsa (1982) for exterior joints.

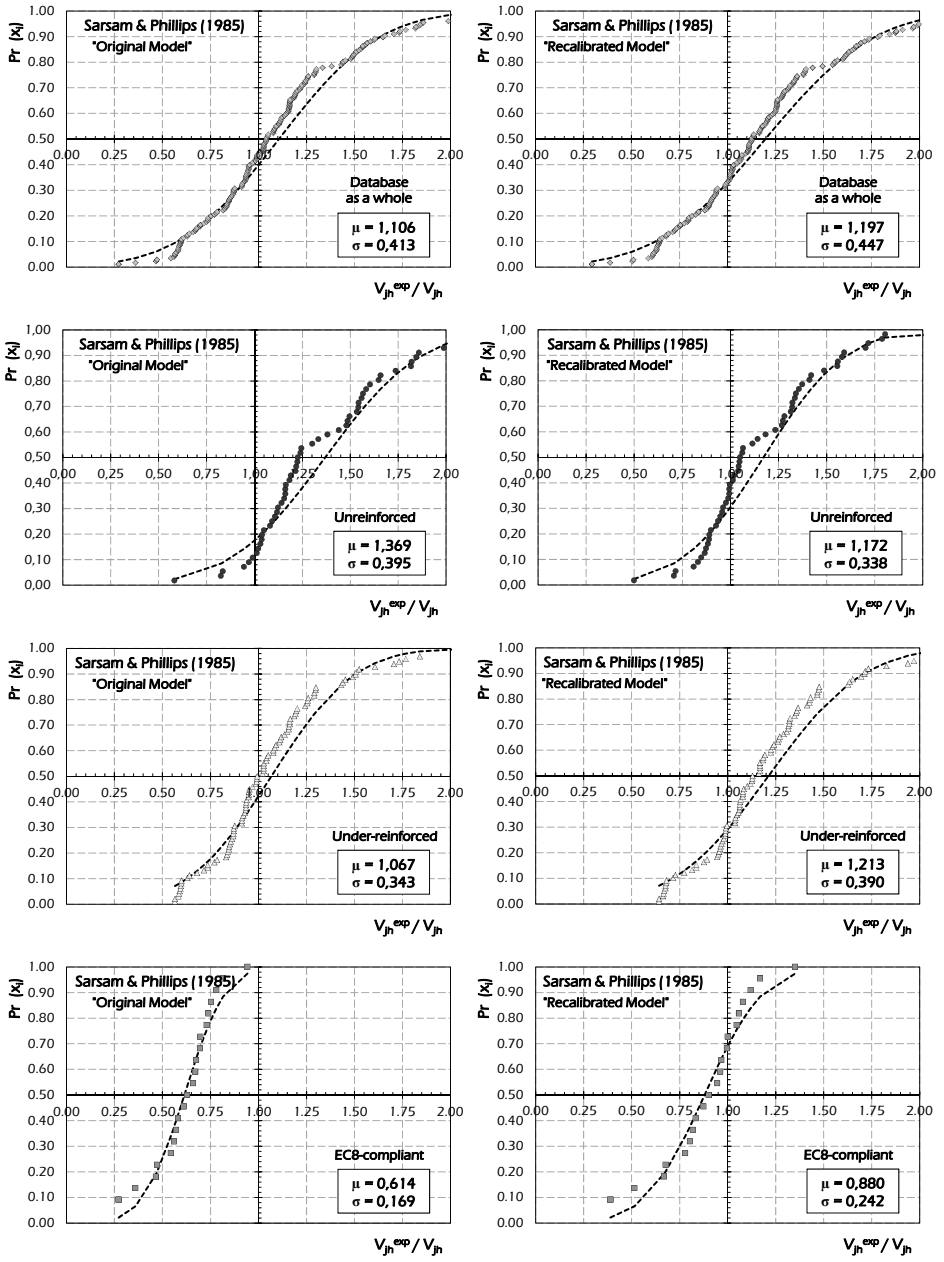

Fig. 6.65: Probabilistic Assessment of the original and recalibrated model by Sarsam & Phillips (1985) for exterior joints.

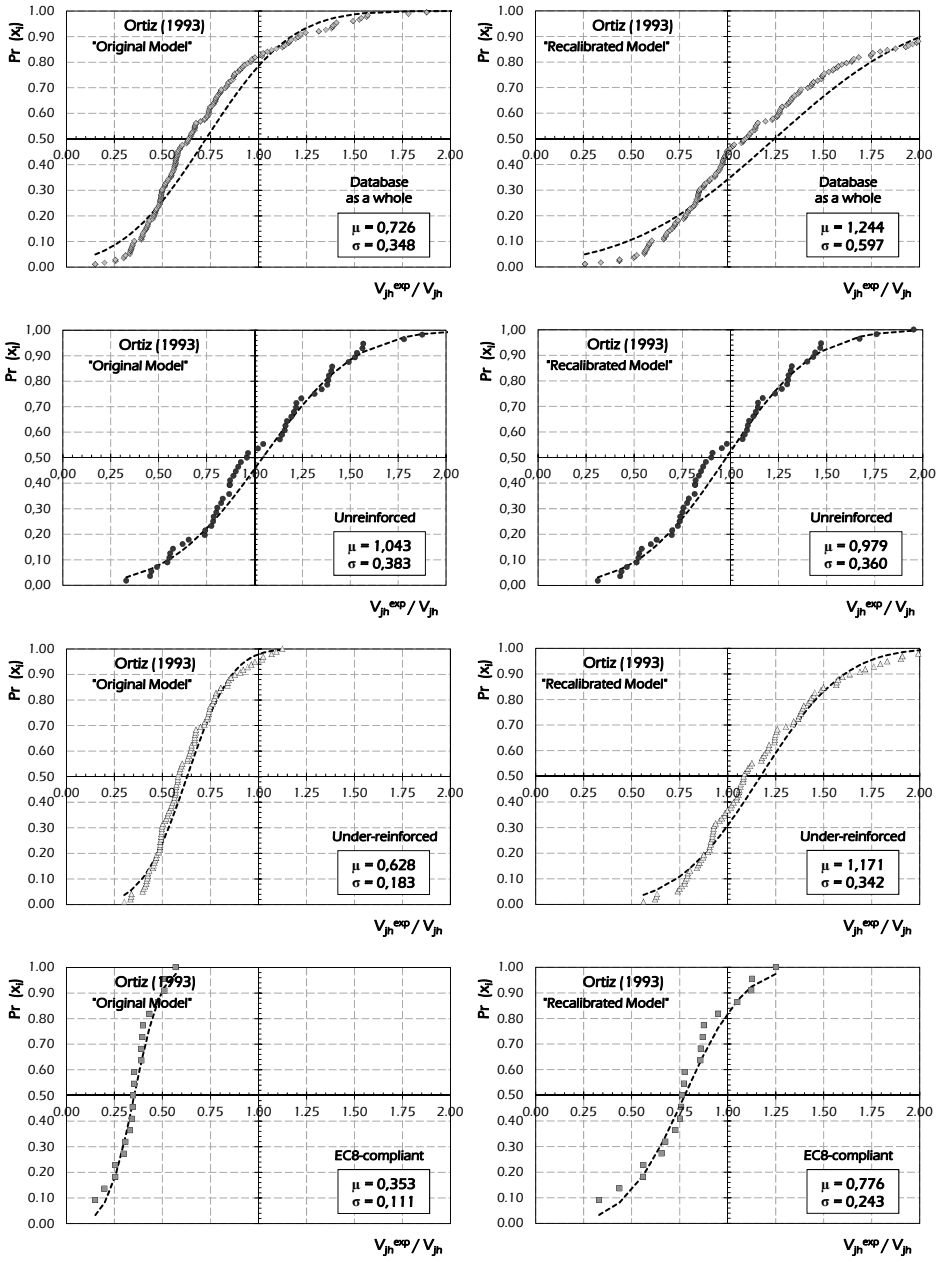

Fig. 6.66: Probabilistic Assessment of the original and recalibrated model by Ortiz (1993) for exterior joints.

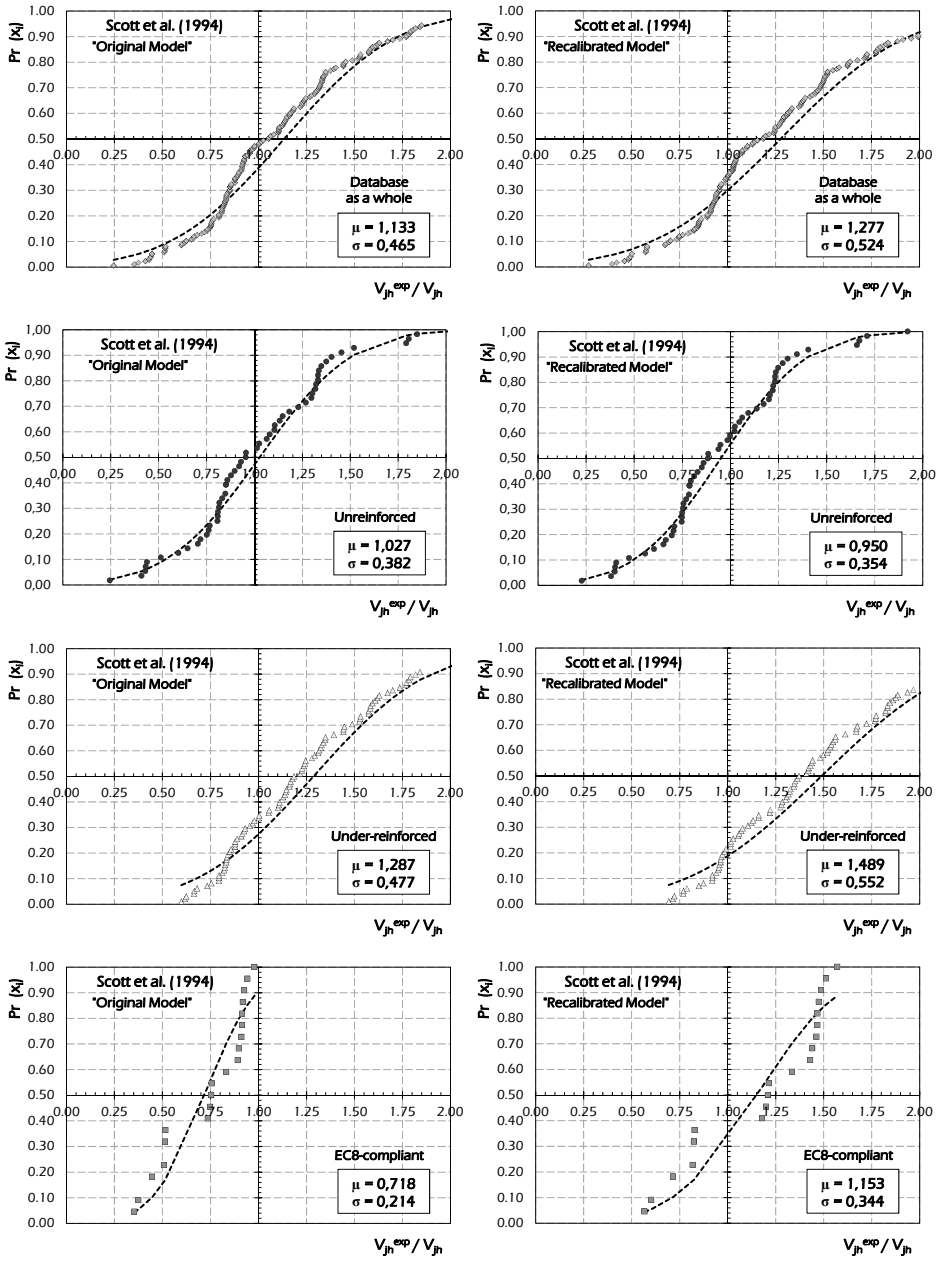

Fig. 6.67: Probabilistic Assessment of the original and recalibrated model by Scott et al. (1994) for exterior joints.

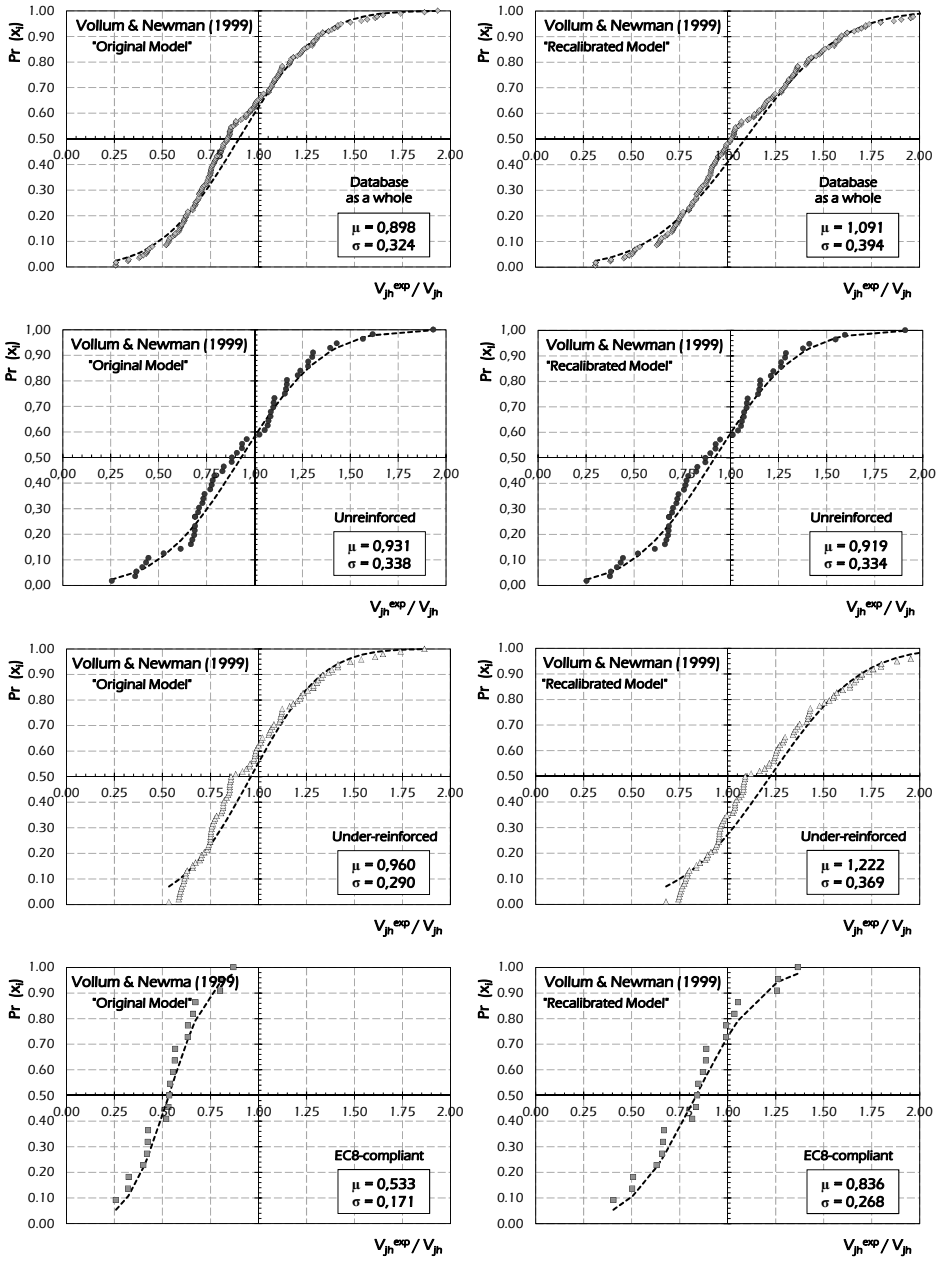

Fig. 6.68: Probabilistic Assessment of the original and recalibrated model by Vollum & Newman (1999) for exterior joints.

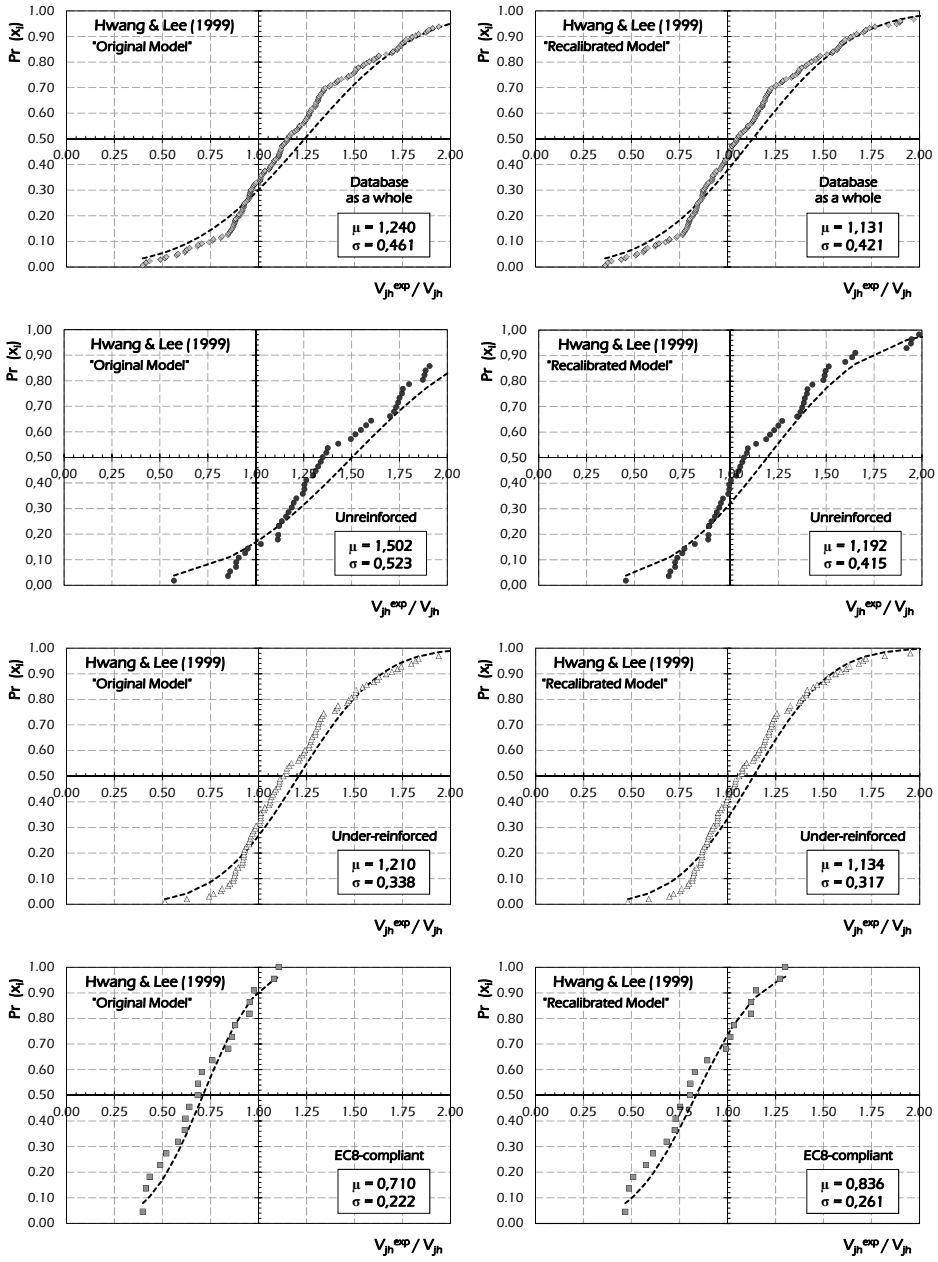

Fig. 6.69: Probabilistic Assessment of the original and recalibrated model by Hwang & Lee (1999) for exterior joints.

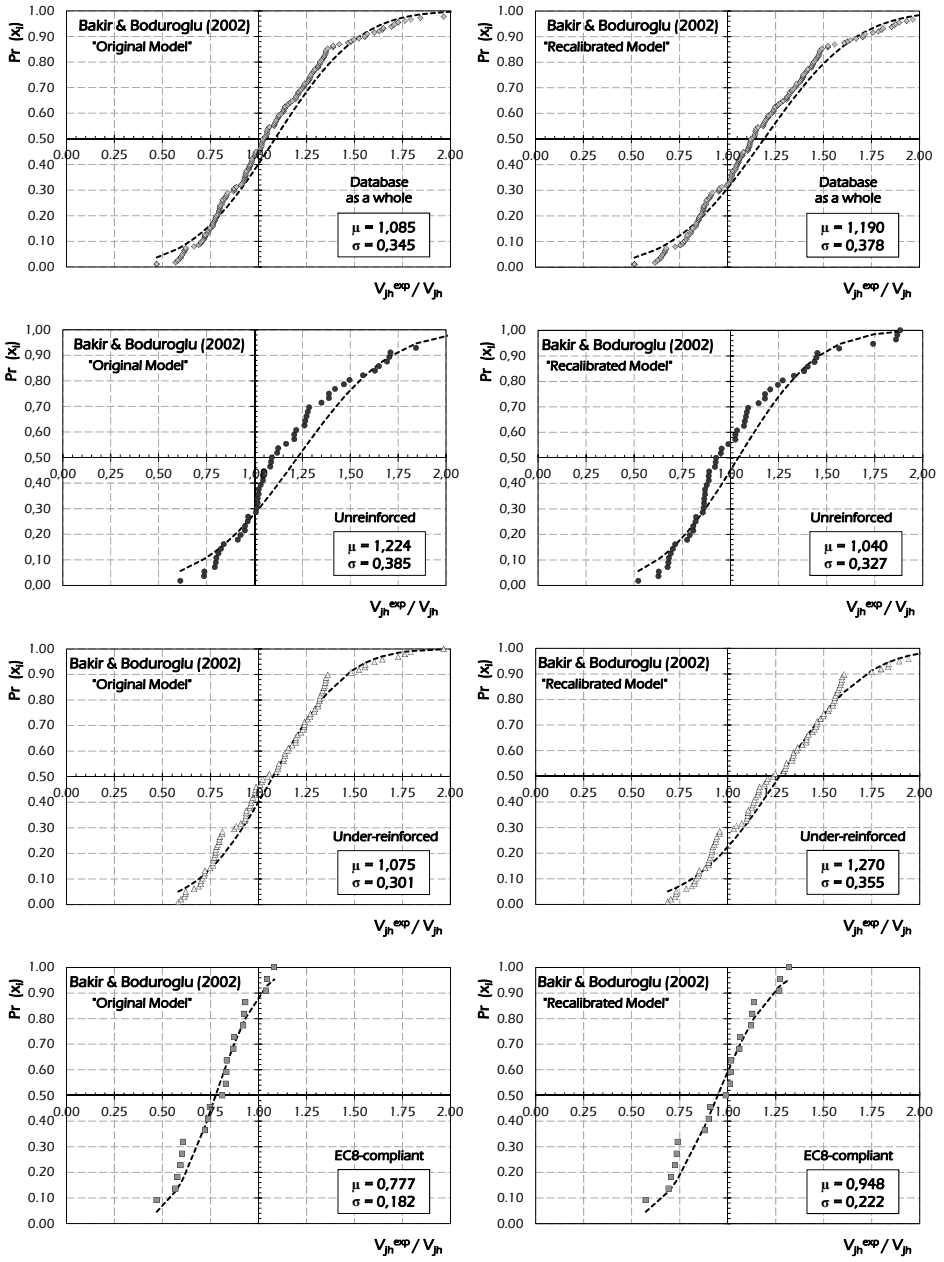

Fig. 6.70: Probabilistic Assessment of the original and recalibrated model by Bakir & Boduroglu (2002) for exterior joints.

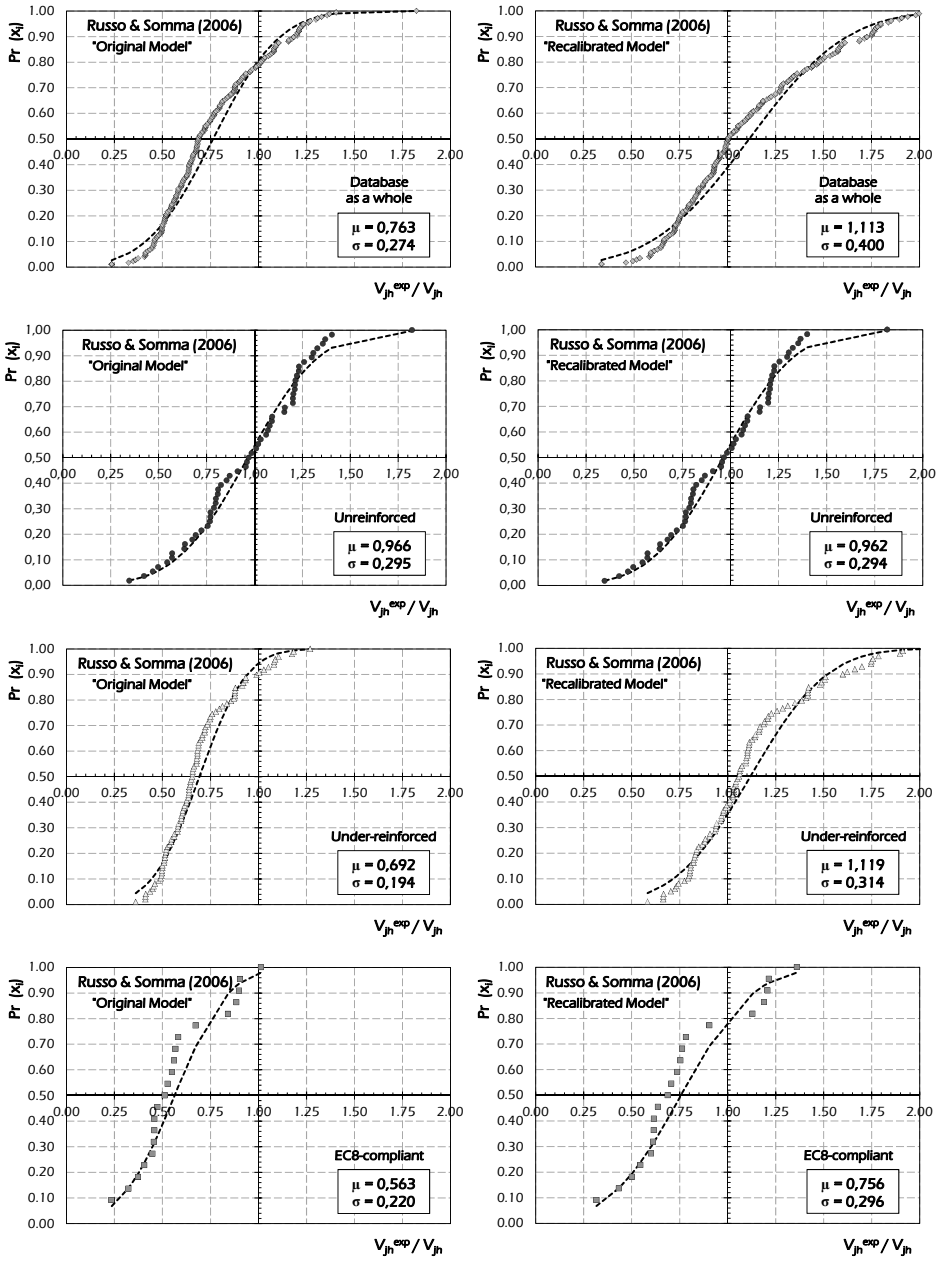

Fig. 6.71: Probabilistic Assessment of the original and recalibrated model by Russo & Somma (2006) for exterior joints.

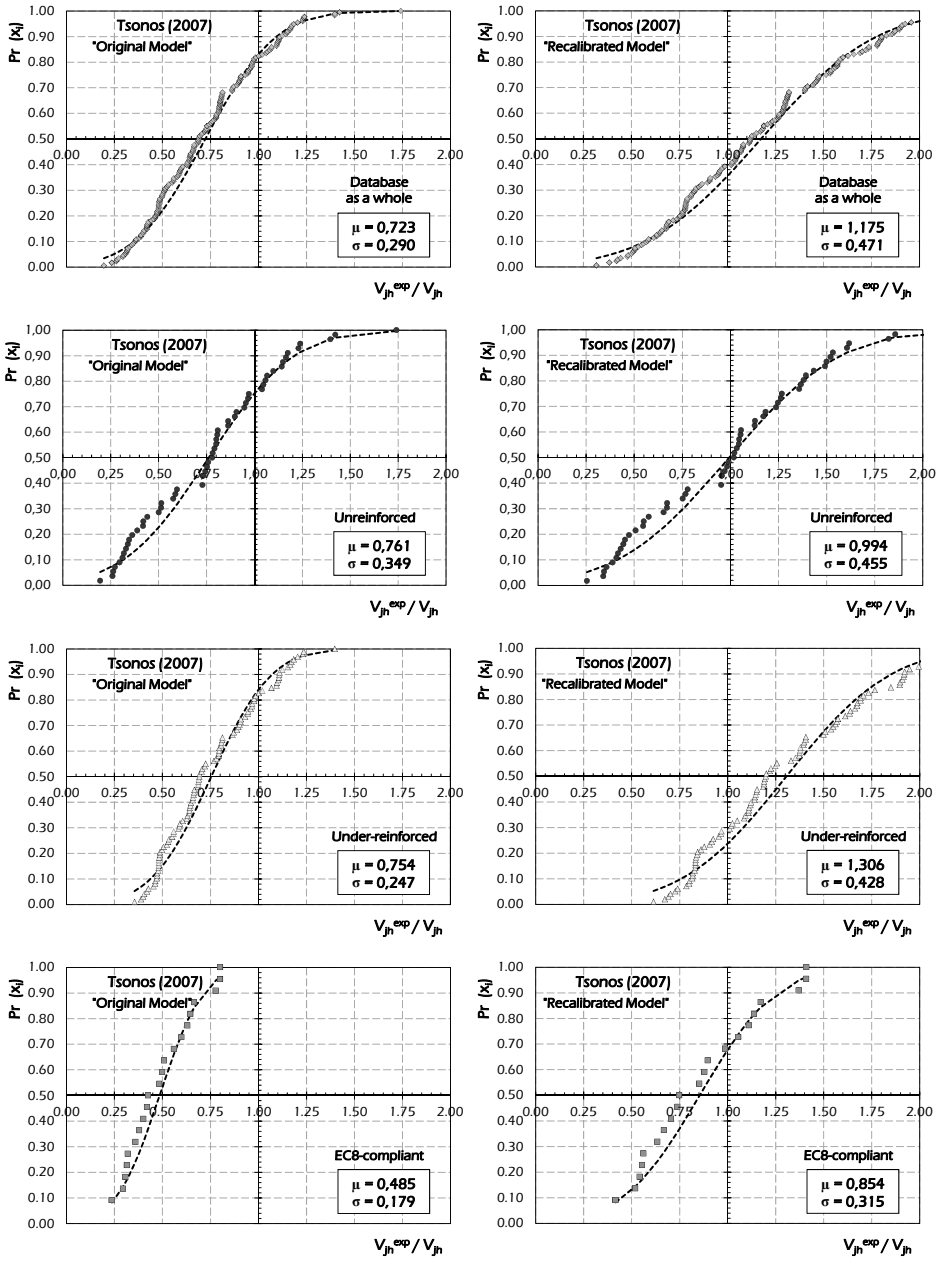

Fig. 6.72: Probabilistic Assessment of the original and recalibrated model by Tsonos (2007) for exterior joints.

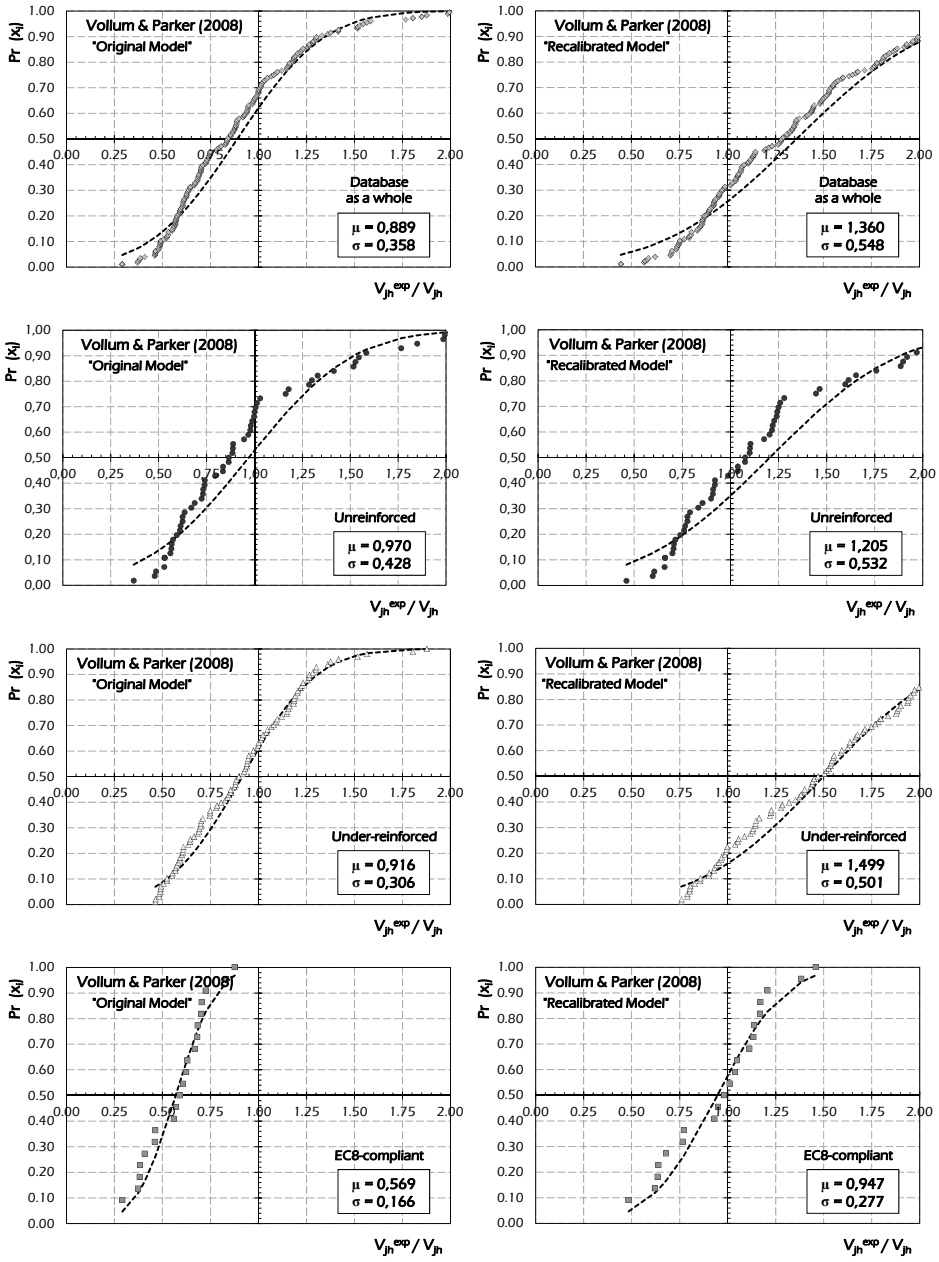

Fig. 6.73: Probabilistic Assessment of the original and recalibrated model by Vollum & Parker (2008) for exterior joints.

6.2.2 Interior Joints

The probabilistic assessment of code formulations and capacity models for interior joints is provided in this section by considering the database as a whole and its three subsections (namely, collecting unreinforced and reinforced specimens).

6.2.2.1 Code Formulations

In the following figures both original code formulations and recalibrated ones are assessed by reporting on each chart the values of mean μ and standard deviation σ.

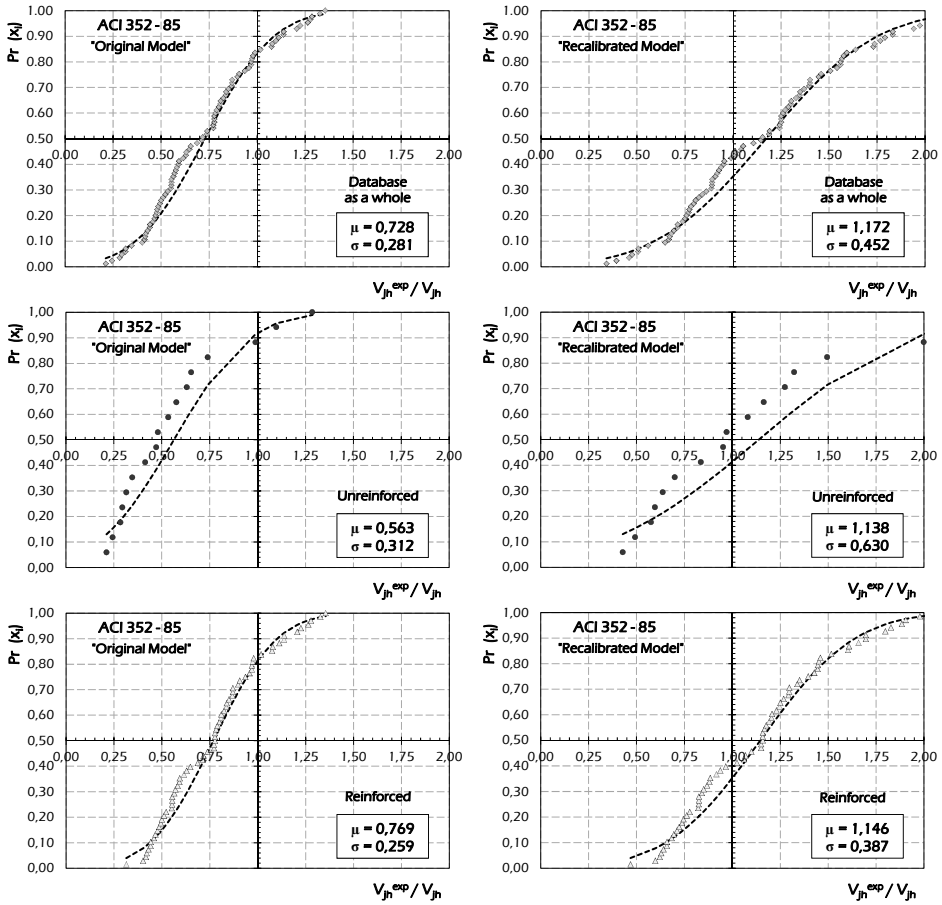

Fig. 6.74: Probabilistic Assessment of the original and recalibrated ACI 352-85 (1985) formulation for interior joints.

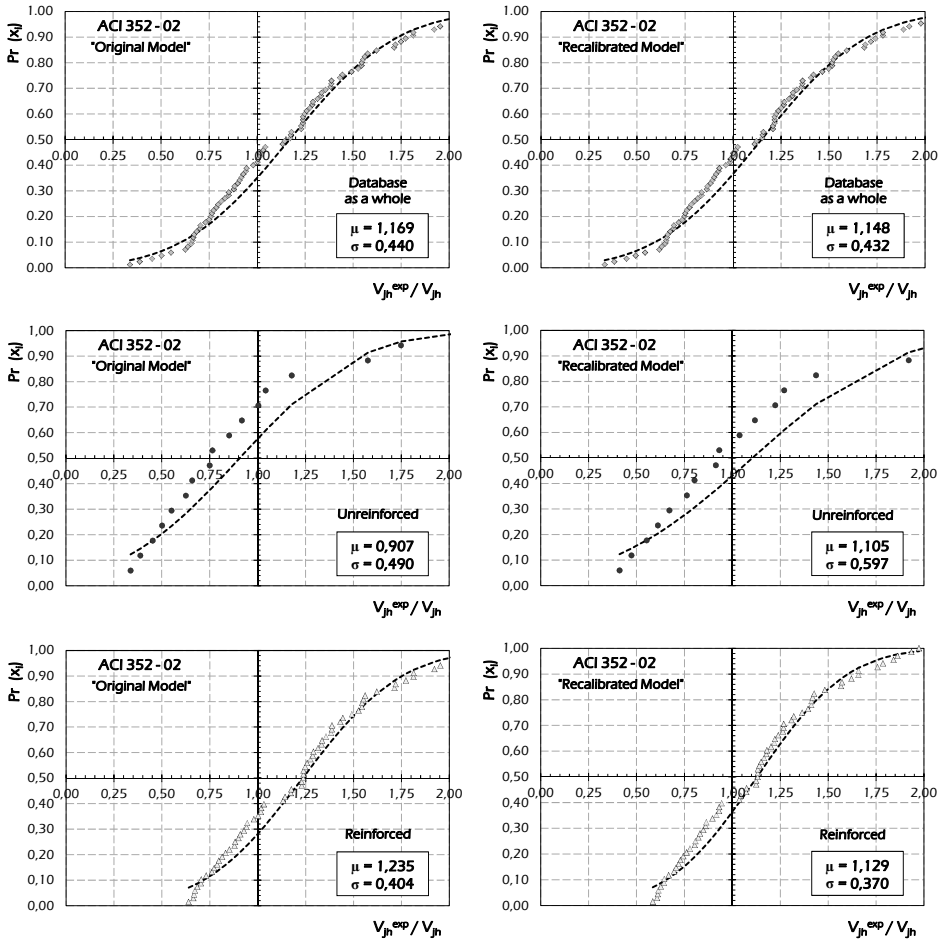

Fig. 6.75: Probabilistic Assessment of the original and recalibrated ACI 352-02 (2002) formulation for interior joints.

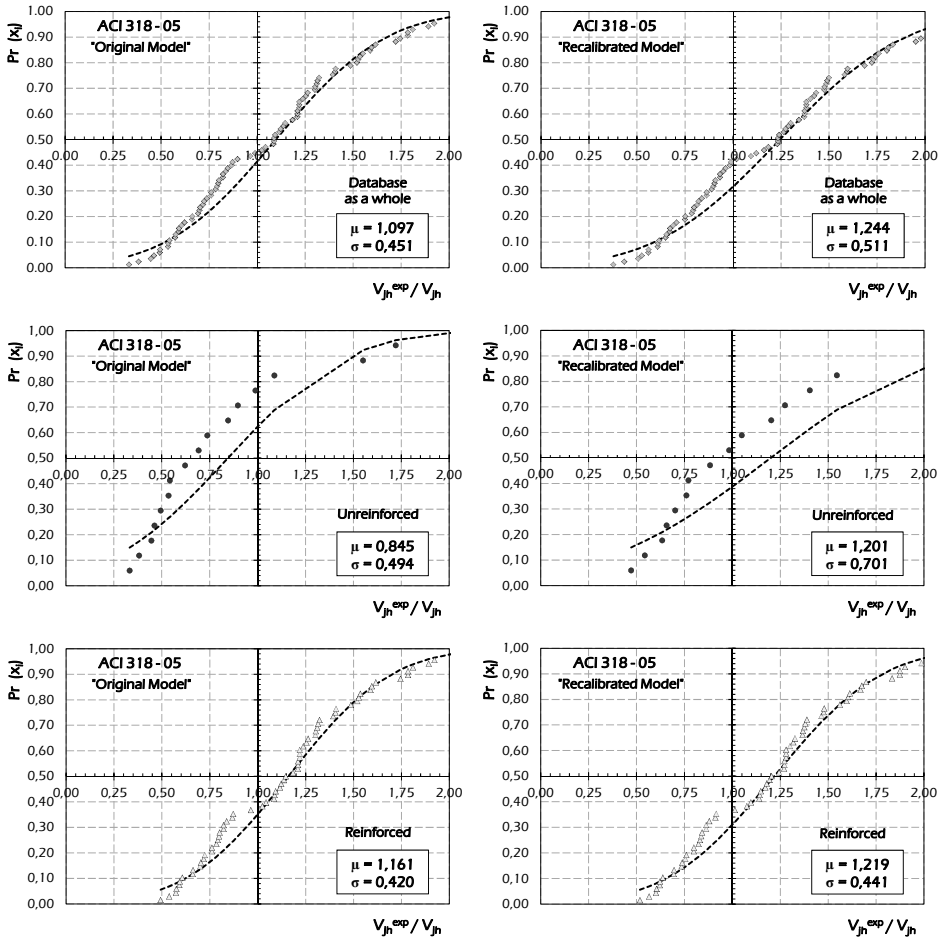

Fig. 6.76: Probabilistic Assessment of the original and recalibrated ACI 318-05 (2005) formulation for interior joints.

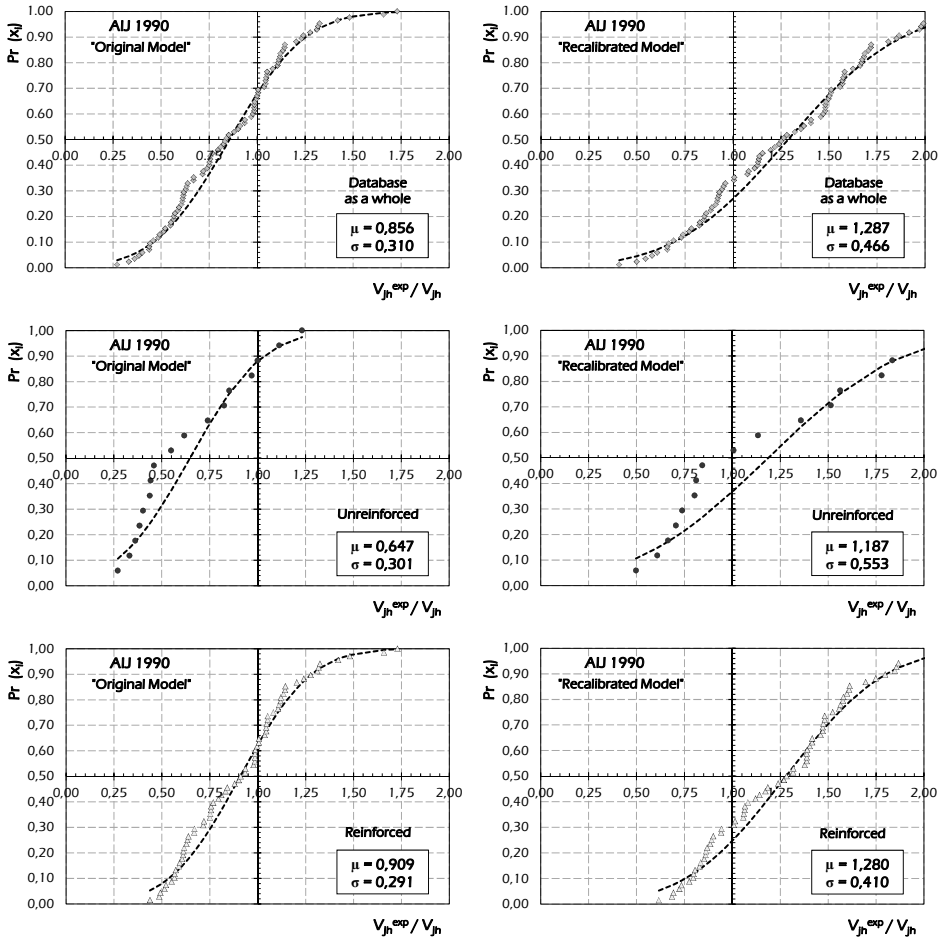

Fig. 6.77: Probabilistic Assessment of the original and recalibrated AIJ 1990 (1990) formulation for interior joints.

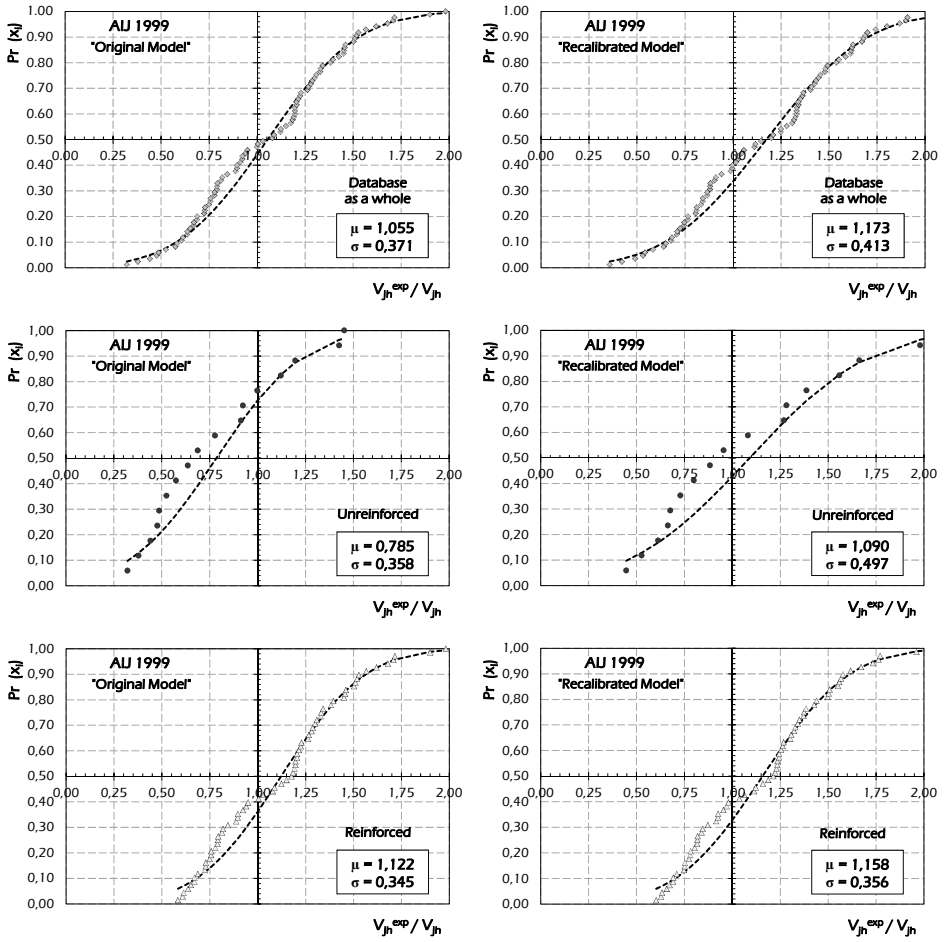

Fig. 6.78: Probabilistic Assessment of the original and recalibrated AIJ 1999 (1999) formulation for interior joints.

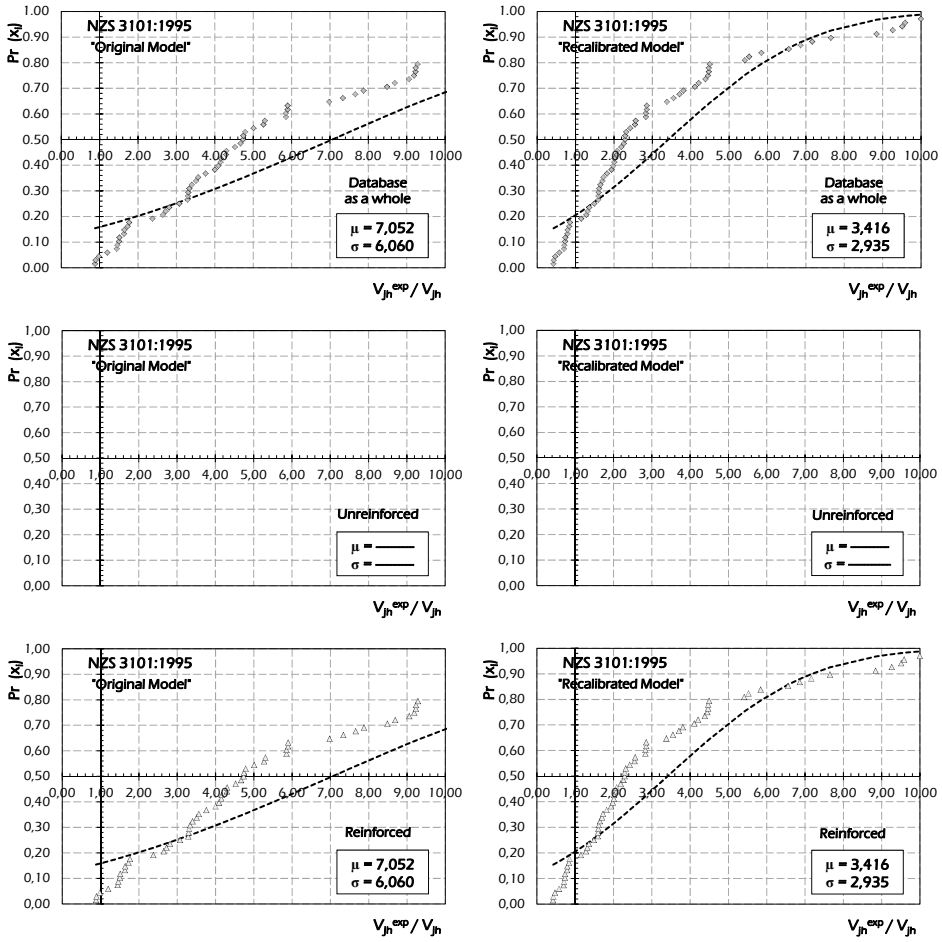

Fig. 6.79: Probabilistic Assessment of the original and recalibrated NZS 3101 (1995) formulation for interior joints.

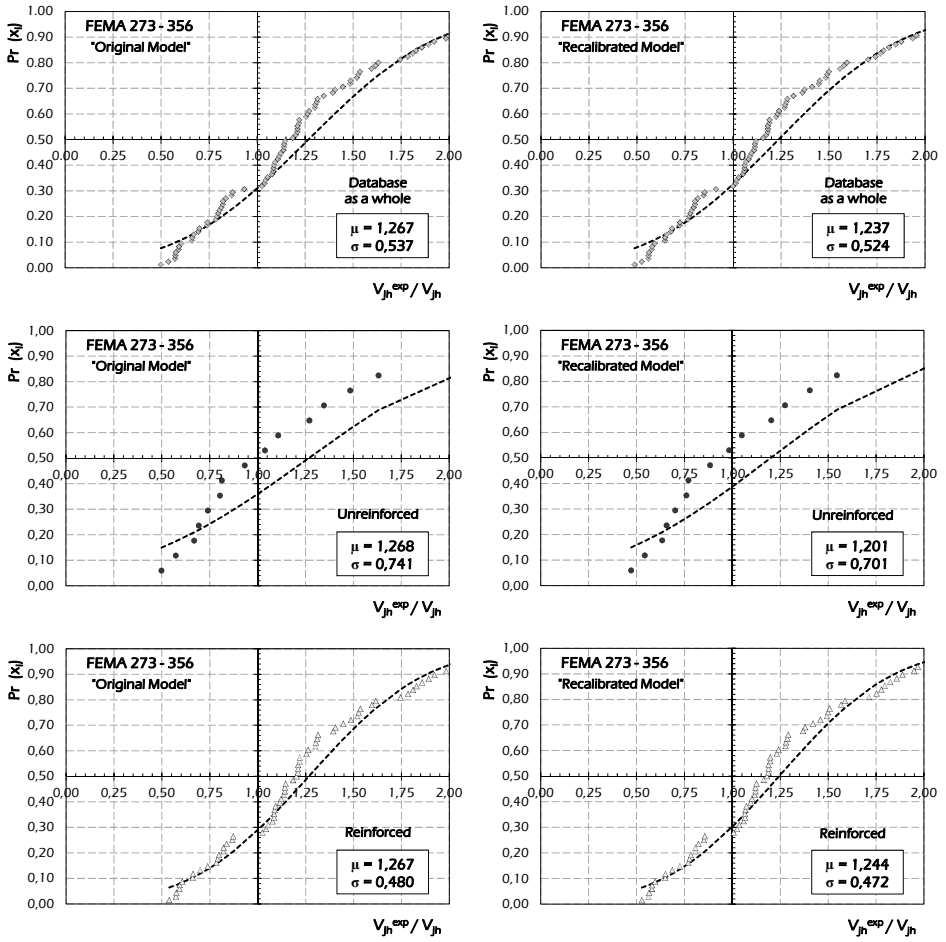

Fig. 6.80: Probabilistic Assessment of the original and recalibrated FEMA 273 (1997) – 356 (2000) formulation for interior joints.

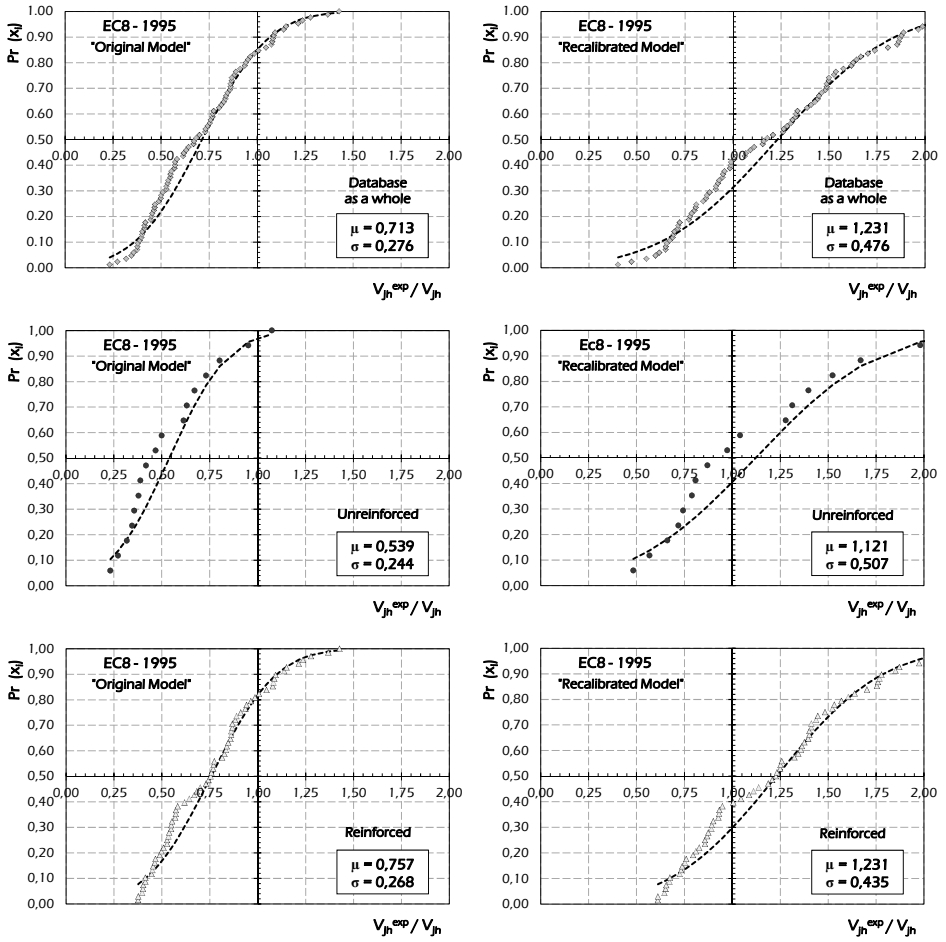

Fig. 6.81: Probabilistic Assessment of the original and recalibrated Eurocode 8 (EN 1995, 1995) formulation for interior joints.

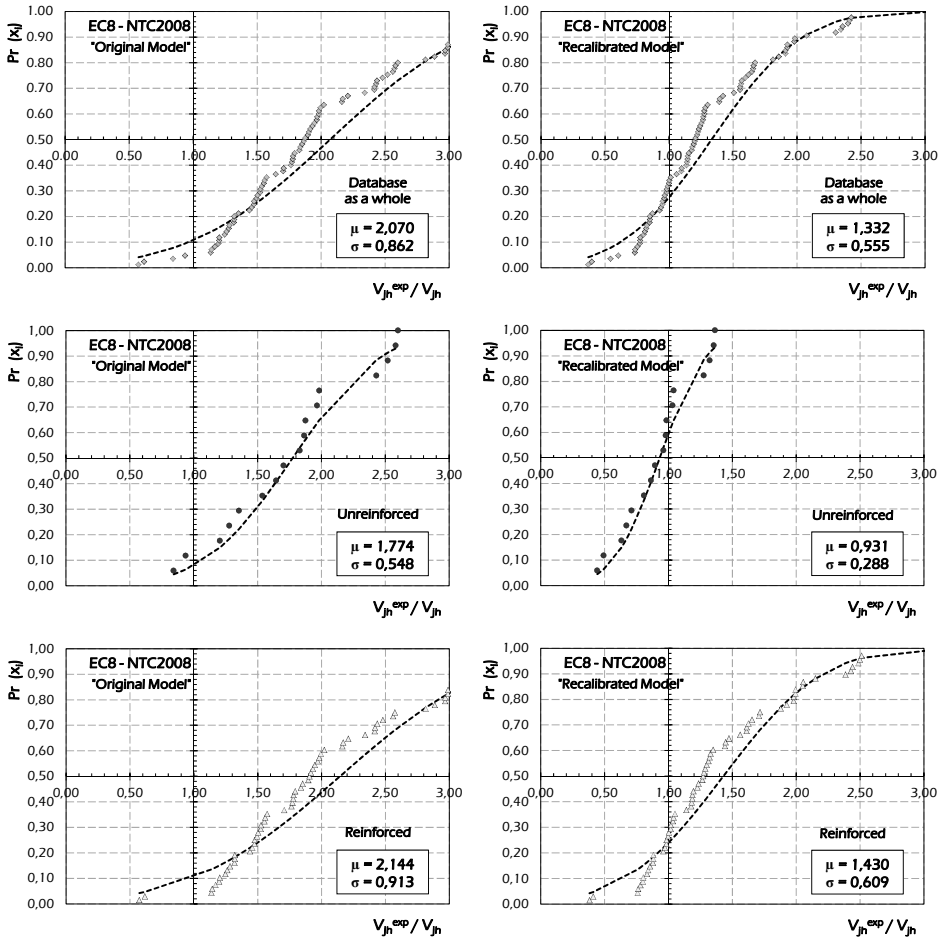

Fig. 6.82: Probabilistic Assessment of the original and recalibrated Eurocode 8 (EN 1998, 2005) and NTC (2008) formulation for interior joints.

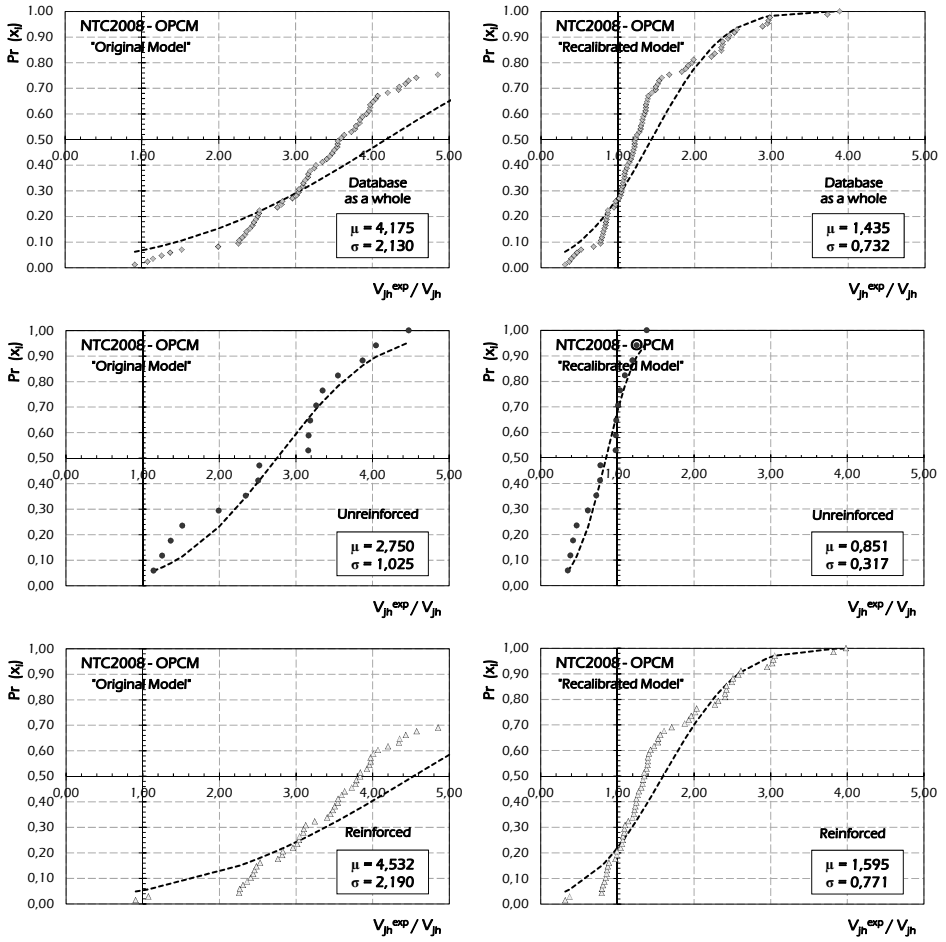

Fig. 6.83: Probabilistic Assessment of the original and recalibrated NTC (2008) and OPCM 3431 (2005) formulation for interior joints.

6.2.2.2 Scientific Literature

In this section, the probabilistic assessment of the capacity models available in the scientific literature for evaluating the shear strength of interior joints is carried out.

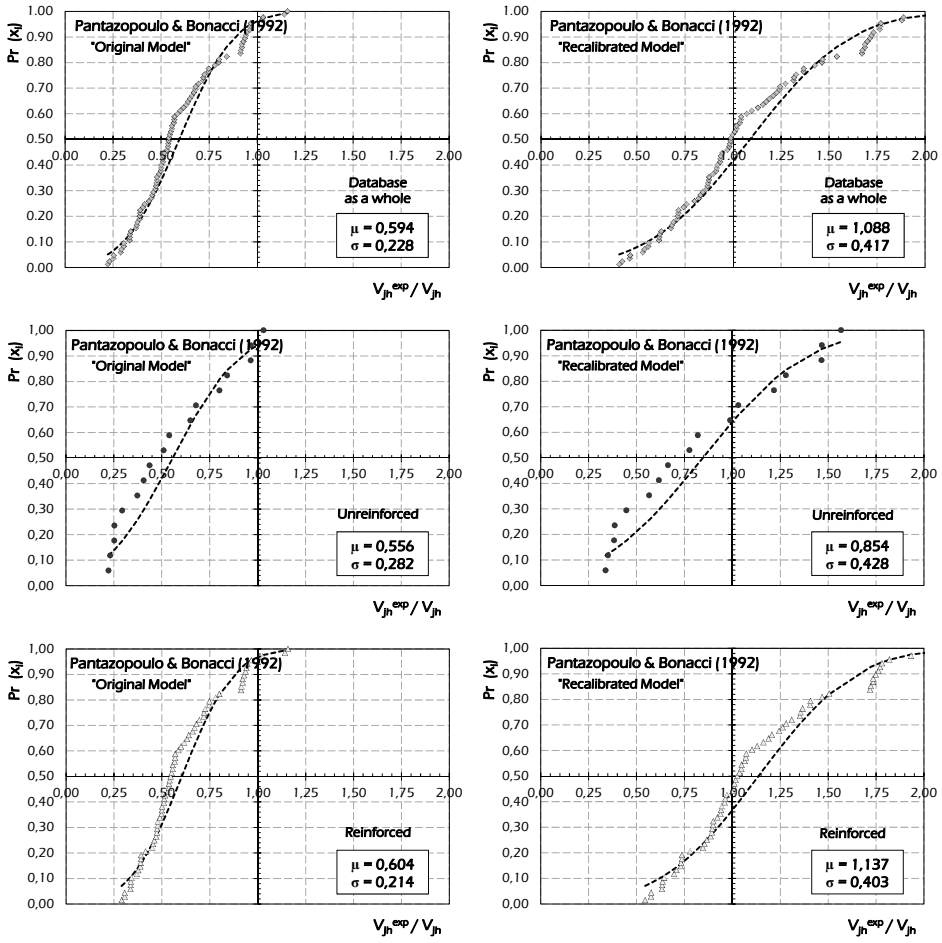

Fig. 6.84: Probabilistic Assessment of the original and recalibrated model by Pantazopoulo & Bonacci (1992) for interior joints.

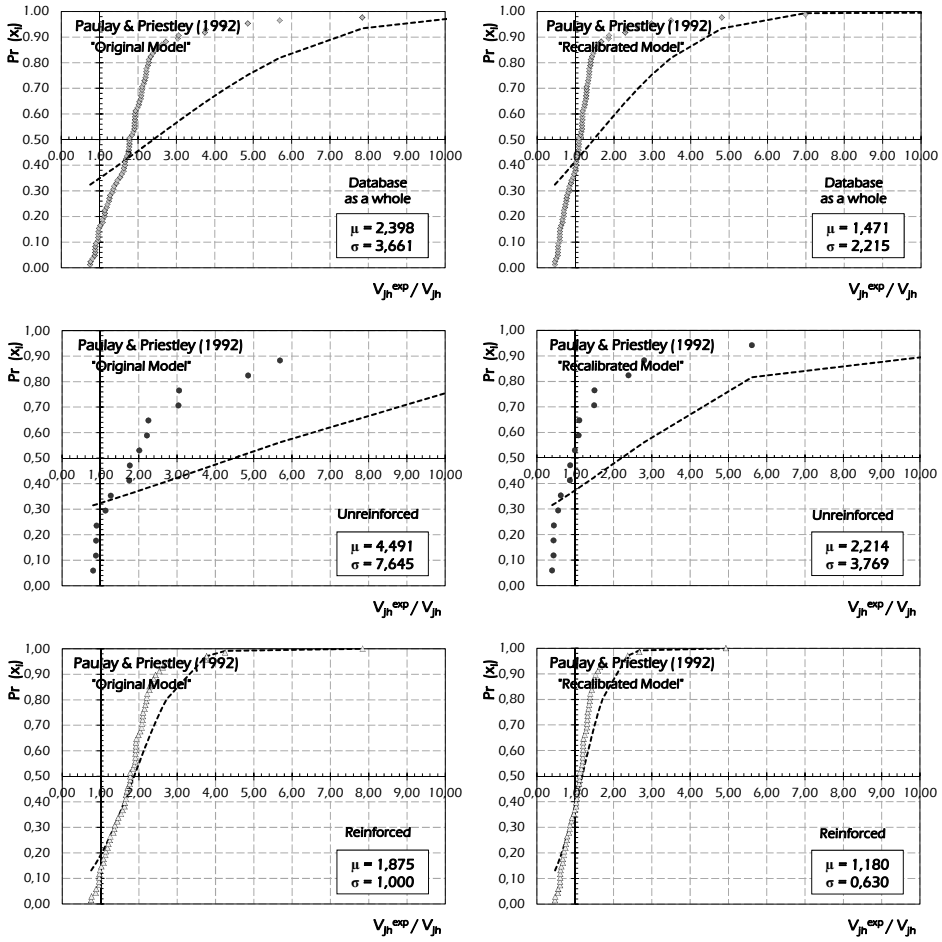

Fig. 6.85: Probabilistic Assessment of the original and recalibrated model by Paulay & Priestley (1992) for interior joints.

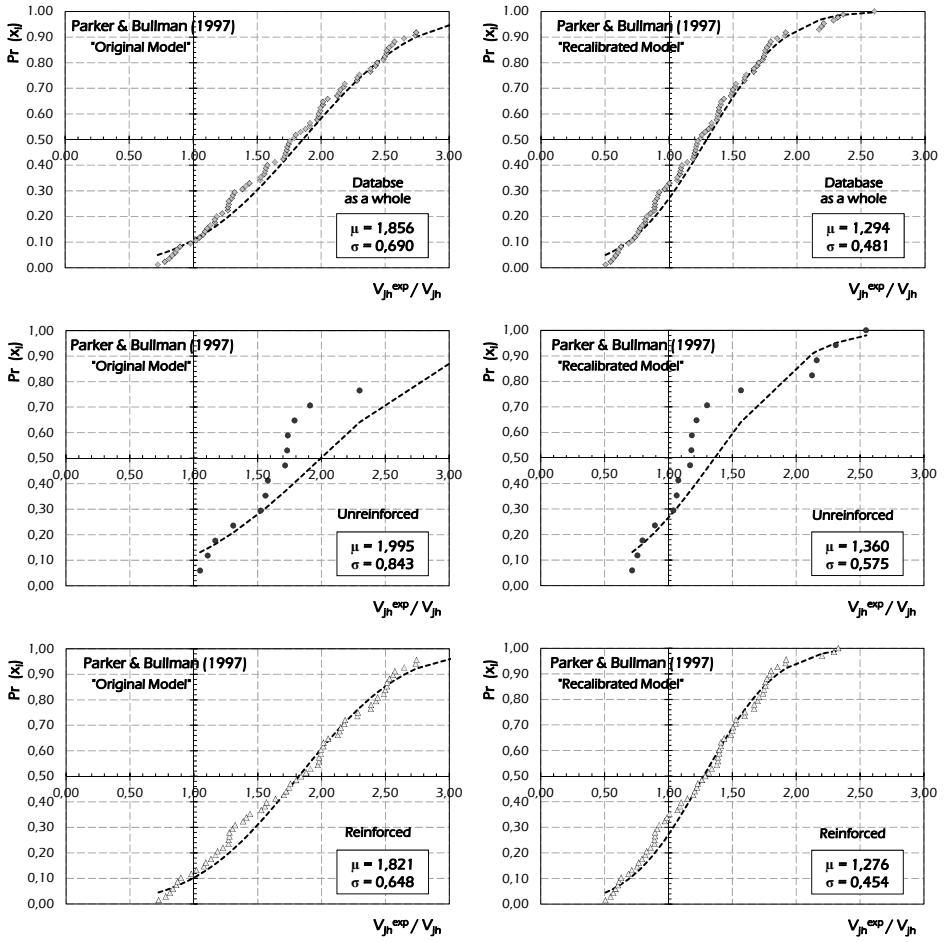

Fig. 6.86: Probabilistic Assessment of the original and recalibrated model by Parker & Bullman (1997) for interior joints.

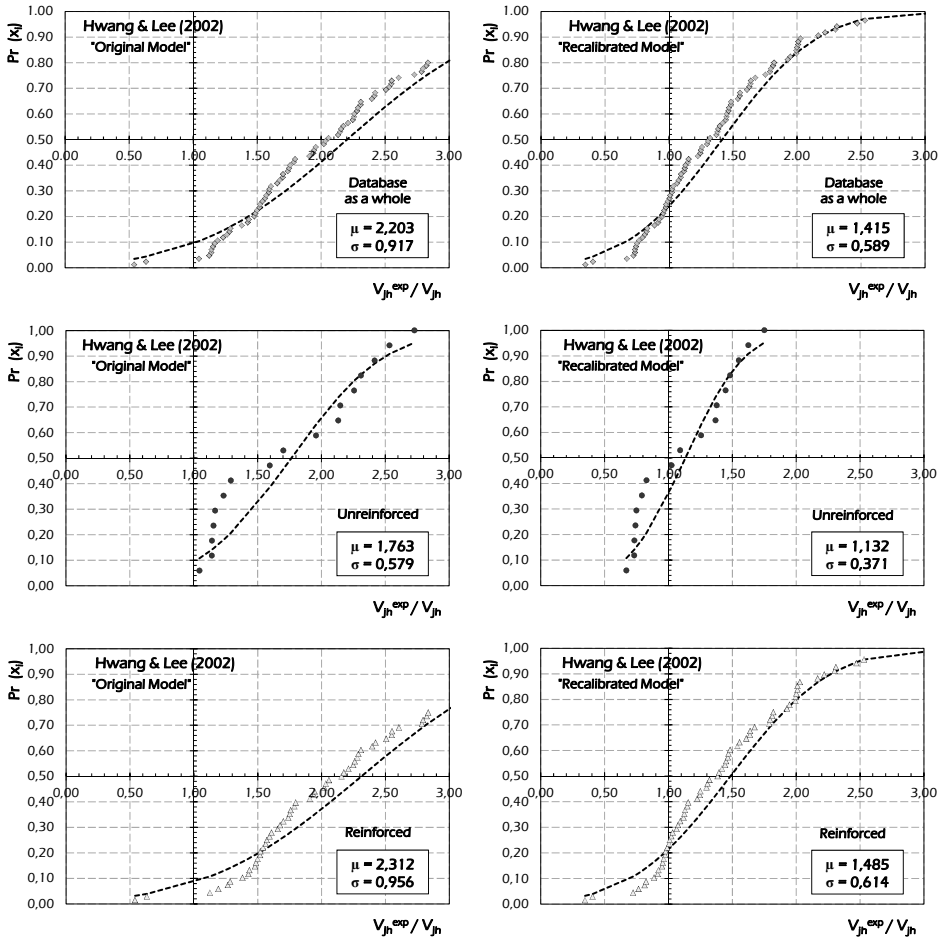

Fig. 6.87: Probabilistic Assessment of the original and recalibrated model by Hwang & Lee (2002) for interior joints.

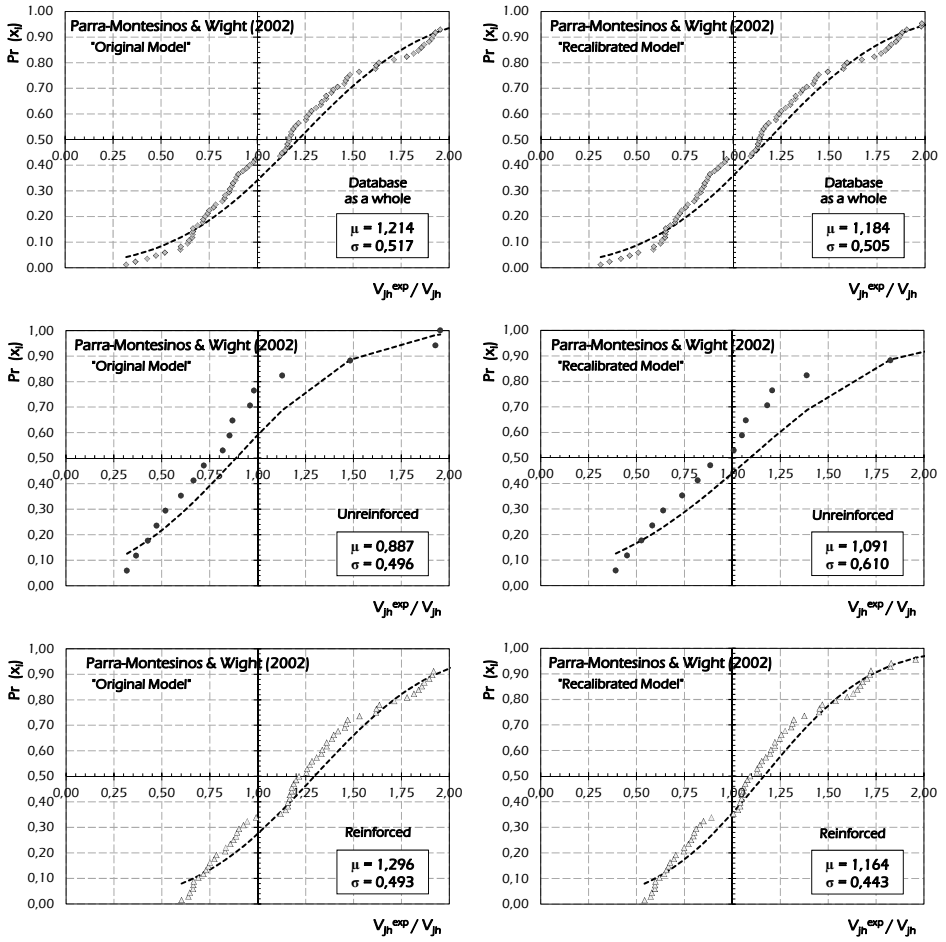

Fig. 6.88: Probabilistic Assessment of the original and recalibrated model by Parra-Montesinos & Wight (2002) for interior joints.

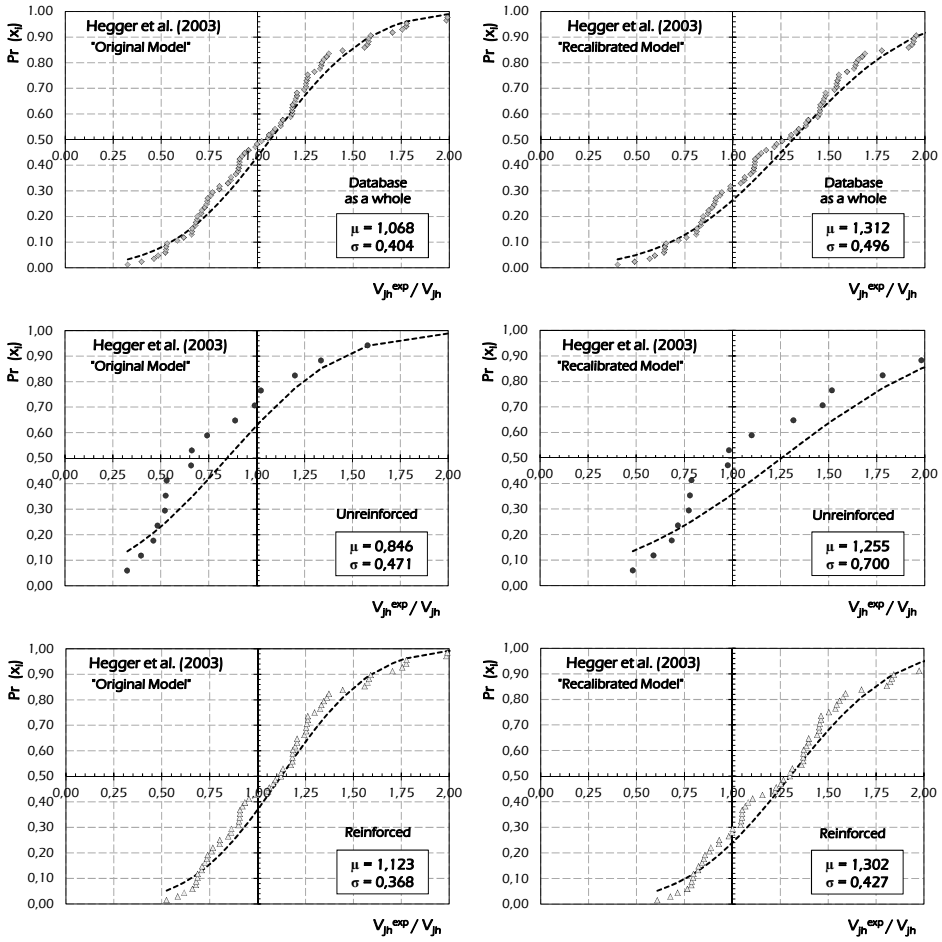

Fig. 6.89: Probabilistic Assessment of the original and recalibrated model by Hegger et al. (2003) for interior joints.

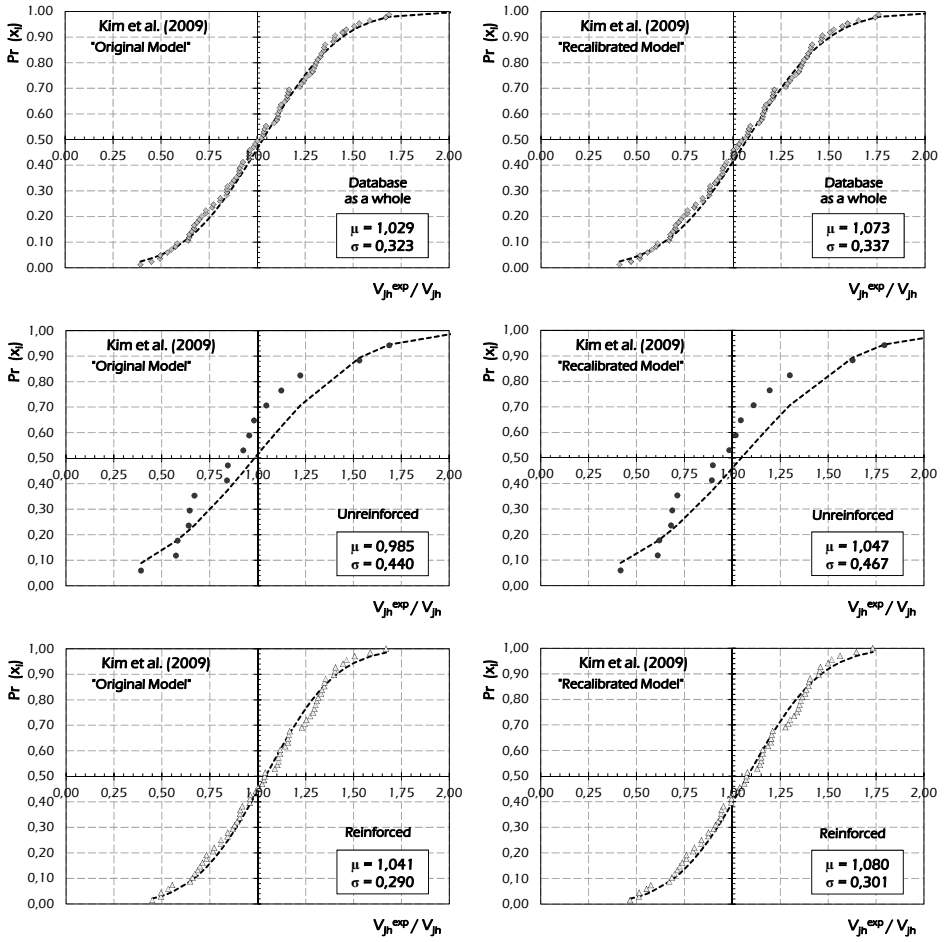

Fig. 6.90: Probabilistic Assessment of the original and recalibrated model by Kim et al. (2009) for interior joints.

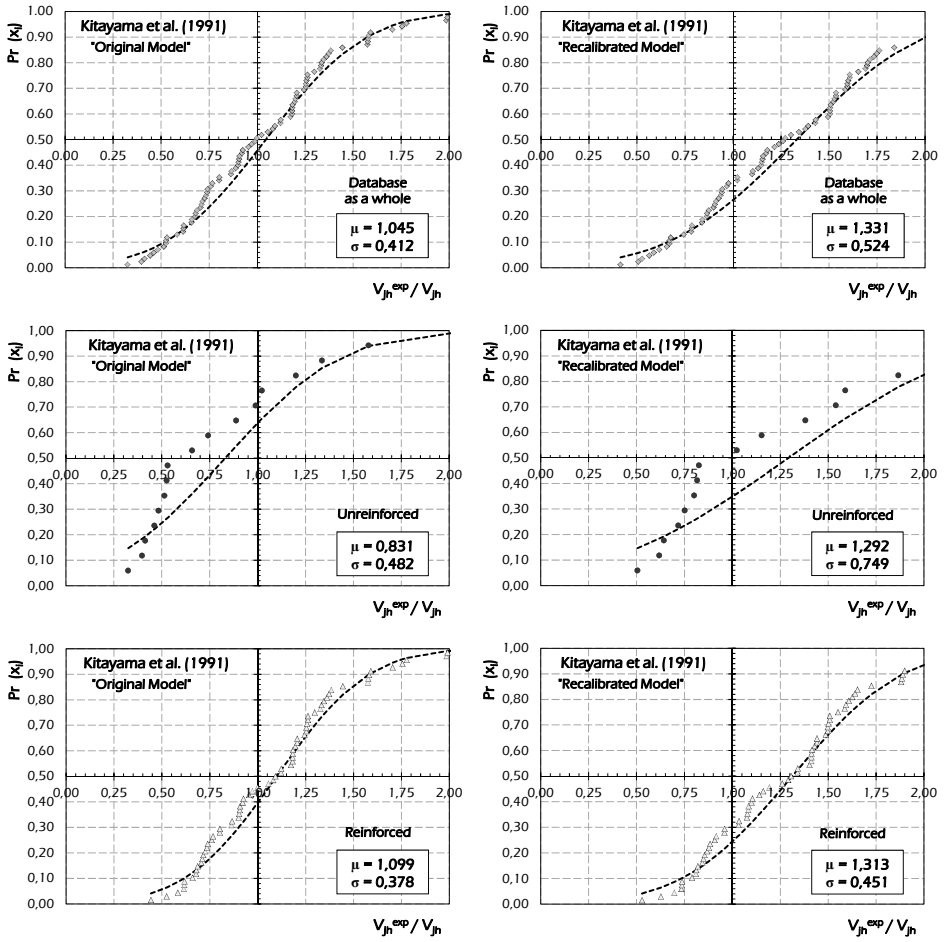

Fig. 6.91: Probabilistic Assessment of the original and recalibrated model by Kitayama et al. (1991) for interior joints.

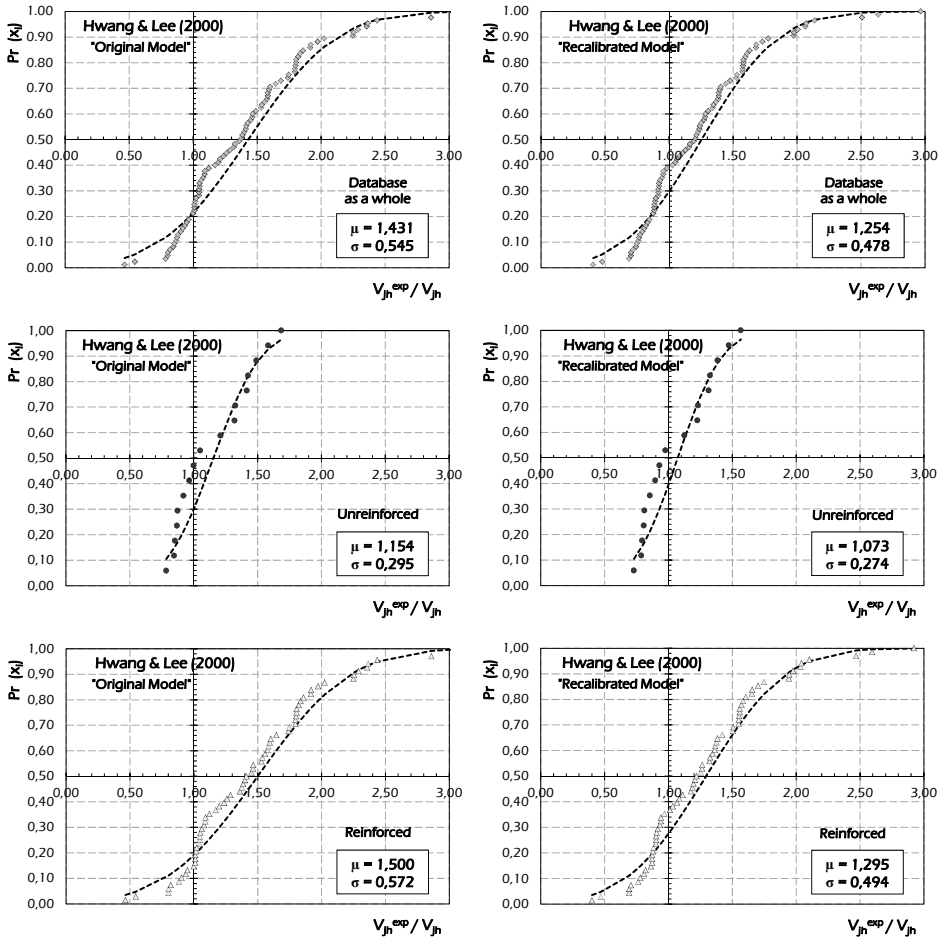

Fig. 6.92: Probabilistic Assessment of the original and recalibrated model by Hwang & Lee (2000) for interior joints.

6.3 The Proposed Formula for Exterior Joints

A model for evaluating the shear strength of exterior joints has been finally developed by using the collected experimental database and starting from the theoretical model by Vollum & Newman (1999). The model is suitable for exterior RC beam-to-column joints both reinforced and unreinforced. In this section, the procedure of estimation of the parameters affecting the proposed formulation is outlined. Model uncertainty is quantified for evaluating the performance of the developed joint shear strength by comparison with other models.

The basic concepts of the model by Vollum & Newman (1999) have been reported in section 2.4.5. Basically the model develops the shear strength V_{jh} of exterior joints as the sum of the two contributions of the concrete strut V_{ch} and of the stirrups into the panel zone V_{sh}:

$$V_{jh} = V_{ch} + V_{sh} \,. \tag{6.10}$$

The joint shear strength without stirrups V_{ch} is defined as follows:

$$V_{ch} = 0.642 \cdot \beta \cdot \left[1 + 0.555 \cdot \left(2 - {h_b}/{h_c}\right)\right] \cdot b_j \cdot h_c \cdot \sqrt{f_c} \tag{6.11}$$

where b_j is the effective joint width evaluated as follows:

$$\begin{aligned} b_j &= \min\left(\frac{b_c + b_b}{2}\,;\, b_b + \frac{h_c}{2}\right) \qquad \text{if } b_b \le b_c \,, \\ b_j &= \min\left(b_b\,;\, b_c + \frac{h_c}{2}\right) \qquad \text{if } b_b > b_c \,. \end{aligned} \tag{6.12}$$

and where β is 1.00 for connection with L bars and 0.90 for connections with U bars.

By analysing Eqn. (6.11), about unreinforced joints, the model does not take into account some important parameters for evaluating the shear strength of joints. In particular, the parametric analysis reported in section 4.4 showed that the following parameters are not taken into account by the model by Vollum & Newman (1999):

- the axial load in the top column;
- the amount of flexural reinforcement in beam;
- the amount of flexural reinforcement in column.

The proposed model, starting from the theoretical formulation of Vollum & Newman (1999) for unreinforced joints, is developed by recalibrating the

numerical coefficients already reported in Eqn. (6.11) and introducing the terms accounting the parameters listed above. In particular, Eqn. (6.11) can be rewritten as follows:

$$V_{ch} = A_1 \cdot \beta \cdot \left[1 + A_2 \cdot \left(2 - {h_b}/{h_c}\right)\right]^{\psi} \cdot b_j \cdot h_c \cdot f_c^{\zeta} \cdot \left(A_3 + \frac{N_c}{b_c \cdot h_c \cdot f_c}\right)^{\gamma_1} \cdot \cdot \left(\frac{A_{sb,\inf} + A_{sb,\sup}}{b_b \cdot h_b \cdot f_c} \cdot f_{yb}\right)^{\gamma_2} \cdot \left(\frac{A_{sc}}{b_c \cdot h_c \cdot f_c} \cdot f_{yc}\right)^{\gamma_3}, \quad (6.13)$$

being A_1, A_2, A_3, ψ, ζ, γ_1, γ_2 and γ_3 some numerical coefficients to improve by minimizing the Average Quadratic Error Δ of the developed model in respect of the collected database of exterior beam-to-column joints:

$$A_1, A_2, A_3, \psi, \zeta, \gamma_1, \gamma_2, \gamma_3 = = \underset{A_1, A_2, A_3, \psi, \zeta, \gamma_1, \gamma_2, \gamma_3}{\arg\min} \left\{ \sqrt{\frac{\sum_{i=1}^{n} \left[V_{jh}(A_1, A_2, A_3, \psi, \zeta, \gamma_1, \gamma_2, \gamma_3) - V_{jh}^{\exp}\right]^2}{n}} \right\}. \quad (6.14)$$

In addition, the following conditions have been imposed:

- the factor of dispersion β_C should be the minimum;
- the mean μ should be equal to 1.000;
- the standard deviation σ should be the minimum.

By performing the procedure the results reported in the following table have been obtained:

Table 6.5: Numerical coefficients and measures of error and dispersion of the basic formula

A_1	A_2	A_3	ψ	ζ	γ_1	γ_2	γ_3
0.446	0.311	0.563	0.854	1.043	1.211	0.653	0.124
Δ [kN]		**β**		**μ**		**σ**	
103.80		0.179		1.000		0.186	

With the aim of simplify the proposed formulation a procedure of reduction of the parameters has been performed by removing the variables less significative and updating the numerical coefficient. No significantly variation of mean, dispersion and average error should be observed.

By removing the amount of longitudinal reinforcement in column the results reported in Table 6.6 have been obtained.

Table 6.6: Numerical coefficients and measures of error and dispersion of the removal process

A_1	A_2	A_3	ψ	ζ	γ_1	γ_2	γ_3
0.491	0.199	0.570	0.802	1.017	1.185	0.755	-
Δ [kN]		β		μ		σ	
115.75		0.186		1.000		0.191	

The process of simplication continues by an approximation of the numerical coefficients; in particular, the following numbers are taken into account and the measures of error and dispersion reported in Table 6.7 have been obtained:

Table 6.7: Numerical coefficients and measures of error and dispersion of the simplified formula

A_1	A_2	A_3	ψ	ζ	γ_1	γ_2	γ_3
0.500	0.150	0.600	1.000	1.000	1.230	0.750	-
Δ [kN]		β		μ		σ	
115.22		0.186		1.006		0.192	

Therefore, Eqn. (6.13) can be converted into the following simple model that can be conveniently used in evaluating shear strength of exterior unreinforced joints:

$$V_{ch} = 0.50 \cdot \beta \cdot \left[1 + 0.15 \cdot \left(2 - {h_b}/{h_c}\right)\right] \cdot b_j \cdot h_c \cdot f_c \cdot \left(0.6 + \frac{N_c}{b_c \cdot h_c \cdot f_c}\right)^{1.23} \cdot \left(\frac{A_{sb,\inf} + A_{sb,\sup}}{b_b \cdot h_b \cdot f_c} \cdot f_{yb}\right)^{0.75} \quad (6.15)$$

By taking into account reinforced exterior joints, the contribution of horizontal stirrups in the panel zone should be considered [Eqn. (6.10)]. This last contribution is evaluated as follows:

$$V_{sh} = B_1 \cdot A_{sjh} \cdot f_{yj} \quad (6.16)$$

in which B_1 is a numerical parameter evaluated by minimizing the Average Quadratic Error Δ obtained by applying the developed model to the database

including only reinforced exterior joints. The minimizing procedure is performed by considering the following additional conditions:

- the factor of dispersion of the capacity β should be the minimum;
- the mean μ should be equal to 1.000;
- the standard deviation σ should be the minimum.

Table 6.8: Numerical coefficients and measures of error and dispersion of the contribution of the horizontal stirrups into the joint

B_1	Δ [kN]	β	μ	σ
0.24	131.96	0.261	1.002	0.272

Finally the proposed model for evaluating the shear strength of exterior beam-to-column joints is the following:

$$V_{jh} = 0.50 \cdot \beta \cdot \left[1 + 0.15 \cdot \left(2 - h_b / h_c\right)\right] \cdot b_j \cdot h_c \cdot f_c \cdot \left(0.6 + \frac{N_c}{b_c \cdot h_c \cdot f_c}\right)^{1.23} \cdot \left(\frac{A_{sb,\inf} + A_{sb,\sup}}{b_b \cdot h_b \cdot f_c} \cdot f_{yb}\right)^{0.75} + 0.24 \cdot A_{sjh} \cdot f_{yj} \tag{6.17}$$

in which the effective width b_j is evaluated according the model by Vollum & Newman (1999) through Eqn. (6.12).

6.3.1 Assessment of the Proposed Formula

The accuracy of the model developed is assessed in the present section by comparing the experimental values of shear strength V_{jh}^{exp} with the corresponding theoretical predictions V_{jh}. The assessment is first of all carried out in a qualitative way by analysing the equivalence charts between the experimental values V_{jh}^{exp} and the corresponding theoretical ones V_{jh}.

The analyses and validations presented in following are reported for exterior joints by specialising the results about the amount of reinforcement in the panel zone in unreinforced, under-reinforced and EC8-compliant exterior joints according to the classification made in section 1.4.

The qualitative results are provided through the so-called equivalence charts in which the experimental shear strength V_{jh}^{exp} is reported on the x-axis while the corresponding theoretical strength V_{jh} evaluated through the analysed capacity model is reported on the y-axis. The equivalence between the experimental evidence and the calculated strength results from the bisector

segment reported in every figure as reference. The model can be deemed as accurate as the bunch of points is close to that segment, being either conservative or non-conservative as the points tend to be manly below or above the same segment, respectively.

Four equivalence charts are made: the first one shows all the analysed specimens while the other ones show the assessment of unreinforced, under-reinforced and EC8-compliant exterior joints.

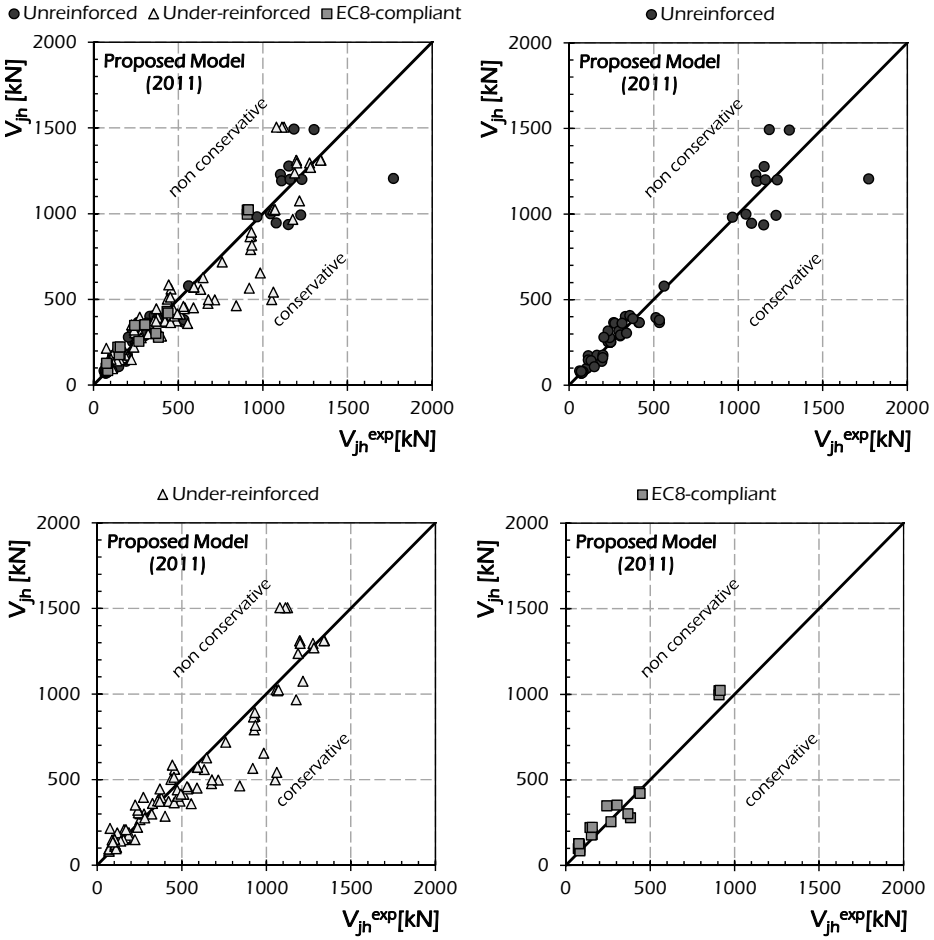

Fig. 6.93: Assessment of the proposed model for exterior joints.

Fig. 6.93 shows the equivalence charts developed by applying the proposed model. About all the specimens on exterior joints, good results are shown, being the bunch of points gathered around the bisector segment. A manly equivalent law is obtained.

Although, there is not difference between unreinforced, under-reinforced and EC8-compliant joints in the results obtained by applying the proposed model (Fig. 6.93).

The proposed model provides results being in good correlation with the experimental evidence; in fact:

- the points representing unreinforced joints gather around the bisector segment;
- the points representing under-reinforced specimens lie around the bisector segment providing a meanly equivalent law;
- the points representing EC8-compliant joints gather near the equivalence segment.

By considering under-reinforced joints, accurate results are obtained but five specimens provide values of the shear strength that the model does not reproduce with accuracy. The corresponding points are reported in a circle in Fig. 6.94.

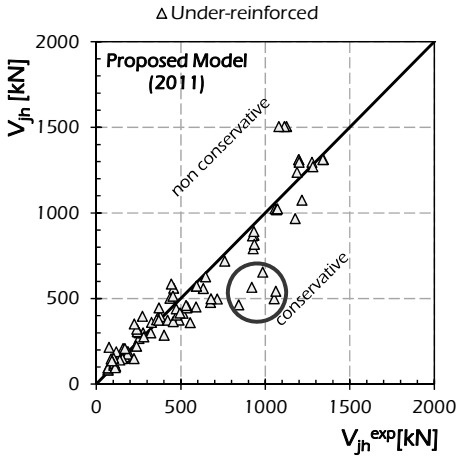

Fig. 6.94: *Assessment of the proposed model for under-reinforced joints.*

This particular condition can be explained by noticing that the joints that provide these particular results are characterized by mechanical anchorages of the longitudinal bars in the beam, defined headed bars. The utilised mechanical anchorages, shown in Fig. 6.95, develop a bond stress higher than the one

generally obtained by conventional details used in seismic design and so high shear strength is provided. For those joints a particular model should be developed accounting the higher strength provided by the headed bars.

Consequently, the model leads to over-conservative predictions in these cases.

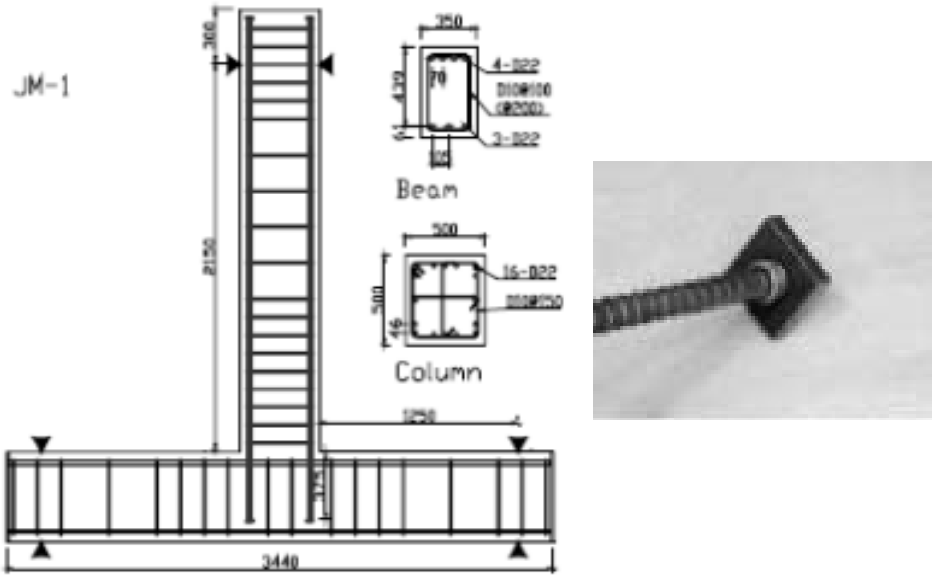

Fig. 6.95: Specimens with headed bars.

Further analyses are provided with the aim of assessing under the quantitative standpoint the accuracy of the model outlined above. The quantitative parameters describing the error and the dispersion are the *Average Quadratic Error* Δ [Eqn. (5.1)], the *Relative Average Quadratic Error* δ [Eqn. (5.2)], the *Coefficient of determination* R^2 [Eqn. (5.4)] and the reliability capacity factor β_C [Eqn. (5.16)].

Table 6.9 reports the measures of error and dispersion evaluated for the proposed model. Very good results are achieved about all the analysed specimens, in particular the model, compared with the capacity models available in the scientific literature and outlined in section 2, provides the lower average quadratic errors and the higher coefficient of determinations. However, very low values of the factor of dispersion β_C have been obtained

demonstrating the powerful of the proposed formulation in performing reliability analyses.

Table 6.9: Measures of error and factor of dispersion of the proposed formulation for exterior joints.

Total				Unreinforced				Under-reinforced				EC8-compliant			
Δ [kN]	δ	R^2	β_C	Δ [kN]	δ	R^2	β_C	Δ [kN]	δ	R^2	β_C	Δ [kN]	δ	R^2	β_C
126.88	0.271	0.899	**0.239**	115.22	0.189	0.927	**0.186**	143.11	0.299	0.871	**0.263**	61.31	0.314	0.970	**0.215**

Finally, Fig. 6.96 shows the probabilistic assessment of the model.

The proposed model develops a meanly equivalent law for all the considered specimens on exterior joints, for unreinforced and non-compliant joints, while a little unconservative trend is observed in the case of compliant joints resulting the mean μ smaller than 1.000. Low values of the standard deviation σ are obtained in all the analysed cases.

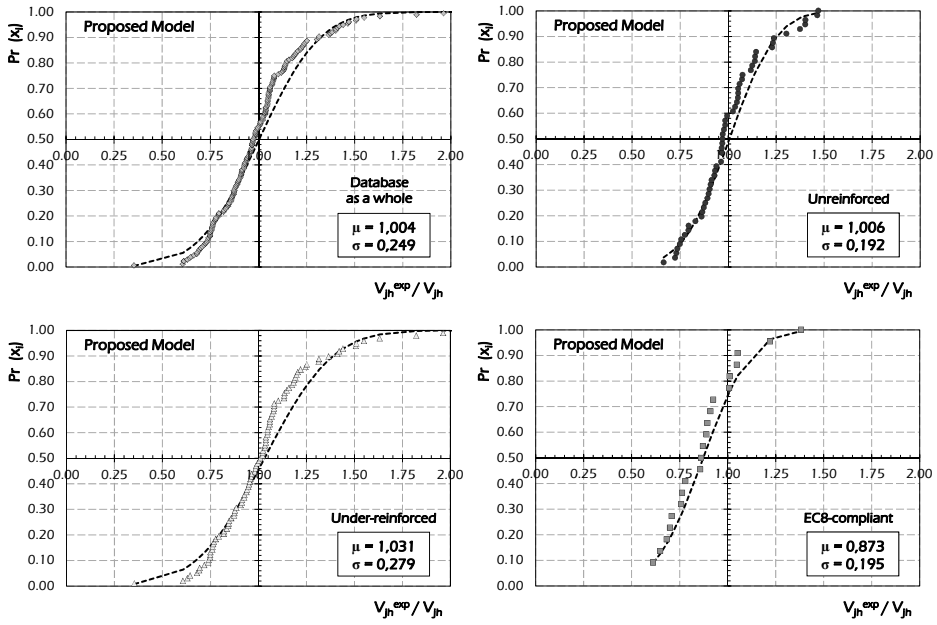

Fig. 6.96: Probabilistic Assessment of the proposed model.

CHAPTER VII

7. Monotonic and Cyclic Strength

Several theoretical models for evaluating the shear strength of exterior and interior beam-to-column joints under monotonically loads have been outlined In the previous sections. An important development in the study of beam-to-column joints is to provide shear strength of these elements under cyclic loads.

In this chapter, starting from the monotonic shear strength, a formulation for evaluating the capacity under cyclic loads is developed; this formulation allows to take into account the strength degradation of joints under seismic actions.

7.1 Specimens Under Cyclic Loads

Most of the specimens collected in the database outlined in section 4 have been tested under cyclic loading; these tests were made in force or displacement control or, in some cases, a combination of these two types, with a first step in force control and displacement control to the next.

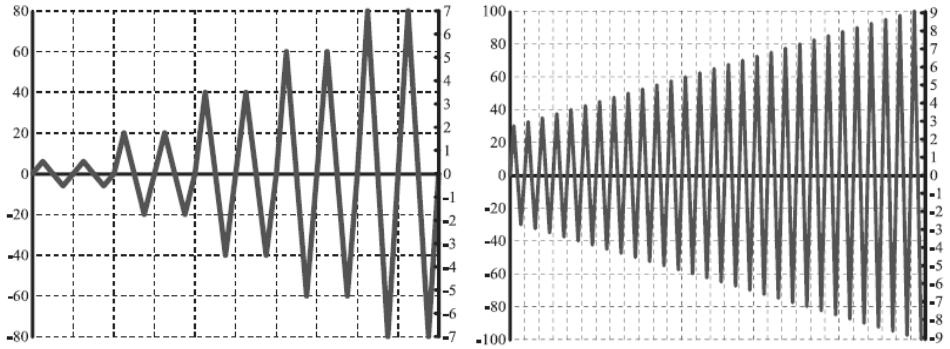

Fig. 7.1: Load histories with 2 constant cycles (left) and variable amplitude (right).

The applied load histories consist of several steps (Fig. 7.1), each of which consists of one or more cycles of full charging with constant intensity or drift. At each step the intensity is changed until the failure of the subassemblages is achieved.

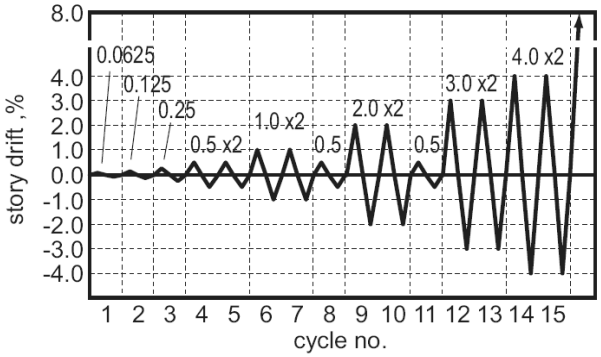

Fig. 7.2: Example of complex load histories.

Complex load histories can be adopted by considering step-by-step increasing of intensity interrupted by one cycle at low intensity (Fig. 7.2). A particular load history consists in a first part of increasing action in force control and a second part in displacement control to complete the failure of the joint (Fig. 7.3).

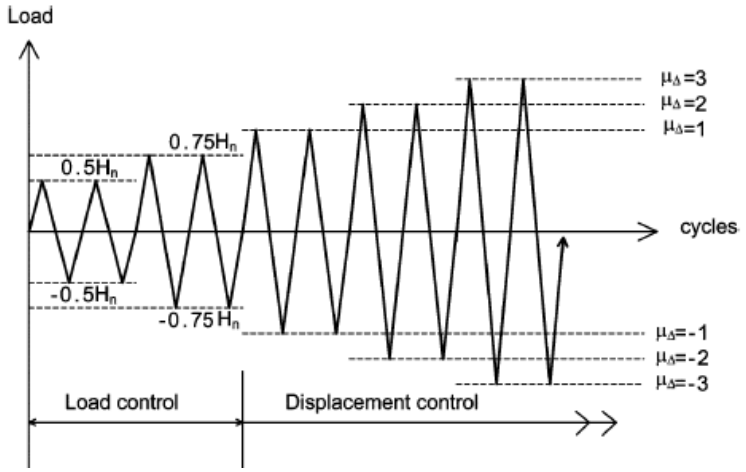

Fig. 7.3: Example of load histories with initial steps in force control and then in displacement control.

With the aim of providing shear strength of beam-to-column joints under cyclic loads, the shear force of cyclic tests is identified for several specimens collected in the database. For specimens tested in displacement control the failure has been considered achieved when the shear force is smaller than 20% of its maximum value.

7.2 Low Cycle Fatigue

Based on the Theory of low cycle fatigue (Miner, 1945), the following equation is assumed for evaluating the shear strength beam-to-column joints:

$$\log(V) = \log(V_{mon}) - \frac{1}{m}\log(N) \tag{7.1}$$

where V_{mon} is the shear strength under monotonic loads, N is the number of cycles with constant intensity V which provide the failure of the joint and m is a parameter accounting the cumulate damage of the joint under cyclic actions. At each intensity of V_i corresponds a number of cycles N_i that provide the joint failure; by increasing the shear V_i the number of cycles N_i needed for achieving joint failure decreases (Fig. 7.4).

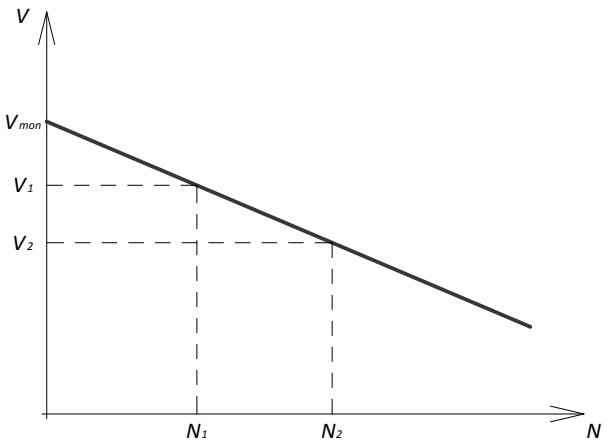

Fig. 7.4: Relationship between shear strength and number of cycles needed for acting joint failure.

According to the hypothesis of Palmgreen-Miner (Miner, 1945 and Palmgreen, 1924), the damage provided by a history of cyclic loading of

constant intensity V_i is proportional to the number of cycles. A number of cycles n_i smaller than N_i, with intensity V_i will make damage equal to:

$$D_i = \frac{n_i}{N_i}. \tag{7.2}$$

By accounting specimens with k steps of load with variable intensity, the joint failure is achieved when:

$$D_1 + D_2 + ... + D_{k-1} + D_k = 1, \tag{7.3}$$

and then, substituting Eqn. (7.2) in Eqn. (7.3):

$$\sum_{j=1}^{k} \frac{n_j}{N_j} = 1. \tag{7.4}$$

The term N_j depended by V_j represents the number of cycles with constant intensity which provides the joint failure, so Eqn. (7.4) can be rewritten as follows by considering the condition of failure:

$$\sum_{j=1}^{k} \frac{n_j}{N\left(V_j\right)} = 1. \tag{7.5}$$

The number of cycles N_j needed for providing the failure under a constant shear V_j can be evaluated from Eqn. (7.1) as follows:

$$\log\left(\frac{V_j}{V_{mon}}\right) = \log\left(N_j^{-\frac{1}{m}}\right), \tag{7.6}$$

$$\frac{V_j}{V_{mon}} = N_j^{-\frac{1}{m}}, \tag{7.7}$$

$$N_j = \left(\frac{V_j}{V_{mon}}\right)^{-m}, \tag{7.8}$$

By substituting Eqn. (7.8) in Eqn. (7.5):

$$\sum_{j=1}^{k} \frac{n_j}{\left(\frac{V_j}{V_{mon}}\right)^{-m}} = 1 \tag{7.9}$$

where k is the number of steps in the load history that provides the failure of the specimen, V_j is the shear force corresponding to the j-th step, n_j is the number of cycles at constant shear force of the j-th step.

In Eqn. (7.9) there are two unknown terms:

- the parameter m;
- the shear strength under monotonic loads V_{mon}.

For obtaining an exact estimation of m, tests in which two identical specimens are tested under both monotonic and cyclic loads are needed; this condition is not achieved for any tests in the selected database, so an estimation of the monotonic shear strength is required for deriving the fatigue curve.

By considering the models outlined and assessed in previous sections the model by Kim et al. (2009) results the most accurate; consequently, the monotonic shear strength of beam-to-column joints will be evaluated according this last model recalibrated by applying the factor α evaluated for all the considered specimens and reported in section 6 for the model by Kim et al. (2009).

7.3 Fatigue Curves

The behaviour of beam-to-column joints under cyclic loading is highly influenced by some seismic details, such as the amount of shear reinforcement and the anchorage of rebars in beam. By considering the huge number of specimens collected in the database it is possible to evaluate different fatigue curves, and so different parameter m, associated to different types of joints.

In the following the analysis will be performed by considering interior and exterior joints; a further classification is made between unreinforced and reinforced elements.

The experimental tests providing information about the load history have been selected in the database outlined in section 4, while those ones providing contradictory or unclear (negative values of m or higher values) results have been neglected. For each specimen the damage parameter m_j has been evaluated, while for each group of joints the mean value m and the standard deviation σ has been provided.

7.3.1 Interior Joints

As an example, Table 7.1 reports the geometric and mechanical characteristics of the cyclic test performed by Durrani & Wight (1982) with the parameter *m* derived by applying the procedure listed above.

Table 7.1: Geometric and mechanical characteristics and parameters of the cyclic behaviour of the specimen X1 provided by Durrani & Wight (1982)

X1			
$L_{col,sup}$ [mm]	1123.95		
$L_{col,inf}$ [mm]	1123.95		
L_b [mm]	1248		
h_{col} [mm]	362		
h_b [mm]	419.1		
A_{sb} [mm^2]	1551		
A_{sbinf} [mm^2]	1139		
λ	1.67		
f_{yb} [Mpa]	330.7		
Horizz. reinfor.	stirrups		
Anchorage			
V_{jh}^{th} [kN]	791.71		
$V_{jh,mon}^{th}$ [kN]	1078.74		
m	***20.58***		
			Σ
δ [mm]	**V_{col} [kN]**	**V_{jh} [kN]**	**1.00**
6.35	40.05	212.67	
-5.08	-40.05	-212.67	3.066E-15
40.64	186.9	992.47	
-38.1	-186.9	-992.47	1.799E-01
50.8	191.35	1016.10	
-50.8	-191.35	-1016.10	2.920E-01
63.5	191.35	1016.10	
-63.5	-191.35	-1016.10	2.920E-01
83.82	186.9	992.47	
-83.82	-186.9	-992.47	1.799E-01
104.14	173.55	921.58	
-101.6	-178	-945.21	5.087E-02
119.38	160.2	850.69	
-119.38	-155.75	-827.06	5.652E-03
134.62	142.4	756.17	
-137.16	-133.5	-708.91	3.473E-04

The value of the displacement δ at the top of column is derived from the graph reporting the load-displacement relationship of the specimen considered, or is derived from the load history in the case of tests performed in displacement control. V_{col} represents the load applied to the top of the column by the actuator, and taken positive and negative, to simulate the cyclic action of the earthquake; finally, V_{jh} is the shear force acting the joint and evaluated by equilibrium as outlined in section 4.3 for interior joints.

The parameter of cumulated damage m of each test is evaluated by imposing the sum of the values reported in the last column of Table 7.1 equal to 1.00. The amounts in the last column are expressed as follows:

$$\frac{n_j}{\left(\frac{V_j}{V_{mon}}\right)^{-m}}, \tag{7.10}$$

by considering each step of constant load, in particular n_j is equal to 1.00 if the load changes at each step.

The following figure shows the fatigue curves derived for interior unreinforced joints; in grey are reported the curves about each individual specimen, the red line shows the average curve and the dashed red line shows the relationship relative to the mean m reduced by the standard deviation σ. The continuous curves have been constructed by designing the following function:

$$\frac{V}{V_{mon}} = N^{-\frac{1}{m}}, \tag{7.11}$$

while the dashed curve has been drawn by representing the equation:

$$\frac{V}{V_{mon}} = N^{-\frac{1}{m-\sigma}}. \tag{7.12}$$

Table 7.2 reports the value of the parameter m derived for the selected specimens on unreinforced interior joints.

Table 7.2: Values of m for specimens on unreinforced interior joints.

TEST	Hakuto et al. (2000)	Li et al. (2002)		Pampanin et al. (2002)
Specimen	O1	A1	A2	C2
m	4.49	3.28	6.22	5.50

Fig. 7.5 shows the fatigue curves derived for unreinforced interior joints.

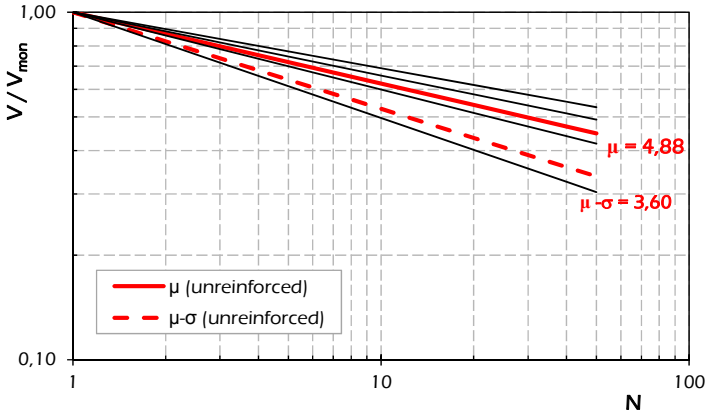

Fig. 7.5: Fatigue curves for interior unreinforced joints

The values of the mean parameter *m* and of the mean parameter reduced by the standard deviation *m* - σ of unreinforced interior joints are:

$$m = 4.88 \quad ; \quad m - \sigma = 3.60.$$

Fig. 7.6 shows the fatigue curves for reinforced interior joints; in particular the grey line are representative of the single analysed specimens, while green continuous and dashed curves reports the mean and the mean reduced by the standard deviation relationships, respectively.

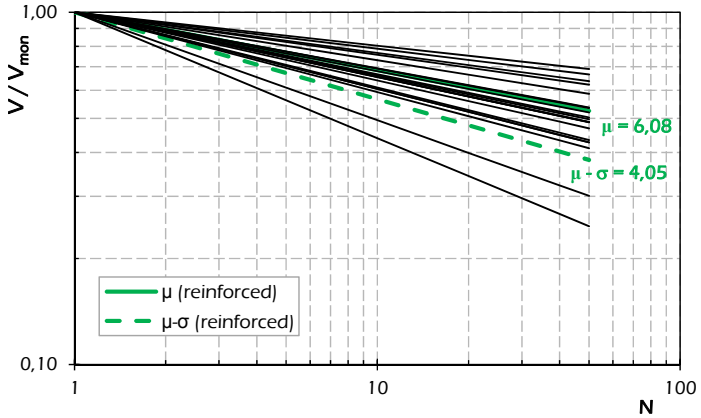

Fig. 7.6: Fatigue curves for interior reinforced joints.

The values of the mean parameter m and of the mean parameter reduced by the standard deviation $m - \sigma$ of reinforced interior joints are:

$$m = 6.08 \quad ; \quad m - \sigma = 4.05.$$

In Table 7.3 are reported the numerical values of m for each specimen on reinforced interior joints.

Table 7.3: Values of m for specimens on reinforced interior joints.

TEST	Durrani & Wight (1982)	Kitayama et al. (1991)	Kusuhara et al. (2004)		
Specimen	X3	J1	JE-0	JE-55	JE-55S
m	10.52	4.40	5.59	6.25	5.97
TEST	Lee et al. (2009)				
Specimen	J1	BJ1	BJ2	BJ3	B1
m	5.16	5.45	5.43	7.34	8.26
TEST	Leon (1990)	Li et al. (2002)		Shin & LaFave (2004)	
Specimen	BCJ3	M1	M2	1	2
m	8.67	2.80	3.26	5.45	5.69
TEST	Shiohara et al. (2000)	Takaine et al. (2008)	Teng & Zhou (2003)		
Specimen	S3	JH1	S1 (Series 1)	S6(Series 2)	
m	4.69	4.60	6.28	9.62	

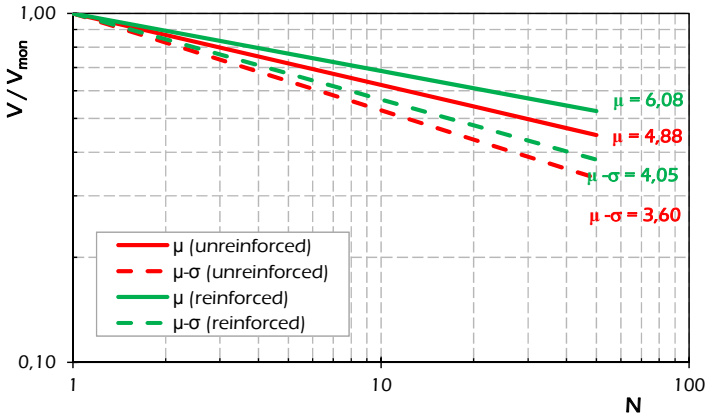

Fig. 7.7: Comparison of the fatigue curves for interior reinforced and unreinforced joints.

In Fig. 7.7 shows the mean fatigue curves of both unreinforced and reinforced interior joints. The unreinforced beam-to-column joints develop degradation higher than the one observed in the cases of reinforced specimens being the red curve located below the green one. The dispersion is almost equivalent between unreinforced and reinforced joints resulting the two dashed line spaced of the same gap observed for the mean curves.

Table 7.4 reports the numerical values of the ratio V / V_{mon} corresponding to the mean μ and the mean reduced by the standard deviation μ - σ curves for both unreinforced and reinforced interior joints when the number of cycles ranges between 1 and 50.

Table 7.4: Mean fatigue curves for interior joints.

N_i	$V(m)/V_{mon}$			
	Unreinforced		Reinforced	
	μ	$\mu - \sigma$	μ	$\mu - \sigma$
1	1.000	1.000	1.000	1.000
10	0.624	0.527	0.685	0.567
20	0.541	0.435	0.611	0.478
40	0.469	0.359	0.545	0.403
50	0.448	0.337	0.525	0.381

The comparison reported in Fig. 7.7 between unreinforced and reinforced interior joints shows values of the shear strength of unreinforced joints smaller than the one achieved for reinforced interior connections. The comparison shows a limited difference between the two cases demonstrating that for interior joints the confinement action provided by beam is a beneficial effect and makes the presence of horizontal reinforcement into the panel zone less important.

7.3.2 Exterior Joints

As an example, Table 7.5 reports the geometric and mechanical properties of the cyclic test performed by Chalioris et al. (2008) with the parameter *m* derived by applying the procedure listed in the previous subsection.

Regarding the values shown in Table 7.5 the same considerations made in section 7.3.1 about interior joints can be drawn out.

Table 7.5: Geometric and mechanical characteristics and parameters of the cyclic behaviour of the specimen JB-s1 provided by Chalioris et al. (2008)

Specimen JB-s1			
L_{col} [mm]	750		
L_b [mm]	1150		
h_{col} [mm]	300		
h_b [mm]	300		
Horizz. reinforc.	stirrups		
Anchorage	L - in		
V_{jh} [kN]	275.34		
$V_{jh,mon}$ [kN]	318.56		
m	***4.061***		
			Σ
δ [mm]	**V_b [kN]**	**V_{jh} [kN]**	**1.00**
6	32	119.78	
-6	-32	-119.78	0.019
6	27	101.06	
-6	-25	-93.58	0.008
20	58	217.10	
-20	-59	-220.85	0.218
20	54	202.13	
-20	-56	-209.62	0.170
40	63	235.82	
-40	-61	-228.33	0.276
40	58	217.10	
-40	-47	-175.93	0.141
60	58	217.10	
-60	-48	-179.67	0.146
60	37	138.50	
-60	-30	-112.29	0.023

The following figures show the fatigue curves evaluated for exterior beam-to-column joints. Similar to the previous paragraph in grey are shown the curves on each individual specimen, in continuous red and green lines are reported the average curve and in dashed red and green lines are shown the curves about the value of the average parameter *m* reduced by the standard deviation σ.

Table 7.6 shows the values of the parameters m relating to the tests conducted on exterior unreinforced joints.

Table 7.6: Values of *m* for specimens on unreinforced exterior joints.

TEST	Karayannis et al. (2008)	Karayannis & Sirkelis (2008)	
Specimen	A0	A1	A2
m	5.320	3.302	2.927

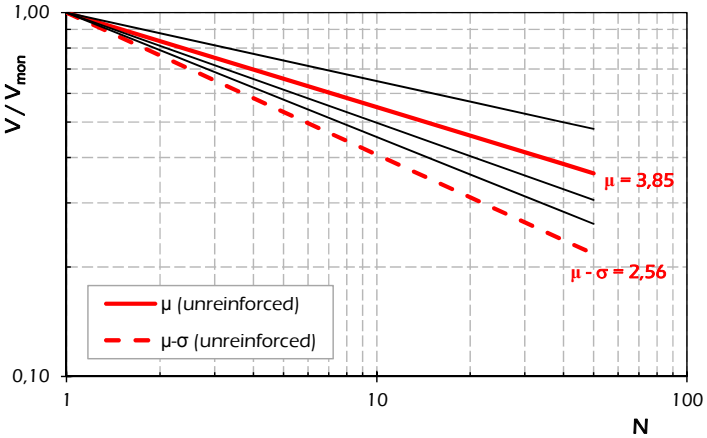

Fig. 7.8: Fatigue curves for exterior unreinforced joints.

Fig. 7.8 shows the fatigue curves of unreinforced exterior joints. The values of the mean parameter *m* and of the mean reduced by the standard deviation *m* - σ of unreinforced exterior joints are:

$$m = 3.85 \quad ; \quad m - \sigma = 2.56.$$

Table 7.7: Values of *m* for specimens on reinforced exterior joints.

TEST	Bindhu & Jaya (2008)				Chalioris et al. (2008)
Specimen	A1	A2	B1	B2	JB-s1
m	2.144	2.144	2.144	2.000	4.061
TEST	**Chun & Kim (2004)**		**Ehsani & Alameddine (1991)**		
Specimen	JC - 2	JM - 2	LL11	HL11	HH14
m	5.693	5.826	5.679	5.376	6.840
TEST	**Ehsani et al. (1987)**			**Ehsani & Wight (1985[a])**	
Specimen	1	2	3	1B	2B
m	8.691	9.699	8.206	5.478	8.169

Table 7.7: Values of *m* for specimens on reinforced exterior joints.

TEST	Ehsani & Wight (1985[b])			Hakuto et al. (2000)	Karayannis et al. (2008)
Specimen	3B	5B	6B	O7	A1
m	9.096	4.021	3.370	1.990	10.433
TEST	**Karayannis et al. (2008)**	**Lee & Ko (2007)**			**Tsonos (2007)**
Specimen	B1	W0	W75	W150	G1
m	4.051	12.634	13.594	10.406	8.023
TEST	**Tsonos et al. (1992)**			**Wong & Kuang (2008)**	
Specimen	S2	S6		BS-L-H1	
m	5.486	7.394		12.127	

Table 7.7 shows the values of the parameter m relating to the tests conducted on exterior reinforced joints, while in Fig. 7.9 are reported the corresponding chart.

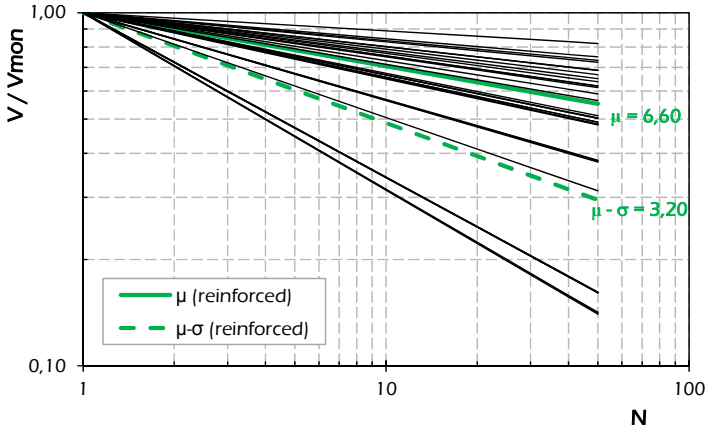

Fig. 7.9: Fatigue curves for exterior reinforced joints.

The values of the mean parameter *m* and of the mean reduced by the standard deviation *m* - σ of reinforced exterior joints are:

$$m = 6.60 \quad ; \quad m - \sigma = 3.20.$$

Table 7.8 shows the values V / V_{mon} corresponding to the average fatigue curves of exterior joints (both unreinforced and reinforced).

Table 7.8: Mean fatigue curves for exterior joints.

N_i	$V(m)/V_{mon}$			
	Unreinforced		Reinforced	
	m	m - σ	m	m - σ
1	1.000	1.000	1.000	1.000
10	0.550	0.407	0.705	0.487
20	0.459	0.311	0.635	0.392
40	0.383	0.237	0.572	0.316
50	0.362	0.217	0.553	0.295

Fig. 7.10 shows the average fatigue curves for both unreinforced and reinforced exterior joints.

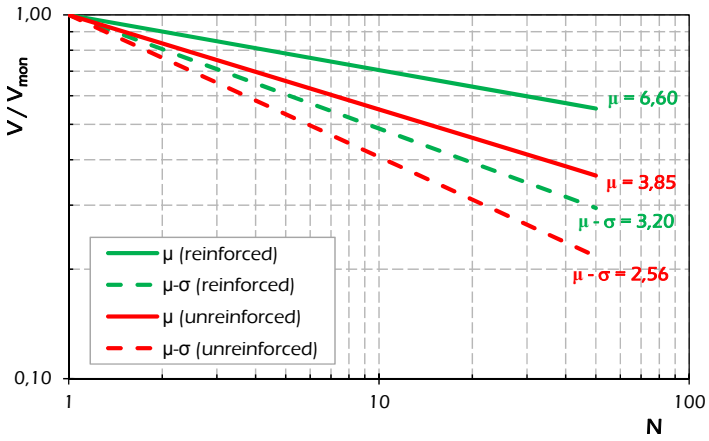

Fig. 7.10: Comparison of the fatigue curves for exterior reinforced and unreinforced joints.

With reference to exterior joints, as expected, the absence of horizontal reinforcement in the panel zone leads to a faster reduction in shear strength under cyclic actions. Unlike what happens for the behaviour of interior joints in this case the gap between the two curves is more marked, this result would comfort about the hypothesis on the beneficial effect of confinement on the shear strength by considering that in exterior joints where there are not lateral beam this effect is guaranteed by only the stirrups.

CHAPTER VIII

8. Modelling Joints in Nonlinear Structural Analyses

Several researches attempt to simulate the behaviour of RC frames by including the actual response of beam-to-column joints. Due to the inherent complex behaviour of RC beam-to-column joints, rotational spring elements have been used to simply represent the shear deformation of the joint panel combined with the rotation due to bar slip.

In the following, the main analytical models available in the scientific literature are outlined. A model that can be successfully and easily implemented in nonlinear static and dynamic analyses of existing multi-storey RC structures for investigating the influence of the finite stiffness and strength of joints is calibrated and purpose as behavioural. The validity and accuracy of the proposed joint element model are demonstrated through a comparison against experimental results of RC exterior beam-to-column joints under cycling loads reported in literature.

8.1 Overview of Joints Models

Over the last four decades, several experimental studies have been carried out and many analytical models have been proposed for modelling the seismic response of RC beam-to-column joints in frame simulation. The inelastic behaviour of joints combined with the effects due to bar slip is often represented by an inelastic rotational spring elements.

Fig. 8.1 shows samples reviews of the models frequently used for simulating beam-to-column joints n frame analyses of reinforced concrete and steel structures. Celik & Ellingwood (2008) and Park & Mosalam (2009) summarised some of them.

Alath & Kunnath (1995) [Fig. 8.1(a)] introduced a model where the relative rotational deformation between the beam and the column is controlled by a zero-length rotational spring and a rigid link to represent joint panel geometry, including joint shear-strain relationship and hysterical degradation evaluated through experimental studies.

Biddah and Ghobarah (1999) [Fig. 8.1(b)] proposed a similar zero-length element considering separately joint shear and bond slip deformations; in particular, for interior joints two rotational spring for bond-slip effects and one spring for joint shear deformation are used. In an exterior joint, one rotational spring for bond-slip deformation and the other one for joint shear deformation are considered. The shear stress-strain relationship of a joint is defined as a trilinear idealization based on the softening truss model (Hsu, 1988). The cyclic behaviour includes hysteretic degradation without pinching effect. The bond-slip relationship was idealized with a bilinear model and cyclic pinching effect.

Youssef & Ghobarah (2001) [Fig. 8.1(c)] provided a frame model of the beam-to-column joint using twelve translational springs to simulate inelastic behaviours due to bond slip and concrete crushing, and two elastic diagonal springs to simulate joint shear deformation.

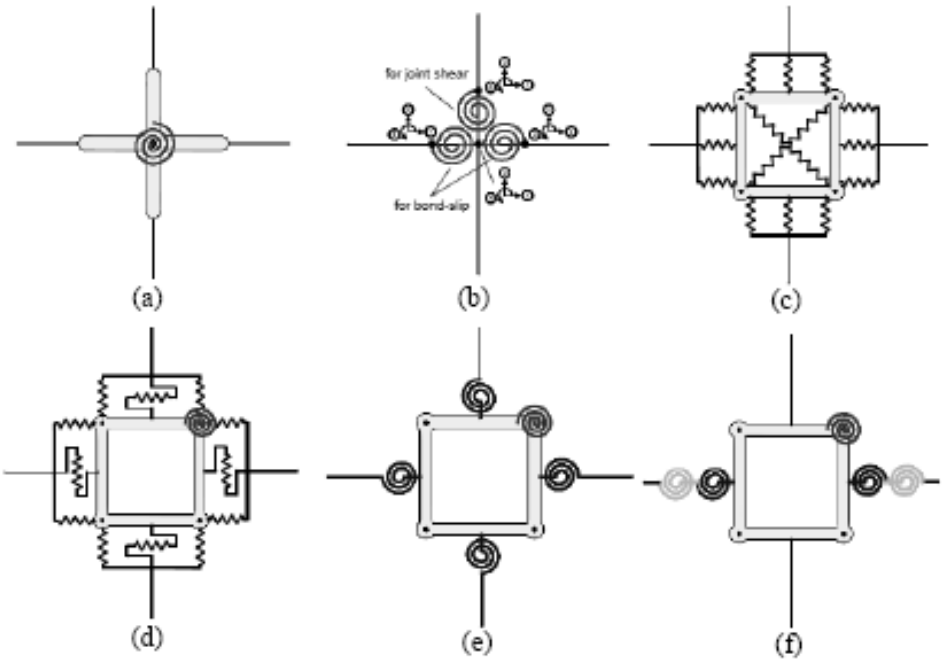

Fig. 8.1: Existing simulation models for beam-column joints (Celik & Ellingwood, 2008).

Lowes & Altoontash (2003) and Mitra & Lowes (2007) [Fig. 8.1(d)] developed a frame model using twelve translation springs, similar to the one proposed by Youssef & Ghobarah (2001), in which a rotational spring replaces the two diagonal springs for simulating joint shear distortion. Lowes & Altoontash (2003) model uses the modified compression field theory (MCFT) developed by Vecchio & Collins (1986) for deriving the constitutive relationship of the joint panel, while the model by Mitra & Lowes (2007) derives empirically diagonal concrete strut strength by accounting the confinement effect of transverse hoops according to Mander et al. (1988).

A simplification of the model by Lowes & Altoontash (2003) was proposed by Altoontash & Deierlein (2003) [Fig. 8.1(e)] in which four rotational springs replace the twelve translational ones.

Finally, Shin & LaFave (2004) [Fig. 8.1(f)] assembled four rigid frames for representing the joint panel and one rotational spring located on one of four hinges; other two rotational springs are located in series between the beam and the joint for simulating bond-slip and inelastic rotation.

Multi-springs models (namely Frame Models) are intended to simulate more realistic behaviour of beam-column joints but need significant calibration per each spring based on test data. Even though the springs are calibrated from test data, they do not ensure the accuracy of the analysis for other test results. Frame Models have also a high possibility of causing numerical divergence during frame analysis. Thus, a single rotational spring with a rigid panel to represent the joint geometry (namely Scissor Models) is adopted by Celik & Elingwood (2008), Theiss (2005), and Pampanin et al. (2003). Hertanto (2005) used the same concept but split the single spring into two springs with identical properties. In the Scissor Models only a nonlinear moment-rotation relationship is needed and frame analyses result faster and more stable than frame analyses performed using multi-spring models for joints.

8.1.1 The Model by Biddha & Ghobarah (1999)

According to Biddha & Ghobarah (1999) the joint is represented by two rotational springs in series, one representing the joint shear deformation and the other representing the reinforcing bars bond-slip. The two springs are only influenced by the relative rotational displacement between the nodes as shown in Fig. 8.2 and Fig. 8.3.

The numbers on the figures represent the degrees of freedom of the model. The moment transmitted by the elements is the moment transferred from the beams to the column. The deformation of the element represents either the

shear deformation of the joint (the change in the angle between the connected beams and columns) or the additional joint rotation due to bond-slip of the longitudinal bars of the beam. In this element, translational displacements of the nodes at both ends of the element are constrained to be identical. The nodal coordinates were also taken to be identical to satisfy equilibrium.

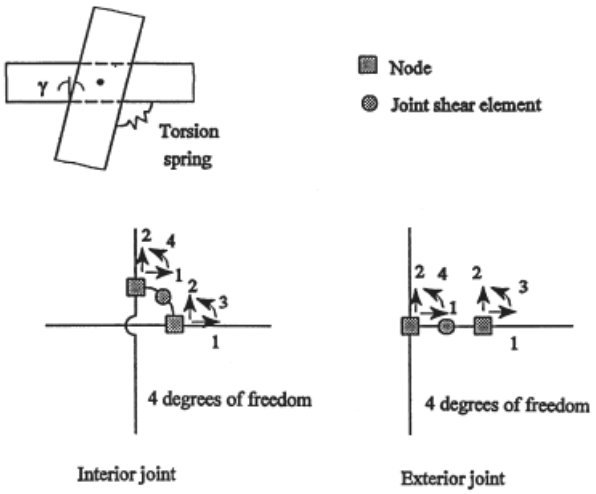

Fig. 8.2: Idealization of the joint shear elements for Biddha & Ghobarah (1999).

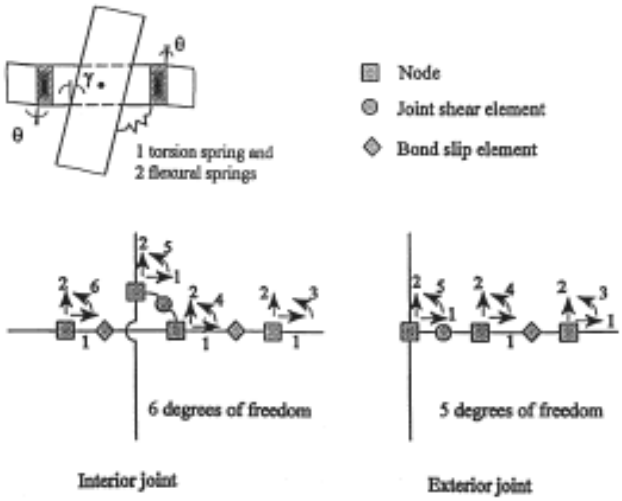

Fig. 8.3: Joint shear and bond-slip elements (Biddha & Ghobarah, 1999).

The joint shear deformation is modelled through a mechanical model using the softened truss model theory (Hsu, 1988) to satisfy both equilibrium of stress resultants and compatibility of deformations within the joint taking in account the constitutive laws of concrete and reinforcement.

The equations used in the softened truss model theory are:

- equilibrium equations assuming steel bars to resist only axial stresses;
- compatibility equations of Collins (1978) to determine the angle of inclination of the concrete struts;
- constitutive laws of materials.

The nonlinear stress-strain relationship for concrete represents the softening of concrete in compression caused by cracking due to the tension in the perpendicular direction (Vecchio & Collins, 1986).

The average principal tensile stress in concrete f_{c1} is related to the principal tensile strain ε_1. Before the cracking, f_{c1} is given by the following expression:

$$f_{c1} = E_c \cdot \varepsilon_1 \,. \tag{8.1}$$

After cracking, f_{c1} is given by:

$$f_{c1} = \frac{\alpha_1 \alpha_2 f_{cr}}{1 + \sqrt{500 \cdot \varepsilon_1}} \tag{8.2}$$

where

$$f_{cr} = 0.33\sqrt{f_c} \quad [MPa] \tag{8.3}$$

in which α_1 and α_2 are factors accounting for the bond characteristics of reinforcement and the type of loading. The value of α_1 is 1.0 for deformed reinforcement bars, 0.7 for plain bars and 0.0 for unbounded reinforcement. The value of α_2 is taken 1.0 for monotonic loading and 0.7 for cyclic loading. The concrete compressive strength in MPa is denoted f_c.

To maintain static equilibrium between the average stresses and the localised stresses the following limit to the value of f_{c1} was considered by the authors (Biddha & Ghobarah, 1999):

$$f_{c1} = \frac{0.18\sqrt{f_c}\tan\theta}{0.3 + \dfrac{24w}{a+16}} \quad [MPa] \tag{8.4}$$

where a is the maximum aggregate size (in mm), $w = \varepsilon_1 \cdot S_{m0}$ the crack width (in mm) and S_{m0} is the spacing of the inclined cracks, which depends on the crack

control characteristics of the reinforcement in both directions and the inclination of the cracks. For evaluating S_{m0} the authors suggested the concrete design code CSA A23.3-94 (1994) procedure.

The softening truss model outlined above has a corresponding moment-rotation relationship that defines the characteristics for the rotational spring to represent the shear deformation in the joint. Fig. 8.4 shows the equilibrium of an interior beam-to-column joint. The length along the beam between the contra flexure points is L_b and that along the column L_c. The shear diagram is plotted in Fig. 8.4(c). Equilibrium of the forces in the horizontal direction gives:

$$V_{jh} = C_b + T_b - V_{col} \,, \tag{8.5}$$

$$C_b = T_b = \frac{M_b}{jd} \,, \tag{8.6}$$

where jd is the moment arm of the beam. Summing the moments in Fig. 8.4 and expressing the shear in terms of an equivalent beam moment results:

$$V_{jh} = 2 \cdot M_b \left[\frac{1}{jd} - \frac{1}{L_c \left(1 - \frac{h_c}{L_b} \right)} \right] . \tag{8.7}$$

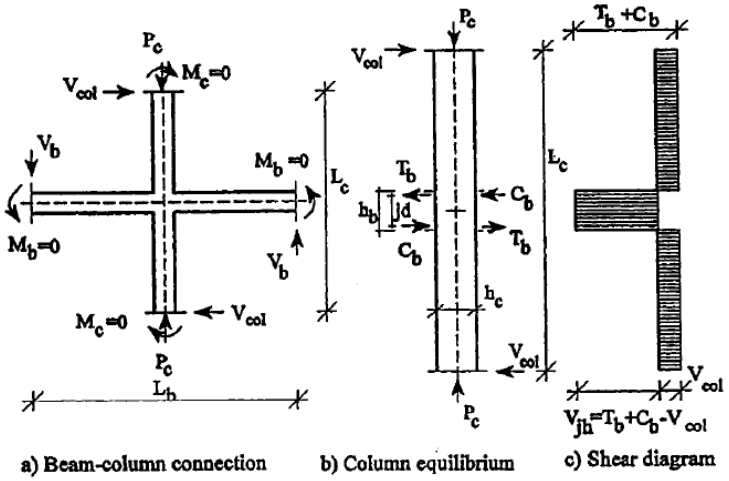

Fig. 8.4: Equilibrium of an interior beam-to-column joint.

Defining ΣM_b as the total beam moment to be transferred to the column by joint shear, it is obtained:

$$\sum M_b = 2 \cdot M_b = \frac{V_{jh}}{\frac{1}{jd} - \frac{1}{L_c\left(1 - \frac{h_c}{L_b}\right)}}. \tag{8.8}$$

Using the same procedure for calculating the total beam moment ΣM_b, as a function of the joint shear force, formulation for the ΣM_b can be made for interior and exterior top floor beam-to-column connections including corner joints.

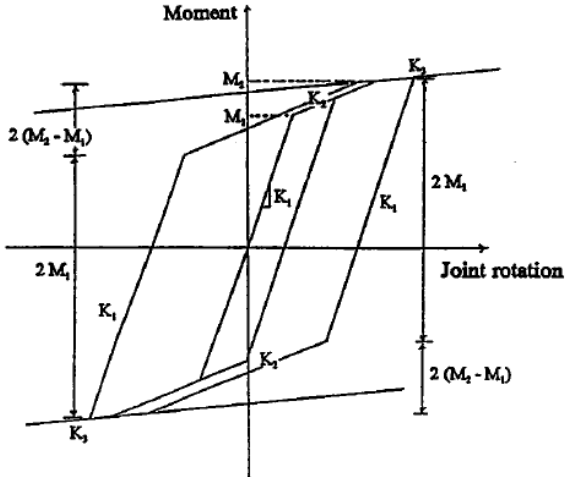

Fig. 8.5: Trilinear moment-rotation relationship for the shear spring.

The calculated shear-deformation envelopes of reinforced concrete joints were compared by the authors (Biddha & Ghobarah, 1999) to several test results. The proposed trilinear model Fig. 8.5 shown to be effective for the analysis of reinforced concrete joints accounting only shear deformation.

A simple analytical approach for evaluating the load-displacement relationship of reinforced concrete beam-to-column joints was developed considering the additional rotation due to anchorage slip of the reinforcing bars in beam. The moment-rotation relationship due to bond-slip is defined by the critical points of cracking (M_{cr}), yielding (M_y, θ_y) and ultimate conditions (M_u, θ_u). A bi-linear idealization is assumed as shown in Fig. 8.6.

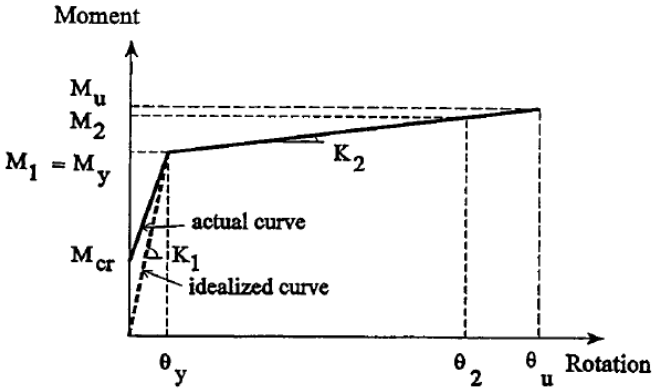

Fig. 8.6: Moment-rotation relationship for simulating bond-slip.

The various constant used in the formulation were evaluated based on analysis and experimental data.

Neglecting the concrete strain along the bar in the joint, the slippage Δ, at the beam-column interface is given by the integration of the steel strain distribution over a length L_s representing the distance from the beam-column interface to the point at which the bar begins to slip (Fig. 8.7).

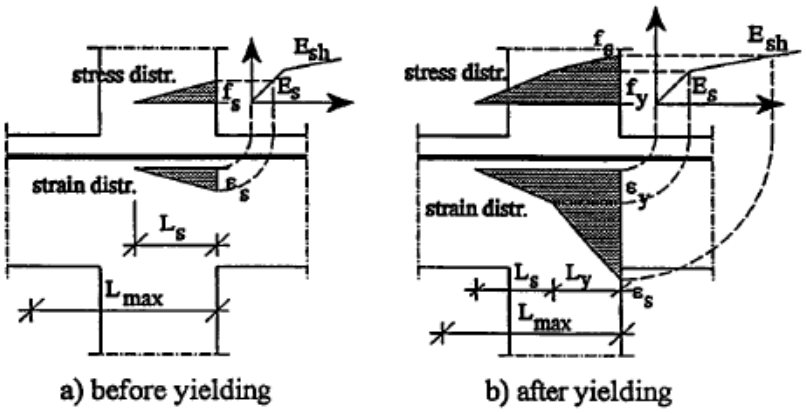

Fig. 8.7: Stress and strain distribution assumption in the joint.

The distance from the beam-column interface to the point at which the bar begins to slip (L_s) is evaluated by Eqn. (8.9) defining the diameter of the bar (d_b) in mm and the Young's modulus and the stress (f_{ys}) of beam reinforcing bars in MPa.

$$L_s = \frac{f_{ys} \cdot A_s}{\sum perimeter \cdot f_b} = \frac{E_s \cdot d_b}{2400 \cdot \sqrt{f_c}}, \tag{8.9}$$

$$\Delta_s = \frac{L_s \cdot \varepsilon_s}{2} = \frac{f_{ys} \cdot d_b}{4800 \cdot \sqrt{f_c}}. \tag{8.10}$$

Before bar yielding ($\varepsilon_s \leq \varepsilon_y$), the bar slippage from the joint in mm is given by Eqn. (8.10); after yielding ($\varepsilon_s \geq \varepsilon_y$), it is assumed that the slope of M - θ relationship depends on the strain hardening characteristics (χ) of the reinforcing bars, the thickness of the concrete cover relative to the dimensions of the cross section confined by the transversal steel, the amount of transverse steel, the size of yielding region, the penetration of yielding into the beam-column connection (L_y) as well as other factors. The upper limit length of the slip region, denoted L_{max}, is provided adding the depth of the column and half depth of the beam for interior joints and the length of bar anchorage for exterior ones Fig. 8.8.

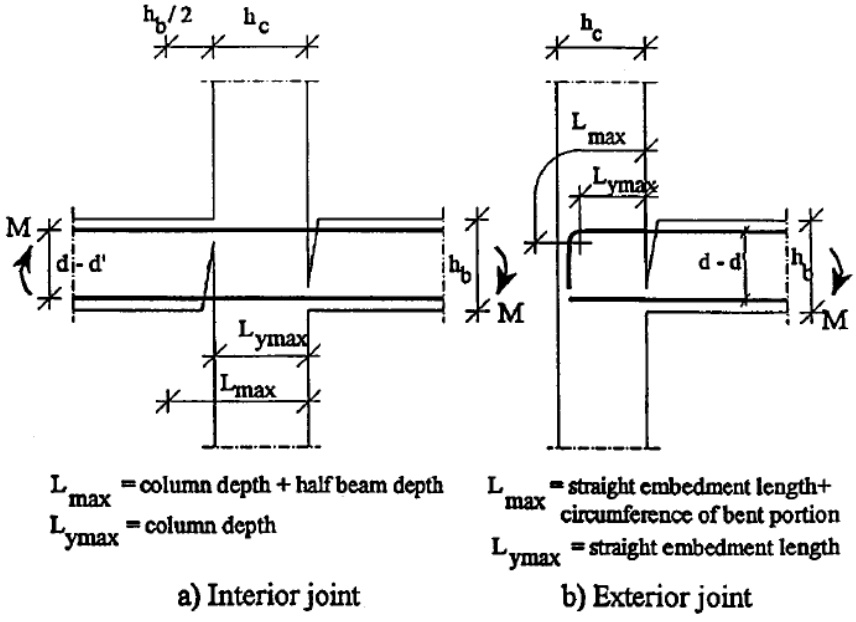

Fig. 8.8: Definition of L_{max} and $L_{y,max}$.

The length of yielding region is assumed as a function of the strain-hardening of bars as reported in Eqn. (8.11)

$$\chi = \frac{f_{us}}{f_{ys}} \rightarrow \begin{cases} for \quad 1 \le \chi \le 1{,}05 \quad \rightarrow \quad L_y = 2000\ \chi - 2000\ mm \\ for \quad \chi > 1{,}05 \quad \rightarrow \quad L_y = 500\ \chi - 425\ mm \end{cases} . \tag{8.11}$$

Therefore, the value of bar slippage from the joint after the yielding can be calculated by Eqn. (8.12) where E_{sh} is the slope of the strain hardening branch of the stress-strain behaviour of steel.

$$\Delta_s = \left[\frac{L_s + 2 \cdot L_y}{E_s} + (\chi - 1) \frac{L_y}{E_{sh}} \right] \frac{f_y}{2} . \tag{8.12}$$

The length of yielding region L_y should not exceed the maximum limit $L_{y,max}$ equal to the depth of the column for interior joints and the depth of the column minus the concrete cover for exterior ones (Fig. 8.8); furthermore it must be assumed $L_s + L_y \leq L_{max}$.

Two different cases can be observed: yielding of the reinforce before slippage ($L_s \leq L_{max}$) and pull-out before yielding ($L_s > L_{max}$).

In the first case the stiffness before the yielding K_1 is evaluated by Eqn. (8.13) and the flexural moment at yielding is provided by Eqn. (8.14) in which (d-d') is the effective depth of the beam, and d_b and n are the bar diameter and number or reinforcing bars in the beam respectively

$$K_1 = 1200 \cdot \pi \cdot n \cdot d_b (d - d')^2 \sqrt{f_c} , \tag{8.13}$$

$$M_y = n \cdot A_s \cdot f_{ys} (d - d') . \tag{8.14}$$

After yielding, the stiffness K_2 is evaluated by Eqn. (8.15) defining the χ factor as the ratio between the ultimate and the yielding moment [Eqn. (8.16)].

$$\begin{aligned} K_2 &= \frac{2(\chi_2 - 1) n \cdot A_s (d - d')^2 E_s}{2 \cdot L_{y,max} + \left(\frac{\chi_2 - 1}{\zeta} \right) L_{y,max}} \quad if \quad L_s + L_{y,max} \le L_{max} , \\ K_2 &= \frac{2(\chi_2 - 1) n \cdot A_s (d - d')^2 E_s}{(L_{max} - L_s) + \left[2 + \left(\frac{\chi_2 - 1}{\zeta} \right) \right]} \quad if \quad L_s + L_{y,max} > L_{max} , \end{aligned} \tag{8.15}$$

$$\chi_2 = \frac{M_u}{M_y} \le \frac{f_{us}}{f_{ys}} . \tag{8.16}$$

In the second case in which bars pull-out before yielding ($L_s > L_{max}$ and $K_2 = 0$), the moment at yielding M_y and the stiffness K_1 can be calculated as follows:

$$K_1 = \frac{2 \cdot n \cdot A_s \cdot E_s \left(d - d'\right)^2}{L_{max}}, \tag{8.17}$$

$$M_y = n \cdot A_s \cdot f_{ys} \left(d - d'\right) \frac{L_{max}}{L_s}. \tag{8.18}$$

The model developed by Chung et al. (1987) was adopted to represent the hysteretic behaviour of the rotational spring accounting the bond slip. The model is capable of including the effects of stiffness degradation, strength deterioration and pinching. An input parameter which ranges between 0.0 and 0.1 governs the strength deterioration, where a value of 0.0 means no strength deterioration.

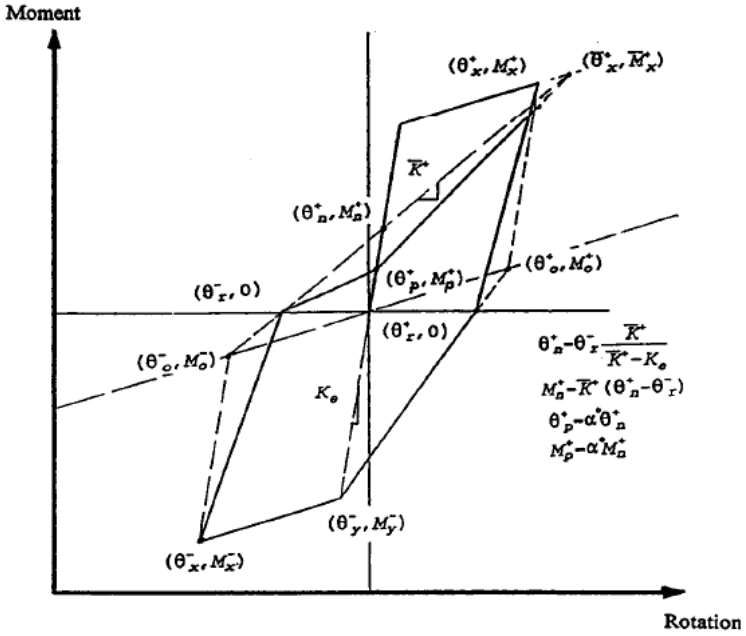

Fig. 8.9: Hysteretic model accounting pinching effects.

The pinching effect is introduced in the loops by an input parameter α^* ranging between 0.0 and 1.0 as shown in Fig. 8.9, where a value of 1.0 means no pinching.

8.1.2 The Model by Youssef & Ghobarah (2001)

The model proposed by Youssef & Ghobarah (2001) simulates the behaviour of the joint region as represented by four rigid members enclosing the joint as shown in Fig. 8.10.

Beams and columns are idealized using elastic elements. Bond slip and concrete crushing are idealised in the connection between the beam or the column and the rigid members enclosing the joint. The connection between the joint and beam or column is represented using three concrete springs and three steel springs. The connections between these rigid members are assumed pinned with shear springs connecting the diagonals as shown in Fig. 8.10.

Each of the concrete and steel springs represents the stiffness of the effective group reinforcing bars and the effective concrete in compression. The capacity of the edge concrete springs is calculated as the concrete compression force at ultimate condition for a given axial load. The capacity of the central concrete spring is calculated as the difference between the total capacity of the concrete section and the capacity of the edge springs. The distance between the edge springs is calculated such that the ultimate moment of the transformed section (consisting of the steel and concrete springs) will be the same as that of the actual section.

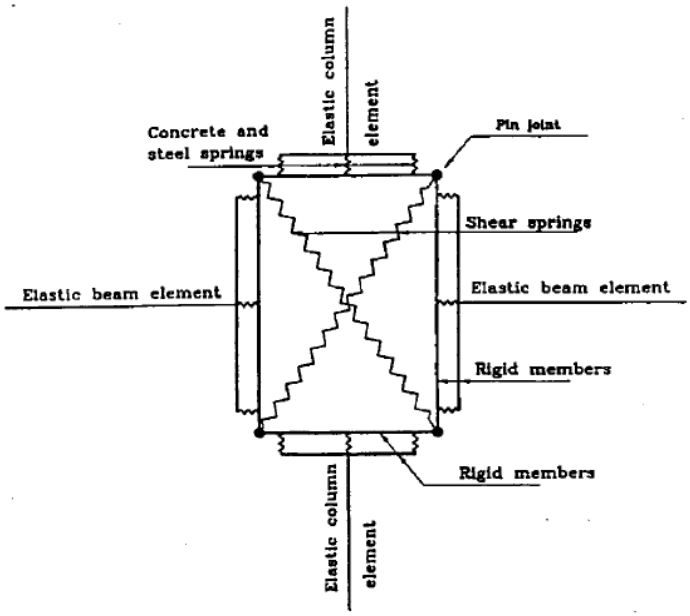

Fig. 8.10: Joint model developed by Youssef & Ghobarah (2001).

From simple geometry, as shown in Fig. 8.11, the elongation (|d1+d2|) in one of the diagonal springs is equal to the contraction (|d3+d4|) in the other spring.

$$\Delta D = |d1 + d2| = |d3 + d4| . \tag{8.19}$$

The shear deformation γ can be calculated using the following equation:

$$\gamma = \frac{\gamma_{h1} + \gamma_{h2}}{2} + \frac{\gamma_{v1} + \gamma_{v2}}{2} = \frac{2 \cdot \Delta D}{D \cdot \sin(2\varphi)} \tag{8.20}$$

where the average of γ_{h1} and γ_{h2} is the horizontal shear deformation, the average of γ_{v1} and γ_{v2} is the vertical shear deformation, D is the undistorted diagonal length and φ is the angle between the diagonal and the horizontal.

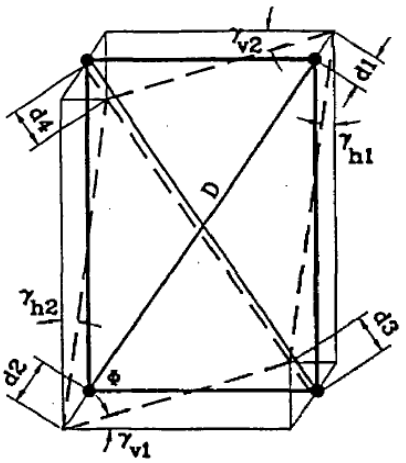

Fig. 8.11: Geometry of the model by Youssef & Ghobarah (2001).

During the analysis, the shear force V corresponding to a given shear deformation in the joint can be calculated. The force in each of the diagonal springs F can be calculated from simple equilibrium:

$$F = \frac{V}{2 \cdot \cos\varphi} . \tag{8.21}$$

In the developed models, the reinforcement steel in the form of a group of bars is represented by steel springs which idealise the relationship between the force in the steel bars and the bond slip. In effect, the model is intended to represent the behaviour of the group of steel reinforcement bars and is not a

pure material model. The steel spring model is shown in Fig. 8.12 depending on the bar size, the amount of confinement. The concrete strength, the development length and the steel yield stress, the steel element parameters such as the elastic stiffness K_s, the steel yield force P_{sy}, the post yielding stiffness K_{s2}, the force and displacement after which bond-slip softening starts P_{su} and d_{su}, the residual force after complete slippage P_{s0} and α_s (a parameter controlling the rate of degradation) can be defined. The detailed methodology for determining these parameters is explained by Youssef and Ghobarah (1999).

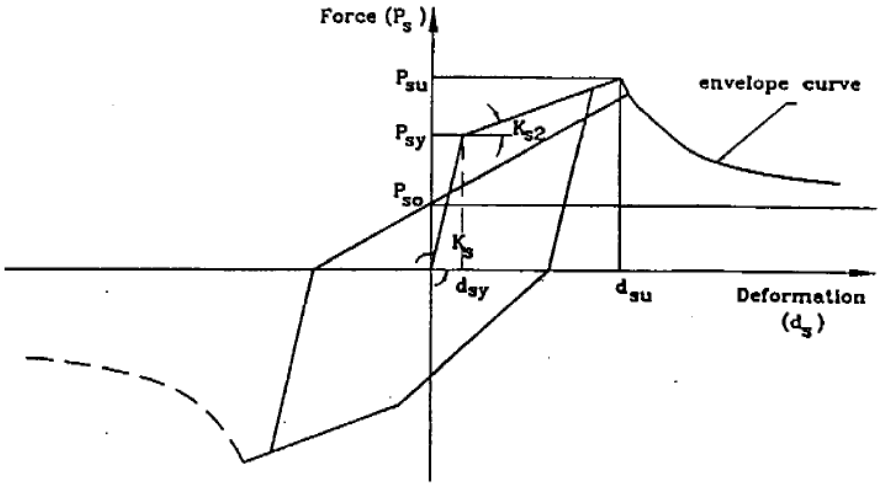

Fig. 8.12: Hysteretic model for the steel spring.

Bond-slip softening is defined as the point at which steel spring force degradation starts.

To define the post slip failure behaviour of the steel spring element ($d_s > d_{su}$), it is suggested that the steel spring force P_s corresponding to a displacement d_s is given by:

$$P_s = P_{sy}\left(R_{s0} + \frac{1-R_{s0}}{1+\alpha_s\left(d_s - d_{su}\right)^2}\right) \tag{8.22}$$

where R_{so} is the ratio between the residual force P_{so} in the steel bars after complete slippage and the maximum load attained P_{su}, a_s is a softening factor which depends on the degree by which the steel loses its force, d_{su} is the displacement at which strength softening due to bond slip starts. All these factors can be determined from the bond slip-steel stress curve.

In this cycle (Fig. 8.12), loading starts in the positive direction (tension) with stiffness K_s until the yield load P_{sy} is reached and then the post yielding curve is followed at stiffness K_{s2}. As the load direction is reversed, unloading proceeds with the same initial stiffness K_s. When loading starts in the negative direction (compression), the stiffness changes and aims at the yield point in the first cycle or at the previous unloading point on the negative envelope. Unloading from the negative envelope will be parallel to the initial stiffness K_s until zero force. Loading in tension will begin aiming at the previous unloading point, or if the additional stiffness degradation starts (after reaching yield), loading will be with degraded stiffness K_{so} until reaching the envelope curve. As the load direction is reversed, unloading will proceed in the same manner described previously. The difference between the hysteretic model for the steel spring and that of an ideal elastic-plastic rule was implemented to represent the pinching effect due bond slip.

The additional stiffness deterioration is taken into account in cycles following the cycle when the yield load is exceeded. A formula similar to that presented by Park et al. (1985) is adopted:

$$f = 1.0 - \lambda_s \frac{d_{s1}}{d_{sy}} \tag{8.23}$$

where f is a reduction factor to be multiplied by the maximum load reached in the preceding cycle as shown in Fig. 8.12, λ_s is the strength deterioration parameter, the maximum achieved displacement in the preceding cycle d_{s1} corresponds to load P_{s1}, and d_{sy} is the yield displacement corresponding to yield load P_{sy}.

In the absence of test data, typical values for λ_s to be used are:

- 0.0 for no degradation;
- 0.0001 for slight degradation;
- 0.01 for moderate degradation;
- 0.1 for substantially increased degradation.

Once the deteriorated strength $f P_{s1}$ is determined, the stiffness for the next cycle can be defined.

A concrete spring represents the relationship between the axial force on an identified concrete strut and the axial displacement of that strut. The characteristics of the concrete spring model are shown in Fig. 8.13. The yield force of the concrete spring in compression is P_{cy}, the concrete compressive yield displacement after which concrete softening starts with a degrading slope Z is d_{cy} and the tensile cracking load is P_{ty}. Confinement effect was taken into

account using a parameter K_h. Concrete softening in compression is defined as the point at which concrete spring force degradation starts.

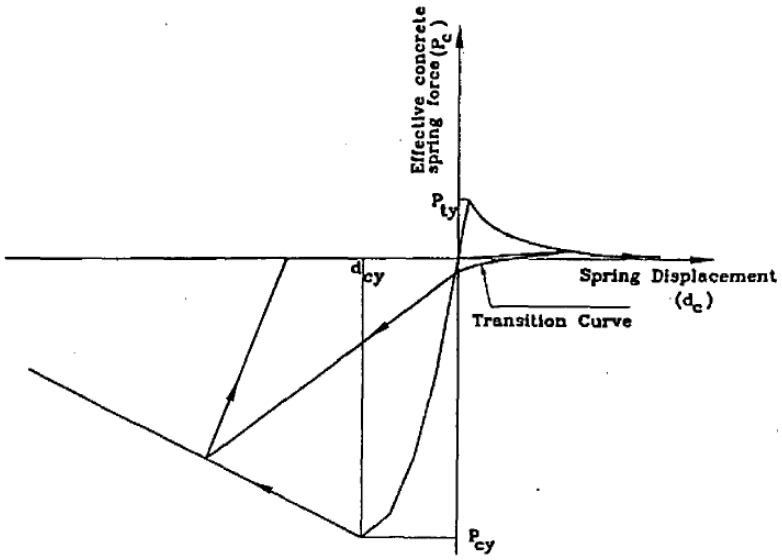

Fig. 8.13: Hysteretic model for the concrete spring.

The main function of the concrete spring is to represent the opening and closing of cracks. The concrete model includes a defined envelope in tension and in compression. The monotonic concrete stress-strain relation in compression is described by two regions as shown in Fig. 8.14:

$$f_c = K_h f_c' \left[2.0\left(\frac{\varepsilon_c}{\varepsilon_0}\right) - \left(\frac{\varepsilon_c}{\varepsilon_0}\right)^2 \right], \quad \varepsilon_c \le \varepsilon_0 \,, \tag{8.24}$$

$$f_c = K_h f_c' \left[1 - Z\left(\varepsilon_c - \varepsilon_0\right)\right] \ge 0.2 \cdot K_h f_c', \quad \varepsilon_0 \le \varepsilon_c \le \varepsilon_u \,, \tag{8.25}$$

where f_c' is the concrete compressive cylinder strength in MPa and the concrete strain at maximum stress ε_o is:

$$\varepsilon_0 = 0.002 \cdot K_h \,, \tag{8.26}$$

and the strength increase due to confinement is determined by the factor K_h:

$$K_h = 1 + \frac{\rho_s \cdot f_{yh}}{f_c'} \,, \tag{8.27}$$

where f_{yh} is the yield strength of transverse reinforcement in MPa, and ρ_s is the ratio of the volume of hoop reinforcement to the volume of concrete core measured to outside of the ties.

The slope of the strain softening branch Z is calculated as:

$$Z = \frac{0.5}{\frac{3+0.29\cdot f_c'}{145\cdot f_c'-1000}+0.75\cdot\rho_s\sqrt{\frac{h'}{S_h}}-0.002\cdot K_h} \tag{8.28}$$

where h' is the width of the concrete core measured to outside of the ties, and S_h is the centre-to-centre spacing of the ties or hoop sets.

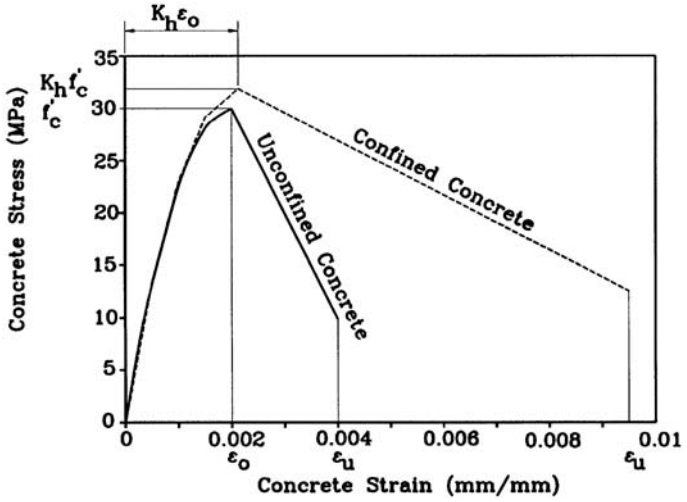

Fig. 8.14: Stress-strain relation for confined and unconfined concrete with f_c' = 30 MPa.

Transformation from stress to force and from strain to displacement should be made by applying the set of Eqns. (8.24) to (8.28). The force transformation factor is taken equal to the concrete area represented by the spring A_c multiplied by 0.85. The yield force of the concrete spring in compression P_{cy} is:

$$P_{cy} = 0.85\cdot A_c\cdot K_h\cdot f_c'. \tag{8.29}$$

The plastic deformation of the concrete member is assumed to be fully concentrated within the inelastic element at the beam-column joint. The plastic deformation of the effective concrete spring is postulated to represent the accumulated crushing behaviour of the concrete over the plastic hinge length.

The methodology used for determining the concrete compressive yield displacement d_{cy} that corresponds to the compressive yield force P_{cy} depends on the fact that the displacement is the integration of the strain over the length. Thus, the concrete strain values are obtained by assuming that:

- the point of contra-flexure is at the middle of the concrete member;
- by applying the given axial load on half the member with the transformed section simultaneously with a lateral load, which will cause compression failure to the member;
- the value of d_{cy} is determined;
- the displacement transformation factor is taken as d_{cy}/ε_o by integrating these values along half the member length.

The monotonic force-displacement relationship in tension includes a linear branch until the cracking load P_{ty} is reached and a softening branch that describes the post cracking stage. The formula describing the softening branch is:

$$f_{cr} = 0.33\sqrt{f_c'}\,, \tag{8.30}$$

$$f_t = f_{cr}\left[0.95\cdot e^{-1000\cdot(\varepsilon_c-\varepsilon_{cr})}+0.05\right]. \tag{8.31}$$

In the hysteretic cycle shown in Fig. 8.13, loading starts in the positive direction until the cracking load P_{ty} is reached and the post cracking curve is followed. When the load direction is reversed, loading proceeds in the negative direction until the opened cracks are closed. Crack closing is characterised by an abrupt change in the stiffness from very low stiffness to the initial stiffness that may cause convergence difficulties. To overcome this problem, a smooth transition curve that represents gradual change in stiffness is used. This transition curve is followed until the envelope curve is reached. If loading continues in the same direction, the yield force P_{cy} is reached and the post yield branch is followed. If the load direction is reversed at displacement d_r corresponding to strain ε_r, unloading takes place aiming at displacement d_p corresponding to strain ε_p on the zero load axis. The strain ε_p is calculated using the following equations:

$$\frac{\varepsilon_p}{\varepsilon_0} = 0.145\left(\frac{\varepsilon_r}{\varepsilon_0}\right)^2 + 0.13\left(\frac{\varepsilon_r}{\varepsilon_0}\right), \qquad for \quad \left(\frac{\varepsilon_r}{\varepsilon_0}\right) < 2\,, \tag{8.32}$$

$$\frac{\varepsilon_p}{\varepsilon_0} = 0.707\left(\frac{\varepsilon_r}{\varepsilon_0}-2\right)+0.834, \qquad for \quad \left(\frac{\varepsilon_r}{\varepsilon_0}\right) \geq 2\,. \tag{8.33}$$

Loading then proceeds with zero stiffness until the displacement changes from negative (compression) to positive (tension). The loading line then aims at the point on the post crack branch where unloading started in the previous cycle. If unloading occurs again, the transition curve is again followed until the monotonic envelope curve is reached and then the loading line aims at the previous unloading point on the post yield branch of the previous cycle. The remaining part of the cycle follows the same route previously described.

About shear springs, the shear model used by Ghobarah & Youssef (1999) is adopted. During each cycle of the iteration process, the shear force corresponding to a specified shear deformation calculated by the structural model based on the element deformation is determined using the modified compression field theory. The solution strategy to determine the shear force corresponding to a specified shear strain at equilibrium uses an iterative procedure. Iterations are carried out over an incrementally increasing average principal tensile strain, ε_1. For each iteration, the longitudinal strain at mid-depth of section, ε_x is calculated then the axial force corresponding to ε_x is calculated using sectional analysis. This procedure is repeated until for a certain ε_1, the axial force on the section is equal to the acting force.

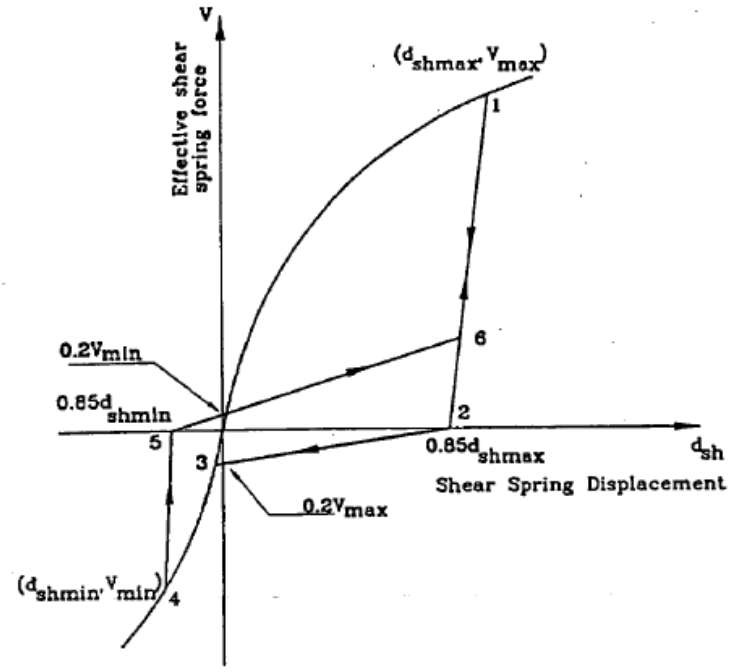

Fig. 8.15: Hysteretic shear model by Youssef & Ghobarah (1999).

The outlined solution strategy establishes the primary curve for the shear spring element. Each point on this curve is evaluated for the corresponding axial force acting on the element represented by the shear spring. To account for continually varying stiffness and energy absorption characteristics under cyclic loading, the hysteretic model developed by Ghobarah & Youssef (1999) and shown in Fig. 8.15 is adopted. Shear failure is assumed when degradation in the shear envelope starts.

The proposed hysteretic macro-element provides an accurate representation of the behaviour of RC joints under cyclic actions. The model is particularly efficacy in analysing existing structures where the shear and bond-slip effects are important.

All the parameters affecting the model by Youssef & Ghobarah (2001) are evaluated using theoretical procedures without calibrating experimental values.

8.1.3 The Model by Pampanin et al. (2003)

The authors (2003) developed an alternative simplified analytical model for joint behaviour as a viable and useful tool for extensive parametric studies on the seismic response of such frame systems.

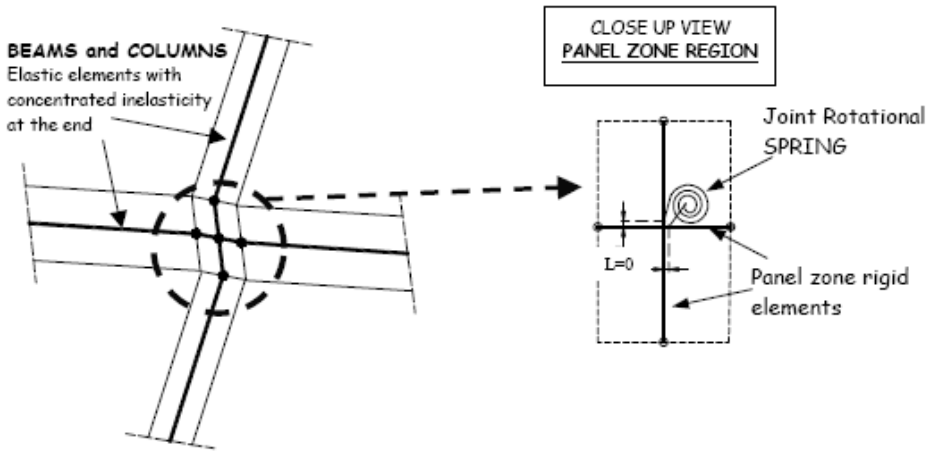

Fig. 8.16: Model for joint behaviour proposed by Pampanin et al. (2003).

An equivalent moment rotational spring, governing the relative rotation of beams and columns, is adopted to represent the joint behaviour either in the linear and non-linear range. As shown in Fig. 8.16, beam and column elements

converging in the joint are modelled as one-dimensional frame elements with concentrated inelasticity at the critical section interface, defined through appropriate moment-curvature curves based on section analysis. The effects of moment-axial load interaction are taken into account for columns. Rigid elements are adopted to model the portion of beam and column elements comprising the panel zone region.

The moment-rotation characteristics of the joint spring can be directly derived, based on equilibrium considerations, from the corresponding principal tensile stress vs. shear deformation curve (i.e. Fig. 8.17):

- the equivalent joint spring moment corresponding to a defined level of principal tensile (or compression) stress in the joint (first cracking or higher damage level) is taken as the sum of the column moments (equal to the sum of the beam moments);
- joint spring rotation corresponds to the joint shear deformation if a joint shear distortion mechanism is assumed to govern at higher level of deformation (i.e. it is predominant when compared to pure flexural joint behaviour).

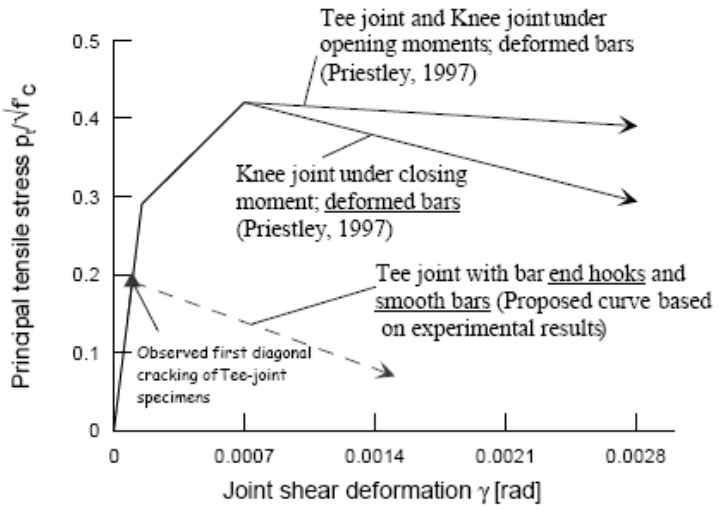

Fig. 8.17: Strength degradation curve for exterior joints.

The principal tensile stress at first cracking is defined as:

$$p_t = 0.2\sqrt{f_c'} \quad \textit{for exterior} \text{ joints}, \tag{8.34}$$

$$p_t = 0.29\sqrt{f_c'} \quad \textit{for interior} \text{ joints}. \tag{8.35}$$

After first cracking occurs, a hardening behaviour until

$$p_t = 0.42\sqrt{f_c'} \tag{8.36}$$

is assumed for interior joint, where alternative shear transfer mechanisms can be activated, while elastic-plastic behaviour or an appropriate strength degradation model can be adopted for exterior Tee-joints.

The cyclic behaviour will then be modelled by an appropriate hysteresis rule able to represent the "pinching" effect due to slip of the reinforcement and shear cracking in the joint (Fig. 8.18).

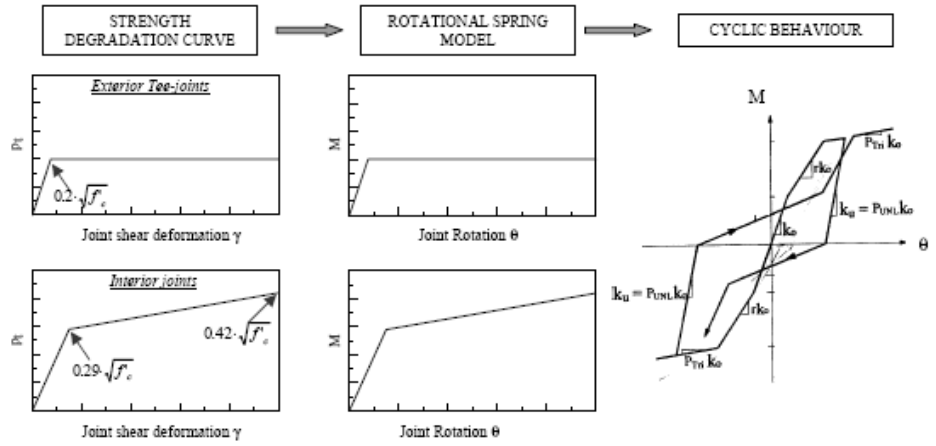

Fig. 8.18: Monotonic and cyclic behaviour of the shear hinge model.

It is noted that the rotational spring connects two nodes that are respectively the conjunction of beams and columns, so it is possible to transfer the axial load through the column without affecting the spring element. To solve this problem Trowland (2003) introduced another model with concentrated plasticity, slightly more complex, (see section 8.1.5): the spring was divided into two parts which are respectively interposed between the node connecting beams and the top and bottom column.

8.1.4 The Model by Lowes & Altoontash (2003) and Mitra & Lowes (2007)

The authors (Lowes & Altoontash, 2003 and Mitra & Lowes, 2007) developed a joint model able of simulating nonlinear behaviour of beam-to-column joints in nonlinear analyses of plane RC frames. The mechanisms

affecting the behaviour of interior and exterior joints have been accounted modelling the joint shear panel and the bar slip. In the model are developed constitutive laws based on the concrete and steel properties and the geometrical characteristics to define these two mechanisms.

The model takes into account two nonlinear mechanisms of failure:

- the failure of the joint panel under shear forces;
- the failure of longitudinal reinforcement in beam and column through the joint.

Lowes & Altoontash (2003) presented a four-node, 12 degrees-of-freedom element for use in modelling the response of reinforced concrete beam–column joints in two-dimensional structural analyses. The joint element comprises:

- a shear-panel component that simulates strength and stiffness loss due to failure of the joint core;
- eight bar-slip springs that simulate stiffness and strength loss due to anchorage-zone damage;
- four interface-shear springs that simulate reduced capacity for shear transfer at the joint perimeter due to crack opening.

Fig. 8.19 shows the model developed by Lowes & Altoontash (2003), including revisions accomplished as part of the study provided by Mitra & Lowes (2007).

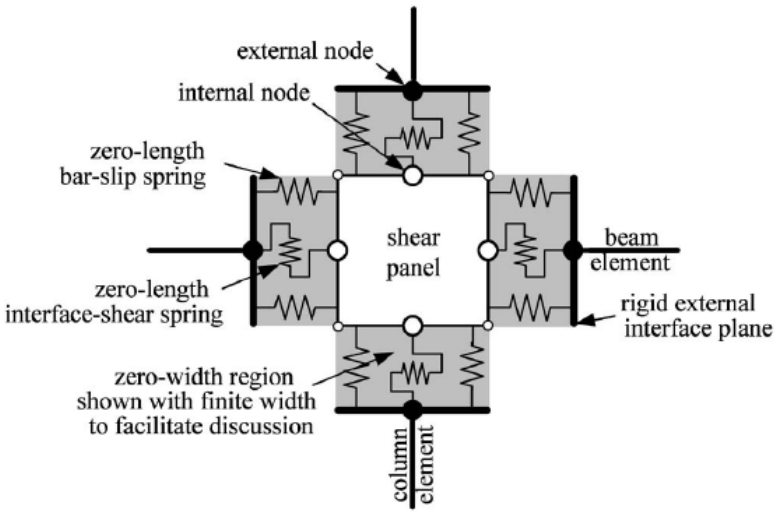

Fig. 8.19: Beam-to-column joint element proposed by Mitra & Lowes (2007).

A general one-dimensional load-deformation response model is used to predict the behaviour of the components that make up the joint element (Lowes & Altoontash, 2003). This one-dimensional model is defined by a multi-linear response envelope, a trilinear unload-reload path, and three damage rules that control the evolution of the response path. The unload-reload path is defined by three parameters:

1. *rDisp*, the ratio of the deformation at which reloading occurs to the maximum (minimum) historic deformation;
2. *rForce*, the ratio of the load at which reloading occurs to the maximum (minimum) historic load;
3. *uForce*, the ratio of the load developed upon unloading, from a negative (positive) load, to the maximum (minimum) of the load envelope.

Three damage rules simulate deterioration in the unloading stiffness (unloading stiffness degradation), deterioration in the strength developed in the vicinity of the maximum and minimum deformation demands (reloading stiffness degradation), and deterioration in the strength achieved at previously unachieved deformation demands (strength degradation).

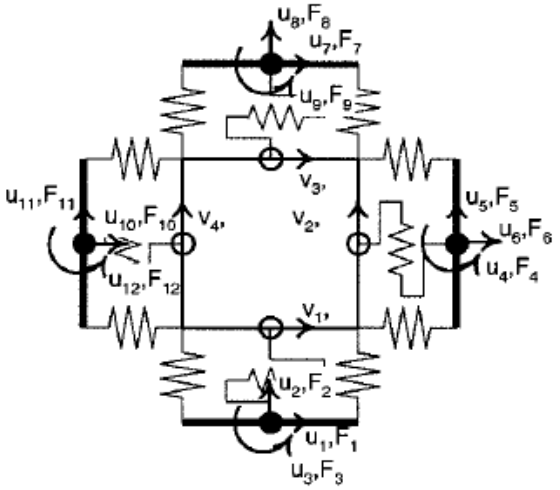

Fig. 8.20: Internal and external generalized displacements resultants.

Procedures are required to calibrate the general load-deformation response model for each of the element components. For joints with moderate to high volumes of transverse reinforcement, Lowes & Altoontash (2003) recommend using the Modified Compression Field Theory (MCFT) (Vecchio & Collins, 1986) to define the response of the shear panel and provide parameters for use in

simulating cyclic response. Bond-slip spring response is defined assuming a constant, or piecewise constant, bond-stress distribution within the joint. Bond strength values are provided for different bond-zone conditions, and parameters are provided to enable simulation of response under cyclic loading. Interface-shear springs are considered elastic due to lack of experimental data for use in calibrating these components.

The material state of the joint element is defined uniquely by the generalized displacement history of the four external and four internal element nodes Fig. 8.20. These displacements define the deformation history of the eight bar-slip springs, four interface shear springs and one shear-panel component that compose the joint model [Fig. 8.21(a)] as follows:

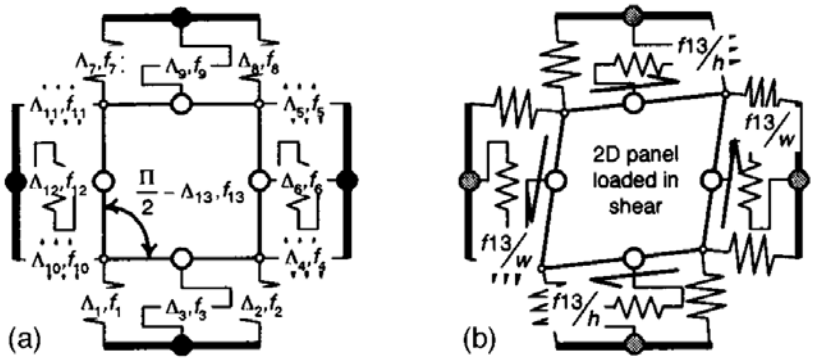

Fig. 8.21: Definition of component deformations and generalized forces: (a) Component deformations and forces, (b) Shear forces acting on shear-panel component.

$$\Delta = \mathbf{A} \cdot \begin{Bmatrix} \mathbf{u} \\ \mathbf{v} \end{Bmatrix} \tag{8.37}$$

where $\mathbf{u}$ and $\mathbf{v}$ refer, respectively, to external and internal nodal displacements; Δ is the vector of component deformations function of the joint height h and the joint width w. One-dimensional material constitutive relationships define component forces f_i [Fig. 8.21(a)] as a function of the component deformation histories. For the shear panel, the complementary component force, f_{13}, is the nominal shear stress developed within the joint core multiplied by the volume of the joint core [Fig. 8.21(b)].

To facilitate the constitutive modelling process, a general one-dimensional hysteretic load-deformation model was used to represent the response of each of the components that compose the element. A response envelope, an

unload–reload path, and three damage rules that control evolution of these paths define the one-dimensional material model (Fig. 8.22). Calibration of the model requires 16 parameters to define the response envelope [states 1 and 2 in Fig. 8.22(a)], 6 parameters to define the two unload–reload paths [states 3 and 4 in Fig. 8.22(a)], and 12 parameters to define the hysteretic damage rules [Fig. 8.22(b)].

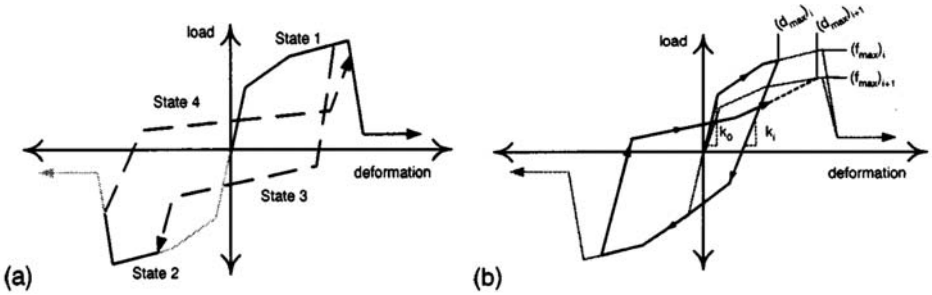

Fig. 8.22: One-dimensional material model: (a) Material states, (b) Impact of hysteretic damage rules on load-deformation response.

Fig. 8.22(a) shows the four material states that define the one-dimensional material model. Load-deformation paths for states 1 and 2 are defined at the beginning of the analysis and modified during the analysis to simulate hysteretic strength loss. For states 3 and 4, the load path is redefined each time there is a deformation reversal. The load-deformation point at which the reversal occurs defines one endpoint for state 3 (state 4); the state 3 – state 2 (state 4 – state 1) transition defines the other. Two additional load-deformation points define the state 3 (state 4) load path: the point reached once substantial unloading has occurred and the point at which substantial reloading occurs. For state 3 (state 4), the load developed upon unloading is defined as a fraction of the minimum (maximum) strength that can be developed. With the unloading stiffness defined, this establishes the end of the substantial unload phase. The load-deformation point at which substantial reloading occurs for state 3 (state 4) is defined as a fraction of the minimum (maximum) historic deformation demand and a fraction of the load developed at the minimum (maximum) deformation demand.

Hysteretic damage is simulated through deterioration in unloading stiffness (unloading stiffness degradation), deterioration in strength achieved at previously unachieved deformation demands (strength degradation), and deterioration in the strength developed in the vicinity of the maximum and minimum deformation demands (reloading strength degradation). Fig. 8.22(b)

shows the impact of these three different damage modes on the hysteretic response.

A generalisation of the damage index proposed by Park & Ang (1985) is used to define hysteretic damage:

$$\delta_i = \left(\alpha 1 \cdot \left(\overline{d}_{\max} \right)^{\alpha 3} + \alpha 2 \cdot \left(\frac{E_i}{\alpha 5 \cdot E_{monotonic}} \right)^{\alpha 4} \right) \leq \lim it \tag{8.38}$$

where

$$\overline{d}_{\max} = \text{maximum} \left[\frac{(d_{\max})_i}{def_{\max}}, \frac{(d_{\min})_i}{def_{\min}} \right], \tag{8.39}$$

$$E_i = \int_{load\ history} dE\ , \tag{8.40}$$

and i refers to the current displacement increment, δ_i is defined damage index; limit defines the maximum value of the damage index, α_s is a parameters for use in fitting the damage rule to experimental data, E_i is the accumulated hysteretic energy, $E_{monotonic}$ represents the energy required to achieve the deformation that defines failure, def_{max} and def_{min} are the positive and negative deformations that define failure, respectively, and $/d_{max}/_i$ and $/d_{min}/_i$ are the maximum and minimum historic deformation demands.

For the case of stiffness degradation [Fig. 8.22(b)]:

$$k_i = k_0 \cdot (1 - \delta k_i) \tag{8.41}$$

where k_i = current unloading stiffness, k_0 = initial unloading stiffness and δk_i = current value of the stiffness damage index. Envelope strength is simulated in the same way [Fig. 8.22(b)]:

$$(f_{\max})_i = (f_{\max})_0 \cdot (1 - \delta f_i) \tag{8.42}$$

where $/f_{max}/_i$ = current envelope maximum strength; $/f_{max}/_0$ = initial envelope maximum strength; and δf_i = current value of the strength damage index. The reduction in strength that is observed upon reloading is simulated by applying the damage rule to define an increase in the maximum (decrease in the minimum) historic deformation [Fig. 8.22(b)]

$$(d_{\max})_i = (d_{\max})_0 \cdot (1 - \delta d_i) \tag{8.43}$$

where $(d_{max})_i$ = current deformation that defines the end of the reload cycle for increasing deformation demand; $(d_{max})_0$ = maximum historic deformation demand; and δd_i = current value of the reloading-strength damage index.

Earthquake loading of a joint results in substantial shear loading of the joint core; the inelastic response of the joint core is simulated by the shear-panel component (Fig. 8.20).

A constitutive model was developed that employs the Modified Compression Field Theory (MCFT) (Vecchio & Collins, 1986) to define the envelope to the shear stress versus strain history of the joint core, and experimental data provided by Stevens et al. (1991) were used to define response under cyclic loading. This procedure allows a user to define behaviour using material properties, joint geometry, and joint reinforcing steel ratio.

The Stevens et al. (1991) data show an extremely pinched shear stress–strain history. This behaviour is attributed to the opening and closing of cracks in the concrete–steel composite. This behaviour is represented using the one-dimensional material model with parameters defined as follows:

- unloading stiffness: assumed equal to the initial stiffness;
- shear strain at which reloading occurs: defined to be 0.25 of maximum historic shear strain;
- shear stress at which reloading occurs: defined to be 0.0;
- displacement damage rule: $\alpha1$=0.12, $\alpha2$=0.0, $\alpha3$=0.23, $\alpha4$=0.0, $\alpha5$=10, and limit=0.95;
- stiffness damage rule: defined such that the minimum unloading stiffness is equal to the secant stiffness at the point of maximum shear strength;
- strength damage rule: $\alpha1$=1.11, $\alpha2$=0.0, $\alpha3$=0.32, $\alpha4$=0.1, $\alpha5$=10, and limit=0.125.

About bond slip, the envelope to the bar-stress versus –slip relationship is developed on the basis of several simplifying assumptions about joint anchorage-zone response:

1. bond stress along the anchored length of a reinforcing bar is assumed to be uniform for reinforcement that remains elastic or piecewise uniform for reinforcement loaded beyond yield;
2. slip is assumed to define the relative movement of the reinforcing bar with respect to the perimeter of the joint and is a function of the strain distribution along the bar;
3. the bar is assumed to exhibit zero slip at the point of zero-bar stress.

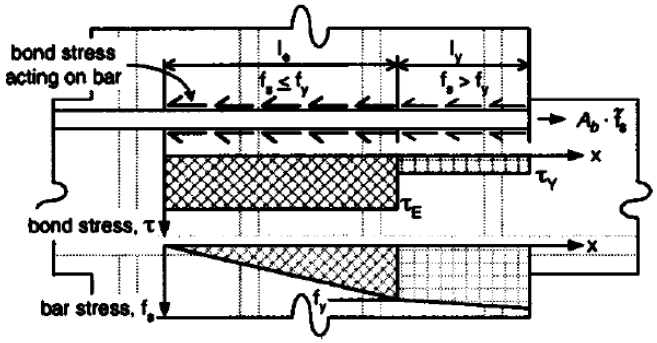

Fig. 8.23: Bond stress and bar stress distribution for a bar anchored in a beam-to-column joint.

Fig. 8.23 shows an idealization of the bond stress and resulting bar stress distribution for an anchored bar loaded beyond yield. Employing these simplifying assumptions, the bar-stress versus -slip relationship is defined as follows:

for $\bar{f}_s < f_y$

$$slip = \int_0^{l_{fs}} \tau_E \frac{\pi \cdot d_b}{A_b} \cdot \frac{1}{E} x dx = 2 \frac{\tau_E}{E} \frac{l_{fs}^2}{d_b}, \tag{8.44}$$

for $\bar{f}_s \ge f_y$

$$slip = \int_0^{l_e} \frac{4}{d_b} \frac{\tau_E}{E} x dx + \int_{l_e}^{l_y + l_e} \frac{f_y}{E} + \tau_y \frac{4}{d_b} \frac{1}{E_h} (x - l_e) dx = \tag{8.45}$$

$$= 2 \frac{\tau_E}{E} \frac{l_e^2}{d_b} + \frac{f_y}{E} l_y + 2 \frac{\tau_y}{E_h} \frac{l_y^2}{d_b},$$

with

$$l_{fs} = \frac{\bar{f}_s}{\tau_{ET}} \cdot \frac{A_b}{\pi \cdot d_b}, \tag{8.46}$$

$$l_e = \frac{f_y}{\tau_{ET}} \cdot \frac{A_b}{\pi \cdot d_b}, \tag{8.47}$$

$$l_y = \frac{\bar{f}_s - f_y}{\tau_{YT}} \cdot \frac{A_b}{\pi \cdot d_b}, \tag{8.48}$$

where $\bar{f}_s$ = bar stress at the joint perimeter; f_y = steel yield strength; E = steel elastic modulus; E_h = steel hardening modulus assuming a bilinear stress–strain response; τ_E = bond strength for elastic steel; τ_Y = bond strength for yielded steel; A_b = nominal bar area; and d_b = nominal bar diameter. l_e and l_y define, respectively, the lengths along the reinforcing bar for which steel stress is less than and greater than the yield stress. For the case of $l_e + l_y$ greater than the width of the joint, the deterioration of bond strength under cyclic loading will be much more severe. In this case, it may be appropriate to assume reduced bond strength in the elastic region of the reinforcing bar.

Average bond strength values for regions where the reinforcing bar is elastic are computed using the empirically defined maximum bond strength for elastic reinforcement and the assumption that zero to maximum bond strength is developed along the elastic length. This results in average bond strength equal to 71% of the maximum bond strength. Average bond strength values for regions where the reinforcing bar has yielded are defined equal to the observed maximum bond strength value for yielded reinforcement (Table 8.1).

Table 8.1: Average Bond Strengths as a Function of Steel Stress State.

Bar Stress, f_s (f_y = tensile yield strength)	Average bond strength Mpa (f_c in Mpa)
Tension, $f_s < f_y$	$\tau_{ET} = 1.8\sqrt{f_c}$
Tension, $f_s > f_y$	$\tau_{YT} = 0.4\sqrt{f_c}$ *to* $0.05\sqrt{f_c}$
Compression, $-f_s < f_y$	$\tau_{EC} = 2.2\sqrt{f_c}$
Compression, $-f_s > f_y$	$\tau_{YC} = 3.6\sqrt{f_c}$

Extension of the monotonic bar-stress versus -slip history for the case of reversed-cyclic loading required calibration of the unload–reload path and the hysteretic damage rules. Observed response was simulated using the one-dimensional material model Fig. 8.22 with model parameters defined as follows:

- unloading stiffness: assumed equal to the elastic stiffness;
- residual bar stress: computed assuming that a uniform residual bond stress of $0.15\sqrt{f_c}$ in MPa;
- slip at which reloading occurs as a fraction of maximum historic slip: defined to be 0.25;
- force at which reloading occurs as a fraction of the force developed at the maximum historic slip: defined to be 0.25;

- displacement damage rule: $\alpha 1$=0.6, $\alpha 2$=0.0, $\alpha 3$=0.2, $\alpha 4$=0.0, $\alpha 5$=10, and limit=0.25;
- stiffness damage rule: $\alpha 1$=0.3, $\alpha 2$=0.0, $\alpha 3$=0.1, $\alpha 4$=0.0, $\alpha 5$=10, and limit=0.40;
- strength damage rule: limit=0.0.

Development of the bar-slip spring constitutive model is completed by definition of the relationship between the bar stress and spring force. The tensile and compressive spring forces equilibrate the axial and flexural loads carried by the beams and columns framing into the joint. The bar stress defines the load carried by the framing-member longitudinal reinforcement that is transferred into the joint through bond. For the case of a tensile spring force, it is appropriate to assume that all of the spring force is carried by the reinforcing steel and transferred into the joint through bond. However, for the case of a compressive spring force, load is distributed between concrete and reinforcing steel. Thus, only a fraction of the total spring force is transferred into the joint through bond, and only a fraction of the total spring force contributes to anchorage-zone damage.

To define the spring-force versus bar-stress relationship for the case of compressive load, the fraction of the frame-member cross section compression resultant force carried by the reinforcing steel for loading at nominal flexural strength is assumed valid for all load levels. The recommendations of ACI Committee 318 (2005) were used as a basis for defining the stress distribution at the joint perimeter of the joint. Using this model, the concrete compression resultant, C_c , and steel compression resultant, C_s' , are defined as follows:

$$C_c = 0.85 \cdot f_c' \beta \cdot c \cdot w \,, \tag{8.49}$$

$$C_s' = f_s' A_s' = 0.003 \frac{c - d'}{c} E_s A_s' \,, \tag{8.50}$$

where f_c'=nominal concrete compressive strength; β=scale factor to account for the use of a uniform concrete compressive stress distribution in place of the true stress distribution; c=neutral axis depth; w=width of the frame member; d'=depth to centroid of the compression reinforcement; E_s=reinforcing steel elastic modulus; and A_s'=area of reinforcing steel carrying compression. Assuming that the centroid of the total compression force is defined by the concrete–stress distribution, the compressive spring force, C, is defined as a function of the compressive bar stress:

$$C = C_s' + C_c = f_s' A_s' \left(1 + \frac{0.85 \cdot f_c' \cdot d \cdot w}{E_s \cdot A_s'} \cdot \frac{2(1-j)}{0.003 \cdot \beta \left(1 - \frac{d'}{d} \frac{\beta}{2(1-j)} \right)} \right) \tag{8.51}$$

where d=depth to the tension reinforcement and $j \cdot d$ =distance between tension and compression resultants acting on the cross section. Typically, in designing reinforced concrete sections, j is assumed to be constant with j=0.85 for beams and j=0.75 for columns. Employing these assumptions, a constant-value relationship between compressive bar stress and compressive spring force is obtained from Eqn. (8.51).

Following studies provided by Mitra & Lowes (2007) suggested ways to modify the joint model to improve prediction of response for joints with a wide range of design parameters. These recommendations resulted in three major modifications to the originally proposed model:

- a new joint element formulation was proposed in which bar slip springs are located at the centroid of beam and column flexural tension and compression zones rather than at the perimeter of the joint. This improves simulation of bar-slip spring force demands;
- a new model was proposed for calibration of the joint-panel component. This model assumes a diagonal compression strut mechanism for load transfer within the joint (Paulay et al., 1978) rather than a uniform shear stress field, as is the case for the MCFT-based model proposed by Lowes & Altoontash (2003). The new model simulates strength loss resulting from cyclic loading as well as anchorage-zone damage;
- a new bar-slip response model was proposed. This new model combines hysteretic strength-loss with a response model that does not exhibit negative stiffness prior to reinforcing steel reaching ultimate strength. This eliminates numerical instability problems that resulted from the softening model proposed by Lowes & Altoontash (2003). Additionally, the new bond-slip model modifies the unload-reload model to provide accurate simulation of frictional resistance for bars loaded in tension and compression.

Further details about the models can be through in the original works of the authors (Lowes & Altoontash, 2003 and Mitra & Lowes, 2007).

8.1.5 The Model by Trowland (2003)

In the model by Trowland (2003) the end of the top column is rigidly connected to the bottom column. The beam is connected to the column through a rotational spring being continuous through the joint. This particular configuration allows transferring the action from the column to the beam only through the spring. The axial load is controlled by an axial spring.

The springs are considered zero-length elements and the effective dimensional of the joint panel are modelled by using rigid links.

Beam and column are modelled with elastic elements, while the nonlinear behaviour is concentrated at the ends in the plastic hinge regions which length is evaluated as follows (Paulay & Priestley, 1992):

$$L_p = 0.08\frac{L}{2} + 0.22 \cdot f_{yl} \cdot d_{bl} \ . \tag{8.52}$$

The behaviour under monotonic loading was defined with a moment-curvature sectional analysis.

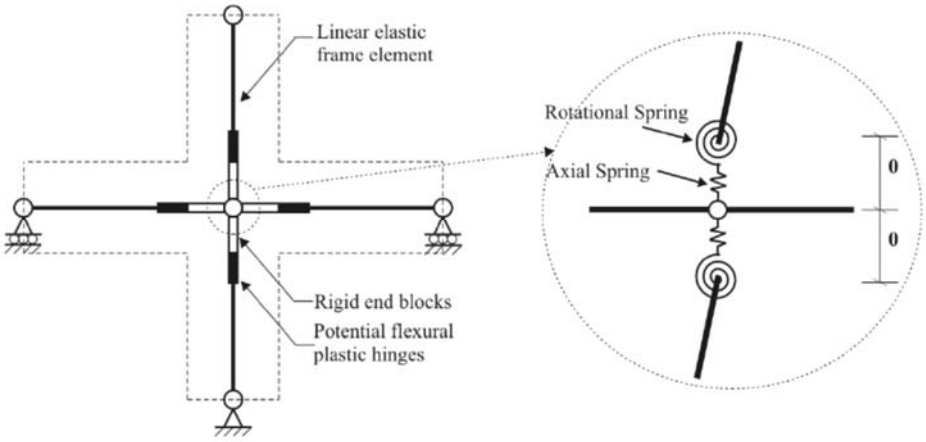

Fig. 8.24: Joint model developed by Trowland (2003).

The elastic stiffness is the secant stiffness with the yielding point. The cyclic behaviour is described by the hysteretic curve of Takeda (Takeda et al., 1970)

The elastic stiffness of the rotational spring of the joint is evaluated as follows:

$$K = G\left(\frac{0.9 \cdot d_b \cdot H}{H - 0.9 \cdot d_b}\right) A_c \tag{8.53}$$

where G is the elastic shear modulus of the concrete, A_c is the cross section of the column, H is the interstory height and d_b is the beam depth.

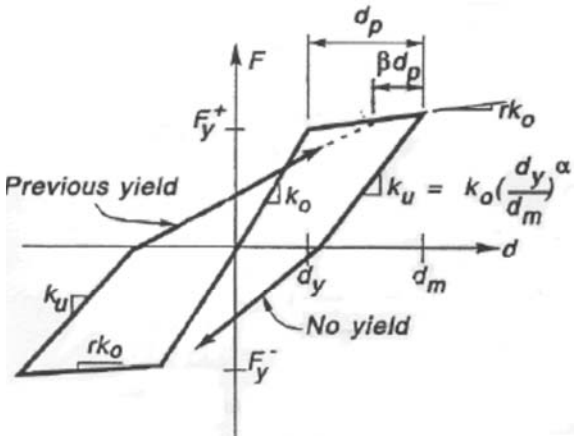

Fig. 8.25: Hysteretic behaviour of Takeda et al. (1970).

The axial stiffness of the translational springs is considered equal to the axial stiffness of the column:

$$K = \frac{E \cdot A_c}{L} \tag{8.54}$$

in which E=elastic modulus of concrete, A_c=cross section of the column and L=half height of the joint panel.

8.1.6 The Model by Shin & LaFave (2004)

The model consists of four rigid frames to represent the joint panel and one rotational spring located on one of four hinges; other two rotational springs are located in series between the beam and the joint to represent bar slip and inelastic rotation.

The authors (Shin & LaFave, 2004) tested four RC edge beam-column-slab connection subassemblies subjected to simulated lateral loading; hysteretic joint shear behaviour was investigated based on these tests and other laboratory tests reported in the literature. An analytical scheme employing the modified

compression field theory (MCFT) was proposed to approximate joint shear stress vs. joint shear strain curves and was verified based on the experimental investigations.

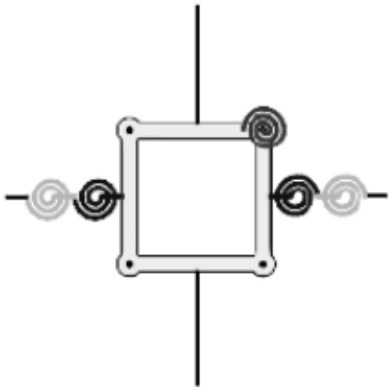

Fig. 8.26: Joint model by Shin & LaFave (2004).

The joint shear failure mechanism is described in terms of physical phenomena such as concrete damage and reinforcement yielding.

Fig. 8.27 plots the envelope τ_j–γ curve for specimens SL2 constructed by the authors (Shin & LaFave, 2004) by connecting the peak drift point of each cycle.

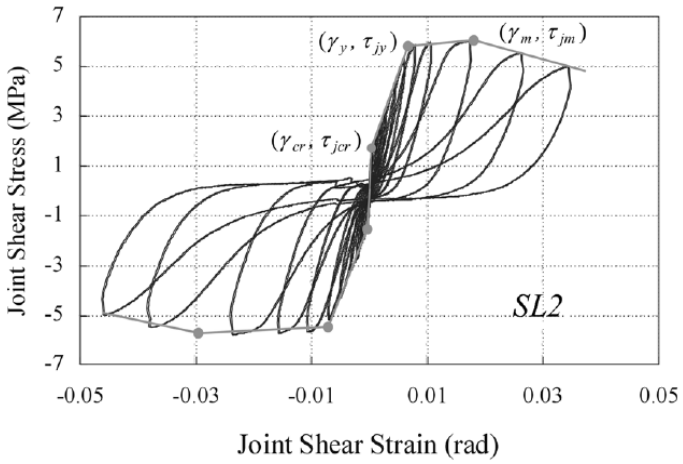

Fig. 8.27: Simplified envelope joint shear stress vs. strain relationship.

The envelope is simplified (for use in analysis) as four linear segments, starting from the origin and connecting three key points, so-called as joint shear

cracking (γ_{cr}, τ_{jcr}), reinforcement yielding (γ_y, τ_{jy}), and joint shear strength (γ_m, τ_{jm}). After the point of joint shear strength, the envelope curves typically show gradually descending inclination; this part of the envelope curve can be represented by a straight line with a modest negative slope. In the case of joint shear failure after beam hinging, the second key point has been found to correspond to longitudinal beam bar yielding (Shin & LaFave, 2004). In the case of joint shear failure without prior beam hinging, the joint reinforcement typically yields near the second key point (joint shear failure is defined as a condition wherein a joint cannot resist higher joint shear stress; this condition occurs at the third key point, joint shear strength).

The joint shear stress at shear crack initiation, τ_{jcr}, varied widely with concrete strength and column axial load, and the γ_{cr} value was typically very small (on the order of 0.0005 radians); τ_{jcr} and γ_{cr} values are not included in the table due to lack of consistent data. The γ_y values ranged from 0.002 to 0.010 radians, and γ_m was typically between 0.01 and 0.03 radians. (For most of the specimens, 0.01 radians of joint shear deformation alone would produce nearly 1% story drift.) The τ_{jy} values were approximately equal to 90% of τ_{jm} (the joint shear stress when the joint shear strength had been reached). The average of the τ_{jm} values, when normalized by the square root of the concrete compressive strength, was about $1.85\sqrt{f_c}$ [MPa] in J-type failure mode specimens, while it was about 20% less in BJ-type failure mode specimens. After the point of joint shear strength (γ_m, τ_{jm}), the envelope $\tau_j - \gamma$ curves typically became flat or showed slightly descending inclination; the slope of this part (called the "post-peak slope") ranged from zero (horizontal) on up to about half of the average (secant) ascending slope from the origin to the point of joint shear strength; the average descending slope was about 15% of the secant ascending slope. The largest joint shear deformations were typically about 0.03 to 0.05 radians.

Some researchers (Fujii & Morita, 1991 and Teraoka & Fujii 2000) have proposed fixed values (0.005 and 0.028 radians; 0.004 and 0.01 radians, respectively) for the joint shear strains corresponding to the "reinforcement yielding" and "joint shear strength" points. However, using fixed values for the key strain points, regardless of joint details, is not reasonable in light of the above observations; therefore, a rational approach to estimate the envelope $\tau_j - \gamma$ curve of any given joint is preferred.

As a general solution scheme, the key point ordinates of an RC beam-column connection envelope $\tau_j - \gamma$ curve can be approximately obtained by employing the modified compression field theory (MCFT) developed by Vecchio & Collins

(1986). An RC joint core is considered as a two-dimensional (2-D) concrete panel element with uniformly distributed orthogonal reinforcement; the joint transverse reinforcement and the longitudinal column bars are regarded as the distributed horizontal and vertical reinforcement, respectively. Presuming that the middle region of a joint (away from the longitudinal beam bars) limits joint shear strength and controls the joint shear failure mechanism, the volumetric steel ratio of horizontal reinforcement (ρ_x) was taken as the total cross-sectional area of joint transverse reinforcement in a layer divided by the product of vertical spacing and column width. The volumetric steel ratio of vertical reinforcement (ρ_y), which was taken as the total cross-sectional area of longitudinal column bars divided by the product of column width and column depth, was typically two to five times larger than that of horizontal reinforcement, so the analytical joint shear behaviour was governed by the horizontal reinforcement in most cases.

Fig. 8.28 explains the equilibrium equations, compatibility conditions, and material constitutive laws used for the analyses (note that "v_{xy}" is the average shear stress, equivalent to τ_j). In keeping with the MCFT, it is assumed that:

1. principal stress directions in the concrete coincide with principal strain directions;
2. average concrete strain in the direction of reinforcement is equal to average reinforcement strain;
3. reinforcing steel does not resist shear (dowel action is neglected).

Additionally, to simplify the analysis process, a joint core is assumed to be under uniform in-plane stress along each of the joint boundaries, as proposed by Vecchio & Collins (1988) who applied the MCFT for predicting the response of RC beams; actual stress conditions in a joint will vary locally at each particular loading stage (because every joint boundary is actually under coupled compressive and tensile forces transmitted from the top and bottom (or left and right) of each beam (or column)). Then, the monotonic joint shear stress (τ_j) vs. strain (γ) relationship may be acquired for a given set of average normal (axial) stresses at the joint boundaries.

Concrete cracking starts when the principal tensile stress in the joint concrete (f_{c1}) reaches its proportional limit with respect to the principal tensile strain (ε_1):

$$f_{c1} = \begin{cases} E_c \cdot \varepsilon_1 & \left(\varepsilon_1 \le \varepsilon_{cr}\right) \\ \dfrac{\alpha_1 \cdot \alpha_2 \cdot f_{cr}}{1+\sqrt{500 \cdot \varepsilon_1}} & \left(\varepsilon_1 > \varepsilon_{cr}\right) \end{cases}. \tag{8.55}$$

Here, E_c is the modulus of elasticity of concrete (initial tangent stiffness equal to $2f_c'/\varepsilon_o$); ε_o is the strain in concrete corresponding to the concrete compressive strength (f_c) from a standard cylinder test; f_{cr} is the concrete (tensile) cracking stress, taken as 0.5 times the square root of f_c' (in MPa); ε_{cr} is the concrete cracking strain computed by f_{cr}/E_c; and α_1 and α_2 are factors accounting for bond characteristics of the reinforcement and type of loading, respectively.

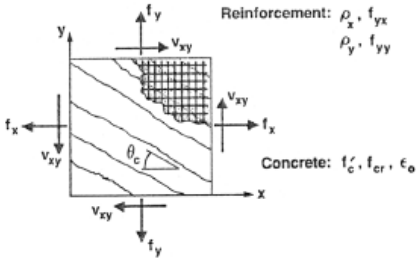

(a) Cracked reinforced concrete element

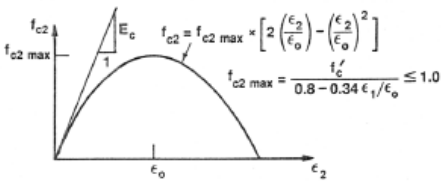

(d) Concrete in principal compressive direction

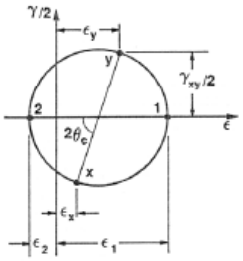

(b) Mohr's circle of average strains

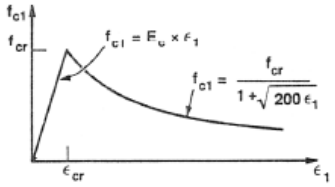

(e) Concrete in principal tensile direction

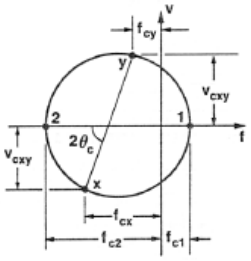

(c) Mohr's circle of average concrete stresses

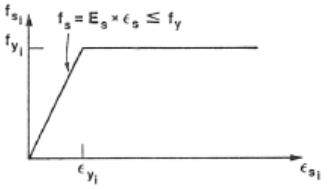

(f) Reinforcing steel

Fig. 8.28: Modified compression field theory proposed by Vecchio & Collins (1986).

As joint boundary stresses get higher, the compressive strength of joint concrete (f_{c2max}) decays with increasing principal tensile strain (ε_1) in the transverse direction:

$$f_{c2\max} = \frac{f_c'}{0.8 - 0.34 \cdot \varepsilon_1 / \varepsilon_o} \le f_c' . \tag{8.56}$$

The analysis stops when the principal compressive stress in concrete (f_{c2}) exceeds the reduced concrete compressive strength (f_{c2max}); in other words, the analysis cannot compute further joint shear response after the joint concrete reaches compression failure.

As mentioned earlier, the MCFT cannot compute further joint shear response after the joint concrete reaches compression failure. Thus, this part of the analytical joint shear stress vs. strain curve is assumed to be a straight line with a negative slope equal to 5% of the secant ascending slope up to the joint shear strength point; this line forms the fourth segment of the quad-linear analytical envelope curve, as plotted in Fig. 8.27.

The hysteretic joint shear behaviour consists of a monotonic (envelope) joint shear response analytically computed by the MCFT, and hysteretic properties calibrated based on experimental data. It is further assumed that all inelastic beam and column deformations occur in the vicinity of beam/joint or column/joint interfaces.

Fig. 8.29 illustrates the computer model for a typical cruciform RC beam-column connection subassembly subjected to lateral loading developed by Shin & LaFave (2004). The joint is represented by four rigid link elements located along the joint edges and three nonlinear rotational springs embedded in one of the four hinges connecting adjacent rigid elements. Three such springs connected in parallel are used to represent hysteretic joint shear behaviour. The hysteretic joint shear force (V_j) vs. strain (γ) curve is first determined from a hysteretic $\tau_j - \gamma$ curve described by the analytically computed and simplified (quad-linear) envelope; V_j is calculated by multiplying the joint shear stress (τ_j) by the product of column depth and effective joint width (average of the beam and column widths). Then the hysteretic moment (M_s) vs. rotation (θ_s) curve to be expressed by the combination of the three joint springs is acquired from the joint shear force (V_j) vs. strain (γ) curve by:

$$\begin{aligned} \theta_s &= \gamma , \\ M_s &= V_j \cdot jd . \end{aligned} \tag{8.57}$$

Here, *jd* is assumed to be the average of positive and negative beam moment arms at beam/joint interfaces.

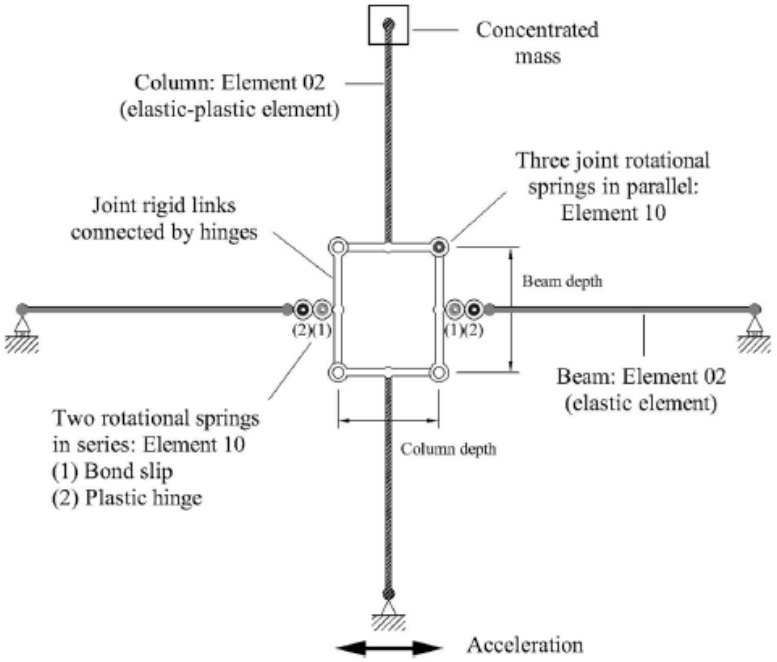

Fig. 8.29: Model by Shin & LaFave (2004) for a beam-column connection subassembly.

Fig. 8.30 illustrates the way the three joint springs (each with a bilinear envelope) combine to express a quad-linear envelope $M_s - \theta_s$ curve. Two of the springs are elastic and then perfectly plastic, while the third spring has a negative second slope equal to that of the fourth linear segment in the quad-linear envelope $M_s - \theta_s$ curve.

Outside of the joint itself, each beam is modelled using an elastic part and two nonlinear rotational springs located at the beam/joint interface; the three elements are connected in series. One of the nonlinear rotational springs represents fixed end rotations arising at the beam/joint interface due to bond slip and yielding of longitudinal beam bars in the joint, while the other represents plastic hinge rotations near the end of the beam. The vertical position of the beam elements and the horizontal position of the column elements are simply located at the beam mid-depth and the column mid-depth, respectively. This beam model is similar to one proposed by Filippou et al.

(1999), which consisted of three sub-elements (elastic, spread plastic, and interface bond-slip) connected in series. However, Filippou et al. (1999) did not address hysteretic joint shear behaviour, assuming that joints could be designed and detailed in order that joint shear deformations would remain small.

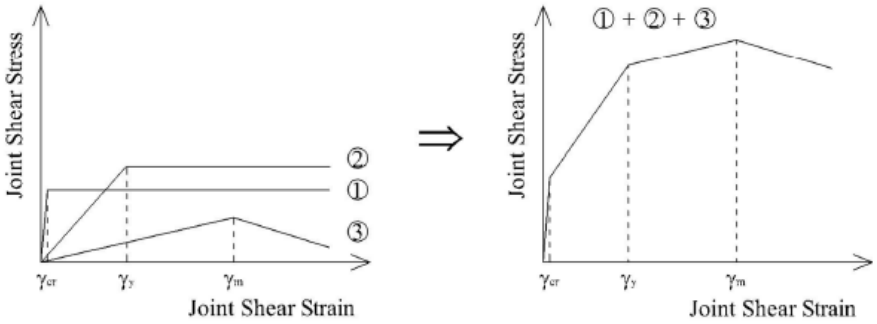

Fig. 8.30: Combination of three bilinear joint springs in parallel.

The necessary input parameters are initial stiffness (k_1), strain-hardening ratio (k_2/k_1), positive and negative yield moments (M_y^+ and M_y^-), strength degradation factor, and positive and negative pinching moments (M_g^+ and M_g^-), as illustrated in Fig. 8.31. The strength degradation factor is defined as the ratio of the second to the first cycle moment at the maximum rotation reached during the first cycle, for two consecutive loading cycles (for example, the ratio between moments at the points labelled as "9" and "2" in Fig. 8.31). The positive and negative pinching moments determine the extent of pinching in the middle part of each hysteretic loop, by designating the direction of reloading branches in conjunction with the maximum rotations reached during the previous cycle (for example, the negative pinching moment in Fig. 8.31 specifies the slope of the line connecting the points labelled as "3" and "4"). The extent of stiffness degradation during reloading is necessarily determined from assigning pinching moments, while stiffness during unloading is kept as a constant value equal to the initial stiffness (k_1).

All input parameters for the three joint rotational springs, except the strength degradation factors and the M_g^+ and M_g^- values, are determined from the quad-linear envelope $M_s - \theta_s$ curve, with k_2/k_1 values for the first two springs set to zero (see Fig. 8.30). For the two elastic and perfectly plastic springs, the strength degradation factor is specified as 0.95 and the pinching moments are assumed as one-fifth of the yielding moments of each spring, while neither strength degradation nor pinching is considered for the third spring (with a negative

k_2/k_1 value); values for these two parameters have been approximately determined from investigating the test results of the specimens.

The positive and negative input values for each joint spring are identical because the $\tau_j - \gamma$ curves are assumed symmetric for positive and negative loading.

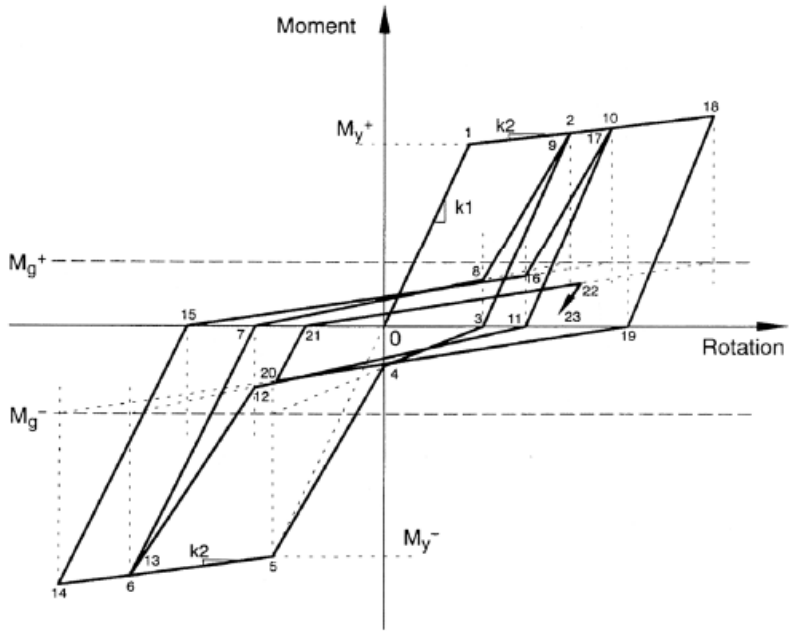

Fig. 8.31: Hysteretic behaviour of the joint model.

Input parameters for the bond slip rotational spring are determined according to the formulation proposed by Morita & Kaku (1984), with some modifications. Fig. 8.32 illustrates the assumed stress and strain distributions of a longitudinal beam reinforcing bar (after yielding) in an interior joint. These and additional assumptions used to compute the moment vs. rotation relation of the bond slip spring can be summarized as follows:

- the tensile stress distribution in a longitudinal beam bar along the column depth is linear before yielding and bilinear after yielding (zero at the location where the bar begins to slip, and maximum at the beam/joint interface);
- the bond stress in the joint is uniformly distributed, and its magnitude is proportional to the reinforcing bar tensile strain at the beam/joint interface (ε_{sl});

- the amount of beam bar pull-out slip at the beam/joint interface is computed by integrating beam bar strains from where bond slip starts to the interface. For interior joints, L_y (the length within which beam bar yielding occurs in the joint) is limited to the column depth, and the sum of L_s and L_y (the distance from where bond slip starts to the interface) is limited to L_{cs} (the column depth plus half the beam depth);
- rotations are estimated by the amount of pull-out slip divided by the distance between top and bottom beam bars, neglecting the push-in of reinforcing bars in compression;
- the moment-rotation curve of the bond slip spring is assumed bi-linear (two lines meeting at the point of beam reinforcement yielding), even though the post-yield part of the curve is actually nonlinear because the amount of pull-out slip after yielding depends on the maximum-to-yield stress ratio;
- the pinching moments (M_g) for the bond slip spring are determined as a function of the length of the bond slip region (L_s). For most specimens, with column depth to beam bar diameter ratios greater than about 15, this resulted in no pinching of the bond slip spring. Strength degradation is not considered in the bond slip spring.

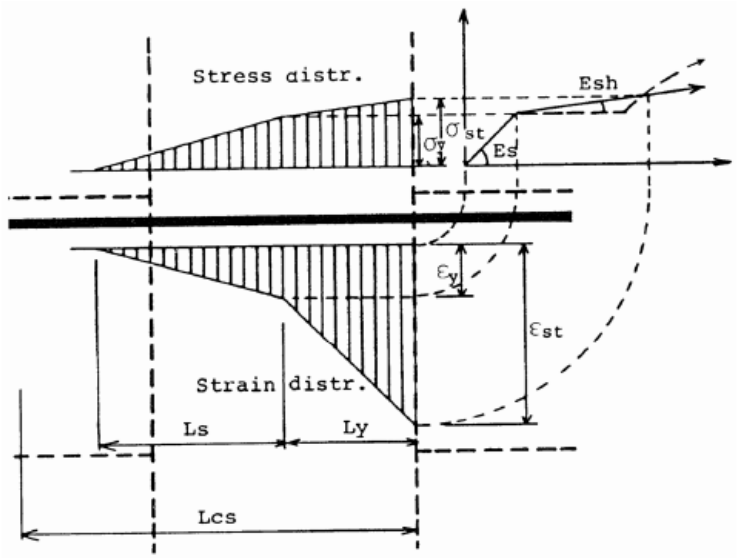

Fig. 8.32: Stress and strain distributions (after yielding) assumed by Morita & Kaku (1984).

Modifying Morita & Kaku (1984), the yield moments of the bond slip spring are taken equal to the yield moments of the plastic hinge spring in this study; the stiffness of the bond slip spring is computed with beam reinforcement only.

8.2 Preliminary Simulation of the Cyclic Behaviour of Joints

As a preliminary study about the simulation of nonlinear behaviour of beam-to-column joints, two selected samples from the database (one exterior and one interior) have been analysed with suitable modelling software that allows to perform nonlinear structural analyses.

A Static Time-History Analysis has been carried out, where in addition to the permanent gravitational loads a history load has been applied at the end of the beam or column depending on type of test layout (section 4.3). The user defines the Time-History curve (loaded from a text file .txt) and the corresponding curve multiplier (scale factor).

The software used for this preliminary analysis is SeismoStruct 5.0.4. SeismoStruct is a software for calculating the structural finite elements to predict the static and dynamic behaviour of plane and three-dimensional frames subjected to large displacements considering both the effects of geometric and mechanical non-linearity.

A distributed plasticity model, the so-called "fiber approach" has been used for modelling nonlinear behaviour of RC frames. The fiber model estimates results with a great accuracy, but requires more computational costs compared to a concentrated plasticity model.

8.2.1 Simulation of the Model by Biddha & Ghobarah (1999)

The comparison between analytical and experimental non-linear behaviour of the joints is provided by applying the model by Biddah & Ghobarah (1999), which simulates the shear deformation of the panel and the bond-slip through a rotational zero-length spring.

The hysteretic behaviour, with pinching effect, is given by the definition of a trilinear asymmetric law assigned to the rotational spring. The trilinear curve adopted, shown in Fig. 8.33, requires 10 parameters for it complete definition:

- the initial positive stiffness (K_0^+);
- the displacement at the end of the elastic positive range (d_1^+);
- the stiffness of the second positive branch (K_1^+);

- the displacement corresponding to the end of the second positive branch (d_2^+);
- the stiffness of the third positive branch (K_2^+);
- the initial negative stiffness (K_0^-);
- the displacement at the end of the elastic negative range (d_1^-);
- the stiffness of the second negative branch (K_1^-);
- the displacement corresponding to the end of the second negative branch (d_2^-);
- the stiffness of the third negative branch (K_2^-).

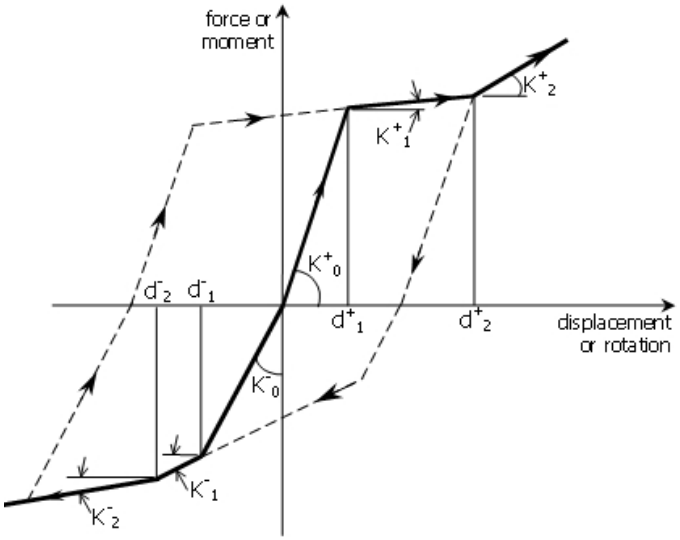

Fig. 8.33: Trilinear asymmetric curve available in SeismoStruct.

In the following, the comparison between the experimental and simulated behaviour of two specimens is carried out; in particular the test O4 provided by Hakuto et al. (2000) and the test JC-2 by Chun & Kim (2004) have been selected to represent interior and exterior joints, respectively.

8.2.2 Simulation of Interior Joint

Fig. 8.34 shows the geometrical characteristics of the analysed specimen for interior joint, while Fig. 8.35 reports the cyclic load-displacement curve.

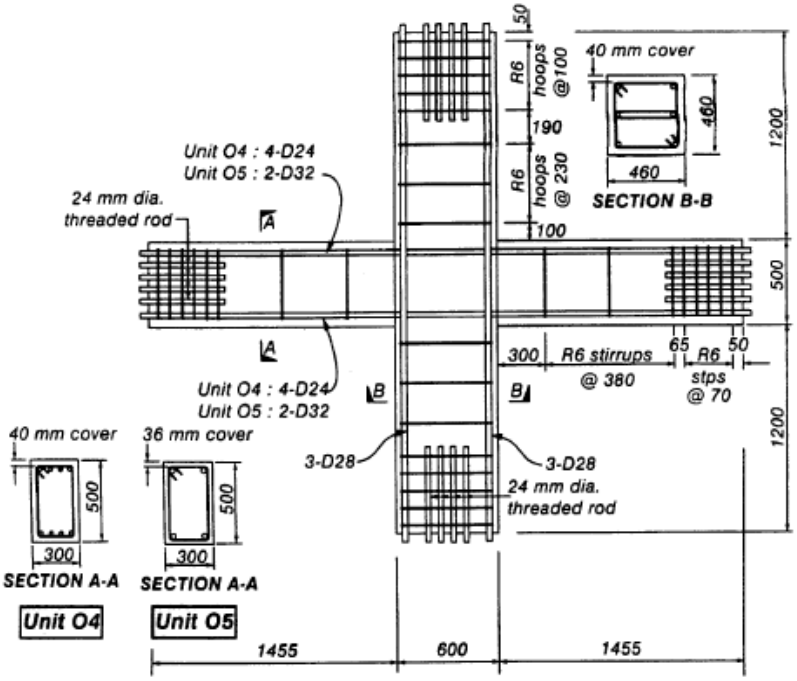

Fig. 8.34: Details of specimens O4 and O5 provided by Hakuto et al. (2000).

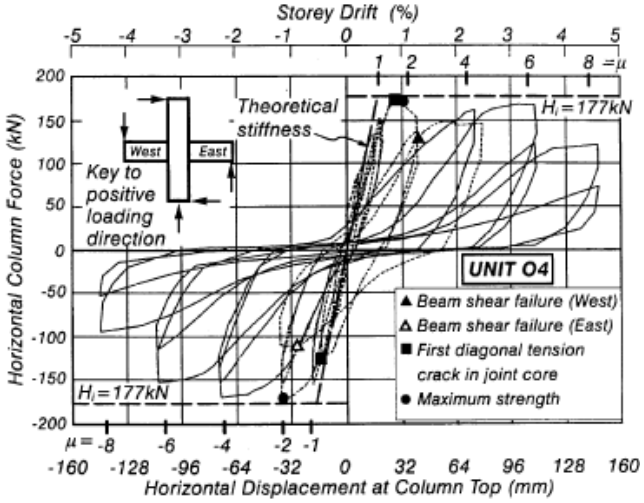

Fig. 8.35: Cyclic response of the specimens O4.

Table 8.2 reports the main geometric and mechanical characteristics of the analysed specimen needed for calibrating the parameters affecting the hysteretic response.

Table 8.2: Geometric and mechanical characteristics of the specimen O4.

COLUMN					
b_c [mm]	h_c [mm]	$L_{col,inf}$ [mm]	$L_{col,sup}$ [mm]	$A'_{s,c}$ [mm^2]	$A_{s,c}$ [mm^2]
460	460	1600	1600	1847	1847

BEAM								
b_b [mm]	h_b [mm]	L_b [mm]	$n_{bars,inf}$	$n_{bars,sup}$	$\phi_{sup,b}$ [mm]	$\phi_{inf,b}$ [mm]	$A_{s,b,inf}$ [mm^2]	$A_{s,b,sup}$ [mm^2]
300	500	1905	4	4	24	24	1810	1810

MECHANICAL PROPERTIES								
COLUMN		BEAM			JOINT		E_s [MPa]	E_c [MPa]
$f_{y,col}$ [MPa]	f'_c [MPa]	$f_{y,b}$ [MPa]	λ_0 [-]	f'_c [MPa]	$f_{y,j}$ MPa]	f'_c MPa]		
321	53	308	1.25	53	339	53	210000	37846

The model of the interior joints developed in SeismoStruct is shown Fig. 8.36, while Table 8.3 reports the 10 parameters needed for defining the nonlinear behaviour of the joint and evaluated by applying the model by Biddha & Ghobarah (1999).

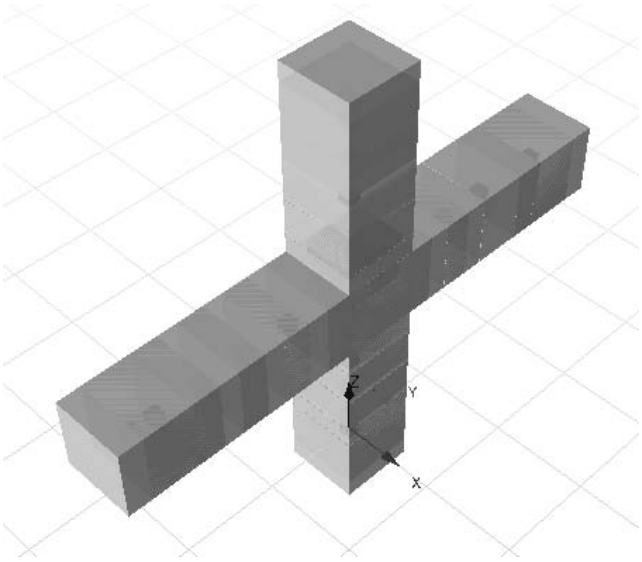

Fig. 8.36: Model of interior joint developed in SeismoStruct.

Table 8.3: Calibrated parameters of the hysteretic bond-slip curve.

K_1^- [kNm]	K_1^+ [kNm]	K_2^- [kNm]	K_2^+ [kNm]	K_3^- [kNm]	K_3^+ [kNm]
464771	464771	3129	3129	0.00	0.00
θ_y^- [rad]	θ_y^+ [rad]	θ_u^- [rad]	θ_u^+ [rad]		
0.00050	0.00050	0.091	0.091		

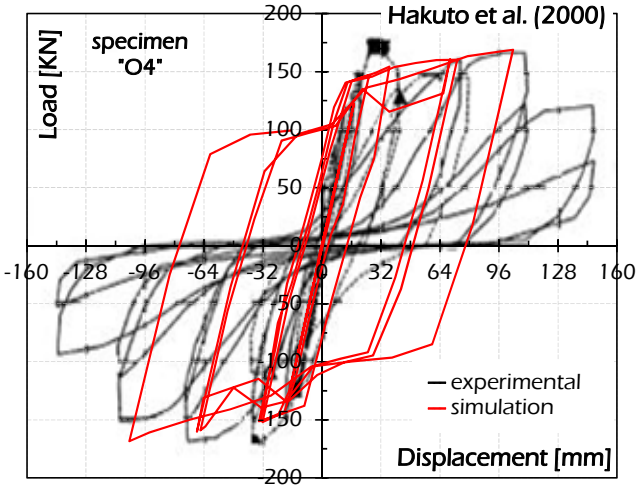

Fig. 8.37: Comparison between analytical and experimental cyclic behaviour for the specimen O4.

In Fig. 8.37 is shown the comparison between the analytical simulation and the experimental evidence. A good simulation is shown about the peak points in each loading cycle, but by the simulation in SeismoStruct does not result the pinching effect.

8.2.3 Simulation of Exterior Joint

In Fig. 8.38 are shown the geometric details, the cyclic loading and the cyclic response of the analysed specimen of Chun & Kim (2004) namely JC-2. In particular the loading history is characterised by three complete loading cycles for each step of load, while the cyclic response reports the relationship between the displacement and the applied load at the end of the beam.

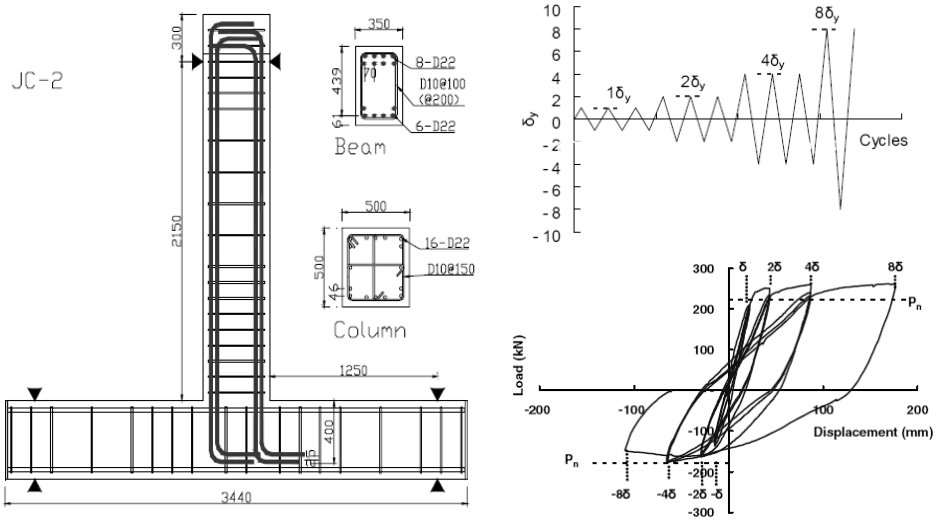

Fig. 8.38: Details of the specimen JC-2 provided by Chun & Kim (2004).

Table 8.4: Geometric and mechanical characteristics of the specimen JC-2.

COLUMN					
b_c [mm]	h_c [mm]	d'_c [mm]	L_c [mm]	$A'_{s,c}$ [mm^2]	$A_{s,c}$ [mm^2]
500	500	61	1500	1901	1901

BEAM								
b_b [mm]	h_b [mm]	L_b [mm]	$n_{bars,inf}$	$n_{bars,sup}$	$\phi_{sup,b}$ [mm]	$\phi_{inf,b}$ [mm]	$A_{s,b,inf}$ [mm^2]	$A_{s,b,sup}$ [mm^2]
350	500	2400	6	8	22	22	2281	3041

MECHANICAL PROPERTIES								
COLUMN		BEAM		JOINT				
$f_{y,col}$ [MPa]	f'_c [MPa]	$f_{y,b}$ [MPa]	λ_0 [-]	f'_c [MPa]	$f_{y,j}$ [MPa]	f'_c [MPa]	E_s [MPa]	E_c [MPa]
403	60	403	1.25	60	384	60	210000	39117

In Table 8.4 are reported the main geometric and mechanical characteristics of the specimen taken into account for providing the comparison between the simulated joint model and the experimental evidence.

Fig. 8.39 shows the model of the specimen JC-2 built in SeismoStruct.

Table 8.5 reports the parameters of the trilinear curve used for simulating the rotational spring modelling the hysteretic behaviour.

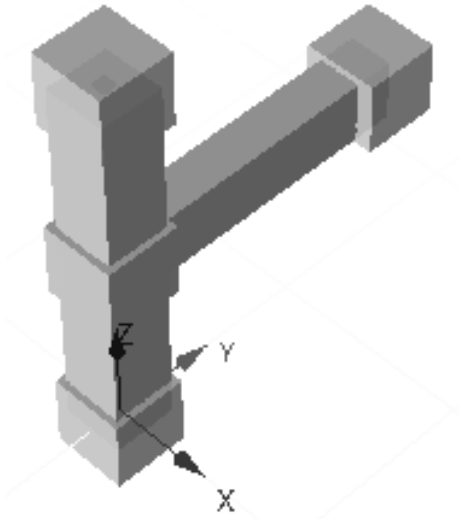

Fig. 8.39: Model of the exterior joint JC-2 built in SeismoStruct.

Table 8.5: Calibrated parameters of the hysteretic bond-slip curve for specimen JC-2.

K_1^- [kNm]	K_1^+ [kNm]	K_2^- [kNm]	K_2^+ [kNm]	K_3^- [kNm]	K_3^+ [kNm]
734962	551221	7133	5540	0.00	0.00
θ_y^- [rad]	θ_y^+ [rad]	θ_u^- [rad]	θ_u^+ [rad]		
0.00063	0.00063	0.021	0.048		

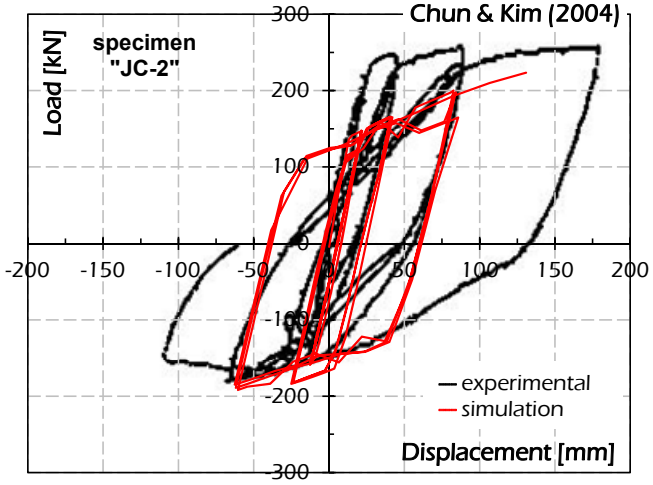

Fig. 8.40: Comparison between analytical simulation and experimental response of JC-2 specimen.

Finally, Fig. 8.40 shows the comparison between the analytical simulation and the experimental evidence resulting by the scientific literature. A good simulation is shown about the peak points in each loading cycle, but, as already observed for interior joints, by the simulation in SeismoStruct does not result the pinching effect.

8.3 Development and Assessment of a Hysteretic Nonlinear Model for Exterior Joints

The present section is mainly intended at calibrating a behavioural model that can be successfully and easily implemented in nonlinear static and dynamic analyses of existing multi-storey RC structures for investigating the influence of the finite stiffness and strength of joints on the global behaviour of structures.

The proposed response model has been implemented in the advanced program for nonlinear static and dynamic analysis of structures ADAPTIC (Izzuddin, 1991), which incorporates novel features for the nonlinear analysis of RC frames.

The sameness and accuracy of the proposed joint model are demonstrated through a comparison against experimental results of 12 RC exterior beam-to-column joints under cycling loads reported in the literature and mentioned in the following.

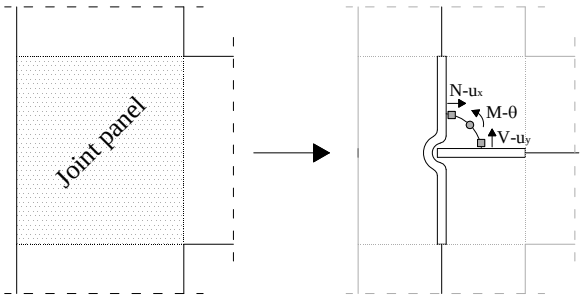

Fig. 8.41: Idealization of exterior joint element in frame analysis.

In the modelling of exterior joints, the strategy suggested in Favvata et al. (2008) is employed. The enhanced joint element can be considered as a spring element with zero length, it is defined by two nodes with the same coordinates, and is only influenced by the relative rotational displacements between the nodes. The moment transmitted by the element is the moment transferred from

the beam to the column. The entire seismic behaviour of the joint is described by the proposed joint model, and therefore rigid elements are adopted to simulate the portions of the beam and column inside the joint core area (Fig. 8.41).

The Pivot model (Dowel et al., 1998) is used for representing the nonlinear behaviour of the joint. Fig. 8.42 shows a nonlinear moment-rotation curve drawn according to this model.

The monotonic response is asymmetric; elastic and plastic moment $M_{yp(n)}$ and $M_{pp(n)}$ should be defined together with the Pivot Points which allow the determination of the stiffness degradation, caused by the damage evolution in the joint. Points P_{1p} and P_{1n} describe the linear-elastic branches of the moment-rotation relationship, while P_{2p} and P_{2n} control the unloading response. The position of the pivot points can be determined considering the elastic moments and the amplification parameters α_1 and α_2. Two moment values $\beta_1 M_{yn}$ and $\beta_2 M_{yp}$ are also defined for controlling the pinching effect in the cyclic response. Three stiffness values $K_{ep(n)}$, $K_{pp(n)}$ and $K_{hp(n)}$ characterize the monotonic laws in the elastic, plastic and hardening phase.

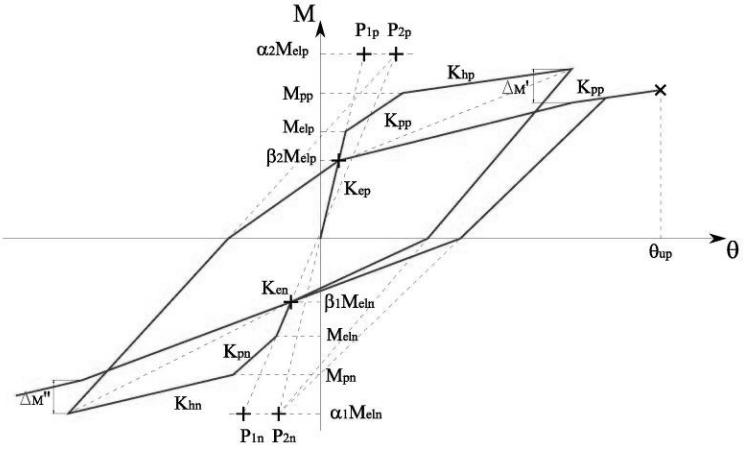

Fig. 8.42: Pivot Model.

Moreover, a multi-parametric strength degradation formulation is used for taking into account the reduction of the joint strength according to Eqn. (8.58):

$$\Delta M = M_y \cdot \gamma \left[1 - \left(1 - \left(\frac{E_\rho}{E_{um} + E_\rho} \right)^{\varepsilon} \right) \cdot \left(1 - \left(\frac{\theta_{max}}{\theta_{um}} \right)^{\delta} \right) \right] \quad , \tag{8.58}$$

where the coefficients γ, ε and δ are the strength, energy and displacement degradation parameters, E_p is the dissipated energy, E_{um} is the dissipated energy under monotonic loading, θ_{max} is the maximum rotation experienced by the joint in previous cycles, and θ_{um} is the ultimate rotation under monotonic loading.

When using the Pivot model for representing the nonlinear behaviour of the joint, strength and stiffness can be calculated employing specific analytical formulations, while the degradation parameters should be calibrated considering experimental data.

The authors (Dowel et al., 1998) provide various values, variable from 1,50 to 5,00 for α and 0,50 to 0,55 for β, to estimate the degradation parameter derived by specimen tests; furthermore two charts for circular reinforced concrete column are available for evaluating the degradation parameters depending by longitudinal steel ratio.

8.3.1 Joint Strength Model

The model proposed by Vollum & Newman (1999) has been used for evaluating the ultimate shear strength V_{jh} for the beam-to-column joints. This model is based on an empirical formulation calibrated against a large experimental database incorporating results of many tests reported in the technical literature. According to this model, the shear strength of the joint is determined considering two contributions, the shear strength of the concrete panel and the tensile strength of the stirrups inside the connection, as given by:

$$V_{jh} = V_{c,jh} + V_{s,jh} \,. \tag{8.59}$$

The concrete contribution $V_{c,jh}$ depends on the ultimate strength of the compressed strut which can be evaluated as follows:

$$V_{c,jh} = 0.642 \cdot \beta \cdot \left[1 + 0.555 \cdot \left(2 - {h_b}/{h_{col}}\right)\right] \cdot b_{eff} \cdot h_{col} \cdot \sqrt{f_c} \,, \tag{8.60}$$

where parameter β is assumed equal to 0.8, and h_b and h_{col} represent the depth of the beam and the column, respectively. The effective width b_{eff} is conventionally assumed as the average of the beam and column widths, while f_c is the compressive strength of concrete.

$$V_{s,jh} = A_{w,jh} \cdot f_{sy} \,. \tag{8.61}$$

The shear strength provided by any stirrups into the joint can be simply evaluated from the steel force at yielding, similar to Eqn. (8.61).

8.3.2 Joint Stiffness Model

The model proposed by Biddah & Ghobarah (1999) has been considered for determining the joint stiffness. As it is strongly affected by potential slip of rebars throughout the joint, the authors proposed an accurate model for relating the loss of stiffness to the bars slip (section 8.1.1). This model depends on several mechanical parameters such as the anchorage length L_{max}, the steel-to-concrete bond strength f_b, and the overstrength ratio λ of rebars, and it consists of two different formulations in the case of slip onset before or after yielding. In particular, if slip occurs before bar yielding, as the anchorage length L_{max} is smaller than the minimum anchorage length L_s resulting in rebars yielding, the initial elastic stiffness K_e and the yield moment M_y developed in the joint are given by:

$$K_1 = \frac{2 \cdot n \cdot A_s \cdot E_s \left(d - d'\right)^2}{L_{max}}, \tag{8.62}$$

$$M_y = n \cdot A_s \cdot f_{ys} \left(d - d'\right) \frac{L_{max}}{L_s}. \tag{8.63}$$

After bond slip the behaviour is perfectly plastic.

Conversely, when the bar yielding occurs before slippage, the stiffness K_e and the yield moment M_y are evaluated as follows:

$$K_1 = 1200 \cdot \pi \cdot n \cdot d_b \left(d - d'\right)^2 \sqrt{f_c}, \tag{8.64}$$

$$M_y = n \cdot A_s \cdot f_{ys} \left(d - d'\right). \tag{8.65}$$

After yielding, the stiffness K_p depends on the minimum anchorage length L_s, the maximum length $L_{y,max}$ of the yielded region and the ratio χ_2 between the ultimate and the yielding moment (see section 8.1.1).

8.3.3 The Experimental Database

The specimens reproduce exterior beam-to-column subassemblages, they have different characteristics and where tested under cyclic loads.

The selected database consists in 12 subassemblages simulating exterior joints tested by various authors from 1985 to 2004 (Table 8.6)

Table 8.6: Database for exterior beam-to-column joints under cyclic loading.

Authors (year)	Number of specimens	Name of specimens
Chun & Kim (2004)	2	JC-1
		JC-2
Hwang et al. (2004)	1	28-0T0
Chutarat & Aboutaha (2003)	2	1
		A
Clyde et al. (2000)	2	Test #4
		Test #5
Economou et al. (1998)	1	A5
Ehsani et al. (1987)	2	1
		2
Ehsani & Wight (1985)	2	1B
		2B

Fig. 8.43 shows the subassemblage used by Chun & Kim (2004) to test exterior beam-to-column joints in horizontal configuration (section 4.3).

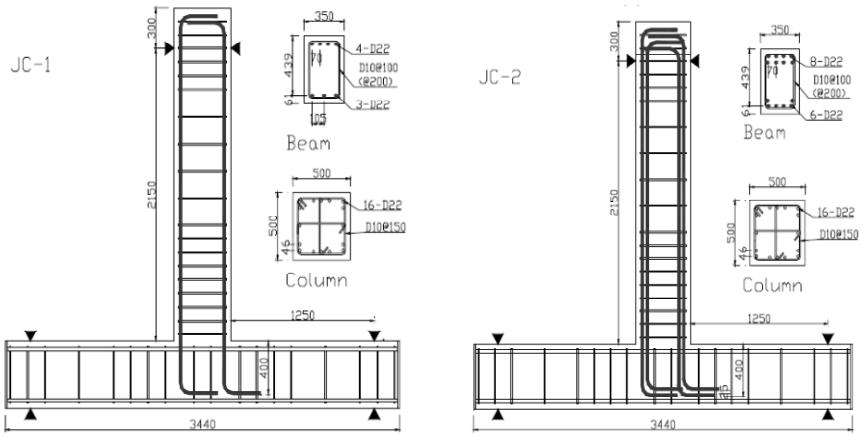

Fig. 8.43: Experimental tests provided by Chun & Kim (2004).

Fig. 8.44 shows the geometric characteristics of the specimen provided by Hwang et al. (2004), the loading history applied at the end of the beam in

displacement control and the picture representing the failure mode observed at the end of the test. The cracks shown demonstrate the joint failure achieved by the specimen.

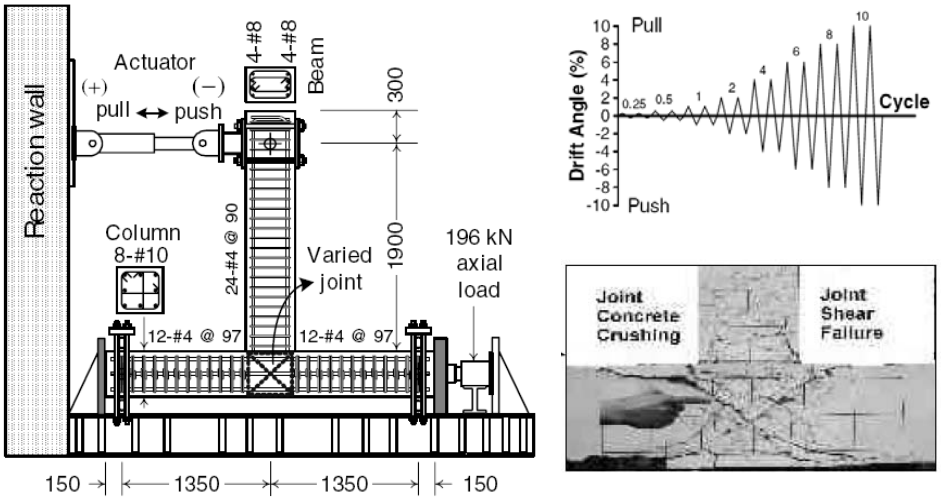

Fig. 8.44: Experimental test provided by Hwang et al. (2004)

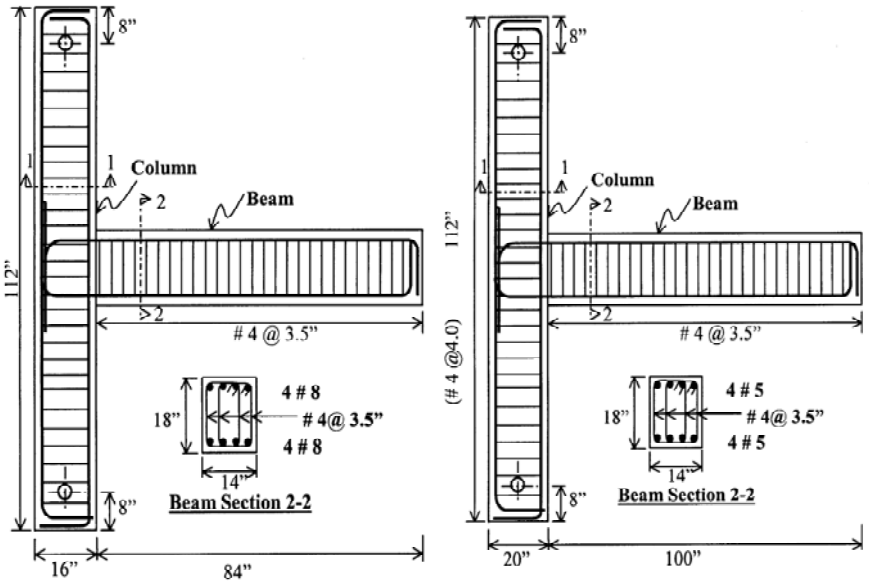

Fig. 8.45: Experimental tests provided by Chutarat & Aboutaha (2003): specimen 1 (on the left) and specimen namely A (on the right).

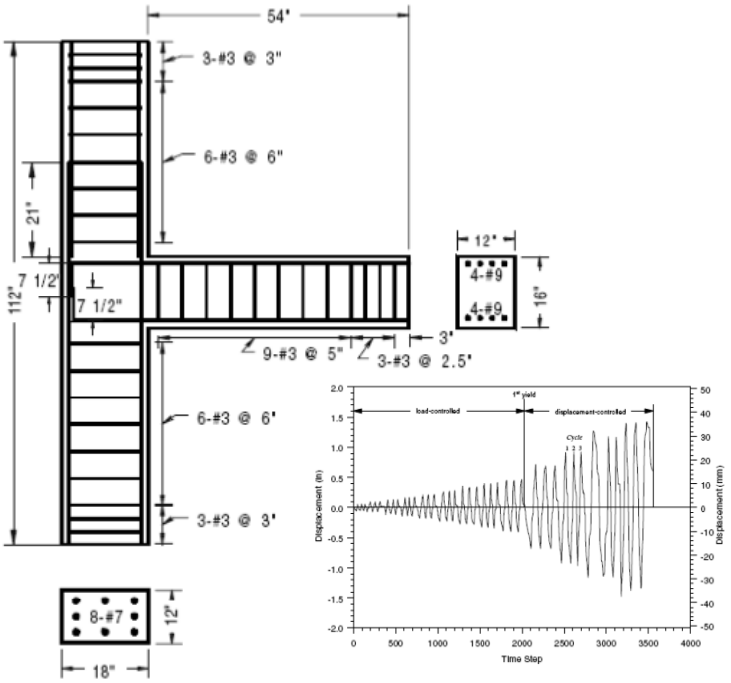

Fig. 8.46: Characteristics of the specimens provided by Clyde et al. (2000).

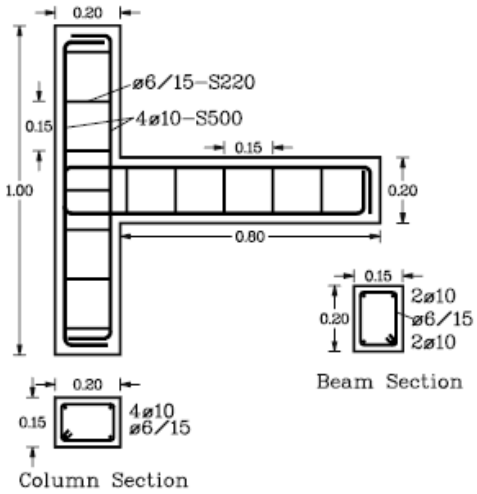

Fig. 8.47: Specimen provided by Economou et al. (1998).

Fig. 8.46 reports the geometric characteristics and the load history of the specimens namely 1 and A developed by Clyde et al. (2000); in this case the two specimens have the same dimensions and amount of reinforcement, while the concrete strength is different.

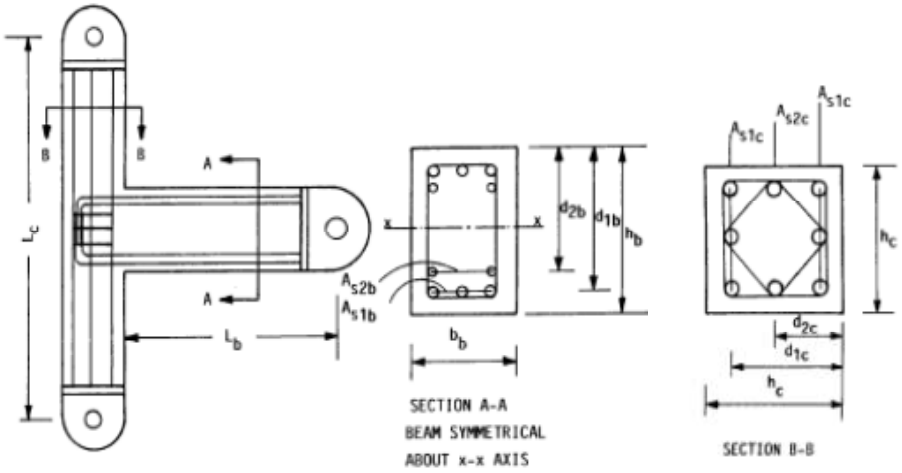

Fig. 8.48: Characteristics of the specimens provided by Ehsani et al. (1987).

The geometric characteristics of the two specimens provided by Ehsani et al. (1987) are shown in Fig. 8.48. In particular the specimens namely 1 and 2 by the authors (Ehsani et al., 1987) are characterised by the same geometric dimensions and material with different diameters of the bars in beam and column.

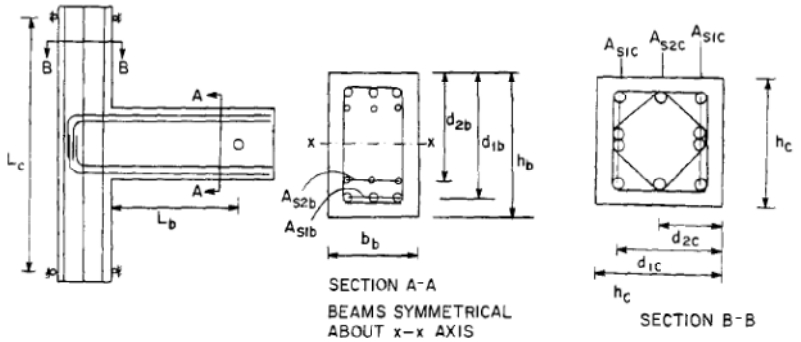

Fig. 8.49: Sketch of the specimens provided by Ehsani & Wigth (1985).

Designation	Specimen number 1B	2B
L_c, in.	84.0	84.0
h_c, in.	11.8	11.8
d_{1c}, in.	9.6	9.6
d_{2c}, in.	5.9	5.9
A_{s1c}*	3#6	4#6
A_{s2c}*	2#6	2#6
L_b, in.	60.0	60.0
h_b, in.	18.9	17.3
b_b, in.	10.2	10.2
d_{1b}, in.	16.9	15.4
d_{2b}, in.	15.0	13.4
A_{s1b}†	3#7	3#7
A_{s2b}†	3#6	3#6
Hoops‡	2	2
f'_c, psi	4870	5070

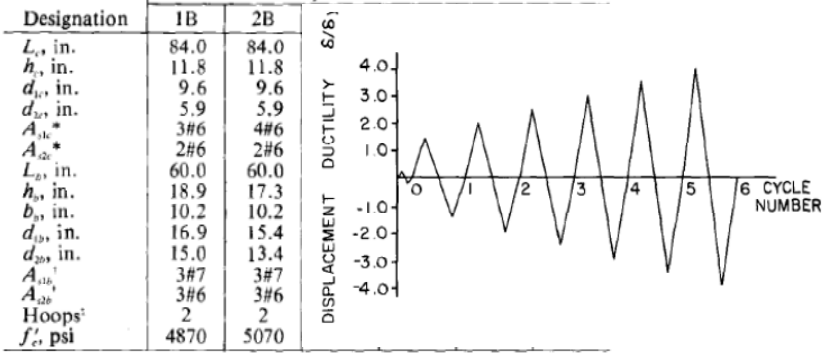

Note: 1 in. = 25.4 mm; 1 psi = 0.0069 MPa.
*Summary of column steel yield stress, in ksi; bar size #6 = 71.0, #8 = 60.0.
†Summary of beam steel yield stress, in ksi; bar size #6 = 50.0, #7 = 48.0.
‡Number of sets of #4 hoops in the joint with yield stress of 63.4 ksi.

Fig. 8.50: Characteristics of the specimens provided by Ehsani & Wigth (1985).

Finally, Fig. 8.49 and Fig. 8.50 show the geometric and mechanical characteristics and the loading history of the specimens namely 1B and 2B provided by Ehsani & Wight (1985).

Further details about the considered specimens are available in the original paper of the authors which references are reported in the special section of the present thesis.

8.3.4 Calibration of Model Parameters

The applications reported in the following are developed by using the scissor model shown in Fig. 8.41 to simulate the nonlinear behaviour of exterior joints; in particular the two degree of freedom restrained by the two translational springs are considered fixed and only the behaviour of the rotational spring is calibrated using a *M-θ* Pivot relationship. The selected Pivot model is characterized by a lot of parameters that are not provided by authors (Dowel et al., 1998) for reinforced concrete beam-to-column joints; in particular stiffness, strength and degradation parameters are required.

As long as stiffness and strength are easily evaluable by using Biddah & Ghobarah (1999) and Vollum & Newman (1999) formulations, respectively [the ultimate moment is calculated by equilibrium as shown in Eqn. (8.66)], the calibration of the degradation parameters requires a comparison study using experimental data available in the scientific literature and the results provided by the numerical simulation.

$$M_u = V_{jh} \cdot (h_b - 2d') . \tag{8.66}$$

The nonlinear model has been implemented in the advanced program for nonlinear static and dynamic analysis of structure ADAPTIC (Izzuddin, 1991), which already incorporates Pivot model for nonlinear analysis of RC frames. The joint element is considered as a zero length spring element defined by two nodes with the same coordinate and therefore rigid elements are adopted to simulate the portion of the beam and column inside the joint panel area. Beam elements which account for both material and geometric nonlinearity have been used for representing the spread of plasticity along beams and columns.

Table 8.7: Strength and stiffness for Pivot model in analysed specimens (units in N-mm).

Specimen JC-1	K_{ep}	K_{pp}	M_{yp}	M_{up}	U_{mp}
	296E+9	2,60E+9	1,74E+8	3,27E+8	4,77E-1
	K_{en}	K_{pn}	M_{yn}	M_{un}	U_{mn}
	395E+9	3,44E+9	-2,32E+8	-3,85E+8	3,61E-1
Specimen JC-2	K_{ep}	K_{pp}	M_{yp}	M_{up}	U_{mp}
	585E+9	5,13E+9	3,47E+8	4,99E+8	2,41E-1
	K_{en}	K_{pn}	M_{yn}	M_{un}	U_{mn}
	780E+9	6,75E+9	-4,63E+8	-6,15E+8	1,84E-1
Specimen 28-0T0	K_{ep}	K_{pp}	M_{yp}	M_{up}	U_{mp}
	388E+9	8,26E+9	4,18E+8	5,84E+8	1,69E-1
	K_{en}	K_{pn}	M_{yn}	M_{un}	U_{mn}
	388E+9	8,26E+9	-4,18E+8	-5,84E+8	1,69E-1
Specimen 1	K_{ep}	K_{pp}	M_{yp}	M_{up}	U_{mp}
	418E+9	11,4E+9	3,89E+8	4,57E+8	5,52E-2
	K_{en}	K_{pn}	M_{yn}	M_{un}	U_{mn}
	418E+9	11,4E+9	-3,89E+8	-4,57E+8	5,52E-2
Specimen A	K_{ep}	K_{pp}	M_{yp}	M_{up}	U_{mp}
	281E+9	1,51E+9	1,52E+8	2,92E+8	7,51E-1
	K_{en}	K_{pn}	M_{yn}	M_{un}	U_{mn}
	281E+9	1,51E+9	-1,52E+8	-2,92E+8	7,51E-1
Specimen Test #4	K_{ep}	K_{pp}	M_{yp}	M_{up}	U_{mp}
	332E+9	5,90E+9	4,06E+8	4,11E+8	1,68E-2
	K_{en}	K_{pn}	M_{yn}	M_{un}	U_{mn}
	332E+9	5,90E+9	-4,06E+8	-4,11E+8	1,68E-2
Specimen Test #5	K_{ep}	K_{pp}	M_{yp}	M_{up}	U_{mp}
	315E+9	0,00E-0	4,06E+8	4,06E+8	1,03E-2

Table 8.7: Strength and stiffness for Pivot model in analysed specimens (units in N-mm).

	K_{en}	K_{pn}	M_{yn}	M_{un}	U_{mn}
	315E+9	0,00E-0	-4,06E+8	-4,06E+8	1,03E-2
Specimen A5	K_{ep}	K_{pp}	M_{yp}	M_{up}	U_{mp}
	12,3E+9	1,76E+8	1,13E+7	1,72E+7	2,76E-1
	K_{en}	K_{pn}	M_{yn}	M_{un}	U_{mn}
	12,3E+9	1,76E+8	-1,13E+7	-1,72E+7	2,76E-1
Specimen 1	K_{ep}	K_{pp}	M_{yp}	M_{up}	U_{mp}
	495E+9	3,02E+9	1,99E+8	2,21E+8	6,31E-2
	K_{en}	K_{pn}	M_{yn}	M_{un}	U_{mn}
	495E+9	3,02E+9	-1,99E+8	-2,21E+8	6,31E-2
Specimen 2	K_{ep}	K_{pp}	M_{yp}	M_{up}	U_{mp}
	547E+9	3,86E+9	2,43E+8	2,65E+8	5,04E-2
	K_{en}	K_{pn}	M_{yn}	M_{un}	U_{mn}
	547E+9	3,86E+9	-2,43E+8	-2,65E+8	5,04E-2
Specimen 1B	K_{ep}	K_{pp}	M_{yp}	M_{up}	U_{mp}
	436E+9	0,00E-0	2,57E+8	2,57E+8	4,73E-3
	K_{en}	K_{pn}	M_{yn}	M_{un}	U_{mn}
	436E+9	0,00E-0	-2,57E+8	-2,57E+8	4,73E-3
Specimen 2B	K_{ep}	K_{pp}	M_{yp}	M_{up}	U_{mp}
	363E+9	27,3E+9	2,33E+8	2,39E+8	6,85E-3
	K_{en}	K_{pn}	M_{yn}	M_{un}	U_{mn}
	363E+9	27,3E+9	-2,33E+8	-2,39E+8	6,85E-3

The stiffness K_e, and K_p and the yielding M_y and ultimate M_p moments evaluated for simulating the Pivot model are reported in Table 8.7 in which the subscripts p and n denote the positive and negative branches, respectively. For the used model K_{hp} and K_{hn} equal to zero have been assumed.

Table 8.8: Degradation parameters for Pivot model in analysed specimens.

	α_1	β_1	γ_p	ε_p	δ_p
Specimen JC-1	3,00	0,50	0,10	15	1,50
	α_2	β_2	γ_n	ε_n	δ_n
	3,00	0,50	0,10	15	1,50
Specimen JC-2	α_1	β_1	γ_p	ε_p	δ_p
	3,00	0,50	0,05	15	1,30
	α_2	β_2	γ_n	ε_n	δ_n
	3,00	0,50	0,05	15	1,30
Specimen	α_1	β_1	γ_p	ε_p	δ_p

Table 8.8: Degradation parameters for Pivot model in analysed specimens.

28-0T0	3,00	0,50	0,80	15	1,50
	α_2	β_2	γ_n	ε_n	δ_n
	3,00	0,50	0,80	15	1,50
	α_1	β_1	γ_p	ε_p	δ_p
Specimen 1	3,00	0,50	0,05	15	1,50
	α_2	β_2	γ_n	ε_n	δ_n
	3,00	0,50	0,05	15	1,50
	α_1	β_1	γ_p	ε_p	δ_p
Specimen A	3,00	0,50	0,05	15	1,50
	α_2	β_2	γ_n	ε_n	δ_n
	3,00	0,50	0,05	15	1,50
	α_1	β_1	γ_p	ε_p	δ_p
Specimen Test #4	3,00	0,50	0,30	15	1,50
	α_2	β_2	γ_n	ε_n	δ_n
	3,00	0,50	0,30	15	1,50
	α_1	β_1	γ_p	ε_p	δ_p
Specimen Test #5	3,00	0,50	0,25	15	1,50
	α_2	β_2	γ_n	ε_n	δ_n
	3,00	0,50	0,25	15	1,50
	α_1	β_1	γ_p	ε_p	δ_p
Specimen A5	3,00	0,50	0,20	15	1,50
	α_2	β_2	γ_n	ε_n	δ_n
	3,00	0,50	0,20	15	1,50
	α_1	β_1	γ_p	ε_p	δ_p
Specimen 1	3,00	0,50	0,00	15	1,25
	α_2	β_2	γ_n	ε_n	δ_n
	3,00	0,50	0,00	15	1,25
	α_1	β_1	γ_p	ε_p	δ_p
Specimen 2	3,00	0,50	0,00	15	1,30
	α_2	β_2	γ_n	ε_n	δ_n
	3,00	0,50	0,00	15	1,30
	α_1	β_1	γ_p	ε_p	δ_p
Specimen 1B	3,00	0,30	0,10	5	1,50
	α_2	β_2	γ_n	ε_n	δ_n
	3,00	0,30	0,10	5	1,50
	α_1	β_1	γ_p	ε_p	δ_p
Specimen 2B	3,00	0,50	0,06	15	1,50
	α_2	β_2	γ_n	ε_n	δ_n
	3,00	0,50	0,06	15	1,50

Table 8.8 reports the degradation values obtained from the model calibration, which can be adopted for simulating the exterior joints behaviour using the Pivot model. Parameters with subscripts p and n refer to the positive and negative branches of the relationship, respectively. In particular, parameter α can be assumed equal to 3.00, while β ranges between 0.30 and 0.50. Furthermore, the γ strength degradation parameter is between 0.00 and 0.80, the energy degradation parameter ε between 5 and 15 and the displacement degradation parameter δ between 1.25 and 1.50.

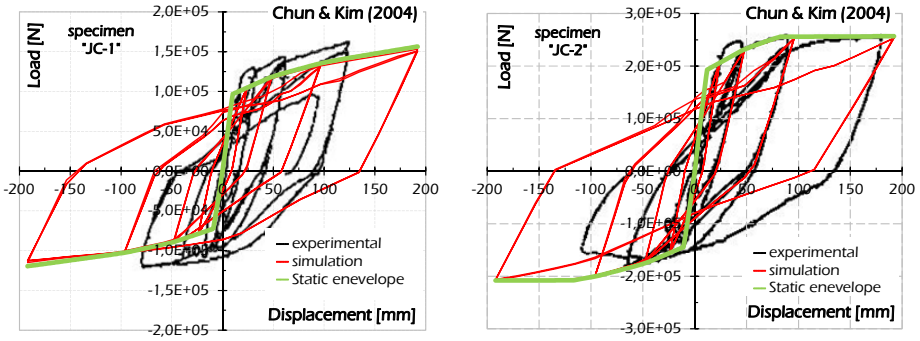

Fig. 8.51: Simulated and observed response for specimens provided by Chun & Kim (2004).

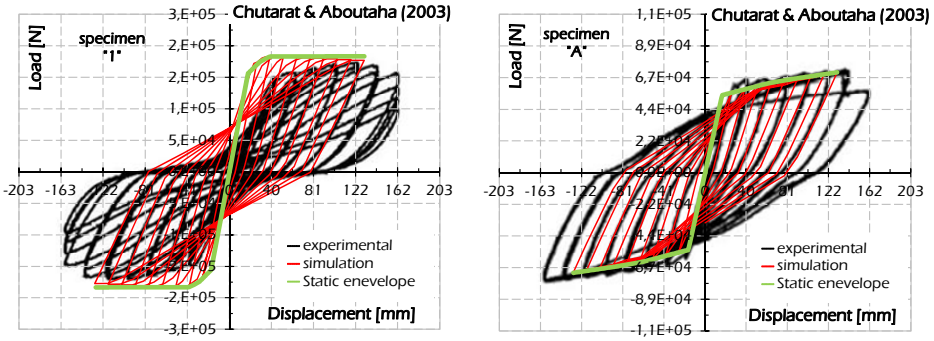

Fig. 8.52: Simulated and observed response for specimens provided by Chutarat & Aboutaha (2003).

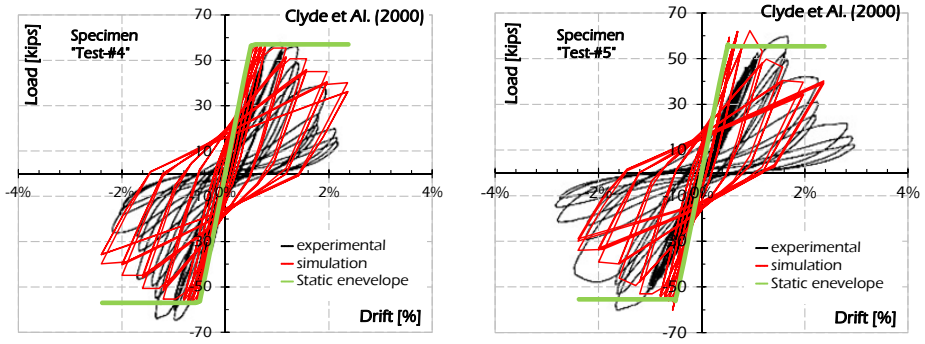

Fig. 8.53: Simulated and observed response for specimens provided by Clyde et al. (2000).

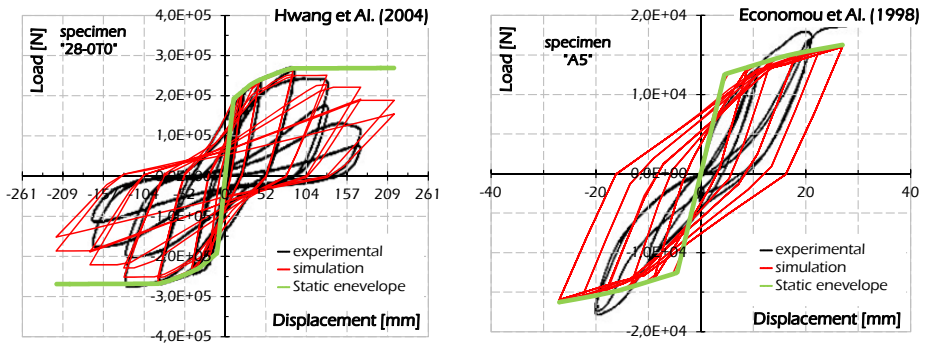

Fig. 8.54: Simulated and observed response for specimens provided by Hwang et al. (2004) and Economou et al. (1998).

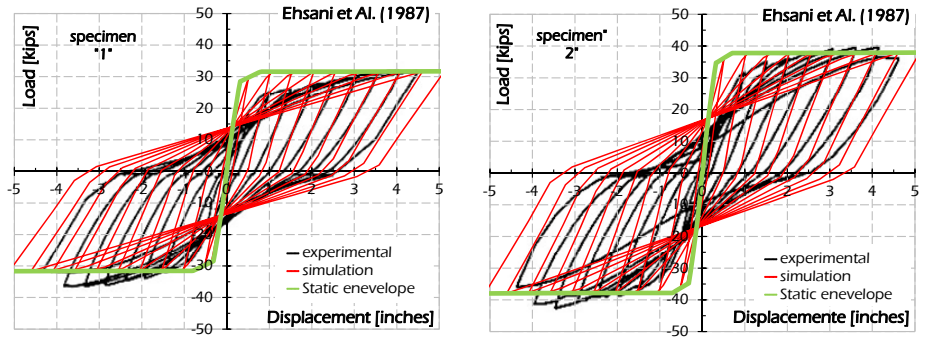

Fig. 8.55: Simulated and observed response for specimens provided by Ehsani et al. (1987).

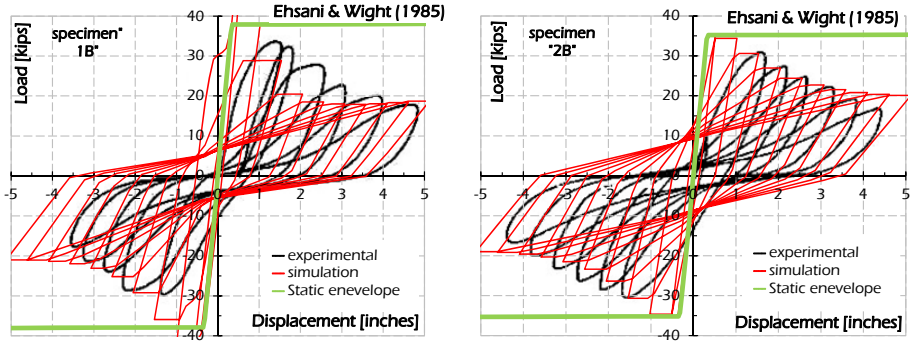

Fig. 8.56: Simulated and observed response for specimens provided by Ehsani & Wight (1985).

In Fig. 8.51 to Fig. 8.56 the numerical-experimental comparisons are shown, where the red line represents the numerical curve under cyclic loads, while the green curve denotes numerical response under monotonic loading conditions. These figures show how the calibrated Pivot model can be effectively employed for representing the actual behaviour of the exterior joint, both in the case of relevant and negligible pinching effect. Moreover, a good agreement between ultimate experimental strength and the corresponding value calculated using the Vollum & Newman model (1999) can be observed.

CHAPTER IX

9. Joint Behaviour in Frame Analyses

The behaviour of beam-to-column joints is usually neglected in nonlinear static or dynamic analyses of frame structures, as the beam-column intersection are supposed to be infinitely resistant and fixed. Studies that include the influence of the damage and failure of joints on the seismic response of reinforced concrete multi-storey structures (Favvata et al., 2008) typically adopt simple rotational spring elements for this purpose.

Using the joint Pivot model proposed in the previous section, the influence of the local response of connections on the seismic behaviour of reinforced concrete structures is presented through static and dynamic analyses provided considering two, three and four-storey plane frame structure. Additionally a vulnerability assessment according the Italian Code (NTC, 2008) is developed showing the influence of the damage of exterior RC joints with reduced capacity on the overall seismic response, on the failure mode and on the ductility capacity and demand of columns.

9.1 Seismic Analysis of Frame Structures

The knowledge of values of structural response parameters are of primary interest in structural design and assessment (such as the maximum shear at the base or the displacement of a particular point). For that purpose it is necessary to choose the type of analysis most appropriate to use. The types of existing methodologies are:

- Static Linear Analysis;
- Dynamic Linear Analysis with assigned Response Spectrum;
- Static Nonlinear Analysis (namely PushOver Analysis);
- Dynamic Nonlinear Analysis (namely Nonlinear Time History Analysis).

Several researches led to the formulation of different methodologies that have the possibility of finding accurate solutions depending on the level of detail available. It is noted that currently the reference method in seismic design remains the Nonlinear Dynamic Analysis for the accuracy of the results compared to other proposed, although it is still object of researches the possibility of using simplified methods based on Nonlinear Static Analysis.

Under the above considerations, in recent years simplified procedures for performing Nonlinear Static Analysis has been developed (Nonlinear Static Procedures - NSP). These procedures represent a tool for quickly assessing the overall response of structures in plastic field. In this context, the approximate methods may play a central role, especially in advanced seismic codes that allow to explicitly linking the different levels of risk with the required performance targets (Performance-Based Design - PBD).

9.1.1 Static Nonlinear Analysis

In Static Nonlinear Analyses a system of horizontal forces is applied to the structure in addition to gravitational loads. The pattern of horizontal forces is then monotonically increased with the aim of increasing the displacement of a node assumed as control point until the ultimate conditions have been reached. This procedure allows to consider also the post elastic behaviour and hence the ductility of the structure allowing to capture the structural behaviour when the structural elements, or parts of them, are subject to deformations that change the stiffness of the system. The methodology consists mainly in the following steps:

- evaluation of the capacity curve generally relating the base shear and the displacement of the control point;
- evaluation of the maximum response in terms of displacement through simplified methods;
- assessment of the structures through the comparison between the capacity and the demand in terms of displacements for ductile mechanisms and of force for brittle ones.

Structures in which the response is governed mainly by the fundamental modal shape in the considered direction the distribution of equivalent static forces can be expressed as follows:

$$F_i = \frac{m_i \cdot \Phi_i}{\sum_{j=1}^{N} m_j \cdot \Phi_j} \cdot V \qquad (9.1)$$

in which F_i, m_i and Φ_i are the lateral force, the mass and the component of the fundamental mode of the i-th floor, respectively, V is the base shear and N represents the number of floors.

The contribution of the superior vibration modes can be considered performing more analyses in which distributions of forces proportional to the component of the higher mode of vibration have been applied to the structure; the response of each considered mode can be obtained by adding the effects through the normal rules of modal superposition. Alternative procedures plan to perform the structural analysis only once by applying a system of lateral forces proportional to the modal shape according to the SRSS modal combination (Faella et al., 2008).

When the increase of the loads is interrupted in order to achieve the limit value of lateral deformation, the inability to support the vertical loads or degradation of the strength of structural elements, the system shows a sharp reduction in strength. The pushover analysis, however, may continue to introduce new characteristics of strength and reduce the level of lateral actions. In this case, the capacity curve has a saw tooth shape due to the subsequent loss of strength.

When ultimate condition is achieved the capacity curve is obtained in which is possible to distinguish the maximum displacement δ_i and the base shear V that the structure can reach before the collapse. At this point there are several methods of bi-linearization of the force-displacement relationship and evaluation of the response that, in most cases, transform the real system (MDOF) in an equivalent simple oscillator characterised by an equivalent single degree of freedom system (SDOF).

One of the most popular variants for evaluating the demand, also incorporated in Eurocode 8 (EN 1995, 2005) is the N2-Method (Fajfar, 1999) so called because the initials N2 indicates that the method is non-linear (N) and uses "2" computational models of the structure (the MDOF system and the equivalent SDOF). The operations can be divided into two steps:

- the transformation of the MDOF system in an equivalent SDOF system;
- the evaluation of lateral nonlinear response.

The first part of the method is based on two assumptions: the distribution of horizontal forces is invariant and assumed to be proportional to the first mode of vibration through the masses concentrated at each floor and the components of the vector representative of the first modal shape[1]

[1] The codes that integrate the N2-Method prescribe specifically to consider different distributions of forces.

$$\mathbf{f}(u) = \mathbf{M} \cdot \Phi \cdot \lambda(u); \tag{9.2}$$

the distribution of the displacements is assumed invariant and is described by the first modal shape (this hypothesis is exact until the structure is elastic)

$$\mathbf{u} = \Phi \cdot u. \tag{9.3}$$

Neglecting the viscous damping for simplicity of exposition, the equation of the dynamic equilibrium of the MDOF system is expressed as follows:

$$\mathbf{M}\ddot{\mathbf{u}} + \mathbf{f}(u) = -\mathbf{M}\mathbf{1}\ddot{u}_g(t) \tag{9.4}$$

where $\mathbf{1}$ is the unit vector and $\ddot{u}_g(t)$ the acceleration of the seismic input.

Under the assumptions underlying the method and pre multiplying Eqn. (9.50) for $\Phi^{\mathbf{T}}$ it is obtained:

$$\left(\Phi^{\mathbf{T}}\mathbf{M}\Phi\right)\ddot{u} + \left(\Phi^{\mathbf{T}}\mathbf{M}\Phi\right)\lambda(u) = -\left(\Phi^{\mathbf{T}}\mathbf{M}\mathbf{1}\right)\ddot{u}_g(t). \tag{9.5}$$

By defining the modal participation factor Γ, the equation can be easily transformed into:

$$\Gamma = \frac{\left(\Phi^{\mathbf{T}}\mathbf{M}\mathbf{1}\right)}{\left(\Phi^{\mathbf{T}}\mathbf{M}\Phi\right)}, \tag{9.6}$$

$$\left(\Phi^{\mathbf{T}}\mathbf{M}\mathbf{1}\right)\frac{\ddot{u}}{\Gamma} + \left(\Phi^{\mathbf{T}}\mathbf{M}\mathbf{1}\right)\frac{\lambda(u)}{\Gamma} = -\left(\Phi^{\mathbf{T}}\mathbf{M}\mathbf{1}\right)\ddot{u}_g(t), \tag{9.7}$$

where $\left(\Phi^{\mathbf{T}}\mathbf{M}\mathbf{1}\right)\lambda(u) = \sum_i f_i(u) = V_b(u)$ is the base shear. Considering the assumptions made in Eqn. (9.8), Eqn. (9.9) and Eqn. (9.10) the dynamic equilibrium equation of an equivalent simple oscillator characterized by a nonlinear force-displacement relationship is achieved [Eqn. (9.11)].

$$m^* = \Phi^{\mathbf{T}}\mathbf{M}\mathbf{1} = \sum_i m_i \Phi_i, \tag{9.8}$$

$$d^* = \frac{u}{\Gamma}, \tag{9.9}$$

$$F^*\left(\Gamma d^*\right) = \frac{V_b(u)}{\Gamma}, \tag{9.10}$$

$$m^* \ddot{d}^* + F^* \left(\Gamma d^* \right) = -m^* \ddot{u}_g (t) . \tag{9.11}$$

The displacement u and the base shear V_b are obtained from the pushover analysis performed on the three-dimensional structure subjected to the distribution of forces consistent with that taken as the assumptions underlying the method.

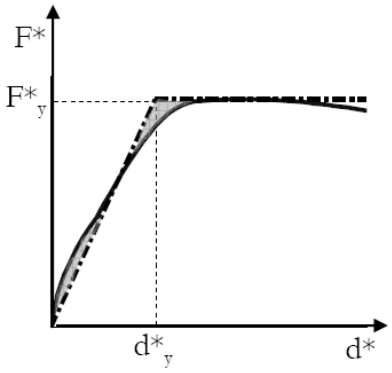

Fig. 9.1: Bi-linearization of the PushOver curve according to the N2-Method.

The second part of the method consists of determining the response of SDOF system, which requires some assumptions on the cyclic behaviour, after which the solution can be found through numerical integrations from an appropriate set of acceleration records or by using an appropriate inelastic response spectrum as prescribed in the literature (Fajfar, 1999). With the aim of simplifying the method is appropriate to approximate the capacity curve in a simple bilinear relationship. In the N2-Method the bi-linearization consists in approximating the curve into two linear sections, the first branch elastic and perfectly plastic the other one on the basis of equality of energy at maximum displacement (Fig. 9.1).

The elastic stiffness and hence the natural period of vibration of the simplified SDOF system can be evaluated as follows:

$$T^* = 2\pi \sqrt{\frac{m^* d_y^*}{F_y^*}} . \tag{9.12}$$

The response in terms of displacement is evaluated by the inelastic response spectrum, it can be obtained in simplified way from the elastic one with the various methods available in scientific literature whose general form is:

$$S_d\left(T^*\right)=\frac{S_{d,e}\left(T^*\right)}{R_\mu}\left[1+\frac{1}{c_1}\left(R_\mu^{c_2}-1\right)\right]^{\frac{1}{c_3}}\geq\frac{S_{d,e}\left(T^*\right)}{R_\mu} \tag{9.13}$$

where R_μ is the factor of reduction of forces, S_d and $S_{d,e}$ are the ordinates of the elastic and inelastic response spectrum corresponding to the period T^*, respectively, and c_1, c_2 and c_3 are coefficients that depend on the period T_c of transition between pseudo constant acceleration and constant velocity defined by Krawinkler & Nasser (1992).

$$\begin{aligned} &c_1=c_2=\frac{T^{*a}}{1+T^{*a}}+\frac{b}{T^*}, \\ &c_3=1. \end{aligned} \tag{9.14}$$

A simple version of the evaluation of the response adopted in Eurocode 8 (EN 1998, 2005) and OPCM 3431/05 (2005), in which the determination of the seismic response of SDOF system is extremely easy when the period is greater than T_c (period of transition from the constant pseudo-acceleration to the constant pseudo-velocity), is given in the following:

$$S_d\left(T^*\right)=\frac{\mu}{R_\mu}S_{d,e}\left(T^*\right) \tag{9.15}$$

where μ is the ductility of the system in terms of displacement taken equal to:

$$\begin{cases} \mu=1+\left(R_\mu-1\right)\dfrac{T_c}{T^*} & \text{for } T^*<T_c \\ \mu=R_\mu & \text{for } T^*\geq T_c \end{cases}. \tag{9.16}$$

When the maximum response d_{max}^* of SDOF system is known the maximum displacement at the top of the building is given by:

$$u_{\max}=\Gamma d_{\max}^*. \tag{9.17}$$

Once evaluated the maximum displacement demanded to the structure, the vulnerability assessment can be developed using the procedures outlined in section 9.1.3.

9.1.2 Nonlinear Time History Analysis

Nonlinear Time History Analysis is most accurate approach for simulating the behaviour of a structure under seismic actions in post-yielding field. It submits the structure to a story of accelerations at the base making a step integration of the dynamic equation, and upgrading the mechanical characteristics of the control sections step-by-step. The analysis requires a very accurate model and very long processing time; it is also very sensitive, as well as the acceleration history impressed at the base, the detail of the elements constituting the structure as well as the approximations made, and then the constitutive laws of materials and their evolution during the analysis. Much attention should be made at the definition of the system damping and the hysteretic behaviour of the structure which strongly influence the results.

From the considerations made above, it is shown that this method requires models more and more conform to the reality that they are often difficult to achieve. It follows that for this type of analysis the uncertainties associated with those data are greater than those related to the method itself. Therefore, the mentioned reasons lead the Nonlinear Time History Analysis to be more used in scientific research and rarely used in practice as it seeks to achieve the structural behaviour using methods less expensive and more intuitive.

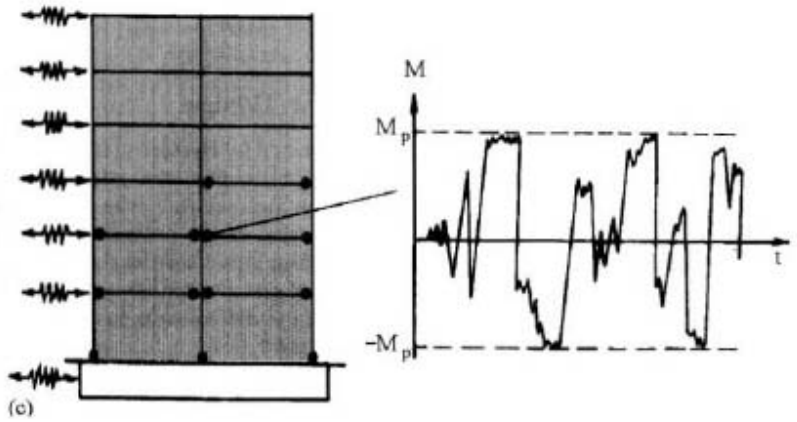

Fig. 9.2: Graphical example of the structural response achieved through NLTH analysis.

The execution of a dynamic analysis involves the following steps:

- *accurate definition of the geometric model* (performing a complex analysis using a not accurate model provides not significant results);

- *definition of the masses involved in earthquake event and their application to the model*;
- *definition of the damping of the structure,* pointing out that the solution of the problem requires an integration step-to-step:

$$\begin{aligned} &M\ddot{x}(t)+C\dot{x}(t)+F\left[x(t)\right]=-M\ddot{a}_g(t), \\ &x(0)=x_0, \\ &\dot{x}(0)=\dot{x}_0. \end{aligned} \tag{9.18}$$

  Also the matrix *C* of the system that allows modelling the damping offered by the system should be defined. It is generally defined as proportional to stiffness and masses [model by Rayleigh (Clough & Penzien, 1995)];
- *definition of the non-linear constitutive laws of materials for fiber models and the position of plastic hinges for the concentrated plasticity models*;
- *definition of the seismic input*, the model should be called simultaneously by two horizontal seismic events and, in some cases, even from a vertical one: it should be considered groups of two or three different accelerograms applied in the main directions simultaneously; these accelerograms may be artificial, simulated or natural;
- *verification of the structure*, carrying out the analysis and calculating the time response of the structure is possible to know the effects of the earthquake at each time on each element of the structure (bending, shear, displacements and rotations) and identifying the maximum values.

In step-by-step integration method (finite difference methods) of Eqn. (9.18) it is assumed that the acceleration varies according to some predetermined criterion in the time interval Δt, so that they can be integrated to find the velocity and displacement at the time $t+\Delta t$.

The direct integration methods do not provide any transformation of coordinates and equations before numerical integration and can be divided essentially in explicit methods (central difference) and implicit methods in which the vector of the displacements is function of the displacement known at the previous step and the current velocities and accelerations (unknown). The formers require very small time steps for stability of the solution and essentially are:

- the Central Differences Method;

- the Method by Hilber Hurghens Taylor.

The implicit methods, however, generally require time steps limited only by reasons of accuracy of results and tend to be unconditionally stable.

The integration schemes commonly used are:

- the Method by Newmark[2] (best-known and used);
- the Method by Wilson;
- the Method by Hubolt.

The integration scheme of Newmark depends on two variables: γ and α. The following conditions can occur:

$$\begin{aligned}
&\gamma = 1/2, \quad \alpha = 1/4, && \text{acceleration constant in } \Delta t ;\\
&\gamma = 1/2, \quad \alpha = 1/6, && \text{acceleration linearly variable in } \Delta t ;\\
&\gamma = 1/2, \quad \alpha = 1/8, && \begin{cases} \text{acceleration constant in the first step } \Delta t/2 \\ \text{with value evaluated at time t} \\ \text{and constant in the second step of } \Delta t/2 \\ \text{with value evaluated at time t+}\Delta\text{t} ; \end{cases}
\end{aligned} \tag{9.19}$$

This type of analysis appears to be the most refined, but on a factual level is affected by many uncertainties and complexity. The results, not easy to use, may not be as precise as they should, especially in proportion to the costs required from the analysis.

In Nonlinear Dynamic Analysis the response is not obtained as a superposition of decoupled modal responses, and the damping cannot be expressed in terms of damping rate but an explicit damping matrix must be define. In these cases the easiest way to determine the damping matrix is to consider it proportional to the masses and stiffness because for the un-damped mode shapes they are orthogonal with respect to these.

$$\mathbf{C} = \alpha\mathbf{M} \quad ; \quad \mathbf{C} = \beta\mathbf{K} . \tag{9.20}$$

By taking into account the orthogonality of mode shapes with the stiffness and mass matrices are worth Eqn. (9.21) and Eqn. (9.22).

$$C_n = \phi_n^T c \phi_n = \alpha \phi_n^T \mathbf{M} \phi_n , \tag{9.21}$$

$$C_n = \phi_n^T c \phi_n = \beta \phi_n^T \mathbf{K} \phi_n . \tag{9.22}$$

[2] The method by Newmark has been used to perform the dynamic analyses made in the following sections.

By considering the following definition of the factor of damping 0

$$\xi_n = \frac{c_n}{c_{cr}} = \frac{c_n}{2\sqrt{K_n M_n}} = \frac{c_n}{2\sqrt{\frac{K_n}{M_n} M_n}} = \frac{c_n}{2\omega_n M_n} = \frac{\alpha M_n}{2\omega_n M_n}, \tag{9.23}$$

$$\begin{matrix} 2\omega_n \mathbf{M_n} \xi_n = \alpha \mathbf{M_n} \\ 2\omega_n \mathbf{K_n} \xi_n = \alpha \mathbf{K_n} \end{matrix} \quad \text{where } \mathbf{K_n} = \omega_n^2 \mathbf{M}, \tag{9.24}$$

it is possible to achieve the parameters α and β:

$$\alpha = 2\omega_n \xi_n, \tag{9.25}$$

$$\beta = \frac{2\xi_n}{\omega_n}. \tag{9.26}$$

A development of the formulation outlined above is the assumption of the combined proportional law between the damping and both masses and stiffness:

$$\mathbf{C} = \alpha \mathbf{M} + \beta \mathbf{K}. \tag{9.27}$$

The definition of damping through Eqn. (9.27) is called Rayleigh Damping and was proposed by Lord Raylegh (Clough & Penzien, 1995). Similar to the development of Eqn. (9.23) and Eqns. (9.25) and (9.26) the parameters α and β must be such as to satisfy:

$$\xi_n = \frac{\alpha}{2\omega_n} + \frac{\beta\omega_n}{2}. \tag{9.28}$$

By Eqn. (9.28) the values of the two parameters are evaluable by solving the following system:

$$\begin{cases} \alpha = \dfrac{2\omega_i\omega_j\left(\xi_j\omega_j - \xi_i\omega_i\right)}{\omega_i^2 - \omega_j^2} \\ \beta = \dfrac{2\left(\xi_j\omega_j - \xi_i\omega_i\right)}{\omega_i^2 - \omega_j^2}. \end{cases} \tag{9.29}$$

The graphic relations described by Eqn. (9.29) are shown in Fig. 9.3.

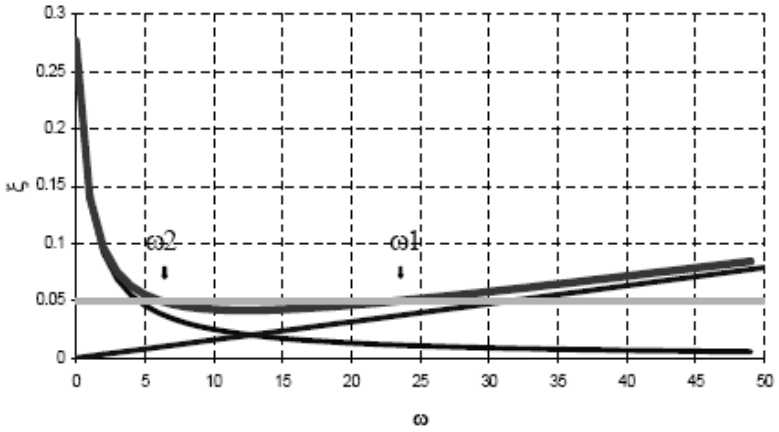

Fig. 9.3: Relationship between pulsation and damping equal to 5%.

The two factors of Rayleigh can be evaluated through the system of equations associated with two specific frequencies (modes) ω_i and ω_j. Generally, the modes are chosen to have the desired damping calibrated on the main modes of the structure, this amounts to calibrate the coefficients α and β for a given damping (5% for reinforced concrete buildings and about 2% for steel buildings) on the first two mode shapes.

9.1.3 Vulnerability Evaluation

The capacity curve obtained through Nonlinear Static Analyses (PushOver), generally relating the top displacement and the base shear, can be used as starting point for applying the simplified methods allowing to evaluate the displacement that the structure attains under the expected earthquake. Some of these methods have been reported and compared by Faella et al. (2008); in the following the N2-Method (Fajfar, 1999) will be used by considering the performance levels (Limit States) defined by Eurocode 8 (EN 1998, 2005) and NTC (2008).

The response spectrum in respect of the vulnerability assessment is made is evaluated according the NTC (2008). Eqns. (9.30) to (9.33) represent the bunch of the response spectrum:

$$0 \le T < T_B \quad S_{a,e}(T) = a_g \cdot S \cdot \eta \cdot F_0 \cdot \left[\frac{T}{T_B} + \frac{1}{\eta \cdot F_0} \left(1 - \frac{T}{T_B} \right) \right] , \tag{9.30}$$

$$T_B \le T < T_C \quad S_{a,e}(T) = a_g \cdot S \cdot \eta \cdot F_0 \ , \tag{9.31}$$

$$T_C \le T < T_D \quad S_{a,e}(T) = a_g \cdot S \cdot \eta \cdot F_0 \cdot \frac{T_C}{T} \tag{9.32}$$

$$T_D \le T \quad S_{a,e}(T) = a_g \cdot S \cdot \eta \cdot F_0 \cdot \left(\frac{T_C \cdot T_D}{T^2} \right) \tag{9.33}$$

where T_B, T_C and T_D represent the characteristic spectral periods, F_0 is the coefficient of dynamic amplification and η is a coefficient accounting the viscous damping through the following relation:

$$\eta = \sqrt{10/(5+\xi)} \ge 0.55 \, . \tag{9.34}$$

The factor S is evaluated from the stratigraphic amplification factor S_s and the topographic amplification factor S_T . The evaluation of the spectral shape depends on the type of structure and the Limit State of interest; in the following applications the Limit State of Damage Limitation (SLD), the Limit State of Life Safety (SLV) and the limit State of Collapse (SLC) are taken into account.

Both the Eurocode 8 (EN 1998, 2005) and the NTC (2008) require two different shapes in performing Nonlinear Static Analysis:

- distribution defined **Uniform** based on force proportional to the masses concentrated at each floor;
- distribution defined **Modal**, in which the applied forces are proportional to the masses multiplied by the displacements vector of the fundamental mode of vibration determined by elastic analysis.

The capacity curve of the SDOF system can then be modified in an elastic-plastic model using the principle of energy equality (see section 9.1.1).

The curve obtained can be represented in the ADRS format by dividing the base shear for the mass m^* of the equivalent SDOF, the same format can be used to represent the demand curve (elastic spectrum in ADRS format). The displacement demand, or performance point, for a general Limit State can then be evaluated by applying the N2-Method through the intersection of the spectrum and the inelastic capacity curve (Faella et al., 2009).

Many parameters and indices can be used as a measure of structural performance under seismic actions (Faella et al., 2008). In this work the chord rotation is taken as the control parameter derived in accordance with the formula prescribed in Eurocode 8 (EN 1998, 2005) and NTC (2008) under which the three Limit States of interest can be identified for existing structures using three measures of chord rotation briefly described below.

The general structure reaches a defined limit, when the first structural element reaches the correspondent level of engagement. In this thesis is also considered the possibility of reaching brittle failure related primarily to overcome the shear limit in the structural elements, in this case it is assumed to match this condition to the SLC.

The capacity of a single element can be described in terms of chord rotation (i.e. the line joining the node with the point on the frame placed at a distance equal to the shear length L_V). Here are briefly outlined the relations reported Eurocode 8 (EN 1998, 2005) for defining the basic values of the rotational capacity of structural members.

The chord rotation related to the yield limit is provided by the sum of three terms related to the flexural deformability, the shear deformation and the bond slip:

$$\theta_y = \phi_y \frac{L_V + a_V z}{3} + 0.00135\left(1+1.5\frac{h}{L_V}\right) + \frac{\varepsilon_y}{d-d'}\frac{d_b f_y}{6\sqrt{f_c}}. \tag{9.35}$$

In Eqn. (9.35), ϕ_y is the curvature of the section corresponding to the yielding of rebars, L_V is the shear length, h is the depth of the section, d_b is the average diameter of the longitudinal reinforcement, while f_y and f_c are the yielding stress of steel and the compression concrete strength of concrete, respectively. In Eqn. (9.35), furthermore, it is possible to individuate the moment arm of the section z and the Boolean operator a_V allowing to take into account the effects of shear.

The ultimate chord rotation is proposed in two alternative formulations:

$$\theta_u = \frac{1}{\gamma_{el}} 0.016\left(0.3^{\upsilon}\right)\left[\frac{\max(0.01;\omega')}{\max(0.01;\omega)}\right]^{0.225}\left(\frac{L_V}{h}\right)^{0.35} 25^{\left(\alpha\rho_{sx}f_{yw}/f_c\right)}\left(1.25^{100\rho_d}\right) \tag{9.36}$$

$$\theta_u = \frac{1}{\gamma_{el}}\left(\theta_y + \left(\phi_u - \phi_y\right)L_{pl}\left(1-\frac{0.5L_{pl}}{L_V}\right)\right). \tag{9.37}$$

Eqn. (9.36) is entirely empirical and is derived from calibration with respect to experimental results, while Eqn. (9.37) is based on the theoretical link between the rotation and the curvature by defining the length of the plastic hinge L_p in accordance with the following relationship derived from experimental results:

$$L_{pl} = 0.1L_V + 0.17h + 0.24\frac{d_{bL}f_y}{\sqrt{f_c}}. \tag{9.38}$$

The equations introduced above are used to define the values at which a specified Limit State SL (NTC, 2008) is achieved:

- the chord rotation at the SLD corresponds to the chord rotation at the yielding limit $\theta_{DL} = \theta_y$;
- the chord rotation at the SLV corresponds to $\theta_{LS} = 3/4\,\theta_u$;
- the chord rotation at the SLC is equal to the ultimate rotation $\theta_{NC} = \theta_u$.

The following equation can be used for evaluating the shear strength V_R in brittle mechanisms:

$$V_R = \frac{1}{\gamma_{el}}\left[\begin{array}{l}\dfrac{h-x}{2L_V}\min\left(N;0{,}55A_c f_c\right)+\left(1-0{,}05\min\left(5;\mu_\Delta^{pl}\right)\right)\cdot \\ \left[0{,}16\max\left(0{,}5;100\rho_{tot}\right)\left(1-0{,}16\min\left(5;\dfrac{L_V}{h}\right)\right)\sqrt{f_c}\,A_c+V_w\right]\end{array}\right], \qquad (9.39)$$

where μ_Δ^{pl} is the ratio between the post-elastic part of the chord rotation and the yielding rotation, γ_{el} is equal to 1.15 for structural elements and 1.00, h is the depth of the section, x is the neutral axis, N is the axial load, A_c is the area of the core section of concrete, ρ_{tot} the geometric ratio of the longitudinal reinforcement and V_w the shear strength due to the hoops:

$$V_w = \rho_w \cdot b_w \cdot z \cdot f_{yw}\,. \qquad (9.40)$$

The shear strength cannot overlap the following value:

$$V_{R,\max} = \frac{4}{7}\frac{\left(1-0{,}02\min\left(5;\mu_\Delta^{pl}\right)\right)}{\gamma_{el}}\left(1+1{,}35\frac{N}{A_c f_c}\right) \qquad (9.41)$$
$$\left(1+0{,}45\left(100\rho_{tot}\right)\right)\sqrt{\min\left(40;f_c\right)}\,b_w z\sin 2\delta\,.$$

The seismic assessment of existing structures involves the need to define parameters to identify the "degree of inadequacy" of the structure. With this objective in the following two parameters are introduced aimed at quantifying two aspects of the seismic response of the structure. On the one hand, we define a parameter that expresses the distance between the displacement capacity with reference to the attainment of a certain Limit State and the demand on it requested by an earthquake hazard commensurate to that Limit State. On the other hand it is considered important to introduce a parameter that measures the extension of the damage or the number of elements with a

capacity smaller than the demand when the structure requires a capacity value equal to that required and evaluated through an extrapolation of the capacity curve after reaching the failure. This parameter, in particular, assumes a high importance if viewed from the standpoint of a future seismic retrofit as an important parameter that allows to choose between measures that increase the capacity of the members (local retrofitting techniques), interventions that reduce demand (global retrofitting techniques) or combined solutions.

The first parameter of vulnerability can be defined as the ratio between demand and capacity in terms of displacement for the generic Limit State:

$$V_{Dsp,LS} = \frac{\Delta_{d,LS}}{\Delta_{c,LS}}. \tag{9.42}$$

By considering that the PushOver analysis involves the application of different distributions of lateral forces in several directions, the vulnerability of the structure is taken as the maximum value of that parameter.

$$V_{Dsp,LS} = \max_{distr,dir}\left\{V_{Dsp,LS}\right\}. \tag{9.43}$$

From the definition [Eqn. (9.42)] is clear that more testing is far from the condition of satisfaction, the greater the value of the parameter V_{Dsp} and, further, to values smaller than 1.00 correspond the satisfaction of the vulnerability assessment. A similar parameter is the best known vulnerability factor α defined by OPCM 3431/05 (EN 1998, 2005). In particular, two parameters of vulnerability are defined: the risk indicator of collapse α_u [Eqn. (9.44)] and the indicator of risk of unavailability of the structure α_e [Eqn. (9.45)].

$$\alpha_u = \min\left\{\frac{PGA_{LS}}{PGA_{10\%}}; \frac{PGA_{NC}}{PGA_{2\%}}\right\}, \tag{9.44}$$

$$\alpha_e = \frac{PGA_{DL}}{PGA_{50\%}}. \tag{9.45}$$

It can easily show that for structures whose period of vibration is within the range of constant pseudo-velocity of the elastic spectrum the parameter α coincides with the reciprocal of the parameter V_{Dsp}.

When verification is not satisfied, it makes sense to define a parameter measuring the extension of the damage, this parameter is determined according to the number of structural elements that are in a condition of exceeding the capacity when the structural response is extrapolated to a

displacement equal to their corresponding value of demand $\Delta_{d,LS}$. Since the modelling is made with reference to the chord rotation is defined by n_{LS} the number of elements in which the demand exceed the limit value of the chord rotation. The vulnerability parameter is then no dimensional in respect the total number of structural elements N_{tot}:

$$\eta_{LS} = \frac{n_{LS}}{n_{tot}}. \tag{9.46}$$

This parameter can also be measured against the brittle mechanisms defining the relationship between the number of elements in which shear stress exceeds the strength when the structural response is extrapolated up to a demand of displacement calculated with reference to the Limit State of Collapse (SLC).

The parameter measuring the extension of the damage can range between 0 and 1, depending on whether the damage attempts only a few sections or is extended to various parts of the structure.

9.2 Application

With the aim of evaluating the influence of the nonlinear behaviour of exterior beam-to-column joints on the response of RC frames, numerical nonlinear static and dynamic analyses have been carried out using ADAPTIC (Izzuddin, 1991), and the vulnerability of the analysed frames has been determined.

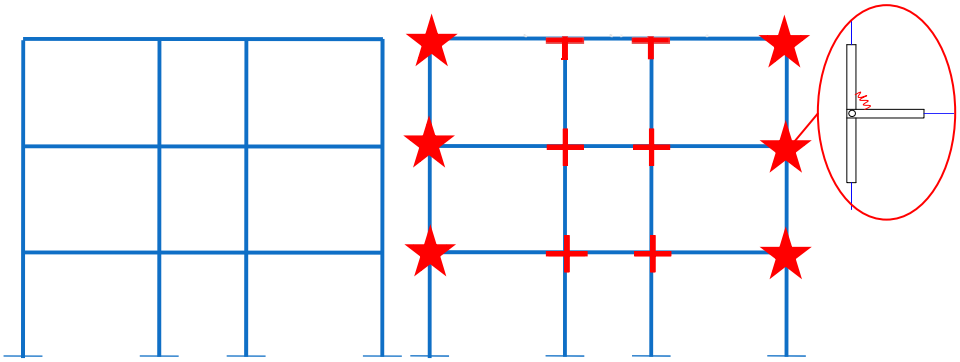

Fig. 9.4: Models of the plane frame without joint damage (on the left) and accounting the nonlinearity of exterior joint.

Nonlinear rotational springs have been included in frame models for investigating the seismic performance of four, three and two storey plane frame structures with three bays. The analysed frames are derived from a set of structures representative of existing buildings built in Italy around the 60's and 70's (Faella et al., 2009). The analyses have been carried out on plane frame structures modelled without accounting joint damage and on the same frames in which exterior beam-to-column joints have been modelled using the Pivot model outlined in the previous chapter (Fig. 9.4).

In all the examined cases, exterior joints without shear reinforcement have been modelled using rotational springs with the Pivot law outlined in the previous chapter in which the following degradation parameters α=3.00, β=0.50, γ=0.30, δ=1.50 and ε=15 have been taken into account.

9.2.1 The Analysed Structure

The plane frames analysed in the present study derives from 3D reinforced concrete structures designed according the old Italian Code (Regio Decreto, 1939). In particular the old code recommendations have been derived by the technical paper used around 60's and 70's (Santarella, 1963)

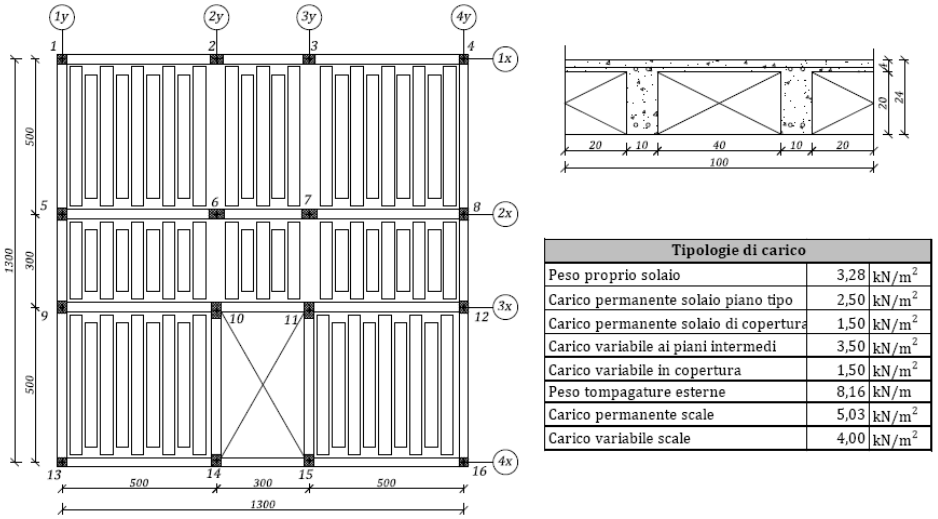

Tipologie di carico		
Peso proprio solaio	3,28	kN/m^2
Carico permanente solaio piano tipo	2,50	kN/m^2
Carico permanente solaio di copertura	1,50	kN/m^2
Carico variabile ai piani intermedi	3,50	kN/m^2
Carico variabile in copertura	1,50	kN/m^2
Peso tompagature esterne	8,16	kN/m
Carico permanente scale	5,03	kN/m^2
Carico variabile scale	4,00	kN/m^2

Fig. 9.5: 3D structure considered in the analysis.

Fig. 9.5 shows the characteristics of the 3D structure from which the plane frame analysed in this study have been derived. Furthermore, it is reported a

typical section of the floor and a table reporting the gravitation load applied to the structures. As shown, four frames are located along the X-direction to form a resistant tool stronger than the one located along the Y-direction in which there are only the two external frames.

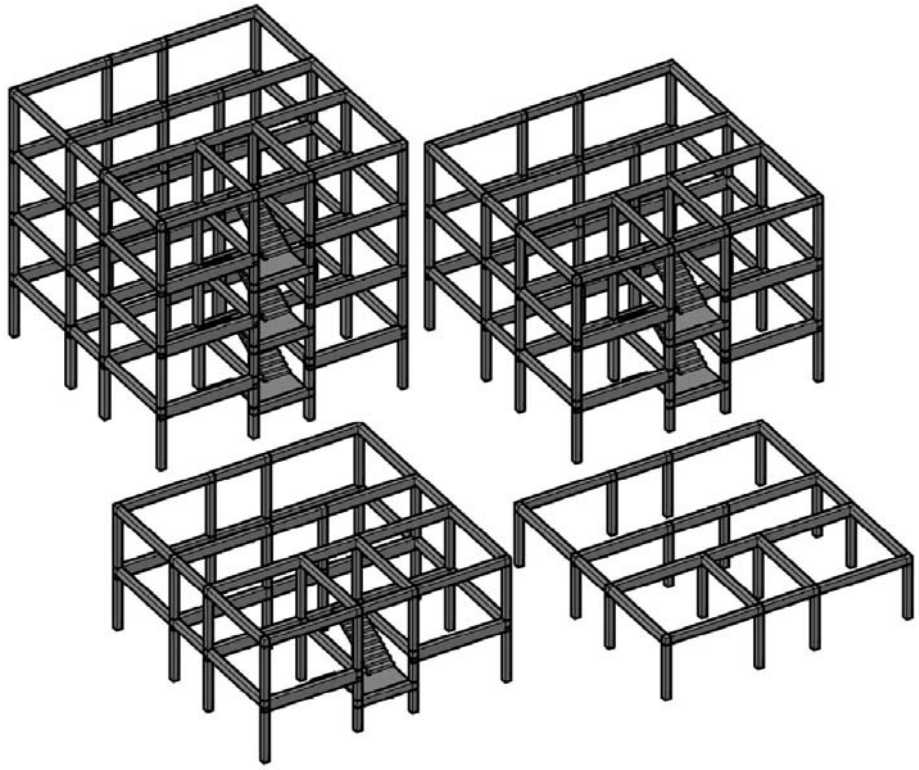

Fig. 9.6: Tri-dimensional representation of the 3D structures.

Fig. 9.6 shows the isometric views of the 3D structures from which the analysed plane frames have been derived.

The geometric characteristics of the structural elements are reported in Table 9.1 and Table 9.2 for column and beams, respectively.

The columns have shear reinforcement made with horizontal two arms hoops ϕ 8 with step equal to 20 cm.

The beams are reinforced with two arms hoops ϕ 8 with step 15 cm at the two ends and 25 cm in the middle.

Table 9.1: Geometric characteristics of the columns.

Section	B [cm]	H [cm]	A_{long}
101	30	30	4 ϕ 16
102	30	40	4 ϕ 16+2 ϕ 12
103	40	30	4 ϕ 16+2 ϕ 12
104	30	50	6 ϕ 16
105	50	30	6 ϕ 16

Table 9.2: Geometric characteristics of the beams.

Section	B [cm]	H [cm]	A_{sup}	A_{inf}
1	30	60	3 ϕ 16	2 ϕ 16
2	30	60	2 ϕ 16	5 ϕ 16+1 ϕ 20
3	30	60	5 ϕ 16+2 ϕ 20	2 ϕ 16
4	30	60	2 ϕ 16	3 ϕ 16
5	30	60	2 ϕ 16	2 ϕ 16
6	30	60	4 ϕ 16	2 ϕ 16
7	30	60	3 ϕ 16	3 ϕ 16
8	30	60	2 ϕ 16	5 ϕ 16
9	30	60	5 ϕ 16+1 ϕ 20	3 ϕ 16
10	30	40	2 ϕ 16	4 ϕ 16
11	30	40	2 ϕ 16	2 ϕ 16
12	30	40	4 ϕ 16	2 ϕ 16
13	30	40	2 ϕ 16	3 ϕ 16
14	30	40	2 ϕ 16	5 ϕ 16
15	30	40	6 ϕ 16	2 ϕ 16
16	30	40	3 ϕ 16	2 ϕ 16
17	30	50	3 ϕ 16	2 ϕ 16
18	30	50	2 ϕ 16	5 ϕ 16
19	30	50	7 ϕ 16	2 ϕ 16
20	30	50	2 ϕ 16	3 ϕ 16
21	30	50	2 ϕ 16	2 ϕ 16

The arrangement of structural elements within the structure is shown in Table 9.3, Table 9.4 and Table 9.5 by considering that buildings with fewer floors can be obtained simply by removing the floors located below.

Table 9.3: Layout of the column in the structure.

Column	1st Floor	2nd Floor	3rd Floor	4th Floor
1	101	101	101	101
2	103	101	101	101
5	102	101	101	101
6	105	103	101	101
9	102	101	101	101
10	104	102	101	101
13	101	101	101	101
14	102	101	101	101

Table 9.4: Layout of the beam in the structure at the roof floor.

Roof Floor							
Allignment	1y		Span	2y			Span
1x	Joint	11	10	15	Joint	15	13
	11						
Span	11						
	11						
2x	Joint	17	18	19	Joint	19	20
	11						
Span	11						
	11						
3x	Joint	17	18	19	Joint	19	20
	11				13		
Span	11				13		
	11				13		
4x	Joint	11	10	15	joint	15	13

The numbering used in Table 9.3, Table 9.4 and Table 9.5 is the one already utilised and shown in Fig. 9.5.

By considering the symmetry of the structure in respect of a vertical plane parallel to the y-axis and passing through the geometric centre of the floor, in Table 9.4 and Table 9.5 are reported only the structural elements located at left of the geometric centre.

About the materials, concrete having a characteristic cube strength R_{ck} equal to 25 MPa and steel type AQ42 (Santarella, 1963) have been considered.

The contribution of the confinement effect provided by stirrups has been taken into account by considering two different constitutive laws for the core and cover concrete; in particular the following equation have been utilised for developing the two constitutive laws (Paulay & Priestley, 1992):

$$f_{cc} = \left[1 + 3.7\left(\frac{0.5\alpha_n\alpha_s\rho_s f_{yt}}{f_c}\right)^{0.86}\right] f_c \,, \tag{9.47}$$

$$\varepsilon_{cu} = 0.004 + 0.5\frac{0.5\alpha_n\alpha_s\rho_s f_{yt}}{f_{cc}} \,, \tag{9.48}$$

$$\varepsilon_{cc} = \varepsilon_{c1}\left[1 + 5\left(\frac{f_{cc}}{f_c} - 1\right)\right]. \tag{9.49}$$

Table 9.5: Layout of the beam in the structure at the intermediate floors.

Other Floors							
Allignment	1y		Span	2y			Span
1x	Joint	1	2	6	Joint	6	5
	11						
Span	10						
	12						
2x	Joint	1	2	6	Joint	6	5
	12						
Span	11						
	12						
3x	Joint	1	2	6	Joint	6	5
	12				13		
Span	10				14		
	11				13		
4x	Joint	7	8	7	Joint	10	10

Basically, the mechanical characteristics of the materials are:

- Cover Concrete
  - f_c = 28.75 MPa;
  - ε_{c0} = 0.002;
  - f_{cu} = 5.75 MPa;
  - ε_{cu} = 0.006;
  - Tensile strength equal to zero.

- Core Concrete
  - f_c = 33.55 MPa;
  - ε_{c0} = 0.0037;
  - f_{cu} = 6.75 MPa;
  - ε_{cu} = 0.0157;
  - Tensile strength equal to zero.
- Steel
  - f_y = 320 MPa;
  - E_s = 210 000 MPa;
  - strength hardening = 1%;

The plane frame considered in the following analyses is the one individuate by the alignment namely 2X in Fig. 9.5. The frame has been modelled in ADAPTIC (Izzuddin, 1991) which provides several linear and nonlinear materials. The ones considered in this study are shown in Fig. 9.7.

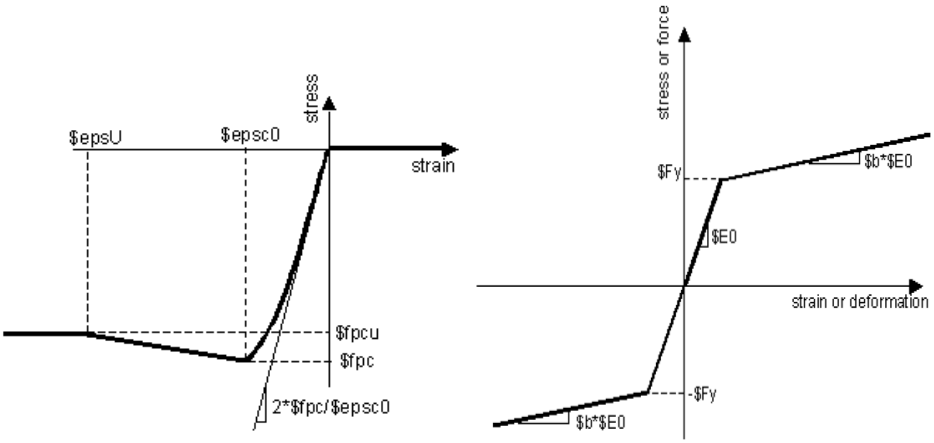

Fig. 9.7: Constitutive laws of concrete (on the left) and steel (on the right).

The masses related to the gravitational load are reported in Fig. 9.5 and have been evaluated according to the NTC (2008) recommendations through Eqn. (9.50)

$$G_k + \sum_j \left(\psi_{2j} Q_{kj} \right) \tag{9.50}$$

in which $\psi_{2i} = 0.6$ has been taken by considering the variable loads at the intermediate floors and $\psi_{2i} = 0.0$ has been considered about the load due to snow on the roof floor.

$$E + G_k + \sum_j \left(\psi_{2\,j} Q_{kj}\right). \tag{9.51}$$

Eqn. (9.51) reports the load combination considered for the superposition of the seismic action and the gravity loads.

9.2.2 Static Nonlinear Analysis Results

Both NTC (2008) and Eurocode 8 (EN 1998, 2005) prescribe two different force patterns to apply to structures: a uniform pattern where forces proportional to the masses on the floor are taken in account and a modal pattern where the applied forces are taken proportional to the masses and the modal shape.

The performance point provided by the N2-Method (Fajfar, 1999) should be compared with the capacity point, this last one is function of the Limit State considered and of the mechanism taken in account; in this work only flexural and shear mechanisms in beams and columns are considered to define the Limit State of Damage Limitation (SLD), of Life Safety (SLV) and Collapse (SLC). The three Limit States considering flexural mechanisms are individuate by the value of yielding chord rotation θ_y [Eqn. (9.52)] and ultimate chord rotation θ_u [Eqn. (9.53)]; in particular yielding chord ration θ_y is used to individuate the SLD, the ultimate chord rotation θ_u denotes the SLC and ¾ θ_u is representative of the SLV.

$$\theta_y = \phi_y \frac{L_V + a_v z}{3} + 0{,}00135\left(1 + 1{,}5\frac{h}{L_V}\right) + \frac{\varepsilon_y}{d - d'}\frac{d_b f_y}{6\sqrt{f_c}}, \tag{9.52}$$

$$\theta_u = \frac{1}{\gamma_{el}} 0{,}016\left(0{,}3^{\nu}\right)\left[\frac{max\left(0{,}01;\omega'\right)}{max\left(0{,}01;\omega\right)}\right]^{0{,}225}\left(\frac{L_V}{h}\right)^{0{,}35} 25^{\left(\alpha\rho_{sx} f_{yw}/f_c\right)}\left(1{,}25^{100\rho_d}\right). \tag{9.53}$$

The brittle failure is controlled by the shear stress in the elements; in particular a shear collapse is verified if the interior shear force in a column exceeds the resistance value provided by Eqn. 5.3.

$$V_R = \frac{1}{\gamma_{el}}\left[\begin{array}{c} \frac{h - x}{2L_V} min\left(N; 0{,}55 A_c f_c\right) + \left(1 - 0{,}05\, min\left(5; \mu_\Delta^{pl}\right)\right)\cdot \\ \cdot 0{,}16\, max\left(0{,}05; 100\rho_{tot}\right)\left(1 - 0{,}16\, min\left(5; \frac{L_V}{h}\right)\right)\sqrt{f_c} A_c + V_w \end{array}\right]. \tag{9.54}$$

Further information about symbols, equations, analyses and vulnerability evaluation parameters used in this thesis can be found in Faella et al. (2009).

Fig. 9.8 shows the capacity curve provided by PushOver analyses of the plane frames without joint modelling (black lines) and with exterior beam-to-column modelling (red lines); both uniform (continuous lines) and modal (dashed line) forces patterns are taken in account. Furthermore the points of the first element that exceed flexural and shear capacity for each Limit State are reported.

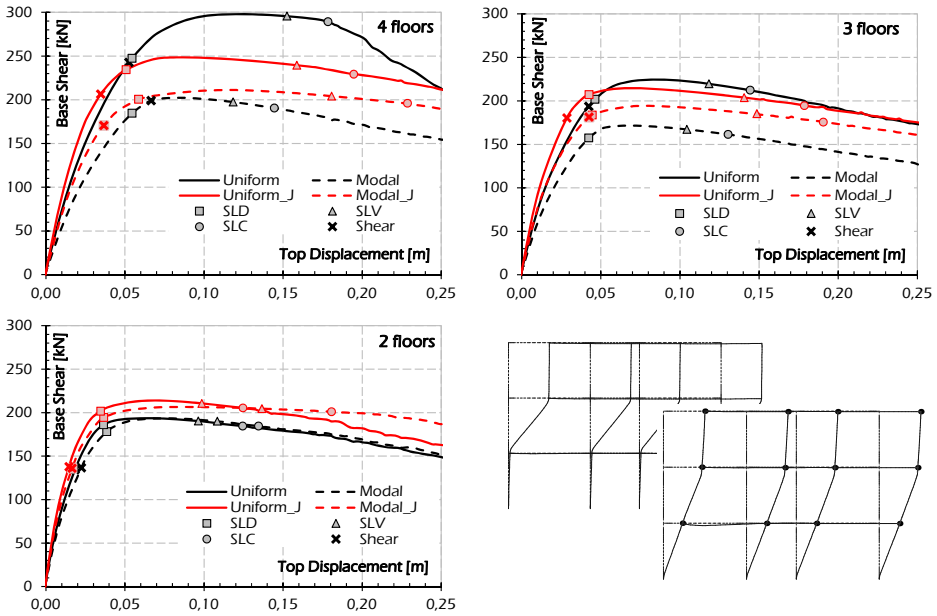

Fig. 9.8: Capacity curve with and without joint behaviour.

For all the analysed structures in which the damage of exterior beam to column joints has been taken in account it is easily observable an initial stiffness of the nonlinear behaviour greater than the one developed in traditional analyses where the joint behaviour is neglected. Indeed, the effects of the deformability of joints are equilibrated by the introduced rigid link simulating the panel zone. Another important effect is that in joint modelling the two curves obtained by the two different force patterns are more coincident than other ones derived for the frames without exterior joint behaviour simulation.

Finally, also the deformed shape of the three storey plane frame corresponding to the capacity point of Life Safety is shown in Fig. 9.8. The use of

a nonlinear rotational spring for representing the actual behaviour of exterior joint leads to a significant change in the failure mode. In the analysis of the frame with rigid joints, a floor mechanism characterizes the collapse of the structures; conversely a global mechanism determines the performance of the frames modelled accounting for the damage in the joints.

9.2.3 Results of Seismic Assessment

For all the structures a seismic vulnerability assessment using N2-Method is carried out and the level of inadequacy is represented by the risk index α (Faella et al., 2009).

Table 9.6: Parameters of the seismic action.

Limit State	SLD	SLV	SLC
a_g	0,125 g	0,300 g	0,381 g
F_0	2,316	2,384	2,425
T_{C^*}	0,290 s	0,356 s	0,373 s
S_S	1,200	1,114	1,030
C_c	1,409	1,352	1,340
S_T	1,200	1,200	1,200
S	1,440	1,337	1,236
η	1,00	1,00	1,00
T_B	0,136 s	0,161 s	0,166 s
T_C	0,409 s	0,482 s	0,499 s
T_D	2,100 s	2,799 s	3,124 s

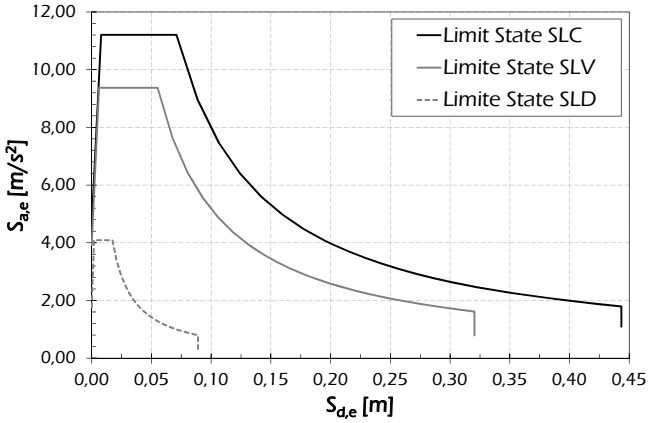

Fig. 9.9: Elastic ADRS spectra.

For this purpose we assumed the three structures located at L'Aquila (Italy) where a strong earthquake happened on April 2009; the seismic inputs for the three Limit States considered in this analyses are evaluated using NTC (2008) parameters that provide spectra function of the geographic coordinates of the site and of the soil category; in particular the parameters of the considered seismic action are reported in Table 9.6 and the corresponding spectra are shown in Fig. 9.9.

Fig. 9.10 to Fig. 9.12 compare the vulnerability of the frames determined using different models, either accounting for the nonlinear joint behaviour (red histograms) or assuming rigid and resistant joints (black histograms). The former modelling approach leads to higher α values and therefore lower vulnerability in assessing flexural mechanisms, but to higher vulnerability when considering shear failure. The lower vulnerability gained at SLV and SLC when using frame models accounting for joint damage is due to the lower ductility demand for beams and columns caused by the joint deformability. A more limited reduction in vulnerability is obtained at SLD because the performance at that limit state is not associated with the ductility capacity but with the stiffness of the analysed structure.

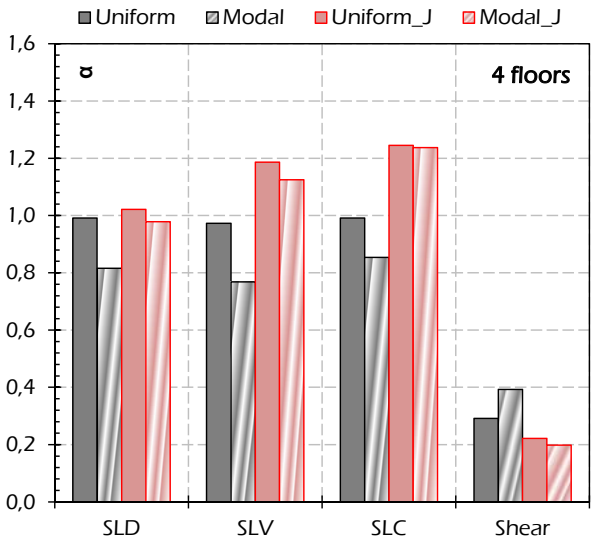

Fig. 9.10: Vulnerability parameter α at different limit states, considering flexural and shear failure mechanisms for frame with 4 floors.

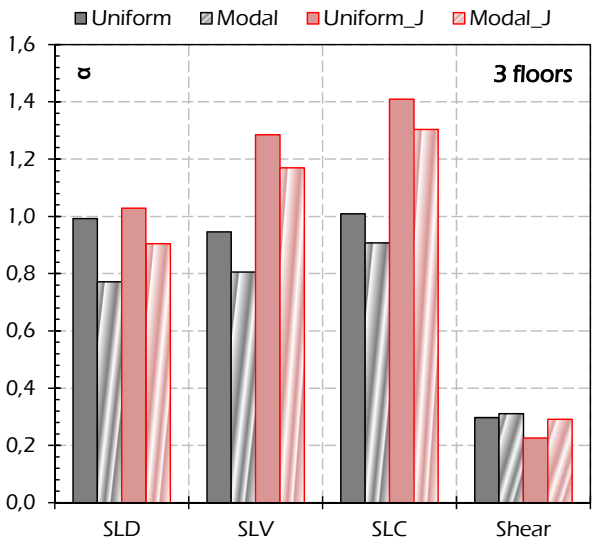

Fig. 9.11: Vulnerability parameter α at different limit states, considering flexural and shear failure mechanisms for frame with 3 floors.

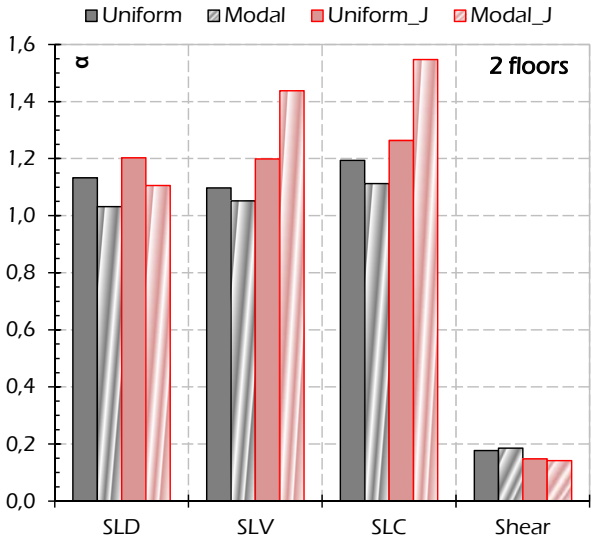

Fig. 9.12: Vulnerability parameter α at different limit states, considering flexural and shear failure mechanisms for frame with 2 floors.

9.2.4 Nonlinear Time History Analysis Results

The effects of the local response of the exterior joints with reduced capacity on the seismic behaviour of 4, 3 and 2-storey frame structures are investigated for the seismic excitation of ElCentro-1940 (Chopra, 1995). For comparison purpose the response of the multi-storey frame structures is also studied for the case without the joint effect and without rigid zones.

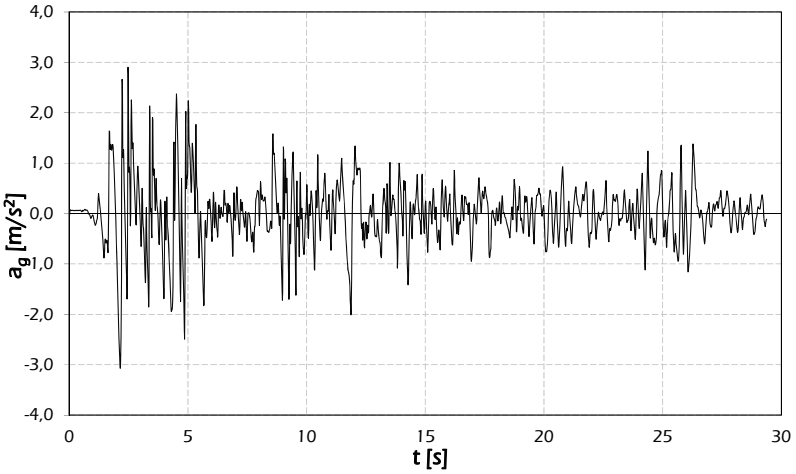

Fig. 9.13: Accelerograms of El Centro-1940 (Chopra, 1995).

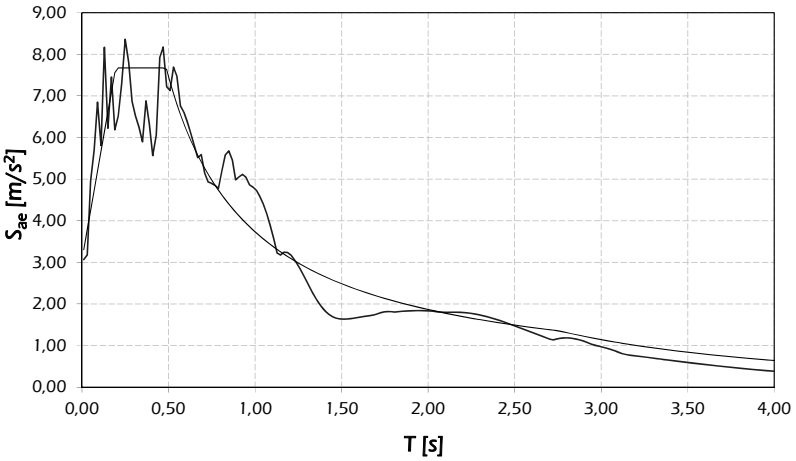

Fig. 9.14: Response spectrum of El Centro-1940 (Chopra, 1995) and corresponding response spectrum of Newmark & Hall (1982).

The effects of the exterior beam-to-column connections on the maximum displacement and on the maximum interstory drift is presented in Fig. 9.15 in which it is observed that in any case the joint results in approximately equality top displacement than ones without joint effect.

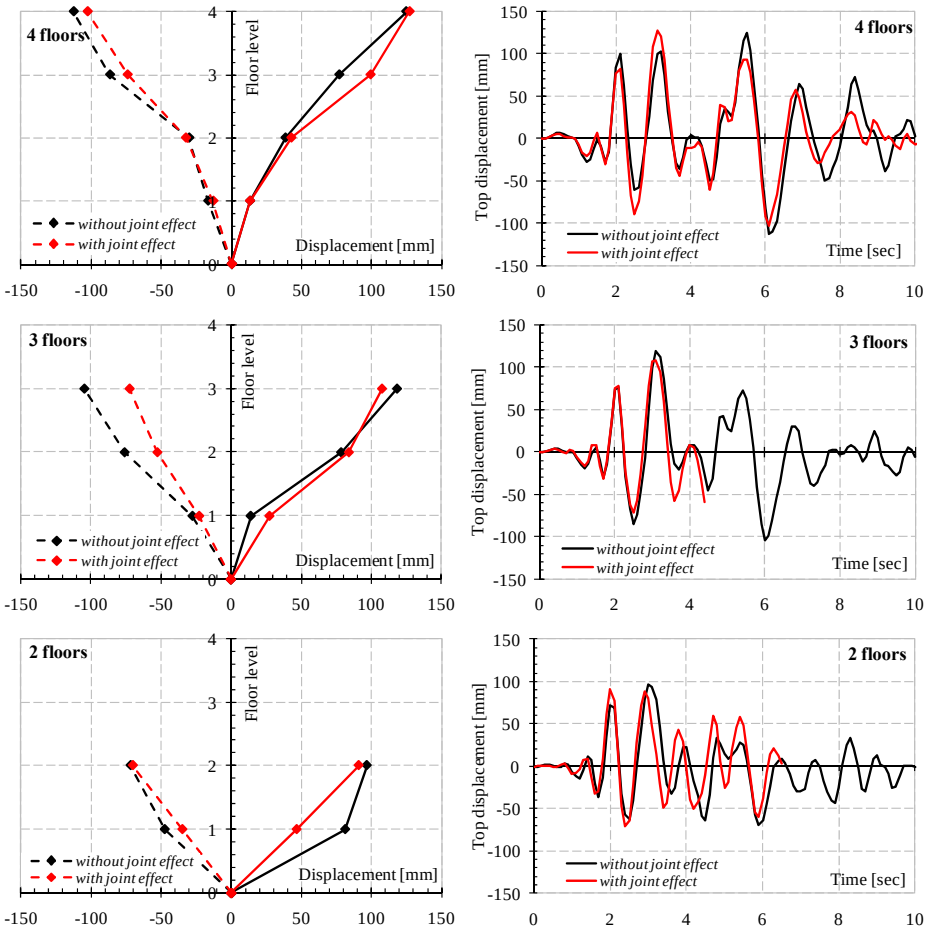

Fig. 9.15: Comparison of time history analysis

By Fig. 9.15 it can be observed that in spite of the equal top displacement developed for both analysed cases, the interstory drift measured for 2-storey frame in which joint nonlinearity is taken in account is smaller than one provided by the frame without joint effect.

CHAPTER X

10. Conclusions

In this thesis, reinforced concrete beam-to-column joints have been analysed. A wide database collecting 224 experimental tests on exterior joints and 85 specimens on interior connections has been collected. The available test data on the strength of exterior and interior beam-to-column connections is far from being comprehensive and there is a clear need for further tests.

The results collected herein have been firstly used for assessing the behaviour of joints individuating the parameters that affect their ultimate shear capacity. Shear strength of both interior and exterior joints depends on joint dimensions, concrete strength, joint shear reinforcement, joint aspect ratio and detailing of beam and column reinforcement. Less sensitive correlation was found between column axial load and joint shear strength.

The main code formulations and capacity models available in the scientific literature have been outlined and explained also using flow charts that report the procedure used for evaluating the shear strength of joints. The models have been studied and compared with the aim of individuating the parameters taken into account by them. All the models generally account the sensitivity dependent by the geometrical dimensions, the concrete strength and the amount of stirrups in the panel zone.

The capacity models have been assessed in qualitative and quantitative ways by comparing the theoretical shear strength V_{jh} with the experimental one V_{jh}^{exp} derived from the collected database. Error and correlation indices have been defined and evaluated for each model. Further analyses have been provided regarding to the parameters needed to perform reliability analysis; in this context important tools have been carried out. Furthermore, a new formulation has been proposed for evaluating the shear strength of exterior joints both reinforced and unreinforced.

In chapter 7 the behaviour under cyclic loading has been analysed. A general law relating the cyclic degradation to the monotonic strength has been calibrated by providing the parameter of degradation needed for evaluating the shear strength of joints after a specified number of loading and unloading cycles.

Finally, the modelling of nonlinear behaviour of exterior and interior beam-to-column joints in rc frames analyses is discussed. The most known models available in the scientific literature have been outlined. Furthermore, a general model for accounting beam-to-column joints in nonlinear analyses has been calibrated showing the results obtained by comparing the experimental dynamic response and the theoretical one. The calibrated model has been used in the application on a plane frame outlined in chapter 9. The influence of the joint modelling on the global response has been shown with reference to static and dynamic nonlinear analyses by performing also a vulnerability analysis according to European and Italian codes.

The main results obtained in this work can be considered subdivided in five fundamental parts:

- assessment and validation of capacity models for evaluating the shear strength of beam-to-column joints;
- recalibration and assessment of the recalibrated models and of the proposed formulation for exterior joints;
- study of the models with the aim of performing reliability analyses;
- evaluation of the cyclic shear strength starting from the monotonic one and the number of cycles;
- and the part in which the dynamic cyclic behaviour of beam-to-column joints is taken in account with the aim of performing nonlinear analyses on structures accounting the damage of joints.

In the following the main results are synthetically resumed through tables and charts.

10.1 Assessment of Capacity Models

A set of capacity models for evaluating the shear capacity of reinforced beam-to-column joints either available in the scientific literature or adopted by seismic codes have been assessed by considering exterior and interior subassemblies. By analysing exterior joints the collected database has been subdivided in unreinforced, under-reinforced and reinforced joints compliant with Eurocode 8 recommendations (namely, EC8-compliant). Interior joints, instead, have been considered divided in reinforced and unreinforced

connections. The Average Quadratic Error and the Coefficient of Determination (Everitt, 2002) have been evaluated for each model and type of joint as a quantitative measure of the accuracy of the original formulations both recommended by seismic codes and available in the scientific literature.

Fig. 10.1 shows the values of the Average Quadratic Error Δ (Everitt, 2002) provided by the code formulations evaluated with reference to exterior joints by considering the total number of specimens on exterior joints taken into account and the groups individuate taking into account the amount of horizontal reinforcement in the panel zone.

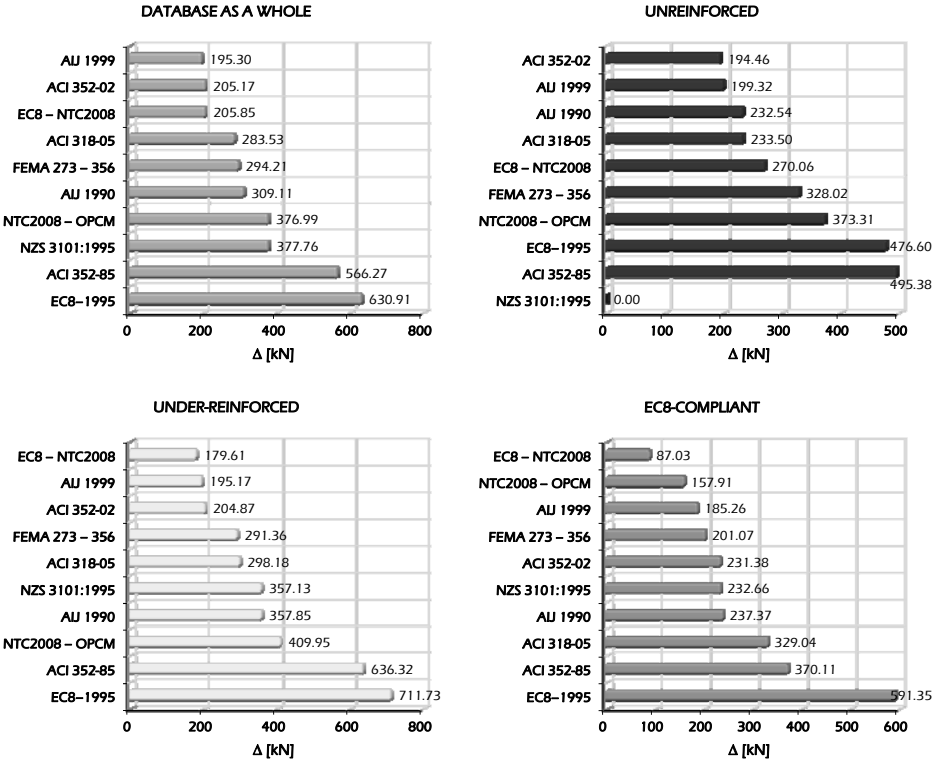

Fig. 10.1: Average Quadratic Error Δ of Code Formulations for exterior joints.

The formulation proposed by the AIJ 1999 (1999) provides the lower error for the total specimens on exterior joints, while the higher Δ is achieved by the formulation recommended by Eurocode 8 (EN 1995, 1995). The lower Average Quadratic Error Δ for unreinforced exterior joints is achieved by the ACI 352-02

(2002) formulation, while by considering reinforced joints both under-reinforced and EC8-compliant, the Eurocode 8 (EN 1998, 2005) and NTC (2008) provide the lower error. On the contrary, the models by Eurocode 8 (EN 1995, 1995) and ACI 352-85 (1985) results the less accurate as they provide the higher Δ in all the analysed cases. By considering unreinforced exterior joints it is noted that the formulation reported in NZS 3101 (1995) does not account shear strength in connections without hoops.

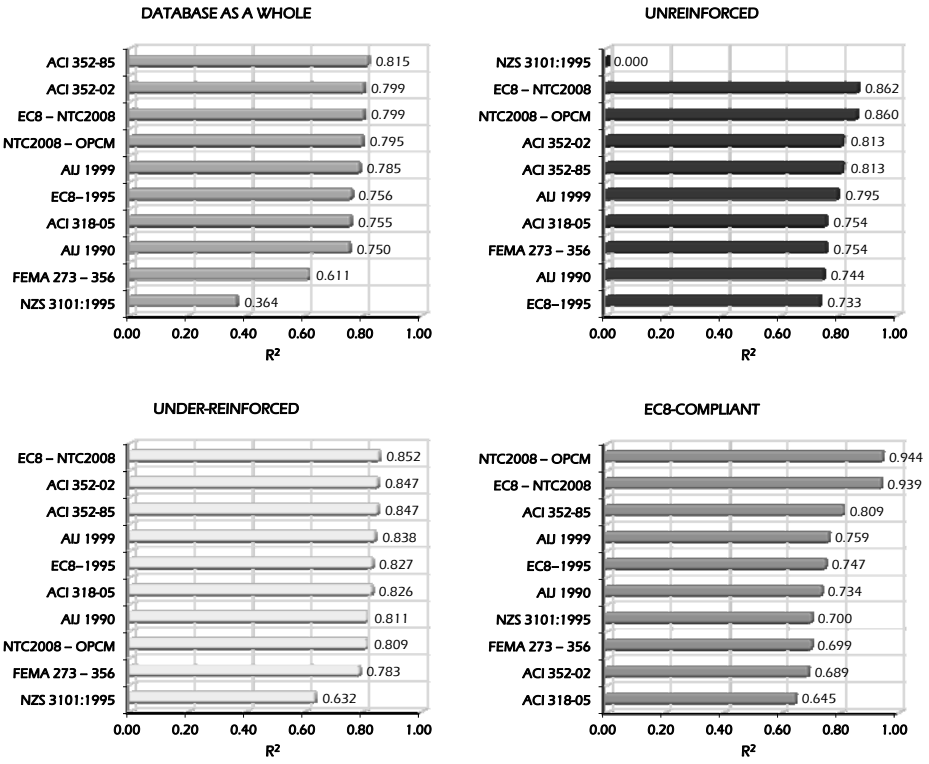

Fig. 10.2: Coefficient of Determination R^2 of Code Formulations for exterior joints.

Fig. 10.2 shows the histograms reporting the Coefficient of Determination R^2 of code formulations in evaluating the shear strength of exterior joints. The higher R^2 is achieved by the ACI352-85 (1985) for the total specimens, by Eurocode 8 (EN 1998, 2005) and NTC (2008) for unreinforced and under-reinforced exterior joints and by the NTC (2008) and OPCM 3431/05 (2005) formulation for existing joints in the case of EC8-compliant connections. The formulation provided by NZS

3101 (1995) allows to the lower value of R^2 for the total specimens on exterior joints taken into account and the under-reinforced joints. The lower Coefficient of determination R^2 for unreinforced exterior joints is developed by the formulations provided by Eurocode 8 (EN 1995, 1995), while the American codes ACI 352-02 (2002) and ACI 318-05 (2005) provide the lower R^2 for EC8-compliant joints.

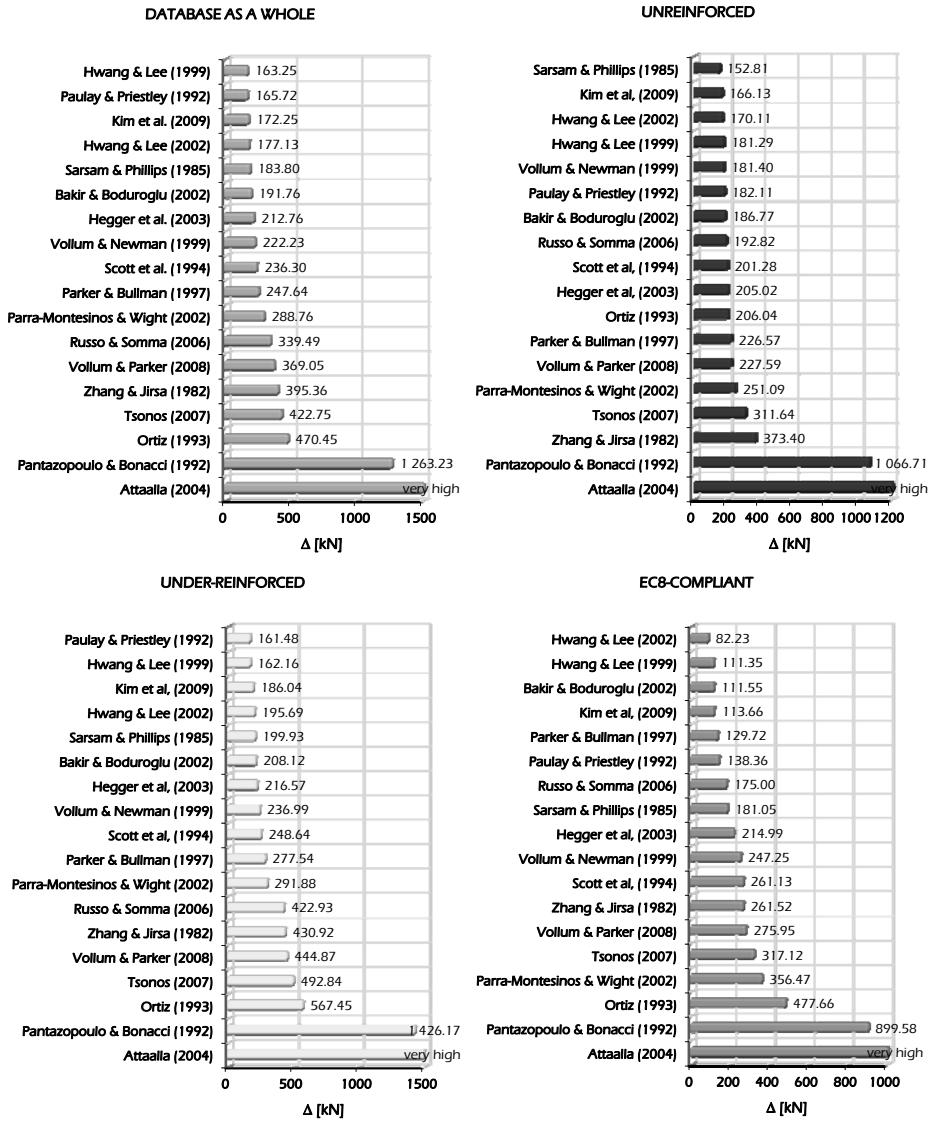

Fig. 10.3: *Average Quadratic Error Δ of Capacity Models for exterior joints.*

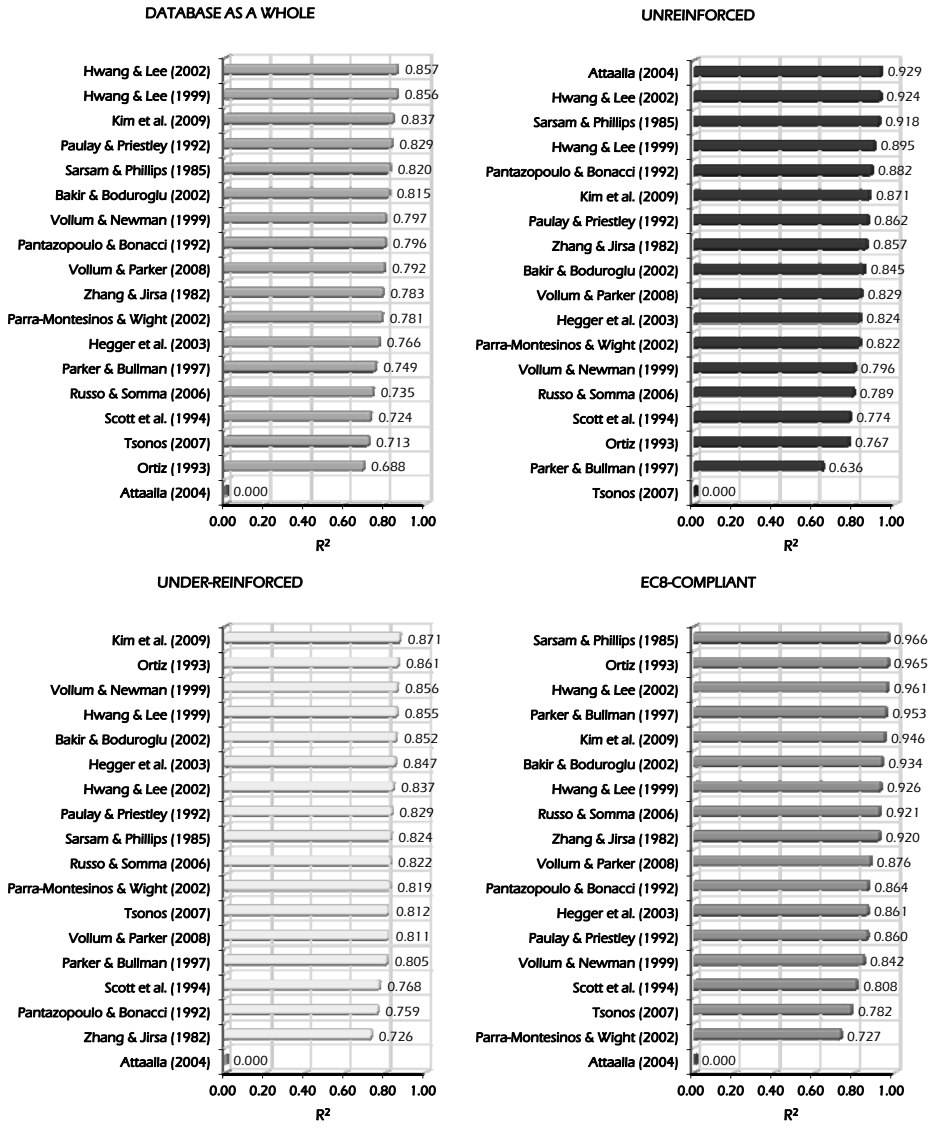

Fig. 10.4: Coefficient of Determination R^2 of Capacity Models for exterior joints.

Fig. 10.3 shows the Average Quadratic Error calculated for the capacity models available in the scientific literature for evaluating the shear strength of exterior reinforced concrete beam-to-column joints.

The model by Hwang & Lee (1999) is the most accurate in evaluating the shear strength of exterior joints by taking into account the total set of specimens

about exterior joints. The lower Δ is provided by the model by Sarsam & Phillips (1985) for unreinforced joints, by the model by Paulay & Priestley (1992) for non-compliant joints and by the model by Hwang & Lee (2002) taking into account compliant joints.

In all the analysed cases the models by Attalla (2004) and Pantazopoulo & Bonacci (1992) are the less accurate providing very high values of the Average Quadratic Error Δ.

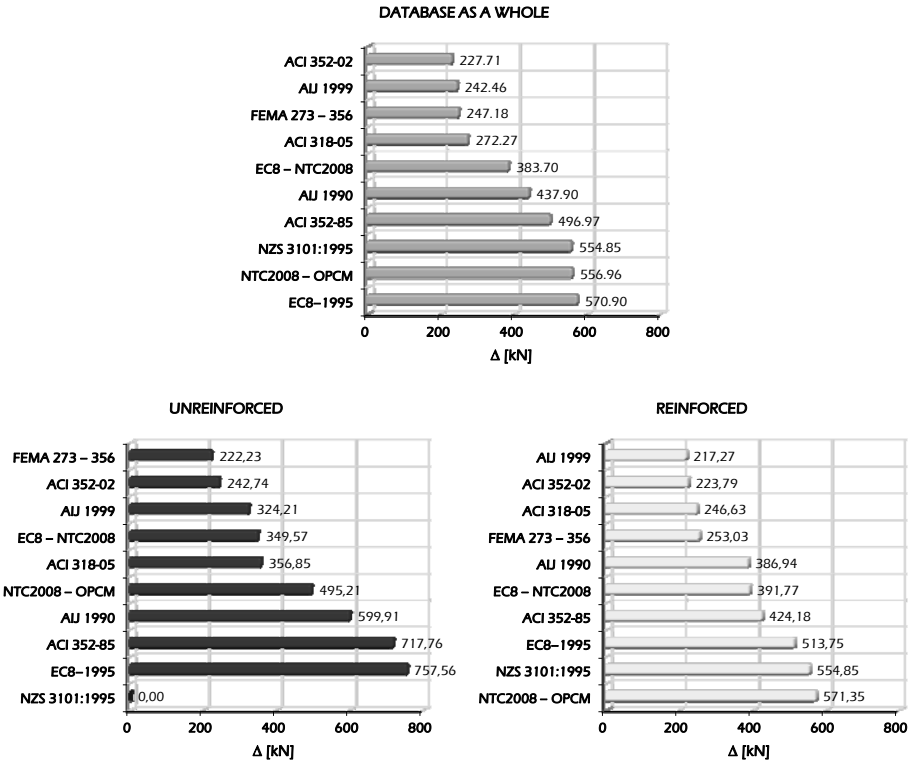

Fig. 10.5: Average Quadratic Error Δ of Code Formulations for interior joints.

Fig. 10.4 shows the Coefficient of Determination R^2 evaluated for the capacity models for exterior beam-to-column joints. In particular the higher R^2 is obtained by the model by Hwang & Lee (2002) for the total specimens and unreinforced joints, while accounting compliant joints very high values of the Coefficient of Determination R^2 are obtained by the model by Sarsam & Phillips (1985) in analysing exterior EC8-compliant joints. The higher Coefficient of

Determination for under-reinforced joints is provided by the model by Kim et al. (2009). On the contrary, the lower values of R^2 are obtained by the model by Ortiz (1993) and Tsonos (2007) by considering the total set of specimens and unreinforced joints, respectively, while the model by Zhang & Jirsa (1982) provides the lower R^2 for under-reinforced exterior joints. Finally, the model by Parra-Montesinos & Wight (2002) achieves the lower Coefficient of Determination in the case of reinforced exterior joints compliant with the Eurocode 8 (EN 1998, 2005) recommendations.

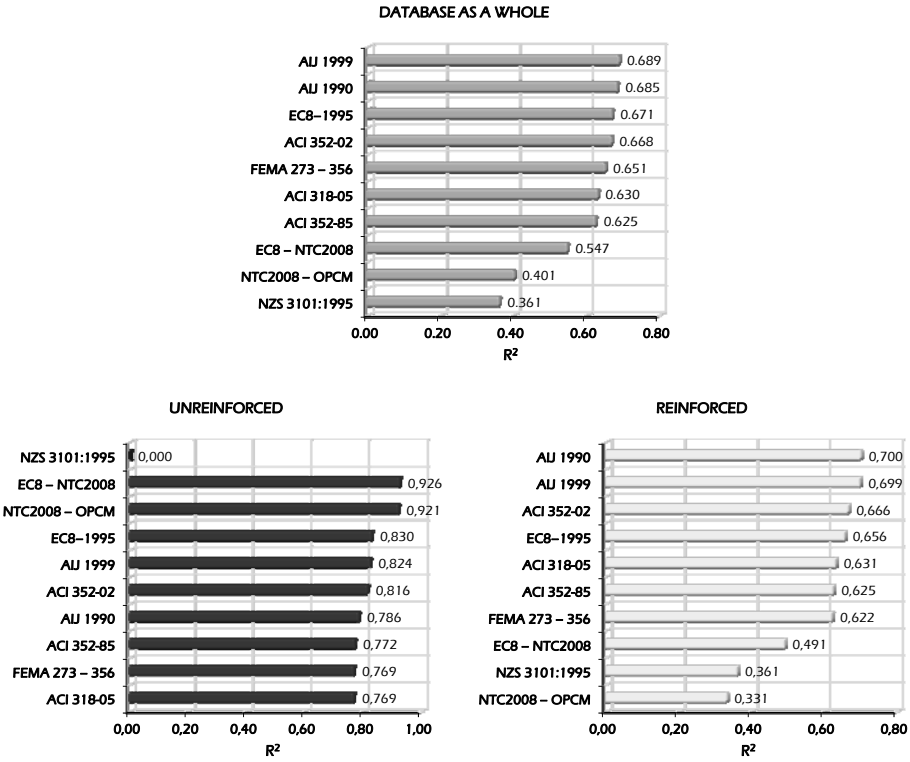

Fig. 10.6: Coefficient of Determination R^2 of Code Formulations for interior joints.

Fig. 10.5 shows the histograms reporting the Average Quadratic Error Δ of the code formulations evaluated for the interior joints collected in the analysed database. By accounting the total number of specimens on interior joints taken into account the lower Δ is provided by the formulation proposed by the ACI 352-02 (2002). The FEMA 273 (1997) and 356 (2000) and the AIJ 1999 (1999)

formulations provide the lower Average Error Δ in the case of unreinforced and reinforced interior joints, respectively.

Instead, the less accurate model for the total number of specimens on interior joints is the one by Eurocode 8 (EN 1995, 1995) providing the higher Δ. This last model is the less accurate also by analysing unreinforced joints, while about reinforced beam-to-column joints the higher Average Error Δ is provided by the formulation recommended by NTC (2008) and OPCM 3431/05 (2005).

Fig. 10.6 shows the values of the Coefficient of Determination R^2 provided by the code formulation for evaluating the shear strength of interior joints.

The higher R^2 is achieved by the models by AIJ 1999 (1999) and AIJ 1990 (1990) for the total number of specimens and only reinforced joints, while the higher correlation in the case on unreinforced joints is obtained by the formulation recommended in Eurocode 8 (EN 1998, 2005) and NTC (2008).

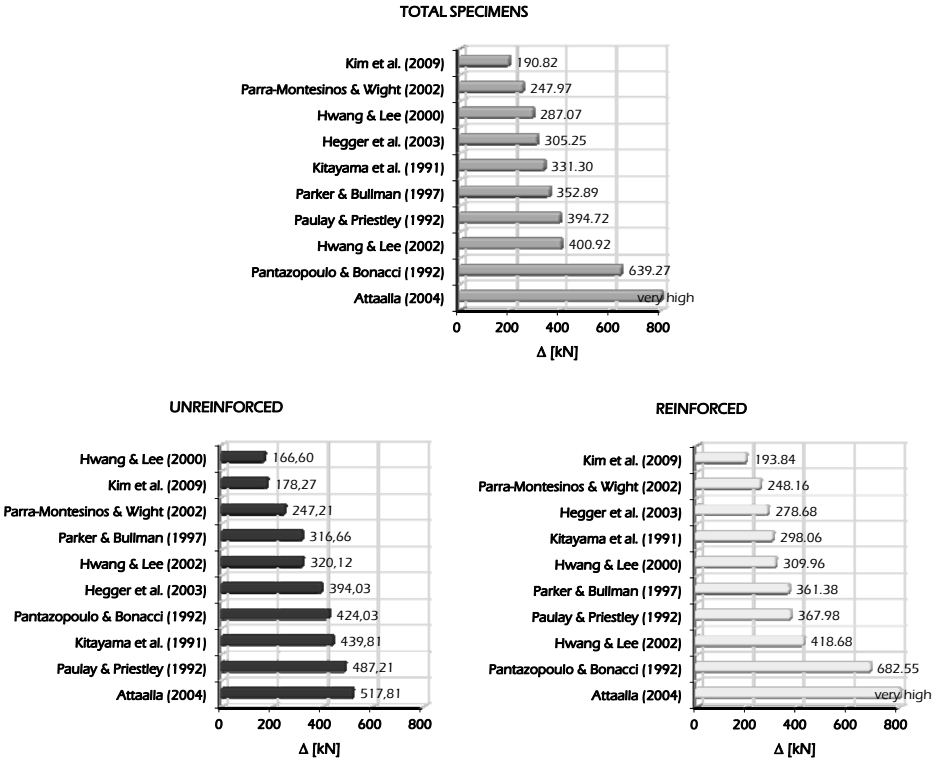

Fig. 10.7: Average Quadratic Error Δ of Capacity Models for interior joints.

Fig. 10.7 shows the histograms reporting the Average Quadratic Error Δ evaluated through the capacity models available in the scientific literature for evaluating the shear strength of interior beam-to-column joints. About the total number of specimens taken into account in the present study the model by Kim et al. (2009) provides the lower average error, while the models by Pantazopoulo & Bonacci (1992) and by Attalla (2004) develop the higher value of Δ being the less accurate between the analysed models. The same behaviour is observed by considering only reinforced interior joints resulting the model by Kim et al. (2009) the most accurate. About unreinforced interior joints, the model by Hwang & Lee (2000) provides the lower Average Quadratic Error is the one, while the models by Attalla (2004) and by Paulay & Priestley (1992) are the less accurate developing the higher Δ.

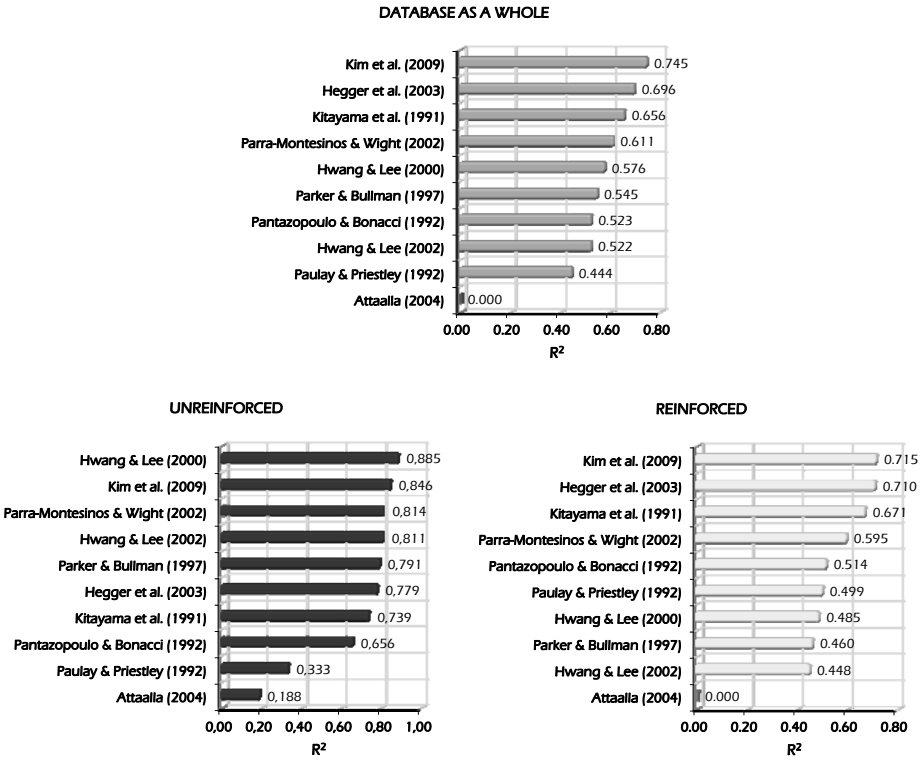

Fig. 10.8: Coefficient of Determination R^2 of Capacity Models for interior joints.

Finally, Fig. 10.8 reports the values of the Coefficient of Determination R^2 derived by evaluating the shear strength of interior beam-to-column joints through the capacity models available in the scientific literature for this purpose.

According to the values shown Fig. 10.7 for the Average Error Δ, the model by Kim et al. (2009) provides the higher R^2 in the case of reinforced joints and by considering all the specimens on interior joints collected in the database.

Based on the values determined for both Average Quadratic Error Δ and Coefficient of Determination R^2, the most accurate model about unreinforced interior joints is the one by Hwang & Lee (2000). Finally, the lower R^2 is developed by the models by Paulay & Priestley (1992), by Attaalla (2004) and by Hwang & Lee (2002) for the database as a whole, unreinforced and reinforced joints, respectively.

10.2 Assessment of Recalibrated Capacity Models and Proposed Formula

The models outlined and verified have been recalibrated in chapter 6 through a coefficient α.

Furthermore the following formulation for evaluating the shear strength of exterior joints both reinforced and reinforced has been proposed and assessed with the recalibrated models:

$$V_{jh} = 0.50 \cdot \beta \cdot \left[1 + 0.15 \cdot \left(2 - {h_b}/{h_c}\right)\right] \cdot b_j \cdot h_c \cdot f_c \cdot \left(0.6 + \frac{N_c}{b_c \cdot h_c \cdot f_c}\right)^{1.23} \cdot \left(\frac{A_{sb,\inf} + A_{sb,\sup}}{b_b \cdot h_b \cdot f_c} \cdot f_{yb}\right)^{0.75} + 0.24 \cdot A_{sjh} \cdot f_{yj} \tag{10.1}$$

In the following are shown the histograms reporting the Average Quadratic Error Δ of the recalibrated models for exterior and interior joints; in particular about exterior joints the results of the assessment of the proposed formula compared with the available capacity models are shown.

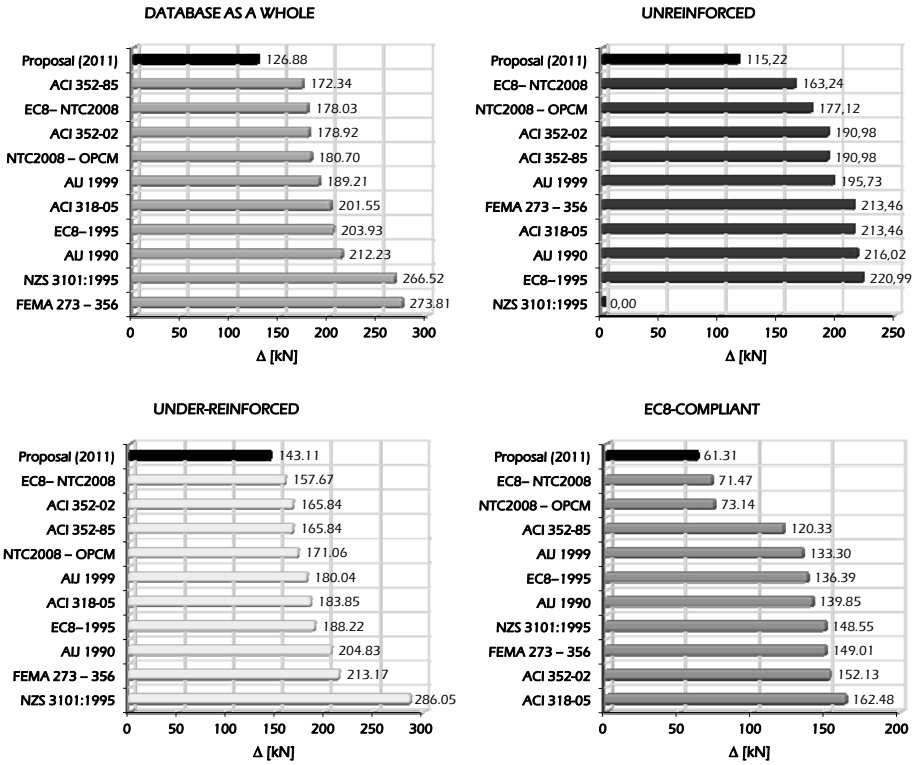

Fig. 10.9: Average Quadratic Error Δ of recalibrated Code Formulations and proposed formula for exterior joints.

Fig. 10.9 and Fig. 10.10 show the Average Quadratic Error Δ evaluated for exterior beam-to-column joints; in particular in Fig. 10.9 are reported the histograms about code formulations while Fig. 10.10 shows the ones reporting the Average Error Δ evaluated for the capacity models available in the scientific literature. Furthermore, in each figure is reported the assessment of the proposed formula showing the accuracy achieved.

The proposed formula for exterior joints leads out a value of the Average Quadratic Error lower than the corresponding value provided by all the analysed code formulations.

Good results of the proposed formula are shown in term of average error by considering the comparison with the recalibrated capacity models available in the scientific literature.

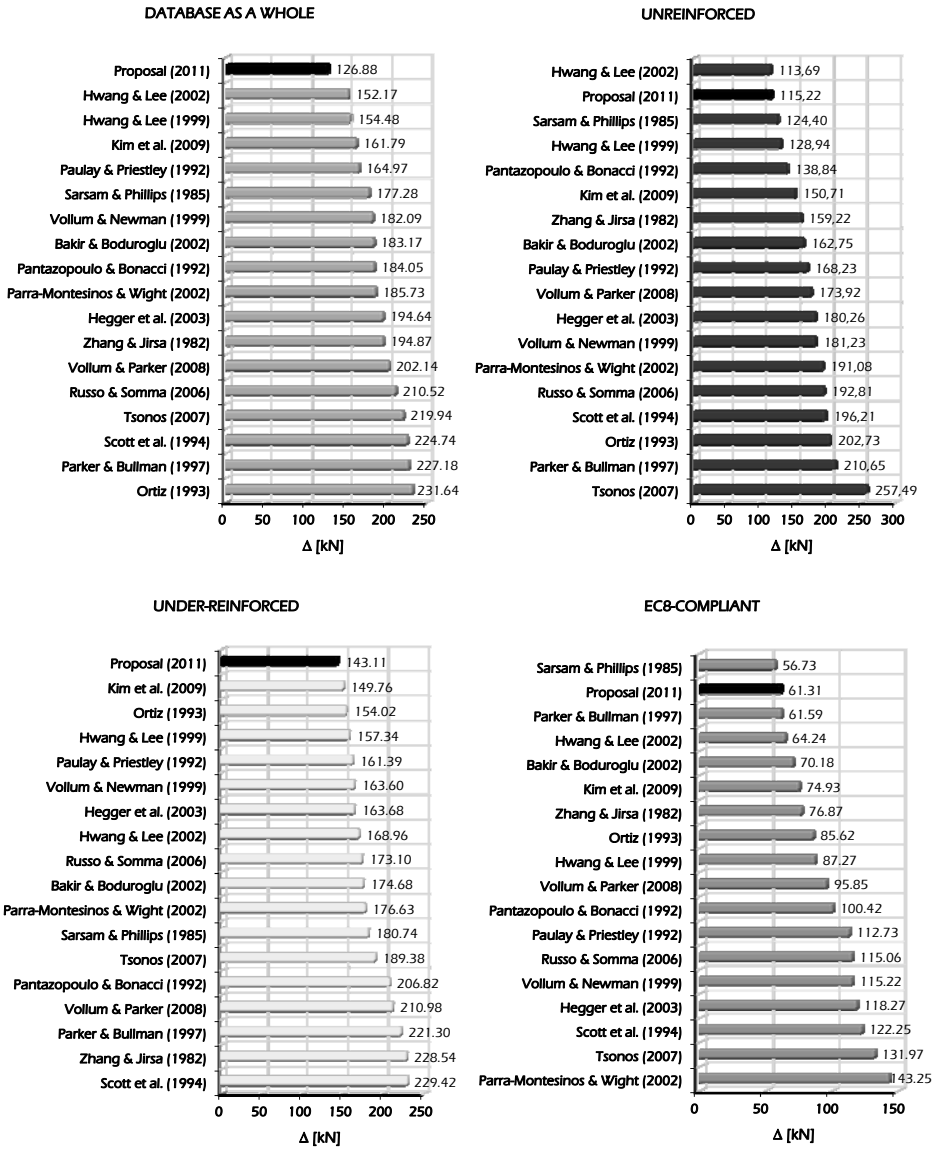

Fig. 10.10: Average Quadratic Error Δ of recalibrated Capacity Models and proposed formula for exterior joints.

The proposed formula provides an average error Δ lower than other capacity models for all the analysed specimens and for under-reinforced joints; while

with reference to unreinforced and EC8-compliant exterior joints the proposed formula is placed at the 2nd place in terms of accuracy resulting the recalibrated models by Hwang & Lee (2002) and by Sarsam & Phillips (1985) the most accurate for unreinforced and compliant joints, respectively.

Finally, it is noted that the recalibration made allows to obtain very low values of the Average Quadratic Error Δ.

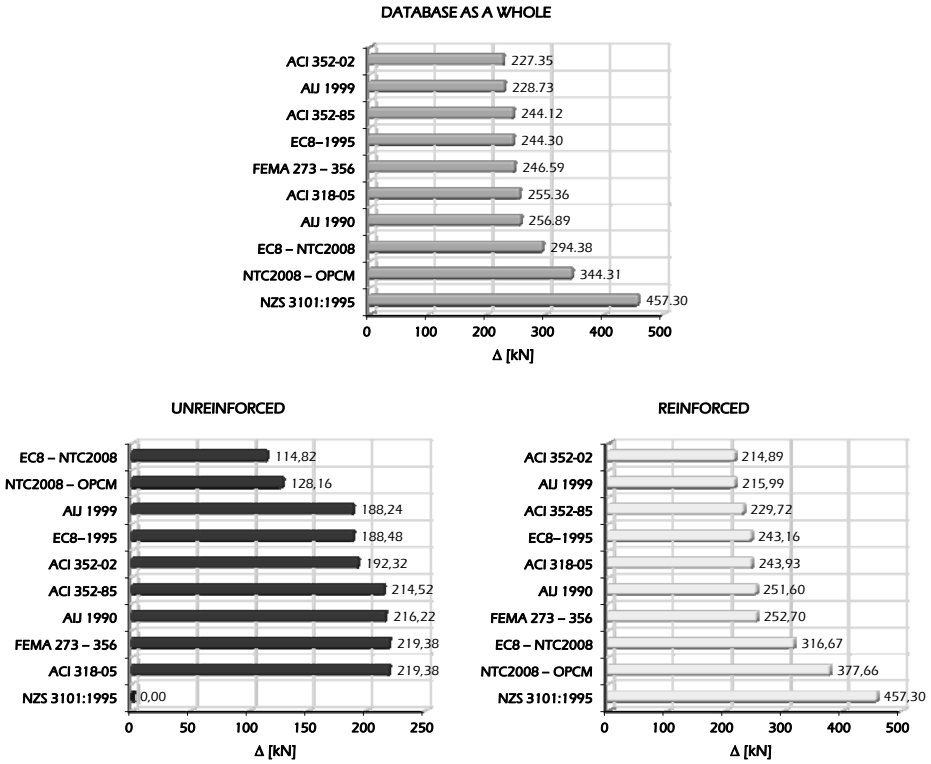

Fig. 10.11: Average Quadratic Error Δ of recalibrated Code Formulations for interior joints.

The resume of the assessment of the recalibrated code formulations for evaluating the shear strength of interior beam-to-column joints is shown in Fig. 10.11. The recalibrated models provide low values of Average Quadratic Error Δ; in particular the lower Δ for all the specimens is provided by the ACI 352-02 (2002), while the lower average error for unreinforced and reinforced interior

joints is achieved by the model by Eurocode 8 (EN 1998, 2005) and NTC (2008) and by ACI 352-02 (2002), respectively.

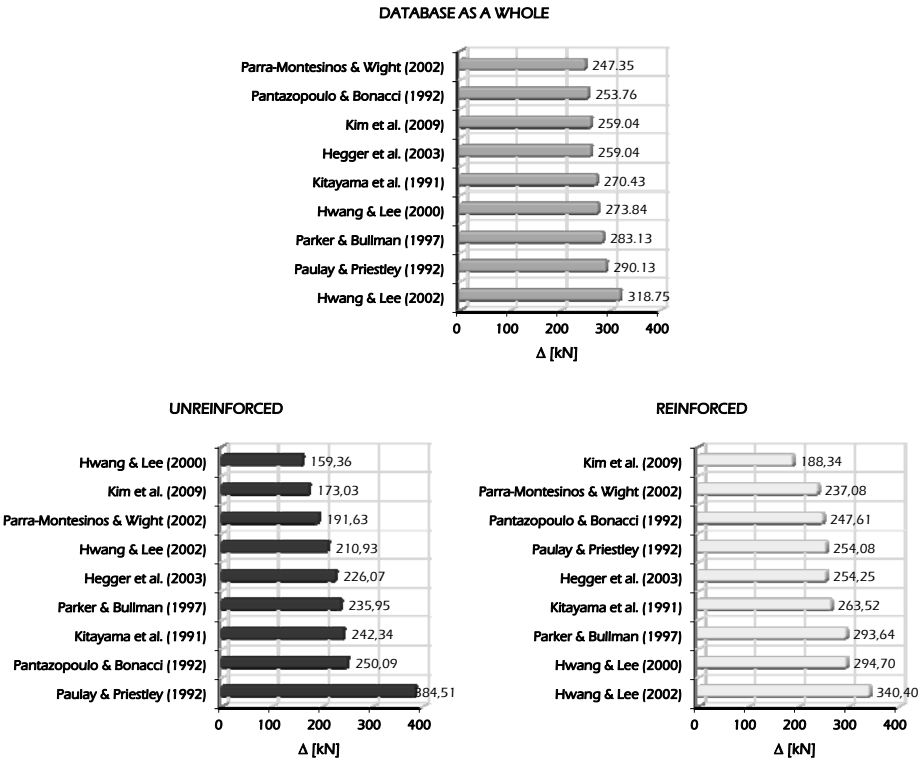

Fig. 10.12: Average Quadratic Error Δ of recalibrated Capacity Models for interior joints.

Finally, the Average Quadratic Errors Δ of the recalibrated capacity models for interior joints are shown in Fig. 10.12. The lower Δ are achieved by the recalibrated models by Parra-Montesinos & Wight (2002), Hwang & Lee (2000) and Kim et al. (2009) for the total set of specimens, unreinforced and reinforced interior beam-to-column joints, respectively.

10.3 Reliability Analysis

By specialising the assessment of the capacity models for beam-to-column joints with the aim of providing tools for performing reliability analyses, the reliability capacity factor β_C has been evaluated.

The following figures show the histograms reporting values of the factor of dispersion of the capacity β_C for both exterior and interior joints.

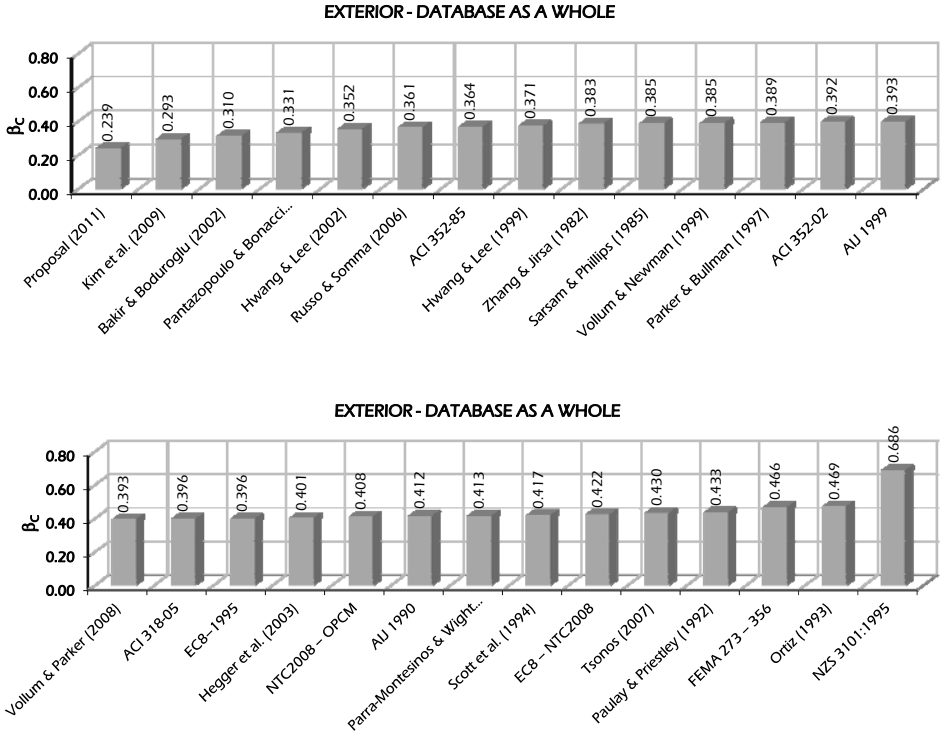

Fig. 10.13: Factor of dispersion of the capacity β_C for the total set of specimens on exterior joints.

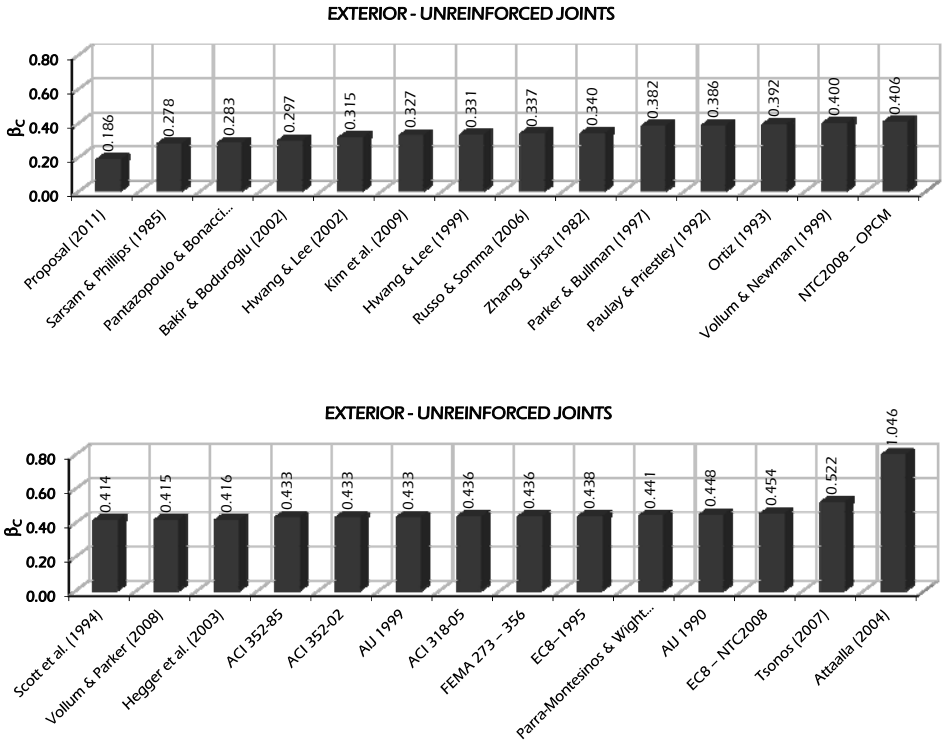

Fig. 10.14: Factor of dispersion of the capacity β_C for unreinforced exterior joints.

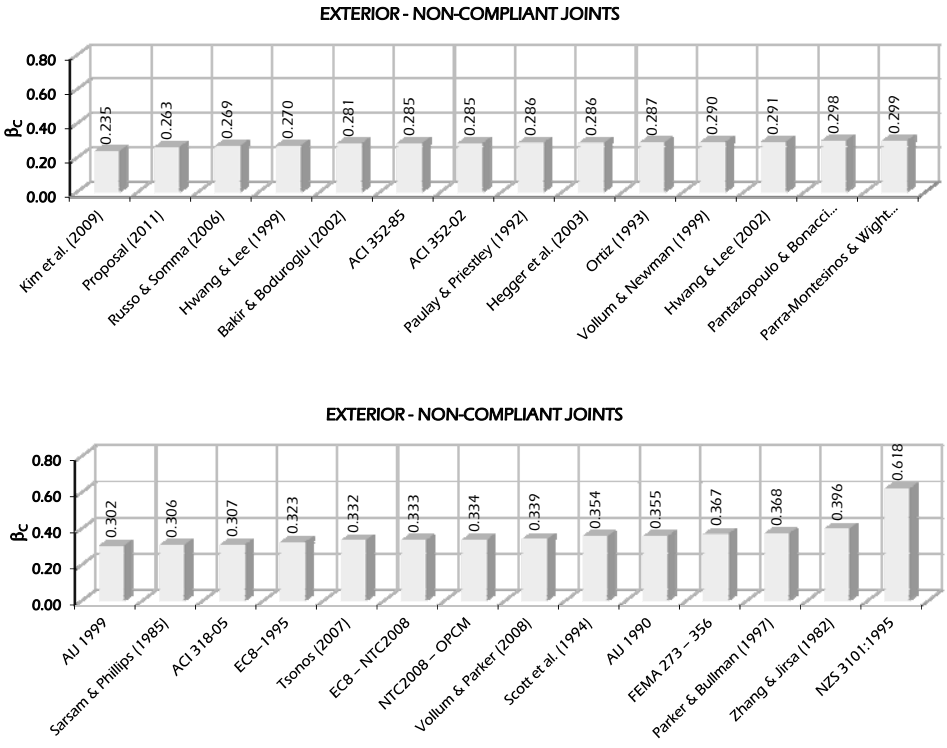

Fig. 10.15: Factor of dispersion of the capacity β_C for under-reinforced exterior joints.

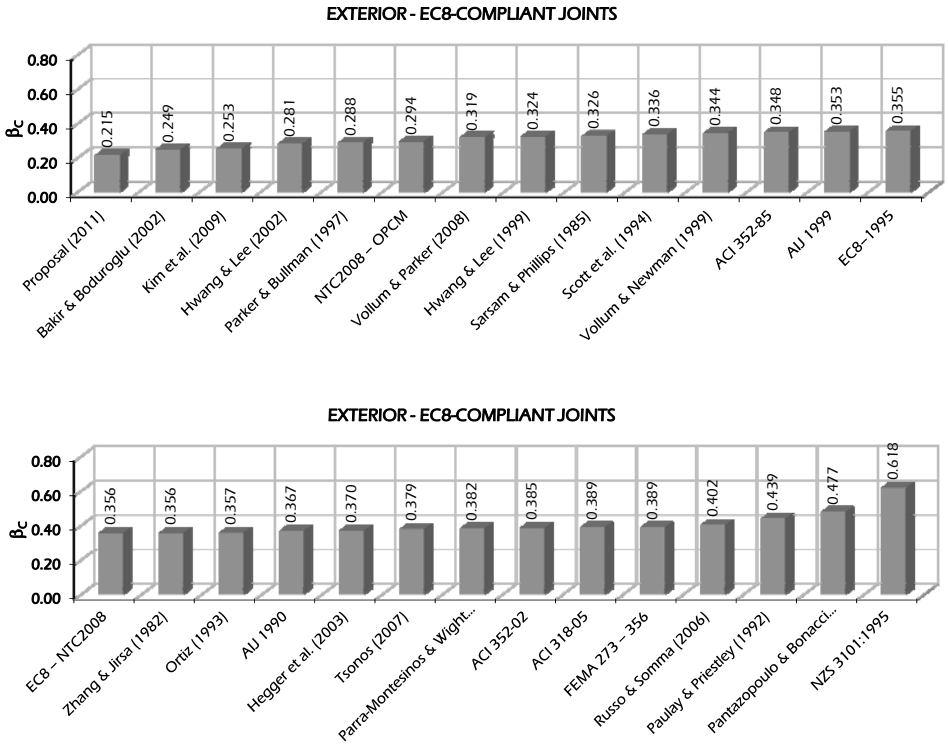

Fig. 10.16: Factor of dispersion of the capacity β_C for EC8-compliant exterior joints.

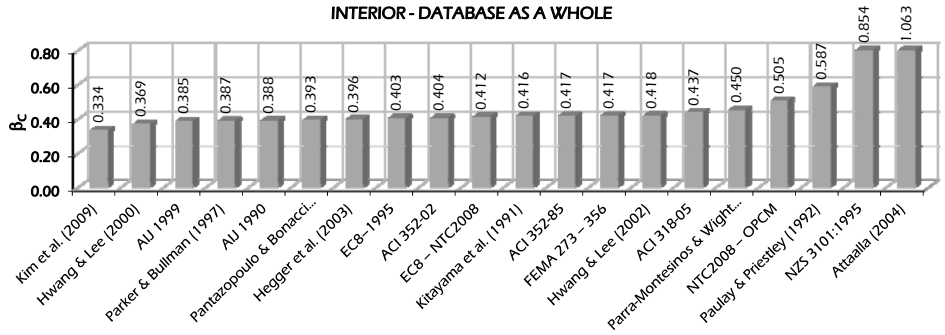

Fig. 10.17: Factor of dispersion of the capacity β_C for the total set of specimens on interior joints.

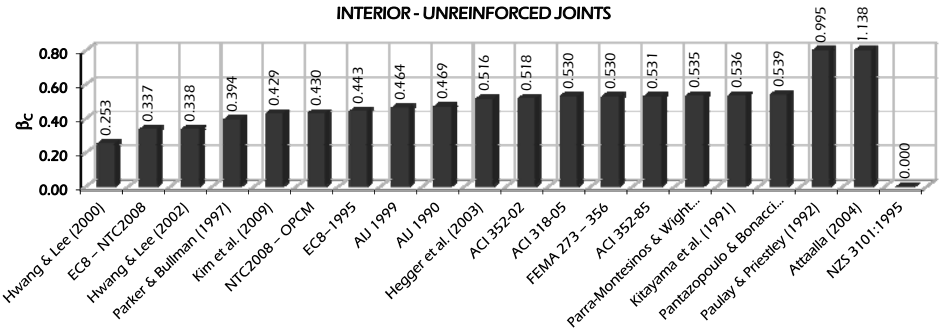

Fig. 10.18: Factor of dispersion of the capacity β_C for unreinforced interior joints.

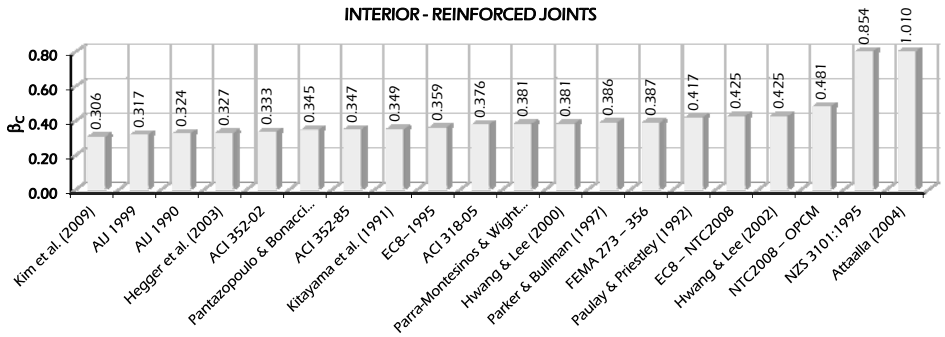

Fig. 10.19: Factor of dispersion of the capacity β_C for reinforced interior joints.

About exterior joints, the proposed formula and the model by Kim et al. (2009) provides the lower dispersion of the capacity, while by analysing interior joints the lower factor of dispersion of the capacity β_C is achieved by applying the models by Kim et al. (2009) and Hwang & Lee (2000).

10.4 Monotonic and Cyclic Strength

Important developments in the study of beam-to-column joints addressed the issue of evaluating the shear strength of these elements under cyclic loads.

Starting from the monotonic shear strength, a formulation for evaluating the capacity under cyclic loads has been assessed; this formulation allows to take into account the strength degradation of joints under seismic actions.

The results that allow to define the log-normal degradation law outlined in Chapter 7 are shown in the following figures.

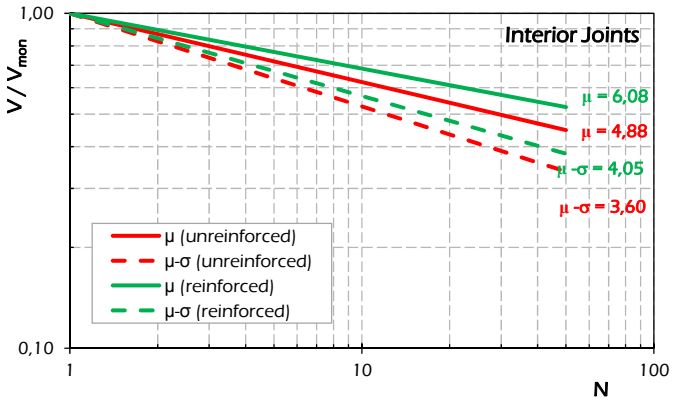

Fig. 10.20: Fatigue curves for interior joints both reinforced and unreinforced.

Fig. 10.20 and Fig. 10.21 show the fatigue curves evaluated for interior and exterior joints, respectively. In particular continuous lines denote the average behaviour derived from the analysed specimens, while the dashed curves indicate the characteristic behaviour evaluated from the average values minus the standard deviation. On the charts are also reported the values of the angular coefficient *m* of the log-normal linear relationship.

The results show a degradation in the strength of unreinforced joints greater than the one observed in the case of reinforced joint. This behaviour is less evident for interior joints. Finally, it can be noted that the confinement effects

made by stirrups and lateral beams in interior joints allow to obtained a ductile joint behaviour.

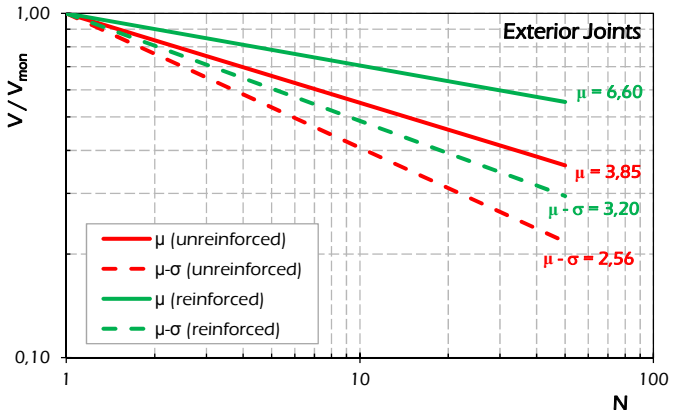

Fig. 10.21: Fatigue curves for exterior joints both reinforced and unreinforced.

10.5 Nonlinear Joints in Seismic Analysis of Frames

The seismic performance of existing RC frames has been investigated accounting for the external joint damage. A scissor nonlinear single-spring model based on the Pivot law (Dowel et al., 1998) has been employed for representing the nonlinear behaviour of exterior RC beam-to-column joints. The parameters of the Pivot model have been determined through calibration of numerical simulations against the results of 12 cyclic tests on RC sub-assemblages. It has been observed that the degradation parameters do not depend on the geometry and mechanical properties of the analysed joints; consequently, these can be employed in general analysis of exiting frames.

The parameters suggested for modelling exterior reinforced concrete beam-to-column joints are:

- α=3.00;
- β=0.50;
- γ=0.30;
- δ=1.50;
- ε=15.

The outcomes of nonlinear static and dynamic analyses, carried out on plane frame structures assuming either rigid joints or nonlinear springs for exterior joints, reveal that:

- the failure mode of the multi-storey frames substantially changes from a floor mechanism in the case of model with rigid joints to a global mechanism considering joint damage;
- considering the so-called "ductile" failure modes, the analyses based on models accounting for joints damage led to lower vulnerability values (indeed higher α); on the contrary, non-conservative vulnerability assessment related to "brittle" failure modes generally results by neglecting the effects of joints damage;
- no significant variation in the overall frame response under low intensity ground motion has been observed using either model for exterior joints.

Appendix A1- Database for Exterior Joints

LOAD TYPE, NOTES AND FAILURE TYPE				
Authors	Name	Load Type	Notes	Failure Type
Alva, 2004	LVP1	C	-	J
Alva et al., 2007	LVP2	C	-	J
	LVP3	C	-	J
	LVP4	C	-	J
	LVP5	C	-	J
Binbhu & Jaya, 2008	A1	C	one-third scaled	BJ
	A2	C	one-third scaled	B
	B1	C	one-third scaled - X-bars	B
	B2	C	one-third scaled - X-bars	B
Calvi et al., 2001	T1	C	2/3 scaled-50's & 70's	BJ
Chalioris et al., 2008	JA-0	C	-	J
	JA-s5	C	-	BJ
	JA-X12	C	X-bars	BJ
	JA-X14	C	X-bars	BJ
	JB-0	C	-	J
	JB-s1	C	-	J
	JB-X10	C	X-bars	BJ
	JB-X12	C	X-bars	BJ
	JCa-0	C	-	J
	JCa-X10	C	X-bars	BJ
	JCa-s1	C	-	BJ
	JCa-s1-X10	C	X-bars	BJ
	JCa-s2	C	-	BJ
	JCa-s2-X10	C	X-bars	BJ
	JCb-0	C	-	J
	JCb-X10	C	X-bars	BJ
	JCb-s1	C	-	J
	JCb-s1-X10	C	X-bars	BJ
	JCb-s2	C	-	J
	JCb-s2-X10	C	X-bars	BJ
Chun & Kim, 2004	JC-1	C	-	B
	JM-1	C	headed bars	B
	JC-2	C	-	J
	JM-2	C	headed bars	J
Chun et al., 2007	JC-1	C	-	B
	JM-1	C	headed bars	B
	JC-2	C	-	J
	JM-2	C	headed bars	J
	JC-No. 11-1	C	-	J
	JM-No. 11-1a	C	headed bars	BJ
	JM-No. 11-1b	C	headed bars	BJ
Chutarat & Aboutaha, 2003	A -Group 2	C	-	B
	B - Group 2	C	headed bars	B
	I -Group 1	C	-	J
	II - Group 1	C	headed bars	J
Clyde et al., 2000	#2	C	0,5 scaled, bad anchorage of longitudinal beam bars in the connection	J
	#4	C		J
	#5	C		J

LOAD TYPE, NOTES AND FAILURE TYPE				
Authors	Name	Load Type	Notes	Failure Type
	#6	C		J
Durrani & Zerbe, 1987	J1	C	-	BJ
	J2	C	transv. beams of 1778mm tot. length	BJ
	J5	C	transv. beams+slab of 1168,4mm width	BJ
	J7	C	transv. beams+slab of 1778mm width	BJ
Ehsani & Alameddine, 1991	LL8	C	CLS high str.	U
	LH8	C	CLS high str.	U
	HL8	C	CLS high str.	U
	HH8	C	CLS high str.	U
	LL11	C	CLS high str.	BJ
	LH11	C	CLS high str.	BJ
	HL11	C	CLS high str.	BJ
	HH14	C	CLS high str.	BJ
	LL14	C	CLS high str.	BJ
	LH14	C	CLS high str.	BJ
	HH11	C	CLS high str.	U
Ehsani et al., 1987	1	C	CLS high str.	BJ
	2	C	CLS high str.	BJ
	3	C	CLS high str.	BJ
	4	C	CLS high str.	J
	5	C	-	BJ
Ehsani & Wight, 1985(a)	1S	C	transverse beams and slab	BJ
	2S	C	transverse beams and slab	BJ
	3S	C	transverse beams and slab	BJ
	6S	C	transverse beams and slab	BJ
Ehsani & Wight, 1985(b)	1B	C	specimens designed in the fall of 1978	BJ
	2B	C	specimens designed in the fall of 1979	BJ
	3B	C	specimens designed in the fall of 1980	BJ
	4B	C	specimens designed in the fall of 1981	BJ
	5B	C	specimens designed in the fall of 1982	BJ
	6B	C	specimens designed in the fall of 1983	BJ
Genesan et al., 2007	HPr	C	high performance concrete	B
Gencoglu & Eren, 2002	#1	C	-	B
	#2	C	-	J
Hamil, 2000	C6LN0	C	U-bars for the main beam steel	J
	C6LN1	C	U-bars for the main beam steel	J
	C6LN3	C	U-bars for the main beam steel	J
	C6LN5	C	U-bars for the main beam steel	J
	C6LH0	C	U-bars for the main beam steel	J
	C6LH1	C	U-bars for the main beam steel	J

LOAD TYPE, NOTES AND FAILURE TYPE				
Authors	Name	Load Type	Notes	Failure Type
	C6LH3	C	U-bars for the main beam steel	J
	C6LH5	C	U-bars for the main beam steel	B
	C4ALN0	C	the main beam steel bent down into the column (D)	J
	C4ALN1	C	the main beam steel bent down into the column (D)	J
	C4ALN3	C	the main beam steel bent down into the column (D)	J
	C4ALN5	C	the main beam steel bent down into the column (D)	J
	C4ALH0	C	the main beam steel bent down into the column (D)	J
	C4ALH1	C	the main beam steel bent down into the column (D)	B
	C4ALH3	C	the main beam steel bent down into the column (D)	B
	C4ALH5	C	the main beam steel bent down into the column (D)	B
Hakuto et al., 2000	O6	C	-	BJ
	O7	C	-	BJ
Hegger et al., 2003	RK1	M	-	B
	RK2	M	U bar column+ diagonal bar beam	B
	RK3	M	-	B
	RK4	M	-	J
	RK5	M	-	J
	RK6	M	-	J
	RK7	M	-	J
	RK8	M	-	J
Hwang et al., 2004	70-3T44	C	-	B
	70-3T4	C	-	B
	70-2T5	C	-	BJ
	70-1T55	C	-	BJ
	28-3T4	C	-	BJ
	28 - 0T0	C	-	J
Hwang et al., 2005	0T0	C	-	BJ
	3T44	C	-	B
	1B8	C	-	BJ
	3T3	C	-	BJ
	2T4	C	-	BJ
	1T44	C	-	BJ
	3T4	C	-	B
	2T5	C	-	B
	1T55	C	-	B
Idayani, 2007	S1	M	-	J
	S2	M	-	J
	S3	M	-	J
Karayannis et al., 2008	A0	C	-	J
	A1	C	-	BJ
	A2	C	-	BJ

LOAD TYPE, NOTES AND FAILURE TYPE				
Authors	Name	Load Type	Notes	Failure Type
	A3	C	-	BJ
	B0	C	-	J
	B1	C	-	J
	C0	C	-	J
	C2	C	-	BJ
	C3	C	-	BJ
	C5	C	-	BJ
Karayannis & Sirkelis, 2005	AJ1sp	C	rectangular spiral shear reinforcement	B
	AJ1s	C	-	J
Karayannis & Sirkelis, 2008	A1	C	-	J
	A2	C	-	J
	B1	C	-	BJ
	B2	C	-	BJ
Kuang & Wong, 2006	BS-OL	C	Beam bars bent away from joint	J
	BS-LL	C	beam bars bent into joint	J
	BS-U	C	U-anchorage	J
	BS-L-LS	C	Beam bars bent into joint; Laps in column bars at end zone of upper column	J
Kusuhara & Shiohara, 2008	E1	C	-	J
	E2	C	-	J
	B2	C	-	J
Lee & Ko, 2007	S0	C	e_b=0mm	B
	S50	C	e_b=50mm	B
	W0	C	e_b=0mm	BJ
	W75	C	e_b=75mm	BJ
	W150	C	e_b=150mm	BJ
Liu, 2006	RC - 1	C	-	J
	RC - 6	C	-	B
	NZ - 7	C	was designed by New Zealand concrete design code NZS3101:1995	B
Masi et al., 2009	T1	C	ERD: NE; Tipo trave: RB	B
	T2	C	ERD: Z2; Tipo trave: RB	B
	T3	C	ERD: Z2; Tipo trave: FB	B
	T4	C	ERD: Z4; Tipo trave: FB	B
	T5	C	ERD: Z2; Tipo trave: RB	BJ
	T6	C	ERD: NE; Tipo trave: RB	B
	T7	C	ERD: NE; Tipo trave: FB	B
	T8	C	ERD: Z4; Tipo trave: FB	B
	T9	C	ERD: Z2; Tipo trave: RB	BJ
	T10	C	ERD: Z2; Tipo trave: RB	BJ
Pampanin et al., 2002	T2	C	2/3 scaled-50's & 70's	J
Pantelides et al., 2002	1	C	$l_{anch.}$ bottom beam bar=152,4mm;	J
	2	C	upper beam bar U-bent type	J
	3	C	$l_{anch.}$ bottom beam bar=355,6mm;	J
	4	C	upper beam bar U-bent type	CJ
	5	C	bottom beam bar and upper beam	BJ

LOAD TYPE, NOTES AND FAILURE TYPE				
Authors	Name	Load Type	Notes	Failure Type
	6	C	bar U-bent type	CJ
Parker & Bullman, 1997	4a	M	-	J
	4b	M	-	J
	4c	M	-	J
	4d	M	-	J
	4e	M	-	J
	4f	M	-	J
	5a	M	-	J
	5b	M	-	J
	5c	M	-	J
	5d	M	-	J
	5e	M	-	J
	5f	M	-	J
Scott, 1996	C1	M	beam reinf. bent down into column	B
	C1A	M	beam reinf. bent down into column	B
	C1AL	M	beam reinf. bent down into column	J
	C2	M	beam reinf. bent up into column	J
	C3	M	beam reinf. Bent into U-bar	B
	C3L	M	beam reinf. Bent into U-bar	J
	C4	M	beam reinf. bent down into column	J
	C4A	M	beam reinf. bent down into column	J
	C4AL	M	beam reinf. bent down into column	J
	C5	M	beam reinf. bent up into column	J
	C6	M	beam reinf. Bent into U-bar	J
	C6L	M	beam reinf. Bent into U-bar	J
	C7	M	beam reinf. bent down into column	J
	C8	M	beam reinf. bent up into column	J
	C9	M	beam reinf. Bent into U-bar	J
Tsonos, 1999	M1	C	-	CJ
	M2	C	-	CJ
Tsonos, 2007	A1	C	-	BJ
	E2	C	-	BJ
	E1	C	-	J
	G1	C	-	J
Tsonos et al., 1992	S1	C	-	BJ
	X1	C	INCL. BARS	B
	S2	C	-	J
	X2	C	INCL. BARS	B
	S6	C	-	J
	X6	C	INCL. BARS	J
	S'6	C	-	J
	F2	C	-	J
Wong and Kuang, 2008	BS-L-300	C	-	J
	BS-L-450	C	-	J
	BS-L-600	C	-	J
	BS-L-V2	C	-	J
	BS-L-V4	C	-	J
	BS-L-H1	C	-	J

LOAD TYPE, NOTES AND FAILURE TYPE				
Authors	Name	Load Type	Notes	Failure Type
	BS-L-H2	C	-	J
Wallace et al., 1998	BCEJ1	C	stub beam + headed bars	B
	BCEJ2	C	stub beam + headed bars	U

Load Type: **M** = Monotonic; **C** = Cyclic;
Failure Type: **B** = Beam; **BJ** = Beam-Joint; **C** = Column; **CJ** = Column-Joint; **J** = Joint; **U** = Unknown.

GEOMETRIC DETAILS OF THE COLUMN							
Authors	Name	Column					
		b_c [mm]	h_c [mm]	d'_c [mm]	L_c [mm]	$A'_{s,c}$ [mm^2]	$A_{s,c}$ [mm^2]
Alva, 2004	LVP1	200	300	36	1250	603	603
Alva et al., 2007	LVP2	200	300	36	1250	603	603
	LVP3	200	300	36	1250	603	603
	LVP4	200	300	36	1250	603	603
	LVP5	200	300	36	1250	603	603
Binbhu & Jaya, 2008	A1	100	150	15	500	129	129
	A2	100	150	15	500	129	129
	B1	100	150	15	500	129	129
	B2	100	150	15	500	129	129
Calvi et al., 2001	T1	200	200	20	1165	151	151
Chalioris et al., 2008	JA-0	200	300	50	750	308	308
	JA-s5	200	300	50	750	308	308
	JA-X12	200	300	50	750	534	534
	JA-X14	200	300	50	750	616	616
	JB-0	200	300	30	750	157	157
	JB-s1	200	300	30	750	157	157
	JB-X10	200	300	30	750	314	314
	JB-X12	200	300	30	750	383	383
	JCa-0	100	200	30	750	157	157
	JCa-X10	100	200	30	750	314	314
	JCa-s1	100	200	30	750	157	157
	JCa-s1-X10	100	200	30	750	314	314
	JCa-s2	100	200	30	750	157	157
	JCa-s2-X10	100	200	30	750	314	314
	JCb-0	100	200	30	750	157	157
	JCb-X10	100	200	30	750	314	314
	JCb-s1	100	200	30	750	157	157
	JCb-s1-X10	100	200	30	750	314	314
	JCb-s2	100	200	30	750	157	157
	JCb-s2-X10	100	200	30	750	314	314
Chun & Kim, 2004	JC-1	500	500	61	1500	1901	1901
	JM-1	500	500	61	1500	1901	1901
	JC-2	500	500	61	1500	1901	1901
	JM-2	500	500	61	1500	1901	1901
Chun et al., 2007	JC-1	500	500	35	1303	1521	1521
	JM-1	500	500	35	1303	1521	1521
	JC-2	500	500	35	1303	1521	1521
	JM-2	500	500	35	1303	1521	1521
	JC-No. 11-1	650	520	35	1303	3167	3167
	JM-No. 11-1a	650	520	35	1303	3167	3167
	JM-No. 11-1b	650	520	35	1303	3167	3167
Chutarat & Aboutaha, 2003	A -Group 2	508	406	30	1219	1161	1161
	B - Group 2	508	406	30	1219	1161	1161
	I -Group 1	406	406	30	1219	1548	1548
	II - Group 1	406	406	30	1219	1548	1548
Clyde et al., 2000	#2	305	457	57	1283	1161	1161
	#4	305	457	57	1283	1161	1161

GEOMETRIC DETAILS OF THE COLUMN							
Authors	Name	Column					
		b_c [mm]	h_c [mm]	d'_c [mm]	L_c [mm]	$A'_{s,c}$ [mm^2]	$A_{s,c}$ [mm^2]
	#5	305	457	57	1283	1161	1161
	#6	305	457	57	1283	1161	1161
Durrani & Zerbe, 1987	J1	305	305	30	1219	1520	1520
	J2	305	305	30	1219	1520	1520
	J5	305	305	30	1219	1520	1520
	J7	305	305	30	1219	1520	1520
Ehsani & Alameddine, 1991	LL8	356	356	64	1791	1400	1400
	LH8	356	356	64	1791	1400	1400
	HL8	356	356	64	1791	1519	1519
	HH8	356	356	64	1791	1519	1519
	LL11	356	356	64	1791	1400	1400
	LH11	356	356	64	1791	1400	1400
	HL11	356	356	64	1791	1519	1519
	HH14	356	356	64	1791	1519	1519
	LL14	356	356	64	1791	1400	1400
	LH14	356	356	64	1791	1400	1400
	HH11	356	356	64	1791	1519	1519
Ehsani et al., 1987	1	340	340	51	1727	1061	1061
	2	340	340	51	1727	1061	1061
	3	300	300	51	1727	1061	1061
	4	300	300	51	1727	1400	1400
	5	300	300	51	1067	1146	1146
Ehsani & Wight, 1985(a)	1S	300	300	51	1105	860	860
	2S	300	300	51	1105	860	860
	3S	300	300	51	1105	1146	1146
	6S	340	340	51	1105	860	860
Ehsani & Wight, 1985(b)	1B	300	300	56	1067	860	860
	2B	300	300	56	1067	1146	1146
	3B	300	300	56	1067	860	860
	4B	300	300	56	1067	1146	1146
	5B	340	340	51	1105	2027	2027
	6B	340	340	51	1105	860	860
Genesan et al., 2007	HPr	150	200	30	500	226	226
Gencoglu & Eren, 2002	#1	250	400	30	1500	603.19	603.19
	#2	250	400	30	1500	603.19	603.19
Hamil, 2000	C6LN0	150	150	30	850	402	402
	C6LN1	150	150	30	850	402	402
	C6LN3	150	150	30	850	402	402
	C6LN5	150	150	30	850	402	402
	C6LH0	150	150	30	850	402	402
	C6LH1	150	150	30	850	402	402
	C6LH3	150	150	30	850	402	402
	C6LH5	150	150	30	850	402	402
	C4ALN0	150	150	30	850	402	402
	C4ALN1	150	150	30	850	402	402
	C4ALN3	150	150	30	850	402	402

GEOMETRIC DETAILS OF THE COLUMN							
Authors	Name	Column					
		b_c [mm]	h_c [mm]	d'_c [mm]	L_c [mm]	$A'_{s,c}$ [mm^2]	$A_{s,c}$ [mm^2]
	C4ALN5	150	150	30	850	402	402
	C4ALH0	150	150	30	850	402	402
	C4ALH1	150	150	30	850	402	402
	C4ALH3	150	150	30	850	402	402
	C4ALH5	150	150	30	850	402	402
Hakuto et al., 2000	O6	460	460	40	1600	905	905
	O7	460	460	40	1600	905	905
Hegger et al., 2003	RK1	150	240	30	830	402	402
	RK2	150	240	30	830	402.12	402.12
	RK3	150	240	30	830	402.12	402.12
	RK4	150	200	30	830	402.12	402.12
	RK5	150	200	30	830	402.12	402.12
	RK6	150	200	30	830	402.12	402.12
	RK7	150	200	30	830	402.12	402.12
	RK8	150	200	30	830	402.12	402.12
Hwang et al., 2004	70-3T44	420	420	56	1350	2458	2458
	70-3T4	450	450	56	1350	2458	2458
	70-2T5	450	450	56	1350	2458	2458
	70-1T55	450	450	56	1350	2458	2458
	28-3T4	550	550	56	1350	3278	3278
	28 - 0T0	550	550	56	1350	3278	3278
Hwang et al., 2005	0T0	420	420	71	1350	2458	2458
	3T44	420	420	71	1350	2458	2458
	1B8	420	420	71	1350	2458	2458
	3T3	420	420	71	1350	2458	2458
	2T4	420	420	71	1350	2458	2458
	1T44	420	420	71	1350	2458	2458
	3T4	450	450	69	1350	2458	2458
	2T5	450	450	69	1350	2458	2458
	1T55	450	450	69	1350	2458	2458
Idayani, 2007	S1	180	180	38	865	402	402
	S2	180	180	38	865	402	402
	S3	180	180	38	865	402	402
Karayannis et al., 2008	A0	200	200	30	750	157	157
	A1	200	200	30	750	157	157
	A2	200	200	30	750	157	157
	A3	200	200	30	750	157	157
	B0	200	300	30	750	157	157
	B1	200	300	30	750	157	157
	C0	200	300	50	750	308	308
	C2	200	300	50	750	308	308
	C3	200	300	50	750	308	308
	C5	200	300	50	750	308	308
Karayannis & Sirkelis, 2005	AJ1sp	200	200	30	900	157	157
	AJ1s	200	200	30	900	157	157
Karayannis & Sirkelis, 2008	A1	200	200	30	750	157	157
	A2	200	200	30	750	157	157

GEOMETRIC DETAILS OF THE COLUMN							
Authors	Name	Column					
		b_c [mm]	h_c [mm]	d'_c [mm]	L_c [mm]	$A'_{s,c}$ [mm^2]	$A_{s,c}$ [mm^2]
	B1	200	200	30	750	339	339
	B2	200	200	30	750	339	339
Kuang & Wong, 2006	BS-OL	300	300	30	1550	982	982
	BS-LL	300	300	30	1550	982	982
	BS-U	300	300	30	1550	982	982
	BS-L-LS	300	300	30	1550	982	982
Kusuhara & Shiohara, 2008	E1	300	300	35	735	265	265
	E2	300	300	35	735	265	265
	B2	300	300	35	735	398	398
Lee & Ko, 2007	S0	400	600	50	1350	1140	1140
	S50	400	600	50	1350	1140	1140
	W0	600	400	50	1350	1901	1901
	W75	600	400	50	1350	1901	1901
	W150	600	400	50	1350	1901	1901
Liu, 2006	RC - 1	230	230	25	1000	236	236
	RC - 6	250	250	30	1000	452	452
	NZ - 7	250	250	30	1000	452	452
Masi et al., 2009	T1	300	300	30	1600	308	308
	T2	300	300	30	1600	462	462
	T3	300	300	30	1600	462	462
	T4	300	300	30	1600	308	308
	T5	300	300	30	1600	462	462
	T6	300	300	30	1600	308	308
	T7	300	300	30	1600	308	308
	T8	300	300	30	1600	308	308
	T9	300	300	30	1600	462	462
	T10	300	300	30	1600	462	462
Pampanin et al., 2002	T2	200	200	20	1245	151	151
Pantelides et al., 2002	1	406	406	60	1600	2027	2027
	2	406	406	60	1600	2027	2027
	3	406	406	60	1600	2027	2027
	4	406	406	60	1600	2027	2027
	5	406	406	60	1600	2027	2027
	6	406	406	60	1600	2027	2027
Parker & Bullman, 1997	4a	300	300	55	1000	402	402
	4b	300	300	55	1000	402	402
	4c	300	300	55	1000	402	402
	4d	300	300	55	1000	1608	1608
	4e	300	300	55	1000	1608	1608
	4f	300	300	55	1000	1608	1608
	5a	300	300	55	1000	982	982
	5b	300	300	55	1000	982	982
	5c	300	300	55	1000	982	982
	5d	300	300	55	1000	982	982
	5e	300	300	55	1000	982	982
	5f	300	300	55	1000	982	982

GEOMETRIC DETAILS OF THE COLUMN							
Authors	Name	Column					
		b_c [mm]	h_c [mm]	d'_c [mm]	L_c [mm]	$A'_{s,c}$ [mm^2]	$A_{s,c}$ [mm^2]
Scott, 1996	C1	150	150	30	850	402	402
	C1A	150	150	30	850	402	402
	C1AL	150	150	30	850	402	402
	C2	150	150	30	850	402	402
	C3	150	150	30	850	402	402
	C3L	150	150	30	850	402	402
	C4	150	150	30	850	402	402
	C4A	150	150	30	850	402	402
	C4AL	150	150	30	850	402	402
	C5	150	150	30	850	402	402
	C6	150	150	30	850	402	402
	C6L	150	150	30	850	402	402
	C7	150	150	30	850	402	402
	C8	150	150	30	850	402	402
	C9	150	150	30	850	402	402
Tsonos, 1999	M1	200	200	30	650	157.08	157.08
	M2	200	200	30	650	157.08	157.08
Tsonos, 2007	A1	200	200	30	700	236	236
	E2	200	200	30	700	462	462
	E1	200	200	30	700	462	462
	G1	200	200	30	700	462	462
Tsonos et al., 1992	S1	200	200	30	650	462	462
	X1	200	200	30	650	462	462
	S2	200	200	30	650	157	157
	X2	200	200	30	650	157	157
	S6	200	200	30	650	308	308
	X6	200	200	30	650	308	308
	S'6	200	200	30	650	616	616
	F2	200	200	30	650	308	308
Wong and Kuang, 2008	BS-L-300	300	300	30	1550	982	982
	BS-L-450	300	300	30	1550	982	982
	BS-L-600	300	300	30	1550	982	982
	BS-L-V2	300	300	30	1550	982	982
	BS-L-V4	300	300	30	1550	982	982
	BS-L-H1	300	300	30	1550	982	982
	BS-L-H2	300	300	30	1550	982	982
Wallace et al., 1998	BCEJ1	457	457	64	1524	1927.27	1927.27
	BCEJ2	457	457	64	1524	1927.27	1927.27

b_c = column width;
h_c = column depth;
d'_c = cover concrete;
L_c = total length of the column;
$A'_{s,c}$ = $A_{s,c}$ = longitudinal reinforcement in column.

GEOMETRIC DETAILS OF THE BEAM										
Authors	Name	Beam								
		b_b [mm]	h_b [mm]	d'_b [mm]	L_b [mm]	e_b [mm]	$d_{b,sup}$ [mm]	$d_{b,inf}$ [mm]	$A_{sb,inf}$ [mm^2]	$A_{sb,sup}$ [mm^2]
Alva, 2004	LVP1	200	400	36	1700	0	16.0	16.0	804	804
Alva et al., 2007	LVP2	200	400	36	1700	0	16.0	16.0	804	804
	LVP3	200	400	36	1700	0	16.0	16.0	804	804
	LVP4	200	400	36	1700	0	16.0	16.0	804	804
	LVP5	200	400	36	1700	0	16.0	16.0	804	804
Binbhu & Jaya, 2008	A1	100	150	15	625	0	8.0	6.0	157	157
	A2	100	150	15	625	0	8.0	6.0	157	157
	B1	100	150	15	625	0	8.0	6.0	157	157
	B2	100	150	15	625	0	8.0	6.0	157	157
Calvi et al., 2001	T1	200	330	20	1700	0	12.0	8.0	327	327
Chalioris et al., 2008	JA-0	200	300	50	1150	0	12.0	12.0	452	452
	JA-s5	200	300	50	1150	0	12.0	12.0	452	452
	JA-X12	200	300	50	1150	0	12.0	12.0	452	452
	JA-X14	200	300	50	1150	0	12.0	12.0	452	452
	JB-0	200	300	30	1150	0	10.0	10.0	471	471
	JB-s1	200	300	30	1150	0	10.0	10.0	471	471
	JB-X10	200	300	30	1150	0	10.0	10.0	471	471
	JB-X12	200	300	30	1150	0	10.0	10.0	471	471
	JCa-0	100	200	30	1100	0	10.0	10.0	157	157
	JCa-X10	100	200	30	1100	0	10.0	10.0	157	157
	JCa-s1	100	200	30	1100	0	10.0	10.0	157	157
	JCa-s1-X10	100	200	30	1100	0	10.0	10.0	157	157
	JCa-s2	100	200	30	1100	0	10.0	10.0	157	157
	JCa-s2-X10	100	200	30	1100	0	10.0	10.0	157	157
	JCb-0	100	200	30	1100	0	10.0	10.0	236	236
	JCb-X10	100	200	30	1100	0	10.0	10.0	236	236
	JCb-s1	100	200	30	1100	0	10.0	10.0	236	236
	JCb-s1-X10	100	200	30	1100	0	10.0	10.0	236	236
	JCb-s2	100	200	30	1100	0	10.0	10.0	236	236
	JCb-s2-X10	100	200	30	1100	0	10.0	10.0	236	236
Chun & Kim, 2004	JC-1	350	500	61	2400	0	22.0	22.0	1140	1521
	JM-1	350	500	61	2400	0	22.0	22.0	1140	1521
	JC-2	350	500	61	2400	0	22.0	22.0	2281	3041
	JM-2	350	500	61	2400	0	22.0	22.0	2281	3041
Chun et al., 2007	JC-1	350	500	40	2250	0	22.0	22.0	1521	1140
	JM-1	350	500	40	2250	0	22.0	22.0	1521	1140
	JC-2	350	500	40	2250	0	22.0	22.0	3041	2281
	JM-2	350	500	40	2250	0	22.0	22.0	3041	2281
	JC-No.11-1	450	505	40	2260	0	34.9	34.9	2870	2870
	JM-No.11-1a	450	505	40	2260	0	34.9	34.9	2870	2870
	JM-No.11-1b	450	505	40	2260	0	34.9	34.9	2870	2870
Chutarat & Aboutaha, 2003	A -Group 2	356	457	30	2337	0	12.7	12.7	507	507
	B - Group 2	356	457	30	2337	0	12.7	22.2	2055	2055
	I -Group 1	356	457	30	2337	0	25.4	25.4	2027	2027

GEOMETRIC DETAILS OF THE BEAM										
Authors	Name	Beam								
		b_b [mm]	h_b [mm]	d'_b [mm]	L_b [mm]	e_b [mm]	$d_{b,sup}$ [mm]	$d_{b,inf}$ [mm]	$A_{sb,inf}$ [mm^2]	$A_{sb,sup}$ [mm^2]
	II - Group 1	356	457	30	2337	0	25.4	22.2	3575	3575
Clyde et al., 2000	#2	305	406	38	1499	0	28.7	28.7	2588	2588
	#4	305	406	38	1499	0	28.7	28.7	2588	2588
	#5	305	406	38	1499	0	28.7	28.7	2588	2588
	#6	305	406	38	1499	0	28.7	28.7	2588	2588
Durrani & Zerbe, 1987	J1	254	381	30	1829	0	19.1	19.1	1146	1146
	J2	254	381	30	1829	0	19.1	19.1	1146	1146
	J5	254	381	30	1829	0	19.1	12.7	1146	1906
	J7	254	381	30	1829	0	19.1	12.7	1146	2413
Ehsani & Alameddine, 1991	LL8	318	508	76	1778	0	25.4	25.4	2026	2026
	LH8	318	508	76	1778	0	25.4	25.4	2026	2026
	HL8	318	508	76	1778	0	28.7	28.7	2586	2586
	HH8	318	508	76	1778	0	28.7	28.7	2586	2586
	LL11	318	508	76	1778	0	25.4	25.4	2026	2026
	LH11	318	508	76	1778	0	25.4	25.4	2026	2026
	HL11	318	508	76	1778	0	28.7	28.7	2586	2586
	HH14	318	508	76	1778	0	28.7	28.7	2586	2586
	LL14	318	508	76	1778	0	25.4	25.4	2026	2026
	LH14	318	508	76	1778	0	25.4	25.4	2026	2026
	HH11	318	508	76	1778	0	28.7	28.7	2586	2586
Ehsani et al., 1987	1	300	480	67	1745	0	19.1	15.9	1169	1169
	2	300	480	70	1745	0	19.1	19.1	1433	1433
	3	259	439	64	1725	0	19.1	15.9	1257	1257
	4	259	439	61	1725	0	22.2	15.9	1558	1558
	5	259	439	70	1674	0	22.2	19.1	2021	2021
Ehsani & Wight, 1985(a)	1S	259	480	51	1217	0	19.1	19.1	860	860
	2S	259	480	51	1217	0	19.1	19.1	860	860
	3S	259	439	51	1217	0	19.1	19.1	860	860
	6S	300	480	51	1237	0	22.2	22.2	1161	1161
Ehsani & Wight, 1985(b)	1B	259	480	71	1674	0	22.2	19.1	2021	2021
	2B	259	439	69	1674	0	22.2	19.1	2021	2021
	3B	259	480	71	1674	0	22.2	19.1	2021	2021
	4B	259	439	76	1674	0	22.2	19.1	2021	2021
	5B	300	480	58	1237	0	22.2	22.2	2322	2322
	6B	300	480	66	1237	0	22.2	19.1	1734	1734
Genesan et al., 2007	HPr	150	200	30	650	0	12.0	12.0	226	226
Gencoglu & Eren, 2002	#1	250	600	30	1200	0	14.0	14.0	462	462
	#2	250	600	30	1200	0	14.0	14.0	462	462
Hamil, 2000	C6LN0	110	210	30	825	0	16.0	16.0	402	402
	C6LN1	110	210	30	825	0	16.0	16.0	402	402
	C6LN3	110	210	30	825	0	16.0	16.0	402	402
	C6LN5	110	210	30	825	0	16.0	16.0	402	402
	C6LH0	110	210	30	825	0	16.0	16.0	402	402
	C6LH1	110	210	30	825	0	16.0	16.0	402	402
	C6LH3	110	210	30	825	0	16.0	16.0	402	402
	C6LH5	110	210	30	825	0	16.0	16.0	402	402

GEOMETRIC DETAILS OF THE BEAM										
Authors	Name	Beam								
		b_b [mm]	h_b [mm]	d'_b [mm]	L_b [mm]	e_b [mm]	$d_{b,sup}$ [mm]	$d_{b,inf}$ [mm]	$A_{sb,inf}$ [mm^2]	$A_{sb,sup}$ [mm^2]
	C4ALN0	110	210	30	825	0	16.0	16.0	402	402
	C4ALN1	110	210	30	825	0	16.0	16.0	402	402
	C4ALN3	110	210	30	825	0	16.0	16.0	402	402
	C4ALN5	110	210	30	825	0	16.0	16.0	402	402
	C4ALH0	110	210	30	825	0	16.0	16.0	402	402
	C4ALH1	110	210	30	825	0	16.0	16.0	402	402
	C4ALH3	110	210	30	825	0	16.0	16.0	402	402
	C4ALH5	110	210	30	825	0	16.0	16.0	402	402
Hakuto et al., 2000	O6	300	500	40	1905	0	24.0	24.0	905	1357
	O7	300	500	40	1905	0	24.0	24.0	905	1357
Hegger et al., 2003	RK1	150	300	30	970	0	20.0	20.0	628	628
	RK2	150	300	30	970.0	0	20.0	20.0	628	628
	RK3	150	300	30	970.0	0	20.0	20.0	628	628
	RK4	150	300	30	950.0	0	20.0	20.0	628	628
	RK5	150	300	30	950.0	0	20.0	20.0	628	628
	RK6	150	300	30	950.0	0	20.0	20.0	628	628
	RK7	150	400	30	950.0	0	20.0	20.0	628	628
	RK8	150	300	30	950.0	0	20.0	20.0	628	628
Hwang et al., 2004	70-3T44	320	450	56	2110	0	25.4	25.4	2027	2027
	70-3T4	320	450	56	2125	0	25.4	25.4	2027	2027
	70-2T5	320	450	56	2125	0	25.4	25.4	2027	2027
	70-1T55	320	450	56	2125	0	25.4	25.4	2027	2027
	28-3T4	380	500	56	2175	0	25.4	25.4	2027	2027
	28 - 0T0	380	500	66	2175	0	25.4	25.4	2027	2027
Hwang et al., 2005	0T0	320	450	66	2110	0	25.4	25.4	2027	2027
	3T44	320	450	66	2110	0	25.4	25.4	2027	2027
	1B8	320	450	66	2110	0	25.4	25.4	2027	2027
	3T3	320	450	66	2110	0	25.4	25.4	2027	2027
	2T4	320	450	66	2110	0	25.4	25.4	2027	2027
	1T44	320	450	66	2110	0	25.4	25.4	2027	2027
	3T4	320	450	66	2125	0	25.4	25.4	2027	2027
	2T5	320	450	66	2125	0	25.4	25.4	2027	2027
	1T55	320	450	66	2125	0	25.4	25.4	2027	2027
Idayani, 2007	S1	150	300	40	1000	0	20.0	16.0	402	628
	S2	150	300	40	1000	0	20.0	16.0	402	628
	S3	150	300	40	1000	0	20.0	16.0	402	628
Karayannis et al., 2008	A0	200	300	30	1100	0	10.0	10.0	157	157
	A1	200	300	30	1100	0	10.0	10.0	157	157
	A2	200	300	30	1100	0	10.0	10.0	157	157
	A3	200	300	30	1100	0	10.0	10.0	157	157
	B0	200	300	30	1150	0	10.0	10.0	471	471
	B1	200	300	30	1150	0	10.0	10.0	471	471
	C0	200	300	50	1150	0	12.0	12.0	452	452
	C2	200	300	50	1150	0	12.0	12.0	452	452
	C3	200	300	50	1150	0	12.0	12.0	452	452
	C5	200	300	50	1150	0	12.0	12.0	452	452
Karayannis	AJ1sp	200	300	30	1100	0	10.0	10.0	157	157

GEOMETRIC DETAILS OF THE BEAM										
		Beam								
Authors	Name	b_b [mm]	h_b [mm]	d'_b [mm]	L_b [mm]	e_b [mm]	$d_{b,sup}$ [mm]	$d_{b,inf}$ [mm]	$A_{sb,inf}$ [mm^2]	$A_{sb,sup}$ [mm^2]
& Sirkelis, 2005	AJ1s	200	300	30	1100	0	10.0	10.0	157	157
Karayannis & Sirkelis, 2008	A1	200	300	30	1100	0	10.0	10.0	157	157
	A2	200	300	30	1100	0	10.0	10.0	157	157
	B1	200	300	30	1100	0	10.0	10.0	157	157
	B2	200	300	30	1100	0	10.0	10.0	157	157
Kuang & Wong, 2006	BS-OL	260	450	30	1650	0	20.0	20.0	942	942
	BS-LL	260	450	30	1650	0	20.0	20.0	942	942
	BS-U	260	450	30	1650	0	20.0	20.0	942	942
	BS-L-LS	260	450	30	1650	0	20.0	20.0	942	942
Kusuhara & Shiohara, 2008	E1	300	300	47	1350	0	16.0	16.0	1206	1206
	E2	300	300	47	1350	0	16.0	16.0	1206	1206
	B2	300	300	47	1350	0	13.0	13.0	796	796
Lee & Ko, 2007	S0	300	450	50	2150	0	22.0	22.0	1521	1521
	S50	300	450	50	2150	50	22.0	22.0	1521	1521
	W0	300	450	50	2150	0	22.0	22.0	1521	1521
	W75	300	450	50	2150	75	22.0	22.0	1521	1521
	W150	300	450	50	2150	150	22.0	22.0	1521	1521
Liu, 2006	RC - 1	200	330	25	1525	0	10.0	10.0	471	471
	RC - 6	250	330	30	1525	0	12.0	12.0	452	452
	NZ - 7	250	330	30	1525	0	12.0	12.0	452	452
Masi et al., 2009	T1	300	500	30	2150	0	12.0	12.0	226	226
	T2	300	500	30	2150	0	16.0	12.0	515	603
	T3	600	240	30	2150	0	16.0	12.0	515	603
	T4	600	240	30	2150	0	12.0	12.0	226	226
	T5	300	500	30	2150	0	16.0	12.0	515	603
	T6	300	500	30	2150	0	12.0	12.0	226	226
	T7	600	240	30	2150	0	12.0	12.0	226	226
	T8	600	240	30	2150	0	12.0	12.0	226	226
	T9	300	500	30	2150	0	16.0	12.0	515	603
	T10	300	500	30	2150	0	16.0	12.0	515	603
Pampanin et al., 2002	T2	200	330	20	1700	0	12.0	8.0	327	327
Pantelides et al., 2002	1	406	406	60	1880	0	28.7	28.7	2588	2588
	2	406	406	60	1880	0	28.7	28.7	2588	2588
	3	406	406	60	1880	0	28.7	28.7	2588	2588
	4	406	406	60	1880	0	28.7	28.7	2588	2588
	5	406	406	60	1880	0	28.7	28.7	2588	2588
	6	406	406	60	1880	0	28.7	28.7	2588	2588
Parker & Bullman, 1997	4a	250	500	55	1000	0	25.0	25.0	982	982
	4b	250	500	55	1000	0	25.0	25.0	982	982
	4c	250	500	55	1000	0	25.0	25.0	982	982
	4d	250	500	55	1000	0	25.0	25.0	982	982
	4e	250	500	55	1000	0	25.0	25.0	982	982
	4f	250	500	55	1000	0	25.0	25.0	982	982
	5a	250	500	55	1000	0	25.0	25.0	982	982
	5b	250	500	55	1000	0	25.0	25.0	982	982

GEOMETRIC DETAILS OF THE BEAM										
Authors	Name	Beam								
		b_b [mm]	h_b [mm]	d'_b [mm]	L_b [mm]	e_b [mm]	$d_{b,sup}$ [mm]	$d_{b,inf}$ [mm]	$A_{sb,inf}$ [mm^2]	$A_{sb,sup}$ [mm^2]
	5c	250	500	55	1000	0	25.0	25.0	982	982
	5d	250	500	55	1000	0	32.0	32.0	1608	1608
	5e	250	500	55	1000	0	32.0	32.0	1608	1608
	5f	250	500	55	1000	0	32.0	32.0	1608	1608
Scott, 1996	C1	110	210	30	925	0	12.0	12.0	226	226
	C1A	110	210	30	925	0	12.0	12.0	226	226
	C1AL	110	210	30	925	0	12.0	12.0	226	226
	C2	110	210	30	925	0	12.0	12.0	226	226
	C3	110	210	30	925	0	12.0	12.0	226	226
	C3L	110	210	30	925	0	12.0	12.0	226	226
	C4	110	210	30	925	0	16.0	16.0	402	402
	C4A	110	210	30	925	0	16.0	16.0	402	402
	C4AL	110	210	30	925	0	16.0	16.0	402	402
	C5	110	210	30	925	0	16.0	16.0	402	402
	C6	110	210	30	925	0	16.0	16.0	402	402
	C6L	110	210	30	925	0	16.0	16.0	402	402
	C7	110	300	30	925	0	16.0	16.0	402	402
	C8	110	300	30	925	0	16.0	16.0	402	402
	C9	110	300	30	925	0	16.0	16.0	402	402
Tsonos, 1999	M1	200	300	30	1100	0	12.0	10.0	383	383
	M2	200	300	30	1100	0	14.0	14.0	616	616
Tsonos, 2007	A1	200	300	30	1000	0	10.0	10.0	314	314
	E2	200	300	30	1000	0	14.0	14.0	308	308
	E1	200	300	30	1000	0	14.0	14.0	462	462
	G1	200	300	30	1000	0	14.0	14.0	462	462
Tsonos et al., 1992	S1	200	300	30	1150	0	14.0	14.0	308	308
	X1	200	300	30	1150	0	14.0	14.0	308	308
	S2	200	300	30	1150	0	12.0	10.0	305	305
	X2	200	300	30	1150	0	12.0	10.0	305	305
	S6	200	300	30	1150	0	14.0	14.0	616	616
	X6	200	300	30	1150	0	14.0	14.0	616	616
	S'6	200	300	30	1150	0	14.0	14.0	616	616
	F2	200	300	30	1150	0	14.0	14.0	616	616
Wong and Kuang, 2008	BS-L-300	260	300	30	1650	0	20.0	20.0	942	942
	BS-L-450	260	450	30	1650	0	20.0	20.0	942	942
	BS-L-600	260	600	30	1650	0	20.0	20.0	942	942
	BS-L-V2	260	450	30	1650	0	20.0	20.0	942	942
	BS-L-V4	260	450	30	1650	0	20.0	20.0	942	942
	BS-L-H1	260	450	30	1650	0	20.0	20.0	942	942
	BS-L-H2	260	450	30	1650	0	20.0	20.0	942	942
Wallace et al., 1998	BCEJ1	457	610	64	3276.5	0	25.4	25.4	1520	2027
	BCEJ2	457	610	64	3276.5	0	25.4	25.4	1520	2027

b_b = beam width;
h_b = beam depth;
d'_b = cover concrete;

GEOMETRIC DETAILS OF THE BEAM										
Authors	Name	Beam								
		b_b [mm]	h_b [mm]	d'_b [mm]	L_b [mm]	e_b [mm]	$d_{b,sup}$ [mm]	$d_{b,inf}$ [mm]	$A_{sb,inf}$ [mm^2]	$A_{sb,sup}$ [mm^2]

L_b = total length of the beam;
e_b = eccentricity of the beam;
$d_{b,sup}$ = diameter of the top bars;
$d_{b,inf}$ = diameter of the bottom bars;
$A_{sb,inf}$ = reinforcement at the bottom;
$A_{sb,sup}$ = reinforcement at the top.

GEOMETRIC DETAILS OF THE JOINT							
Authors	Name	Joint					
		$d_{bw,j}$ [mm]	$p_{w,j}$ [mm]	R [mm]	$A_{sj,h}$ [mm^2]	$A_{sj,v}$ [mm^2]	$A_{sj,incl}$ [mm^2]
Alva, 2004	LVP1	8.0	100	120	402	804	0
Alva et al., 2007	LVP2	8.0	150	120	201	804	0
	LVP3	8.0	75	120	402	804	0
	LVP4	8.0	150	120	201	804	0
	LVP5	8.0	75	120	402	804	0
Binbhu & Jaya, 2008	A1	6.0	30	28	339	57	0
	A2	6.0	30	28	339	57	0
	B1	6.0	120	28	85	57	101
	B2	6.0	120	28	85	57	101
Calvi et al., 2001	T1	0.0	0	42	0	0	0
Chalioris et al., 2008	JA-0	0.0	0	72	0	157	0
	JA-s5	8.0	50	72	503	157	0
	JA-X12	0.0	0	72	0	157	226
	JA-X14	0.0	0	72	0	157	308
	JB-0	0.0	0	100	0	0	0
	JB-s1	8.0	150	100	101	0	0
	JB-X10	0.0	0	100	0	0	157
	JB-X12	0.0	0	100	0	0	226
	JCa-0	0.0	0	50	0	0	0
	JCa-X10	0.0	0	50	0	0	157
	JCa-s1	8.0	100	50	101	0	0
	JCa-s1-X10	8.0	100	50	101	0	157
	JCa-s2	8.0	67	50	201	0	0
	JCa-s2-X10	8.0	67	50	201	0	157
	JCb-0	0.0	0	50	0	0	0
	JCb-X10	0.0	0	50	0	0	157
	JCb-s1	8.0	100	50	101	0	0
	JCb-s1-X10	8.0	100	50	101	0	157
	JCb-s2	8.0	67	50	201	0	0
	JCb-s2-X10	8.0	67	50	201	0	157
Chun & Kim, 2004	JC-1	10.0	150	77	471	2281	0
	JM-1	10.0	150	77	471	2281	0
	JC-2	10.0	150	77	471	2281	0
	JM-2	10.0	150	77	471	2281	0
Chun et al., 2007	JC-1	12.7	150	77	1013	3041	0
	JM-1	12.7	150	77	1013	3041	0
	JC-2	12.7	150	77	1013	3041	0
	JM-2	12.7	150	77	1013	3041	0
	JC-No. 11-1	12.7	120	122	1520	1583	0
	JM-No. 11-1a	12.7	120	122	1520	1583	0
	JM-No. 11-1b	12.7	120	122	1520	1583	0
Chutarat & Aboutaha, 2003	A -Group 2	12.7	102	44	2027	774	0
	B - Group 2	12.7	102	44	2027	774	0
	I -Group 1	12.7	102	89	2027	1548	0
	II - Group 1	12.7	102	89	2027	1548	0
Clyde et al., 2000	#2	0.0	0	100	0	774	0
	#4	0.0	0	100	0	774	0

GEOMETRIC DETAILS OF THE JOINT							
Authors	Name	Joint					
		$d_{bw,j}$ [mm]	$p_{w,j}$ [mm]	R [mm]	$A_{sj,h}$ [mm^2]	$A_{sj,v}$ [mm^2]	$A_{sj,incl}$ [mm^2]
	#5	0.0	0	100	0	774	0
	#6	0.0	0	100	0	774	0
Durrani & Zerbe, 1987	J1	12.7	76	67	1267	1013	0
	J2	12.7	76	67	1267	1013	0
	J5	12.7	76	67	1267	1013	0
	J7	12.7	76	67	1267	1013	0
Ehsani & Alameddine, 1991	LL8	12.7	127	88	1520	774	0
	LH8	12.7	85	88	2280	774	0
	HL8	12.7	127	99	1520	1013	0
	HH8	12.7	85	99	2280	1013	0
	LL11	12.7	127	88	1520	774	0
	LH11	12.7	85	88	2280	774	0
	HL11	12.7	127	99	1520	1013	0
	HH14	12.7	85	99	2280	1013	0
	LL14	12.7	127	88	1520	774	0
	LH14	12.7	85	88	2280	774	0
	HH11	12.7	85	99	2280	1013	0
Ehsani et al., 1987	1	12.7	115	67	760	573	0
	2	12.7	113	67	760	573	0
	3	12.7	104	67	760	573	0
	4	12.7	106	78	760	774	0
	5	12.7	100	78	760	573	0
Ehsani & Wight, 1985(a)	1S	12.7	160	67	507	573	0
	2S	12.7	120	67	760	573	0
	3S	12.7	146	67	507	573	0
	6S	12.7	160	78	507	573	0
Ehsani & Wight, 1985(b)	1B	12.7	160	78	507	573	0
	2B	12.7	146	78	507	573	0
	3B	12.7	120	78	760	573	0
	4B	12.7	110	78	760	573	0
	5B	12.7	160	78	507	1013	0
	6B	12.7	160	78	507	573	0
Genesan et al., 2007	HPr	6.0	125	42	57	0	0
Gencoglu & Eren, 2002	#1	8.0	10	49	503	0	0
	#2	0.0	0	49	0	0	0
Hamil, 2000	C6LN0	6.0	0	56	0	0	0
	C6LN1	6.0	150	56	57	0	0
	C6LN3	6.0	75	56	170	0	0
	C6LN5	6.0	38	56	283	0	0
	C6LH0	6.0	0	56	0	0	0
	C6LH1	6.0	150	56	57	0	0
	C6LH3	6.0	75	56	170	0	0
	C6LH5	6.0	38	56	283	0	0
	C4ALN0	6.0	0	56	0	0	0
	C4ALN1	6.0	150	56	57	0	0
	C4ALN3	6.0	75	56	170	0	0
	C4ALN5	6.0	38	56	283	0	0

GEOMETRIC DETAILS OF THE JOINT							
Authors	Name	Joint					
		$d_{bw,j}$ [mm]	$p_{w,j}$ [mm]	R [mm]	$A_{sj,h}$ [mm^2]	$A_{sj,v}$ [mm^2]	$A_{sj,incl}$ [mm^2]
	C4ALH0	6.0	0	56	0	0	0
	C4ALH1	6.0	150	56	57	0	0
	C4ALH3	6.0	75	56	170	0	0
	C4ALH5	6.0	38	56	283	0	0
Hakuto et al., 2000	O6	6.0	305	84	57	0	0
	O7	6.0	305	84	57	0	0
Hegger et al., 2003	RK1	10.0	80	70	628	402	0
	RK2	8.0	80	70	402	353	0
	RK3	10.0	80	70	628	402	0
	RK4	10.0	80	70	628	402	0
	RK5	10.0	80	70	628	402	0
	RK6	10.0	80	70	628	402	0
	RK7	10.0	113	70	628	402	0
	RK8	10.0	80	70	628	402	0
Hwang et al., 2004	70-3T44	12.7	97	89	2280	1639	0
	70-3T4	12.7	97	89	1140	1639	0
	70-2T5	15.9	146	89	792	1639	0
	70-1T55	15.9	293	89	792	1639	0
	28-3T4	12.7	122	89	760	3278	0
	28 - 0T0	0.0	0	89	0	3278	0
Hwang et al., 2005	0T0	0.0	0	89	0	1639	0
	3T44	12.7	97	89	1140	1639	0
	1B8	0.0	0	89	0	1639	0
	3T3	9.5	97	89	638	1639	0
	2T4	12.7	146	89	507	1639	0
	1T44	12.7	293	89	507	1639	0
	3T4	12.7	97	89	1140	1639	0
	2T5	15.9	146	89	792	1639	0
	1T55	15.9	293	89	792	1639	0
Idayani, 2007	S1	0.0	0	70	0	0	0
	S2	0.0	0	70	0	0	0
	S3	6.0	55	70	170	0	0
Karayannis et al., 2008	A0	0.0	0	100	0	0	0
	A1	8.0	150	100	101	0	0
	A2	8.0	100	100	201	0	0
	A3	8.0	75	100	302	0	0
	B0	0.0	0	100	0	0	0
	B1	8.0	150	100	101	0	0
	C0	0.0	0	72	0	157	0
	C2	8.0	100	72	201	157	0
	C3	8.0	75	72	302	157	0
	C5	8.0	50	72	503	157	0
Karayannis & Sirkelis, 2005	AJ1sp	8.0	15	35	0	0	0
	AJ1s	8.0	15	35	101	0	0
Karayannis & Sirkelis, 2008	A1	0.0	0	35	0	0	0
	A2	0.0	0	35	0	0	0
	B1	8.0	60	35	402	0	0

GEOMETRIC DETAILS OF THE JOINT							
Authors	Name	Joint					
		$d_{bw,j}$ [mm]	$p_{w,j}$ [mm]	R [mm]	$A_{sj,h}$ [mm^2]	$A_{sj,v}$ [mm^2]	$A_{sj,incl}$ [mm^2]
	B2	8.0	60	35	402	0	0
Kuang & Wong, 2006	BS-OL	0.0	0	70	0	0	0
	BS-LL	0.0	0	70	0	0	0
	BS-U	0.0	0	70	0	0	0
	BS-L-LS	0.0	0	70	0	0	0
Kusuhara & Shiohara, 2008	E1	6.0	50	56	170	265	0
	E2	6.0	50	56	170	265	0
	B2	6.0	50	46	170	265	0
Lee & Ko, 2007	S0	10.0	100	77	1571	2281	0
	S50	10.0	100	77	1571	2281	0
	W0	10.0	100	77	942	760	0
	W75	10.0	100	77	628	760	0
	W150	10.0	100	77	942	760	0
Liu, 2006	RC - 1	0.0	0	35	0	0	0
	RC - 6	6.0	165	42	57	226	0
	NZ - 7	6.0	50	42	283	226	0
Masi et al., 2009	T1	0.0	0	42	0	0	0
	T2	8.0	75	56	603	0	0
	T3	8.0	75	56	603	0	0
	T4	8.0	75	42	603	0	0
	T5	8.0	75	56	603	0	0
	T6	0.0	0	42	0	0	0
	T7	0.0	0	42	0	0	0
	T8	8.0	75	42	603	0	0
	T9	8.0	75	56	603	0	0
	T10	8.0	75	56	603	0	0
Pampanin et al., 2002	T2	0.0	0	42	0	0	0
Pantelides et al., 2002	1	0.0	0	100	0	0	0
	2	0.0	0	100	0	0	0
	3	0.0	0	100	0	0	0
	4	0.0	0	100	0	0	0
	5	0.0	0	100	0	0	0
	6	0.0	0	100	0	0	0
Parker & Bullman, 1997	4a	0.0	0	106	0	0	0
	4b	0.0	0	106	0	0	0
	4c	0.0	0	106	0	0	0
	4d	0.0	0	106	0	0	0
	4e	0.0	0	106	0	0	0
	4f	0.0	0	106	0	0	0
	5a	12.0	150	88	679	0	0
	5b	12.0	150	88	679	0	0
	5c	12.0	150	88	679	0	0
	5d	12.0	100	112	679	0	0
	5e	12.0	100	112	679	0	0
	5f	12.0	100	112	679	0	0
Scott, 1996	C1	6.0	150	42	57	0	0
	C1A	6.0	150	42	57	0	0

GEOMETRIC DETAILS OF THE JOINT							
Authors	Name	Joint					
		$d_{bw,j}$ [mm]	$p_{w,j}$ [mm]	R [mm]	$A_{sj,h}$ [mm^2]	$A_{sj,v}$ [mm^2]	$A_{sj,incl}$ [mm^2]
	C1AL	6.0	150	42	57	0	0
	C2	6.0	150	42	57	0	0
	C3	6.0	150	42	57	0	0
	C3L	6.0	150	42	57	0	0
	C4	6.0	150	56	57	0	0
	C4A	6.0	150	56	57	0	0
	C4AL	6.0	150	56	57	0	0
	C5	6.0	150	56	57	0	0
	C6	6.0	150	56	57	0	0
	C6L	6.0	150	56	57	0	0
	C7	6.0	150	56	57	0	0
	C8	6.0	150	56	57	0	0
	C9	6.0	150	56	57	0	0
Tsonos, 1999	M1	8.0	70	42	402	0	0
	M2	8.0	70	49	402	0	0
Tsonos, 2007	A1	6.0	50	35	424	157	0
	E2	6.0	48	49	424	308	0
	E1	6.0	50	49	424	308	0
	G1	8.0	100	49	452	308	0
Tsonos et al., 1992	S1	8.0	100	49	302	616	0
	X1	8.0	100	49	302	0	616
	S2	8.0	100	42	402	616	0
	X2	8.0	100	42	302	0	616
	S6	8.0	100	49	402	616	0
	X6	8.0	100	49	0	0	616
	S'6	8.0	100	49	0	0	0
	F2	8.0	100	49	0	0	0
Wong and Kuang, 2008	BS-L-300	0.0	0	70	0	0	0
	BS-L-450	0.0	0	70	0	0	0
	BS-L-600	0.0	0	70	0	0	0
	BS-L-V2	0.0	0	70	0	314	0
	BS-L-V4	0.0	0	70	0	628	0
	BS-L-H1	10.0	250	70	157	0	0
	BS-L-H2	10.0	150	70	314	0	0
Wallace et al., 1998	BCEJ1	12.7	102	89	1520	1285	0
	BCEJ2	12.7	152	89	760	1285	0

$d_{bw,j}$ = diameter of the horizontal stirrups;
$p_{w,j}$ = spacing of horizontal stirrups in the panel zone;
R = radius of curvature of beam bars bent in the joint;
$A_{sj,h}$ = horizontal reinforcement in the joint;
$A_{sj,v}$ = vertical reinforcement in the joint;
$A_{sj,incl}$ = area of inclined bars into the joint.

MECHANICAL PROPERTIES						
Authors	Name	Column	Beam		Joint	
		$f_{y,col}$ [MPa]	$f_{y,b}$ [MPa]	λ_0 [-]	$f_{y,j}$ [MPa]	f'_c [MPa]
Alva, 2004	LVP1	630.0	630.0	1.17	610.0	40.4
Alva et al., 2007	LVP2	594.0	594.0	1.18	602.0	44.2
	LVP3	594.0	594.0	1.18	602.0	23.9
	LVP4	594.0	594.0	1.18	602.0	24.6
	LVP5	594.0	594.0	1.18	602.0	25.9
Binbhu & Jaya, 2008	A1	432.0	432.0	1.25	432.0	36.7
	A2	432.0	432.0	1.25	432.0	36.7
	B1	432.0	432.0	1.25	432.0	36.7
	B2	432.0	432.0	1.25	432.0	36.7
Calvi et al., 2001	T1	386.0	366.0	1.24	366.0	23.9
Chalioris et al., 2008	JA-0	580.0	580.0	1.10	580.0	34.0
	JA-s5	580.0	580.0	1.10	580.0	34.0
	JA-X12	580.0	580.0	1.10	580.0	34.0
	JA-X14	580.0	580.0	1.10	580.0	34.0
	JB-0	580.0	580.0	1.10	580.0	31.6
	JB-s1	580.0	580.0	1.10	580.0	31.6
	JB-X10	580.0	580.0	1.10	580.0	31.6
	JB-X12	580.0	580.0	1.10	580.0	31.6
	JCa-0	470.0	470.0	1.06	470.0	20.6
	JCa-X10	470.0	470.0	1.06	470.0	20.6
	JCa-s1	470.0	470.0	1.06	470.0	20.6
	JCa-s1-X10	470.0	470.0	1.06	470.0	20.6
	JCa-s2	470.0	470.0	1.06	470.0	20.6
	JCa-s2-X10	470.0	470.0	1.06	470.0	20.6
	JCb-0	470.0	470.0	1.06	470.0	23.0
	JCb-X10	470.0	470.0	1.06	470.0	23.0
	JCb-s1	470.0	470.0	1.06	470.0	23.0
	JCb-s1-X10	470.0	470.0	1.06	470.0	23.0
	JCb-s2	470.0	470.0	1.06	470.0	23.0
	JCb-s2-X10	470.0	470.0	1.06	470.0	23.0
Chun & Kim, 2004	JC-1	402.9	402.9	1.25	383.9	61.7
	JM-1	402.9	402.9	1.25	383.9	61.7
	JC-2	402.9	402.9	1.25	383.9	60.1
	JM-2	402.9	402.9	1.25	383.9	60.1
Chun et al., 2007	JC-1	402.9	402.9	1.54	500.0	61.7
	JM-1	402.9	402.9	1.54	500.0	61.7
	JC-2	402.9	402.9	1.54	500.0	60.1
	JM-2	402.9	402.9	1.54	500.0	60.1
	JC-No. 11-1	458.0	458.0	1.42	500.0	32.8
	JM-No. 11-1a	458.0	458.0	1.42	500.0	32.8
	JM-No. 11-1b	458.0	458.0	1.42	500.0	32.8
Chutarat & Aboutaha, 2003	A -Group 2	482.7	482.7	1.14	365.4	33.1
	B - Group 2	482.7	482.7	1.14	365.4	33.1
	I -Group 1	482.7	482.7	1.14	365.4	27.6
	II - Group 1	482.7	482.7	1.14	365.4	27.6
Clyde et al., 2000	#2	469.5	454.4	1.64	454.4	55.7
	#4	469.5	454.4	1.64	454.4	49.4

MECHANICAL PROPERTIES						
Authors	Name	Column	Beam		Joint	
		$f_{y,col}$ [MPa]	$f_{y,b}$ [MPa]	λ_0 [-]	$f_{y,j}$ [MPa]	f'_c [MPa]
	#5	469.5	454.4	1.64	454.4	44.6
	#6	469.5	454.4	1.64	454.4	48.3
Durrani & Zerbe, 1987	J1	483.0	414.0	1.50	531.3	47.4
	J2	483.0	414.0	1.50	531.3	47.0
	J5	483.0	414.0	1.50	531.3	46.6
	J7	483.0	414.0	1.50	531.3	49.0
Ehsani & Alameddine, 1991	LL8	421.0	421.0	1.25	421.0	55.1
	LH8	421.0	421.0	1.25	421.0	55.1
	HL8	421.0	421.0	1.25	421.0	55.1
	HH8	421.0	421.0	1.25	421.0	55.1
	LL11	421.0	421.0	1.25	421.0	75.8
	LH11	421.0	421.0	1.25	421.0	75.8
	HL11	421.0	421.0	1.25	421.0	75.8
	HH14	421.0	421.0	1.25	421.0	96.5
	LL14	421.0	421.0	1.25	421.0	96.5
	LH14	421.0	421.0	1.25	421.0	96.5
	HH11	421.0	421.0	1.25	421.0	96.5
Ehsani et al., 1987	1	428.0	428.0	1.50	428.0	64.6
	2	428.0	428.0	1.50	428.0	67.2
	3	428.0	428.0	1.50	428.0	64.6
	4	428.0	428.0	1.50	428.0	67.2
	5	428.0	276.0	1.75	428.0	44.6
Ehsani & Wight, 1985(a)	1S	489.9	345.0	1.75	437.1	51.4
	2S	489.9	345.0	1.75	437.1	47.6
	3S	489.9	345.0	1.75	437.1	34.9
	6S	489.9	331.2	1.75	437.1	42.3
Ehsani & Wight, 1985(b)	1B	489.9	338.1	1.75	437.5	40.5
	2B	489.9	338.1	1.75	437.5	42.1
	3B	489.9	338.1	1.75	437.5	49.3
	4B	489.9	338.1	1.75	437.5	53.8
	5B	414.0	331.2	1.75	437.5	29.3
	6B	489.9	338.1	1.75	437.5	48.0
Genesan et al., 2007	HPr	428.0	428.0	1.50	428.0	76.2
Gencoglu & Eren, 2002	#1	500.0	500.0	1.25	500.0	29.5
	#2	500.0	500.0	1.25	500.0	29.5
Hamil, 2000	C6LN0	525.0	525.0	1.25	414.0	53.1
	C6LN1	525.0	525.0	1.25	414.0	53.1
	C6LN3	525.0	525.0	1.25	414.0	50.6
	C6LN5	525.0	525.0	1.25	414.0	38.2
	C6LH0	525.0	525.0	1.25	414.0	104.6
	C6LH1	525.0	525.0	1.25	414.0	105.4
	C6LH3	525.0	525.0	1.25	414.0	100.4
	C6LH5	525.0	525.0	1.25	414.0	103.8
	C4ALN0	525.0	525.0	1.25	414.0	44.0
	C4ALN1	525.0	525.0	1.25	414.0	47.3
	C4ALN3	525.0	525.0	1.25	414.0	43.2
	C4ALN5	525.0	525.0	1.25	414.0	52.3

MECHANICAL PROPERTIES						
Authors	Name	Column	Beam		Joint	
		$f_{y,col}$ [MPa]	$f_{y,b}$ [MPa]	λ_0 [-]	$f_{y,j}$ [MPa]	f'_c [MPa]
	C4ALH0	525.0	525.0	1.25	414.0	107.9
	C4ALH1	525.0	525.0	1.25	414.0	98.8
	C4ALH3	525.0	525.0	1.25	414.0	109.6
	C4ALH5	525.0	525.0	1.25	414.0	102.1
Hakuto et al., 2000	O6	308.0	308.0	1.25	398.0	41.0
	O7	308.0	308.0	1.25	398.0	37.3
Hegger et al., 2003	RK1	530.0	530.0	1.25	530.0	57.9
	RK2	530.0	530.0	1.25	530.0	57.4
	RK3	530.0	530.0	1.25	530.0	57.2
	RK4	530.0	530.0	1.25	530.0	51.7
	RK5	530.0	530.0	1.25	530.0	54.9
	RK6	530.0	530.0	1.25	530.0	86.5
	RK7	530.0	530.0	1.25	530.0	54.7
	RK8	530.0	530.0	1.25	530.0	38.6
Hwang et al., 2004	70-3T44	421.0	430.0	1.41	498.0	92.5
	70-3T4	458.0	491.0	1.46	436.0	90.6
	70-2T5	458.0	491.0	1.46	469.0	92.3
	70-1T55	458.0	491.0	1.46	469.0	84.0
	28-3T4	458.0	491.0	1.46	436.0	42.2
	28 - 0T0	458.0	491.0	1.46	458.0	39.8
Hwang et al., 2005	0T0	421.0	430.0	1.41	430.0	81.1
	3T44	421.0	430.0	1.51	498.0	92.5
	1B8	430.0	435.0	1.52	435.0	74.5
	3T3	421.0	430.0	1.41	471.0	83.1
	2T4	421.0	430.0	1.41	498.0	85.5
	1T44	421.0	430.0	1.41	498.0	87.7
	3T4	458.0	491.0	1.46	436.0	90.7
	2T5	458.0	491.0	1.46	469.0	92.3
	1T55	458.0	491.0	1.46	469.0	84.0
Idayani, 2007	S1	460.0	460.0	1.25	250.0	36.1
	S2	460.0	460.0	1.25	250.0	94.0
	S3	460.0	460.0	1.25	250.0	36.1
Karayannis et al., 2008	A0	580.0	580.0	1.10	580.0	31.6
	A1	580.0	580.0	1.10	580.0	31.6
	A2	580.0	580.0	1.10	580.0	31.6
	A3	580.0	580.0	1.10	580.0	31.6
	B0	580.0	580.0	1.10	580.0	31.6
	B1	580.0	580.0	1.10	580.0	31.6
	C0	580.0	580.0	1.10	580.0	31.6
	C2	580.0	580.0	1.10	580.0	31.6
	C3	580.0	580.0	1.10	580.0	31.6
	C5	580.0	580.0	1.10	580.0	31.6
Karayannis & Sirkelis, 2005	AJ1sp	580.0	580.0	1.10	580.0	32.8
	AJ1s	580.0	580.0	1.10	580.0	32.8
Karayannis & Sirkelis, 2008	A1	574.0	574.0	1.10	574.0	36.4
	A2	574.0	574.0	1.10	574.0	36.4
	B1	574.0	574.0	1.10	574.0	36.4

MECHANICAL PROPERTIES						
		Column	Beam		Joint	
Authors	Name	$f_{y,col}$ [MPa]	$f_{y,b}$ [MPa]	λ_0 [-]	$f_{y,j}$ [MPa]	f'_c [MPa]
	B2	574.0	574.0	1.10	574.0	36.4
Kuang & Wong, 2006	BS-OL	520.0	520.0	1.25	520.0	30.9
	BS-LL	520.0	520.0	1.25	520.0	30.9
	BS-U	520.0	520.0	1.25	520.0	30.9
	BS-L-LS	520.0	520.0	1.25	520.0	30.9
Kusuhara & Shiohara, 2008	E1	375.0	379.0	1.47	366.0	30.4
	E2	375.0	379.0	1.47	366.0	30.4
	B2	357.0	456.0	1.28	326.0	28.3
Lee & Ko, 2007	S0	455.0	455.0	1.50	471.0	32.6
	S50	455.0	455.0	1.50	471.0	34.2
	W0	455.0	455.0	1.50	471.0	34.8
	W75	455.0	455.0	1.50	471.0	36.6
	W150	455.0	455.0	1.50	471.0	35.1
Liu, 2006	RC - 1	323.8	323.8	1.25	383.7	18.0
	RC - 6	306.7	306.7	1.25	383.7	25.0
	NZ - 7	306.7	306.7	1.25	383.7	25.0
Masi et al., 2009	T1	478.0	478.0	1.23	478.0	21.5
	T2	478.0	478.0	1.23	478.0	21.5
	T3	478.0	478.0	1.23	478.0	21.5
	T4	478.0	478.0	1.23	478.0	21.5
	T5	478.0	478.0	1.23	478.0	21.5
	T6	478.0	478.0	1.23	478.0	21.5
	T7	478.0	478.0	1.23	478.0	21.5
	T8	478.0	478.0	1.23	478.0	21.5
	T9	580.0	580.0	1.12	580.0	21.5
	T10	580.0	580.0	1.12	580.0	21.5
Pampanin et al., 2002	T2	386.0	366.0	1.24	366.0	29.1
Pantelides et al., 2002	1	469.9	458.9	1.66	458.9	39.9
	2	469.9	458.9	1.66	458.9	36.4
	3	469.9	458.9	1.66	458.9	41.0
	4	469.9	458.9	1.66	458.9	38.1
	5	469.9	458.9	1.66	458.9	38.2
	6	469.9	458.9	1.66	458.9	37.3
Parker & Bullman, 1997	4a	550.0	570.0	1.25	560.0	49.0
	4b	550.0	570.0	1.25	560.0	49.0
	4c	550.0	570.0	1.25	560.0	46.0
	4d	580.0	570.0	1.25	560.0	49.0
	4e	580.0	570.0	1.25	560.0	50.0
	4f	580.0	570.0	1.25	560.0	47.0
	5a	485.0	485.0	1.25	480.0	53.0
	5b	485.0	485.0	1.25	480.0	54.0
	5c	485.0	485.0	1.25	480.0	54.0
	5d	485.0	515.0	1.25	480.0	54.0
	5e	485.0	515.0	1.25	480.0	56.0
	5f	485.0	515.0	1.25	480.0	54.0
Scott, 1996	C1	525.0	575.0	1.25	414.0	49.9
	C1A	525.0	575.0	1.25	414.0	60.0

MECHANICAL PROPERTIES						
Authors	Name	Column	Beam		Joint	
		$f_{y,col}$ [MPa]	$f_{y,b}$ [MPa]	λ_0 [-]	$f_{y,j}$ [MPa]	f'_c [MPa]
	C1AL	525.0	575.0	1.25	414.0	41.7
	C2	525.0	575.0	1.25	414.0	61.7
	C3	525.0	575.0	1.25	414.0	45.4
	C3L	525.0	575.0	1.25	414.0	44.4
	C4	525.0	525.0	1.25	414.0	51.8
	C4A	525.0	525.0	1.25	414.0	55.4
	C4AL	525.0	525.0	1.25	414.0	44.7
	C5	525.0	525.0	1.25	414.0	41.3
	C6	525.0	525.0	1.25	414.0	49.8
	C6L	525.0	525.0	1.25	414.0	57.3
	C7	525.0	525.0	1.25	414.0	44.0
	C8	525.0	525.0	1.25	414.0	55.6
	C9	525.0	525.0	1.25	414.0	44.9
Tsonos, 1999	M1	465.1	465.1	1.25	494.6	34.0
	M2	465.1	484.7	1.25	494.6	33.5
Tsonos, 2007	A1	500.0	500.0	1.25	540.0	35.0
	E2	495.0	495.0	1.25	540.0	35.0
	E1	495.0	495.0	1.25	540.0	26.5
	G1	495.0	495.0	1.25	500.0	26.5
Tsonos et al., 1992	S1	485.0	485.0	1.25	494.7	44.6
	X1	484.7	485.0	1.25	494.6	44.6
	S2	465.0	507.7	1.25	494.7	31.3
	X2	465.1	496.8	1.25	494.6	31.3
	S6	485.0	485.0	1.25	494.7	39.8
	X6	485.0	485.0	1.25	494.7	32.5
	S'6	485.0	485.0	1.25	494.7	34.9
	F2	485.0	485.0	1.25	494.7	28.9
Wong and Kuang, 2008	BS-L-300	520.0	520.0	1.25	500.0	42.6
	BS-L-450	520.0	520.0	1.25	500.0	38.6
	BS-L-600	520.0	520.0	1.25	500.0	45.5
	BS-L-V2	520.0	520.0	1.25	500.0	40.7
	BS-L-V4	520.0	520.0	1.25	500.0	35.4
	BS-L-H1	520.0	520.0	1.25	500.0	41.6
	BS-L-H2	520.0	520.0	1.25	500.0	52.6
Wallace et al., 1998	BCEJ1	455.0	483.0	1.25	462.0	35.8
	BCEJ2	455.0	483.0	1.25	462.0	33.6

$f_{y,col}$ = strength of the steel in the column;
$f_{y,b}$ = strength of the steel in the beam;
λ_0 = overstrength of the steel in the beam;
$f_{y,j}$ = strength of the steel in the joint;
f'_c = strength of the concrete in the joint;

EXTERANAL LOAD							
			M	C			
Authors	Name	N_{col} [KN]	P^{exp} [KN]	$P^{exp,U}$ [KN]	$P^{exp,max}$ [KN]	V_j^{exp} [kN]	Classification
Alva, 2004	LVP1	360.00	-	-	112.84	539.50	Under-reinforced
Alva et al., 2007	LVP2	397.62	-	-	131.00	514.10	Under-reinforced
	LVP3	215.01	-	-	90.00	364.40	Under-reinforced
	LVP4	221.58	-	-	81.00	327.20	Under-reinforced
	LVP5	233.19	-	-	93.90	380.40	Under-reinforced
Binbhu & Jaya, 2008	A1	15.92	-	16.18	16.18	74.71	EC8-compliant
	A2	15.92	-	18.63	18.63	73.18	EC8-compliant
	B1	53.06	-	17.65	19.62	72.56	Under-reinforced
	B2	53.06	-	18.64	18.64	73.17	Under-reinforced
Calvi et al., 2001	T1	120.00	-	-	11.95	62.29	Unreinforced
Chalioris et al., 2008	JA-0	102.00	-	20.00	63.00	241.23	Unreinforced
	JA-s5	102.00	-	13.00	61.00	242.76	Under-reinforced
	JA-X12	102.00	-	9.00	63.00	241.23	Unreinforced
	JA-X14	102.00	-	12.00	64.00	240.46	Unreinforced
	JB-0	94.80	-	14.00	58.00	230.97	Unreinforced
	JB-s1	94.80	-	38.00	64.00	252.53	Under-reinforced
	JB-X10	94.80	-	24.00	71.00	247.16	Unreinforced
	JB-X12	94.80	-	35.00	73.00	245.63	Unreinforced
	JCa-0	41.20	-	4.00	12.00	69.74	Unreinforced
	JCa-X10	41.20	-	5.00	11.00	70.47	Unreinforced
	JCa-s1	41.20	-	3.00	12.50	69.37	Under-reinforced
	JCa-s1-X10	41.20	-	6.00	11.00	70.47	Under-reinforced
	JCa-s2	41.20	-	5.50	13.00	69.01	Under-reinforced
	JCa-s2-X10	41.20	-	4.00	11.50	70.11	Under-reinforced
	JCb-0	46.00	-	2.00	15.20	105.77	Unreinforced
	JCb-X10	46.00	-	5.50	15.00	103.86	Unreinforced
	JCb-s1	46.00	-	4.00	17.50	104.98	Under-reinforced
	JCb-s1-X10	46.00	-	5.50	17.00	105.34	Under-reinforced
	JCb-s2	46.00	-	2.50	16.00	106.08	Under-reinforced
	JCb-s2-X10	46.00	-	7.50	15.50	106.44	Under-reinforced

EXTERANAL LOAD							
Authors	Name	N_{col} [KN]	M	C		V_j^{exp} [kN]	Classification
			P^{exp} [KN]	$P^{exp,U}$ [KN]	$P^{exp,max}$ [KN]		
Chun & Kim, 2004	JC-1	490.00	-	-	150.42	645.44	EC8-compliant
	JM-1	490.00	-	-	139.58	654.11	EC8-compliant
	JC-2	490.00	-	-	234.58	1343.89	Under-reinforced
	JM-2	490.00	-	-	236.67	1342.22	Under-reinforced
Chun et al., 2007	JC-1	0.00	-	-	160.44	569.43	EC8-compliant
	JM-1	0.00	-	-	148.89	579.41	EC8-compliant
	JC-2	0.00	-	-	250.22	1199.90	Under-reinforced
	JM-2	0.00	-	-	252.89	1197.60	Under-reinforced
	JC-No. 11-1	0.00	-	137.80	245.58	1125.63	Under-reinforced
	JM-No. 11-1a	0.00	-	-	244.69	1113.89	Under-reinforced
	JM-No. 11-1b	0.00	-	222.20	238.94	1080.40	Under-reinforced
Chutarat & Aboutaha, 2003	A -Group 2	0.00	-	61.17	77.28	204.77	EC8-compliant
	B - Group 2	0.00	-	80.69	92.84	471.51	Under-reinforced
	I -Group 1	0.00	-	110.90	190.80	932.47	Under-reinforced
	II - Group 1	0.00	-	115.40	231.40	1188.60	Under-reinforced
Clyde et al., 2000	#2	689.00	-	134.00	267.00	1154.34	Unreinforced
	#4	1380.00	-	102.00	276.00	1302.61	Unreinforced
	#5	1357.00	-	98.00	267.00	1184.77	Unreinforced
	#6	587.00	-	129.00	262.00	1104.49	Unreinforced
Durrani & Zerbe, 1987	J1	175.00	-	86.80	86.80	457.79	Under-reinforced
	J2	175.00	-	101.70	101.70	633.50	Under-reinforced
	J5	175.00	-	153.00	153.00	985.98	Under-reinforced
	J7	175.00	-	144.60	146.80	760.57	Under-reinforced
Ehsani & Alameddine, 1991	LL8	293.70	-	-	248.00	942.96	Under-reinforced
	LH8	293.70	-	-	240.00	946.93	Under-reinforced
	HL8	507.30	-	-	262.00	1231.02	Under-reinforced
	HH8	507.30	-	-	264.00	1230.02	Under-reinforced
	LL11	285.00	-	142.00	213.00	929.15	Under-reinforced
	LH11	276.00	-	267.00	284.00	925.09	Under-

EXTERANAL LOAD							
Authors	Name	N_{col} [KN]	M	C		V_j^{exp} [kN]	Classification
			P^{exp} [KN]	$P^{exp,U}$ [KN]	$P^{exp,max}$ [KN]		
							reinforced
	HL11	587.00	-	147.00	263.00	1177.46	Under-reinforced
	HH14	605.00	-	200.00	289.00	1217.61	Under-reinforced
	LL14	236.00	-	205.00	261.00	936.50	Under-reinforced
	LH14	222.00	-	214.00	267.00	933.53	Under-reinforced
	HH11	605.20	-	-	289.00	1217.61	Under-reinforced
Ehsani et al., 1987	1	133.00	-	146.80	146.80	676.16	Under-reinforced
	2	338.00	-	122.40	136.50	592.68	Under-reinforced
	3	383.00	-	164.60	181.30	716.27	Under-reinforced
	4	325.00	-	110.60	159.20	920.97	Under-reinforced
	5	222.00	-	130.80	169.00	843.45	Under-reinforced
Ehsani & Wight, 1985(a)	1S	222.00	-	210.14	244.10	384.56	EC8-compliant
	2S	222.00	-	242.28	272.62	368.86	EC8-compliant
	3S	222.00	-	185.80	212.13	402.16	Under-reinforced
	6S	303.31	-	297.97	325.84	490.65	Under-reinforced
Ehsani & Wight, 1985(b)	1B	177.87	-	78.70	146.80	591.21	Under-reinforced
	2B	221.87	-	76.60	135.70	679.47	Under-reinforced
	3B	221.87	-	89.00	180.90	1053.73	Under-reinforced
	4B	221.87	-	128.20	170.10	1062.20	Under-reinforced
	5B	356.58	-	112.60	158.50	444.27	Under-reinforced
	6B	303.82	-	138.10	156.80	437.01	Under-reinforced
Genesan et al., 2007	HPr	15.70	-	23.54	23.54	81.12	EC8-compliant
Gencoglu & Eren, 2002	#1	150.00	-	53.38	57.45	105.82	EC8-compliant
	#2	150.00	-	54.35	61.91	114.04	Unreinforced
Hamil, 2000	C6LN0	50.00	-	-	24.00	113.90	Unreinforced
	C6LN1	50.00	-	-	25.00	118.65	Under-reinforced
	C6LN3	50.00	-	-	29.00	137.86	Under-reinforced

EXTERANAL LOAD							
Authors	Name	N_{col} [KN]	M	C		V_j^{exp} [kN]	Classification
			P^{exp} [KN]	$P^{exp,U}$ [KN]	$P^{exp,max}$ [KN]		
	C6LN5	50.00	-	-	34.00	164.68	Under-reinforced
	C6LH0	100.00	-	-	36.00	163.86	Unreinforced
	C6LH1	100.00	-	-	37.00	169.07	Under-reinforced
	C6LH3	100.00	-	-	41.00	187.65	Under-reinforced
	C6LH5	100.00	-	-	51.00	239.14	Under-reinforced
	C4ALN0	50.00	-	-	27.00	129.60	Unreinforced
	C4ALN1	50.00	-	-	34.00	162.26	Under-reinforced
	C4ALN3	50.00	-	-	35.00	168.30	Under-reinforced
	C4ALN5	50.00	-	-	39.00	185.17	Under-reinforced
	C4ALH0	100.00	-	-	43.00	200.98	Unreinforced
	C4ALH1	100.00	-	-	43.00	204.90	Under-reinforced
	C4ALH3	100.00	-	-	46.00	229.83	Under-reinforced
	C4ALH5	100.00	-	-	49.00	240.11	Under-reinforced
Hakuto et al., 2000	O6	0.00	-	44.26	104.15	434.30	EC8-compliant
	O7	0.00	-	25.50	104.15	440.24	EC8-compliant
Hegger et al., 2003	RK1	500.00	131.70	-	-	374.00	EC8-compliant
	RK2	500.00	146.10	-	-	417.00	Under-reinforced
	RK3	500.00	137.40	-	-	402.00	EC8-compliant
	RK4	500.00	118.50	-	-	357.00	Under-reinforced
	RK5	500.00	131.50	-	-	423.00	Under-reinforced
	RK6	500.00	181.90	-	-	556.00	Under-reinforced
	RK7	500.00	144.40	-	-	277.00	Under-reinforced
	RK8	500.00	86.90	-	-	273.00	Under-reinforced
Hwang et al., 2004	70-3T44	196.00	-	86.21	205.00	1066.03	EC8-compliant
	70-3T4	196.00	-	136.69	214.00	1284.53	Under-reinforced
	70-2T5	196.00	-	135.52	224.00	1276.66	Under-reinforced
	70-1T55	196.00	-	91.21	217.00	1282.17	Under-reinforced
	28-3T4	196.00	-	139.97	313.00	1200.81	Under-reinforced
	28 - 0T0	196.00	-	85.40	276.00	1230.62	Unreinforced

EXTERANAL LOAD							
Authors	Name	N_{col} [KN]	M	C		V_j^{exp} [kN]	Classification
			P^{exp} [KN]	$P^{exp,U}$ [KN]	$P^{exp,max}$ [KN]		
Hwang et al., 2005	0T0	196.00	-	90.00	192.00	1078.82	Unreinforced
	3T44	196.00	-	86.95	205.00	1157.24	Under-reinforced
	1B8	196.00	-	110.00	242.00	1151.02	Unreinforced
	3T3	196.00	-	110.00	218.00	1058.50	Under-reinforced
	2T4	196.00	-	90.00	208.00	1066.32	Under-reinforced
	1T44	196.00	-	80.00	200.00	1072.57	Under-reinforced
	3T4	196.00	-	134.48	214.00	1280.76	Under-reinforced
	2T5	196.00	-	134.48	224.00	1272.89	Under-reinforced
	1T55	196.00	-	90.80	217.00	1278.40	Under-reinforced
Idayani, 2007	S1	90.00	50.80	-	-	194.08	Unreinforced
	S2	90.00	52.10	-	-	199.04	Unreinforced
	S3	90.00	58.60	-	-	223.87	Under-reinforced
Karayannis et al., 2008	A0	152.29	-	5.00	24.50	82.56	Unreinforced
	A1	126.40	-	8.00	24.00	82.93	EC8-compliant
	A2	152.29	-	4.00	24.00	82.93	EC8-compliant
	A3	152.29	-	12.00	25.00	82.20	EC8-compliant
	B0	228.43	-	13.00	58.00	227.81	Unreinforced
	B1	228.43	-	38.00	63.00	253.29	Under-reinforced
	C0	228.43	-	18.00	65.00	239.70	Unreinforced
	C2	228.43	-	40.00	61.00	242.76	Under-reinforced
	C3	228.43	-	50.00	65.00	239.70	Under-reinforced
	C5	228.43	-	10.00	60.00	243.53	EC8-compliant
Karayannis & Sirkelis, 2005	AJ1sp	70.00	-	-	23.92	85.60	Unreinforced
	AJ1s	70.00	-	-	25.18	84.83	EC8-compliant
Karayannis & Sirkelis, 2008	A1	70.00	-	8.50	21.00	74.95	Unreinforced
	A2	70.00	-	7.50	21.50	76.07	Unreinforced
	B1	70.00	-	21.50	22.00	77.19	EC8-compliant
	B2	70.00	-	21.00	22.00	77.19	EC8-compliant
Kuang & Wong, 2006	BS-OL	402.98	-	-	70.10	264.21	Unreinforced
	BS-LL	402.98	-	-	127.50	534.59	Unreinforced
	BS-U	402.98	-	-	109.10	411.21	Unreinforced
	BS-L-LS	402.98	-	-	110.30	415.73	Unreinforced
Kusuhara & Shiohara, 2008	E1	216.00	-	60.68	80.44	535.55	Under-reinforced
	E2	216.00	-	70.40	70.40	371.13	Under-reinforced
	B2	216.00	-	69.51	101.78	370.03	Under-

EXTERANAL LOAD							
Authors	Name	N_{col} [KN]	M	C		V_j^{exp} [kN]	Classification
			P^{exp} [KN]	$P^{exp,U}$ [KN]	$P^{exp,max}$ [KN]		
							reinforced
Lee & Ko, 2007	S0	942.65	-	114.56	192.76	883.51	EC8-compliant
	S50	988.92	-	102.94	189.60	886.02	EC8-compliant
	W0	835.20	-	93.50	163.17	907.83	EC8-compliant
	W75	878.40	-	97.60	163.17	907.83	EC8-compliant
	W150	842.40	-	37.40	154.35	914.85	EC8-compliant
Liu, 2006	RC - 1	75.00	-	-	29.48	148.71	Unreinforced
	RC - 6	100.00	-	-	32.21	148.85	Under-reinforced
	NZ - 7	100.00	-	-	34.14	147.38	EC8-compliant
Masi et al., 2009	T1	290.25	-	-	28.13	103.80	Unreinforced
	T2	580.50	-	-	59.83	264.80	EC8-compliant
	T3	580.50	-	-	57.90	282.00	EC8-compliant
	T4	580.50	-	-	63.85	235.60	EC8-compliant
	T5	290.25	-	-	59.24	267.90	EC8-compliant
	T6	580.50	-	-	31.70	103.30	Unreinforced
	T7	290.25	-	-	31.70	104.60	Unreinforced
	T8	580.50	-	-	63.70	248.50	EC8-compliant
	T9	580.50	-	-	71.89	303.20	EC8-compliant
	T10	290.25	-	-	72.78	322.50	Under-reinforced
Pampanin et al., 2002	T2	100.00	-	1.60	13.79	72.09	Unreinforced
Pantelides et al., 2002	1	546.70	-	30.70	194.80	1224.55	Unreinforced
	2	1247.00	-	16.20	189.90	1110.45	Unreinforced
	3	561.50	-	8.90	184.20	1045.82	Unreinforced
	4	1304.80	-	54.80	211.30	1771.78	Unreinforced
	5	523.60	-	25.00	169.90	966.87	Unreinforced
	6	1280.00	-	30.50	191.70	1160.64	Unreinforced
Parker & Bullman, 1997	4a	0.00	118.00	-	-	231.27	Unreinforced
	4b	300.00	138.00	-	-	270.47	Unreinforced
	4c	570.00	170.00	-	-	333.19	Unreinforced
	4d	0.00	150.00	-	-	293.99	Unreinforced
	4e	300.00	160.00	-	-	313.59	Unreinforced
	4f	600.00	183.00	-	-	358.67	Unreinforced
	5a	0.00	213.00	-	-	455.89	Under-reinforced
	5b	300.00	236.00	-	-	477.18	Under-reinforced
	5c	600.00	242.00	-	-	474.18	Under-reinforced
	5d	0.00	226.00	-	-	454.57	Under-reinforced
	5e	300.00	295.00	-	-	593.36	Under-reinforced
	5f	600.00	322.00	-	-	647.67	Under-reinforced
Scott, 1996	C1	275.00	26.20	-	-	148.32	Under-

EXTERANAL LOAD							
Authors	Name	N_{col} [KN]	M	C		V_j^{exp} [kN]	Classification
			P^{exp} [KN]	$P^{exp,U}$ [KN]	$P^{exp,max}$ [KN]		
							reinforced
	C1A	275.00	26.80	-	-	148.00	Under-reinforced
	C1AL	50.00	22.00	-	-	114.65	Under-reinforced
	C2	275.00	21.60	-	-	110.36	Under-reinforced
	C3	275.00	25.90	-	-	148.48	Under-reinforced
	C3L	50.00	21.60	-	-	112.31	Under-reinforced
	C4	275.00	30.00	-	-	159.63	Under-reinforced
	C4A	275.00	32.00	-	-	169.61	Under-reinforced
	C4AL	50.00	28.80	-	-	154.26	Under-reinforced
	C5	275.00	14.00	-	-	75.62	Under-reinforced
	C6	275.00	22.20	-	-	118.66	Under-reinforced
	C6L	50.00	26.50	-	-	140.17	Under-reinforced
	C7	275.00	32.00	-	-	104.38	Under-reinforced
	C8	275.00	27.50	-	-	89.04	Under-reinforced
	C9	275.00	28.20	-	-	92.21	Under-reinforced
Tsonos, 1999	M1	300.00	-	27.68	81.72	153.66	EC8-compliant
	M2	300.00	-	21.08	107.46	282.15	Under-reinforced
Tsonos, 2007	A1	200.00	-	40.00	54.70	157.28	EC8-compliant
	E2	200.00	-	30.50	53.20	152.50	EC8-compliant
	E1	200.00	-	50.00	72.50	233.96	Under-reinforced
	G1	200.00	-	35.00	65.00	239.32	Under-reinforced
Tsonos et al., 1992	S1	713.60	-	31.80	48.90	143.39	EC8-compliant
	X1	713.60	-	46.35	57.10	136.14	EC8-compliant
	S2	500.80	-	28.20	40.90	157.20	EC8-compliant
	X2	500.80	-	37.37	43.60	150.65	EC8-compliant
	S6	636.80	-	32.30	58.60	225.60	Under-reinforced
	X6	520.00	-	72.90	80.00	302.53	Unreinforced
	S'6	558.40	-	34.30	78.60	303.77	Unreinforced
	F2	462.40	-	30.00	52.90	205.55	Unreinforced
Wong and	BS-L-300	575.10	-	45.00	95.40	561.83	Unreinforced

EXTERANAL LOAD							
Authors	Name	N_{col} [KN]	M	C		V_j^{exp} [kN]	Classification
			P^{exp} [KN]	$P^{exp,U}$ [KN]	$P^{exp,max}$ [KN]		
Kuang, 2008	BS-L-450	521.10	-	50.00	100.90	377.44	Unreinforced
	BS-L-600	614.25	-	45.00	132.70	340.12	Unreinforced
	BS-L-V2	549.45	-	53.00	127.00	514.18	Unreinforced
	BS-L-V4	477.90	-	60.00	128.80	533.80	Unreinforced
	BS-L-H1	561.60	-	55.00	124.50	495.48	Under-reinforced
	BS-L-H2	710.10	-	55.00	153.20	531.07	Under-reinforced
Wallace et al., 1998	BCEJ1	0.00	-	-	133.93	741.89	Under-reinforced
	BCEJ2	0.00	-	-	142.43	790.53	Under-reinforced

N_{col} = axial load of the top column;
M = monotonic load;
C = cyclic load;
P^{exp} = maximum force in monotonic tests (subsection 2.3);
$P^{exp,U}$ = ultimate external force in cyclic tests;
$P^{exp,max}$ = maximum force in cyclic tests;
V_j^{exp} = experimental shear strength;
EC8-compliant = classification about the amount of horizontal stirrups in the panel zone.

Appendix A2- Database for Interior Joints

LOAD TYPE, NOTES AND FAILURE TYPE				
Authors	Name	Load Type	Notes	Failure Type
Benevant et al., 2008	IL	C	3/5 scaled - wide beam	J
	IU	C	3/5 scaled - wide beam	J
Durrani & Wight, 1982	X1	C	-	J
	X2	C	-	J
	X3	C	-	J
	S1	C	with slab and transverse beam	J
	S2	C	with slab and transverse beam	BJ
	S3	C	with slab and transverse beam	J
Hakuto et al., 2000	O1	C	-	J
	O4	C	-	J
	O5	C	-	CJ
Hegger et al., 2003	RA1	M		J
	RA2	M	-	J
	RA3	M	-	J
	RA4	M	-	J
	RA5	M	-	J
	RA6	M	-	J
	RA7	M	-	J
Kitayama et al., 1991	J1	C	-	J
	C1	C	-	BJ
	B1/B2	C	only legged ties	BJ
	B3	C	only legged ties	BJ
Kusuhara et al., 2004	JE-0	C	-	J
	JE-55	C	eccentric beams	J
	JE-55S	C	eccentric beams - additional reinforcement	J
Kusuhara & Shiohara, 2008	A1	C	-	BJ
	A2	C		BJ
	A3	C		J
	C1	C	transverse beam	J
	D1	C	-	J
	D2	C	anchor plates in the joint	J
	B1	C		BJ
Lee et al., 2009	J1	C	-	J
	BJ1	C	-	BJ
	BJ2	C	-	BJ
	BJ3	C	-	BJ
	B1	C	-	BJ
Leon, 1990	BCJ2	C	-	J
	BCJ3	C	-	J
	BCJ4	C	-	BJ
Li et al., 2002	A1	C	Beam bottom bar lap spliced within joint	J
	M1	C	-	J
	A2	C	Beam bottom bar lap spliced within joint	BJ
	M2	C	-	BJ

LOAD TYPE, NOTES AND FAILURE TYPE				
Authors	Name	Load Type	Notes	Failure Type
Pampanin et al., 2002	C2	C	2/3 scaled-50's & 70's - Continuous reinforcement	CJ
Pampanin et al., 2007	C4	C	2/3 scaled-50's & 70's - End Hocked bars	CJ
Shannag & Alhassan, 2005	S1	C	-	CJ
	S2	C	Discontinuous beam bottom steel	J
	S5	C	Discontinuous beam bottom steel	J
	S8	C	Discontinuous beam bottom steel	J
Shin & LaFave, 2004	1	C	eccentric beams with slab	J
	2	C	eccentric beams with slab	J
Shiohara et al., 2000	S3	C	-	J
Soleimani et al., 1979	BC2	C	-	BJ
	BC3	C	-	BJ
Takaine et al., 2008	JH1	C	-	BJ
Teng & Zhou, 2003	S1 (Series 1)	C	-	J
	S2 (Series 1)	C	eccentric beams	J
	S3 (Series 1)	C	eccentric beams	J
	S5 (Series 2)	C	eccentric beams	J
	S6 (Series 2)	C	eccentric beams	J
Wang & Hsu, 2009	Ko-JI1	C	-	CJ
	Ho-JI1	C	-	J
Supuviriyakit & Pimanmas, 2007	Control	C	-	J
	Debond	C	-	BJ
Shiohara & Kusuhara, 2008	B01	C	-	J
	B02	C	-	J
	B03	C	-	J
	B04	C	-	J
	B05	C	-	J
	B06	C	-	J
	B07	C	-	J
	B08	C	-	J
	B09	C	-	J
	B10	C	-	J
	C01	C	-	J
	C03	C	-	J
	D01	C	-	J
	D02	C	-	J
	D03	C	-	J
	D04	C	-	J
	D05	C	-	J
	D06	C	-	J
	D07	C	-	J
	D08	C	-	J

Load Type: **M** = Monotonic; **C** = Cyclic;
Failure Type: **B** = Beam; **BJ** = Beam-Joint; **C** = Column; **CJ** = Column-Joint; **J** = Joint; **U** = Unknown.

GEOMETRIC DETAILS OF THE COLUMN								
Authors	Name	Column						
		b_c [mm]	h_c [mm]	d'_c [mm]	$L_{c,inf}$ [mm]	$L_{c,sup}$ [mm]	$A'_{s,c}$ [mm^2]	$A_{s,c}$ [mm^2]
Benevant et al., 2008	IL	270	270	24	900	900	804	804
	IU	210	210	24	900	900	515	515
Durrani & Wight, 1982	X1	362	362	25	1124	1124	1520	1520
	X2	362	362	25	1124	1124	1520	1520
	X3	362	362	25	1124	1124	1061	1061
	S1	362	362	25	1124	1124	1520	1520
	S2	362	362	25	1124	1124	1520	1520
	S3	362	362	25	1124	1124	1164	1164
Hakuto et al., 2000	O1	460	300	40	1600	1600	1357	1357
	O4	460	460	40	1600	1600	1847	1847
	O5	460	460	40	1600	1600	1847	1847
Hegger et al., 2003	RA1	150	240	30	830	830	1257	1257
	RA2	150	240	30	830	830	1257	1257
	RA3	150	240	30	830	830	1257	1257
	RA4	150	240	30	830	830	1232	1232
	RA5	150	240	30	830	830	1257	1257
	RA6	150	300	30	830	830	1257	1257
	RA7	150	240	30	830	830	1257	1257
Kitayama et al., 1991	J1	300	300	30	735	735	664	664
	C1	300	300	30	735	735	393	393
	B1/B2	300	300	30	735	735	664	664
	B3	300	300	30	735	735	393	393
Kusuhara et al., 2004	JE-0	320	280	33	735	735	796	796
	JE-55	320	280	33	735	735	796	796
	JE-55S	320	280	33	735	735	796	796
Kusuhara & Shiohara, 2008	A1	300	300	35	735	735	664	664
	A2	300	300	35	735	735	664	664
	A3	300	300	35	735	735	664	664
	C1	300	300	35	735	735	664	664
	D1	300	300	35	735	735	664	664
	D2	300	300	35	735	735	664	664
	B1	300	300	35	735	735	398	398
Lee et al., 2009	J1	350	350	30	780	780	2642	2642
	BJ1	350	350	30	780	780	2642	2642
	BJ2	350	350	30	780	780	2642	2642
	BJ3	350	350	30	780	780	2642	2642
	B1	350	350	30	780	780	2642	2642
Leon, 1990	BCJ2	254	254	25	1232	1232	1267	1267
	BCJ3	305	254	25	1232	1232	1267	1267
	BCJ4	356	254	25	1232	1232	1013	1013
Li et al., 2002	A1	900	300	30	1250	1250	3436	3436
	M1	900	300	30	1250	1250	3436	3436
	A2	300	900	30	1250	1250	982	982
	M2	300	900	30	1250	1250	982	982
Pampanin et al., 2002	C2	200	200	20	925	1245	151	151
Pampanin et al., 2007	C4	200	200	20	925	1245	151	151
Shannag & Alhassan,	S1	125	150	30	373	373	308	308

GEOMETRIC DETAILS OF THE COLUMN								
Authors	Name	Column						
		b_c [mm]	h_c [mm]	d'_c [mm]	$L_{c,inf}$ [mm]	$L_{c,sup}$ [mm]	$A'_{s,c}$ [mm^2]	$A_{s,c}$ [mm^2]
2005	S2	125	150	30	373	373	308	308
	S5	125	150	30	373	373	308	308
	S8	125	150	30	373	373	308	308
Shin & LaFave, 2004	1	457	330	38	1232	1715	855	855
	2	457	330	38	1232	1715	855	855
Shiohara et al., 2000	S3	300	300	35	735	735	1134	1134
Soleimani et al., 1979	BC2	432	432	19	914	914	1140	1140
	BC3	432	432	19	914	914	1140	1140
Takaine et al., 2008	JH1	500	500	30	750	750	1134	1134
Teng & Zhou, 2003	S1 (Series 1)	300	300	30	1313	1313	1571	1571
	S2 (Series 1)	400	300	30	1313	1313	1571	1571
	S3 (Series 1)	400	300	30	1313	1313	1571	1571
	S5 (Series 2)	400	200	30	1313	1313	1571	1571
	S6 (Series 2)	400	200	30	1313	1313	1571	1571
Wang & Hsu, 2009	Ko-JI1	300	300	30	1230	1230	1473	1473
	Ho-JI1	400	400	30	1215	1215	1473	1473
Supuviriyakit & Pimanmas, 2007	Control	200	350	30	680	890	565	565
	Debond	200	350	30	680	890	565	565
Shiohara & Kusuhara, 2008	B01	240	240	30	700	700	531	531
	B02	240	240	30	700	700	664	664
	B03	240	240	30	700	700	1005	1005
	B04	240	240	30	700	700	796	796
	B05	240	240	30	700	700	664	664
	B06	240	240	30	700	700	664	664
	B07	240	240	30	700	700	531	531
	B08	240	240	30	700	700	531	531
	B09	240	240	30	700	700	1005	1005
	B10	240	240	30	700	700	1005	1005
	C01	240	240	30	700	700	664	664
	C03	240	240	30	700	700	664	664
	D01	240	340	30	700	700	265	265
	D02	240	340	30	700	700	398	398
	D03	240	340	30	700	700	664	664
	D04	240	340	30	700	700	265	265
	D05	240	340	30	700	700	398	398
	D06	240	340	30	700	700	531	531
	D07	240	340	30	700	700	796	796
	D08	240	340	30	700	700	603	603

b_c = column width;
h_c = column depth;
d'_c = cover concrete;
$L_{c,inf}$ = length of the bottom column;
$L_{c,sup}$ = length of the top column;
$A'_{s,c}$ = $A_{s,c}$ = longitudinal reinforcement in column.

GEOMETRIC DETAILS OF THE BEAM										
Authors	Name	Beam								
		b_b [mm]	h_b [mm]	d'_b [mm]	L_b [mm]	e_b [mm]	$d_{b,1}$ [mm]	$d_{b,2}$ [mm]	$A_{sb,inf}$ [mm^2]	$A_{sb,sup}$ [mm^2]
Benevant et al., 2008	IL	480	180	24	1650	0	12.0	-	1017	1583
	IU	360	180	24	1650	0	12.0	-	452	1130
Durrani & Wight, 1982	X1	279	419	25	1248	0	22.2	19.1	1140	1551
	X2	279	419	25	1248	0	22.2	19.1	1140	1551
	X3	279	419	25	1248	0	22.2	19.1	855	1163
	S1	279	419	25	1248	0	22.2	19.1	1140	1535
	S2	279	419	25	1248	0	22.2	19.1	1140	1535
	S3	279	419	25	1248	0	22.2	19.1	855	1282
Hakuto et al., 2000	O1	300	500	40	1905	0	24.0	-	904	1809
	O4	300	500	40	1905	0	24.0	-	1809	1809
	O5	300	500	36	1905	0	32.0	-	1608	1608
Hegger et al., 2003	RA1	150	300	30	970	0	14.0	20.0	929	929
	RA2	150	300	30	970	0	14.0	-	615	615
	RA3	150	300	30	970	0	14.0	12.0	728	728
	RA4	150	300	30	970	0	20.0	16.0	1030	1030
	RA5	150	300	30	970	0	12.0	-	565	565
	RA6	150	300	30	1000	0	14.0	-	615	615
	RA7	150	300	30	970	0	16.0	12.0	917	917
Kitayama et al., 1991	J1	200	300	30	1350	0	13.0	-	398	1061
	C1	200	300	30	1350	0	10.0	-	471	942
	B1/B2	200	300	30	1350	0	13.0	-	1061	1061
	B3	200	300	30	1350	0	10.0	-	942	942
Kusuhara et al., 2004	JE-0	180	300	51	1350	0	10.0	-	785	785
	JE-55	180	300	51	1350	55	10.0	-	785	785
	JE-55S	180	300	51	1350	55	10.0	-	785	785
Kusuhara & Shiohara, 2008	A1	300	300	53	1350	0	13.0	-	1062	1062
	A2	300	300	53	1350	0	13.0	-	1062	1062
	A3	300	300	53	1350	0	13.0	-	1062	1062
	C1	300	300	53	1350	0	13.0	-	1062	1062
	D1	300	300	47	1350	0	16.0	-	1206	1206
	D2	300	300	47	1350	0	16.0	-	1206	1206
	B1	300	300	53	1350	0	13.0	-	1327	1327
Lee et al., 2009	J1	300	400	45	1250	0	16.0	-	2010	2010
	BJ1	300	400	40	1250	0	16.0	-	1206	1206
	BJ2	300	400	30	1250	0	16.0	-	1005	1005
	BJ3	300	400	30	1250	0	16.0	-	804	804
	B1	300	400	30	1250	0	16.0	-	603	603
Leon, 1990	BCJ2	203	305	25	1016	0	12.7	9.5	285	506
	BCJ3	203	305	25	1016	0	12.7	9.5	285	506
	BCJ4	203	305	25	1016	0	12.7	9.5	285	506
Li et al., 2002	A1	300	600	30	2000	0	16.0	-	603	1005
	M1	300	600	30	2000	0	16.0	-	603	1005
	A2	300	600	30	2000	0	25.0	16.0	1472	1874
	M2	300	600	30	2000	0	25.0	16.0	1472	1874
Pampanin et al., 2002	C2	200	330	20	1700	0	12.0	8.0	276	327
Pampanin et	C4	200	330	20	1700	0	12.0	8.0	276	327

GEOMETRIC DETAILS OF THE BEAM										
Authors	Name	Beam								
		b_b [mm]	h_b [mm]	d'_b [mm]	L_b [mm]	e_b [mm]	$d_{b,1}$ [mm]	$d_{b,2}$ [mm]	$A_{sb,inf}$ [mm^2]	$A_{sb,sup}$ [mm^2]
al., 2007										
Shannag & Alhassan, 2005	S1	125	200	30	800	0	14.0	-	308	308
	S2	125	200	30	800	0	14.0	-	308	308
	S5	125	200	30	800	0	14.0	-	308	308
	S8	125	200	30	800	0	14.0	-	308	308
Shin & LaFave, 2004	1	279	406	38	2337	89	15.9	-	396	791
	2	178	406	57	2337	140	15.9	-	396	791
Shiohara et al., 2000	S3	200	300	49	1350	0	16.0	-	1005	1005
Soleimani et al., 1979	BC2	229	406	41	1829	0	19.1	15.9	593	1140
	BC3	229	406	41	1829	0	19.1	15.9	593	1140
Takaine et al., 2008	JH1	285	500	45	1500	0	16.0	-	1608	1608
Teng & Zhou, 2003	S1 (Series 1)	200	400	45	2000	0	16.0	-	603	1005
	S2 (Series 1)	200	400	45	2000	50	16.0	-	603	1005
	S3 (Series 1)	200	400	45	2000	100	16.0	-	603	1005
	S5 (Series 2)	200	400	30	2000	50	13.0	-	398	663
	S6 (Series 2)	200	400	30	2000	100	13.0	-	398	663
Wang & Hsu, 2009	Ko-JI1	300	500	30	1750	0	25.0	-	1963	1963
	Ho-JI1	300	400	30	1750	0	19.0	-	1134	1134
Supuviriyakit & Pimanmas, 2007	Control	175	300	30	1500	0	12.0	-	452	679
	Debond	175	300	30	1500	0	12.0	-	452	679
Shiohara & Kusuhara, 2008	B01	240	240	30	700	0	13.0	-	531	531
	B02	240	240	30	700	0	13.0	-	664	664
	B03	240	240	30	700	0	16.0	-	1005	1005
	B04	240	240	30	700	0	13.0	-	531	531
	B05	240	240	30	700	0	13.0	-	664	664
	B06	240	240	30	700	0	13.0	-	664	664
	B07	240	240	30	700	0	13.0	-	531	531
	B08	240	240	30	700	0	13.0	-	531	531
	B09	240	240	30	700	0	16.0	-	1005	1005
	B10	240	240	30	700	0	16.0	-	1005	1005
	C01	120	240	30	700	0	13.0	-	664	664
	C03	240	240	30	700	0	13.0	-	664	664
	D01	170	240	30	700	0	13.0	-	664	664
	D02	170	240	30	700	0	13.0	-	664	664
	D03	170	240	30	700	0	13.0	-	664	664
	D04	170	240	30	700	0	13.0	-	929	929
	D05	170	240	30	700	0	13.0	-	929	929
	D06	170	240	30	700	0	13.0	-	929	929
	D07	170	240	30	700	0	13.0	-	929	929
	D08	170	240	30	700	0	16.0	-	1407	1407

b_b = beam width;
h_b = beam depth;
d'_b = cover concrete;
L_b = total length of the beam;

GEOMETRIC DETAILS OF THE BEAM										
Authors	Name	Beam								
		b_b [mm]	h_b [mm]	d'_b [mm]	L_b [mm]	e_b [mm]	$d_{b,1}$ [mm]	$d_{b,2}$ [mm]	$A_{sb,inf}$ [mm^2]	$A_{sb,sup}$ [mm^2]

e_b = eccentricity of the beam;
$d_{b,1}$ = primary diameter of the steel bars;
$d_{b,2}$ = secondary diameter of the steel bars;
$A_{sb,inf}$ = reinforcement at the bottom;
$A_{sb,sup}$ = reinforcement at the top.

GEOMETRIC DETAILS OF THE JOINT							
Authors	Name	Joint					
		$d_{bw,i}$ [mm]	$p_{w,i}$ [mm]	R [mm]	$A_{si,h}$ [mm^2]	$A_{si,v}$ [mm^2]	$A_{si,incl}$ [mm^2]
Benevant et al., 2008	IL	0	0	0	0	402	0
	IU	0	0	0	0	804	0
Durrani & Wight, 1982	X1	9,5	368	0	428	1013	0
	X2	9,5	184	0	641	1013	0
	X3	9,5	368	0	428	570	0
	S1	9,5	368	0	428	1013	0
	S2	9,5	184	0	641	1013	0
	S3	9,5	368	0	428	776	0
Hakuto et al., 2000	O1	0	0	0	0	0	0
	O4	0	0	0	0	0	0
	O5	0	0	0	0	0	0
Hegger et al., 2003	RA1	0	0	0	0	0	0
	RA2	6	80	0	226	0	0
	RA3	8	60	0	503	0	0
	RA4	8	60	0	503	0	0
	RA5	6	60	0	283	0	0
	RA6	6	60	0	283	0	0
	RA7	10	60	0	785	0	0
Kitayama et al., 1991	J1	6	100	0	170	796	0
	C1	6	100	0	170	471	0
	B1/B2	6	75	0	226	796	0
	B3	6	43	0	594	471	0
Kusuhara et al., 2004	JE-0	6	100	0	170	531	0
	JE-55	6	100	0	170	531	0
	JE-55S	6	100	0	254	531	0
Kusuhara & Shiohara, 2008	A1	6	50	0	170	796	0
	A2	6	50	0	170	796	1
	A3	6	50	0	170	796	2
	C1	6	50	0	170	796	0
	D1	6	50	0	170	531	0
	D2	6	50	0	170	531	0
	B1	6	50	0	170	265	0
Lee et al., 2009	J1	10	50	0	942	2641	0
	BJ1	10	50	0	942	2641	0
	BJ2	10	75	0	628	2641	0
	BJ3	10	75	0	628	2641	0
	B1	10	75	0	628	2641	0
Leon, 1990	BCJ2	6,4	85	0	253	506	0
	BCJ3	6,4	85	0	253	506	0
	BCJ4	6,4	85	0	253	506	0
Li et al., 2002	A1	0	0	0	0	0	0
	M1	8	150	0	302	0	0
	A2	0	0	0	0	4906	0
	M2	8	150	0	302	4906	0
Pampanin et al., 2002	C2	0	0	0	0	0	0
Pampanin et al., 2007	C4	0	0	0	0	0	0
Shannag & Alhassan, 2005	S1	8	200	0	101	100	0

GEOMETRIC DETAILS OF THE JOINT							
Authors	Name	Joint					
		$d_{bw,j}$ [mm]	$p_{w,j}$ [mm]	R [mm]	$A_{sj,h}$ [mm^2]	$A_{sj,v}$ [mm^2]	$A_{sj,incl}$ [mm^2]
	S2	0	0	0	0	0	0
	S5	0	0	0	0	0	0
	S8	0	0	0	0	0	0
Shin & LaFave, 2004	1	9,5	83	0	641	570	0
	2	9,5	83	0	641	570	0
Shiohara et al., 2000	S3	6,0	40	0	452	1134	0
Soleimani et al., 1979	BC2	6,4	56	0	633	1140	0
	BC3	6,4	56	0	633	1140	0
Takaine et al., 2008	JH1	10,0	50	0	785	1134	0
Teng & Zhou, 2003	S1 (Series 1)	10,0	75	0	1178	628	0
	S2 (Series 1)	10,0	75	0	1178	628	0
	S3 (Series 1)	10,0	75	0	1178	628	0
	S5 (Series 2)	10,0	50	0	1414	628	0
	S6 (Series 2)	10,0	50	0	1414	628	0
Wang & Hsu, 2009	Ko-JI1	0,0	0	0	0	0	0
	Ho-JI1	0,0	0	0	0	981	0
Supuviriyakit & Pimanmas, 2007	Control	0,0	0	0	0	905	0
	Debond	0,0	0	0	0	905	0
Shiohara & Kusuhara, 2008	B01	6,0	60	0	226	0	0
	B02	6,0	60	0	226	0	0
	B03	6,0	60	0	226	0	0
	B04	6,0	60	0	226	0	0
	B05	6,0	60	0	226	531	0
	B06	6,0	60	0	226	1327	0
	B07	6,0	60	0	226	0	0
	B08	6,0	60	0	226	0	0
	B09	6,0	60	0	226	0	0
	B10	6,0	60	0	226	0	0
	C01	6,0	60	0	226	0	0
	C03	6,0	60	0	226	0	0
	D01	6,0	60	0	226	0	0
	D02	6,0	60	0	226	0	0
	D03	6,0	60	0	226	0	0
	D04	6,0	60	0	226	0	0
	D05	6,0	60	0	226	0	0
	D06	6,0	60	0	226	0	0
	D07	6,0	60	0	226	0	0
	D08	6,0	60	0	226	0	0

$d_{bw,j}$ = diameter of the horizontal stirrups;
$p_{w,j}$ = spacing of horizontal stirrups in the panel zone;
R = radius of curvature of beam bars bent in the joint;
$A_{sj,h}$ = horizontal reinforcement in the joint;
$A_{sj,v}$ = vertical reinforcement in the joint;
$A_{sj,incl}$ = area of inclined bars into the joint.

MECHANICAL PROPERTIES						
Authors	Name	Column	Beam		Joint	
		f'_c [MPa]	$f_{y,b}$ [MPa]	λ_0 [-]	$f_{y,j}$ [MPa]	f'_c [MPa]
Benevant et al., 2008	IL	24.9	404.0	1.25	404.0	24.9
	IU	24.9	404.0	1.25	404.0	24.9
Durrani & Wight, 1982	X1	34.3	330.7	1.67	503.0	34.3
	X2	33.6	330.7	1.67	503.0	33.6
	X3	31.0	330.7	1.67	503.0	31.0
	S1	41.5	346.2	1.57	503.0	41.5
	S2	30.7	346.2	1.57	503.0	30.7
	S3	28.2	344.5	1.58	503.0	28.2
Hakuto et al., 2000	O1	41.0	325.0	1.25	339.0	41.0
	O4	53.0	308.0	1.25	339.0	53.0
	O5	33.0	306.0	1.25	339.0	33.0
Hegger et al., 2003	RA1	53.1	530.0	1.25	530.0	53.1
	RA2	66.1	530.0	1.25	530.0	66.1
	RA3	43.6	530.0	1.25	530.0	43.6
	RA4	66.1	530.0	1.25	530.0	66.1
	RA5	56.2	530.0	1.25	530.0	56.2
	RA6	56.2	530.0	1.25	530.0	56.2
	RA7	79.7	530.0	1.25	530.0	79.7
Kitayama et al., 1991	J1	26.2	375.0	1.25	375.0	26.2
	C1	26.1	330.0	1.25	330.0	26.1
	B1/B2	25.0	498.0	1.25	240.0	25.0
	B3	25.0	498.0	1.25	240.0	25.0
Kusuhara et al., 2004	JE-0	24.0	387.0	1.40	364.0	24.0
	JE-55	24.0	387.0	1.40	364.0	24.0
	JE-55S	24.0	387.0	1.40	364.0	24.0
Kusuhara & Shiohara, 2008	A1	28.3	456.0	1.28	326.0	28.3
	A2	28.3	456.0	1.28	326.0	28.3
	A3	28.3	456.0	1.28	326.0	28.3
	C1	28.3	456.0	1.28	326.0	28.3
	D1	30.4	379.0	1.47	366.0	30.4
	D2	30.4	379.0	1.47	366.0	30.4
	B1	28.3	456.0	1.28	326.0	28.3
Lee et al., 2009	J1	40.0	509.9	1.25	510.4	40.0
	BJ1	40.0	509.9	1.25	510.4	40.0
	BJ2	40.0	509.9	1.25	510.4	40.0
	BJ3	40.0	509.9	1.25	510.4	40.0
	B1	40.0	509.9	1.25	510.4	40.0
Leon, 1990	BCJ2	27.6	498.1	1.25	498.1	27.6
	BCJ3	27.6	498.1	1.25	498.1	27.6
	BCJ4	27.6	498.1	1.25	498.1	27.6
Li et al., 2002	A1	32.3	503.0	1.25	499.0	32.3
	M1	32.0	503.0	1.25	499.0	32.0
	A2	32.5	477.2	1.32	499.0	32.5
	M2	30.3	477.2	1.32	499.0	30.3
Pampanin et al., 2002	C2	24.2	365.8	1.24	385.6	24.2
Pampanin et al., 2007	C4	23.9	365.8	1.24	385.6	23.9
Shannag & Alhassan, 2005	S1	27.0	310.0	1.25	310.0	27.0

MECHANICAL PROPERTIES						
Authors	Name	Column	Beam		Joint	
		f'_c [MPa]	$f_{y,b}$ [MPa]	λ_0 [-]	$f_{y,j}$ [MPa]	f'_c [MPa]
	S2	27.0	310.0	1.25	310.0	27.0
	S5	27.0	310.0	1.25	310.0	27.0
	S8	27.0	310.0	1.25	310.0	27.0
Shin & LaFave, 2004	1	32.9	500.0	1.32	450.0	29.9
	2	38.5	500.0	1.32	450.0	36.2
Shiohara et al., 2000	S3	23.2	470.0	1.40	390.0	23.2
Soleimani et al., 1979	BC2	26.8	465.3	1.43	445.1	26.8
	BC3	29.9	490.4	1.41	445.1	29.9
Takaine et al., 2008	JH1	78.3	738.7	1.25	888.0	78.3
Teng & Zhou, 2003	S1 (Series 1)	33.0	510.0	1.25	440.0	33.0
	S2 (Series 1)	34.0	510.0	1.25	440.0	34.0
	S3 (Series 1)	35.0	510.0	1.25	440.0	35.0
	S5 (Series 2)	39.0	425.0	1.25	440.0	39.0
	S6 (Series 2)	38.0	425.0	1.25	440.0	38.0
Wang & Hsu, 2009	Ko-JI1	32.0	533.0	1.33	533.0	32.0
	Ho-JI1	26.0	514.0	1.27	514.0	26.0
Supuviriyakit & Pimanmas, 2007	Control	19.5	488.6	1.30	312.0	19.5
	Debond	21.5	488.6	1.30	312.0	21.5
Shiohara & Kusuhara, 2008	B01	24.1	378.0	1.25	399.0	24.1
	B02	24.1	378.0	1.25	399.0	24.1
	B03	24.1	425.0	1.25	399.0	24.1
	B04	24.1	378.0	1.25	399.0	24.1
	B05	24.1	378.0	1.25	399.0	24.1
	B06	24.1	378.0	1.25	399.0	24.1
	B07	24.1	378.0	1.25	399.0	24.1
	B08	24.1	378.0	1.25	399.0	24.1
	B09	24.1	425.0	1.25	399.0	24.1
	B10	24.1	425.0	1.25	399.0	24.1
	C01	25.7	378.0	1.25	399.0	25.7
	C03	25.7	378.0	1.25	399.0	25.7
	D01	26.9	378.0	1.25	399.0	26.9
	D02	26.9	378.0	1.25	399.0	26.9
	D03	26.9	378.0	1.25	399.0	26.9
	D04	26.9	378.0	1.25	399.0	26.9
	D05	26.9	378.0	1.25	399.0	26.9
	D06	26.9	378.0	1.25	399.0	26.9
	D07	26.9	378.0	1.25	399.0	26.9
	D08	26.9	425.0	1.25	399.0	26.9

$f_{y,col}$ = strength of the steel in the column;
$f_{y,b}$ = strength of the steel in the beam;
λ_0 = overstrength of the steel in the beam;
$f_{y,j}$ = strength of the steel in the joint;
f'_c = strength of the concrete in the joint;

EXTERANAL LOAD							
Authors	Name	N_{col} [KN]	M	C		$V_{j,h}^{exp}$ [kN]	Classification
			F^{exp} [KN]	$F^{exp,U}$ [KN]	$F^{exp,max}$ [KN]		
Benevant et al., 2008	IL	296.00	-	17.00	72.00	932.15	Unreinforced
	IU	74.00	-	12.00	35.00	433.70	Unreinforced
Durrani & Wight, 1982	X1	244.75	-	142.40	186.90	1117.79	Reinforced
	X2	244.75	-	160.20	195.80	1167.34	Reinforced
	X3	214.49	-	133.50	164.65	949.77	Reinforced
	S1	311.50	-	209.15	244.75	1204.67	Reinforced
	S2	311.50	-	200.25	249.20	1200.22	Reinforced
	S3	240.30	-	182.45	198.03	962.50	Reinforced
Hakuto et al., 2000	O1	0.00	-	65.00	89.00	601.60	Unreinforced
	O4	0.00	-	70.00	175.00	1217.65	Unreinforced
	O5	0.00	-	57.00	160.00	1069.88	Unreinforced
Hegger et al., 2003	RA1	497.00	96.65	-	-	573.79	Unreinforced
	RA2	458.00	111.96	-	-	703.50	Reinforced
	RA3	502.00	91.04	-	-	538.92	Reinforced
	RA4	336.00	133.70	-	-	789.88	Reinforced
	RA5	499.00	94.43	-	-	598.41	Reinforced
	RA6	641.00	131.57	-	-	683.89	Reinforced
	RA7	457.00	143.75	-	-	850.07	Reinforced
Kitayama et al., 1991	J1	180.00	-	99.00	119.00	445.41	Reinforced
	C1	180.00	-	102.00	102.00	422.80	Reinforced
	B1/B2	180.00	-	112.00	130.00	677.38	Reinforced
	B3	180.00	-	105.00	120.00	625.15	Reinforced
Kusuhara et al., 2004	JE-0	0.00	-	55.00	93.90	737.41	Reinforced
	JE-55	0.00	-	47.00	88.90	581.48	Reinforced
	JE-55S	0.00	-	56.00	91.50	662.56	Reinforced
Kusuhara & Shiohara, 2008	A1	216.00	-	80.00	126.60	753.22	Reinforced
	A2	216.00	-	75.93	77.79	462.82	Reinforced
	A3	216.00	-	163.37	176.69	437.27	Reinforced
	C1	216.00	-	120.00	150.30	1085.70	Reinforced
	D1	216.00	-	95.00	133.90	768.50	Reinforced
	D2	216.00	-	100.00	140.20	887.97	Reinforced
	B1	216.00	-	89.32	96.92	586.79	Reinforced
Lee et al., 2009	J1	0.00	-	270.00	344.20	1372.59	Reinforced
	BJ1	0.00	-	142.00	293.30	1243.74	Reinforced
	BJ2	0.00	-	148.00	253.30	1027.57	Reinforced
	BJ3	0.00	-	145.00	215.60	809.10	Reinforced
	B1	0.00	-	65.00	171.10	597.42	Reinforced
Leon, 1990	BCJ2	0.00	-	-	46.73	360.38	Reinforced
	BCJ3	0.00	-	-	55.63	424.56	Reinforced
	BCJ4	0.00	-	-	68.98	423.70	Reinforced
Li et al., 2002	A1	0.00	-	-	162.40	601.43	Unreinforced
	M1	0.00	-	-	188.70	637.77	Reinforced
	A2	0.00	-	-	367.60	1444.56	Unreinforced
	M2	0.00	-	-	389.70	1513.16	Reinforced
Pampanin et al., 2002	C2	120.00	-	-	17.00	111.52	Unreinforced
Pampanin et al.,	C4	100.00	-	-	14.51	95.08	Unreinforced

EXTERANAL LOAD							
Authors	Name	N_{col} [KN]	M	C		$V_{j,h}^{exp}$ [kN]	Classification
			F^{exp} [KN]	$F^{exp,U}$ [KN]	$F^{exp,max}$ [KN]		
2007							
Shannag & Alhassan, 2005	S1	75.00	-	-	23.83	97.08	Reinforced
	S2	75.00	-	-	15.02	61.19	Unreinforced
	S5	120.00	-	-	16.50	67.22	Unreinforced
	S8	0.00	-	-	10.10	41.14	Unreinforced
Shin & LaFave, 2004	1	0.00	-	62.30	86.78	558.75	Reinforced
	2	0.00	-	55.63	83.22	586.09	Reinforced
Shiohara et al., 2000	S3	100.00	-	87.00	128.40	774.95	Reinforced
Soleimani et al., 1979	BC2	2002.50	-	-	164.65	702.32	Reinforced
	BC3	2002.50	-	71.20	204.70	856.71	Reinforced
Takaine et al., 2008	JH1	0.00	-	614.00	727.20	2241.78	Reinforced
Teng & Zhou, 2003	S1 (Series 1)	441.00	-	89.00	113.00	746.90	Reinforced
	S2 (Series 1)	441.00	-	88.00	112.20	743.99	Reinforced
	S3 (Series 1)	441.00	-	91.00	107.60	729.10	Reinforced
	S5 (Series 2)	343.00	-	68.00	69.90	413.04	Reinforced
	S6 (Series 2)	343.00	-	51.00	68.00	408.16	Reinforced
Wang & Hsu, 2009	Ko-JI1	403.20	-	70.00	134.00	639.73	Unreinforced
	Ho-JI1	0.00	-	105.00	148.00	930.85	Unreinforced
Supuviriyakit & Pimanmas, 2007	Control	300.00	-	44.00	72.00	426.89	Unreinforced
	Debond	300.00	-	67.00	62.00	349.33	Unreinforced
Shiohara & Kusuhara, 2008	B01	0.00	-	-	63.95	437.78	Reinforced
	B02	0.00	-	-	75.78	551.38	Reinforced
	B03	0.00	-	-	70.00	472.08	Reinforced
	B04	0.00	-	-	67.13	434.60	Reinforced
	B05	0.00	-	-	78.92	548.24	Reinforced
	B06	0.00	-	-	81.40	545.76	Reinforced
	B07	0.00	-	-	63.97	437.76	Reinforced
	B08	0.00	-	-	67.16	434.57	Reinforced
	B09	0.00	-	-	102.33	690.12	Reinforced
	B10	0.00	-	-	106.70	719.59	Reinforced
	C01	0.00	-	-	75.34	551.82	Reinforced
	C03	0.00	-	-	67.56	465.84	Reinforced
	D01	0.00	-	-	46.18	309.55	Reinforced
	D02	0.00	-	-	56.11	376.11	Reinforced
	D03	0.00	-	-	63.50	425.64	Reinforced
	D04	0.00	-	-	46.89	317.93	Reinforced
	D05	0.00	-	-	42.64	289.11	Reinforced
	D06	0.00	-	-	46.98	318.54	Reinforced
	D07	0.00	-	-	52.53	356.17	Reinforced
	D08	0.00	-	-	85.35	583.31	Reinforced

N_{col} = axial load of the top column;
M = monotonic load;
C = cyclic load;

EXTERANAL LOAD							
Authors	Name	N_{col} [KN]	M	C		$V_{j,h}^{exp}$ [kN]	Classification
			F^{exp} [KN]	$F^{exp,U}$ [KN]	$F^{exp,max}$ [KN]		

P^{exp} = maximum force applied at the top column in monotonic tests (subsection 2.3);
$P^{exp,U}$ = ultimate external force applied at the top column in cyclic tests;
$P^{exp,max}$ = maximum force applied at the top column in cyclic tests;
V_j^{exp} = experimental shear strength;
EC8-compliant = classification about the amount of horizontal stirrups in the panel zone.

References

ACI-ASCEE COMMITTEE 352, (1985), *"Recommendation for design of beam-column joints in monolithic reinforced concrete structures* (ACI 352-85)*"*, American Concrete Institute, Farmington Hills, MI.

ACI-ASCEE COMMITTEE 352, (2002), "Recommendation for design of beam-column joints in monolithic reinforced concrete structures (ACI 352R-02)", American Concrete Institute, Farmington Hills, MI.

ACI-ASCEE COMMITTEE 318, (2005), "Building code requirements for reinforced concrete (ACI 318-05) and commentary (ACI 318R-05)", American Concrete Institute, Farmington Hills, MI.

AIJ 1990, (1990), "Design guidelines for earthquake resistant reinforced concrete building based on ultimate strength concept and commentary (AIJ 1990)"

AIJ 1999, (1999), "Design guidelines for earthquake resistant reinforced concrete building based on ultimate strength concept and commentary (AIJ 1999)"

ADIN M.A., YANKELEVSKY D.Z. & FARHEY D.N., (1993), "Cyclic behaviour of epoxy-repaired reinforced concrete beam-column joints", ACI Structural Journal, V. 90, n. 2, p. 170-179, Mar-Apr 1993.

ALATH S. & KUNNATH S.K., (1995), "Modeling inelastic shear deformation in RC beam-column joints", Engineering Mechanics: Proceedings of 10th Conference, University of Colorado at Boulter, ASCE, V. 2, p. 822-825, 1995.

ALTOONTASH A. & DEIERLEIN G.G., (2003), "A versatile model for beam-column joints", ASCE Structures Congress Proceedings, Seattle, Washington, 2003.

ALVA G.M.S., (2004), (in Portuguese) "Estudo teorico-experimental do comportamento de nos de portico de concreto armado submetidos a acoes ciclicas", PhD thesis, Departamento de Engenharia de Estruturas, Sao Carlos, 2004

ALVA G.M.S., EL DEBS A.L.H. DE CRESCE & EL DEBS M.K., (2007), "An experimental study on cyclic behaviour of reinforced concrete connections", Can. J. Civ. Eng., V. 34, p. 565-575, May 2007.

AMANAT K.M. & ENAM B., (1999), "Study of the semi-rigid properties of reinforced concrete beam-column joints", Journal of Civil Engineering, The Institute of Engineers, Bangladesh, V. CE27, n. 1, p. 59-69, 1999.

ATTAALLA S.A., (2004), "General analytical model for nominal shear stress of type 2 normal- and high-strength concrete beam-to-column joints", ACI Structural Journal, V. 101, n.1, p. 65-75, Jan-Feb 2004.

AYCARDI L.E., MANDER J.B. & REINHORN A.M., (1994), "Seismic resistance of reinforced concrete frame structures designed only for gravity loads: experimental performance of subassemblages", V. 91, n. 5, p. 552-563, Sep-Oct 1994.

BAKIR P.G. & BODUROGLU H.M., (2002), "A new design equation for predicting the joint shear strength of monotonically loaded exterior beam-to-column joints", Engineering Structures, V. 24, p. 1105-1117, Mar 2002.

BAKIR P.G. & BODUROGLU H.M., (2005), "Nonlinear analysis of beam–column joints using softened truss model", Mechanics Research Communications, V. 33, p. 134–147, 2006, Available on line Oct 2005.

BENEVANT A.C., CAHIS X. & ZAHRAN R., (2008), "Seismic performance of old interior wide beam-column connections under seismic loading", The 14th WCEE, October 12-17, 2008, Beijing, China

BIDDHA A. & GHOBARAH A., (1999), "Modelling of shear deformation and bond slip in reinforced concrete joints", Structural Engineering and Mechanics, V. 7, n. 4, p. 413-432, 1999

BIDDHA A. & GHOBARAH A., (1999), "Dynamic analysis of reinforced concrete frames including joint shear deformation", Engineering Structures, V. 21, p. 971–987, 1999.

BINDHU K.R. & JAYA K.P., (2008), "Performance of exterior beam column joints with cross-inclined bars under seismic type loading", Journal of Engineering and Applied Sciences, V. 7, p. 591-597, 2008.

BOUSRI Y. & SMITH J.W., (1995), "The use of double U-bar stirrups in seismically loaded reinforced concrete beam-column joints", V. 7, n. 2, p. 131-143, Mar 1995.

BRAGA F., DE CARLO G., CORRADO G.F., GIGLIOTTI R., LATERZA M. & NIGRO D., (2001), "Meccanismi di risposta di nodi trave-pilastro in c.a. di strutture non antisismiche", X Congresso Nazionale L'ingegneria Sismica in Italia, Potenza-Matera 9-13 Settembre 2001, Italy, 2001.

BURSI O.S., DUSATTI T. & PUCINOTTI R., (2009), "A reconnaissance report. The April 6, 2009, L'Aquila Earthquake, Italy", http://www.reluis.it.

CALVI G.M., MAGENES G. & PAMPANIN S., (2001), (in Italian), "Studio sperimentale sulla risposta sismica di edifici a telaio in cemento armato progettati per soli carichi da gravità", X Congresso Nazionale 'L'ingegneria sismica in Italia', Potenza-Matera 9-13 Settembre 2001, Italy, 2001.

CALVI G.M., MAGENES G. & PAMPANIN S., (2002), "Experimental test on a three storey rc frame designed for gravity only", 12th European Conference on Earthquake Engineering, paper 727, 2002.

CASTRO J.M., ELGHAZOULI A.Y. & IZZUDDIN B.A., (2005), "Modelling of the panel zone in steel and composite moment frames", Engineering Structures, V. 27, p. 129-144, 2005.

CEB-FIP, (1990), "Model code for concrete structures, CEB-FIP International Recommendations", 1990.

CELIK O.C. & ELLINGWOOD B.R., (2008), "Modelling beam-column joints in fragility assessment of gravity load designed reinforced concrete frame", Journal of Earthquake Engineering, V. 12, n. 3, p. 357-381, 2008.

CHALIORIS C.E., FAVVATA M.J. & KARAYANNIS C.G., (2008), "Reinforced concrete beam-column joints with crossed-inclined bars under cyclic deformations", Earthquake Engineering and Structural Dynamics, V. 37, p. 881-897, Feb. 2008.

CHOPRA A.K., (1995), "Dynamics of structures", 1st Edition, Prentice Hall, 1995.

CHUN S.C. & KIM D.Y., (2004), "Evaluation of mechanical anchorage of reinforcement by exterior beam-column joint experiments", 13th World Conference on Earthquake Engineering, Paper n. 0326, Vancouver, B.C., Canada, Aug. 1-6, 2004.

CHUN S.C., LEE S.H., KANG T.H.-K., OH B. & WALLACE J.W., (2007), "Mechanical anchorage in exterior beam-column joints subjected to cyclic loading", ACI Structural Journal, V. 104, n. 1, p. 102-112, Jan-Feb 2007.

CHUNG Y.S., MEYER C. & SHINOZUKA M., (1987), "Seismic damage assessment of reinforced concrete members", Report No. NCEER-88-0022, National Center for Earthquake Engineering Research, State University of New York at Buffalo, NY 1987.

CHUTARAT N. & ABOUTAHA R.S., (2003), "Cyclic response of exterior reinforced concrete beam-column joints reinforced with headed bars – experimental investigation", ACI Structural Journal, V. 100, n. 2, p. 259-264, Mar-Apr 2003.

CIMELLARO G.P., (2009), "Field reconnaissance following the April 6, 2009 L'Aquila Earthquake in Italy", Lecture in Room 140, Ketter Hall, North Campus, Buffalo NY, Jun 2009.

CLOUGH R.W. & PENZIEN J., (1995), "Dynamics of structures", Computer & Structures Inc., University Ave., Berkeley CA, USA, 1995.

CLYDE C., PANTELIDES C.P. & REAVELEY L.D., (2000), "Performance-based evaluation of exterior reinforced concrete building joints for seismic excitation", PEER - Pacific Earthquake Engineering Research Center, Report 2000/05, University of California, Berkeley, Jul 2000.

COLLINS M.P., (1978), "Toward a rational theory of reinforced concrete members in shear", ASCE Journal of the Structural Division, V. 104, p. 649-666.

CORNELL C.A., JALAYER F., HAMBURGER R.O. & FOUTCH D.A., (2002), "The probabilistic basis for the 2000 SAC/FEMA steel moment frame guidelines", Journal of Structural Engineering, V. 128, n. 4, p. 526-533, Apr. 2002.

CSA A23.3-94, (1994), "Design of concrete structures", Canadian Standard Associations, Rexdale, Ontario, Canada, 1994.

DECRETO MINISTERIALE 14 GENNAIO 2008, NTC 2008, (2008), "Norme tecniche per le costruzioni (NTC 2008)", G.U. n.29 del 4 febbraio 2008.

DEIERLEIN G., ELWOOD K., LEHMAN D. & WALLACE J., (2006), "Evaluation of Existing Reinforced Concrete Buildings", 8NCEE - Tutorial, April 21, 2006.

DOWEL R.K., SEIBLE F. & WILSON E.L., (1998), "Pivot hysteresis model for reinforced concrete members", ACI Structural Journal, V. 95, n. S55, p. 607-617, 1998.

DURRANI A.J. & WIGHT J.K., (1982), "Experimental and analytical study of internal beam-to-column connections subjected to reversed cyclic loading", Report UMEE 82R3, Department of Civil Engineering, University of Michigan, July 1982.

DURRANI A.J. & ZERBE H.E., (1987), "Seismic resistance of RC exterior connections with floor slab", Journal of Structural Engineering, V. 113, n. 8, p. 1850-1864, Aug 1987.

ECONOMOU C.M., PRINOU C., CHALIORIS C.E. & KARAYANNIS, C.G., (1998), "Capacity decrease of RC joints due to seismic actions in the curing period", 11th European Conference on Earthquake Engineering, ISBN 90 5410 982 3, 1998.

EHSANI M.R. & ALAMEDDINE F., (1991), "Design recommendations for type 2 high-strength reinforced concrete connections", ACI Structural Journal, V. 88, n. 3, p. 227-291, May-Jun 1991.

EHSANI M.R., MOUSSA A.E. & VALLENILLA C.R., (1987), "Comparison of inelastic behavior of reinforced ordinary- and high-strength concrete frames", ACI Structural Journal, V. 84, s17, p. 161-169, Mar-Apr 1987.

EHSANI M.R. & WIGHT J.K., (1985 [a]), "Effect of transverse beam and slab on behavior of reinforced concrete beam-to-column connections", ACI Structural Journal, V. 82, n. 17, p. 188-195, Mar-Apr 1985.

EHSANI M.R. & WIGHT J.K., (1985 [b]), "Exterior reinforced concrete beam-to-column connections subjected to earthquake type loading", ACI Structural Journal, V. 82, n. 43, p. 492-499, Jul-Aug 1985.

EUROCODE 2, (2004), "Design of concrete structures. Part. 1-1: General rules and rules for buildings", prEN 1992.

EUROCODE 8, (1995), "Design of structures for earthquake resistance - part I: general rules, seismic actions and rules for building", prEN 1995.

EUROCODE 8, (2005), "Design of structures for earthquake resistance - part I: general rules, seismic actions and rules for building", prEN 1998.

EUROCODE 0, (2006), "Basis of structural design", prEN 1990.

EVERITT B.S., (2002), "Cambridge Dictionary of Statistics (2nd Edition)", CUP, ISBN 0-521-81099-X, 2002.

FAELLA C., LIMA C. & MARTINELLI E., (2009), "DEFINIZIONE E VALUTAZIONE PARAMETRICA DI MISURE DI VULNERABILITÀ SISMICA PER EDIFICI ESISTENTI IN CEMENTO ARMATO", XIII CONVEGNO ANIDIS, PAPER S14.14, 2009.

FAELLA C., LIMA C., MARTINELLI E. & NIGRO E., (2008), "Comparative application of capacity models for seismic vulnerability evaluation of existing rc structures", Seismic Engineering International Conference, Messina and Reggio Calabria (Italy) 8-11 July 2008, pp. 1187-1194 – ISBN: 978-0-7354-0542-4

FAELLA C., LIMA C., MARTINELLI E. & NIGRO E., (2008), "Applicazione comparata di diversi metodi di analisi non-lineare di strutture esistenti in c.a.", Valutazione e riduzione della vulnerabilità sismica di edifici in c.a., Roma (Italy) 29-30 May 2008, pp. 336-343 – ISBN: 978-88-7699-129-5.

FAJFAR P., (1999), "Capacity spectrum method based on inelastic demand spectra", Earthquake Engineering and Structural Dynamics, V. 28, n. 9, p. 979-993, 1999.

FAVVATA M.J., IZZUDDIN B.A. & KARAYANNIS C.G., (2008), "Modelling exterior beam–column joints for seismic analysis of RC frame structures", Earthquake Engineering and Structural Dynamics, V. 37, p. 1527-1548, 2008

FEDERAL EMERGENCY MANAGEMENT AGENCY, (1997), "NEHRP Guidelines for the seismic rehabilitation of building (FEMA 273)", Reston, VA.

FEDERAL EMERGENCY MANAGEMENT AGENCY, (1997), "NEHRP Commentary on the guidelines for the seismic rehabilitation of building (FEMA 274)", Reston, VA.

FEDERAL EMERGENCY MANAGEMENT AGENCY, (2000), "Prestandard and commentary for the seismic rehabilitation of buildings (FEMA 356)", Reston, VA.

FILIPPOU F.C., D'AMBRISI A. & ISSA A., (1999), "Effects of reinforcement slip on hysteretic behavior of reinforced concrete frame members", ACI Structural Journal, V. 96, n. 3, p. 327-335, 1999.

FUJII S. & MORITA H., (1991), "Comparison between interior and exterior RC beam-column joint behavior", Design of Beam-Column Joints for Seismic Resistance (SP-123), American Concrete Institute, Detroit, Michigan, p. 145-165, 1991.

GENESAN N., INDIRA P.V. & ABRAHAM R., (2007), "Steel fibre reinforced high performance concrete beam-column joints subjected to cyclic loading", ISET Journal of Earthquake Technology, V. 44, n. 3-4, p. 445-456, Sept-Dec 2007.

GENCOGLU M. & EREN I., (2002), "An experimental study on the effect of steel fiber reinforced concrete on the behavior of the exterior beam-column joints subjected to reversal cyclic loading", Turkish J. Eng. Env. Sci., V. 26, p. 493-502, Feb 2002.

HAKUTO S., PARK R. & TANAKA H., (2000), "Seismic load tests on interior and exterior beam-column joints with substandard reinforcing details", ACI Structural Journal, V. 97, n. 1, p. 11-25, Jan-Feb 2000.

HAMIL S.J., (2000), "Reinforced concrete beam-column connection behaviour", PhD Thesis, University of Durham, United Kingdom, 2000.

HANSON W. & CONNOR H.W., (1967), "Seismic resistance of reinforced concrete beam-column joints", Journal of the Structural Division, Oct 1967.

HEGGER J., SHERIF A. & ROESER W., (2003), "Nonseismic design of beam-column joints", ACI Structural Journal, V. 100, n.5, p. 654-664, Sep-Oct 2003.

HERTANTO E., (2005), "Seismic assessment of pre-1970s reinforced concrete structures", MSCE thesis, University of Canterbury, 2005.

HSU T.T.C., (1988), "Softened truss model theory for shear and torsion", ACI Structural Journal, V. 85, n. 6, p. 624-634, Nov-Dec 1988.

HWANG S.J. & LEE H.J., (1999), "Analytical model for predicting shear strength of exterior reinforced concrete beam-column joints for seismic resistance", ACI Structural Journal, V. 96, n.5, Sep-Oct 1999.

HWANG S.J. & LEE H.J., (2000), "Analytical model for predicting shear strength of interior reinforced concrete beam-column joints for seismic resistance", ACI Structural Journal, V. 97, n.1, Jan-Feb 2000.

HWANG S.J. & LEE H.J., (2002), "Strength prediction for discontinuity regions by softened strut-and-tie model", Journal of Structural Engineer, V. 128, n.12, Dec 2002.

HWANG S.J., LEE H.J. & WANG K.C., (2004), "Seismic design and detailing of exterior reinforced concrete beam-column joints", 13th World Conference on Earthquake Engineering, Paper n. 0397, Vancouver, B.C., Canada, Aug. 1-6, 2004

HWANG S.J., LEE H.J, LIAO T.F., WANG K.C. & TSAI H.H., (2005), "Role of hops on shear strength of reinforced concrete beam-column joints", ACI Structural Journal, V. 102, n. 3, p. 445-453, May-Jun 2005.

IDAYANI B.S., (2007), "The influence of concrete strength on the behaviour of external beam-column joints", Degree Master of Engineering, University of Malaysia, May 2007.

IZZUDDIN B.A., (1991), "Nonlinear Dynamic Analysis of Framed Structures", Department of Civil Engineering, Imperial College, University of London, 1991.

KARAYANNIS C.G., CHALIORIS C.E. & SIRKELIS G.M., (2008), "Local retrofit of exterior RC beam-column joints using thin RC jackets – An experimental study", Earthquake Engineering and Structural Dynamics, V. 37, p. 727-746, 2008.

KARAYANNIS C.G. & SIRKELIS G.M., (2005), "Response of column and joints with spiral shear reinforcement", CMEM Conference on Computational Methods and Experimental Measurements, Malta, 2005.

KARAYANNIS C.G. & SIRKELIS G.M., (2008), "Strengthening and rehabilitation of RC beam-column joints using carbon-FRP jacketing and epoxy resin injection", Earthquake Engineering and Structural Dynamics, V. 37, p. 769-790, 2008

KIM J., LAFAVE J.M. & SONG J., (2007), "A new statistical approach for joint shear strength determination of RC beam-column connections subjected to lateral earthquake loading", Structural Engineering and Mechanics, V. 27, n.4, p. 439-456, 2007.

KIM J. & LAFAVE J.M., (2007), "Key influence parameters for the joint shear behaviour of reinforced concrete (RC) beam-column connections", Engineering Structures, V. 29, p. 2523-2539, 2007.

KIM J. & LAFAVE J.M., (2009), "Joint shear behaviour of reinforced concrete beam-column connections subjected to seismic lateral loading", Newmark Structural Engineering Laboratory - NSEL Report Series, NSEL-020, 2009.

KIM J., LAFAVE J.M. & SONG J., (2009), "Joint shear behaviour of reinforced concrete beam-column connections", Magazine of Concrete Research, V. 61, n.2, p. 119-132, Mar 2009.

KITAYAMA K., OTANI S. & AOYAMA H., (1991), "Development of design criteria for rc interior beam-column joints", America Concrete Institute, p. 97-123, James O. Jirsa Editor, Michigan, 1991.

KRAWINKLER H. & NASSER A.A., (1992), "Seismic Design Based on Ductility and Cumulative Damage Demands and Capacities", in Nonlinear Seismic Analysis and Design of Reinforced Concrete Buildings, Elsevier Science Publishers Ltd., New York, N.Y., p. 23-40, 1992.

KUANG J.S. & WONG H.F., (2006), "Effects of beam bar anchorage on beam-column joint behaviour", Proceedings of the Institution of Civil Engineering, Structures and Building 159, Paper 14045, p. 115-124, Apr. 2006.

KUSUHARA F., AZUWARA K., SHIOHARA H. & OTANI S., (2004), "Tests of reinforced concrete interior beam-column joint subassemblage with eccentric beams", 13th WCEE, August 1-6, 2004, Vancouver, Canada

KUSUHARA F. & SHIOHARA H., (2008), "Tests of R/C beam-column joints with variant boundary conditions and irregular details on anchorage of beam bars", The 14th World Conference on Earthquake Engineering, Beijing, China, Oct 12-17, 2008.

LEE H.J. & KO J.W., (2007), "Eccentric reinforced concrete beam-column connections subjected to cyclic loading in Principal directions", ACI Structural Journal, V. 104, n. 4, Jul-Aug 2007.

LEE J.Y., KIM J.Y. & OH G.J., (2009), "Strength deterioration of reinforced concrete beam-column joints subjected to cyclic loading, Engineering Structures, doi:10.1016, 2009

LEON R.T., (1990), "Shear strength and hysteretic behaviour of interior beam-column joints", ACI Structural Journal, V. 87, n. 1, pp. 3-11, Jan-Feb 1990

LI B., WU Y. & PAN T.C., (2002), "Seismic behavior of nonseismically detailed interior beam-wide column joints – Part 1: experimental results and observed behavior", ACI Structural Journal, V. 99, n. 6, pp. 791-802, Nov-Dec 2002

LIMA C., MARTINELLI E., MACORINI L. & IZZUDDIN B.A., (2010), "Seismic performance of existing rc frames: influence of beam-to-column joint modelling", 14th European Conference on Earthquake Engineering, 30 Aug - 3 Sep, 2010, Ohrid, Macedonia – ISBN: 978-608-65185-1-6.

LIMA C., FAELLA C. & MARTINELLI E., (2010), "Validation of capacity models for monotonic and cyclic behaviour of rc beam-to-column joints", 14th European Conference on Earthquake Engineering, 30 Aug - 3 Sep, 2010, Ohrid, Macedonia - ISBN: 978-608-65185-1-6.

LIMA C., MARTINELLI E., MACORINI L. & IZZUDDIN B.A., (2010), "Comportamento non lineare di nodi esterni trave-colonna in c.a.: modelli locali di capacità ed influenza sulla risposta sismica globale", 18° Congresso CTE, 11 - 13 Nov 2010, pp. 693-702 - ISBN: 978-88-903647-6-1.

LIMA C., MARTINELLI E. & FAELLA C., (2010), "Validazione sperimentale di modelli di capacità per nodi interni trave-colonna di strutture in cemento armato", 18° Congresso CTE, 11 - 13 Nov 2010, pp. 173-182 - ISBN: 978-88-903647-6-1.

LIU C., (2006), "Seismic behaviour of beam-column joint subassemblies reinforced with steel fibres", Thesis for the Degree of Master of Engineering, University of Canterbury, New Zealand, 2006.

LOWES L.N. & ALTOONTASH A., (2003), "Modelling reinforced-concrete beam-column joints subjected to cyclic loading", ASCE Journal of Structural Engineering, V. 129, n. 12, p. 1686-1697, Dec 2003.

MANDER J.B., PRIESTLEY M.J.N. & PARK R., (1988), "Theoretical stress-strain model for confined concrete", ASCE Journal of Structural Engineering, V. 114, n. 8, p. 1804-1826, Aug 1988.

MASI A., SANTARSIERO G., MORONI C. & NIGRO D., (2009), (in Italian), "Meccanismi di collasso di nodi esterni trave-colonna in c.a. sottoposti a test ciclici", Anidis Convegno L'ingegneria Sismica in Italia, Bologna, 2009.

MINER M.A., (1945) "Cumulative damage in fatigue", Journal of Applied Mechanics, 1945, Vol. 67, pag. 159-164.

MITRA N. & LOWES L.N., (2007), "Evaluation, calibration and verification of a reinforced concrete beam-column joint model", ASCE Journal of Structural Engineering, V. 133, n. 1, p. 105-120, Jan 2007.

MONTI G., ALESSANDRI S. & SANTINI S., (2009), "Design by testing: a procedure for the statistical determination of capacity models", Construction and Building Materials, V. 23, p. 1487-1494, 2009.

MORITA S. & KAKU T. (1984), "Slippage of reinforcement in beam-column joint of reinforced concrete frame", Eighth World Conf. on Earthquake Engineering, San Francisco, CA, p. 477-484, 1984.

NEWMARK N. M. & HALL W.J., (1982), "Earthquake Spectra and Design", Engineering Monographs on Earthquake Criteria, Structural Design, and Strong Motion Records, V. 3, Earthquake Engineering Research Institute, Oakland, CA, 1982.

NZS 3101, (1995), "Concrete structures standard – part. 1", Standard Associations of New Zealand, Willington, New Zealand.

ORDINANZA DEL PRESIDENTE DEL CONSIGLIO DEI MINISTRI N.3431, (2005), "Ulteriori modifiche ed integrazioni all'O.P.C.M. 20 marzo del 2003, recante 'Primi elementi in materia di criteri generali per la classificazione sismica del territorio nazionale e di normative tecniche per le costruzioni in zona sismica' (O.P.C.M. 3431/05)".

ORTIZ (REYES DE) I., (1993), "Strut and tie modelling of reinforced concrete short beams and beam-column joints", PhD Thesis, University of Westminster, 1993.

PALMGREN A., (1924), "Die Lebensdauer von Kugellagern", Verfahrenstechnik, Berlin, 1924, Vol. 68, p. 339-341.

PAMPANIN S., CALVI G.M. & MORATTI M., (2002), "Seismic behaviour of RC beam-column joints designed for gravity loads", 12th European Conference on Earthquake Engineering, Paper 726, London, 2002.

PAMPANIN S., MAGENES G & CARR A., (2003), "Modeling of shear hinge mechanism in poorly detailed RC beam column joints", FIB Symposium, Concrete Structures in Seismic Regions, Athens, 2003.

PAMPANIN S., BOLOGNINI D. & PAVESE A., (2007), "Performance-based seismic retrofit strategy for existing reinforced concrete frame systems using fiber-reinforced polymer composites", Journal of Composites for Structures, V. 11, n. 2, pp. 1-16, Apr 2007

PANTAZOPOULO S. & BONACCI J., (1992), "Considerations of questions about beam-column joints", ACI Structural Journal, V. 89, n.1, p. 27-36, Jan-Feb 1992.

PANTELIDES C.P., HANSEN J., NADAULT J. & REAVELEY L.D., (2002), "Assessment of reinforced concrete building exterior joints with substandard details", PEER - Pacific Earthquake Engineering Research Center, Report 2002/18, University of California, Berkeley, May 2002.

PARK Y. J. & ANG A. H. S., (1985), ''Mechanistic seismic damage model for reinforced concrete", Journal of Structural Engineering, V. 111,n. 4, p. 722–739, 1985.

PARK Y. J., REINHORN A. M. & KUNNATH S. K., (1987), "IDARC: Inelastic Damage Analysis of Reinforced Concrete Frame—Shear-Wall Structures", Technical Report NCEER-87-0008, State University of New York at Buffalo, 1987.

PARK S. & MOSALAM K.M., (2009), "Shear strength models of exterior beam-column joints without transverse reinforcement", Pacific Earthquake Engineering Research Center, PEER 2009/106 report, University of California, Berkeley, Nov 2009.

PARKER D.E. & BULLMAN P.J.M., (1995), "Shear strength of reinforced concrete-the influence of shear span", The Structural Engineer, V. 73, n.23-24, p. 413-, Dec 1995.

PARKER D.E. & BULLMAN P.J.M., (1997), "Shear strength within reinforced concrete beam-column joints", The Structural Engineer, V. 75, n.4, p. 53-57, Feb 1997.

PARRA-MONTESINOS G.J. & WIGHT J.K., (2002), "Prediction of strength and shear distortion in R/C beam-column joints. In behaviour and design of concrete structures for seismic performance", American Concrete Institute, sp. 197, p. 191-214, Detroit, Michigan, 2002.

PAULAY T., PARK R. & PRIESTLEY M. J. N., (1978), "Reinforced concrete beam-column joints under seismic actions", ACI Journal, V. 75, n. 11, p. 585–593, 1978.

PAULAY T, (1989), "Equilibrium criteria for reinforced concrete beam-column joints", ACI Structural Journal, V. 86, n. 6, p. 635-643, Nov-Dec 1989.

PAULAY T. & PRIESTLEY M.J.N., (1992), "Seismic design of reinforced concrete and masonry building", John Wiley & Sons, inc., New York, 1992.

PINTO P.E., GIANNINI R. & FRANCHIN P., (2004), "Seismic reliability analysis of structures", IUSS Press, Pavia, 2004.

REGIO DECRETO 16/11/1939 N.2229, "Norme per la esecuzione delle opere in conglomerato cementizio semplice ed armato", 1939.

RUSSO G. & SOMMA G., (2006), "Shear strength of exterior beam-column joints under seismic loading", Fib – Federation Internationale du Beton, Proceedings of the 2nd International Congress, Naples, Italy, 5-8 Jun 2006.

SANTARELLA L., (1963), "Prontuario del Cemento Armato", XXV Edizione U. Hoepli – Milano, 1963.

SARSAM K.F. & PHILLIPS M.E., (1985), "The shear design of in-situ reinforced beam-column joints subjected to monotonic loading", Magazine of Concrete Research, V. 37, n.130, p. 16-28, Mar 1985.

SCOTT R.H., FELTHAM I. & WHITTLE R.T., (1994), "Reinforced beam-column connections and BS 8110", The Structural Engineer, V. 72, n.4, p. 55-60, Feb 1994.

SCOTT R.H., (1996), "Intrinsic mechanisms in reinforced concrete beam-column connection behavior", ACI Structural Journal, V. 93, n. 3, p. 1-11, May-Jun 1996.

SEISMOSTRUCT, "SEISMOSOFT, Earthquake Engineering Software Solutions", www.seismosoft.com.

SHANNAG M.J. & ALHASSAN M.A., (2005), "Seismic upgrade of interior beam-column subassemblages with high-performance fiber-reinforced concrete jackets", ACI Structural Journal, V. 102, n. 1, pp. 131-138, Jan-Feb 2005

SHIN M. & LAFAVE J.M., (2004), "Seismic performance of reinforced concrete eccentric beam-column connections with floor slabs", ACI Structural Journal, V. 101, n. 3, pp. 403-412, May-June 2004

SHIOHARA H., ZAID S. & OTANI S., (2000), "Test of an innovative reinforcing detail for high-performance RC interior beam-column connections subjected to seismic action", Report of University of Tokio, Japan

SHIOHARA H. & KUSUHARA F., (2008), "Comprehensive series of tests on seismic performance of reinforced concrete beam column joints", Report of University of Tokio, Japan.

SIVASELVAN M.V. & REINHORN A.M., (2000), "Hysteretic models for deteriorating inelastic structures", Journal of Engineering Mechanics, V. 126, n. 6, p. 633-640, Jun 2000.

SOLEIMANI D., POPOV E.P. & BERTERO V.V., (1979), "Hysteretic behavior of reinforced concrete beam-column subassemblages", ACI Journal, n. 76-48, pp. 1179-1195, Nov 1979

STEVENS N. J., UZUMERI S. M. & COLLINS M. P., (1991), "Reinforced concrete subjected to reversed-cyclic shear—Experiments and constitutive model", ACI Structural Journal, V. 88, n. 2, p. 135–146, 1991.

SUPUVIRIYAKIT T. & PIMANMAS A., (2007), "Comparative performance of a substandard beam-column joint with and without initial bond between beam bars and concrete in the joint core", Thammasat Int. J. Sc. Tech., V. 12, n. 1, Jan-Mar 2007

TAKAINE Y., NAGAI S. & MARUTA M., (2008), "Structural performance of RC beams and beam-column subassemblages using reinforcement with sleeve joints at the end of beams", The 14th WCEE, 12-17 October 2008, Beijing, China

TAKEDA T., SOZEN M.A. & NIELSEN N.N., (1970), "Reinforced concrete response to simulated earthquakes", Journal of Structural Engineering Division, ASCE, v.96, n.12, p. 2557–2573, 1970.

TENG S. & ZHOU H., (2003), "Eccentric reinforced concrete beam-column joints subjected to cyclic loading", ACI Structural Journal, V. 100, n. 2, pp. 139-148, Mar-Apr 2003

TERAOKA M. & FUJII S., (2000), "Seismic damage and performance evaluation of R/C beam-column joints", The Second U.S.-Japan Workshop on Performance-Based Engineering for Reinforced Concrete Building Structures, Hokkaido, Japan, p. 379-390, 2000.

THEISS A.G., (2005), "Modeling the earthquake response of older reinforced concrete beam-column buildings joints", MSCE thesis, University of Washington, 2005.

TROWLAND M., (2003), "Modelling the Shear Hinge in Beam Column Joints". Third Professional Year Project, Department of Civil Engineering, University of Canterbury, New Zealand, 2003.

TSONOS A.G., TEGOS I.A. & PENELIS G.G., (1992), "Seismic resistance of type 2 exterior beam-column joints reinforced with inclined bars", ACI Structural Journal, V. 89, n. 1, Jan-Feb 1992.

TSONOS A.G., (1999), "Lateral load response of strengthened reinforced concrete beam-to-column joints", ACI Structural Journal, V. 96, n. 1, p. 46-56, Jan-Feb 1999.

TSONOS A.G., (2007), "Cyclic load behaviour of reinforced concrete beam-column subassemblages of modern structures", ACI Structural Journal, V. 104, n. 4, Jul-Aug 2007.

VECCHIO F.J. & COLLINS M.P., (1986), "The modified compression-field theory of reinforced concrete elements subjected to shear", ACI Structural Journal, V. 83, n. 2, p. 219-231, Mar-Apr 1986.

VECCHIO F.J. & COLLINS M.P., (1988), "Predicting the response of reinforced concrete beams subjected to shear using modified compression field theory", ACI Structural Journal, V. 85, n. 3, p. 258-268, 1988.

VOLLUM R.L., (1998), "Design and analysis of reinforced concrete beam-column joints", PhD Thesis, Concrete Structures Section, Department of Civil Engineering, Imperial College London, 1998.

VOLLUM R.L. & NEWMAN J.B., (1999), "The design of external, reinforced concrete beam-column joints", The Structural Engineer, V. 77, n.23-24, p. 21-27, Dec 1999.

VOLLUM R. & PARKER D., (2008), "External beam-column joints: design to Eurocode 2", Magazine of Concrete Research, V. 60, n.7, p. 511-521, Sep 2008.

WALLACE J.W., MCCONNEL S.W., GUPTA P. & COTE P.A., (1998), "Use of headed reinforcement in beam-column joints subjected to earthquake loads", ACI Structural Journal, V. 95, n. 5, p. 590-606, Sept-Oct 1998.

WANG Y.C. & HSU K., (2009), "Shear strength of RC jacketed interior beam-column joints without horizontal shear reinforcement", ACI Structural Journal, V. 106, n. 2, pp. 222-232, Mar-Apr 2009

WONG H.F. & KUANG J.S., (2008), "Effects of beam-column depth ratio on joint seismic behaviour", Proceedings of the Institution of Civil Engineers, Structures and Buildings 161, Paper 700010, p. 91-101, Apr 2008.

YOUSSEF M. & GHOBARAH A., (1999), "Strength deterioration due to bon slip and concrete crushing in modelling of RC members", ACI Structural Journal, V. 96, n. 6, p. 956-966, 1999.

YOUSSEF M. & GHOBARAH A., (2001), "Modelling of RC beam-column joints and structural walls", Journal of Earthquake Engineering, V. 5, n. 1, p. 93-111, 2001.

ZHANG L. & JIRSA J.O., (1982), "A study of shear behaviour of rc beam-column joints", PMFSEL Report No. 82-1, University of Texas at Austin, Feb 1982.

ZHANG L. & HSU T.C., (1998), "Behavior and analysis of 100 MPa concrete membrane elements", Journal of Structural Engineering, ASCE, V. 124, n.1, p. 24-34, Jan 1998.

List of Figures

Fig. 1.1: Joint failure and wrong detail of stirrup (Bursi et al., 2009). 4

Fig. 1.2: Soft story mechanisms due to the earthquake of L'Aquila (Bursi et al., 2009). 5

Fig. 1.3: Joint failures due to the earthquake of L'Aquila (Bursi et al., 2009). 5

Fig. 1.4: Shear failure of squat column due to seismic events (Cimellaro, 2009). 6

Fig. 1.5: Modes of collapse of RC frame structures. 7

Fig. 1.6: Comparison between old and compliant with recent seismic codes joint details (Deierlin et al., 2006)....8

Fig. 1.7: Comparison between old and compliant with recent seismic codes joint details (Deierlin et al., 2006)....9

Fig. 1.8: Beam-to-column connections in RC structures (Kim et al., 2009). 10

Fig. 1.9: Exterior beam-to-column joints (Paulay & Priestley, 1992). 11

Fig. 1.10: Interior beam-to-column joints (Paulay & Priestley, 1992)..... 11

Fig. 1.11: Features of column and joint behaviour (Paulay & Priestley, 1992). 12

Fig. 1.12: Equilibrium for interior (a) and exterior (b) joints..... 13

Fig. 2.1: Joint geometry (Pantazopoulo & Bonacci, 1992). 26

Fig. 2.2: Stress equilibrium: (a) in vertical direction, (b) in horizontal direction (Pantazopoulo & Bonacci, 1992). 27

Fig. 2.3: Evaluating the shear strength according to Pantazopoulo & Bonacci (1992)..... 30

Fig. 2.4: Paulay and Priestley mechanisms of shear transfer at an interior joint: concrete strut (a) and diagonal compression field (b). (Paulay & Priestley, 1992) 31

Fig. 2.5: External actions and internal stress resultants at an interior joint (Paulay & Priestley, 1992). 32

Fig. 2.6: Mechanism for exterior joint (Paulay & Priestley, 1992) 34

Fig. 2.7: Evaluating the shear strength according to Paulay & Priestley (1992)..... 36

Fig. 2.8: Evaluating the shear strength according to Parker & Bullman (1997). 38

Fig. 2.9: Hwang & Lee's strut-and-tie modelling of interior joint (Hwang & Lee, 2002). 39

Fig. 2.10: Evaluating the shear strength according to Hwang & Lee (2002) 43

Fig. 2.11: Evaluating shear strength according to Parra-Montesinos & Wight (2002) 47

Fig. 2.12: Evaluating shear strength according to Hegger et al. (2003) 49

Fig. 2.13: Evaluating shear strength according Attaalla (2004). 52

Fig. 2.14: Evaluating shear strength according to Kim et al. (2009). 55

Fig. 2.15: Determination of areas of horizontal and vertical ties. 57

Fig. 2.16: Evaluating shear strength according to Hwang & Lee (2000). 59

Fig. 2.17: Algorithm for post-yielding cases according to Hwang & Lee (2000). 60

Fig. 2.18: Evaluating shear strength according to Zhang & Jirsa (1982). 62

Fig. 2.19: Definition of the Ortiz (1993) strut-and-tie model. 64

Fig. 2.20: Evaluating shear strength according to Ortiz (1993). 66

Fig. 2.21: Evaluating shear strength according to Vollum & Newman (1999). 68

Fig. 2.22: Joint shear resisting mechanisms: (a) diagonal mechanism, (b) horizontal mechanism and (c) vertical mechanism (Hwang & Lee, 1999). 69

Fig. 2.23: Evaluating shear strength according to Hwang & Lee (1999). 72

Fig. 2.24: Algorithm of Hwang & Lee (1999) for post yielding cases. 73

Fig. 2.25: Biaxial strength of concrete (Russo & Somma, 2006). 76

Fig. 2.26: Evaluating shear strength according to Russo & Somma (2006) 78

Fig. 2.27: Exterior beam-to-column joint: (a) resultant of seismic action; (b) internal forces; (c) two mechanisms of shear transfer; (d) forces acting in joint core through section I-I (Tsonos, 2007) 79

Fig. 2.28: Evaluating shear strength according to Tsonos (2007). 82

Fig. 2.29: Strut and tie model for external beam-to-column joint without stirrups (a) and with stirrups (b) (Vollum & Parker, 2008). 84

Fig. 2.30: Evaluating shear strength according to Vollum & Parker (2008) – part.1. 86

Fig. 2.31: Evaluating shear strength according to Vollum & Parker (2008) – part.2. 87

Fig. 3.1: Sketch of the original specimen provided by Ehsani et al. (1987) 93

Fig. 3.2: Models for exterior joints: sensitivity to the column width b_c 94

Fig. 3.3: Models for exterior joints: sensitivity to the beam width b_b 95

Fig. 3.4: Models for exterior joints: sensitivity to the joint aspect ratio h_b / h_c 96

Fig. 3.5: Models for exterior joints: sensitivity to the Horizontal Reinforcement Index *HRI*. 97

Fig. 3.6: Models for exterior joints: sensitivity to the Beam Reinforcement Index *BRI* 99

Fig. 3.7: Models for exterior joints: sensitivity to the Column Reinforcement Index *CRI*. 100

Fig. 3.8: Models for exterior joints: sensitivity to the non-dimensional axial stress ν in the top column. 101

Fig. 3.9: Models for exterior joints: sensitivity to the concrete strength f_c 102

Fig. 3.10: Sketch of the original specimen provided by Kitayama et al. (1991). 103

Fig. 3.11: Models for interior joints: sensitivity to the column width b_c 104

Fig. 3.12: Models for interior joints: sensitivity to the beam width b_b 105

Fig. 3.13: Models for interior joints: sensitivity to the joint aspect ratio h_b / h_c 106

Fig. 3.14: Models for interior joints: sensitivity to the Horizontal Reinforcement Index *HRI* 108

Fig. 3.15: Models for interior joints: sensitivity to the Beam Reinforcement Index *BRI* 109

Fig. 3.16: Models for interior joints: sensitivity to the Column Reinforcement Index *CRI* 110

Fig. 3.17: Models for interior joints: sensitivity to the non-dimensional axial stress in the top column ν 111

Fig. 3.18: Models for interior joints: sensitivity to the concrete strength f_c 112

Fig. 4.1: Ductility capacity function of type of failure (Lee et al., 2009) 122

Fig. 4.2: Type of loading and failure for the database of exterior joints 123

Fig. 4.3: Type of loading and failure for the reduced database of exterior joints 123

Fig. 4.4: Amount of stirrups in respect of Eurocode 8 requirements. 124

Fig. 4.5: Type of loading and failure for the database of interior joints 127

Fig. 4.6: Amount of horizontal stirrups into the panel zone 127

Fig. 4.7: Horizontal test configuration for exterior joints 128

Fig. 4.8: Vertical test configuration for exterior joints 129

Fig. 4.9: Distribution of the experimental shear strength about the column base for exterior joints 131

Fig. 4.10: Distribution of the experimental shear strength about the beam base for exterior joints. 131

Fig. 4.11: Distribution of the experimental shear strength about the joint aspect ratio for exterior joints 132

Fig. 4.12: Distribution of the experimental shear strength about the horizontal reinforcement index for exterior joints. 133

Fig. 4.13: Distribution of the experimental shear strength about the Beam Reinforcement Index for exterior joints. 133

Fig. 4.14: Distribution of the experimental shear strength about the Column Reinforcement Index for exterior joints. 134

Fig. 4.15: Distribution of the experimental shear strength about the axial load for exterior joints. 134

Fig. 4.16: Distribution of the experimental shear strength about the concrete strength for exterior joints. 135

Fig. 4.17: Distribution of the experimental shear strength about the column base for interior joints. 136

Fig. 4.18: Distribution of the experimental shear strength about the beam base for interior joints. 136

Fig. 4.19: Distribution of the experimental shear strength about the joint aspect ratio for interior joints. 137

Fig. 4.20: Distribution of the experimental shear strength about the Horizontal Reinforcement Index (HRI) for interior joints. 138

Fig. 4.21: Distribution of the experimental shear strength about the Beam Reinforcement Index (BRI) for interior joints 138

Fig. 4.22: Distribution of the experimental shear strength about the Column Reinforcement Index (CRI) for interior joints 139

Fig. 4.23: Distribution of the experimental shear strength about the axial load for interior joints. 139

Fig. 4.24: Distribution of the experimental shear strength about the concrete strength for interior joints. 140

Fig. 5.1: Assessment of the ACI 352-85 (1985) for exterior joints. 145
Fig. 5.2: Assessment of the ACI 352-02 (2002) for exterior joints. 146
Fig. 5.3: Assessment of the ACI 318-05 0 for exterior joints. 147
Fig. 5.4: Assessment of the AIJ 1990 (1990) for exterior joints..... 148
Fig. 5.5: Assessment of the AIJ 1999 (1999) for exterior joints..... 149
Fig. 5.6: Assessment of the NZS 3101 (1995) for exterior joints..... 150
Fig. 5.7: Assessment of the FEMA 273 (1997) - 356 (2000) for exterior joints..... 151
Fig. 5.8: Assessment of the Eurocode 8 (EN 1995-1, 1995) for exterior joints..... 152
Fig. 5.9: Assessment of the Eurocode 8 (EN 1998-3, 2005) and NTC (2008) for exterior joints. 153
Fig. 5.10: Assessment of the NTC (2008) and OPCM 3431/05 (2005) for exterior joints. 154
Fig. 5.11: Assessment of the model by Pantazopoulo & Bonacci (1992) for exterior joints. 156
Fig. 5.12: Assessment of the model by Paulay & Priestley (1992) for exterior joints. 157
Fig. 5.13: Assessment of the model by Parker & Bullman (1997) for exterior joints. 158
Fig. 5.14: Assessment of the model by Hwang & Lee (2002) for exterior joints. 159
Fig. 5.15: Assessment of the model by Parra-Montesinos & Wight (2002) for exterior joints. 160
Fig. 5.16: Assessment of the model by Hegger et al. (2003) for exterior joints. 161
Fig. 5.17: Assessment of the model by Attaalla (2004) for exterior joints. 162
Fig. 5.18: Assessment of the model by Kim et al. (2009) for exterior joints. 163
Fig. 5.19: Assessment of the model by Zhang & Jirsa (1982) for exterior joints. 165
Fig. 5.20: Assessment of the model by Sarsam & Phillips (1985) for exterior joints..... 166
Fig. 5.21: Assessment of the model by Ortiz (1993) for exterior joints..... 167
Fig. 5.22: Assessment of the model by Scott et al. (1994) for exterior joints. 168
Fig. 5.23: Assessment of the model by Vollum & Newman (1999) for exterior joints. 169
Fig. 5.24: Assessment of the model by Hwang & Lee (1999) for exterior joints. 170
Fig. 5.25: Assessment of the model by Bakir & Boduroglu (2002) for exterior joints. 171
Fig. 5.26: Assessment of the model by Russo & Somma (2006) for exterior joints. 172

Fig. 5.27: Assessment of the model by Tsonos (2007) for exterior joints. 173

Fig. 5.28: Assessment of the model by Vollum & Parker (2008) for exterior joints..... 174

Fig. 5.29: Assessment of the ACI 352–85 (1985) for interior joints. 175

Fig. 5.30: Assessment of the ACI 352–02 (2002) for interior joints. 176

Fig. 5.31: Assessment of the ACI 318–05 (2005) for interior joints. 177

Fig. 5.32: Assessment of the AIJ 1990 (1990) for interior joints. 179

Fig. 5.33: Assessment of the AIJ 1999 (1999) for interior joints. 180

Fig. 5.34: Assessment of the NZS 3101 (1995) for interior joints. 181

Fig. 5.35: Assessment of the FEMA 273 (1997) – FEMA 356 (2000) for interior joints. 182

Fig. 5.36: Assessment of the Eurocode 8 (EN 1995-1, 1995) for interior joints. 183

Fig. 5.37: Assessment of the Eurocode 8 (EN 1998-3, 2005) and NTC (2008) for interior joints. 184

Fig. 5.38: Assessment of the NTC (2008) and OPCM 3431/05 (2005) for interior joints. 185

Fig. 5.39: Assessment of the model by Pantazopoulo & Bonacci (1992) for interior joints. 187

Fig. 5.40: Assessment of the model by Paulay & Priestley (1992) for interior joints. 188

Fig. 5.41: Assessment of the model by Parker & Bullman (1997) for interior joints. 189

Fig. 5.42: Assessment of the model by Hwang & Lee (2002) for interior joints. 190

Fig. 5.43: Assessment of the model by Parra-Montesinos & Wight (2002) for interior joints. 191

Fig. 5.44: Assessment of the model by Hegger et al. (2003) for interior joints. 192

Fig. 5.45: Assessment of the model by Attaalla (2004) for interior joints. 193

Fig. 5.46: Assessment of the model by Kim et al. (2009) for interior joints. 194

Fig. 5.47: Assessment of the model by Kitayama et al. (1991) for interior joints. 195

Fig. 5.48: Assessment of the model by Hwang & Lee (2000) for interior joints. 196

Fig. 6.1: Assessment of the recalibrated ACI 352-85 (1985) formulation for exterior joints. 229

Fig. 6.2: Assessment of the recalibrated ACI 352-02 (2002) formulation for exterior joints. 230

Fig. 6.3: Assessment of the recalibrated ACI 318-05 (2005) formulation for exterior joints. 231

Fig. 6.4: Assessment of the recalibrated AIJ 1990 (1990) formulation for exterior joints. 232

Fig. 6.5: Assessment of the recalibrated AIJ 1999 (1999) formulation for exterior joints. 233

Fig. 6.6: Assessment of the recalibrated NZS 3101 (1995) formulation for exterior joints. 234

Fig. 6.7: Assessment of the recalibrated FEMA 273 (1997) and 356 (2000) formulation for exterior joints. 235

Fig. 6.8: Assessment of the recalibrated Eurocode 8 (EN 1995, 1995) formulation for exterior joints. 236

Fig. 6.9: Assessment of the recalibrated Eurocode 8 (EN 1998, 2005) and NTC (2008) formulation for exterior joints. 237

Fig. 6.10: Assessment of the recalibrated NTC (2008) and OPCM 3431/05 (2005) formulation for exterior joints. 238

Fig. 6.11: Assessment of the recalibrated model by Pantazopoulo & Bonacci (1992) for exterior joints. 243

Fig. 6.12: Assessment of the recalibrated model by Paulay & Priestley (1992) for exterior joints. 244

Fig. 6.13: Assessment of the recalibrated model by Parker & Bullman (1997) for exterior joints. 245

Fig. 6.14: Assessment of the recalibrated model by Hwang & Lee (2002) for exterior joints. 246

Fig. 6.15: Assessment of the recalibrated model by Parra-Montesinos & Wight (2002) for exterior joints. 247

Fig. 6.16: Assessment of the recalibrated model by Hegger et al. (2003) for exterior joints. 248

Fig. 6.17: Assessment of the recalibrated model by Kim et al. (2009) for exterior joints. 249

Fig. 6.18: Assessment of the recalibrated model by Zhang & Jirsa (1982) for exterior joints. 250

Fig. 6.19: Assessment of the recalibrated model by Sarsam & Phillips (1985) for exterior joints. 251

Fig. 6.20: Assessment of the recalibrated model by Ortiz (1993) for exterior joints. 252

Fig. 6.21: Assessment of the recalibrated model by Scott et al. (1994) for exterior joints. 253

Fig. 6.22: Assessment of the recalibrated model by Vollum & Newman (1999) for exterior joints. 254

Fig. 6.23: Assessment of the recalibrated model by Hwang & Lee (1999) for exterior joints. 255

Fig. 6.24: Assessment of the recalibrated model by Bakir & Boduroglu (2002) for exterior joints. 256

Fig. 6.25: Assessment of the recalibrated model by Russo & Somma (2006) for exterior joints. 257

Fig. 6.26: Assessment of the recalibrated model by Tsonos (2007) for exterior joints. 258

Fig. 6.27: Assessment of the recalibrated model by Vollum & Parker (2008) for exterior joints. 259

Fig. 6.28: Assessment of the recalibrated ACI 352-85 (1985) formulation for interior joints. 261

Fig. 6.29: Assessment of the recalibrated ACI 352-02 (2002) formulation for interior joints. 262

Fig. 6.30: Assessment of the recalibrated ACI 318-05 (2005) formulation for interior joints. 263

Fig. 6.31: Assessment of the recalibrated AIJ 1990 (1990) formulation for interior joints. 264

Fig. 6.32: Assessment of the recalibrated AIJ 1999 (1999) formulation for interior joints. 265

Fig. 6.33: Assessment of the recalibrated NZS 3101 (1995) formulation for interior joints. 266

Fig. 6.34: Assessment of the recalibrated FEMA 273 (1997) – 356 (2000) formulation for interior joints. 267

Fig. 6.35: Assessment of the recalibrated Eurocode 8 (EN 1995, 1995) formulation for interior joints. 268

Fig. 6.36: Assessment of the recalibrated Eurocode 8 (EN 1998, 2005) and NTC (2008) formulation for interior joints 269

Fig. 6.37: Assessment of the recalibrated NTC (2008) and OPCM 3431/05 (2005) formulation for interior joints. 270

Fig. 6.38: Assessment of the recalibrated model by Pantazopoulo & Bonacci (1992) for interior joints. 273

Fig. 6.39: Assessment of the recalibrated model by Paulay & Priestley (1992) for interior joints. 274

Fig. 6.40: Assessment of the recalibrated model by Parker & Bullman (1997) for interior joints. 275

Fig. 6.41: Assessment of the recalibrated model by Hwang & Lee (2002) for interior joints. 276

Fig. 6.42: Assessment of the recalibrated model by Parra-Montesinos & Wight (2002) for interior joints. 277

Fig. 6.43: Assessment of the recalibrated model by Hegger et al. (2003) for interior joints. 278

Fig. 6.44: Assessment of the recalibrated model by Kim et al. (2009) for interior joints. 279

Fig. 6.45: Assessment of the recalibrated model by Kitayama et al. (1991) for interior joints. 280

Fig. 6.46: Assessment of the recalibrated model by Hwang & Lee (2000) for interior joints. 281

Fig. 6.47: Probabilistic Assessment of the original and recalibrated ACI 352-85 (1985) formulation for exterior joints. 284

Fig. 6.48: Probabilistic Assessment of the original and recalibrated ACI 352-02 (2002) formulation for exterior joints. 285

Fig. 6.49: Probabilistic Assessment of the original and recalibrated ACI 318-05 (2005) formulation for exterior joints. 286

Fig. 6.50: Probabilistic Assessment of the original and recalibrated AIJ 1990 (1990) formulation for exterior joints. 287

Fig. 6.51: Probabilistic Assessment of the original and recalibrated AIJ 1999 (1999) formulation for exterior joints. 288

Fig. 6.52: Probabilistic Assessment of the original and recalibrated NZS 3101 (1995) formulation for exterior joints. 289

Fig. 6.53: Probabilistic Assessment of the original and recalibrated FEMA 273 (1997) – 356 (2000) formulation for exterior joints. 290

Fig. 6.54: Probabilistic Assessment of the original and recalibrated Eurocode 8 (EN 1995, 1995) formulation for exterior joints. 291

Fig. 6.55: Probabilistic Assessment of the original and recalibrated Eurocode 8 (EN 1998, 2005) and NTC (2008) formulation for exterior joints. 292

Fig. 6.56: Probabilistic Assessment of the original and recalibrated NTC (2008) and OPCM 3431 (2005) formulation for exterior joints. 293

Fig. 6.57: Probabilistic Assessment of the original and recalibrated model by Pantazopoulo & Bonacci (1992) for exterior joints. 294

Fig. 6.58: Probabilistic Assessment of the original and recalibrated model by Paulay & Priestley (1992) for exterior joints. 295

Fig. 6.59: Probabilistic Assessment of the original and recalibrated model by Parker & Bullman (1997) for exterior joints. 296

Fig. 6.60: Probabilistic Assessment of the original and recalibrated model by Hwang & Lee (2002) for exterior joints. 297

Fig. 6.61: Probabilistic Assessment of the original and recalibrated model by Parra-Montesinos & Wight (2002) for exterior joints. 298

Fig. 6.62: Probabilistic Assessment of the original and recalibrated model by Hegger et al. (2003) for exterior joints. 299

Fig. 6.63: Probabilistic Assessment of the original and recalibrated model by Kim et al. (2009) for exterior joints. 300

Fig. 6.64: Probabilistic Assessment of the original and recalibrated model by Zhang & Jirsa (1982) for exterior joints. 301

Fig. 6.65: Probabilistic Assessment of the original and recalibrated model by Sarsam & Phillips (1985) for exterior joints. 302

Fig. 6.66: Probabilistic Assessment of the original and recalibrated model by Ortiz (1993) for exterior joints. 303

Fig. 6.67: Probabilistic Assessment of the original and recalibrated model by Scott et al. (1994) for exterior joints. 304

Fig. 6.68: Probabilistic Assessment of the original and recalibrated model by Vollum & Newman (1999) for exterior joints. 305

Fig. 6.69: Probabilistic Assessment of the original and recalibrated model by Hwang & Lee (1999) for exterior joints. 306

Fig. 6.70: Probabilistic Assessment of the original and recalibrated model by Bakir & Boduroglu (2002) for exterior joints. 307

Fig. 6.71: Probabilistic Assessment of the original and recalibrated model by Russo & Somma (2006) for exterior joints. 308

Fig. 6.72: Probabilistic Assessment of the original and recalibrated model by Tsonos (2007) for exterior joints. 309

Fig. 6.73: Probabilistic Assessment of the original and recalibrated model by Vollum & Parker (2008) for exterior joints. 310

Fig. 6.74: Probabilistic Assessment of the original and recalibrated ACI 352-85 (1985) formulation for interior joints 311

Fig. 6.75: Probabilistic Assessment of the original and recalibrated ACI 352-02 (2002) formulation for interior joints 312

Fig. 6.76: Probabilistic Assessment of the original and recalibrated ACI 318-05 (2005) formulation for interior joints 313

Fig. 6.77: Probabilistic Assessment of the original and recalibrated AIJ 1990 (1990) formulation for interior joints. 314

Fig. 6.78: Probabilistic Assessment of the original and recalibrated AIJ 1999 (1999) formulation for interior joints. 315

Fig. 6.79: Probabilistic Assessment of the original and recalibrated NZS 3101 (1995) formulation for interior joints 316

Fig. 6.80: Probabilistic Assessment of the original and recalibrated FEMA 273 (1997) – 356 (2000) formulation for interior joints. 317

Fig. 6.81: Probabilistic Assessment of the original and recalibrated Eurocode 8 (EN 1995, 1995) formulation for interior joints 318

Fig. 6.82: Probabilistic Assessment of the original and recalibrated Eurocode 8 (EN 1998, 2005) and NTC (2008) formulation for interior joints 319

Fig. 6.83: Probabilistic Assessment of the original and recalibrated NTC (2008) and OPCM 3431 (2005) formulation for interior joints. 320

Fig. 6.84: Probabilistic Assessment of the original and recalibrated model by Pantazopoulo & Bonacci (1992) for interior joints 321

Fig. 6.85: Probabilistic Assessment of the original and recalibrated model by Paulay & Priestley (1992) for interior joints. 322

Fig. 6.86: Probabilistic Assessment of the original and recalibrated model by Parker & Bullman (1997) for interior joints 323

Fig. 6.87: Probabilistic Assessment of the original and recalibrated model by Hwang & Lee (2002) for interior joints 324

Fig. 6.88: Probabilistic Assessment of the original and recalibrated model by Parra-Montesinos & Wight (2002) for interior joints 325

Fig. 6.89: Probabilistic Assessment of the original and recalibrated model by Hegger et al. (2003) for interior joints. 326

Fig. 6.90: Probabilistic Assessment of the original and recalibrated model by Kim et al. (2009) for interior joints. 327

Fig. 6.91: Probabilistic Assessment of the original and recalibrated model by Kitayama et al. (1991) for interior joints. 328

Fig. 6.92: Probabilistic Assessment of the original and recalibrated model by Hwang & Lee (2000) for interior joints. 329

Fig. 6.93: Assessment of the proposed model for exterior joints. 334

Fig. 6.94: Assessment of the proposed model for under-reinforced joints. 335

Fig. 6.95: Specimens with headed bars. 336

Fig. 6.96: Probabilistic Assessment of the proposed model. 337

Fig. 7.1: Load histories with 2 constant cycles (left) and variable amplitude (right). 339

Fig. 7.2: Example of complex load histories. 340

Fig. 7.3: Example of load histories with initial steps in force control and then in displacement control. 340

Fig. 7.4: Relationship between shear strength and number of cycles needed for acting joint failure. 341

Fig. 7.5: Fatigue curves for interior unreinforced joints 346

Fig. 7.6: Fatigue curves for interior reinforced joints. 346

Fig. 7.7: Comparison of the fatigue curves for interior reinforced and unreinforced joints. 347

Fig. 7.8: Fatigue curves for exterior unreinforced joints. 350

Fig. 7.9: Fatigue curves for exterior reinforced joints. 351

Fig. 7.10: Comparison of the fatigue curves for exterior reinforced and unreinforced joints. 352

Fig. 8.1: Existing simulation models for beam-column joints (Celik & Ellingwood, 2008). 354

Fig. 8.2: Idealization of the joint shear elements for Biddha & Ghobarah (1999). 356

Fig. 8.3: Joint shear and bond-slip elements (Biddha & Ghobarah, 1999). 356

Fig. 8.4: Equilibrium of an interior beam-to-column joint. 358

Fig. 8.5: Trilinear moment-rotation relationship for the shear spring. 359

Fig. 8.6: Moment-rotation relationship for simulating bond-slip. 360

Fig. 8.7: Stress and strain distribution assumption in the joint. 360

Fig. 8.8: Definition of L_{max} and $L_{y,max}$. 361

Fig. 8.9: Hysteretic model accounting pinching effects. 363

Fig. 8.10: Joint model developed by Youssef & Ghobarah (2001). 364

Fig. 8.11: Geometry of the model by Youssef & Ghobarah (2001). 365

Fig. 8.12: Hysteretic model for the steel spring. 366

Fig. 8.13: Hysteretic model for the concrete spring. 368

Fig. 8.14: Stress-strain relation for confined and unconfined concrete with $f_c' = 30$ MPa. 369

Fig. 8.15: Hysteretic shear model by Youssef & Ghobarah (1999). 371

Fig. 8.16: Model for joint behaviour proposed by Pampanin et al. (2003). 372

Fig. 8.17: Strength degradation curve for exterior joints. 373

Fig. 8.18: Monotonic and cyclic behaviour of the shear hinge model. 374

Fig. 8.19: Beam-to-column joint element proposed by Mitra & Lowes (2007). 375

Fig. 8.20: Internal and external generalized displacements resultants. 376

Fig. 8.21: Definition of component deformations and generalized forces: (a) Component deformations and forces, (b) Shear forces acting on shear-panel component. 377

Fig. 8.22: One-dimensional material model: (a) Material states, (b) Impact of hysteretic damage rules on load-deformation response. 378

Fig. 8.23: Bond stress and bar stress distribution for a bar anchored in a beam-to-column joint. 381

Fig. 8.24: Joint model developed by Trowland (2003). 385

Fig. 8.25: Hysteretic behaviour of Takeda et al. (1970). 386

Fig. 8.26: Joint model by Shin & LaFave (2004). 387

Fig. 8.27: Simplified envelope joint shear stress vs. strain relationship. 387

Fig. 8.28: Modified compression field theory proposed by Vecchio & Collins (1986). 390

Fig. 8.29: Model by Shin & LaFave (2004) for a beam-column connection subassembly. 392

Fig. 8.30: Combination of three bilinear joint springs in parallel. 393

Fig. 8.31: Hysteretic behaviour of the joint model..... 394

Fig. 8.32: Stress and strain distributions (after yielding) assumed by Morita & Kaku (1984)..... 395

Fig. 8.33: Trilinear asymmetric curve available in SeismoStruct. 397

Fig. 8.34: Details of specimens O4 and O5 provided by Hakuto et al. (2000). 398

Fig. 8.35: Cyclic response of the specimens O4. 398

Fig. 8.36: Model of interior joint developed in SeismoStruct. 399

Fig. 8.37: Comparison between analytical and experimental cyclic behaviour for the specimen O4. 400

Fig. 8.38: Details of the specimen JC-2 provided by Chun & Kim (2004). 401

Fig. 8.39: Model of the exterior joint JC-2 built in SeismoStruct. 402

Fig. 8.40: Comparison between analytical simulation and experimental response of JC-2 specimen..... 402

Fig. 8.41: Idealization of exterior joint element in frame analysis. 403

Fig. 8.42: Pivot Model..... 404

Fig. 8.43: Experimental tests provided by Chun & Kim (2004). 407

Fig. 8.44: Experimental test provided by Hwang et al. (2004)..... 408

Fig. 8.45: Experimental tests provided by Chutarat & Aboutaha (2003): specimen 1 (on the left) and specimen namely A (on the right). 408

Fig. 8.46: Characteristics of the specimens provided by Clyde et al. (2000). 409

Fig. 8.47: Specimen provided by Economou et al. (1998). 409

Fig. 8.48: Characteristics of the specimens provided by Ehsani et al. (1987). 410

Fig. 8.49: Sketch of the specimens provided by Ehsani & Wigth (1985). 410

Fig. 8.50: Characteristics of the specimens provided by Ehsani & Wigth (1985). 411

Fig. 8.51: Simulated and observed response for specimens provided by Chun & Kim (2004). 415

Fig. 8.52: Simulated and observed response for specimens provided by Chutarat & Aboutaha (2003). 415

Fig. 8.53: Simulated and observed response for specimens provided by Clyde et al. (2000)..... 416

Fig. 8.54: Simulated and observed response for specimens provided by Hwang et al. (2004) and Economou et al. (1998)..... 416

Fig. 8.55: Simulated and observed response for specimens provided by Ehsani et al. (1987)..... 416

Fig. 8.56: Simulated and observed response for specimens provided by Ehsani & Wight (1985)..... 417

Fig. 9.1: Bi-linearization of the PushOver curve according to the N2-Method..... 423

Fig. 9.2: Graphical example of the structural response achieved through NLTH analysis..... 425

Fig. 9.3: Relationship between pulsation and damping equal to 5%..... 429

Fig. 9.4: Models of the plane frame without joint damage (on the left) and accounting the nonlinearity of exterior joint..... 434

Fig. 9.5: 3D structure considered in the analysis..... 435

Fig. 9.6: Tri-dimensional representation of the 3D structures..... 436

Fig. 9.7: Constitutive laws of concrete (on the left) and steel (on the right)..... 440

Fig. 9.8: Capacity curve with and without joint behaviour..... 442

Fig. 9.9: Elastic ADRS spectra..... 443

Fig. 9.10: Vulnerability parameter α at different limit states, considering flexural and shear failure mechanisms for frame with 4 floors..... 444

Fig. 9.11: Vulnerability parameter α at different limit states, considering flexural and shear failure mechanisms for frame with 3 floors..... 445

Fig. 9.12: Vulnerability parameter α at different limit states, considering flexural and shear failure mechanisms for frame with 2 floors..... 445

Fig. 9.13: Accelerograms of El Centro-1940 (Chopra, 1995)..... 446

Fig. 9.14: Response spectrum of El Centro-1940 (Chopra, 1995) and corresponding response spectrum of Newmark & Hall (1982)..... 446

Fig. 9.15: Comparison of time history analysis..... 447

Fig. 10.1: Average Quadratic Error Δ of Code Formulations for exterior joints..... 451

Fig. 10.2: Coefficient of Determination R^2 of Code Formulations for exterior joints..... 452

Fig. 10.3: Average Quadratic Error Δ of Capacity Models for exterior joints..... 453

Fig. 10.4: Coefficient of Determination R^2 of Capacity Models for exterior joints..... 454

Fig. 10.5: Average Quadratic Error Δ of Code Formulations for interior joints..... 455

Fig. 10.6: Coefficient of Determination R^2 of Code Formulations for interior joints..... 456

Fig. 10.7: Average Quadratic Error Δ of Capacity Models for interior joints..... 457

Fig. 10.8: Coefficient of Determination R^2 of Capacity Models for interior joints..... 458

Fig. 10.9: Average Quadratic Error Δ of recalibrated Code Formulations and proposed formula for exterior joints..... 460

Fig. 10.10: Average Quadratic Error Δ of recalibrated Capacity Models and proposed formula for exterior joints..... 461

Fig. 10.11: Average Quadratic Error Δ of recalibrated Code Formulations for interior joints..... 462

Fig. 10.12: Average Quadratic Error Δ of recalibrated Capacity Models for interior joints..... 463

Fig. 10.13: Factor of dispersion of the capacity β_C for the total set of specimens on exterior joints..... 464

Fig. 10.14: Factor of dispersion of the capacity β_C for unreinforced exterior joints..... 465

Fig. 10.15: Factor of dispersion of the capacity β_C for under-reinforced exterior joints..... 466

Fig. 10.16: Factor of dispersion of the capacity β_C for EC8-compliant exterior joints..... 467

Fig. 10.17: Factor of dispersion of the capacity β_C for the total set of specimens on interior joints..... 468

Fig. 10.18: Factor of dispersion of the capacity β_C for unreinforced interior joints..... 468

Fig. 10.19: Factor of dispersion of the capacity β_C for reinforced interior joints..... 468

Fig. 10.20: Fatigue curves for interior joints both reinforced and unreinforced..... 469

Fig. 10.21: Fatigue curves for exterior joints both reinforced and unreinforced..... 470

List of Tables

Table 2.1: Values of γ for beam-to-column joints provided by ACI 352-85. (1985) 19

Table 2.2: Values of γ for beam-to-column joints provided by ACI 352-02 (2002). 20

Table 2.3: Values of γ for beam-to-column joints provided by FEMA 273 (1997)..... 23

Table 2.4: Shear reinforcement coefficient factor α_2..... 49

Table 3.1: Original specimen provided by Ehsani et al. (1987). 92

Table 3.2: Original specimen provided by Kitayama et al. (1991). 103

Table 4.1: Experimental database collecting exterior beam-to-column joints..... 115

Table 4.2: Experimental database collecting interior beam-to-column joints. 124

Table 5.1: Error and scatter measures for Code Formulation for exterior joints..... 198

Table 5.2: Error and dispersion measures for the Capacity Models available in literature for exterior joints. 200

Table 5.3: Error and dispersion measures for Code Formulation for interior joints. 205

Table 5.4: Error and dispersion measures for the Capacity Models available in literature for interior joints. 207

Table 5.5: Measures of error and factor of dispersion of the capacity for code formulations for exterior joints. 214

Table 5.6: Measures of error and factor of dispersion of the capacity for the capacity models for exterior joints. 216

Table 5.7: Measures of error and factor of dispersion of the capacity for code formulations for interior joints. 219

Table 5.8: Measures of error and factor of dispersion of the capacity for the capacity models about interior joints. 221

Table 6.1: Recalibration factors and Average Quadratic Error of the recalibrated Code Formulation for exterior joints. 226

Table 6.2: Recalibration factors and Average Quadratic Error of the recalibrated Capacity Models for exterior joints. 239

Table 6.3: Recalibration factors and Average Quadratic Error of the recalibrated Code Formulation for interior joints. 260

Table 6.4: Recalibration factors and Average Quadratic Error of the recalibrated Capacity Models for interior joints..... 271

Table 6.5: Numerical coefficients and measures of error and dispersion of the basic formula..... 331

Table 6.6: Numerical coefficients and measures of error and dispersion of the removal process..... 332

Table 6.7: Numerical coefficients and measures of error and dispersion of the simplified formula..... 332

Table 6.8: Numerical coefficients and measures of error and dispersion of the contribution of the horizontal stirrups into the joint..... 333

Table 6.9: Measures of error and factor of dispersion of the proposed formulation for exterior joints..... 337

Table 7.1: Geometric and mechanical characteristics and parameters of the cyclic behaviour of the specimen X1 provided by Durrani & Wight (1982)..... 344

Table 7.2: Values of *m* for specimens on unreinforced interior joints..... 345

Table 7.3: Values of *m* for specimens on reinforced interior joints..... 347

Table 7.4: Mean fatigue curves for interior joints..... 348

Table 7.5: Geometric and mechanical characteristics and parameters of the cyclic behaviour of the specimen JB-s1 provided by Chalioris et al. (2008)..... 349

Table 7.6: Values of *m* for specimens on unreinforced exterior joints..... 350

Table 7.7: Values of *m* for specimens on reinforced exterior joints..... 350

Table 7.8: Mean fatigue curves for exterior joints..... 352

Table 8.1: Average Bond Strengths as a Function of Steel Stress State..... 382

Table 8.2: Geometric and mechanical characteristics of the specimen O4..... 399

Table 8.3: Calibrated parameters of the hysteretic bond-slip curve..... 400

Table 8.4: Geometric and mechanical characteristics of the specimen JC-2..... 401

Table 8.5: Calibrated parameters of the hysteretic bond-slip curve for specimen JC-2..... 402

Table 8.6: Database for exterior beam-to-column joints under cyclic loading..... 407

Table 8.7: Strength and stiffness for Pivot model in analysed specimens (units in N-mm)..... 412

Table 8.8: Degradation parameters for Pivot model in analysed specimens..... 413

Table 9.1: Geometric characteristics of the columns..... 437
Table 9.2: Geometric characteristics of the beams. 437
Table 9.3: Layout of the column in the structure. 438
Table 9.4: Layout of the beam in the structure at the roof floor. 438
Table 9.5: Layout of the beam in the structure at the intermediate floors..... 439
Table 9.6: Parameters of the seismic action. 443